CARBONIFEROUS SEDIMENT DISPERSAL INTO THE OUACHITA BASIN AND TECTONIC EVOLUTION OF THE OUACHITA FOLD-AND-THRUST BELT, OKLAHOMA

A Dissertation

by

HAROLD EVERETT JOHNSON II

Submitted to the Office of Graduate and Professional Studies of
Texas A&M University
in partial fulfillment of the requirements for the degree of

DOCTOR OF PHILOSOPHY

Chair of Committee,	Michael Pope
Committee Members,	Julie Newman
	Brent Miller
	Mitch Malone
Head of Department,	Michael Pope

August 2019

Major Subject: Geology

ABSTRACT

The highly-deformed rocks of western Arkansas to eastern Oklahoma, record the Late Paleozoic tectonic history of the southern boundary of the North American Craton. The Mississippian rocks (i.e., Stanley Group) were deposited in the Ouachita Basin, a basin located adjacent to the North American Craton. Detrital zircon and muscovite spectra indicate a shift in sediment sourcing from Gondwanan crust in Mississippian to Laurentian crust during deposition of the Pennsylvanian Jackfork Group. This provenance shift suggests the craton was exposed and distal sediments were carried 100s of kilometers by large rivers to the Ouachita Basin. A lack of Alleghanian-aged sediment precludes a paleo-drainage linking the Ouachita Basins to any eastward basins indicating that the Cincinnati Arch served as the drainage divide.

Thermal maturation, illite and chlorite 'crystallinity', indicate sufficient burial to reach temperatures ~ 300°C. Using a reasonable range for the geothermal gradient of 15 to 40°C, an estimated 8-14km of overburden were removed from above the present-day Benton Uplift, western Arkansas. Folding and thrust faulting of the Stanley and Jackfork groups occurred during the final stages of the Ouachita orogenesis. As the Ouachita Orogen evolved, wedge models predict the shape and sequence of internal structure development. Thermochronology was used to date the cooling of the rocks through temperatures of approximately 205°C, 180°C, and 110°C using techniques of zircon fission track, (U-Th)/He zircon, and apatite fission track, respectively. Zircon fission track minimum ages (259 ± 34 Ma to 365± 66 Ma) were determined from 643 grain

analyses. (U-Th)/He zircon dates span 181.6 ± 14.53 Ma to 1964.2 ± 157.13 Ma, with the youngest date for each sample providing a range from 181.6 ± 14.53 Ma to 347.6 Ma. Zircon fission track minimum ages record development of the fold and thrust belt (FTB) wedge, whereas the (U-Th)/He dates give paleotopography of the critical wedge. Thus, the internal motion of thrusts and folding of the FTB occurred Pennsylvanian to Early Permian. Paleotopography slope was foreland-directed with the present-day surface of the Broken Bow Uplift buried at ~9 km during Late Triassic-Middle Jurassic, assuming geothermal gradient of 20°C/km and zircon (U-Th)/He closure of ~180°C.

DEDICATION

For Dr. David Vilander Wiltschko – mentor and friend, in memoriam.

How will you search for it, Socrates,

When you have no idea what it is?

What kind of thing from among those you are ignorant of will you set

before yourself to look for?

And even if you happened exactly upon it, how

would you recognize that this is what you didn't know?

- Plato, *Meno*

ACKNOWLEDGEMENTS

With admiration, I express sincere gratitude to Dr. David V. Wiltschko for his extraordinary mentorship as my graduate advisor, and for sharing his genuine passion of geology with me. Dave was responsible for introducing me to the complex geology of the Ouachita Orogenic Belt and its much debated tectonic evolution. I cherished the weekly meetings where we discussed research topics, including means to improve my manuscript writing, ideas for more succinct figures, and his stylistic presentation changes for better comprehension. He served as my advisor during my MSc Geology and the early part of my PhD before his unforeseen passing. Besides my family, Dr. Wiltschko is the only person who has so greatly impacted my life.

My entire committee is thanked for providing edits on complete manuscripts. I thank Dr. Mike Pope for suggestions on early manuscript drafts of the provenance project and the thermochronology project. A special thank you to Dr. John P. Harris for use of his clay mineralogy lab at Sam Houston State University and for his significant contribution to the crystallinity manuscript, including submission to a peer-reviewed journal. I thank Dr. Mitch Malone for his willingness to be my outside committee member on short notice because of changes to my committee, and for his comments that materially improved all of the enclosed manuscripts.

For the provenance research project (manuscript #1), I appreciate the time taken by Dr. Willis Hames to teach me the separation and dating of detrital muscovite in his argon lab at Auburn University. I thank Tim Wuenscher, Geary Evans, and Simon

Murillo for aiding in picking 32 muscovite separates to aid this project. Backscatter electron imaging done by Dr. Andrew Mott at the TAMU Materials Characterization Facility provided a grain location map during U-Pb analysis and his help is sincerely appreciated. Luz Romero provided technical guidance for LA-ICP-MS and her suggestions are very much appreciated. Dawid Szafranski and Eric Peavey provided edits to an early manuscript, and they are sincerely thanked for their comments.

For the crystallinity research project (manuscript #2), H. J. Kisch (Ben-Gurion University of the Negev, Israel) kindly provided illite 'crystallinity' calibration standards. R. N. Guillemette and R.K. Popp helped with the XRD analyses. Jennifer Piper allowed us to collect samples on her sample collection trip. AAPG James E. Hooks Memorial Research Grant to H. Johnson and M.T. Halbouty Chair in geology to D. Wiltschko funded this project. Constructive comments from J. Hill (SHSU) and an anonymous reviewer helped improve this manuscript.

The thermochronology research project (manuscript #3) was influenced from earlier discussions with the late Dr. David Wiltschko. Sampling was permitted because of the generosity of Weyerhaeuser NR Company and we extend our gratitude to William Willis, who arranged permission on our behalf. Jacob Thompson was of foremost help in sampling, and his effort are much appreciated. Project completion would not have been possible without the use of research labs overseen by S.Thomson (Univ. of Arizona) and D. Stockli (Univ. of Texas - Austin). Both research labs accommodated several visits for the author to learn the methods and have the opportunity for research discussions. TAMU facilities were used to separate heavy minerals from bulk rock.

Undergraduates were involved on different steps of the project with direct supervision by H. Johnson: A. Kourakis (rock crushing), J. Thompson (rock crushing, heavy liquids, mineral picking, zircon descriptions, jacketing zircons), T. Wuenscher (mineral picking, jacketing zircons), G. Evans (mineral picking), C. Merrill (sampling), B.Terrell (rock crushing), and J. Sanchez (drill cutting pulverizing, zircon descriptions).

William Willis (Weyerhaeuser) provided his personal cabin to the author and J. Thompson for final two weeks of sampling. His kindness was very much appreciated, and he is thanked for use of his cabin at no expense.

Lastly, there are many people who provided support and general discussion while I completed my graduate study. My parents, Harold Sr. and Diana, have always been supportive of my goals and I am very thankful for their encouragement. I was fortunate to have interacted with many excellent students, undergraduate and graduate, and to have learned from them along the way. One of the most fruitful learning experiences was field mapping with Dr. Michael Heaney and many undergraduates. On these trips, it was common to approach (geologic) problems in two ways: 1) Do what feels right, and 2) Adapt, modify, and overcome. I am very appreciative to have been given the opportunity to study interesting geology in Mason TX, Dillon MT, and Costa Rica while serving as a graduate teaching assistant and field camp instructor.

CONTRIBUTORS AND FUNDING SOURCES

Contributors

This work was supervised by a thesis dissertation committee consisting of Drs. Michael Pope (advisor), Julie Newman, and Brent Miller of the Department of Geology and Geophysics, Dr. Mitch Malone of the Department of Oceanography, and Dr. John P. Harris (clay mineralogy expert) of the Department of Geography and Geology at Sam Houston State University.

Isotopic data presented in Chapter 2 were measured using mass spectrometers in labs at TAMU and Auburn University. Specialized steps in the analyses depicted in Chapter 4 were determined in part by Drs. Daniel Stockli and Stuart Thomson.

All other work conducted for the dissertation was completed by the student independently.

Funding Sources

Graduate study was supported by a Marathon Fellowship (2012), Energy Cup Fellowship (2013), Unocal Graduate Fellowship (2013), Association of Former Students Pooled Scholarship (2014-15), Claude Scruggs Scholarship (2014), Kenneth P. Pipes Fellowship (2015), and graduate teaching assistantship from Texas A&M University.

NSF Grant (EAR-0929922) to S. Thomson aided in fission track data acquisition. Travel funding for bulk rock sample collection by H. Johnson was from a Bush Foundation Travel Grant (HJ), a Sigma Xi Grants-in-Aid of Research Grant (HJ), an American Association of Petroleum Geologists Thomas A. Hendricks Grant (HJ), and a

portion of a NSF Grant (EAR-0643309) to D. Thomas, E. Grossman, B. Miller, T. Olszewski, and T. Yancey. This work was also made possible in part by National Science Foundation under Grant Numbers EAR-0929922 and EAR-0643309. Its contents are solely the responsibility of the authors and do not necessarily represent the official views of the National Science Foundation.

Travel to research labs (one 2-week trip to Univ. of Arizona, two 5-day trips to Auburn Univ., and six 1-day trips to Univ. of Texas – Austin) to get samples processed for data analysis were primarily paid with personal funds. A reduced rate for fission track analysis was granted to me by Dr. Stuart Thomson in absence of research funds for analytical steps. Co-authors, Drs. Daniel Stockli and Willis Hames, funded respective analytical costs with internal funds. Funding gained through an opportunity to serve as TAMU field camp instructor was used to pay for expenses related to collection of Weyerhaeuser 1-22 wet drill cuttings, which entailed of 3 trips to Hot Springs AR and 1.5 months of on-site laboratory work.

TABLE OF CONTENTS

Page

1. INTRODUCTION

Late Paleozoic orogenesis on the southern margin of Laurussia during collision with Gondwana and closure of the Rheic Ocean formed the supercontinent Pangea (Arbenz, 1989). The Ouachita orogen of western Arkansas and eastern Oklahoma record the evolution along this trend as the Ouachita remnant ocean basin evolved into the Carboniferous Ouachita fold and thrust belt (FTB).

Sedimentary basins adjacent to tectonically active margins preserve sediments that record progression of orogenesis and subsequent modification of regional drainage patterns (Archer and Greb, 1995). Dating of detrital minerals from sediments within these basins identify shifts in sediment provenance, which indicates major tectonic events. The Ouachita Basin has a pronounced provenance change from mixed crustal grains in the Mississippi Stanley Group to primarily Laurussian crustal grains in the Pennsylvanian Jackfork Group.

To complement the sedimentary record, the basin thermal history provides temperature and timing of heating, maximum temperatures, and timing of cooling of the syntectonic rocks (Pevear, 1999). Thermal maturation, such as vitrinite reflectance, illite and chlorite ‘crystallinity’, and clay mineralogy, provides a measure of maximum temperatures. Assumptions of the appropriate geothermal gradient and lack of anomalous heat source (e.g., igneous plutons) overprint are used to calculate an estimated depth of burial. The maximum temperature calculated from both illite and chlorite ‘crystallinity’ is ~300°C in the Ouachita orogen, Arkansas. Moreover, there is a

decrease in ‘crystallinity’ away from the axial trace of the Benton Uplift, a crustal-scale anticlinal structure.

Timing of the cooling of the rock, such as by uplift toward the surface caused by thrust motion, is resolved by thermochronology (e.g., Reiners et al., 2018). Specific radiometric systems (e.g., (U-Th)/He and fission track) retain daughter product(s) at specific closure temperatures making these systems useful in understanding uplift pathways. Timing of cooling may be used to test wedge model theory, whereby a critical taper forelandward away from the thicker hinterland occurs during active orogenesis as well as a predictable deformation sequence (Elliot, 1976; Chapple, 1978). Zircon fission track, zircon (U-Th)/He, and apatite fission track thermochronometers for the Ouachita FTB give record development of the FTB wedge, whereas the (U-Th)/He dates give paleotopography of the critical wedge.

The wedge model paradigm, coupled with thermal maturation (i.e., ‘crystallinity) and thermochronology, is a robust method of observing ancient FTBs by indirectly creating better structural interpretations, especially where internal subsurface structures are poorly known. A most complete tectonic history is possible to delineate with the addition of detrital geochronology and insight into the provenance shift during active tectonics.

2. SEDIMENTATION AND TECTONIC IMPLICATIONS OF A MISSISSIPPIAN STANLEY GROUP TO PENNSYLVANIAN JACKFORK GROUP PROVENANCE SHIFT IN THE OUACHITA BASIN, OKLAHOMA

2.1. Overview

Early Carboniferous increased sedimentation rates associated with turbidite deposition into the Ouachita Basin record the closure of the Paleo-Tethys-Rheic (Theic) Ocean during collision of Laurussia (North America and Baltica) and Gondwana to form the supercontinent Pangea. Continued removal of sediments in source areas following a significant relative sea-level drop accelerated weathering of the Laurussia craton, resulting in a provenance shift to more distal sources. This study investigates the closure of the Ouachita Basin and subsequent modification of continent-scale drainage patterns as sediments in this basin preserve a record of major Carboniferous tectonic events for North America.

Geochronologic ages for zircon and muscovite from the detritus of both the Mississippian Stanley Group (320.7 ± 2.5 Ma to ca. 330 Ma) and Pennsylvanian Jackfork Group (ca. 310 Ma to ca. 320 Ma) of the Ouachita Basin indicate age of the source areas. Multi-sourced provenance of the Mississippian Stanley Group is well-documented because the detritus comprises a mix of Laurentian and Gondwanan crustal grains. The Pennsylvanian Jackfork Group lacks an Alleghanian component, especially in the muscovite spectrum, which constrains the sediment pathway to bypass the Greater Black Warrior Basin; this basin contains abundant Alleghanian muscovite. Recycling of

sediments within the proximal Illinois Basin, medial Michigan Basin, or distal headwaters originating in the Maritime Province of Canada are all possible Laurussian provenances for the Pennsylvanian Jackfork Group sediment carried by a continental-scale drainage, the Michigan River.

2.2. Introduction

There are different types of sedimentary basins, but their common attribute is that all basins are infilled with detritus, sourced from local to more distal sources (e.g., Archer and Greb, 1995; Leighton, 1996; Ingersoll et al., 2003). Detritus, collectively preserved sedimentary packages, provides insight into the geologic evolution of the basin, the extent of drainage catchments, and influence of external factors (e.g., tectonics or sea-level change) on the sediment provenance (Archer and Greb, 1995; Miall and Blakey, 2019; Gehrels, 2012, 2014).

A large-scale global collisional tectonic event, such as the formation of a supercontinent, uplifts large portions of the crust along this active plate boundary for erosion, and thus supplies great volumes of detritus to large rivers that traverse the supercontinent (Fig. 1; Archer and Greb, 1995; Rainbird et al., 2014). Minerals, such as zircon and muscovite, are common within these sedimentary deposits, and each grain/flake age (i.e. U-Pb zircon and $^{40}Ar/^{39}Ar$ muscovite) represents the timing of crystallization and in situ cooling of the grain within the original source rock (McDougal and Harrison, 1999; Schoene, 2014). A population of detrital ages for a given sample may be used to distinguish the source areas, or provenance that contribute detritus (e.g., Archer and Greb, 1995).

A modern example of active basin development is the Himalayan orogeny located between the northward-moving Indian Plate relative to the Eurasian Plate (Fig. 2A; Graham et al., 1975; Graham et al., 1976). The hinterland is in the vicinity of the suture lines on Figure 2A and mountain ranges meet at a location called a syntaxis (Graham et al., 1975; Graham et al., 1976). A majority of the sediments shed off of the hinterland and indo-gangetic lowland, shown in Figure 2A, are transported by the Ganges River, a continent-scale river system, to the basin containing the Bengal Fan (Graham et al., 1975). An eastern subduction zone subducts the eastern edge of the Indian Plate and overlying Bengal Fan underneath the Eurasian Plate (Graham et al., 1975). A similar plate configuration formed in the Mississippian when the Ouachita basin became a remnant ocean basin as the Paleo-Tethys-Rheic (Theic) Ocean closed (Fig. 2B; Graham et al., 1975; Blakey, 2008). The Late Mississippian paleogeography (Fig. 2B) illustrates similarities between the Himalayan and Appalachian-Ouachita orogenies (Graham et al., 1975). Tectonic elements shared between both orogenies include the presence of a hinterland, a peripheral foreland basin, a syntaxis, and a remnant basin.

The region to the southwest of the Appalachian hinterland represents the estimated geometry of the Ouachita Basin (dashed square outline). A block model of this area is shown to better illustrate the geologic setting during this Late Mississippian depositional environment (Fig. 2C; Graham et al., 1975). Because of the relative close proximity to the Ouachita Basin, sediments may be sourced from the exposed portions of the Gondwanan and Laurussian margins along with additional sediment contribution

from the Black Warrior Basin (Fig. 1C). A volcanic arc (Fig. 3B) on the Gondwanan margin formed because of the subduction of Rheic Oceanic crust as the Ouachita remnant basin closed (Shaulis et al., 2012). Drainage networks were modified as Gondwana collided with Laurussia (Fig. 3C). The Middle Carboniferous eustatic event (MCEE) occurs at this time, coeval with sea level drop and contemporaneous change in availability of exposed strata for weathering (Fig. 2; Miall, 2019 and references therein; Ettensohn et al., 2019 and references therein; Blake and Beuthin, 2008). As a result, provenance changed and more sediments were sourced from within the Laurussian craton. The sediments overlying the Mississippian Stanley Group in that Ouachita Basin are rocks of the Pennsylvanian Jackfork Group (ca. 318-322 Ma). Sediment provenance shifted toward Laurussian cratonic ages, including Grenville and Midcontinent sources, with little influence on sediments sourced from the Alleghanian (ca. 320 Ma) rocks located adjacent to the Appalachian Basin (Fig. 2B).

This study provides geochronologic ages for zircon and muscovite grains of both the Mississippian Stanley Group (320.7 ± 2.5 Ma and 330 Ma) and Pennsylvanian Jackfork Group (ca. 318 Ma to 322 Ma) located in south-eastern Oklahoma (Fig. 3D; Viele and Thomas, 1989). Carboniferous syn-tectonic deep-water units (Stanley and Jackfork Groups) correlate chronostratigraphically with the Mississippian Parkwood and Pennsylvanian Pottsville formations in the Black Warrior Basin to the east (Fig. 3E; Thomas, 1972; Stone et al., 1981; Hatch and Pawlewicz, 2007; Pashin and Gastaldo, 2009). Across the Mississippian-Pennsylvanian boundary, there was a global drop in sea-level penecontemporaneous with increase in precipitation and tectonism (Fig. S1;

Gordon, 1974; Sutherland and Manger, 1979; Arbenz, 1989a; Cecil and Eble, 1989; Ross and Ross, 1987; Coleman et al., 1994).

Available published detrital zircon spectra for the Appalachians and intracratonic basins, and a suite of detrital muscovite spectra from the rocks of the Greater Black Warrior Basin are helpful in distinguish potential source areas and drainage pathways. The rationale for age-dating of two detrital mineral types is that the zircons are mostly multi-cycle (recycled) to provide a more complete provenance record, whereas the first-cycle muscovite that was weathered from Alleghanian plutons give a more detailed provenance history during this late stage of Appalachian orogenesis (Becker et al., 2005; Uddin et al., 2016). We identified a provenance shift to more Laurussian sources during the deposition of the Pennsylvanian Jackfork Group because of rapid regression, resulting major restructuring of drainage, and far-traveled sediment transport by continental-scale river systems on Laurussia (Fig. 1; Archer and Greb, 1995).

2.3. Geological Background

The Ouachita Basin, a remnant deep-water ocean basin located on the present-day southern (geographic orientations are present-day) margin of the North American craton, was created during collision of Laurussia (North America and Baltica) and Gondwana (Fig. 3B; Arbenz, 1989a; Miall, 2019; Miall and Blakey, 2019). Prior to the formation of the Ouachita Basin, this basin was the Theic Ocean. The Theic Ocean, characterized as a deep-water basin that was sediment-starved, had a carbonate platform form on the passive margin of North American craton during the Early Paleozoic (Colman, 2000). From the Middle Cambrian through the Mississippian, the Ouachita

Basin was infilled with a thin pre-orogenic sequence of interbedded carbonate, shale, chert, and minor sandstone units (Honess, 1923; Flawn et al., 1961; Lowe, 1989).

Increased sedimentation from Carboniferous turbidites deposited in the Ouachita Basin recorded the closing of the Theic Ocean as peri-Gondwanan terranes (microcontinents) approached Laurussia to assemble as the supercontinent Pangea (Figs. 2C, 3C,D; Viele and Thomas, 1989; Miall and Blakey, 2019). The earliest recognition of an unknown southern terrane was based on the sediments preserved in the southern Ouachitas and this southern source was named "Llanoria" (Miser, 1921). Modern plate-tectonic reconstructions (e.g., Miall and Blakey, 2019) suggest a volcanic arc and a series of terranes, including the Yucatan Block being concealed beneath the Gulf Coastal Plain sediments. Turbidite sequences from both the Stanley and Jackfork groups are classified as flysch deposits; these are characteristic marine deposits of interbedded sand and shale deposited in late-stage orogenic belts (van Waterschoot van der Gracht, 1931).

Several published studies (e.g., Morris, 1971, 1974a, 1974b; Thomas, 1977; Lowe, 1985; 1989) refer to the closing of the Ouachita Ocean as a trough implying that it is a narrower and elongate basin between the North American craton and an unknown collider (Bates and Jackson, 1987). The Ouachita basin has a south-dipping subduction zone, and associated Carboniferous-aged accretionary prism, which evolved into the present-day peripheral foreland basin named the Arkoma Basin (Figs. 2B,C, 3D; Ingersoll, 1988, 2012; Arbenz, 1989b; Ingersoll et al., 2003). To avoid confusion, this study uses the classification scheme of Ingersoll (2012) and acknowledges that 'trough' is a more descriptive for a narrow remnant ocean basin. The flysch facies, including

Stanley and Jackfork groups, are described in detail of petrology and general paleo flow direction from published work. Much of the flysch in the Ouachita basin was deformed by the synorogenic Late Carboniferous Ouachita orogenesis that translated allochtonous rock units to the north along thrust faults (Morris, 1989).

In the southern Ouachita orogenic belt, the complete Carboniferous section (Figs. 3E, 4), oldest to youngest, is the Arkansas Novaculite (MDa), the Stanley Group (Ms), the Jackfork Group (IPj), the Johns Valley Formation (IPj), and the Atoka Formation (Arbenz, 1989a; Morris, 1989; Arbenz, 2008). The base of the Jackfork Group corresponds to the Kaskaskia-Absaroka sequence boundary, a significant regional unconformity within the Mississippian-Pennsylvanian stratigraphy (Sloss, 1963). Further eastward on the eastern margin of the North American craton, this same unconformity is present and is coincident with a Late Paleozoic ice age. This major glacio-eustatic sea-level drop is recognized as the mid Carboniferous eustatic event (MCEE; Blake and Beuthin, 2008).

The age of the Stanley Group is bracketed between 320.7 ± 2.5 Ma and 330 Ma (Late Chesterian) based on U-Pb zircon ages from tuffs and biostratigraphy (Niem, 1976, 1977; Shaulis et al., 2012). At its base, the Carboniferous strata unconformably overlie the Mississippian-Devonian Arkansas Novaculite (Morris, 1989). A compilation of many petrographic studies of the Stanley Group indicated that the flysch deposits were sourced extracratonically (i.e., island arc, microcontinent) because of numerous feldspathic and lithic rock fragments (Fig. 5A,B; Morris, 1974b and references therein; Morris, 1989). The age of the Jackfork Group is ca. 318 Ma to 322 Ma (Early

Morrowan) based on relative dating from stratigraphic relationships (Arbenz, 1989a; Sutherland, 1988; Coleman, 1990). Paleo flow structures (Fig. 5C) for both the Stanley and Jackfork groups indicate a westward transport direction (Briggs and Cline, 1967; Morris, 1971; Morris, 1974; Hatcher et al., 1989)

2.4. Sample Selection

Carboniferous sandstone and shale samples from 35 surface outcrop exposures from eastern Oklahoma were processed for this study (Fig. 4). Six samples for detrital zircon analysis and two samples for detrital muscovite were selected (Table 1; Fig. 4). Stratigraphic age of samples (Plate 2, Arbenz, 2008) are the Upper Mississippian Stanley Group and the Lower Pennsylvanian Jackfork Group. Targeted sampling was adjacent to the lithologic contact between these units to ensure the same relative position within the stratigraphy, especially in areas of complex thrusting (Fig. 4). Between 15 to 25 kg of bulk rock were collected from each outcrop to have a representative sample at that location and to provide enough material for multiple analyses following mineral separation.

2.5. Geochronology Methodology

Zircons were separated at Texas A&M University using standard rock disaggregation techniques and gravity settling (e.g., Fedo et al., 2004; Appendix 1, Donelick et al., 2005). Heavy liquids, lithium heteropolytundstates (LST) and methylene iodide (MEI), used have specific gravities of 2.85 and 3.32, respectively. Magnetic separation by neodymium magnets removed primary magnetic particles. Photomicrographs of zircons representative of each sample were first taken on a

binocular microscope and then used for macroscopic characterization of each grain population (Table 2; Corfu et al., 2003). Heavy mineral descriptions aid in the identification of the mineral species by comparison of grain morphology, color, and other macroscopic properties to published petrographic properties (Mange and Maurer, 1992).

Polished epoxy pucks were made of sample zircons and zircon references: FC-1 (primary), R33 (secondary), and 91500 (secondary; Paces and Miller, 1993; Wiedenbeck et al., 1995, and Black et al., 2004). Glass standard, NIST 612, is included in each puck to calibrate the laser ablation system. Laser-ablation-inductively coupled plasma-mass spectrometry (LA-ICP-MS) at the Ken Williams Radiogenic Isotope Lab, Texas A&M University was used for depth profiling of selected grains to yield U-Pb ratios measurements (Arevalo, 2014). This raw isotopic data was reduced using an Excel macro (Chang et al., 2006). A 193 nm wavelength laser at 10 Hz repetition rate produced a 29.6 µm spot diameter that was used to ablate grains for 40 seconds. Detailed instrument settings as recommended for U-Pb data reporting by Horstwood et al. (2016) are provided in the supplementary material section.

One hundred and twenty random zircon grains were analyzed for each sample to ensure a representative sampling from all age populations (Vermeesch, 2004). Zircon age data were plotted using Kernel Density Estimator (KDE) software (Vermeesch, 2012). The n-value for zircon KDE plots is the number of grains analyzed with less than 10% discordance of grains younger than 1000 Ma and less than 20% discordance on

grains older than 1000 Ma. A bandwidth of 10 m.y. was used to construct distribution curves between 0-4000 Ma for this study.

Aliquots of mixed light minerals (e.g., quartz, feldspar, and mica) from crushed bulk rock samples were collected after separation on Wilfley table. Aliquots were sieved using standard sieve sizes: #40 (420 µm mesh), #60 (250 µm mesh), and #80 (177 µm mesh). Grain sizes between 420 µm - 250 µm were preferred; most samples yielded primarily the smaller size fraction of muscovite, so it was necessary to use grains smaller than 250 µm. Sieved material was placed on common laboratory filter paper and lightly tapped to aid in removing the quartz and feldspar grains by them rolling off of the paper. Muscovite that remaining on the textured filter paper was placed in a glass petri dish to minimize electrical static, and handpicked to provide at least 200 grains for each sample.

Petrographic techniques, including cross-polarized light and dry grain picking (no alcohol), aided in selection of the very small muscovite grains. All picked muscovite was sent to Auburn University, Alabama to be packed into aluminum packages, and then sent for irradiation at United States Geologic Survey TRIGA reactor in Denver, Colorado (Moore, 2012). Detailed instrument settings recommended for $^{40}Ar/^{39}Ar$ data reporting by Hodges et al. (2005) provided in the supplementary material section. 112 random irradiated muscovite grains were analyzed by the Auburn Noble Isotope Mass Analysis Laboratory (ANIMAL) using single-crystal laser ablation for $^{40}Ar/^{39}Ar$ method (McDougal and Harrison, 1999; Vermeesch, 2004; Ruhl and Hodges, 2005). Muscovite KDE plots used all grain ages and n-value is the number of grains. A bandwidth of 2 m.y. is used for muscovite ages across a 300-550 Ma range.

2.6. Detrital Zircon Results

Concordant zircon ages of the Mississippian Stanley Group span ca. 320 to 3200 Ma, primarily as a suite of weak to moderate detrital zircon age peaks (Appendix A; Figs. 6A). Two apparent age clusters are at ca. 400-700 Ma and ca. 880-1100 Ma. The Pennsylvanian Jackfork Group has concordant detrital zircon ages that mainly cluster between 1000-1300 Ma (Fig. 6A). This range may be extended for the Jackfork group to 1800 Ma based on the strong peak ages present in OK12-14. Minor detrital zircon age peaks are at ca. 400-500 Ma, ca. 1800-2100 Ma, and ca. 2800 Ma.

2.7. Detrital Muscovite Results

The Mississippian Stanley Group has a strong detrital muscovite age peak at ca. 435 Ma (Fig. 6D) and a suite of moderate peaks between ca. 430 to 490 Ma. A majority of the detrital muscovite ages are between ca. 400-525 Ma (Figs. 6B,C). The Pennsylvanian Jackfork Group has a strong detrital muscovite age peak at ca. 365 Ma and a majority of the detrital muscovite ages between 360-450 Ma (Figs. 6B,C,D).

2.8. Detrital Zircon Interpretation

Four hundred and eighty-four new concordant U-Pb grain ages were determined for detrital zircons from the Ouachita Carboniferous stratigraphy (Table 2; Appendix A). Four samples from the Mississippian Stanley Group yielded 283 detrital zircon U-Pb ages that range from Pennsylvanian (ca. 300 Ma) to Mesoarchean (ca. 3000 Ma). Two samples collected from the Pennsylvanian Jackfork Group have 201 detrital zircon U-Pb ages that span Mississippian (ca. 350 Ma) to Neoarchean (ca. 2700 Ma). Seven age components, corresponding to major tectonic events with magmatic activity, are used to

group the zircons into discrete populations: A, Appalachian-Ouachita (265-500 Ma); B, Pan-Africa (500-700 Ma); C, Grenville (950-1300 Ma); D, Midcontinent (1300-1500 Ma); E, Yavapai-Mazatzal (1600-1800 Ma); and F, Shield (>1800 Ma). Major accretion events for the Appalachian-Ouachita age population are identified as sub-groups: A1, Alleghanian (265-327 Ma); A2, Acadian (350-380 Ma); A4, Taconic (440-465 Ma). A3 (381-439 Ma) and A5 (466-499 Ma) are informal provinces with zircon populations that have not been associated with any specific accretion or rifting event. These age classifications are used in the comparison of detrital samples, but do not necessarily restrict zircon sourcing to these crustal sources alone.

Peak determinations made for the five or more largest peak intensities of each sample, and these peaks are always listed in order of greatest intensity. Several samples have peak age clustering, which necessitate delineation of sub-groups and major peak identification within each sub-groups. In the Stanley Group, OK12-54 is sub-divided into three age groups: 410-660 Ma, 968-1159 Ma, and 1683-1908 Ma (Fig. 6). Both Jackfork Group samples are divided into subgroups. Sample OK12-14 is sub-divided into four age groups: 1615-1735 Ma, 1498 Ma, 1025-1350 Ma, and 421-527 Ma. Sample OK12-39 is divided into three age groups: 410-660 Ma, 968-1159 Ma, and 1683-1908 Ma.

2.8.1. Mississippian Stanley Group

The Middle Cambrian to Early Permian zircons consist of 13% of all U-Pb ages for the Stanley Group, representing a moderate age component (Tables 3, 4; Fig. 6). While mostly older Taconic (A4) zircons, there are an equal percentage of zircons in the

unknown event(s) from both 381-439 Ma (A3) and 466-499 Ma (A5). The youngest age population is a weak peak above background at ca. 375 Ma in OK12-57. Prominent age peaks occur in all samples from Late Cambrian to Middle Ordovician to representing zircon populations at approximately 460-490 Ma. There are weak peaks, with same signal intensity, for OK12-16 at ca. 427 Ma and ca. 459 Ma in OK12-16. An age peak at ca. 489 Ma in OK12-52 is strong. OK12-54 has two strong age peaks at ca. 464 Ma and ca. 410 Ma (second strongest in this spectrum). For OK12-57, a moderate peak is at ca. 495 Ma.

Late Neoproterozoic to Cambrian zircons are a 17% age component of the Stanley Group and are interpreted as Pan-Africa Province (B). There are moderate to weak peak ages for OK12-16, OK12-52, and OK12-54. Moderate peak ages at ca. 568 Ma and ca. 676 Ma occur for OK12-16. At ca. 610 Ma and ca. 648 Ma, OK12-52 has moderate peak ages. Three moderate peak ages at ca. 597 Ma, ca. 537 Ma, and ca. 657 Ma are given for OK12-54. Neoproterozoic zircons provide additional weak age peaks at ca. 800 Ma and ca. 882 Ma in OK12-16 and OK12-57, respectively.

Mesoproterozoic zircons from the Grenville Province (C) account for 22% of all zircons (Tables 3, 4; Fig. 6). Both OK12-16 and OK12-52 have strong peak ages at ca. 960 Ma and ca. 949 Ma, respectively. A second age peak for OK12-52 at ca. 1270 Ma is significantly less intense. Three peak ages at ca. 1159 Ma, ca. 1048 Ma, and ca. 1095 Ma occur in OK12-54. In contrast, a second Mesoproterozoic zircon age population accounting for 4% of all zircons and lacks age peaks above background is the Midcontinent Province (D). The Yavapai-Mazatzal Province (E) constitutes 6% of all

zircons and has a moderate amount of Late Paleoproterozoic zircons; both OK12-54 and OK12-57 have moderate age peaks at ca. 1683 Ma. OK12-54 has weak age peaks at ca. 1908 Ma, ca. 1714 Ma, and ca. 1714 Ma. For OK12-57, another age peak is present at ca. 1705 Ma, but its intensity is much lower than the first peak age.

A substantial portion, exactly 22% of the Stanley Formation zircons, are from sources older than 1800 Ma. In this province (F), there are significant Paleoproterozoic Neoarchean components, including peaks at ca. 2484 Ma and ca. 2522 Ma for OK12-16, and ca. 1908 Ma for OK12-54. Zircon ages not corresponding to the selected provinces make up 16% of all the grains; identifiable age peaks above background spectra are absent.

2.8.2. Pennsylvanian Jackfork Group

Middle Cambrian to Devonian zircons account for 6% of the combined U-Pb ages for the Jackfork Group, which represents a small age component from Taconic Province (A4), Pan-Africa Province (B) and two unknown events (Provinces A3 and A5; Tables 3,4 ; Fig. 6). Three age peaks for OK12-14 are ca. 527 Ma, ca. 421 Ma, and ca. 479 Ma. A single prominent peak age for OK12-39 is at ca. 441 Ma. Cambrian to Late Neoproterozoic zircons comprise a 3% age component for the spectrum and absent of peak ages.

Mesoproterozoic zircons represent a significant age component at 66% of the Jackfork Group zircons. The Grenville Province (C) sourced 43% of the zircons, while the Midcontinent provided the remaining 23% of the zircons. One subgroup for OK12-14 has a suite of peak ages, given in order of greatest intensity: ca. 1028 Ma, ca. 1258

Ma, ca. 1172 Ma, ca. 1083 Ma, and ca. 1217 Ma. For OK12-39, one subgroup has multiple age peaks, in order of greatest intensity, at ca. 1143 Ma, ca. 1178 Ma, ca. 1232 Ma, ca. 1032 Ma, and ca. 1067 Ma. Zircons from the Midcontinent Province (D) are found in both samples. A subgroup in OK12-14 has a strong age peak at ca. 1498 Ma. Subgroup for OK12-39 has peak ages at ca. 1454 Ma, ca. 1375 Ma, and ca. 1318 Ma.

Late Paleoproterozoic zircons amount to a 17% age component; 9% of that component sourced from the Yavapai-Mazatzal Province (E). OK12-14 has one subgroup with representative peak ages for this province at ca. 1615 Ma, ca. 1697 Ma, and ca. 1735 Ma. The remaining 6% zircon population falls within the "Others" age component, which indicates zircons that do not fit into any of the defined provinces.

2.9. Detrital Muscovite Interpretation

Two samples, OK12-54 from the upper portion of the Mississippian Stanley Group and OK12-39 from the lower portion of the Pennsylvanian Jackfork Group, yielded detrital muscovite dated using single-fused $^{40}Ar/^{39}Ar$ analysis. There are 217 new $^{40}Ar/^{39}Ar$ grain ages for detrital muscovite from the Ouachita Carboniferous stratigraphy that range from Cambrian to Early Pennsylvanian (Appendix B). Major accretion events for the Appalachian-Ouachita age population are identified as sub-groups: A1, Alleghanian (265-327 Ma); A2, Acadian (350-380 Ma); A4, Taconic (440-465 Ma). A3 (381-439 Ma) and A5 (466-499 Ma) are informal provinces with zircon populations that have not been associated with any specific accretion or rifting event. The Pan-African Province is denoted as population B, starting at 500 Ma and older grains for these KDE plots. These age classifications are used in the comparison of

detrital samples and not necessarily restrict muscovite sourcing from these crustal sources alone.

2.9.1. Mississippian Stanley Group

Detrital muscovite grain ages from OK12-54, collected within Stanley Group, range between Cambrian to Early Pennsylvanian, though a majority of these grain ages are older than Early Devonian (Table 5; Fig. 6B,C,D). Late Devonian to Early Pennsylvanian muscovite sourced from both Alleghanian (A1) and Acadian (A2) populations are at a sparse 1% and 3%, respectively. The first significant population at 28% of all muscovite consists of Silurian to Middle Devonian grains, indicating crystallization events occurred between 381-439 Ma (informally Province A3). There is a moderate peak age at ca. 426 Ma and two lower intensity peaks in this province.

Middle Ordovician to Early Silurian muscovite comprises 28% of the population and is derived from the Taconic accretion (A4). The strongest peak age is present at ca. 440 Ma with an additional moderate peak age at ca. 461 Ma. Early Cambrian to Middle Ordovician muscovite from crystallization event(s) recognized informally as Province A5 comprises 27% of the muscovite. Moderate peaks ages in this province are at ca. 488 Ma and ca. 469 Ma. Middle Cambrian muscovite, 13% of entire population, is sourced from the Pan-African Province (B).

2.9.2. Pennsylvanian Jackfork Group

The Pennsylvanian Jackfork Group yields Middle Ordovician to Early Mississippian detrital muscovite grain ages (Fig. 6B,C,D). Late Devonian to Early Mississippian muscovite sourced from the Acadian Province (A2) composes 44% of the

total detrital muscovite. A single peak age at ca. 365 Ma is prominent. Multiple crystallization events of the informal Province A3, as suggested by the suite of peak ages, make up another 44% of the total detrital muscovite. Moderate peak ages are at ca. 379 Ma, ca. 387 Ma, and ca. 425 Ma. A population of Middle Ordovician to Early Silurian muscovite represent 10% of the total detrital muscovite and give a moderate peak age at ca. 447 Ma. A Middle Ordovician muscovite grain from a crystallization event sourced from Province A5 (informal) consists of a 1 % contribution to the total detrital muscovite.

Late Neoproterozoic to Late Cambrian muscovite from the Pan-African Province (B) are absent. Only two muscovite grains are sourced from crustal sources older than 1800 Ma (i.e., Province F), comprising 2% of the overall detrital muscovite. The Mesoarchean muscovite and Mesoproterozoic muscovite have grain ages of 2926 ± 212 Ma and 1310.91 ± 31.47 Ma, respectively.

2.10. Geochronological Provinces

2.10.1. Appalachian-Ouachita Province (A; 265-500 Ma)

Zircon grains and muscovite flakes, with ages between 265-500 Ma, correspond to several major episodes of Paleozoic orogenesis. These main tectonic events are recorded in the deformed metasedimentary rocks along the present-day eastern North America, a result primarily from three Appalachian orogenies (A1, 265-327 Ma – Alleghanian; A2, 350-380 Ma – Acadian; A4, 440-465 Ma – Taconic) and Ouachita orogeny (ca. A1, 267-328 Ma; Denison et al, 1977; Hatcher, 1987, 2010; Eriksson et al., 2003; Thomas et al., 2004; Park et al., 2010; Thomas, 2011). Most of the Appalachian

terranes are well exposed in the Appalachian Mountains, and Ouachita exposures are limited to the Marathon Uplift, Texas, and the Ouachita Mountains, Arkansas and Oklahoma.

2.10.1.1. Alleghanian (A1, 265-327 Ma)

This last major orogenic event records the final closing of the Paleo-Tethys-Rheic (Theic) Ocean during the suture between the Gondwana and Laurussia (Figs. 3B, C) in the Late Carboniferous (Blakey, 2008; Hatcher, 2010; Nance et al., 2010). This collision resulted in fold and thrust belts formation along the suture, and the most mountain-building occurred in the locality of the central to southern Appalachian belt (Hatcher et al., 1989) and further to present-day southeast in the Ouachita orogen (Viele and Thomas, 1989).

The sequence of deformation is considered to be "zippered" rather than orthogonal; the suture started from the northeast and progressed southwestward during closure of the Theic Ocean (Fig. 3C, Hatcher, 2002). If this is true, metamorphism occurred first in the northeast, following the suture pattern southwestward toward the incipient southern Appalachians. Plutons that formed during this orogenesis are found in the Southern Appalachians (Speer and Hoff, 1997).

2.10.1.2. Acadian (A2, 350-380 Ma)

This orogenesis was between Laurussia and the microcontinent Avalonia during the closing of the Iapetus Ocean (Blakey, 2008). Late Devonian to Early Mississippian stratigraphy of the Northern Appalachians, including New England, records Acadian

tectonic events best since these sediments are less overprinted by the Alleghanian orogeny (Osberg et al., 1989).

2.10.1.3. Informal Province (A3, 381-439 Ma)

Many relatively small tectonic events during this period may have contributed these crystallization ages, such as small microcontinents or island arc collisions with Laurentia. A major potential source for sediments are those shed from the rocks uplifted during the Caledonian Orogeny; this collision occurred between Laurentia and Baltica from 390-490 Ma (Blakey, 2008). The main tectonic activity, known as the Scandian (Scandinavia) / Grampian (Britain) phase, occurred between Late Silurian to Early Devonian when Avalonia and Laurentia collided (McKerrow et al., 2000). A continuation of this orogenic event in North America, starting at ~380 Ma, is the Acadian orogenesis (i.e., Province A2).

2.10.1.4. Taconic (A4, 440-465 Ma)

The earliest of the major events in forming the Appalachian orogen is the Taconic Orogeny, an arc accretion to Laurentia (Rankin et al., 1989; Hatcher, 2010). Both the Blountian and Penobscottian events (possibly called orogenies) comprise two major collisions based on tectonic record from metasedimentary rocks or preserved sediments in syn- and post-tectonic clastic wedges, respectively (Rankin et al., 1989).

2.10.1.5. Informal Province (A5, 466-499 Ma)

One potential source of sediments from this province is material being shed from rocks uplifted during the Caledonian orogeny. This orogenesis began the Late Cambrian (ca. 500 Ma) Finnmarkian phase recognized in metasedimentary rocks of British Isles

and Scandinavia (McKerrow et al., 2000). Sediments may also be derived from the main phase of the Famatinian Orogeny, associated with the collision of Occidentalia terrane (including the Precordillera), and Gondwana at ~460-490 Ma (Thomas and Astini, 1996; Dalziel, 1997; Dalla Salda et al., 1998; Keller, 1999; Thomas et al., 2004; Dahlquist et al., 2008). The similarities in age between the Famatinian rocks in present-day Argentina and Taconic rocks in eastern North America suggest that the collisional belts formed from a common tectonic event (Dalla Salda et al., 1998; Keller, 1999).

2.10.2. Pan-Africa Province (B; 500-700 Ma)

The Pan-Africa Province has a range of mineral crystallization ages from 500-700 Ma. These ages represent several geologic events, including: 1) Rifting along the Iapetan margin, 2) Eastern Laurentian margin magmatism, and 3) Formation of Gondwana (Hoffman, 1989; Park et al., 2010). During the formation of the supercontinent Gondwana, several older cratons (>1950 Ma) sutured to form several major mountain belts during the Pan-African/Brasiliano Orogeny (Trompette, 2000).

2.10.3. Grenville Province (C; 950-1300 Ma)

Zircon ages between 950-1300 Ma are sourced from Laurentian basement rocks (Fig. 7), formed during the assembly of Rodina (Hoffman, 1989; Dickinson and Gehrels, 2009). The Grenville orogeny resulted in: 1) several regions of moderate to high-grade metamorphic rocks, 2) widespread magmatism (e.g. Keweenawan rift), and 3) a significant supply of detritus for supporting a (proposed) continental-scale Grenvillian river system (Rainbird et al., 2014).

2.10.4. Midcontinent Province (D; 1300-1500 Ma)

Mesoproterozoic granites and rhyolites yield zircons ages between 1300-1500 Ma (Bickford et al., 1986; Van Schmus et al., 1996). These igneous source rocks are basement rock in the North American midcontinent, with the best exposures in the St. Francois Mountains of eastern Missouri. As much of the midcontinent is concealed by sedimentary cover, a more likely source of 1300-1500 Ma zircons are a suite of intrusive granite rocks in the midcontinent, including the St. Francois Mountains (Fig. 7; Bickford et al., 1986; Hoffman, 1989; Karlstrom et al., 1997; Karlstrom et al., 2004).

2.10.5. Yavapai-Mazatzal Province (E; 1600-1800 Ma)

Assembly of primarily juvenile crust to Laurentia (Fig. 7) in the Late Paleoproterozoic occurred during two main orogenies: Yavapai orogeny (1700-1800 Ma) and the Mazatzal orogeny (1600-1700 Ma). An amalgamation of juvenile crust in island arcs is dominant for the Yavapai orogeny, but at least one example in southern Colorado indicates the occurrence of a small volume of reworked crust (Hill and Bickford, 2001). In contrast, the Mazatzal orogeny is better classified as intercratonic tectonism because of the co-occurrence of thick metasedimentary rock sequences and extensive plutonic activity (Karlstrom et al., 2004).

2.10.6. Shield Province (F; >1800 Ma)

Several orogenies occur prior to 1800 Ma that may have sourced these Paleoproterozoic and older zircon crystallization ages (Fig. 7). One major orogeny is the Trans-Hudson orogeny (1800-1900 Ma), a collisional event involving Archean crust of the Superior, Wyoming, and Hearne provinces (Whitmeyer and Karlstrom, 2007). A

second major orogeny, the Penokean orogeny (1800-1900 Ma), consisted of suturing of several Wisconsin magmatic terranes (Pembine-Wausau and Marshfield) to the southern margin of Laurentia (Hoffman, 1989). Minor orogenies are Torngat orogeny (> 2400 Ma) in eastern North America and several others located further away from the eastern margin of the craton (Hoffman, 1989).

2.11. Potential Sediment Sources

Detrital zircon U-Pb grain ages for 4 Stanley Group samples and 2 Jackfork Group samples from the Ouachita orogenic belt display a shift in sediment source. Coupled with detrital muscovite $^{40}Ar/^{39}Ar$ grain ages for 1 sample from both the Stanley and Jackfork groups, a provenance shift is even more evident. Both techniques provide insight into the Carboniferous drainage system evolution and aids in understanding the regional sediment sources.

First-cycle sources include Laurentian crust (Fig. 7) and peri-gondwanan terranes (Blakey, 2008). Recycled sources are from sedimentary rocks, such as sandstones that formed in peripheral foreland basins of the Appalachians during the Acadian and Taconic orogenies (Park et al., 2010). Basement sources are considered first followed by discussion of recycled sources.

2.11.1. Mississippian Stanley Group

The Stanley Group is characterized by a high proportion of Pan-Africa Province and Grenville Province components, and by ages older than 1800 Ma for detrital zircons (Table 4; Fig. 11). Published U-Pb zircon data for the Stanley Group has a slightly different spectra than this study because their research focus was on dating the

interbedded tuffs, so sample collection was biased toward equant grains (Shaulis et al., 2012). For detrital muscovite, the Stanley Group is characterized by high proportions of Taconic age component (grain ages of 381-439 Ma and 466-499 Ma), and moderate proportion for Pan-Africa age component (grain ages of 500-700 Ma, Table 4, Fig. 13). A spectrum of detrital muscovite from 381 Ma to 499 Ma indicates continuous sediment supply of first cycle sedimentation during the Caledonian, Famatinian, and Taconic orogenies. Although Taconic sediments are locally sourced, others must have traveled several thousand kilometers from distal source areas during the Caledonian orogeny (Drake et al., 1989; McKerrow et al., 2000).

Pan-African zircon grains and muscovite flakes are likely sourced directly into the closing Ouachita Basin from approaching peri-Gondwanan terranes to south and southeast of Laurentia (Fig. 2B; Miall, 2019). These terranes formed earlier during assembly of Gondwana in either the Pan-African or Cadomian-Avalonian orogenies (Blakey, 2008). There are 34 of 283 detrital zircons that have a crystallization age between 700 Ma and 950 Ma, which is outside of a defined province. These grain ages may represent magmatic activity related intracratonic extension and subsequent rifting of Rodina during the Neoproterozoic (Aleinikoff et al, 1995; Torsvik, 2003; Cawood et al., 2007).

Grenville zircons represent a major, global-scale orogeny during the formation of the supercontinent Rodina (Cawood et al., 2007). This Late Mesoproterozoic orogeny is well-preserved in detrital zircon sedimentary record of Laurentia; this result of extensive mountain building facilitated erosion and supplied large amounts of siliciclastic material

to proximal syn-collision basins (Rainbird et al., 2014; Spencer et al., 2015). Both Grenvillian basement rocks on the North America margin (C, Fig. 7), and proximal basement rocks north of the Ouachita Basin, are comprised of granite and rhyolite Laurentian crust (D, Fig. 7); this crust sourced the Midcontinent zircons (Hoffman, 1989; Van Schmus et al., 1993; Thomas et al., 2004). Zircons of the Yavapai-Mazatzal basement are medial sourced and derived from the interior portions of the Laurentian craton (E, Fig. 7; Hoffman, 1989; Van Schmus et al., 1993; Thomas et al., 2004).

Detrital zircon grain ages older than 1800 Ma from the shield represent the early stages of assembly for the North American craton. Zircons with ages between 1800 Ma to 1900 Ma may have been sourced from reworked Archean crust in the north-central portion of Laurentia, whereas zircons of 1900 - 2000 Ma ages are from juvenile arc accretions located between the reworked rocks and the Yavapai-Mazatzal rocks (Whitmeyer and Karlstrom, 2007). Zircons that are older than 2000 Ma may have been derived from Archean cratons, such as the nearby Wyoming and Superior provinces (Karlstrom et al., 2004; Whitmeyer and Karlstrom, 2007).

Published U-Pb detrital zircon grain age data and $^{40}Ar/^{39}Ar$ detrital muscovite grain age data (Black Warrior Basin only) were replotted as Kernel Density Estimate (KDE) graphs, with the identical settings (e.g., bandwidth). These KDE plots characterize Early Pennsylvanian and older sediments from Northwest Arkansas, Ouachita Basin (pre-Carboniferous), Black Warrior Basin, Appalachian Basin, Newfoundland, and New England (Fig. 8; Gray and Zeitler, 1997; Cawood and

Nemchin, 2001; Gleason et al., 2001; McLennan et al., 2001; Eriksson et al., 2004; Park et al., 2010; Moore, 2012; Xie et al., 2016a; Xie et al., 2016b).

Recycled sources, considered relative to their geographic position to the Ouachita Basin, are proximal sources and offer a simpler explanation for the source of sediments. Reworking of Ordovician and Silurian rocks within the Ouachita Basin may have contributed sediment as Grenville and Midcontinent signatures are present (Figs. 8, S6; Gleason et al., 2001). Deltaic deposits from the Mississippian Wedington Member, Fayetteville Formation have a large Grenville population and moderate populations of Midcontinent and Yavapai-Mazatzal zircons (Figs. 8, S7; Xie et al., 2016b). Several samples have a minor Taconic population and sparse amount of zircons older than 1800 Ma, which partially fits detrital zircon signal from the Stanley Group (Fig. 6A).

The Black Warrior Basin, further to the east, yields zircons from Mississippian sandstones with a stronger Appalachian signal (Fig. 8). These units closely match the KDE spectrum of the Wedington Member, Fayetteville Formation, and offer another possible source of detrital zircons (Figs. S7, S8; Xie et al., 2016a). Detrital muscovite population from the Mississippian Parkwood Formation has primarily Taconic and Acadian components (Fig. 9; Moore, 2012).

In the Appalachian Basin, detrital zircon data range from Precambrian - Mississippian. Early to Middle Paleozoic Appalachian units have fairly uniform detrital KDE plots with a large population of Grenville zircons and a moderate amount of Midcontinent zircons (Figs. 8, S9; Eriksson et al., 2004; Park et al., 2010). Taconic and Yavapai-Mazatzal zircons appear in the sediments of the Appalachian Basin during the

Devonian (Park et al., 2010). Similar KDE patterns are found for the Mississippian Appalachian units, with few differences. Although the Appalachian signal is represented by both Acadian and Taconic components (Fig. S10; Park et al., 2010). The sample from the Hinton Formation has a several zircons with ages at ca. 2700 Ma. Further, the Yavapai-Mazatzal show up in approximate half of the sampled Mississippian units.

In the north, the New England Foreland Basin with Cambrian - Devonian strata previously reported in detrital studies (Fig. 8; Gray and Zeitler, 1997; McLennan et al., 2001). The main component in all five units is Grenville. The oldest unit, the Poughquag Quartzite, has a significant component of Midcontinent zircons, whereas the youngest unit, the Walton Formation of the Catskill Group, has a strong Taconic signal (Fig. S11; McLennan et al., 2001). In the Maritimes of Canada (Figs. 7, 8), the Precambrian - Ordovician strata of Newfoundland have roughly equal zircon abundances from the Grenville and Shield provinces, with a minor component from the Midcontinent (Fig. S11; Cawood and Nemchin, 2001).

Interpretation of sediment provenance is complex because of the multiple sources of siliciclastic input, both first-cycle and recycled. It is important to consider the provenance history of same age or older sedimentary rocks as these rocks preserve an earlier sediment history that may contribute to overall detrital age spectrum. Absence of a component provides insight into the drainages that precluded sediments, even proximal-sourced ones, from being a source of clastic material. The three main components of the Mississippian Stanley Group are Grenville, Pan-Africa, and Shield (Tables 3, 4; Fig. 8). Stanley Group detrital muscovite signals range between Pan-

African to Taconic provinces, in contrast to the Mississippian Parkwood Formation in the Black Warrior Basin (Fig. 9; Moore, 2012).

At least two sources (Laurentian and Gondwanan) contributed sediment as no single drainage is sufficient to erode all components represented in the detrital ages of the Stanley Group. Multidimensional-scaling statistics (MDS) was used to guide the interpretation further and a discussion of the results is presented in the next major section of this paper.

2.11.2. Pennsylvanian Jackfork Group

Major components of Grenville, Midcontinent, and Yavapai-Mazatzal (only OK12-14 sample) are found in the detrital zircons of the Jackfork Group (Table 4; Fig. 11). Moderate Appalachian signal occurs with a small component of Taconic zircons and very few ages older than 1800 Ma (i.e., Shield Province). A strong Appalachian signal, Acadian through Taconic, provides a better constraint on the provenance than simply using the detrital zircon spectra (Tables 3,4; Fig. 11).

Similarly to the Stanley Group, detritus from erosion of basement rocks are a first-cycle source (Fig. 7). Reworking from underlying Stanley Group strata is an additional, probable sediment source. Source proximity is the most influential factor in delineation of provenance for the Ouachita Basin, as per Occam's Razor. The Pennsylvanian Caseyville Formation is preserved within the Illinois Basin, an intracratonic basin located to the north of the Ouachita Basin (Fig. 2B; Kolata and Nelson, 1990; Nelson and Jacobson, 2010). The detrital zircon spectrum of the Caseyville Formation has a major Grenville component, a moderate Appalachian

component, and minor components of Midcontinent, Yavapai-Mazatazal, and Shield (Figs. 8, S7; Kissock, 2016). This spectrum closely resembles the detrital zircon spectra of the Jackfork Group.

Detrital zircon spectra from Pennsylvania stratigraphy in the Black Warrior Basin has a large Grenville component with small Midcontinent- and Taconic-derived components (Figs. 8, S8; Becker et al., 2005). Compilation of detrital muscovite data (N = 19) from the Pennsylvanian Pottsville Formation provides a large provenance dataset (n = 2027) for the Black Warrior Basin (Moore, 2012; Uddin et al., 2016). Collectively, the Pottsville Formation has three primary components: Taconic, Acadian, and Alleghanian (Fig. 9). Although the detrital zircon data only indicates sediments from Taconic rocks, detrital muscovite provides evidence for Acadian and Alleghanian sediments being deposited into the Black Warrior Basin during the Pennsylvanian. Pennsylvanian sedimentation into the nearby Appalachian Basin has Taconic to Acadian signal for both the Appalachian and Grenville components (Figs. 8, S10; Gray and Zeitler, 1997; Thomas et al., 2004; Becker et al., 2005).

In the Carboniferous stratigraphy of eastern North America, Grenville and Midcontinent zircons are more common than Shield Province zircons (Fig. 10, S12; Gray and Zeitler, 1997; Eriksson et al., 2004; Thomas et al., 2004; Becker et al., 2005; Park et al., 2010; Kissock, 2016; Shaulis et al., 2012; Xie et al., 2016a; Xie et al., 2016b). Zircon grain ages from the end of the Pan-African Province to the start of the Grenville Province are absent in the Jackfork Group; this is in contrast to the underlying Stanley Group which has a less-constrained provenance. There are also neither

Alleghanian zircons nor muscovite in the Jackfork Group. The Pennsylvanian Pottsville Formation, time-correlative to the Jackfork Group, has detrital muscovite with a strong Alleghanian signal. While multiple source areas may contribute sediment to the Jackfork Group, a drainage boundary must separate the Ouachita and Black Warrior basins, and possibly the Appalachian Basin, during the Early Jackfork Group deposition.

2.12. Multi-dimensional Scaling (MDS): Comparing detrital provenances

A fundamental difficulty in provenance studies utilizing radiometric dating is presenting and interpreting of large datasets (n > 1000), especially when comparing between samples or provenance techniques (e.g., detrital zircon age spectrum vs. heavy mineral percentages) on the same sample (Vermeesch and Garzanti, 2015). Recent provenance analysis tools enable multi-type plots for provenance data visualization, some of which use statistics for improved data trend interpretation (Vermeesch, 2012; Vermeesch et al., 2016).

MDS is a statistical technique that simplifies discrete sample comparisons in datasets not easily discernable by a human observer. For example, it is possible to compare the 6 Ouachita detrital zircon samples as 15 comparison pairs determined by n*(n-1) / 2, where n represents total number of samples (Vermeesch, 2012). These 6 samples compared with the 31 Carboniferous samples (Fig. 12C) are 465 possible pairs, and including all of eastern part of North America detrital zircon data (N=67) are 2211 possible pairs (Fig. 12D). ‘Provenance’, a geostatistical program used in an R environment at recommended settings compared the Ouachita detrital spectra to possible

source areas (Vermeesch et al., 2016). The results of the MDS yield increasing sample comparisons for each plot generated in succession (Figure 12).

2.12.1. Detrital Zircon Multi-Dimensional Scaling

Comparison of the Ouachita detrital samples, 2 from the Jackfork Group and 4 from the Stanley Group, show two broad groups (Fig. 12A). Location clustering of detrital zircon data aids discussion, but is based on subjective picks. In this sample set, OK12-54 is more closely related to the Jackfork Group based on detrital components because its two closest neighbors are the Jackfork Group samples. Group II indicates that the three remaining Stanley Group samples are comprised of similar detrital zircon components to those of the Jackfork Group.

New Ouachita detrital zircon data are compared with U-Pb detrital zircon data from the Illinois Basin, Black Warrior Basin, and northwest Arkansas (Fig. 12B; Becker et al., 2005; Kissock, 2016; Xie et al., 2016a; Xie et al., 2016b). The three Stanley Group samples remain clustered together in Group I, without addition of new samples. Detrital zircon data from the adjacent basins plot together with the Jackfork Group samples suggesting a common provenance.

To determine similarities between the Ouachita samples, and Carboniferous stratigraphy of eastern Laurentia (including strata within the Appalachian Basin), a third MDS was constructed (Fig. 12C; Gray and Zeitler, 1997; Eriksson et al., 2004; Thomas et al., 2004; Becker et al., 2005; Park et al., 2010; Shaulis et al., 2012; Xie et al., 2016b). In group IV, the Stanley Group samples remain clustered, whereas Jackfork samples and OK12-54 have more variation between nearest neighbors (other Carboniferous samples).

Five Stanley Group samples from published work are shown in this plot because the zircons were preferentially selected from tuffs, which biased these detrital zircon spectra (Shaulis et al., 2012). These additional samples cluster in a broad pattern in group III.

A complete comparison of published detrital zircon spectra from Precambrian to Carboniferous for Laurentia, Fig. 12D, provides a regional comparison to aid interpretation from all available stratigraphy as the Ouachita Basin was filled (Gray and Zeitler, 1997; Gleason et al., 2001; Eriksson et al., 2004; Thomas et al., 2004; Becker et al., 2005; Park et al., 2010; Shaulis et al., 2012; Xie et al., 2016b). Sample density on this plot made selection of groups difficult, and it is best to study the overall positions of the Ouachita samples and to make note their nearest neighbors.

2.12.2. Detrital Muscovite Multi-Dimensional Scaling

Provenance studies of Carboniferous stratigraphy utilizing muscovite are limited to the Greater Black Warrior Basin (GBWB; includes the Cahaba Synclinorium). These studies have identified Taconic, Acadian, and Alleghanian components (Fig. 13; Moore, 2012; Uddin et al., 2016). Comparison of the Ouachita samples by MDS will determine the likeliest GBWB sediments for a common provenance.

Three broad groups have been used to place each detrital muscovite sample of both Ouachita and Greater Black Warrior basins on the MDS plot (Fig. 13). OK12-54, a sample from the Stanley Group, is in group I; this sample is most like the Pennsylvanian Pottsville Formation in the Cahaba Synclinorium. Several samples analyzed from the Brooks Core, Black Warrior Basin are included in group I as they have a major Taconic

component, weak Acadian component, and lack an Alleghanian component (Figs. 9, 13; Moore, 2012; Uddin et al., 2016).

Group II has Pennsylvanian Jackfork Group sample OK12-39, Mississippian Parkwood Formation sample from Brooks Core, Black Warrior Basin, and several Pennsylvanian Pottsville Formation samples analyzed from both the Cahaba Synclinorium, and Brooks Core, Black Warrior Basin (Fig. 13; Moore, 2012; Uddin et al., 2016). Characteristics of these detrital muscovite spectra shared by these samples are Taconic through Acadian components, including ages for unknown crystallization events of Province A3. It is worth noting that all of these samples, except BRK 698, have no Alleghanian component (Fig. 9; Moore, 2012). Group III has the remaining detrital muscovite samples from the GBWB, and the main distinction being a significant Alleghanian component (Figs. 9, 13; Moore, 2012, Uddin et al., 2016).

2.13. Drainage systems of the Late Mississippian – Early Pennsylvanian in the Ouachita Basin

Coupled detrital techniques utilizing zircon and muscovite have aided in understanding large-scale drainage networks and paleogeography of the Mid-Carboniferous. Earlier provenance studies focused on petrography and sedimentary structures (e.g., flute casts, cross-bedding, ripple marks) to investigate possible sediment sources, which can be constrained with use of geochronology ((Fig. 14; modified from Donaldson and Shumaker, 1981 and references therein).

In the Late Mississippian, much of Laurussia is covered by shallow water with land to the north (craton) and the east (Appalachians; Fig. 14C). The shallow sea that

covered a portion of present-day Ohio, West Virginia, and eastern Kentucky began to fill with sediments derived from erosion of the rocks in northeast (e.g., Maritimes Province). A large river system, the Ontario River, paralleled the Appalachian front and supplied sediments further south into the Appalachian Basin (Williamson, 1974; Dennison and Wheeler, 1975; Kepferle, 1977; Sable, 1979). To the west of the Cincinnati Arch (shown as a ca. 300 km peninsula in Fig. 14), a second continental-scale river system, the Michigan River, deposited clastic material reworked from the Michigan Basin, first-cycle sediments from basement rocks, and possibly the Northern Appalachians/ Maritimes into the Illinois Basin (Kay, 1942; Swann, 1963; Swann et al., 1965; Pryor and Sable, 1974).

A rapid drop in relative sea-level near ca. 323 Ma is recorded globally; the emergent exposure of the Laurussian craton facilitated extensive erosion following relative sea-level fall (Fig. S1; Rygel et al., 2008; Cohen et al., 2013). Concurrent with this sea-level drop, the craton tilted to the southwest caused by loading the Laurussian margin from the collision with Gondwana during the Alleghanian and Ouachita orogenies (Figs. 3C, 14; Donaldson and Shumaker, 1981; Miall, 2019 and references therein; Hatcher, 2010).

The shape of the Appalachian Basin became defined as it filled with sediments because the Cincinnati Arch and Nashville Dome were topographic highs to the west (Stearns and Reesman, 1986; Shumaker and Wilson, 1996). Southward, the Black Warrior Basin filled with sediments sourced both locally from the adjacent Appalachian Mountains and by the Ontario River system (Figs. 5C, 14B,C; Pepper et al., 1954;

Hatcher et al., 1989 and references therein; Thomas et al., 2004). A widespread network of channels down-cut into the lower portion of the early Illinois Basin to erode the Mississippian stratigraphy (Swan, 1963; Bristol and Howard, 1974). The central portion of eastern North America during the Early Pennsylvanian was exposed to erosion, including basement rocks of the craton and recycling of sediments within intracratonic basins, and this clastic material was transported to southwestward (Potter and Siever, 1956; Meckel, 1967; Arkle, 1974; Milici, 1974; Miller, 1974; Dennison and Wheeler, 1975; Dever et al., 1977; Edmunds et al., 1979; Englund, 1979; Presley, 1979; Houseknecht, 1980).

Across the Mississippi-Pennsylvanian boundary in the Ouachita Basin, the sediments record the change in regional drainage pattern. Both detrital zircons and muscovite record the provenance shift by utilization of component occurrence in each sample analyzed. Detrital zircon results primarily differentiate between Pan-Africa (starting at 500 Ma) and older provinces, while the Late Cambrian to Carboniferous detrital history and tectonism are best recorded by the detrital muscovite spectra. Coupling the detrital results from both techniques, the Mississippian Stanley Group yielded detritus with mainly Taconic, Pan-Africa, Grenville, and Shield components (Tables 4, 5; Figs. 9, 11). In contrast, the Pennsylvanian Jackfork Group sediments have major Acadian, Taconic, Grenville, and Midcontinent components (Tables 4, 5; Figs. 9, 11).

The sandstones from the Stanley Group contain more feldspar and lithic fragments, whereas the Jackfork Group is quartz-rich (Fig. 5A; Morris, 1989). Slight

differences in feldspar composition between these sedimentary packages are illustrated in Fig. 5B (Morris, 1989). Possible tectonic environments based on combination of both petrologic datasets suggests a passive margin along with plutonic, metamorphic, volcanic, and authigenic minerals for the Stanley Group to a cratonic/transcratonic/ recycled orogenic setting for the Jackfork Group (Morris, 1989 and references therein). Regional paleo flow directions within the Ouachita Basin are generally southwest-directed, whereas the Black Warrior Basin has generally south-southeast-directed paleo flow indicators (Fig. 5C; Hatcher et al., 1989). Central and north-central portions of the Appalachians indicate paleo flows traversed the fold belt toward the craton and then moved parallel to the topographic high in the direction of the Black Warrior Basin (southwest; Hatcher et al., 1989).

2.14. Summary and Conclusions

The representative components for each sedimentary group corresponds well with published petrographic work and paleo current data. During deposition of the Mississippian Stanley Group, paleo current data suggest a southern source; petrographic analysis indicates a more proximal source based on higher feldspar content and lithic fragments. Sediments derived off of the margin of Gondwana, are likely sourced from island arcs as oceanic crust subducted under Gondwana during the closure of the Rheic Ocean. This geologic setting explains the minerals of volcanic composition and suite of tuffs present in the Stanley Group.

Cratonic sources contributed sediment into the Ouachita Basin from the north to provide the Laurentian components (i.e., Grenville and Shield). Possible explanations for

a Taconic component are 1) sediments are carried within the Rheic Ocean parallel to Laurussia margin without exposure of Acadian plutons, or 2) a more interior continental-scale river system (Michigan River) transported sediment from the northern Appalachians to the west of the Cincinnati Arch and southward into the Ouachita Basin. The provenance of the Stanley Group comprises at least two sources, as the detritus is a mixture of Laurentian crust and Gondwanan crust.

The high percentage of quartz with scant feldspars indicate highly-weathered sediments; this observation suggests recycling and/or transport of sediments over long distances by a large-scale drainage network. Sediments sourced from the Michigan River system likely enter the north-eastern part of the Ouachita basin, flowing westward as indicated by flute casts during the closure of the Rheic Ocean. The position of the Michigan River nearest the Ouachita Basin may have been influenced by basement structures similar to the present-day drainage lying above the New Madrid area (Fig. 15). A southern source for sediments is possible, but as a secondary source. The detrital ages from zircon are consistent with a major source of the ‘craton’ detritus because there are components of Grenville and Midcontinent.

Absence of an Alleghanian component, especially in the muscovite spectrum, for the Jackfork sandstones constrains the sediment pathway to bypass the GBWB because of the abundant Alleghanian muscovite within its strata. Based on paleo flow data, some sediment from the Appalachian Basin was carried southeastward into the Black Warrior Basin. A topographically high boundary (e.g., Cincinnati Arch and Nashville Dome) separated the Appalachian and Ouachita basins, meaning that there was not significant

Alleghanian sediments transported to the Ouachita Basin during the earliest Pennsylvanian. Recycling of sediments within the proximal Illinois Basin, medial Michigan Basin, or distal headwaters in the Maritimes are all possible provenances for Jackfork Group sediment carried by the Michigan River. The nature of the sediment bypass is not well-constrained because the extension of the Cincinnati Arch and topographic profile of the boundary are poorly defined.

2.15. References

Aleinikoff, J.N., Zartman, R.E., Walter, M., Rankin, D.W., Lyttle, P.T., Burton, W.C., 1995, U-Pb ages of metarhyolites of the Catoctin and Mount Rogers Formations, central and southern Appalachians: evidence for two pulses of Iapetan rifting: American Journal of Science, v. 295, p. 428-454.

Arbenz, J.K., 1989a, The Ouachita System, *in* Bally, A.W., and Palmer, A.R., eds., An Overview, The Geology of North America: Geological Society of America, v. A, p.371-395.

Arbenz, J.K., 1989b, Ouachita thrust belt and Arkoma basin, *in* Hatcher, R.D., Jr., Thomas, W.A., and Viele, G.W., eds., The Appalachian–Ouachita orogen in the United States, The Geology of North America: Geological Society of America, v. F-2, p. 621–634.

Arbenz, J.K., 2008, Structural Framework of the Ouachita Mountains, *in* Suneson, N.H., ed., Stratigraphic and Structural Evolution of the Ouachita Mountains and Arkoma Basin, Southeastern Oklahoma and West-Central Arkansas: Applications to

Petroleum Exploration: 2004 Field Symposium (The Arbenz-Misch/Oles Volume), Circular 112A, Oklahoma Geological Survey, Norman, Oklahoma, p. 4-40.

Archer, A.W., and Greb, S.F., 1995, An Amazon-scale drainage system in the Early Pennsylvanian of central North America: The Journal of Geology, v. 103, p. 611-628.

Arevalo, R., Jr., 2014, Laser ablation ICP-MS and laser fluorination GS-MS, *in* McDonough, W.F., ed., Treatise on geochemistry, Second edition: Reference Module in Earth Systems and Environmental Science, v. 15, Elsevier Publications, Waltham, Massachusetts, p. 425-441, doi:10.1016/B978-0-08-095975-7.01432-7.

Arkle, T.J., 1974, Stratigraphy of the Pennsylvanian and Permian Systems in the Central Appalachians, *in* Briggs, G., ed., Carboniferous of the Southeastern United States: Geological Society of America, Special Paper 148, p. 5-29.

Bates, R.L., and Jackson, J.A, eds., 1987, Glossary of Geology, Third edition: American Geological Institute, Alexandria, Virginia, 788 p.

Becker, T.P., Thomas, W.A., Samson, S.D., and Gehrels, G.E., 2005, Detrital zircon evidence of Laurentian crustal dominance in the Lower Pennsylvanian deposits of the Alleghanian clastic wedge in eastern North America: Sedimentary Geology, v. 182, p. 59-86, doi:10.1016/j.sedgeo.2005.07.014.

Bickford, M.E., Van Schmus, W.R., and Zietz, I., 1986, Proterozoic history of the midcontinent region of North America: Geology, v. 14, p. 492-496, doi:10.1130/0091-7613(1986)14<492:PHOTMR>2.0.CO;2.

Blakey, R.C., 2008, Gondwana paleogeography from assembly to breakup – A 500 m.y. odyssey: Geological Society of America, Special Paper 441, p. 1–28, doi: 10.1130/2008.2441(01).

Black, L.P., Kamo, S.L., Allen, C.M., Davis, D.W., Aleinikoff, J.N., Valley, J.W., Mundil, R., Campbell, I.H., Korsch, R.J., Williams, I.S., and Foudoulis, C., 2004, Improved Pb-206/U-218 microprobe geochronology by the monitoring of a trace-element-related matrix effect; SHRIMP, ID-TIMS, ELA-ICP-MS and oxygen isotope documentation for a series of zircon standards: Chemical Geology, v. 205, p. 115-140.

Blake, B.M., Jr., and Beuthin, J.D., 2008, Deciphering the mid-Carboniferous eustatic event in the central Appalachian foreland basin, southern West Virginia, USA, *in* Fielding, C.R., Frank, T.D., and Isbell, J.L., eds., Resolving the Late Paleozoic ice age in time and space: Geological Society of America, Special Paper 441, p. 249-260, doi:10.1130/2008.2441(17).

Braile, L.W., Hinze, W.J., Keller, G.R., Lidiak, E.G., and Sexton, J.L., 1986, Tectonic development of the New Madrid Rift Complex, Mississippi Embayment, North America: Tectonophysics, v. 131, p. 1-21.

Briggs, G., and Cline, L.M., 1967, Paleocurrents and source areas of Late Paleozoic sediments of the Ouachita Mountains, southeastern Oklahoma: Journal of Sedimentary Petrology, v. 37, p. 985-1000.

Bristol, H.M., and Howard, R.H., 1974, Sub-Pennsylvanian valleys in the Chesterian surface of the Illinois Basin and related Chesterian slump blocks, *in* Briggs, G., ed.,

Carboniferous of the Southeastern United States: Geological Society of America, Special Paper 148, p. 315-335.

Cawood, P.A., and Nemchin, A.A., 2001, Paleogeographic development of the east Laurentian margin: Constraints from U-Pb dating of detrital zircons in the Newfoundland Appalachians: Geological Society of America Bulletin, v. 113, p. 1234-1246.

Cawood, P.A., Nemchin, A.A., Strachan, R., Prave, T., and Krabbendam, M., 2007, Sedimentary basin and detrital zircon record along East Laurentia and Baltica during assembly and breakup of Rodinia: Journal of the Geological Society, London, v. 164, p. 257-275.

Cecil, C.B., AND Eble, C., eds., 1989, Carboniferous geology of the eastern United States: American Geophysical Union, Guidebook T143, Washington D.C., 154 p.

Chang, Z., Vervoort, J.D., Mcclelland, W.C., and Knaack, C., 2006, U-Pb dating of zircon by LA-ICP-MS: Geochemistry, Geophysics, Geosystems, v. 7, 14 p., doi:10.1029/2005GC001100.

Chesnut, D.R., Jr., 1988, Stratigraphic analysis of the Carboniferous rocks of the central Appalachian Basin [Ph.D. dissertation]: University of Kentucky, 297 p.

Cohen, K.M., Finney, S.C., Gibbard, P.L., and Fan, J.-X. (2013) The ICS International Chronostratigraphic Chart. Episodes 36: 199-204.

Coleman, J.L., Jr., 1990, Comparison of depositional elements of an ancient and a "modern" submarine fan complex: Early Pennsylvanian Jackfork and Late

Pleistocene Mississippi fans (abs.): American Association of Petroleum Geologists Bulletin, v. 74, p. 631.

Coleman, J.L., Jr., 2000, Carboniferous Submarine Basin development of the Ouachita mountains of Arkansas and Oklahoma, *in* Bouma, A.H., and Stone, C.G., eds., Fine-grained turbidite systems: American Association of Petroleum Geologists Memoir 72 and Society of Economic Paleontologists and Mineralogists Special Publication 68, p. 21-32.

Coleman, J.L., Jr., Van Swearingen, G., and Breckon, C.E., 1994, The Jackfork Formation of Arkansas: A Test of the Walker-Mutti-Vail Models for Deep-Sea Fan Deposition: Arkansas Geological Commission, Guidebook 94-2, Little Rock, Arkansas, 65 p.

Cook, T.D., and Bally, A.W., 1975, Stratigraphic atlas of North and Central America: Princeton, New Jersey, Princeton University Press, 272 p.

Corfu, F., Hanchar, J.M., Hoskin, P.W.O., and Kinny, P., 2003, Atlas of Zircon Textures, *in* Hanchar, J.M., and Hoskin, P.W.O., eds., Zircon: Reviews in Mineralogy and Geochemistry, v. 53, p. 469-500.

Coler, D.G., and Samson, S.D., 2000, Characterization of the Spring Hope and Roanoke rapids terranes, southern Appalachians: a U-Pb geochronologic and Nd isotopic study: Geological Society of America, Abstracts Program 32, p. 11-12.

Dahlquist, J.A., Pankhurst, R.J., Rapela, C.W., Galindo, C., Alasino, P., Fanning, C.M., Saavedra, J., and Baldo, E., 2008, New SHRIMP U-Pb data for the Famatina Complex: constraining Early-Mid Ordovician Famatinian magmatism in the Sierras

Pampeanas, Argentina: Geologica Acta, v. 6, p. 319-333, doi:10.1344/105.000000260.

Dalla Salda, L.H., Lopez De Luchi, M.G., Cingolani, C.A., Varela, R., 1998, Laurentia-Gondwana collision: the origin of the Famatinian-Appalachian orogenic belt (a review), *in* Pakhurst, R.J. and Rapela, C.W., eds., The Proto-Andean Margin of Gondwana: Geological Society, London, Special Publications 142, p. 219-234.

Dalziel, I.W.D., 1997, Neoproterozoic-Paleozoic geography and tectonics: Review, hypothesis, environmental speculation: Geological Society of America Bulletin, v. 109, p. 16-42.

Denison, J.M., and Wheeler, W.H., 1975, Stratigraphy of Precambrian through Cretaceous strata of probable fluvial origin in southeastern United States and their potential as uranium host rocks: Southeastern Geology, Special Publication 5, 210 p.

Dever, G.R., Hoge, HP, Hester, N.C., and Ettensohn, F.R., 1977, Stratigraphic evidence for Late Paleozoic tectonism in northeastern Kentucky: Kentucky Geological Survey, University of Kentucky, Lexington, 80 p.

Dickinson, W.R., and Suczek, C.A., 1979, Plate tectonics and sandstone compositions: American Association of Petroleum Geologists Bulletin, v. 63, p. 2164-2182.

Donaldson, A.C., and Shumaker, R.C., 1981, Late Paleozoic molasse of central Appalachians: Geological Association of Canada, Special Paper 23, p. 99-124.

Donelick, R.A., O'Sullivan, P.B., and Ketcham, R.A., 2005, Apatite Fission-Track Analysis, *in* Reiners, P.W., and Ehlers, T.A., eds., Low-temperature

thermochronology: Techniques, interpretations, and applications: Reviews in Mineralogy and Geochemistry, v. 58, p. 49-94.

Drake, A.A., Jr., Sinha, A.K., Laird, J., and Guy, R.E., 1989, The Taconic orogeny, *in* Hatcher, R.D., Jr., Thomas, W.A., and Viele, G.W., eds., The Appalachian–Ouachita orogen in the United States, The Geology of North America: Geological Society of America, v. F-2, p. 101–177.

Edmunds, W.E., Berg, T.M., Sevon, W.D., Piotrowski, R.C., Heyman, L. and Rickard, L.V., 1979, The Mississippian and Pennsylvanian Systems in the United States – Pennsylvania and New York: United States Geological Survey, Professional Paper 1110-A-L, p. B1-B33.

Englund, K.J., 1974, Sandstone distribution patterns in the Pocahontas Formation of southwest Virginia and southern West Virginia, *in* Briggs, G., eds., Carboniferous of the Southeastern United States: Geological Society of America, Special Paper 148, p. 31-45.

Englund, K.J., 1979, Mississippian and Pennsylvanian (Carboniferous) Systems in the United States – Virginia: Historical review and summary of areal, stratigraphic, structural, and economic geology of Mississippian and Pennsylvanian rocks in Southwestern Virginia: United States Geological Survey, Professional Paper 1110-A-L, p. C1-C21.

Eriksson, K.A., Campbell, I.H., Palin, J.M., and Allen, C.M., 2003, Predominance of Grenvillian magmatism recorded in detrital zircons from modern Appalachian rivers: Journal of Geology, v. 111, p. 707-717, doi:10.1086/378338.

Ettensohn, F.R., Pashin, J.C., and Gilliam, W., 2019, The Appalachian and Black Warrior Basins: Foreland Basins in the Eastern United States, *in* Miall, A.D., ed., The Sedimentary Basins of the United States and Canada, Sedimentary Basins of the World: Elsevier, p. 129-237, doi: 10.1016/B978-0-444-63895-3.00004-8.

Fedo, C.M., Sircombe, K.N., AND Rainbird, R.H., 2003, Detrital zircon analysis of the sedimentary record, *in* Hanchar, J.M., and Hoskin, P.W.O., eds., Zircon: Reviews in Mineralogy and Geochemistry, v. 53, p. 277-303.

Flawn, P.T., Goldstein, A., JR., King, P.B., and Weaver, C.E., 1961, The Ouachita System, Publication 6120: Bureau of Economic Geology, University of Texas, 401 p.

Gehrels, G., 2012, Detrital zircon U-Pb geochronology: current methods and new opportunities, *in* Busby, C., and Azor, A., eds., Tectonics of Sedimentary Basins: Recent Advances: Wiley-Blackwell, Hoboken, New Jersey, p. 47-62.

Gehrels, G., 2014, Detrital zircon U-Pb geochronology applied to tectonics: Annual Review of Earth and Planetary Sciences, v. 42, p. 127-149, doi: 10.1146/annurev-earth-050212-124012.

Gleason, J.D., Finney, S.C., and Gehrels, G.E., 2001, Paleotectonic implications of a mid- to late-Ordovician provenance shift, as recorded in sedimentary strata of the Ouachita and southern Appalachian mountains: Journal of Geology, v. 110, p. 291-304.

Gordon, Jr., M., 1974, The Mississippian-Pennsylvanian Boundary in the United States: Septième Congrès International de Stratigraphie et de Géologie du Carbonifère, Krefeld, 23-28, August 1971, Compte rendu, v.3, p. 129-141.

Graham, S.A., Dickinson, W.R., and Ingersoll, R.V., 1975, Himalayan-Bengal model for flysch dispersal in the Appalachian-Ouachita system: Geological Society of America Bulletin, v.86, p. 273-286.

Graham, S.A., Ingersol, R.A., and Dickinson, W.R., 1976, Common provenance for lithic grains in Carboniferous sandstones from Ouachita Mountains and Black Warrior Basin: Journal of Sedimentary Petrology, v. 46, p. 620-632.

Gray, M.B., AND Zeitler, P.K., 1997, Comparison of clastic wedge provenance in the Appalachian foreland using U/Pb ages of detrital zircons: Tectonics, v. 16, p. 151-160.

Haley, B.R., Glick, E.E., Bush, W.V., Clardy, R.F., Stone, C.G., Woodward, M.P., and Zachry, D.L., 1976, Geologic map of Arkansas: U.S. Geological Survey and Arkansas Geologic Commission, scale 1:500,000.

Hatch, J.R., and Pawlewicz, M.J., 2007, Introduction to the assessment of undiscovered oil and gas resources of the Black Warrior Basin Province of Alabama and Mississippi, *in* Hatch, J.R., and Pawlewicz, M.J., eds., Geologic assessment of undiscovered oil and gas resources of the Black Warrior Basin Province, Alabama and Mississippi: U.S. Geological Survey Digital Data Series DDS–69–I, Chap. 2, 6 p.

Hatcher, R.D., Jr., 1987, Tectonics of the Southern and Central Appalachian Internides: Annual Review of Earth and Planetary Sciences, v. 15, p. 337-362, doi:10.1146/annurev.ea.15.050187.002005.

Hatcher, R.D., Jr., 2002, Alleghanian (Appalachian) orogeny, a product of zipper tectonics: Rotational transpressive continent-continent collision and closing of ancient oceans along irregular margins, *in* Martínez Catalán, J.R., Hatcher, R.D., Jr., Arenas, R., and Díaz García, F., eds., Variscan-Appalachian dynamics: The building of the Late Paleozoic basement: Geological Society of America, Special Paper 364, p. 199-208.

Hatcher, R.D., Jr., 2010, The Appalachian orogeny: A brief summary, *in* Tollo, R.P., Bartholomew, M.J., Hibbard, J.P., and Karabinos, P.M., eds., From Rodina to Pangea: The Lithotectonic Record of the Appalachian Region: Geological Society of America, Memoir 206, p. 1-19, doi:10.1130/2010.1206(01).

Hatcher, R.D., Jr., Thomas, W.A., Geiser, P.A., Snoke, A.W., Mosher, S., and Wiltschko, D.V., 1989, Alleghanian orogeny, *in* Hatcher, R.D., Jr., Thomas, W.A., and Viele, G.W., eds., The Appalachian–Ouachita orogen in the United States, The Geology of North America: Geological Society of America, v. F-2, p. 233–318.

Hill, B.M., and Bickford, M.E., 2001, Paleoproterozoic rocks of central Colorado: Accreted arcs or extended older crust?: Geology, v. 29, p. 1015-1018.

Hodges, K.V., Ruhl, K.W., Wobus, C.W., and Pringle, M.S., 2005, $^{40}Ar/^{39}Ar$ Thermochronology of Detrital Minerals, *in* Reiners, P.W., and Ehlers, T.A., eds., Low-Temperature Thermochronology: Techniques, Interpretations, and Applications: Reviews in Mineralogy and Geochemistry, v. 58, p. 239-257.

Hoffman, P.F., 1989, Precambrian geology and tectonic history of North America, *in* Bally, A.W., and Palmer, A.R., eds., The Geology of North America - An Overview: Geological Society of America, v. A, p. 447-512.

Honess, C.W., 1923, Geology of the southern Ouachita Mountains of Oklahoma: Oklahoma Geological Survey Bulletin 32, Part I, 278 p., Part II, 76 p.

Horstwood, M.S.A., Kosler, J., Gehrels, G., Jackson, S.E., McLean, N.M., Paton, C., Pearson, N.J., Sircombe, K., Sylvester, P., Vermeesch, P., Bowring, J.F., Condon, D.J., and Schoene, B., 2016, Community-derived standards for LA-ICP-MS U-(Th-) Pb geochronology – Uncertainity propagation, age interpretation, and data reporting: Geostandards and Geoanalytical Research, v. 40, p. 311-332.

Houseknecht, D.W., 1980, Comparative anatomy of a Pottsville lithic arenite and quartz arenite of the Pocahontas Basin, southern West Virginia: Petrographic, depositional, and stratigraphic implications: Journal of Sedimentary Petrology, v. 50, p. 3-20.

Ingersoll, R.V., Dickinson, W.R., and Graham, S.A., 2003, Remnant-ocean submarine fans: Largest sedimentary systems on Earth, *in* Isbell, J.L., Miller, M.F., Wolfe, K.L., and Lenaker, P.A., eds., Extreme depositional environments: Mega end members in geologic time: Geological Society of America, Special Paper 370, p.191-208.

Ingle-Jenkins, S., Mueller, P.A., Heatherington, A.L., Offield, T.W., 1998, Age and origin of the Uwharrie Formation and Albermarle Group, Carolina slate belt: implications from U-Pb and Sm-Nd systematics: Geological Society of America, Abstracts Program 30, p. 239.

Johnson, K.S., ed., 1988, Shelf-to-basin geology and resources of Pennsylvanian strata in the Arkoma Basin and frontal Ouachita Mountains of Oklahoma: Oklahoma Geological Survey, Guidebook 25, Norman, Oklahoma, 105 p.

Kay, G.M., 1942, Ottawa-Bonnechere Graben and Lake Ontario Homocline: Geological Society of America Bulletin, v. 53, p. 585-646.

Keller, M., 1999, Argentine Precordillera: Sedimentary and Plate Tectonic History of a Laurentian Crustal Fragment in South America: Geological Society of America, Special Paper 341, p. 1-131, doi:10.1130/0-8137-2341-8.1.

Kepferle, R.C., 1977, Stratigraphy, petrology, and depositional environment of the Kenwood Siltstone Member Borden Formation (Mississippian) Kentucky and Indiana: United States Geological Survey, Professional Paper 1007, 49p.

Kissock, J.K., 2016, Detrital zircon evidence for the unroofing of the Northern Appalachians in Early-Middle Pennsylvanian sandstones of North America [MS Thesis]: University of Iowa, 220p.

Kolata, D.R., and Nelson, W.J., 1990, Tectonic History of the Illinois Basin, *in* Leighton, M.W., Kolata, D.R., Oltz, D.T., and Eidel, J.J., Interior cratonic basins: American Association of Petroleum Geologists, Memoir 51, p. 263-285.

Leighton, M.W., 1996, Interior cratonic basins: A record of regional tectonic influences, *in* van der Pluijm, B.A., and Catacosinos, P.A., eds., Basements and basins of eastern North America: Geological Society of America, Special Paper 308, p. 77-93.

Lowe, D.R., 1985, Ouachita trough: Part of a Cambrian failed rift system: Geology, v. 13, p.790-793.

Lowe, D.R., 1989, Stratigraphy, sedimentology, and depositional setting of pre-orogenic rocks of the Ouachita Mountains, Arkansas and Oklahoma, *in* Hatcher, R.D., Jr., Thomas, W.A., and Viele, G.W., eds., The Appalachian–Ouachita orogen in the United States, The Geology of North America: Geological Society of America, v. F-2, p. 575–590.

Maynard, J.B., Valloni, R., and Yu, H., 1983, Composition of modern deep-sea sands from arc-related basins, *in* Leggett, J.K., ed., Trench and fore-arc sedimentation: Geological Society of London, Special Publication 10, p. 551-561.

McDougal, I., and Harrison, M., 1999, Geochronology and Thermochronology by the $^{40}Ar/^{39}Ar$ method: Oxford University Press, New York, 271 p.

McKerrow, W.S., Macniocaill, C., and Dewey, J.F., 2000, The Caledonian Orogeny redefined: Journal of the Geological Society, London, v. 157, p. 1149-1154.

McLennan, S.M., Bock, B., Compston, W., Hemming, S.R., and McDaniel, D.K., 2001, Detrital zircon geochronology of Taconian and Acadian foreland sedimentary rocks in New England: Journal of Sedimentary Research, v. 71, p. 305-317.

Meckel, L.D., 1967, Origin of the Pottsville Conglomerates (Pennsylvanian) in the Central Appalachians: Geological Society of America Bulletin, v. 78, p. 223-257.

Miall, A.D., 2019, The Southern Midcontinent, Permian Basin, and Ouachitas, *in* Miall, A.D., ed., The Sedimentary Basins of the United States and Canada, Sedimentary Basins of the World: Elsevier, p. 297-327, doi: 10.1016/B978-0-444-63895-3.00008-5.

Miall, A.D., and Blakey, R.C., 2019, The Phanerozoic tectonic and sedimentary evolution of North America *in* Miall, A.D., ed., The Sedimentary Basins of the United States and Canada, Sedimentary Basins of the World: Elsevier, p. 1-38, doi: 10.1016/B978-0-444-63895-3.00001-2.

Milici, R.C., 1974, Stratigraphy and depositional environments of Upper Mississippian and Lower Pennsylvanian rocks in the southern Cumberland Plateau of Tennessee, Briggs, G., eds., Carboniferous of the Southeastern United States: Geological Society of America, Special Paper 148, p. 115-133.

Miller, M.S., 1974, Stratigraphy and coal beds of Upper Mississippian and Lower Pennsylvanian rocks in southern Virginia: Virginia Division of Mineral Resources, Bulletin 84, 211 p.

Miser, H.D., 1921, Llanoria, the Paleozoic land area in Louisiana and eastern Texas: American Journal of Science, v. 2, p. 61-89.

Moore, M.F., 2012, $^{40}Ar/^{39}Ar$ dating of detrital muscovite and sediment compositional analysis of the Pottsville Formation in the Black Warrior basin in Alabama: Implications for tectonics and sedimentation [MS Thesis]: Auburn University, Alabama, 142 p.

Morris, R.C., 1971, Stratigraphy and sedimentology of Jackfork Group, Arkansas: American Association of Petroleum Geologists Bulletin, v. 55, p. 387-402.

Morris, R.C., 1974a, Carboniferous rocks of the Ouachita mountains, Arkansas: A study of facies patterns along the unstable slope and axis of a flysch trough: Geological Society of America, Special Paper 148, p. 241-279.

Morris, R.C., 1974b, Sedimentary and tectonic history of the Ouachita Mountains: Society of Economic Palentologists and Mineralogists, Special Publication 22, p. 120-142.

Morris, R.C., 1977, Petrography of Stanley-Jackfork sandstones, Ouachita Mountains, Arkansas, *in* Stone, C.G., ed., Symposium of the geology of the Ouachita mountains: Arkansas Geological Commission, Little Rock, Arkansas, p. 146-157.

Morris, R.C., 1989, Stratigraphy and sedimentary history of post-Arkansas Novaculite Carboniferous rocks of the Ouachita Mountains, *in* Hatcher, R.D., Jr., Thomas, W.A., and Viele, G.W., eds., The Appalachian–Ouachita orogen in the United States, The Geology of North America, v. F-2: Geological Society of America, p. 591–602.

Morris, R.C., Proctor, K.E., and Koch, M.R., 1979, Petrology and diagenesis of deep-water sandstones, Ouachita Mountains, Arkansas and Oklahoma: Society of Economic Paleontologists and Mineralogists, Special Publication 26, p. 263-279.

Mueller, P.A., Heatherington, A.L., Wooden, J.L., Shuster, R.D., Nutman, A.P., and Williams, I.S., 1994, Precambrian zircons from the Florida basement: a Gondwanan connection: Geology, v. 22, p. 119-122.

Nance, R.D., and Linnemann, U., 2008, The Rheic Ocean: Origin, Evolution, and Significance: Geological Society of America Today, v. 18, p. 4-12.

Nance, R.D., Gutierrez-Alonso, G., Keppie, J.D., Linneman, U., Murphy, J.B., Quesada, C., Strachan, R.A., and Woodcock, N.H., 2010, Evolution of the Rheic Ocean: Gondwana Research, v. 17, p. 194-222.

Nelson, W.J., and Jacobson, R.J., 2010, Pennsylvanian subsystem and Permian system, *in* Kolata, D.R., and Nimz, C.K., eds., Geology of Illinois: Illinois State Geological Survey, University of Illinois at Urbana-Champaign, p. 187-205.

Niem, A.R., 1976, Patterns of flysch deposition and deep-sea fans in the Lower Stanley Group (Mississippian), Ouachita mountains, Oklahoma and Arkansas: Journal of Sedimentary Petrology, v. 46, p. 633-646.

Niem, A.R., 1977, Mississippian pyroclastic flow and ash-fall deposits in the deep-marine Ouachita flysch basin, Oklahoma and Arkansas: Geological Society of America Bulletin, v. 88, p. 49-61.

Osberg, P.H., Tull, J.F., Robinson, P., Hon, R., and Butler, J.R., 1989, The Acadian orogeny, *in* Hatcher, R.D., Jr., Thomas, W.A., and Viele, G.W., eds., The Appalachian–Ouachita orogen in the United States, The Geology of North America: Geological Society of America, v. F-2, p. 179–232.

Paces, J.B., and Miller, J.D., 1993, Precise U-Pb ages of Duluth Complex and related mafic intrustions, northeastern Minnesota: geochronological insights into physical, petrogenetic, paleomagnetic, and tectonomagnetic processes associated with the 1.1 Ga midcontinent rift system: Journal of Geophysical Research, v. 98, p. 13997-14013.

Pashin, J.C., and Gastaldo, R.A., 2009. Carboniferous of the Black Warrior basin, *in* Greb, S.F., and Chesnut, D.R., Jr., Carboniferous of the Appalachian and Black Warrior Basins: Kentucky Geological Survey, Special Publication 10, Lexington, Kentucky, p.10-21.

Park, H., Barbeau, D.L., Jr., Rickenbaker, A., Bachmann-Krug, D., and Gehrels, G., 2010, Application of foreland basin detrital-zircon geochronology to the reconstruction of the Southern and Central Appalachian Orogen: Journal of Geology, v. 118, p. 23-44.

Potter, P.E., and Siever, R., 1956, Sources of basal Pennsylvanian sediments in the Eastern Interior basin, Part I, Cross-bedding: Journal of Geology, v. 64, p. 225-244.

Presley, M.W., 1979, Facies and depositional systems of Upper Mississippian and Pennsylvanian strata in the Central Appalachians, *in* Donaldson, A.C., Presley, M.W., and Renton, J.J., eds., Carboniferous Coal: West Virginia Geologic Survey, p.1-50.

Pryor, W.A., and Sable, E.G., 1974, Carboniferous of the Eastern Interior basin, *in* Briggs, G., ed., Carboniferous of the Southeastern United States: Geological Society of America, Special Paper 148, p. 281-313.

Rainbird, R., Cawood, P., and Gehrels, G., 2012, The great Grenvillian sedimentation episode: record of supercontinent Rodinia's assembly, *in* Busby, C., and Azor, A., eds., Tectonics of Sedimentary Basins: Recent Advances: Wiley-Blackwell, Hoboken, New Jersey, p. 583-601.

Rankin, D.W., Drake, A.A., Jr., Glover, L., III, Goldsmith, R., Hall, L, Murray, D.P., Ratcliffe, N.M., Read, J.F., Secor, D.T., Jr., and Stanley, R.S., 1989, Pre-orogenic terranes, *in* Hatcher, R.D., Jr., Thomas, W.A., and Viele, G.W., eds., The Appalachian–Ouachita orogen in the United States, The Geology of North America: Geological Society of America, v. F-2, p. 7–100.

Ruhl, K.W., and Hodges, K.V., 2005, The use of detrital mineral cooling ages to evaluate steady state assumptions in active orogens: An example from the central Nepalese Himalaya: Tectonics, v. 24, TC4015, doi:10.1029/2004TC001712.

Ross, C.A., and Ross, J.R.P., 1987, Late Paleozoic sea levels and depositional sequences: Cushman Foundation for Foraminiferal Research, Special Publication 24, Washington D.C., p. 137-149.

Rygel, M.C., Fielding, C.R., Frank, T.D., and Birgenheier, L.P., 2008, The magnitude of Late Paleozoic glacioeustatic fluctuations: A synthesis: Journal of Sedimentary Research, v. 78, p. 500-511, doi:10.2110/jsr.2008.058.

Sable, E.G., 1979, Eastern Interior basin region, *in* Craig, L.C., and Connor, C.W., eds., Paleotectonic investigations of the Mississippian System in the United States, Part I, Introduction and Regional Analyses of the Mississippian System: United States Geological Survey, Professional Paper 1010, p. 59-106.

Samson, S.D., Secor, D.T., and Hamilton, M.A., 2001, Wandering Carolina: tracking exotic terranes with detrital zircons: Geological Society of America, Abstracts Program 33, p. 263.

Schoene, B., 2014, U-Th-Pb geochronology, *in* Rudnick, R.L., ed., Treatise on geochemistry: Reference Module in Earth Systems and Environmental Sciences, v. 4, Elsevier Publications, Waltham, Massachusetts, p. 341-378, doi:10.1016/B978-0-08-095975-7.00310-7.

Scotese, C.R., 1998, Quicktime Computer Animations, PALEOMAP Project: Department of Geology, University of Texas at Arlington, Arlington, Texas.

Scotese, C.R., and Golanka, J., 1992, Paleogeographic Atlas, PALEOMAP Progress report 20-0692: Department of Geology, University of Texas at Arlington, Arlington, Texas, 34 p.

Shaulis, B.J., Lapen, T.J., Casey, J.F., and Reid, D.R., 2012, Timing and Rates of Flysch Sedimentation In the Stanley Group, Ouachita Mountains, Oklahoma and Arkansas, U.S.A.: Constraints from U-Pb Zircon Ages of Subaqueous Ash-Flow Tuffs: Journal of Sedimentary Research, v. 82, p. 833-840., doi:10.2110/jsr.2012.68.

Shumaker, R.C., and Wilson, T.H., 1996, Basement structure of the Appalachian foreland in West Virginia: Its style and effect on sedimentation, *in* van der Pluijm, B.A., and Catacosinos, P.A., eds., Basements and basins of eastern North America: Geological Society of America, Special Paper 308, p. 139-155.

Sloss, L.L., 1963, Sequences in the cratonic interior of North America: Geological Society of America Bulletin, v. 74, p. 93-114.

Speer, J.A, and Hoff, K., 1997, Elemental composition of the Alleghanian granitoid plutons of the southern Appalachians, *in* Sinha, A.K., Whalen, J.B., and Hogan, J.P., eds., The nature of magmatism in the Appalachian orogeny: Geological Society of America, Memoir 191, p. 287-308.

Spencer, C.J., Cawood, P.A., Hawkesworth, C.J., Prave, A.R., Roberts, Z.M.W., Horstwood, M.S.A., Whitehouse, M.J., and EIMF, 2015, Generation and preservation of continental crust in the Grenville orogeny: Geoscience Frontiers, v. 6, p. 357-372, doi:10.1016/j.gsf.2014.12.001.

Stampfli, G.M., Von Raumer, J.F., and Borel, G.D., 2002, Paleozoic evolution of pre-Variscan terranes: from Gondwana to the Variscan collision, *in* Martinez Catalan, J.R., Hatcher, R.D., Arenas, R., and Diaz Garcia, F., eds., Variscan-Appalachian dynamics: the building of the Late Paleozoic basement: Geological Society of America, Special Paper 364, Boulder, Colorado, p. 263-280.

Stearns, R.G., and Reesman, A.L., 1986, Cambrian to Holocene structural and burial history of Nashville Dome: American Association of Petroleum Geologists Bulletin, v. 70, p.143-154.

Stone, C.G., McFarland, J.D., III, and Haley, B.R., 1981, Field guide to the Paleozoic rocks of the Ouachita Mountain and Arkansas Valley Provinces, Arkansas: Arkansas Geological Commission, Guidebook 81-1, Little Rock, Arkansas, 140 p.

Sutherland, P.K., and Manger, W.L., eds., 1979, Mississippian-Pennsylvanian shelf-to-basin transition, Ozark and Ouachita regions, Oklahoma and Arkansas: Oklahoma Geological Survey, Guidebook 19, Norman, Oklahoma, 81 p.

Suneson, N.H., Campbell, J.A., and Tilford, M.J., eds., 1990, Geology and resources of the frontal belt of the western Ouachita Mountains, Oklahoma: Oklahoma Geological Survey, Special Publication 90-1, Norman, Oklahoma, 196 p.

Suneson, N.H., and Hemish, L.A., 1994, Geology and resources of the eastern Ouachita Mountains frontal belt and south-eastern Arkoma Basin, Oklahoma: Oklahoma Geological Survey, Guidebook 29, Norman, Oklahoma, 294 p.

Swann, D.H., 1963, Classification of Genevievian and Chesterian (Late Mississippian) Rocks of Illinois: Illinois State Geological Survey, Report of Investigations 216, p. 91.

Swann, D.H., Lineback, J.A., and Frund, E., 1965, The Borden Siltstone (Mississippian) Delta in southwestern Illinois: Illinois State Geological Survey, Circular 386, 20 p.

Swanson, D.C., 1979, Deltaic deposits in the Pennsylvanian Upper Morrow Formation of the Anadarko Basin, *in* Hyne, N.J., ed., Pennsylvanian Sandstones of the Midcontinent: Tulsa Geological Society, Special Publication 1, Tulsa, Oklahoma, p. 115-168.

Thomas, W.A., 1972, Regional Paleozoic Stratigraphy in Mississippi between Ouachita and Appalachian Mountains: American Association of Petroleum Geologist Bulletin, v. 56, p. 81-106.

Thomas, W.A., 1977, Evolution of Appalachian-Ouachita salient and recesses from reentrants and promontories in the continental margins: America Journal of Science, v. 277, p. 1233-1278.

Thomas, W.A., 2011, Detrital-zircon geochronology and sedimentary provenance: Lithosphere, v. 3, p. 304-308, doi:10.1130/RF.L001.1.

Thomas, W.A., and Astini, R.A., 1996, The Argentine Precordillera: A traveler from the Ouachita Embayment of North American Laurentia: Science, New Series, v. 273, p. 752-757.

Thomas, W.A., Becker, T.P., Samson, S.D., and Hamilton, M.A., 2004, Detrital zircon evidence of a recycled orogenic foreland provenance for Alleghanian clastic-wedge sandstones: Journal of Geology, v. 112, p.23-37, doi:10.1086/379690.

Torsvik, T.H., 2003, The Rodinia Jigsaw Puzzle: Science, v. 300, p. 1379-1381.

Trompette, R., 2000, Gondwana evolution: its assembly at around 600 Ma: Comptes Rendus de l'Academie des sciences, serie II, Sciences de la Terre et des Planetes, v. 330, p. 305-315.

Trevena, A.S., and Nash, W.P., 1981, An electron microprobe study of detrital feldspar: Journal of Sedimentary Petrology, v. 51, p. 137-150.

Uddin, A., Hames, W.E., Peavy, T., and Pashin, J.C., 2016, Detrital history of the Lower Pennsylvanian Pottsville Formation in the Cahaba synclinorium of Alabama, U.S.A.: Journal of Sedimentary Research, v. 86, p. 1287-1297, doi:10.2110/jsr.2016.76.

Valloni, R., and Mezzadri, G., 1984, Compositional suites of terrigenous deep-sea sands of the present continental margins: Sedimentology, v. 31, p. 353-364.

Van Schmus, W.R., Bickford, M.E., and Turek, A., 1996, Proterozoic geology of the east-central midcontinent basement, *in* van der Pluijm, B.A., and Catacosinos, P., eds., Basement and Basins of Eastern North America: Geological Society of America, Special Paper 308, p. 7-32, doi: 10.1130/0-8137-2308-6.7.

Van Schmus, W.R., Bickford, M.E., Anderson, J.L., Bender, E.E., Anderson, R.R., Bauer, P.W., Robertson, J.M., Bowring, S.A., Condie, K.C., Denison, R.E., Gilbert, M.C., Grambling, J.A., Mawer, C.K., Shearer, C.K., Hinze, W.J., Karlstrom, K.E., Kisvarsanyi, E.B., Lidiak, E.G., Reed, J.C., Jr., Sims, P.K., Tweto, O., Silver, L.T.,

Treves, S.B., Williams, M.L., AND Wooden, J.L., 1993, Transcontinental Proterozoic provinces, *in* Reed, J.C., Jr., Bickford, M.E., Houston, R.S., Link, P.K., Rankin, D.W., Sims, P.K., and Van Schmus, W.R., eds., Precambrian: Conterminous U.S.: The Geology of North America: Geological Society of America, v. C-2, p. 171–334.

Van Waterschoot Van Der Gracht, W.A.J.M., 1931, The Permo-Carboniferous orogeny in the south-central United States: American Association of Petroleum Geologists Bulletin, v. 15, p. 991-1057.

Vermeesch, P., 2004, How many grains are needed for a provenance study?: Earth and Planetary Science Letters, v. 224, p. 441-451.

Vermeesch, P., 2012, On the visualization of detrital age distributions: Chemical Geology, v. 312-313, p. 190-194, doi:10.1016/j.chemgeo.2012.04.021.

Vermeesch, P., and Garzanti, E., 2015, Making geological sense of 'Big Data' in sedimentary provenance analysis: Chemical Geology, v. 409, p. 20-27, doi: 10.1016/j.chemgeo.2015.05.004.

Vermeesch, P. Resentini, A., and Garzanti, E., 2016, An R package for statistical provenance analysis: Sedimentary Geology, v. 336, p. 14-25, doi: 10.1016/j.sedgeo.2016.01.009.

Viele, G.W., and Thomas, W.A., 1989, Tectonic synthesis of the Ouachita orogenic belt, *in* Hatcher, R.D., Jr., Thomas, W.A., and Viele, G.W., eds., The Appalachian–Ouachita orogen in the United States, The Geology of North America: Geological Society of America, v. F-2, p. 695–728.

Whitmeyer, S.J., and Karlstrom, K.E., 2007, Tectonic model for the Proterozoic growth of North America: Geosphere, v.3, p. 220-259, doi: 10.1130/GES00055.1.

Wiedenbeck, M., Alle, P., Corfu, F., Griffen, W.L., Meier, M., Oberli, F., Von Quadt, A., Roddick, J.C., and Spiegel, W., 1995, Three natural zircon standards for U-Th-Pb, Lu-Hf, trace element, and REE analyses: Geostandards Newsletter, v. 19, p. 1-23.

Xie, X., O'Connor, P.M., and Alseben, H., 2016a, Carboniferous sediment dispersal in the Appalachian-Ouachita juncture: Provenance of selected Late Mississippian sandstones in the Black Warrior Basin, Mississippi, United States: Sedimentary Geology, v. 342, p. 191-201.

Xie, X., Cains, W., and Manger, W.L., 2016b, U-Pb detrital zircon evidence of transcontinental sediment dispersal: provenance of Late Mississippian Wedington Sandstone member, NW Arkansas: International Geology Review, v. 58, p. 1951-1966.

Williamson, N., 1974, Depositional environments of the Pocono Formation in southern West Virginia [PHD Dissertation]: West Virginia University, 125 p.

Wortman, G.L., Samson, S.D., and Hibbard, J.P., Precise U-Pb zircon constraints on the earliest magmatic history of the Carolina terrane: Journal of Geology, v. 108, p. 321-338.

Ziegler, P.A., 1988 Evolution of the Arctic-North Atlantic and the Western Tethys: American Association of Petroleum Geologists Memoir, v. 43, 198 p.

3. DIAGENETIC TO INCIPIENT METAMORPHIC ZONES OF THE BENTON UPLIFT, OUACHITA OROGEN, ARKANSAS*

3.1. Overview

Vitrinite reflectance analysis and the mean diameter of metamorphosed quartz, suggest that the eastern Ouachita region reached the lower greenschist facies, regardless of burial depth. An increase in 'crystallinity' may explain that the maturation is from the exhumation of the rocks from a greater depth. Shale and sandstone samples collected from outcrops along the crest of the Benton Uplift exhibit illite and chlorite crystallinities that yield higher indices compared to younger rocks adjacent to this crustal-scale anticlinal structure. Illite crystallinity *d*(001) of air-dried, fine (<0.2 μm) authigenic clays (Δ°2Θ (CuKα) = 0.417˚ to 0.875˚) yield a range of conditions from diagenetic temperature to lower anchizone temperatures up to ~200˚C. Air-dried, fine authigenic chlorite clays (Δ°2Θ (CuKα) = 0.259 to 1.570) yield a wide range of diagenetic to metamorphic conditions that span the diagenetic zone through epizone, which indicate a maximum temperature slightly above ~300°C. These results are in contrast to prior thermal maturation data. No additional heat sources, such as from pluton emplacement, were identified by major areas of anomalous high maturation based on crystallinity. Regionally, the illite and chlorite crystallinity increases toward the central axis of the Benton Uplift. Exhumation of the rocks from greater depth is all that is required to explain the illite and chlorite crystallinity data.

*Reprinted with permission from "Diagenetic to incipient metamorphic zones of the Benton Uplift, Ouachita Orogen, Arkansas" by Harold E. Johnson II, David V. Wiltschko, and John P. Harris, 2019. *Geological Society of America Bulletin*, https://doi.org/10.1130/B35174.1, Copyright 2019 by Geological Society of America.

3.2. Introduction

The Ouachita orogen is the largest exposed section of a Late Paleozoic orogeny on the southern margin of North America (Fig. 1; Arbenz, 1989; Viele and Thomas, 1989). The orogen is not as well exposed as the Appalachian Mountains to the east. Also unlike the Appalachian Mountains, the origin and nature of the colliding plate is not well known. It is generally assumed by most authors that the Ouachita orogen is the result of a collision with a large microcontinent during the Late Paleozoic (e.g., Lillie et al., 1983; Arbenz, 2008). The deformation resulting from the collision is not as intense as expressed in the Appalachian Mountains.

Thermal maturation data, vitrinite reflectance and mean diameter of metamorphosed quartz, indicate higher thermal maturation in the eastern Ouachita metamorphic core than the western two-thirds of the exposed core (Houseknecht and Matthews, 1985; Keller et al., 1985). Contoured vitrinite reflectance values, primarily from Carboniferous units, parallel major thrust faults and indicate that rocks in the hanging wall are more thermally mature than rock units in the footwall. In contrast, the vitrinite reflectance contours cut across major structural features in the eastern one-third of the Ouachita orogen and suggest a thermal overprint for the eastern portion (Houseknecht and Matthews, 1985). Keller et al. (1985) sampled pre-tectonic Paleozoic chert and novaculite across the Benton Uplift to determine grain-sizes and textures of quartz because increased grain-size and development of polygonal, triple-point texture are indicators of thermal maturity. Unlike vitrinite reflectance, contoured mean

diameters of metamorphosed quartz grains follow the axial trace of the Benton Uplift, an anticlinal structure (Figs. 1, 2A).

Illite crystallinity can be used to measure thermal maturation in argillaceous sediments of all ages. In contrast, vitrinite reflectance is limited to post-Silurian rocks (much of Benton Uplift is comprised of Ordovician-Silurian stratigraphy). Conodont alteration index, another reliable thermal indicator, relies on conodonts that are only found in Early Cambrian-Triassic rocks.

The objectives of this study are: 1) to use 'crystallinity' of clay minerals as a measure of thermal maturity across the Benton Uplift and adjacent Carboniferous stratigraphy,(2) identify major areas of anomalous high maturation (possibly related to thermal overprint from a pluton emplacement), 3) determine if 'crystallinity' records a thermal pattern coinciding with either vitrinite reflectance, mean diameter of metamorphosed quartz, or a combination of these, and 4) determine if burial and expected overburden are sufficient to explain the regional 'crystallinity' data. The use of 'crystallinity' in a structural context will determine if thermal maturation is a result of burial and overburden and not a thermal overprint from an anomalous heat source.

3.3. Regional Geology

The Ouachita orogen is the easternmost segment of the 3000-km-long late Paleozoic southern Laurentia orogenic system (Fig. 1) that deformed the early to middle Paleozoic southern passive margin of Laurentia during the assembly of Pangea (Viele and Thomas, 1989; Thomas, 2010). Collision proceeded from east to west along an irregular margin

resulting in a variety of along-strike structural styles (Poole et al., 2005). The Ouachita segment of this system deforms rocks that record a rapid transition from relatively thin, passive-margin sedimentation (Collier Shale to Arkansas Novaculite; Fig. 3) to much thicker packages of syn-tectonic sediments (Stanley Group to Atoka Formation; Fig. 3) (Lowe, 1989; Morris, 1989; Viele and Thomas, 1989).

This orogen may be divided into five provinces, shown in Figs. 2A and 2B, based on stratigraphic and structural character (Arbenz, 2008). The northernmost segment, the *Arkoma Basin* (Fig. 1) is a flexural foreland basin situated between the Ozark Dome and the frontal Ouachita thrusts (Sutherland, 1988). South of the Arkoma Basin (Fig. 2), the *Frontal Thrust Zone* encompasses a region of broad north-verging folds of syntectonic sediments with up to 5 km of structural relief. The *Maumelle Chaotic Zone* is an intensely deformed region of Pennsylvanian Johns Valley Formation and Jackfork Group rocks located south of the Frontal Thrust Zone (Viele, 1973; Viele and Thomas, 1989). The *Benton Uplift* is the main anticlinal feature of pre-tectonic rocks, and is a metamorphic core comprised of the oldest and most thermally mature part of the orogen. The southernmost exposures of the Mississippian Stanley Group through Early Pennsylvanian Atoka Formation are the *Southern Ouachitas* (Haley and Stone, 2006).

Lower Paleozoic metamorphic rocks of the Ouachita orogen are classified within the lower greenschist facies. These slates are found to parallel the major anticlinal structures, including the Benton Uplift. Incipent metamorphosed syntectonic rocks flank these large, kilometer-scale structures.

3.4. Illite and Chlorite 'Crystallinity'

A widely used thermal maturation technique for lower temperature conditions, in clay-rich rocks lacking both vitrinite and conodonts, is 'Crystallinity'. There are few petrographic methods to determine the conditions of deformation at lower metamorphic grades, whereas 'crystallinity' is one of the most widely used and useful methods, especially in areas with a range of temperatures (Fig. 4; Frey, 1987).

'Crystallinity' describes the degree of ordering in a crystal lattice of a given clay mineral, commonly illite (Frey, 1987). 'Crystallinity' is commonly measured on an X-ray diffractogram as the full-width half maximum (FWHM) of the characteristic peak and is expressed in °Δ2Θ (i.e., Kübler index) using CuKα radiation. For illite, this peak is at 8.85 °2Θ (CuKα) for basal 10 Å lattice spacing. For chlorite, the center of the peak is typically at 12.65 °2Θ (CuKα) or approximately 7 Å lattice spacing. Samples are typically oriented mineral aggregate preparations of the < 2-μm size fractions (Kübler, 1967, 1968). Several studies show that increased 'crystallinity' is largely controlled by temperature (e.g., Kübler, 1967; Smykatz-Kloss and Althaus, 1974; Schaer and Persoz, 1976; Krumm, 1984). Frey (1987) states that fluid pressure, stress, lithology, crystal chemistry, mineralogy, and time may also play lesser roles. When the term 'crystallinity' was introduced in literature, there was not a clear understanding for the physical attributes affecting the change in the 10 Å peak of illite (Merriman and Peacor, 1999). More recently, Transmission Electron Microscopy (TEM) studies have shown that

narrower *d*(00l) widths occur principally with thicker crystallites of the clay mineral (Merriman and Peacor, 1999).

3.5. Methods

3.5.1. Chemical Pretreatment, Size Fractionation, and Identification of Clay Minerals

For shale and slate samples, approximately a 50 gram aliquot of disaggregated rock yields 1 gram of clay minerals. Sandstones require a larger 100 gram aliquot of disaggregated rock for the same quantity of clay minerals. A series of wet chemical pretreatments outlined by Jackson (1956) removed carbonate and organic cements from the mineral grains. With the cementing material removed, the sample is separated into 4 different size fractions: sand (2 mm to 45 μm), silt (45 to 2 μm), coarse clay (2 to .2 μm), and fine clay (<.2 μm). The bulk sample and sand fraction were crushed with a mortar and pestle until the material passed through a 45 μm mesh sieve.

A Rigaku D/Max-IIIVBX Power X-ray diffractometer (XRD) in the geology and geophysics department at Texas A&M University was used to obtain X-ray diffraction peaks for the specimens. The instrument details and settings are: CuKα, normal focus tube, 40 kV, 20 mA, slit sizes (from shutter to goniometer) are 1˚ divergence slit, 1˚ anti-scatter slit, .08 mm receiving slit, and .06 mm receiving slit on the goniometer, and a graphite-diffracted beam monochronometer. The bulk sample, sand fraction, and silt fraction was side-loaded into an aluminum sample holder for a random oriented mount and continuously scanned from 2˚ to 65˚ 2Θ using a 0.02˚step at 2˚ 2Θ /min (McMurdie

et al., 1986). For both coarse and fine clay fractions, the specimen was sedimented onto a Vicor glass slide at ≥ 2 mg/cm^2 to avoid intersample variation from X-ray absorption of thinly sedimented slides (Moore and Reynolds, 1997). Clay sedimented slides are air dried at room conditions overnight. These slides were continuously scanned from 2˚ to 32˚ 2Θ using a 0.05˚ step at 0.75˚ 2Θ /min. All samples were measured at room temperature and relative humidity.

Each of these fractions along with a whole rock sample is scanned using an X-ray diffractometer to yield diffraction patterns. Sample mineralogy is determined using the Hanawalt Method to qualitatively analyze the diffraction patterns (Hanawalt et al., 1938). Identification of clay minerals was aided by comparison with published clay mineral patterns and an in-house diffractogram of source clay SAz-1 Ca-rich montmorillonite “Cheto” from the Clay Mineral Society. MacDiff XRD analysis software version 4.2.5 was used to process the digital data for peak positions, peak full-width half maximum (FWHM), and the integrated area of the peak after a baseline of intensity was established.

The identification of clay minerals for both the coarse clay and fine clay specimens is confirmed by a comparison of each characteristic peak spectrum produced by the different treatments. A specimen from each clay fraction was 1) saturated with K+ for at least 12 hours, 2) vapor solvated with ethylene glycol for 24 hours in a closed vapor vessel heated to 60˚±10˚C, 4) heat-treated to 300˚C for 2 hours, and finally 5) heat-treated to 550˚C for 2 hours (Dixon and Weed, 1989; Moore and Reynolds, 1997).

Both ethylene glycol vapor solvated and heat-treated specimens are scanned immediately after their removal from the vapor chamber or oven, respectively.

3.5.2. Measure of Thermal Maturation: Clay Mineralogy and Illite/Chlorite Crystallinity

We use two X-ray diffraction techniques to determine burial depth. First, clay samples are treated with glycol vapor to shift the smectite peaks. The location of the smectite peaks identify samples that contain between 10-90% smectite (Środoń, 1980; Hower, 1981). The samples that contain more than 10% smectite indicate the lower diagenetic zone (Merriman and Peacor, 1999). For samples with little smectite, the second technique of illite crystallinity is used (Merriman and Peacor, 1999; Kübler and Jaboyedoff, 2000; Meunier and Velde, 2004). Illite crystallinity is determined by the measurement of the full-width half maximum for the 001 illite peak on an X-ray diffractogram. Values of this measurement, called the Kübler index of crystallinity, decrease with increasing thermal maturation as more smectite is converted to illite (Kübler and Jaboyedoff, 2000).

Kübler (1967) separated his index into three different metapelitic zones: Epizone (> ~300˚C), Anchizone (~200˚- ~300˚C), and Diagenetic Zone (< ~200˚C). A thermal correlation diagram (Fig. 4) compares temperature, clay crystallinity indices, illite percentage, typical XRD pattern, vitrinite reflectance, and metamorphic facies with the metapelitic zones. The temperature is based on computing temperature independently for

metamorphic mineral assemblages in rock for which crystallinity was also determined (see Kisch (1987) for summary; Árkai, 1991).

The estimated range of temperature for the anchizone is ~200˚C to ~300˚C according to Frey (1987). The lower boundary of the anchizone is within the prehnite-pumpellyite facies. The upper boundary of the anchizone lies within the pumpellyite-actinolite facies (Frey, 1987; Árkai, 1991). It is necessary to have the Kübler metapelitic zones because thermal maturation is a relative tool that demonstrates trends in thermal maturation rather than specific temperatures for a given thermal technique value. Only the boundaries of the anchizone are calibrated and these provide a means to determine temperature locally where the boundaries are encountered.

For our samples, the crystallinity of both illite and chlorite were determined by measuring the full-width half maximum above background. The peak width is measured in degrees 2Θ which represents the position of the goniometer during the data recording. We calibrated the anchizone boundaries (Fig. 5) using polished slate standards kindly supplied by Dr. Hanan J. Kisch. Each standard was analyzed, and then removed to rotate 180° before reinserting it into the specimen holder for a total of 6 analyses (i.e., 3 normal and 3 reversed orientations). A calibration curve was constructed by linear regression ($y = 0.9833x + 0.0723$ with $R^2 = 0.9575$) for crystallinity on each sample using values established by recalibrated Kisch values and the values found using our XRD machine (Kisch, 1991; War and Cox, 2016). This line does not go through the origin, suggesting slightly different instrument settings (e.g., time constant, Kisch, 1990). The calibration

of the illite crystallinity (IC) values allows us to use the Kübler metapelitic zones (Kisch, 1991) with the calibrated lower and upper anchizone boundaries for IC of 0.346 °2Θ (CuKα) and 0.538 °2Θ (CuKα), respectively.

The chlorite crystallinity (ChC) values (i.e., Árkai index) offer a second thermal indicator for the same specimen (Árkai, 1991; Árkai et al., 1995). War and Cox (2016) find a positive non- linear correlation curve of $y = .2037\ln(x) + 0.5423$ and $R^2 = 0.79$ between illite (x) and chlorite (y) crystallinity using the metapelitic samples. Other workers show higher thermal maturation using chlorite crystallinity (ChC) that may be related to chemical composition (Frey, 1987). This technique is still useful in determining thermal maturation of a sample lacking illite or when characteristic peaks are obscured by overlapping peaks of other minerals. Using the War and Cox (2016) equation, the anchizone upper and lower boundaries for chlorite are 0.260 °2Θ (CuKα) and 0.336 °2Θ (CuKα) for the 14 Å basal reflection. Many of the air-dried XRD patterns either didn't yield a 14 Å reflection or a low intensity peak resulted, so the greater intensity 7 Å reflection was used.

Peaks of chlorite will overlap and potentially broaden in samples containing kaolinite. Higher-order reflection of chlorite (004) at 25.1°2Θ (CuKα) for the 3.42 Å reflection aid in distinguishing the pattern from the higher-order reflection of kaolinite (002) at 24.8 °2Θ (CuKα) reflection (Moore and Reynolds, 1997). The heat-treated patterns were studied to determine key observations: 1) 7 Å kaolinite reflection absence, and 2) increase intensity of chlorite (001) peak at 14 Å (Moore and Reynolds, 1997).

Chemical treatments, including HCl acid dissolution, and magnetic separation of Fe-rich chlorite were not used because of a limited amount of clays available in the Ouachita samples (Tellier et al., 1988; Moore and Reynolds, 1997).

3.6. Results

A total of 22 clay aliquots from 15 sandstone and shale samples were analyzed by X-ray diffraction (XRD) on oriented glass slide mounts to determine the clay mineralogy and the crystallinity of both illite and chlorite (Table 1). Sand-sized and silt-sized fractions were obtained to identify unknown minerals in the smaller clay-sized samples. Bulk samples were analyzed by X-ray powder diffraction (XRPD) prior to chemical pretreatments. Following chemical pretreatments, the sand- and silt-sized fractions were evaluated using XRPD to identify the mineralogy (Table S1). All clay specimens contained less than 10% smectite in the illite/smectite ratio using the technique of Środoń (1980) and Hower (1981). All of these rocks therefore must have experienced temperatures higher than ~ 100°C according to Merriman and Peacor (1999).

The IC *d*(001) fine clay values (Tables S4-S7; Figs. 6A, 7A, S1-S27) range from 0.417˚ to 0.875˚ Δ°2Θ (CuKα)for air-dried specimens. A few values are in the lower anchizone, while the majority of the values span the diagenetic zone. Illite crystallinity *d*(001) coarse clay values (Tables S4-S7; Figs. 6A, 7B, S1-S27) are between 0.273˚ to 0.688° Δ°2Θ (CuKα) for air-dried specimens. The estimated maximum temperature

using IC coarse clay values is ~300˚C. The estimated maximum temperature based on IC fine clay values is ~200˚C.

Chlorite crystallinity *d*(002) of the fine clay fraction have values (Tables S8-S10; Figs. 7B, 8A, S1-S27) between 0.259 Δ°2Θ (CuKα) to 1.570 Δ°2Θ (CuKα) for air-dried specimens. Chlorite crystallinity *d*(002) coarse clay values (Tables S8-S10; Figs. 6B, 8B, S1-S27) are between 0.202 Δ°2Θ (CuKα) to 1.788 Δ°2Θ (CuKα) for air-dried specimens. Chlorite crystallinity values for the coarse clay fraction span the diagenetic zone to epizone. The maximum metamorphic temperature determined by the chlorite crystallinity of coarse clay and fine clay is slightly higher than ~300°C.

3.7. Discussion

The crystallinities of illite and chlorite decrease away from the Benton Uplift (Fig. 6). Depth plots of the illite crystallinity values (Fig. 7) show a trend of increasing maturation with increasing cumulative stratigraphic thickness. Sediment thicknesses in the Ouachita fold-and-thrust belt are speculative because of the difficulty correlating the relatively thick shale sequences (e.g., Stanley and Jackfork Groups) across numerous thrust faults (see Arbenz, 2008 and references therein). Figs. 7A and 7B illustrates the difference in thermal maturation between the coarse and fine clay fractions. Illite crystallinities *d*(001) of fine and coarse clay fractions increase with increasing stratigraphic thickness with the exception of a few values. These outliers may be recording an older thermal signature from detrital illite. The fine illite fraction records a lower thermal maturation. This difference in crystallinity may be the result of two

thermal events. If the coarse clay is partially detrital, then the fine clay may be more representative of thermal maturation for the area.

The reason for using two size fractions is 1) to separate neocryst clay minerals such as smectite from older clay minerals such as detrital illite, 2) to aid in clay mineral identification by separation of clays to minimize peak overlap, and 3) minimize the effect of grain sorting while pipetting the clay on a glass slide (e.g., coarse grains on bottom and fining upward caused by rapid settling of larger clays) (Moore and Reynolds, 1997). In comparison, the variance of chlorite crystallinity *d*(002) values for both size fractions is larger than that for illite. One possibility is the potential presence of kaolinite with a *d*(001) peak that overlaps with the chlorite *d*(002) peak leading to a broader overall peak at approximately 12.5˚ 2Θ. All samples were heat-treated at 550°C for 2 hours, and the resultant pattern should identify chlorite as the 001 reflection increases and shifts to 6.3-6.4 ˚ 2Θ and any kaolinite (if present) is no longer detected by X-rays. (Moore and Reynolds, 1997).

Unlike illite crystallinity, there is no correlation between chlorite crystallinity with stratigraphic depth (Fig. 8). In some cases, the fine clay value is more thermally mature than the coarse clay counterpart for a given sample. Many of the chlorite peaks were only a few hundred counts above the background spectrum and short peaks. This short peak height contributes to a broad peak as well and thus greater full-width half maximum variability (Tables S8-S10; Figs. S1-S27).

The maximum temperature reached as indicated by both illite crystallinity and chlorite crystallinity is ~300°C and this thermal measurement corresponds to a maximum vitrinite reflectance (Ro) of 4.0-4.1%. Houseknecht and Matthews (1985) found Ro values above 4.0 % east of Hot Springs, Arkansas (Fig. 6). The Ro values decrease to the southwest and away from the culmination of the Benton Uplift. Houseknecht and Matthews (1985) attribute the Ro values to the maximum depth of burial for each sample (western portion), or to an anomalous heat source post-dating burial (eastern portion).

Guthrie et al. (1986) demonstrate the same thermal event/burial is responsible for the IC and vitrinite reflectance (VR) values in the Ouachita syn-tectonic units (e.g., Maumelle Chaotic Zone, Frontal Thrust Zone, and Arkoma Basin). Spötl et al. (1993) measured VR in six industry wells in the northern portion of the Ouachita region. The only Arkansas well, Oxy Danville USA A-1, is located near the Ross Creek Fault (Fig. 2) in the north-central Frontal Thrust Zone. Spötl et al. (1993) found a transition from diagenesis to anchizone (0.8-4.7 % Ro) in the Danville USA A-1 well. The IC did not change with depth and most values lie within the anchizone. Spötl et al. (1993) propose that a high sedimentation rate may preserve clay minerals from the source area and is reflected on X-ray diffractograms as the detrital illite signature, which is present along with authigenic illite. Detrital input is a problem when authigenic illite is used to determine thermal maturation. To minimize error from detrital illite, illite crystallinity and chlorite crystallinity should be restricted to formations older than the Johns Valley

formation. Most of the samples for this study were taken from the pre-tectonic core and adjacent formations (Table 1; Fig. 2); crystallinity should represent the thermal maturation recorded mainly in authigenic illite. Therefore, the crystallinity determined here provides a useful thermal constraint.

The mean apparent diameter of recrystallized quartz taken from chert and novaculite show an increasing crystal size toward the eastern portion of the exposed Ouachita Mountains (Keller et al., 1985). Similar to the contoured vitrinite reflectance values, the mean apparent diameter of recrystallized quartz contours show a trend that follows regional strike and closely follow the shape of the exposed pre-tectonic formations. The mostly linear vitrinite reflectance contours in the central and western Ouachita orogen parallel the thrust faults and culmination of the Benton Uplift. These results suggest that higher temperatures were caused by burial. The burial hypothesis assumes no tectonic burial (i.e. structural thickening from thrust sheets), a uniform regional geothermal gradient, and no stratigraphic variation in cumulative stratigraphic thickness (Houseknecht and Matthews, 1985). The highest gradient for mean apparent diameter of metamorphosed quartz is east of Hot Springs, Arkansas, which suggests thermal maturation increases toward the east (see Fig. 7).

A simple thermal maturation diagram (Fig. 9) presents the ranges in values for crystallinity and vitrinite reflectance, which can be used to evaluate burial depths by the cumulative thickness of the overlying units. Assuming the Savanna Formation and underlying formations were present above the present-day Benton Uplift and then eroded

to their present form, temperatures of 200°C - 350°C are predicted for a geothermal gradient of 25°C/km and 40°C/km, respectively, for units below the lower two-thirds of the Jackfork formation. This diagram implies that a stack of thrust sheets did not exist at the regional scale because higher maturation would be expected than observed. An estimated 8-14 km of material has been eroded above the anticlinal structure based on temperature range of 200°C to 350°C. This amount of material removed is in agreement with Byrnes and Lawyer (1999) who estimate ~12 km of removed material based on unspecified burial models. Therefore, both illite crystallinity and vitrinite reflectance observed across the Benton Uplift are valid measures of maximum burial depth using the given cumulative stratigraphic thickness (Fig. 3).

3.8. Conclusions

(1) The maximum temperature calculated from both illite and chlorite crystallinity is ~300°C in the Ouachita orogen, Arkansas.

(2) No additional heat sources, such as from pluton emplacement, were identified by major areas of anomalous high maturation based on crystallinity.

(3) Illite crystallinity is higher for the fine clay fraction than that of the coarse clay fraction. Although the reason is not known, the coarse clay fraction may have a greater detrital component than the fine clay fraction. If correct, then the fine clay fraction is more nearly recording the thermal maturation of the Benton Uplift.

(4) Regionally, the illite and chlorite crystallinity increases toward the central axis of the Benton Uplift. This increase in crystallinity may be explained by the exhumation of

the rocks from greater depth. Neither a regional thermal fluid flow event nor significant stacking of thrust sheets is required to explain the values or patterns of metamorphism.

3.9. References

Arbenz, J.K., 1989, The Ouachita System, The Geology of North America - An Overview, *in* Bally A.W., and Palmer A.R., eds., The Geology of North America, Volume A: Boulder, Colorado, Geological Society of America, p. 371-396.

Arbenz, J.K., 2008, Structural framework of the Ouachita Mountains, *in* Suneson,N.H.,ed., Stratigraphic and Structural Evolution of the Ouachita Mountains and Arkoma Basin, Southeastern Oklahoma and West-Central Arkansas: Applications to Petroleum Exploration: 2004 Field Symposium, Circular 112A: Norman, Oklahoma, Oklahoma Geological Survey, p.4-40.

Árkai, P., 1991, Chlorite crystallinity: an empirical approach and correlation with illite crystallinity, coal rank, and mineral facies as exemplified by Paleozoic and Mesozoic rocks of northeast Hungary: Journal of Metamorphic Geology, v. 9, p. 723-734.

Árkai, P., Sassi F.P., and Sassi R., 1995, Simultaneous measurements of chlorite and illite crystallinity: a more reliable tool for monitoring low- to very low metamorphisms in metapelites, A case study from the Southern Alps (NE Italy): European Journal of Mineralogy,v. 7, p. 1115-1128.

Barker, C. E., and Pawlewicz, M. J.,1994, Calculation of vitrinite reflectance from thermal histories and peak temperatures – A comparison of methods, *in* Mukhopadhyay, P. K. and Dow, W.G., eds., Vitrinite reflectance as a maturity parameter: Applications and limitations, ACS Symposium Series, American Chemical Society, Washington, DC, pp. 216-229, https://doi.org/10.1021/bk-1994-0570.ch014

Briggs, G., and Roeder, D. H., 1975, Sedimentation and plate tectonics, Ouachita Mountains and Arkoma basin, *in* Briggs, G., McBride, E.F., and Moiola R.J., eds., Sedimentology of Paleozoic flysch and associated deposits, Ouachita Mountains - Arkoma basin, Oklahoma, Dallas Geol. Soc., Dallas, Tex., p. 1-22.

Byrnes, A.P., and Lawyer, G., 1999, Burial, Maturation, and Petroleum Generation History of the Arkoma Basin and Ouachita Foldbelt, Oklahoma and Arkansas: Natural Resources Research, v. 8, p. 3-26

Dixon, J.B., and Weed, S.B., editors, 1989, Minerals in Soil Environments, Second Edition: Madison, Wisconsin, Soil Society of America, 1244 p.

Flawn, P.T., Goldstein, Jr., A., King, P.B., and Weaver, C.E., 1961, The Ouachita System, publication 6120, Univ. of Texas, Austin, Tex.

Frey, M., 1987, Very low-grade metamorphism of clastic sedimentary rocks, *in* Frey, M., ed., Low Temperature Metamorphism: Glasgow and London, United Kingdom, Blackie & Son, p. 9-58.

Guthrie, J.M., Houseknecht, D.W., and Johns, W.D., 1986, Relationships among vitrinite reflectance, illite crystallinity, and organic geochemistry in Carboniferous strata, Ouachita Mountains, Oklahoma and Arkansas: American Association of Petroleum Geologists Bulletin, v.70, p. 26-33.

Haley, B.R., and Stone, C.G., 2006, Geologic Map of the Ouachita Mountain Region and a portion of the Arkansas Valley Region in Arkansas: Arkansas Geological Survey DGM-OMR-001, scale 1:125,000, 1 sheet.

Hanawalt, J.D., Rinn, H.W., and Frevel, L.K., 1938, Chemical analysis by X-ray diffraction: Industrial and Engineering Chemistry, Analytical Edition, v. 10, p. 457-512.

Houseknecht, D.W., and Matthews, S.M., 1985, Thermal maturity of the Carboniferous strata, Ouachita mountains: American Association of Petroleum Geologists Bulletin, v.69, p. 335-345.

Hower, J., 1981, X-ray diffraction identification of mixed-layer clay minerals, *in* Longstaffe, F. J., ed., Short Course in Clay and the Resource Geologist: Calgary, Canada, Mineralogical Association of Canada, p.39-80.

Jackson, M.L., 1956, Soil Chemical Analysis--Advanced Course: Madison, Wisconsin, Published by the author, Department of Soils, University of Wisconsin, p. 930.

Keller, W.D., Stone, C.G., and Hoersch, A.L., 1985, Textures of Paleozoic chert and novaculite in the Ouachita Mountains of Arkansas and Oklahoma and their

geological significance: Geological Society of America Bulletin, v. 96, p. 1353-1363.

Kisch, H.J., 1987, Correlation between indicators of very low-grade metamorphism, *in* Frey, M., ed., Low Temperature Metamorphism: Glasgow and London, United Kingdom, Blackie & Son, p. 227-304.

Kisch, H.J., 1990, Calibration of the anchizone: a critical comparison of illite 'crystallinity' scales used for definition: Journal of Metamorphic Geology, v. 8, p. 31-46.

Kisch, H.J., 1991, Illite crystallinity: recommendations of sample preparation, X-ray diffraction settings, and interlaboratory samples: Journal of Metamorphic Geology, v. 9, p. 665-670.

Kruger, J.M., 1983, Regional anomalies in the Ouachita system and adjacent areas [M.S thesis]: El Paso, Tex., Univ. of Texas.

Krumm, H., 1984, Anchimetamorphoseim Anis und Ladin (Trias) der Nordlichen Kalkalpenzwischen Arlberg und Kaisergebirge-ihre Verbreitung und ihrebaugeschichtliche Bedeutung: Geologische Rundschau, v. 73, p. 223-257.

Kübler, B., 1967, La cristallinité de l'illite et les zones tout a fait supérieures du métamorphisme, *in* Schaer, J.P., ed., Colloque sur les étagestectoniques, Á la Baconniére: Neuchâtel, Switzerland, p. 105-122.

Kübler, B., 1968, Évaluation quantitative du métamorphismepar la cristallinité de l´ illite: Bulletin Centre Recherches Pau – SPNA, v.2, p. 385-397.

Kübler, B., and Jaboyedoff, M., 2000, Cristallinite' de l'illite. Le POINT SUR… (Illite crystallinity concise review paper): ComptesRendus de l'Académie des Sciences-Series IIA-Earth and Planetary Science, v. 331, p. 75-89.

Lillie, R.J., Nelson, K.D., de Voogd, B., Brewer, J.A., Oliver, J.E., Brown, L.D., Kaufman, S., and Viele, G.W., 1983, Crustal structure of Ouachita Mountains, Arkansas: A model based on integration of COCORP reflection profiles and regional geophysical data: American Association of Petroleum Geologists Bulletin, v. 67, p. 907-931.

Lowe, D.R., 1989. Stratigraphy, sedimentology, and depositional setting of pre-orogenic rocks of the Ouachita Mountains, Arkansas and Oklahoma, *in* Hatcher, R.D., Jr., Thomas, W.A., and Viele, G.W., eds., The Appalachian-Ouachita Orogen in the United States: The Geology of North America, Volume F-2: Boulder, Colorado, Geological Society of America, p.695-728.

McMurdie, H.F., Morris, M.C., Evans, E.H., Paretzkin, B., Wong-Ng, W., and Hubbard, C.R., 1986, Methods of producing standard X-ray patterns: Powder Diffraction, v.1, p. 40-43.

Meunier, A., and Velde, B., 2004, Illite: Origins, Evolution, and Metamorphism: Berlin, Germany, Springer-Verlag, p. 286.

Merriman, R.J., and Frey, M., 1999, Patterns of very low-grade metamorphism in metapelitic rocks, *in* Frey, M., and Robinson, D., eds., Low-Grade Metamorphism: Cambridge, Great Britain, Blackwell Science, p.61-107.

Merriman, R.J., and Peacor, D.R., 1999, Very low-grade metapelites: mineralogy, microfabrics and measuring reaction progress, *in* Frey, M., and Robinson, D., eds., Low-Grade Metamorphism: Cambridge, Great Britain, Blackwell Science, p. 10-60.

Moore, D.M., and Reynolds, R.C., Jr., 1997, X-ray Diffraction and the Identification and Analysis of Clay Minerals: New York, Oxford University Press, 378 p.

Morris, R.C., 1974, Sedimentary and Tectonic History of the Ouachita Mountains: Society of Economic Paleontologists and Mineralogists, v. 22, p. 120-142.

Morris, R.C., 1989, Stratigraphy and sedimentary history of post-Arkansas Novaculite Carboniferous rocks of the Ouachita Mountains, *in* Hatcher, R.D., Jr., Thomas, W.A., and Viele, G.W., eds., The Appalachian-Ouachita Orogen in the United States: The Geology of North America, Volume F-2:Boulder, Colorado, Geological Society of America, p. 591-602.

Poole, F.G., Perry, W.J., Madrid, R.J., and Amaya-Martínez, R., 2005, Tectonic synthesis of the Ouachita-Marathon-Sonora orogenic margin of southern Laurentia: Stratigraphic and structural implications for timing of deformational events and plate-tectonic model: Geological Society of America Special Papers, v. 393, p. 543-596.

Schaer, J.P., Persoz, F., 1976, Aspects structuraux et petrographiques du Haut-Atlas calcaire de Midelt (Maroc): Bulletin de la Societé Géologique de France, v. 18, p. 1239-1250.

Smykatz-Kloss, W., and Althaus, E., 1974, Experimental investigation of the temperature dependence of the "crystallinity" of illites and glauconites: Bulletin Groupe Francais des Argiles, v. 26, p. 319-325.

Spötl, C., Houseknecht, D.W., and Jaques, R., 1993, Clay mineralogy and illite crystallinity of the Atoka formation, Arkoma Basin, and Frontal Ouachita Mountains: Clay and Clay Minerals, v.41, p. 745-754.

Środoń, J., 1980, Precise identification of illite/smectite interstratifications by X-ray powder diffraction: Clays and Clay Minerals, v.28, p. 401-411.

Sutherland, P.K., 1988, Late Mississippian and Pennsylvanian depositional history in the Arkoma basin area, Oklahoma and Arkansas: Geological Society of America Bulletin, v. 100, no. 11, p. 1787-1802.

Tellier, K.E., Hulchy, M.M., Walker, J.R., and Reynolds, R.C., 1988, Application of high gradient magnetic separation (HGMS) to structural and compositional studies of clay mineral mixtures: Journal of Sedimentary Petrology, v. 58, p. 761-763.

Thomas, W.A., 1977, Structural and stratigraphic continuity of the Ouachita and Appalachian mountains, *in* Stone C.G., et al., eds., Symposium on the geology of the Ouachita Mountains; Stratigraphy, sedimentology, tectonics, and paleontology, vol. 1, Ark. Geol. Comm., Little Rock, Ark., pp. 9-24

Thomas, W.A., 2010, Interactions between the southern Appalachian–Ouachita orogenic belt and basement faults in the orogenic footwall and foreland, *in* Tollo R.P., Bartholomew, M.J., Hibbard, J.P., and Karabinos, P.M., eds., From Rodinia to

Pangea: The Lithotectonic Record of the Appalachian Region: Geological Society of America Memoir, v. 206, p. 897–916, doi: 10.1130/2010.1206(34).

Viele, G.W., 1973, Structure and tectonic history of the Ouachita Mountains, Arkansas, *in* De Jong, K., and Scholten, R., eds., Gravity and Tectonics: New York, John Wiley, p. 502.

Viele, G.W., 1979, Geologic map and cross section, eastern Ouachita Mountains, Arkansas: map summary: Geological Society of America Bulletin, v. 90, p. 1096-1099.

Viele, G.W., and Thomas, W.A., 1989, Tectonic synthesis of the Ouachita orogenic belt, *in* Hatcher, R.D., Jr., Thomas, W.A., Viele, G.W., eds., The Appalachian-Ouachita Orogen in the United States: The Geology of North America, Volume F-2: Boulder, Colorado, Geological Society of America, p. 695-728.

War, L.N., and Cox, C.C., 2016, Correlating illite (Kübler) and chlorite (Árkai) "crystallinity" indices with metamorphic mineral zones of the South Island, New Zealand: Applied Clay Science, v. 134, p. 164-174, doi: 10.1016/j.clay.2016.06.024.

4. CARBONIFEROUS TECTONIC EVOLUTION OF THE OUACHITA FOLD-AND-THRUST BELT, OKLAHOMA: EXHUMATION DETERMINED BY (U-TH)/HE AND FISSION TRACK THERMOCHRONOLOGY

4.1. Overview

Evolution of fold and thrust belts (FTB) in nature, specifically the mechanical paradox of the inability of rocks within thrust sheets to tolerate the amount of differential stress needed to move km-thick thrust sheets up onto a continental margin above a frictional detachment, is a significant tectonic problem. The goal of this research is to test the wedge model paradigm on an inactive, exhumed FTB, to determine if the predictions (e.g., wedge taper, sequence of thrusting) are accurate. Thermochronological methods constrain timing of wedge development and wedge shape because they provide the cooling time, usually a result of exhumation of the FTB.

We chose the Carboniferous Ouachita FTB in Oklahoma, primarily because interior portions of the wedge are readily available for direct observation at the surface. (U-Th)/He zircon dates span 181.6 ± 14.53 Ma to 1964.2 ± 157.13 Ma, with the youngest date for each sample providing a range from 181.6 ± 14.53 Ma to 347.6 Ma. Zircon fission track minimum ages (259 ± 34 Ma to 365± 66 Ma) were determined from 643 grain analyses. Zircon fission track minimum ages record development of the FTB wedge, whereas the (U-Th)/He dates give paleotopography of the critical wedge. Thus, the internal motion of thrusts and folding of the FTB occurred during the Pennsylvanian

to Early Permian. Paleotopography slope was foreland-directed with the present-day surface of the Broken Bow Uplift buried at ~9 km during Late Triassic-Middle Jurassic, assuming 20°C/km and zircon (U-Th)/He closure of ~180°C.

4.2. Introduction

Evolution of fold and thrust belts (FTB), specifically in what way deformation occurs from the hinterland to foreland, remains an important tectonic question. The mechanical paradox of a FTB is the inability of rocks within thrust sheets to tolerate the amount of differential stress needed to move multiple many-kilometers long by several-kilometers thick thrust sheets up onto the continental margin above a frictional décollement (e.g., Chapple, 1978). The initial hypothesis was gravity sliding as the mechanism to explain thrust sheets sliding off an uplifted metamorphic core complex, rather than being translated by thin-skinned compression along a décollement as a result of the colliding tectonic plates (e.g., De Jong & Scholten, 1973). An alternate concept, the wedge model paradigm, explains the development and evolution of the FTB and predicts many of the first-order observations of both active and ancient orogens (Elliot, 1976; Chapple, 1978).

Wedge models (Figure 1a) have an overall shape of a thickened hinterland and a tapered foreland because the décollement angle (β) dips up in direction of the foreland, while the topography slope angle (α) dips down in direction of the foreland (e.g., DeCelles and Mitra, 1995). The right side of the orogenic wedge (Figure 1a) is under a compressive stress (Elliot, 1976). Factors that influence wedge stability (Figure 1b) are

where S & P move the self-similar deformation line: S = increased strength; P = increased pore pressure at décollement, decrease friction at décollement, or strain softening of décollement; D = increased resilience of topographic surface; E = erosion of topographic surface; F = flexural subsidence (DeCelles & Mitra, 1995 and references therein). The self-similar deformation line (SSDL) represents a critical wedge at steady state, the area below SSDL represents a subcritical wedge that doesn't advance until critical taper is reached, and the area above the SSDL represents a supercritical wedge that translates along the single décollement with the need to internally deform or initiate foreland thrusts (Davis et al., 1983).

Wedge models provide insight into the overall shape of FTBs and predict a general sequence of thrust initiation from hinterland to foreland, yet there are few studies that test these model predictions with field-based observations. The lack of geological data across an entire FTB to constrain geometries of structure, timing of thrust motion, or even absence of sedimentary onlap of datable syntectonic sediments may hinder application of wedge models to actual FTBs (DeCelles & Mitra, 1995). Most geochronologic studies of FTBs focus on isotopic dating either the interior metamorphic core (hinterland), or the more distal parts of the foreland as these geologic provinces are linked to the orogen(e.g., Arne et al., 1997; Blythe et al., 1998; Wiltschko & Dorr, 1983) This indirect dating of tectonic events means the development of the orogenic wedge in between the metamorphic core and the foreland is essentially undetermined.

Higher temperature isotopic dating (e.g., U-Pb zircon) is usually not feasible because of the relatively low metamorphic temperatures in many parts of the FTB. Fortunately, studies of the active Taiwan FTB show encouraging results for applied low-temperature thermochronological methods to tectonics (e.g., Fuller et al., 2006; Lock & Willett, 2008; Rodriguez-Roa & Wiltschko, 2010). For active FTBs, the topographic slope and dip of the décollement may be measured. The surface of inactive FTBs during the critical wedge is missing, yet this same eroded surface exposes the interior of the wedge for direct observation and allows for testing of the wedge model paradigm. To clarify, active FTBs have a poorly exposed interior meaning an exhumed inactive FTBs may prove more useful for thermochronological methods.

The goal of this research is to test the wedge model paradigm of Elliot (1976) and Chapple (1978) on an inactive, exhumed FTB (Figures 1c and 1d) to determine if the predictions (e.g., wedge taper, sequence of thrusting, etc.) are accurate. The Carboniferous Ouachita Orogenic Belt, southeastern Oklahoma, is chosen as the inactive FTB for the following reasons: 1) topography has low total relief minimizing influence of elevation on cooling of the rocks, 2) structures from the hinterland to foreland are exposed, and 3) published thermal maturation, detailed geologic maps of surface, industry subsurface data, published geophysical surveys, and previous isotopic/thermochronologic work constrain crustal-scale interpretations across the entire FTB (Bass & Ferrara, 1967; Cardott, 2013; Denison et al., 1969; Denison et al., 1977; Hendricks et al., 1947; Honess, 1923; Houseknecht & Matthews, 1985; Lillie et al.,

1983; Keller et al., 1985; Miser, 1929; Shelton et al., 1986). Zircon (U-Th)/He and zircon fission track dating results from three regional traverses across the Ouachita FTB are plotted above published cross sections of Arbenz (2008), and timing of cooling discussed in context of the thrust motion and internal building of the critical wedge.

4.3. Geologic Background

4.3.1. Regional Tectonic Setting

The Ouachita orogenic belt (Figure 2) extends as an arcuate trend from a possible connection with the southern Appalachians to southwestern Texas (Flawn et al., 1961). The deformed stratigraphy in western Arkansas and eastern Oklahoma represents the largest exposed area, hinterland to foreland, for direct observation of the Ouachita orogen; a record of a complete orogenic cycle from rifting at ~750 Ma to final orogenesis at ~280 Ma (Viele & Thomas, 1989).

Rifting of the supercontinent Rodina (ca. 750 Ma) resulted in attenuated crust on the margin of the North American craton (Laurentia) and opening of the Iapetus Ocean in the Neoproterozoic (Cawood et al., 2007; Thomas, 2011; Torsvik, 2003). A second major ocean basin, the Rheic Ocean, formed by Late Cambrian to Early Ordovician rifting of the peri-Gondwanan terranes (e.g., Avalonia-Carolinia) from the margin of Gondwana (Nance et al., 2010). As the Rheic Ocean widened in the Early Silurian, Avalonia-Carolinia and Baltica colliding with Laurentia during closure of the Iapetus Ocean (Nance & Linnemann, 2008).

Passive margin sedimentation on the rifted southern (present day) margin in the Rheic Ocean developed into a platform facies, and an off-shelf facies within the deeper water of the Ouachita Basin (Arbenz, 1989b). Lithologies within the platform facies are primarily carbonate, with minor sandstone and shale marking continental regression events (Viele & Thomas, 1989). A sequence of fine-grained clastic rocks, massive and bedded siliceous deposits, and minor intervals of carbonate and sandstone (i.e., Ouachita facies) preserve an Ordovician through Early Mississippian depositional history. Mid- to Late-Ordovician stratigraphy (Blakely, Polk Creek, Blaylock, Womble, & Bigfork formations) within the Ouachita Basin record a shift from proximal mixed cratonic-orogenic sources to distal homogenous Appalachian (Taconic) sources based on a shift of the neodymium isotopic composition (Gleason et al., 2001).

During the Late Paleozoic, the Rheic Ocean closed between Laurussia and Gondwana (Figures 2b and 2c) and the Ouachita Basin evolved from deep-water passive margin sedimentation to a remnant ocean basin being filled by thick, turbidite sequences (Ingersoll et al., 2003; Morris, 1974, 1989b). The relatively slow sedimentation rate of the Ouachita facies changed to a progressively higher sedimentation rate in the Carboniferous, a result of flysch (i.e., syntectonic sedimentation) sourced from the Appalachian-Ouachita orogenesis (Shaulis, 2012). These syntectonic clastic wedge sequences, Mississippian Stanley Group through the Pennsylvanian Atoka Group (Figure 3), are preserved within the Arkoma Basin; a peripheral foreland basin of the Ouachita orogen (e.g., Viele, 1989). Late-stage formation of the Benton-Broken Bow

uplifts in the Early Permian is recorded by isotopic dates that approximate cessation of orogenesis (e.g., Bass & Ferrara, 1967; Denison et al., 1969; Denison et al., 1977; Shelton et al., 1986).

Mesozoic sediments of the Gulf Coastal Plain conceal much of the Ouachita trend, with exception of the exposed orogen in eastern Oklahoma and western Arkansas (Figure 2d). An alkalic igneous suite that post-dates the orogeny is located at western end of the Benton Uplift, AR and within the Gulf Coastal Plain to the south (Eby & Vasconcelos, 2009 and references therein).

4.3.2. Generalized Ouachita Stratigraphy

Stratigraphy in the Ouachita orogenic belt may be divided into a pre-tectonic "Ouachita facies" sequence of Early Mississippian and older rocks, and later syntectonic interval of Carboniferous flysch (Arbenz, 1989b; Flawn et al., 1961). A relatively low sedimentation rate during much of the Early Paleozoic resulted in a sediment-starved basin overlying the southern Laurentian rifted margin (Thomas et al., 2012). An estimated 2.5 km cumulative stratigraphic thickness of Ouachita facies, Cambrian/Ordovician Collier Formation through Early Mississippian Arkansas Novaculite (Figure 3), comprises multiple lithologies, including: shale, sandstone, chert/novaculite, and minor carbonate (Lowe, 1989 and references therein).

The Mississippian Stanley Group, deposited unconformably upon the Ouachita facies, records the onset of syntectonic flysch sedimentation based on stratigraphic position of marine index fossils and radiometric dates of four major tuff units (Morris,

1989a and references therein; Mose, 1969; Shaulis, 2012). The Pennsylvanian Jackfork Group unconformably overlies the Stanley Group (Figure 3) and is distinctly different, both texturally and petrographically (Morris et al., 1979). The Jackfork Group contains turbidite sandstone beds and higher content of quartz, as compared to the underlying Stanley Group that has a more clay-rich matrix (Morris, 1989a). Overlying the Jackfork Group unconformably is the Johns Valley Formation, a thin (125 to 270m) shale-dominant unit with exotic boulders of limestone, chert, and siliclastic rocks (Arbenz, 2008; Harlton, 1933, 1938; Miser, 1934; Morris, 1989a).

The next youngest unit, the Atoka Formation, is sub-divided into informal lower, middle, and upper subdivisions based on interpreted depositional environment in response to structural change (e.g., flexural bending of foredeep in response to tectonic load) as described in detail by Houseknecht (1986) and Sutherland (1988). Collectively, the Atoka Formation is an estimated 5-6 km thick of shale and sandstone (Arbenz, 2008; Viele & Thomas, 1989). Above the Atoka Formation in the Arkoma Basin, the Krebs Group (Hartshorne, McAlester, Savanna, & Boggy formations) was deposited above a minor unconformity as a common molasse, with deltaic complexes (Houseknecht, 1986). Chert-pebble conglomerate beds of the Late Pennsylvanian Thurman Formation (Figure 3) records the local source of detritus from the weathering of uplifted Ouachita facies rocks (i.e., Bigfork Chert & Arkansas Novaculite) that are located southward in the hinterland (Sutherland, 1988).

4.3.3. Structural Provinces

The Ouachita orogen of southwestern Oklahoma (Figure 3) is sub-divided into three tectonic provinces based on the meso-/macro- scale structures and stratigraphy: *Arkoma Basin, Frontal Thrust Zone, and Maumelle Chaotic Zone* (Lillie et al., 1983; Nelson et al., 1982; Viele & Thomas, 1989). There are two anticlinal structures (*Potato Hills and Broken Bow Uplift)* and one ridge (*Black Knob Ridge*), wherein the surface geology is comprised of Early to Middle Paleozoic pre-tectonic rocks (Arbenz, 2008). These uplifted regions are discussed as separate areas with distinct structural boundaries.

4.3.3.1. Arkoma Basin (AB)

The northernmost structural province, the Arkoma Basin (Figure 3), is a foreland basin bounded by the Choctaw Fault to the south (Arbenz, 1989; Sutherland, 1988). This Carboniferous peripheral foreland basin developed from the former Ouachita Basin, a remnant ocean basin that closed from east to west during the Ouachita orogenesis. Syntectonic sediments, Mississippian Stanley Group through Pennsylvanian Krebs Group (e.g., Hartshorne to Boggy formations), are recycled from the active Ouachita orogen are a proximal sediment source, and from sediments carried by the Michigan River system from distal sources within the North American craton (Archer & Greb, 1995 and references therein; Morris, 1971; Potter & Siever, 1956). These sediments are deposited on top of gently south-dipping Cambrian platform carbonate sediments that are locally offset by down-to-the-south normal growth faults (Buchanan & Johnson, 1968; Kruger & Keller, 1986).

4.3.3.2. Frontal Thrust Zone (FTZ)

Bounded between two major thrust faults, the Choctaw Fault and the Windingstair Fault (Figure 3), a region defined by imbricate thrusts and a broad syncline is the Frontal Thrust Zone (Arbenz, 1989). A deep-crustal seismic reflection survey by the Consortium on Continental Reflection Profiling (COCORP) provides seismic imagery of the broad crustal-scale syncline in the subsurface in Arkansas near the state line with Oklahoma (Lillie et al., 1983; Nelson et al., 1982). Members of the Pennsylvania Atoka Formation are mapped at the surface within this province (Hendricks et al., 1947).

4.3.3.3. Maumelle Chaotic Zone (MCZ)

A large region within the Ouachita orogen, south of the Windingstair Fault (Figure 3), is highly deformed by layer parallel shortening, faulting, and by folding into broad synclines (Arbenz, 1989). The Maumelle Chaotic Zone is stratigraphically complex because the rocks are likely a tectonic mélange, olistrome deposits, or a combination of both sediment types (Morris, 1989a; Nielsen et al., 1989; Viele, 1973, 1979). Carboniferous syntectonic sediments of the Stanley Group, Jackfork Group, and the Johns Valley Formation are mapped throughout this zone (Honess, 1923; Ulrich, 1927).

4.3.3.4. Broken Bow Uplift (BBU)

One of the major crustal-scale anticlinal central uplifts within the Ouachita orogen is the Broken Bow uplift (Figure 3); the western portion of an anticlinorium

known as the Benton-Broken Bow uplifts located in western Arkansas to southeastern Oklahoma (Arbenz, 2008). Pre-tectonic rocks from the Ordovician Collier Formation through Mississippian-Devonian Arkansas Novaculite are exposed within the lower green-schist metamorphic core (Honess, 1923; Miser, 1929; Pitt, 1955). The Mississippian Stanley Group borders this central uplift, and overlies a major unconformity (Arbenz, 1989; Honess, 1923; Miser, 1929).

4.3.3.5. Potato Hills (PH)

The Potato Hills, an anticlinorium of pre-tectonic Ordovician through Devonian rocks, occur to the south of the Windingstair Fault near Talihina, Oklahoma (Figure 3). This locality represents the second largest anticlinal structure exposed at the surface in the southwestern Oklahoma portion of the Ouachita FTB (Miser, 1926). At least four thrust faults within the subsurface that duplicate the hanging wall are responsible for the anticlinorium mapped at the surface (Arbenz, 1968). The Mississippian Stanley Group that rims the Potato Hills lies unconformably above the Mississippian-Devonian Arkansas Novaculite and older stratigraphy (Miller, 1955; Miser, 1926, 1954; Roe, 1955; Seely, 1955).

4.3.3.6. Black Knob Ridge (BKR)

A narrow ridge of pre-tectonic, Early Paleozoic rocks in the western part of the Ouachita FTB comprises Black Knob Ridge (Figure 3; Arbenz, 2008). Bounded by the Ti Valley – Choctaw Thrust to the northwest, the Ordovician Womble Formation through Mississippian-Devonian Arkansas Novaculite comprise the interior of this

narrow belt of folded rocks (Hendricks, 1937). The Mississippian Stanley Group that flanks this structure is deposited above a major unconformity (Arbenz, 1989; Honess, 1923; Miser, 1929; Sutherland, 1988).

4.4. Previous Thermal Maturation and Thermochronology

4.4.1. Thermal Maturation

Thermal maturation studies, focused on vitrinite reflectance, coal rank, or clay mineralogy, combined provides the maximum temperature across of Ouachita FTB and are used in basin conceptual models (Figure 4a). The quantification of montmorillonite to illite transformation by X-ray diffraction is the earliest characterization of the thermal maturation of sediments along the Ouachita Trend, Texas and Oklahoma (Weaver, 1960). This semi-quantitative thermal maturation technique uses the "sharpness" of the 10 Å peak as an indicator of increasing metamorphism (see Figure 6 in Weaver, 1960). Presence of kaolinite in foreland basin rocks, and its decrease toward the lower greenschist facies rocks of the central uplifts (surface) and the interior metamorphic zone (subsurface) of the Ouachita Trend (Figure 2d) provide a qualitative measure of thermal maturation (Weaver, 1960).

A detailed regional study of the Ouachita FTB surface rocks indicates vitrinite reflectance (%R_o) increased from west-to-east and toward the central uplifts; values less than 0.5% are in the Frontal Thrust Zone and values greater than 3% are found in the central uplifts (Houseknecht & Matthews, 1985). These vitrinite data show higher maturation in the hanging wall of major thrust faults (i.e., Choctaw and Windingstair

Thrust Faults) in southeastern Oklahoma, yet there is no relationship with structural throw in the vicinity of the Benton Uplift, western Arkansas (Houseknecht & Matthews, 1985). Additional regional illite 'crystallinity' work supports higher maturation in the Benton Uplift area (Guthrie et al., 1986).

Focused thermal maturation studies on the central uplifts and the Arkoma Basin complement the regional studies (e.g., Cardott, 2013; Johnson, 2011; Keller et al., 1985; Spötl et al., 1993). Use of the mean apparent crystal diameter along with the respective chert or novaculite texture establishes a pattern of thermal maturation within the central uplifts, especially for the Benton Uplift (Keller et al., 1977; Keller et al., 1985). The largest apparent crystal diameter, greater than 35 µm, is located northern portion of the Benton Uplift in the eastern end and west of Little Rock, AR. The apparent crystal diameter decreases along the anticlinorial axis of the Benton Uplift to the southwest, and then increases to approximately 20 µm within the southern part of the Broken Bow Uplift (Keller et al., 1985). A triple-point texture is observed within an area surround the central uplifts, and this region parallels the mapping of quartz-filled veins indicating that theses rocks experienced increased temperature (Keller et al., 1985; Miser, 1954).

Illite 'crystallinity' coupled with identification of other clay mineral species indicate temperature greater the epizone (~300°C and higher) in the eastern end of the Benton Uplift and decreasing to anchizone (~200°C to ~300°C) for the western Benton Uplift (Figure 2d; Johnson, 2011). Diagenetic zone (less than ~200°C) temperatures and decrease in illite 'crystallinity' occur in the Carboniferous sediments flanking the Benton

Uplift (Johnson, 2011). Further, Shelton et al. (1986) report a conodont alteration index of 4 from one sample within the central Benton Uplift, which gives a calculated temperature between 190-300°C.

Fluid inclusion and stable isotope studies of syntectonic veins within the Broken Bow and Benton Uplifts provide thermometry and thermobarometry for the conditions at which the veins formed (Cervantes & Wiltschko, 2010; Piper, 2011; Richards et al., 2002). The most recent study indicates temperatures were between 105.6°C to 284.5°C for entrapment of fluid inclusion in quartz and veins precipitated at conditions of 210.6° - 429.2°C and 0.3 - 4.7 kbars (Piper, 2011).

Samples of drill cuttings were analyzed for vitrinite reflectance, clay mineralogy, and illite 'crystallinity' from a suite of industry wells within the Arkoma Basin and Frontal Thrust Zone (Spötl et al., 1993). An increase of vitrinite reflectance from ~0.75-1 $\%R_o$ up to ~4-6$\%R_o$ is observed at approximately 5 km depth, and there is diminished of kaolinite with depth (Spötl et al., 1993). Both illite 'crystallinity', illite polytypes, and percent expandable clays do not correlate well with depth (Spötl et al., 1993).

The Arkoma Basin has thermal maturation indicators of coal rank and vitrinite reflectance for Pennsylvanian Hartshorne Formation of eastern Oklahoma. Coal rank increases toward the east as it matures from high volatile bituminous to a higher rank of low volatile bituminous coal (Cardott, 2013). Mean maximum vitrinite reflectance values, 0.76% Rmax to 2.41% Rmax, from surface and subsurface measurements show an increase of maturation to the eastern part of the Arkoma Basin, OK (see Figure 3 in

Cardott, 2013). Basinal-derived brines were expelled through the Arkoma Basin to elevate the temperatures to 80-170°C because it is suggested that these brines precipitated the Mississippi Valley-type minerals near the Ozark Dome region (Leach and Rowan, 1986; Leach et al., 1985; Leach et al., 2001).

4.4.2. Thermochronology

Higher thermal maturation eastward, the presence of a Cretaceous igneous suite, and the lower greenschist metamorphism of the Benton Uplift, AR support previous thermochronologic studies in western Arkansas because thermochronometers have a greater chance to be reset (Houseknecht & Matthew, 1985 and references therein). These reset thermochronologic ages provide the apparent timing that the rocks experienced heating and subsequent cooling (Gallagher et al., 1998). Apatite fission track analysis of western Arkansas constrains the cooling through the apatite fission track closure temperature to approximately Early Cretaceous, and determined little influence of early Late Cretaceous igneous activity to elevate regional paleo-temperature that would reset the apatite fission track ages (Arne, 1992). Partially reset to reset zircon fission track grain ages from the Benton Uplift indicate Pennsylvanian to Early Permian cooling through the zircon fission track closure temperature (Johnson, 2011).

Isotopic potassium-argon and rubidium-strontium dates for neocryst adularia provide timing of the lower greenschist facies metamorphism from 214-287 Ma and 262 ±10 Ma for the Benton Uplift (Bass & Ferrara, 1969; Shelton et al., 1986). A suite of isotopic ages, potassium-argon and rubidium-strontium measured on samples collected

from wells within the subsurface, interior metamorphic zone of the Ouachita Trend, give a range of potassium-argon ages from Pennsylvanian through Early Permian (Denison et al., 1969; Denison et al., 1977; Flawn et al., 1961; Nicholas & Rozendal, 1975). More recently, U-Pb zircon ages of tuffs from the Mississippian Stanley Group were dated between 320.7 ± 2.5 Ma to 328.5 ± 2.7 Ma (Shaulis et al., 2012).

Timing of emplacement and subsequent cooling of the intrusive igneous bodies (e.g., Magnet Cove, Prairie Creek, and Granite Mountain) was determined by both isotopic and fission-track methods. Potassium-argon, argon-argon, and rubidium-strontium ages on these alkali igneous rocks range from ca. 88-106 Ma (Duke et al, 2014 and references therein). Central ages determined from fission track analysis of apatite, titanite, and zircon give ages between ca. 86-105 Ma (Arne, 1992; Eby, 1987; Eby & Vasconcelos, 2009; Scharon & Hsu, 1969).

4.5. Sample Selection

4.5.1. Surface Outcrops

Three traverses parallel to regional strike are used to position the samples, relative to the structures present (Figure 3). Sampling extends from the interior, metamorphic core of the Broken Bow Uplift to the proximal portions of the Arkoma Basin to the north (Table S1). Sandstone intervals with Carboniferous syntectonic units were primarily targeted, and collection of silty shale were secondary in absence of sandstone. Ordovician to Early Mississippian rocks within the Potato Hills, Black Knob Ridge, and the Broken Bow Uplift are pre-tectonic. Approximately 20 kg of bulk rock

were collected to yield an adequate number of ≥ 60 μm zircon and apatite grains with the heavy mineral separate (Table S2).

4.6. Methods

Heavy minerals were separated at Texas A&M University using standard laboratory procedures with use of lithium heteropolytundstates (LST, ρ = 2.85) and methylene iodide (MEI, ρ = 3.32) (e.g., Bernet & Garver, 2005; Donelick et al., 2005). All bulk rock heavy mineral separates were processed by gravity settling through both LST and MEI to concentrate apatite (ρ = 3.10-3.35) and zircon (ρ = 4.6-4.7) populations (Mange & Maurer, 1992). Zircons from each separate have photomicrographs and morphological descriptions of macroscopic properties (Table S.1; Corfu et al., 2003; Mange & Maurer, 1992). Only one sample, OK12-9, yielded appreciable apatite and those grains were not photographed or described.

Figure 4b illustrates the range of appropriate thermochronometers based on the assumption that maximum temperatures reached were sufficient to reset these thermochronometers. Apatite-zircon fission track and zircon (U-Th)/He thermochronometry were chosen to give exhumation data for the Ouachita orogen.

4.6.1. Fission Track Thermochronometry

The external detector method of determining fission track ages was used, as well as the bulk of the analytical work completed in the Fission Track Lab at the University of Arizona. Aliquots from the zircon separates were mounted into Teflon, step-polished, and fully etched with NaOH:KOH eutectic (Bernet & Garver, 2005; Fleischer et al.,

1975). An aliquot of apatite from OK12-9 was mounted into Teflon, step-polished, and etched with HNO_3 (Donelick et al., 2005). The spontaneous fission tracks within grains are readily observed under an optical microscope. A thin plate of undamaged, low-U muscovite attached to each mount acts as a recorder (i.e., external detector) of induced tracks (Gallagher et al., 1998). Glass dosimeters are placed between individual mounts to characterize the neutron irradiation fluence (Tagami & O'Sullivan, 2005).

The Oregon State University TRIGA reactor, a well-thermalized irradiation facility, was used to induce fission tracks by abundant saturation of neutrons. Irradiated samples, after radioactive cooling, are disassembled and the muscovite detectors etched to determine induced tracks caused by decay of uranium within the corresponding zircon grain. Track densities are determined by selection of tracks on the grain, and corresponding area of mica detector. Fission track age calculations use the ratio of spontaneous tracks to induced tracks in an adjusted radiometric age equation to determine individual grain ages (see equation 13, Tagami & O'Sullivan, 2005). For apatite fission track analysis, the average diameter of the etch pit in same direction as c-axis for each grain is measured as 'Dpar' because this parameter influences the apatite fission track annealing kinetics (Donelick et al., 2005).

It is common to use a representative sample age by combining the grain ages in several ways: (1) Pooled age, (2) Arithmetic mean age, and (3) Central Age (Reiners et al., 2017). A *pooled age* is ratio of the sum of all spontaneous tracks to the sum of all induced tracks. The mean grain ratio is the *arithmetic mean age*. A statistical approach

to a sample age is the c*entral age*, where the weighted mean of a log-normal distribution of a combined dataset of all grain ages and assumes a single population (Galbraith & Laslett, 1993).

Single grain ages plotted to show the discrete age components (i.e., Kernel Density Estimate with histogram) and to show individual grain ages with error combined the central age (i.e., abanico radial plot) are standard means to visualize the thermochronologic data (Galbraith, 1990, 2005; Reiners et al., 2017; Vermeesch, 2009). Computer software programs, BinomFit and Radial Plotter, used to construct these plots have peak-fitting algorithms and population statistics (Brandon, 2002; Vermeesch, 2009).

4.6.2. Zircon (U-Th)/He Thermochronometry

Zircons ($n \approx 6$ per sample), preference to equant grains with smallest dimension > 60 μm, were jacketed in platinum, degassed to measure He released, and isotopic ratios determined. U-Th-Sm isotopes measured using solution inductively coupled plasma mass spectrometry (ICP-MS) in the (U-Th)/He Geo- and Thermochronometry Lab at the University of Texas at Austin, as outlined in the analytical methods of Reiners (2005). Reported dates are initial, calculated dates that were corrected for alpha-ejection (Farley et al., 1996). Diffusion of helium for individual zircon grains shown by a plot of effective uranium (eU) and (U-Th)/He date (Guenthner et al., 2013). Comparison of (U-Th)/He date to Th/U for each zircon is shown by structural province.

4.7. Thermochronometry Results

4.7.1. Apatite Fission Track

Located within the Frontal Thrust Zone, OK12-9 yields a new apatite fission track central age of 193 ± 19.2 Ma from 9 apatite grains (Table S3 and Figure 5).

4.7.2. Zircon Fission Track

Thirty-seven new zircon fission track central ages, 259.3 ± 33.2 Ma to 399.4 ± 39.9 Ma range, determined from 643 grain ages (n) for the Ouachita orogen in Oklahoma (Table S3, and Figure 5a). Figure 5b gives zircon fission track peak ages by separating sample into discrete populations using BINOFIT software (Brandon, 2011 and references therein). The seven new zircon fission track central ages (n = 130) for the Arkoma Basin span 272.2 ± 21.5 Ma (reset) in the central and western portions to 347.5 ± 28.6 Ma (mixed) in the east. Five zircon fission track central ages (n = 100) across the Frontal Thrust Zone are 284.9 ± 20.9 Ma (reset) to 327.0 ± 28.3 Ma (mixed). There are both reset and mixed ages across the Frontal Thrust Zone.

Black Knob Ridge and Potato Hills do not have zircon fission track ages because of poor zircon yield from four samples; each structure has a zircon fission track central age from Carboniferous stratigraphy flanking the structure. A mixed central ages of 327.0 ± 28.3 Ma (n=20) for Black Knob and 311.1 ± 24.7 Ma (n=20) were obtained for Black Knob Ridge and the Potato Hills, respectively. The Maumelle Chaotic Zone with nineteen additional central ages (n = 423) are mostly mixed grain populations. The youngest central age is 273.1 ± 15.4 Ma, interpreted as reset, whereas a mixed age of

399.4 ± 39.9 Ma is the oldest. Two central ages within, and two central ages on the flank of the Broken Bow Uplift (n =31) are between 295.3 ± 25.2 Ma (reset) and 379.0 ± 32.0 Ma (mixed).

4.7.3. Zircon (U-Th)/He

One hundred and fifty-six zircon new (U-Th)/He dates from thirty-five sample localities are shown in Figure 6b. The (U-Th)/He zircon dates are between 181.6 ± 14.53 Ma and 1964.2 ± 157.13 Ma. The youngest (U-Th)/He date for each sample, range from 181.6 ± 14.53 Ma to 347.6 Ma, provided in Table S4. These cooling dates are discussed in context of the respective structural province.

There are seven samples from the Arkoma Basin that contribute forty (U-Th)/He dates. The youngest dates extend from 217.9 ± 17.43 Ma to 334.6 ± 26.77 Ma. The five samples within the Frontal Thrust Zone have twenty-two (U-Th)/He dates, with the youngest date range of 236.2 ± 18.89 Ma to 323.3 ± 25.86 Ma. Black Knob Ridge and Potato Hills do not have zircon fission track ages because of poor zircon yield from three samples. Grain dates from Carboniferous stratigraphy flanking the structure are used.

The Black Knob Ridge has the youngest (U-Th)/He date of 323.3 ± 25.86 Ma. Two samples adjacent to the Potato Hills have the youngest (U-Th)/He dates of 231.8 ± 18.54 Ma and 284.9 ± 22.79 Ma. Nineteen samples within the Maumelle Chaotic Zone give seventy-eight (U-Th)/He dates, where the youngest dates for each sample are between 190.1 ± 15.21 Ma and 343.4 ± 27.47 Ma. A sample that provided six (U-Th)/He dates within the Broken Bow Uplift has the youngest date at 181.6 ± 14.53 Ma. Three

samples adjacent to the Broken Bow Uplift have the youngest (U-Th)/He dates span 190.1 ± 15.21 Ma to 218.1 ± 17.45 Ma.

4.8. Discussion

4.8.1. Exhumation of the Broken Bow Central Uplift

Greenschist facies rocks of the Broken Bow Uplift (Figure 2d) record the history of the interior portions of the orogenic wedge (hinterland). Thermal maturation data indicates maximum temperatures exceeded 300°C meaning zircons were reset for both (U-Th)/He analysis and fission track analysis within this central uplift (Figures 3, 4, & 7; Hodges, 2014 and references therein; Houseknecht & Matthews, 1985).

All thermochronologic data and thermal maturation is initially plotted with respect to elevation and a relationship with the vertical position of each sample evaluated (Figure 8; Arne, 1992; Houseknecht and Matthews, 1985; Johnson, 2011). A relationship between topography and cooling is not evident within the thermochronologic or thermal maturation data. Zircon grain analyzes (Figure 9a, b) illustrate fission track and (U-Th)/He ages in comparison to specified geochemistry given on x-axis of each plot. Figure 9c compares radial and KDE plots by structural province to show differences between each suite of cooling ages.

Cooling ages, plotted above published structural interpretations in Figures 10-12, show clusters of the (U-Th)/He dates, which represent the timing that the rocks record passing through the partial retention zone. Assumptions used, include: 1) rocks pass through a horizontal closure isotherm (Brandon et al., 1998, Figure 1), 2) erosion is

uniform across the FTB for simplicity, 3) geothermal gradient is 20°C/km, and 4) ~205°C for zircon fission track and ~180°C for zircon (U-Th)/He closure temperatures (Hodges, 2014). In reality, isotherms are most likely to parallel large scale topographic features, such as the slope of the taper (Braun, 2005). Thermal history modeling will account for curved isotherms, and therefore are not discussed here.

Use of the assumed geothermal gradient, the depth of the closure isotherm for zircon fission track is at 10.25 km and (U-Th)/He closure isotherm at 9 km. As the rock cooled by the erosion of the overburden, an estimated average exhumation rate of 0.01226 km/m.y. (12.26 m/yr) is presented for the Broken Bow Uplift during Late Permian through Early Jurassic.

4.8.2. Average Rates of Exhumation within the Critical Wedge – Maumelle Chaotic Zone, Frontal Thrust Zone, Potato Hills, and Black Knob Ridge

The youngest cooling ages within error for each thermochronometer will be used in each structural province and determined for each traverse (Tables S4 & S5). Figures 10-12 aid in identifying the youngest representative thermochronologic ages. Exhumation rates are determined using the assumptions stated in section 8.1.

A majority of the new thermochronologic data lies within the large area known as the Maumelle Chaotic Zone, which is fortunate as the rocks are intensely deformed and the geology poorly constrained (Viele, 1973). From east to west, the average rates of exhumation are 0.03456 km/m.y. (34.57 m/yr), 0.03431 km/m.y. (34.31 m/yr), and 0.13256 km/m.y. (132.56 m/yr) during Late Triassic-Middle Jurassic. The eastern and

central traverses cross the Frontal Thrust Zone, and the average rates of exhumation during Early Triassic-Permian are 0.06775 km/m.y. (67.75 m/yr) and 0.05938 km/m.y. (59.38 m/yr), respectively. For sample OK12-9 located within the eastern part of the Frontal Thrust Zone, an apatite fission track minimum age (closure at ~120°C) gives an average exhumation rate of 0.04193 km/m.y. (41.93 m/yr) from Early Triassic to Middle Jurassic. Potato Hills have an average exhumation rate of 0.26151 km/m.y. (261.51 m/yr) and the Black Knob Ridge has 0.03091 km/m.y. (30.91 m/yr) for an average exhumation rate during Permian-Early Triassic.

4.9. Implications

The pattern of (U-Th)/He thermochronologic dates, hinterland to foreland (Figures 10-12) show a foreland-directed sloped topographic surface. These cooling dates become younger toward the Broken Bow Uplift indicating rocks were exhumed first in the foreland as the youngest faults bring thrust sheets toward the surface giving older cooling dates.

Zircon fission track minimum dates, plotted on the same figures, are more difficult to interpret as there is a mix of reset to partially reset grains and some grains are metamict (Table S5). In Figure 12, the pattern of zircon fission track minimum ages between samples 54-57 show cooling ages becoming younger toward the northern Maumelle Chaotic Zone. These samples were collected from the north limb of the Cloudy Syncline, and this broad structure is interpreted to reach 5-6 km (Hendricks et al., 1947; Arbenz, 2008). The pattern of ages mimics the shape of the limb and is

interpreted to represent exhumation by out of sequence thrust motion and folding. Comparison of the representative cooling ages (grey lines in Figures 10-12) broadly define a wedge shape implying that the (U-Th)/He dates give paleotopography of the critical wedge, whereas the zircon fission track minimum ages records internal development of the FTB wedge.

Apatite fission track data for the Ouachita orogen of western Arkansas were reprocessed following the methods of this study to give a minimum ages (Arne, 1992). The apatite fission track data indicate the closure temperature was reached between 184 ± 11 Ma (Arne, 1992, sample 8863-80 Atoka) and 192 ± 19 Ma (OK12-9, this study). The Early Jurassic cooling through the apatite fission track closure temperature continued until Late Cretaceous, and likely a regional cooling event for the midcontinent based on thermochronologic data from the North American craton (Arne, 1992; Zimmerman, 1986).

Zircon fission track minimum dates of mostly reset grains across the Benton Uplift, western Arkansas yield ages record a Pennsylvanian to Early Permian cooling (Johnson, 2011). If zircon fission track data does represent the internal thrust motion and folding, then the Benton Uplift was exhumed earlier than the Broken Bow Uplift.

In contrast, zircon (U-Th)/He dates in the Arkoma Basin report cooling as young as Triassic. Vitrinite reflectance data indicates anomalous and higher than expected thermal maturation in these same Carboniferous rocks (Cardott, 2013; Desborough et al., 1985; Houseknecht et al., 1992; White, 1915). A separate thermal event exceeding the

180°C closure isotherm for the zircon (U-Th)/He thermochronometer is suspected. Maximum peak temperature range between 113°C and 206°C, calculated from the vitrinite reflectance values, supports a secondary thermal event (Barker & Pawlewicz, 1994; Cardott, 2013). If the temperature calculated from vitrinite reflectance is correct, then the zircon fission track minimum ages still reflect orogenic or pre-Carboniferous cooling event (unrest ages).

One explanation for the second thermal event is a topographically-driven fluid flow originating from beneath the hinterland, which transported basinal brines laterally along permeable rocks of the décollement until the fluids are expelled into the foreland (Deming et al., 1990; Dorobek, 1989; Leach and Rowan, 1986; Sharp, 1978). This Ouachita-related fluid flow event is speculated to be the regional event responsible for the Mississippi Valley-type lead-zinc deposits of the Ozark platform (Op on Figure 2d) and combined ages from isotopic and paleomagnetism dating brackets ore mineralization as Late Pennsylvanian-Early Triassic (Leach et al., 2001 and references therein). Further, fluid inclusion homogenization temperatures for sphalerite sampled from these ore deposits indicate fluid temperatures between 80-170°C and that these inclusions were formed at low pressure conditions (Leach & Rowan, 1986 and references therein).

To the east, the large anticlinal structure of pre-Carboniferous rocks that comprise the Benton Uplift, western Arkansas may be explained as maintaining the critical wedge by a anticlinal stack or duplex of Ouachita facies rocks in absence of enough syntectonic material to build the wedge. An alternative explanation is a

reactivation of an out-of-sequence listric normal fault within the rifted Laurentian margin form the crustal-scale anticlinal structure cored with basement rock. We cannot choose between these two hypotheses based on the results from the present study.

Additional (U-Th)/He ages across the western Benton Uplift may help determine the correct choice as a high-fault in basement will make the wedge supercritical and thus have a higher slope angle of the paleotopography than observed in the western part of the Ouachita orogen, Oklahoma.

4.10. Comparison to Low-Temperature Thermochronology in Wichita Mountains, Arbuckle Mountains, and along the Ouachita Trend

Figure 13a summarizes the new thermochronologic cooling data with existing thermal maturation data for the Ouachita FTB of southeastern Oklahoma in the context of known tectonic events (e.g., Ouachita Orogeny, and Gulf of Mexico Rifting). A proposed Cretaceous thermal event of the Bermuda Hotspot that passed beneath the Ouachita FTB is shown in Figure 13a (Cox and van Arsdale, 2002).

Published low-temperature thermochronology studies in the midcontinent have focused on use of apatite fission track dating to understand the thermal history of the Wichita Mountains, southwestern Oklahoma, and post-orogenic unroofing of Marathon Uplift, Llano Uplift, Arbuckle Uplift (Mu, Lu, & AM in Figure 2d, respectively) along the Ouachita trend (Corrigan et al., 1998; Winkler, 1999). The oldest pooled apatite fission track ages are within the Llano Uplift and range from 425 ± 72 Ma to 240 ± 18 Ma, likely a result of a mix of many unreset or partially reset ages (Corrigan et al.,

1998). The apatite fission track pooled ages of the Arbuckle Mountains are between 370 ± 36 Ma to 250 ± 26 Ma, with three out of four ages giving a Permian cooling date (Corrigan et al., 1998). As there are Permian cooling ages both in the Arbuckle Mountains and the Oklahoma portion of the Ouachita Orogen (this study), the surface samples in the Wichita Mountains were at a shallower depth than the surface rocks in the Ouachita orogen based on the different thermochronometers.

The remaining apatite fission track cooling ages are Jurassic - Cretaceous for the Marathon Uplift (127 ± 14 Ma to 112 ± 11 Ma), Wichita Mountains (209 ± 27 to 101 ± 14 Ma), and Ouachita orogen, AR (183.6 ± 11.7 Ma to 87.9 ± 6.4 Ma) from Winkler et al. (1999), Corrigan et al. (1998), and Arne (1992), respectively. The Cretaceous ages are interpreted to represent regional cooling by denudation (Arne, 1992; Zimmerman, 1986). The additional of new thermochronologic dates in Figure 13b is a thermal history summary with cooling rates and denudation rates along the Ouachita trend, modified from Corrigan et al. (1998).

4.11. Conclusions

(1) Zircon fission track minimum ages record development of the FTB wedge, whereas the (U-Th)/He dates define the paleotopography of the critical wedge. As such, the internal motion of thrusts and folding occurred during Pennsylvanian to Late Permian. Paleotopography slopes toward foreland and the present-day surface was buried at 9 km during Late Triassic-Middle Jurassic, assuming 20°C/km and zircon (U-Th)/He closure of ~180°C.

(2) Reset (U-Th)/He dates in the Arkoma Basin correspond to anomalous high maturation and these thermochronologic dates record a second Triassic thermal (fluid flow) event, which exceeded 180°C.

(3) Inactive FTBs did have the critical taper wedge predicted by the wedge paradigm, and as recorded by the trend line of the (U-Th)/He dates.

(4) Thermal maturation coupled with low-temperature thermochronometry and use of the wedge model paradigm together will be an excellent method of observation on ancient FTBs globally by indirectly creating better interpretations, especially where internal structures are poorly known.

4.12. References

Arbenz, J. K. (1989a). Ouachita thrust belt and Arkoma Basin. In R. D. Hatcher Jr., W. A. Thomas, & G. W. Viele (Eds.), *The Appalachian-Ouachita Orogen in the United States, The Geology of North America* (Vol. F-2, pp. 621-634). Boulder, CO: Geological Society of America.

Arbenz, J. K. (1989b). The Ouachita System. In A. W. Bally & A. R. Palmer (Eds.), *The Geology of North America - An Overview, The Geology of North America* (Vol. A, pp. 371-396). Boulder, CO: Geological Society of America.

Arbenz, J. K. (1968). Structural geology of the Potato Hills, Ouachita Mountains, Oklahoma. In L. M. Cline (Ed.), *A guidebook to the geology of the western Arkoma Basin and Ouachita Mountains, Oklahoma* (p. 109-121). Oklahoma City, OK: Oklahoma City Geological Society.

Arbenz, J. K. (2008). Structural framework of the Ouachita Mountains. In N. H. Suneson (Ed.), *Stratigraphic and Structural Evolution of the Ouachita Mountains and Arkoma Basin, Southeastern Oklahoma and West-Central Arkansas: Applications to Petroleum Exploration: 2004 Field Symposium* (Circular 112A, pp. 4-40). Norman, OK: Oklahoma Geological Survey.

Arne, D. C. (1992). Evidence from apatite fission-track analysis for regional Cretaceous cooling in the Ouachita Mountain fold belt and Arkoma Basin of Arkansas. *American Association of Petroleum Geologists Bulletin, 76,* 392-402.

Arne, D., Worley, B., Wilson, C., Chen, S., Foster, D., Luo, Z., et al. (1997). Differential exhumation in response to episodic thrusting along the eastern margin of the Tibetan Plateau. *Tectonophysics*, *280*, 239-256.

Barker, C. E., & Pawlewicz, M. J. (1994). Calculation of vitrinite reflectance from thermal histories and peak temperatures – A comparison of methods. In P. K. Mukhopadhyay, & W.G. Dow (Eds.), *Vitrinite reflectance as a maturity parameter: Applications and limitations, ACS Symposium Series* (pp. 216-229). Washington, DC: American Chemical Society. https://doi.org/10.1021/bk-1994-0570.ch014

Bass, M. N., & Ferrara, G. (1969). Age of the adularia and metamorphism, Ouachita mountains, Arkansas. *American Journal of Science*, *267*, 491-498.

Bernet, M. (2009). A field-based estimate of the zircon fission-track closure temperature. *Chemical Geology*, *259*(3-4), 181-189.

Bernet, M., & Garver, J. I. (2005). Fission-track analysis of detrital zircon. In P. W. Reiner, & T. A., Ehlers (Eds.), *Low-Temperature Thermochronology: Techniques, Interpretations, and Applications*, *Reviews in Mineralogy & Geochemistry* (Vol. 58, pp. 205-238). Chantilly, VA: Mineralogical Society of America.

Blythe, A. E., Bird, J. M., & Omar, G. I. (1998). Constraints on the cooling history on the central Brooks Range, Alaska, from fission-track and $^{40}Ar/^{39}Ar$ analyses. In J. S. Oldow & H. G. Avé Lallemant (Eds.), *Architecture of the Central Brooks Range Fold and Thrust Belt, Arctic Alaska* (Special Paper 324, pp. 163-177). Boulder, CO: Geological Society of America.

Brandon, M. T. (2002). Decomposition of mixed grain age distributions using BINOFIT. *On Track, 24*, 13-18.

Brandon, M. T., Roden-Tice, M. K., & Garver, J. I. (1998). Late Cenozoic exhumation of the Cascadia accretionary wedge in the Olympic Mountains, northwest Washington State. *Geological Society of America Bulletin, 110*(8), 985-1009.

Braun, J. (2005). Quantitative constraints on the rate of landform evolution from low-temperature Thermochronology. In P. W. Reiner, & T. A., Ehlers (Eds.), *Low-Temperature Thermochronology: Techniques, Interpretations, and Applications*, *Reviews in Mineralogy & Geochemistry* (Vol. 58, pp. 351-374). Chantilly, VA: Mineralogical Society of America.

Buchanan, R. S., & Johnson, F. K. (1968). Bonanza gas field - A model for Arkoma Basin growth faulting. In L. M. Kline (Ed.), *A Guidebook to the Geology of the*

Western Arkoma Basin and Ouachita Mountains, Oklahoma (pp. 75-85). Oklahoma City, OK: Oklahoma City Geologic Society.

Cardott, B. J. (2013). Hartshorne coal rank applied to Arkoma basin coalbed methane activity, Oklahoma, USA. *International Journal of Coal Geology, 108*, 35-46.

Cervantes, P., & Wiltschko, D. V. (2010) Tip to midpoint observations on syntectonic veins, Ouachita orogen, Arkansas: Trading space for time. *Journal of Structural Geology, 32*, 1085-1100.

Chapple, W. M. (1978). Mechanics of thin-skinned fold-and-thrust belts. *Geological Society of America Bulletin, 89*(8), 1189-1198.

Cook, T. D., & Balley, A. W. (1975). *Stratigraphic atlas of North and Central America* (272 p.). Princeton, NJ: Princeton University Press.

Corfu, F., Hanchar, J. M., Hoskin, P. W., & Kinny, P. (2003). Atlas of zircon textures. In J. M. Hanchar & P. W. O. Hoskin (Eds.), *Zircon, Reviews in mineralogy and geochemistry*, (Vol. 53, pp. 469-500). Chantilly, VA: Mineralogical Society of America.

Corrigan, J., Cervany, P. F., Donelick, R., & Bergman, S. C. (1998). Postorogenic denudation along the late Paleozoic Ouachita trend, south central United States of America: Magnitude and timing constraints from apatite fission track data. *Tectonics, 17*, 587-603.

Cox, R. T., & Van Arsdale, R. B. (2002). The Mississippi Embayment, North America: A first order continental structure generated by the Cretaceous superplume mantle event. *Journal of Geodynamics*, *34*(2), 163-176.

Dahlen, F. A., Suppe, J., & Davis, D. (1984) Mechanics of fold-and-thrust belts and accretionary wedges: Cohesive coulomb theory. *Journal of Geophysical Research, 89*, 10087-10101.

Davis, D., Suppe, J., & Dahlen, F. A. (1983). Mechanics of fold-and-thrust belts and accretionary wedges. *Journal of Geophysical Research: Solid Earth*, *88*(B2), 1153-1172.

De Jong, K., & Scholten R. (Eds.) (1973), *Gravity and* Tectonics. New York, NY: John Wiley.

DeCelles, P. G., & Mitra, G. (1995) History of the Sevier orogenic wedge in terms of critical taper models, northeast Utah and southwest Wyoming. *Geological Society of America Bulletin, 107,* 454-462.

Deming, D., Nunn, J. A., & Evans, D. G. (1990). Thermal effects of compaction-driven groundwater flow from overthrust belts. *Journal of Geophysical Research, 95*, 6669-6683.

Denison, R. E., Hetherington, E. A., Jr., & Otto, J. B. (1969). Age of the basement rocks in northeastern Oklahoma. *Oklahoma Geology Notes* (Vol. 29, pp. 120-128).

Denison, R. E., Burke, W. H., Otto, J. B., & Hetherington, E. A., Jr. (1977). Age of igneous and metamorphic activity affecting the Ouachita foldbelt. In C. G. Stone et

al. (Eds.), *Symposium on the Geology of the Ouachita Mountains; Stratigraphy, Sedimentology, Tectonics, and Paleontology* (Vol. 1, pp. 25-40) Little Rock, AR: Arkansas Geological Commission.

Donelick, R. A., O'Sullivan, P. B., & Ketcham, R. A. (2005). Apatite fission-track analysis. In P. W. Reiner, & T. A., Ehlers (Eds.), *Low-Temperature Thermochronology: Techniques, Interpretations, and Applications*, *Reviews in Mineralogy & Geochemistry* (Vol. 58, pp. 49-94). Chantilly, VA: Mineralogical Society of America.

Dorobek, S. (1989). Migration of orogenic fluids through the Siluro-Devonian Helderberg Group during late Paleozoic deformation: constraints on fluid sources and implications for thermal histories of sedimentary basins. *Tectonophysics, 159*, 25-45.

Duke, G. I, Carlson, R. W., Frost, C. D., Hearn Jr., B. C., & Eby G. N. (2014). Continental-scale linearity of kimberlite-carbonatite magmatism, mid-continent North America. *Earth and Planetary Letters, 403*, 1-14.

Eby, G. N. (1987) *Fission-track geochronology of the Arkansas alkaline province* (Open-file Report 87-0287, 12 p.). Washington DC: United States Geological Survey

Eby, G. N., & Vasconcelos, P. (2009). Geochronology of the Arkansas Alkaline Province, Southeastern United States. *Journal of Geology, 117*, 615-626.

Elliott, D. (1976). The motion of thrust sheets. *Journal of Geophysical research*, *81*(5), 949-963.

Farley, K. A., Wolf, R. A., & Silver, L. T. (1996). The effects of long alpha-stopping distances on (U-Th)/He ages. *Geochimica et cosmochimica acta*, *60*, 4223-4229.

Fleischer, R. L., Price, P. B., Walker, R. M., & Walker, R. M. (1975). *Nuclear tracks in solids: principles and applications*. University of California Press.

Flawn, P. T., Goldstein Jr., A., King, P. B., & Weaver, C. E. (1961). *The Ouachita System*, (Publication 6120, 401 p., 4 plates). Austin, TX: University of Texas.

Fuller, C. W., Willett, S. D., Fisher, D., & Lu, C.Y. (2006). A thermomechanical wedge model of Taiwan constrained by fission-track thermochronometry. *Tectonophysics, 425*, 1-24.

Galbraith, R. F. (1990). The radial plot: Graphical assessment of spread in ages. *Nuclear Tracks and Radiation Measurements, 17*, 207-214.

Galbraith, R. F. (2005). *Statistics for Fission Track Analysis* (219 p.). London, UK: Chapman & Hall/CRC.

Galbraith, R. F., & Green, P. F. (1990). Estimating the component ages in a finite mixture. *Nuclear Tracks and Radiation Measurements, 17*, 197-206.

Galbraith, R. F., & Laslett, G. M. (1993). Statistical models for mixed fission track ages. *Nuclear Tracks and Radiation Measurements, 21*, 459-470.

Gallagher, K., Brown, R., & Johnson, C. (1998). Fission track analysis and its applications to geological problems. *Annual Review of Earth and Planetary Sciences, 26,* 519-572.

Guenthner, W. R., Reiners, P. W., Ketcham, R. A., Nasdala, L., & Giester, G. (2013). Helium diffusion in natural zircon: Radiation damage, anisotropy, and the interpretation of zircon (U-Th)/He thermochronology. *American Journal of Science*, *313*(3), 145-198.

Guthrie, J. M., Houseknecht, D. W., & Johns, W. D. (1986). Relationships among vitrinite reflectance, illite crystallinity, and organic geochemistry in Carboniferous strata, Ouachita Mountains, Oklahoma and Arkansas. *American Association of Petroleum Geologists Bulletin 70,* 26-33.

Haley, B. R., Glick, E. E., Bush, W. V., Clardy, B. F., Stone, C. G., Woodward, M. B., & Zachary D. L. (1976). *Geologic Map of Arkansas* (Sheet 1, scale 1:500,000). Little Rock, AR: Arkansas Geological Commission & United States Geological Survey.

Haley, B. R., & Stone, C. G. (2006). *Geologic Map of the Ouachita Mountain Region and a portion of the Arkansas Valley Region in Arkansas* (DGM-OMR-001, 1 sheet, scale 1:125,000). Little Rock, AR: Arkansas Geological Survey.

Hendricks, T. A., Gardner, L. S., Knechtel, M. M., & Averitt, P. (1947). *Geology of the western part of the Ouachita Mountains, Oklahoma*. (Oil and Gas Investigation Map OM-66, scale 1:42,240). Washington DC: United States Geological Survey.

Hendricks, T. A., Knechtel, M. M., & Bridge, J. (1937). Geology of Black Knob Ridge, Oklahoma. *American Association of Petroleum Geologists Bulletin*, *21*(1), 1-29.

Hodges, K. V. (2014). Thermochronology in orogenic systems. In *Treatise on Geochemistry: Second Edition*. Elsevier Inc.

Houseknecht, D. W., & Matthews, S. M. (1985). Thermal maturity of the Carboniferous strata, Ouachita mountains. *American Association of Petroleum Geologists Bulletin, 69,* 335-345.

Houseknecht, D. W., Hathon, L. A., & McGilvery, T. A. (1992). Thermal maturity of Paleozoic strata in the Arkoma Basin. In K. S. Johnson & B. J. Cardott (Eds.), *Source rocks in the southern Midcontinent, 1990 symposium* (Circular 93, pp. 122-132). Norman, OK: Oklahoma Geological Survey.

Johnson, H. E., II (2011). *3-D structural analysis of the Benton uplift, Ouachita orogen, Arkansas* (Master's thesis). Retrieved from OAKTrust. (https://oaktrust.library.tamu.edu /handle/1969.1/ETD-TAMU-2011-12-10640). College Station, TX: Texas A&M University.

Keller, W. D., Stone, C. G., & Hoersch, A. L. (1985). Textures of Paleozoic chert and novaculite in the Ouachita Mountains of Arkansas and Oklahoma and their geological significance. *Geological Society of America Bulletin, 96,* 1353-1363.

Keller, W. D., Viele, G. W., & Johnson, C. H. (1977). Texture of Arkansas Novaculite indicates thermally induced metamorphism. *Journal of Sedimentary Petrology, 47* 834-843.

Kruger, J. M., & Keller, G. R. (1986). Interpretation of regional gravity anomalies in the Ouachita Mountains area and adjacent Gulf coastal plain. *American Association of Petroleum Geologists Bulletin, 70,* 667-689.

Leach, D. L., & Rowan, E. L. (1986). Genetic link between Ouachita foldbelt tectonism and the Mississippi Valley–type lead-zinc deposits of the Ozarks. *Geology, 14*(11), 931-935.

Leach, D. L., Rowan, E. L., & Viets, J. G. (1985). Fluid-inclusion evidence for the source of ore fluids for Mississippi Valley-type deposits in Missouri, Arkansas, Kansas, and Oklahoma. In J. A. Martin & W. P. Pratt (Eds.), *Geology and mineral-resource assessment of the Springfield 1° x 2° Quadrangle, Missouri, as appraised in September 1985* (Bulletin 1942, pp. 87-89). Washington DC: United States Geological Survey.

Leach, D. L., Bradley, D., Lewchuk, M. T., Symons, D. T., de Marsily, G., & Brannon, J. (2001). Mississippi Valley-type lead–zinc deposits through geological time: implications from recent age-dating research. *Mineralium Deposita*, *36*(8), 711-740.

Lillie, R. J., Nelson, K. D., De Voogd, B., Brewer, J. A., Oliver, J. E., Brown, L. D., et al. (1983). Crustal structure of Ouachita Mountains, Arkansas: A model based on integration of COCORP reflection profiles and regional geophysical data. *American Association of Petroleum Geologists, 67,* 907-931.

Lock, J. & Willett, S. (2008). Low-temperature thermochronometric ages in fold-and-thrust belts, *Tectonophysics, 456,* 147-162.

Lowe, D. R. (1989). Stratigraphy, sedimentology, and depositional setting of pre-orogenic rocks of the Ouachita Mountains, Arkansas and Oklahoma. In R. D. Hatcher Jr., W. A. Thomas, & G. W. Viele (Eds.), *The Appalachian-Ouachita Orogen in the United States, The Geology of North America* (Vol. F-2, pp. 695-728). Boulder, CO: Geological Society of America.

Ludwig, K. R. (2003). *Isoplot 3.0: A Geochronological Toolkit for Microsoft Excel* (Special Publication No. 4) Berkeley, CA: Berkeley Geochronology Center.

Mange, M. A., & Maurer, H. (2012). *Heavy minerals in colour*. Springer Science & Business Media.

Miall, A. D. (2019). The Southern Midcontinent, Permian Basin, and Ouachitas. In A. D. Miall (Ed.), *The Sedimentary Basins of the United States and Canada, Sedimentary Basins of the World* (pp. 369-399) Amsterdam: Elsevier, doi: 10.1016/B978-0-444-63895-3.00008-5.

Miller, B. W. (1955). *The geology of the western Potato Hills, Pushmataha and Latimer Counties, Oklahoma* (Master's Thesis). Norman, OK: University of Oklahoma.

Miser, H. D. (1926). *Geologic Map of Oklahoma* (1:500,000). United States Geological Survey.

Miser, H. D. (1929). *Structure of the Ouachita Mountains of Oklahoma and Arkansas* (Bulletin 50, 30 p.). Norman, OK: Oklahoma Geological Survey.

Miser, H. D. (1954). *Geologic map of Oklahoma* (1:500,000). Oklahoma Geologic Survey and United States Geologic Survey.

Morris, R. C. (1974) Carboniferous rocks of the Ouachita Mountains, Arkansas: A study of fades patterns along the unstable slope and axis of a flysch trough. In G. Briggs (Ed.), *Carboniferous of the United States* (Special Paper 148, pp. 241-279). Boulder, CO: Geological Society of America.

Morris, R. C. (1989a), Stratigraphy and sedimentary history of post-Arkansas Novaculite Carboniferous rocks of the Ouachita Mountains. In R. D. Hatcher Jr., W. A. Thomas, & G. W. Viele (Eds.), *The Appalachian-Ouachita Orogen in the United States, The Geology of North America* (Vol. F-2, pp. 591-602). Boulder, CO: Geological Society of America.

Morris, R. C. (1989b) *Sedimentary and tectonic history of the Ouachita Mountains* (Special Publication 22, p. 120-142). Tulsa, OK: Society of Economic Paleontonologists and Mineralogists.

Mose, D. (1969). The age of the Hatton Tuff of the Ouachita Mountains, southeastern Oklahoma. *Geological Society of America Bulletin*, *80*(11), 2373-2378.

Nance, R. D., & Linnemann, U. (2008) The Rheic Ocean: Origin, evolution, and significance. *Geological Society of America Today, 18* (12), 4-12.

Nance, R. D., Gutiérrez-Alonso, G., Keppie, J. D., Linnemann, U., Murphy, J. B., Quesada, C., et al. (2010). Evolution of the Rheic ocean. *Gondwana Research*, *17*(2-3), 194-222.

Nelson, K. D., Lillie, R. J., De Voogd, B., Brewer, J. A., Oliver, J. E., Kaufman, S., & Brown L. (1982). COCORP seismic reflection profiling in the Ouachita mountains of western Arkansas: Geometry and geologic interpretations. *Tectonics, 1,* 413-430.

Nielson, K. C., Viele, G. W., & Zimmerman, J. (1989). Structural setting of the Benton-Broken Bow uplifts. In R. D. Hatcher Jr., W. A. Thomas, & G. W. Viele (Eds.), *The Appalachian-Ouachita Orogen in the United States, The Geology of North America* (Vol. F-2, pp. 635-660). Boulder, CO: Geological Society of America.

Nicholas, R. L., & Rozendal, R. A. (1975). Subsurface positive elements within Ouachita Foldbelt in Texas and their relation to Paleozoic cratonic margin. *American Association of Petroleum Geologists, 59,* 193-216.

Pevear, D. R. (1999). Illite and hydrocarbon exploration. *Proceedings of the National Academy of Sciences, 96,* 3440-3446.

Piper, J. (2011). *The thermal evolution of the Ouachita orogen, Arkansas and Oklahoma from quartz-calcite thermometry and fluid inclusion thermobarometry* (Master's thesis). College Station, TX: Texas A&M University.

Pitt, W. D. (1955). *Geology of the core of the Ouachita Mountains of Oklahoma* (Circular 34, 34 p.). Norman, OK: Oklahoma Geological Survey.

Pollard, D. D. (Ed.). (2002). *White Paper: New Departures in Structural Geology and Tectonics*. Retrieved from http://pangea.stanford.edu/~dpollard/NSF/main.html

Purdue, A. H. (1909) The Slates of Arkansas (170 p.). Fayetteville, AR: Geological Survey of Arkansas.

Reiners, P. W., Carlson, R. W., Renne, P. R., Cooper, K. M., Granger, D. E., McLean, N. M., & Schoene, B. (2017). *Geochronology and thermochronology*. John Wiley & Sons.

Richards, I. Connelly, J. B., Gregory, R. T., & Gray, D. R. (2002). The importance of diffusion, advection, and host-rock lithology on vein formation: A stable isotope study from the Paleozoic Ouachita orogenic belt, Arkansas and Oklahoma. *Geological Society of America Bulletin, 114*, 1343-1355.

Roe, N. R. (1955). *Geology of the eastern Potato Hills, Pushmataha and Latimer Counties, Oklahoma* (Master's Thesis). Norman, OK: University of Oklahoma.

Scharon, L., & Hsu, I. (1969) Paleomagnetic investigation of some Arkansas alkali igneous rocks. *Journal of Geophysical Research, 74*, 2774-2779.

Scotese, C. R. (1998). *QuickTime Computer Animations* (PALEOMAP Project). Arlington, TX: University of Texas.

Scotese, C. R., & Golanka, J. (1992). *Paleogeographic Atlas* (PALEOMAP Progress Report 20-0692, 34 p.): Arlington, TX: University of Texas.

Seely, D. R. (1955). Geology of the Talihina area, Pushmataha, Latimer, and LeFlore Counties, Oklahoma (Master's Thesis). Norman, OK: University of Oklahoma.

Sharp Jr., J. M. (1978). Energy and momentum transport model of the Ouachita Basin and its possible impact on formation of economic mineral deposits. *Economic Geology, 73*, 1057-1068.

Shaulis, B. J., Lapen, T. J., Casey, J. F., and Reid, D. R. (2012) Timing and Rates of Flysch Sedimentation In the Stanley Group, Ouachita Mountains, Oklahoma and Arkansas, U.S.A.: Constraints from U-Pb Zircon Ages of Subaqueous Ash-Flow Tuffs. *Journal of Sedimentary Research, 82,* 833-840. https://doi:10.2110/jsr.2012.68

Shelton, K. L., Reader, J. M., Ross, L. M., Viele, G. W., & Seidemann, D. E. (1986). Ba-rich adularia from the Ouachita Mountains, Arkansas: Implications for a postcollisional hydrothermal system. *American Mineralogist, 71,* 916-923.

"Southwest Oklahoma." 34°09'10.00"N and 94°45'00.00"W. **Google Earth.** January 23, 2015. April 25, 2018.

Spötl, C., Houseknecht, D. W., & Jaques R. (1993). Clay mineralogy and illite crystallinity of the Atoka formation, Arkoma Basin, and Frontal Ouachita Mountains. *Clay and Clay Minerals, 41,* 745-754.

Stampfli, G. M., Von Raumer, J. F., & Borel, G. D. (2002). Paleozoic evolution of pre-Variscan terranes: from Gondwana to the Variscan collision. In J. R. Martinez Catalan, R. D. Hatcher, R. Arenas, & F. Diaz Garcia (Eds.), *Variscan-Appalachian dynamics: the building of the Late Paleozoic basement* (Special Paper 364, pp. 263-280). Boulder, CO: Geological Society of America.

Suneson, N. H., Campbell, J. A., & Tilford, M. J. (Eds.). (1990). *Geology and resources of the frontal belt of the western Ouachita Mountains, Oklahoma* (Special Publication 90-1, 196 p.). Norman, OK: Oklahoma Geological Survey.

Suneson, N. H., & Hemish, L. A. (1994). *Geology and resources of the eastern Ouachita Mountains frontal belt and south-eastern Arkoma Basin, Oklahoma* (Guidebook 29, 294 p.). Norman, OK: Oklahoma Geological Survey.

Sutherland, P. K. (1988). Late Mississippian and Pennsylvanian depositional history in the Arkoma basin area, Oklahoma and Arkansas. *Geological Society of America Bulletin, 100,* 1787-1802.

Thomas, W. A. (2011). The Iapetan rifted margin of southern Laurentia. *Geosphere, 7*(1), 97-120.

Thomas, W. A., Tucker, R. D., Astini, R. A., & Denison, R. E. (2012). Ages of pre-rift basement and synrift rocks along the conjugate rift and transform margins of the Argentine Precordillera and Laurentia. *Geosphere, 8*(6), 1366-1383.

Vermeesch, P. (2009). RadialPlotter: A Java application for fission track, luminescence and other radial plots. *Radiation Measurements, 44,* 409-410.

Viele, G. W. (1973). Structure and tectonic history of the Ouachita Mountains, Arkansas. In K. De Jong, & R. Scholten (Eds.), *Gravity and* Tectonics. New York, NY: John Wiley.

Viele, G. W. (1979). Geologic map and cross section, eastern Ouachita Mountains, Arkansas: map summary. *Geological Society of America Bulletin, 90,* 1096-1099.

Viele, G.E. (1989). The Ouachita Orogenic Belt. In R. D. Hatcher Jr., W. A. Thomas, & G. W. Viele (Eds.), *The Appalachian-Ouachita Orogen in the United States, The*

Geology of North America (Vol. F-2, pp. 555–561). Boulder, CO: Geological Society of America.

Viele, G. W., & Thomas, W. A. (1989). Tectonic synthesis of the Ouachita orogenic belt. In R. D. Hatcher Jr., W. A. Thomas, & G. W. Viele (Eds.), *The Appalachian-Ouachita Orogen in the United States, The Geology of North America* (Vol. F-2, pp. 695-728). Boulder, CO: Geological Society of America.

Weaver, C. E. (1960). Possible uses of clay minerals in search of oil. *American Association of Petroleum Geologists Bulletin, 44*, 1505-1518.

White, D. (1915). Some relations in origin between coal and petroleum. *Journal of the Washington Academy of Sciences, 5*, 189-212.

Wiltschko, D. V., & Dorr Jr., J. A. (1983). Timing of deformation in the Overthrust belt and foreland of Idaho, Wyoming, and Utah. *American Association of Petroleum Geologists, 67*, 1304-1322.

Winkler, J. E., Kelley, S. A., & Bergman, S. C. (1999). Cenozoic denudation of the Wichita Mountains, Oklahoma, and southern mid-continent: apatite fission-track thermochronology constraints. *Tectonophysics*, *305*(1-3), 339-353.

Woodward, N. B. (1987) Geological applicability of critical-wedge thrust-belt models. *Geological Society of America Bulletin, 99*, 827-832.

Ziegler, P. A. (1988). Evolution of the Arctic-North Atlantic and the Western Tethys. *American Association of Petroleum Geologists Memoir, 43*, 198 p.

Zimmerman, R. A. (1986). Fission-track dating of samples of the Illinois drill hole core. *United States Geological Survey Bulletin*, *1622*, 100-108.

5. CONCLUSIONS

Zircon and muscovite ages from the detritus of the Mississippian Stanley Group (320.7 ± 2.5 Ma to ca. 330 Ma) within the Ouachita Basin indicate multi-sourced provenance, whereas zircon and muscovite ages from the detritus of the Pennsylvanian Jackfork Group (ca. 310 Ma to ca. 320 Ma) indicate recycling of Laurussian sediments within the proximal Illinois Basin, medial Michigan Basin, and/or distal headwaters originating in the Maritime Province of Canada, and transported by a continental-scale drainage (Michigan River).

Maximum temperature observed within the Ouachita Basin as calculated from both illite and chlorite crystallinity of surface samples is ~300°C. Illite crystallinity is lower for the coarse clay fraction than that of the fine clay fraction. While the reason is not known, the coarse clay fraction may have a greater detrital component than the fine clay fraction meaning the fine clay fraction is more accurately recording the thermal maturation of the Benton Uplift. Regionally, the crystallinity increases toward the central axis of the Benton Uplift and this increase in crystallinity may be explained by the exhumation of the rocks from greater depth. Neither a regional thermal fluid flow event nor significant stacking of thrust sheets is required to explain the values or patterns of metamorphism.

Zircon fission track minimum ages record development of the Ouachita FTB wedge, whereas the (U-Th)/He dates give paleotopography of the critical wedge. The

internal motion of thrusts and folding occurred during Pennsylvanian to Late Permian. Paleotopography slopes forelandward and present-day surface was buried at 9 km during Late Triassic-Middle Jurassic, assuming geothermal gradient of 20°C/km and zircon (U-Th)/He closure of ~180°C. Reset (U-Th)/He dates in the Arkoma Basin correspond to anomalous high maturation; these thermochronologic dates record a second Triassic thermal (fluid flow) event, which exceeded 180°C.

Inactive FTBs did have the critical taper wedge predicted by the wedge paradigm, and as shown by the trend line of the (U-Th)/He dates of the Ouachita FTB that slopes forelandward. Thermal maturation, coupled with low-temperature thermochronometry, and use of the wedge model paradigm together, allows for robust observation of ancient FTBs by indirectly creating better structural interpretations, especially where internal (subsurface) structures are poorly known.

APPENDIX A

MANUSCRIPT #1: FIGURES/TABLES

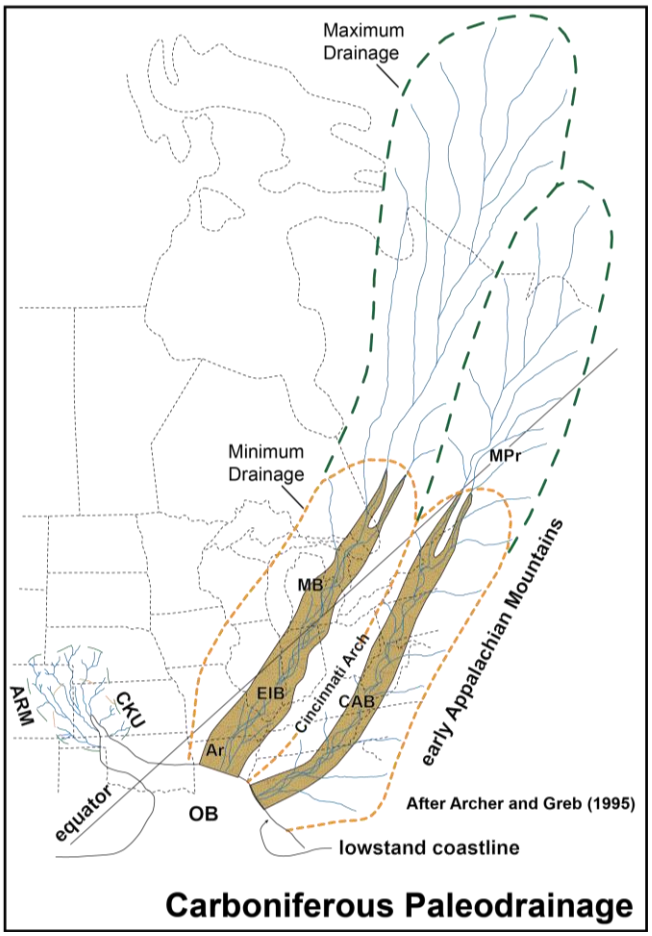

Figure 1. Carboniferous paleodrainage, after Archer and Greb (2005), suggests two major, continental-scale rivers based on preserved basal sandstones, including Lee sandstones (Central Appalachian Basin), Caseyville and equivalent sandstones (Eastern Interior Basin), and Morrow sandstones (Hugoton Embayment). Sedimentary data constraints are from Chesnut (1988) and Swanson (1979). Paleoequator position given in Witzke (1990). Abbreviations -- Ar, Arkansas outcrops of Bloyd Sandstone; ARM, Ancestral Rocky Mountains; CAB, Central Appalachian Basin; CKU, Central Kansas Uplift; EIB, Eastern Interior Basin; MB, Michigan Basin; MPr, Maritime Provinces of Canada; OB, Ouachita Basin. Potential minimum and maximum drainage basins are shown by a dashed line, with northeastward coastline migration across the Appalachian Basin during relatively higher sea-level.

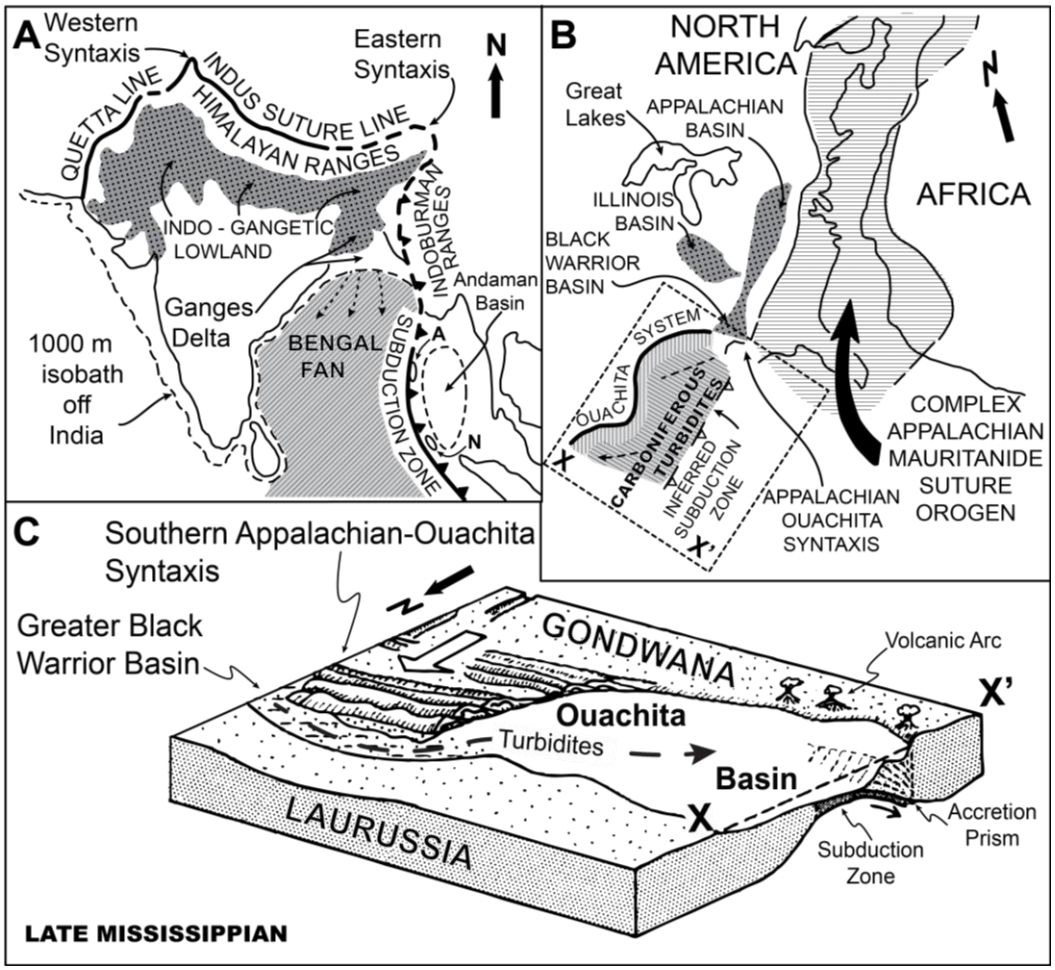

Figure 2. Tectonic map of Cenozoic Himalayan-Bengal system (A) is compared as an analogous tectonic setting at same scale to Appalachian-Ouachita system during the Carboniferous (B; after Graham et al., 1975; 1976). Shallow marine and non-marine depocenters are stippled. Turbidite fans, located in deep-water, are found in area outlined by diagonal line pattern. The Andaman – Nicobar subduction zone, labeled as A and N, is west of the Andaman Basin in the Himalayan-Bengal system. This Cenozoic subduction zone is analogous to the inferred subduction zone to southeast of the Ouachita Basin (C); this zone with the accretionary prism is shown in cross section X-X'. Diagonal lines indicate present-day position of turbidite deposits adjacent to Ouachita thrust front. Idealized block model (C) for Ouachita Basin (location outlined with dashed line in B) during Late Mississippian illustrating sediment input from the Appalachians and through Greater Black Warrior Basin located at Southern Appalachian-Ouachita Syntaxis. Additional sediments may be cratonic from Laurussia and/or Gondwana. Inferred subduction zone with accretionary prism shown in cross section X-X'.

Figure 3. Plate tectonic setting of North America during the Carboniferous. A) Explanation of elements in the plate tectonic maps. B) Late Mississippian. C) Late Pennsylvanian. These maps were created by Miall (2019) using data and ideas from Cook and Bally (1975), Ziegler (1988), Scotese (1998), Scotese and Golanka (1992), and Stampfli et al. (2002). Abbreviations -- AFR, Africa; ANT, Antler terrane; ARM, Ancestral Rocky Mountains; BAL, Baltica; FLA, Florida; GRN, Greenland; HUN, Hunic terranes; NAM, North America (Laurentia); NSL, North slope (Alaska); SAM, South America; YUC, Yucatan. D) Tectonic overview map for the southern margin of North America (modified from Viele and Thomas, 1989). Study area is outlined. Traverse between Arkoma (Ouachita) Basin and Black Warrior Basin is shown as line between positions A and B. Borehole locations are shown with filled triangle and labeled with core abbreviations: B, Brooks; H, Hendrix (Moore, 2012). Abbreviations -- AtF, Appalachian tectonic front; Fb, Frontal belt. Basins: Ab, Arkoma; BWb, Black Warrior; Db, Delaware; FWb, Fort Worth; Kb, Kerr; VVb, Val Verde. Platforms: CBp, Central Basin; Op, Ozark; Tp, Texarkana. Mountains: AM, Arbuckle; WM, Wichita. Uplifts: BBu, Broken Bow; Bu, Benton; DRu, Devil's River; Lu, Llano; Mu, Marathon; Su, Sabine. E) Stratigraphic correlation of Carboniferous strata between Ouachita Basin and proximal Greater Black Warrior Basin. Each basin has two columns, relative time and relative thickness, for stratigraphy to illustrate change in sedimentation accumulation rate across Mississippian-Pennsylvanian boundary (Thomas, 1972; Stone et al., 1981; Hatch, 2007; Pashin and Gastaldo, 2009). Traverse A-B is shown on D.

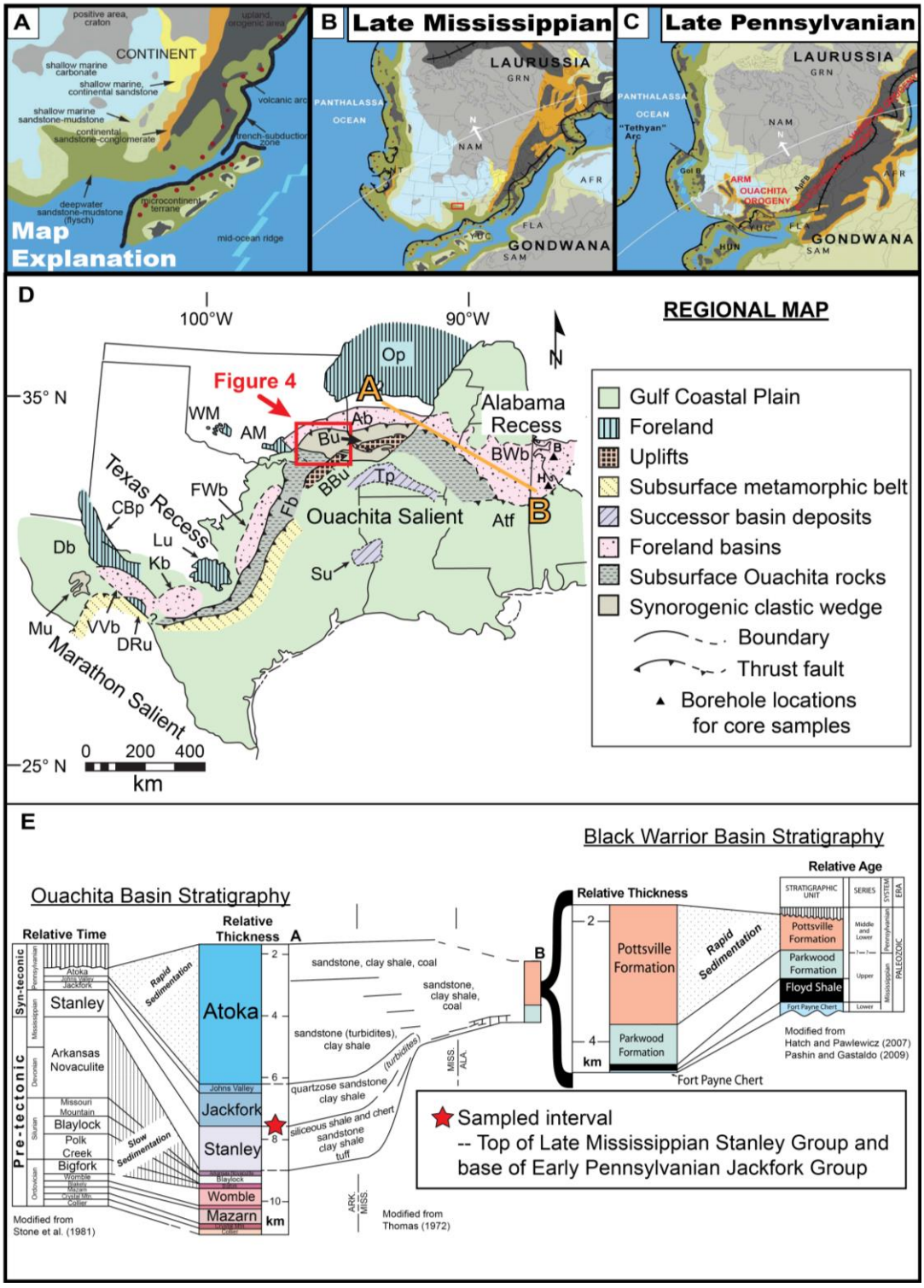
A
positive area, craton
upland, orogenic area
CONTINENT
shallow marine carbonate
shallow marine, continental sandstone
volcanic arc
shallow marine sandstone-mudstone
continental sandstone-conglomerate
trench-subduction zone
deepwater sandstone-mudstone (flysch)
microcontinent terrane
mid-ocean ridge
Map Explanation
B Late Mississippian
LAURUSSIA
GRN
PANTHALASSA OCEAN
NAM
AFR
FLA
GONDWANA
SAM
C Late Pennsylvanian
"Tethyan" Arc
ARM
OUACHITA OROGENY
HUN
D
100°W
90°W
35° N
25° N
0 200 400
km
N
Figure 4
A
B
Op
WM
AM
Bu
Ab
Alabama Recess
BWb
Texas Recess
FWb
CBp
BBu
Tp
Fb
Ouachita Salient
Atf
Db
Lu
Kb
Su
Mu
VVb
DRu
Marathon Salient
REGIONAL MAP
Gulf Coastal Plain
Foreland
Uplifts
Subsurface metamorphic belt
Successor basin deposits
Foreland basins
Subsurface Ouachita rocks
Synorogenic clastic wedge
Boundary
Thrust fault
Borehole locations for core samples
E
Ouachita Basin Stratigraphy
Relative Time
Relative Thickness
A
B
Syn-tectonic
Pre-tectonic
Atoka
Stanley
Arkansas Novaculite
Missouri Mountain
Blaylock
Polk Creek
Bigfork
Womble
Mazarn
Jackfork
Johns Valley
Rapid Sedimentation
Slow Sedimentation
sandstone, clay shale, coal
sandstone, clay shale, coal
sandstone (turbidites), clay shale
(turbidites)
quartzose sandstone clay shale
siliceous shale and chert
sandstone
clay shale
tuff
MISS. ALA.
ARK. MISS.
km
Modified from Stone et al. (1981)
Modified from Thomas (1972)
Black Warrior Basin Stratigraphy
Relative Age
Relative Thickness
Pottsville Formation
Parkwood Formation
Floyd Shale
Fort Payne Chert
Rapid Sedimentation
STRATIGRAPHIC UNIT
SERIES
SYSTEM
ERA
Middle and Lower
Upper
Lower
Pennsylvanian
Mississippian
PALEOZOIC
Modified from Hatch and Pawlewicz (2007) Pashin and Gastaldo (2009)
Sampled interval
-- Top of Late Mississippian Stanley Group and base of Early Pennsylvanian Jackfork Group

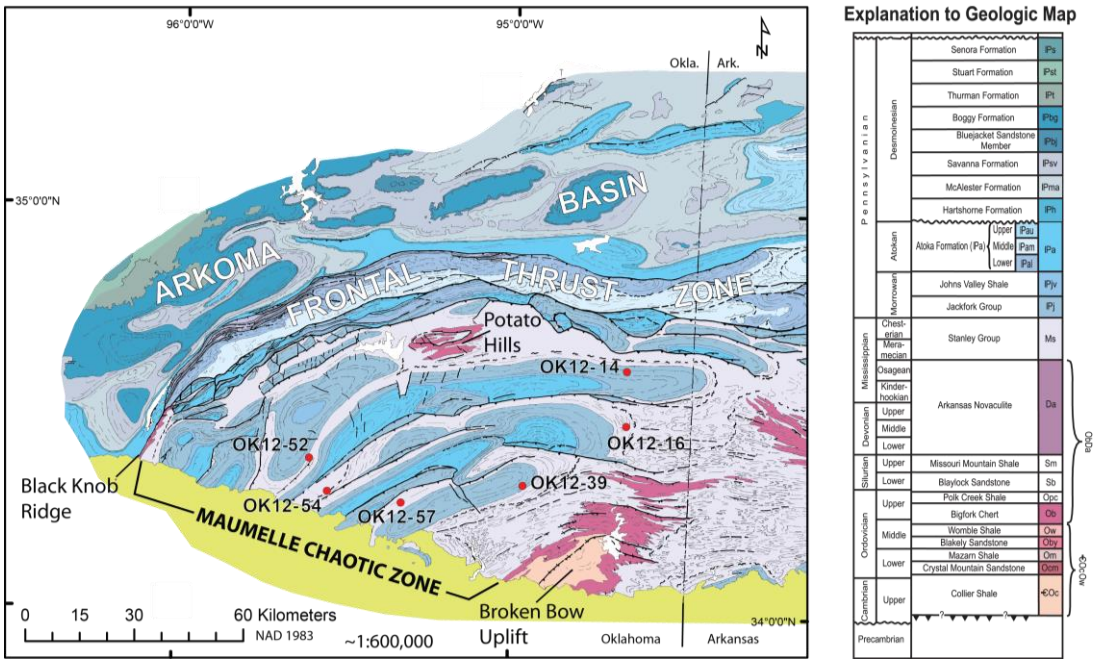

Figure 4. Sample locations in South-Eastern Oklahoma shown on simplified geologic map adapted from Arbenz (2008). Bulk sandstone collected at location marked by filled red dot. Sample number reference is "OK" = Oklahoma, "12" = 2012 collection year, and last number is sample identification. All samples are available in the SESAR database. Surface geology modified from Haley et al., 1976; Stone et al., 1986; Johnson, 1988; Suenson et al., 1990; Suneson et al., 1994; Arbenz, 2008). Areas with sparse surface information or lack of space at this map scale have formations combined and youngest stratigraphy represented. Major tectonic features shown are Black Knob Ridge, Potato Hills, and Broken Bow Uplift.

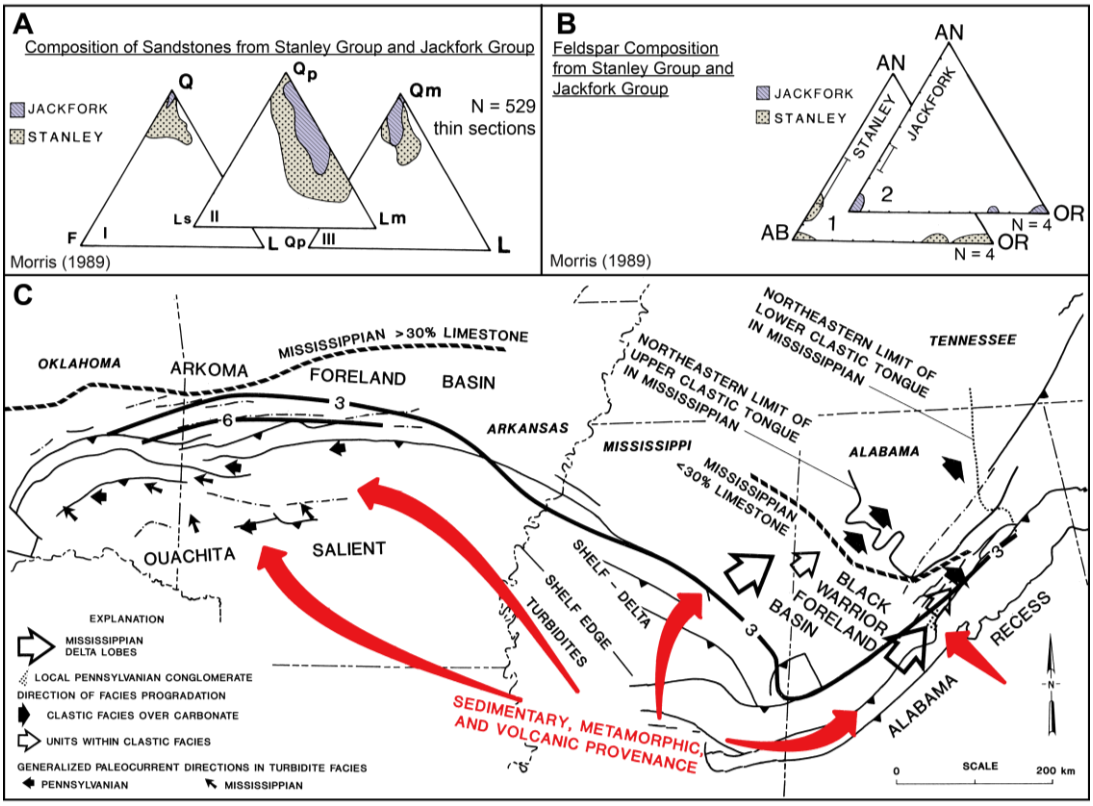

Figure 5. Published Ouachita sandstone petrography of the Stanley and Jackfork Groups (Morris, 1971; Morris, 1974a; Morris, 1974b; Morris et al., 1974; Morris, 1977; Morris et al., 1979; Morris, 1989). A) Petrographic analyses of Stanley (stippled) and Jackfork (diagonal lines) sandstones based on n = 529 thin sections: I, Q-F-L plot of quartz (Q), feldspars (F), and lithic fragments (L); II, Qp-Ls-Lm plot of polycrystalline quartz (Qp), sedimentary lithic fragments (Ls), and metamorphic lithic fragments (Lm); III, Qm-Qp-L plot of monocrystalline quartz (Qm), polycrystalline quartz (Qp), and lithics (L). B) Feldspar composition of Stanley sandstones (N = 4) and Jackfork sandstones (N = 4) determined with microprobe coupled with energy-dispersive spectrometry (MC-EDS). Plagioclase composition, determined optically using the Michel-Levy method from same rocks, are plotted as filled bars. Abbreviations -- AB, albite; AN, anorthoclase; AR, Arkansas; OK, Oklahoma; OR, orthoclase. C) Carboniferous isopach contour values for Ouachita clastic wedge given in kilometers (modified from Hatcher et al, 1989). During Mississippian, the upper part of Ouachita clastic wedge progrades to the northeast and merges with the southwest prograding Pennington-Lee clastic wedge. Paleocurrent indicators and orientation of delta lobes have both a north-eastward and westward sediment dispersal from the south (red arrows) during the Carboniferous.

Figure 6. A) Normalized detrital zircon U-Pb age Kernal Density Estimate (KDE) plots for 4 Mississippian Stanley Group samples and 2 Pennsylvanian Jackfork Group samples covering 0 - 4000 Ma. All y-axes are number of zircons and have the same scale because the plots have been normalized. Plots used KDE bandwidth of 10 m.y. for distribution curves (Vermeesch, 2012); n is the number of grains analyzed with less than 10% discordance on grains younger than 1000 Ma and less than 20% on grains older than 1000 Ma. Geochronologic provinces: A, Appalachian-Ouachita (280-500 Ma); B, Pan-Africa (500-700 Ma); C, Grenville (950-1300 Ma); D, Midcontinent (1300-1500 Ma); E, Yavapai-Mazatzal (1600-1800 Ma); F, Shield (>1800 Ma). Depositional age (not shown) for the Stanley Group is ~ 323 Ma and ~ 310-320 Ma for the overlying Jackfork Group (Arbenz, 1989; Shaulis et al., 2012). Sample locations are shown in Figure 4. U-Pb data are provided in Appendix A. B) Cumulative probability curves of detrital muscovite ages. Detrital muscovite ages from 1 Stanley Group sample (OK12-54) and 1 Jackfork Group sample (OK12-39). Argon data are provided in Appendix B. C) Detrital muscovite grain ages with 1σ error, from youngest to oldest; n is the number of grains analyzed. D) Normalized detrital muscovite laser $^{40}Ar/^{39}Ar$ age KDE plots from 300 Ma to 550 Ma. A bandwidth of 2 m.y. was used to construct both plots (Vermeesch, 2012). The Appalachian-Ouachita geochronologic province includes three major orogenic events: A1, Alleghanian (265-327 Ma); A2, Acadian (350-380 Ma); A4, Taconic (440-465). Province B is Pan-Africa (500-700 Ma). Two muscovite grain ages for OK12-39 are older than 550 Ma and these ages are not represented in the KDE plot.

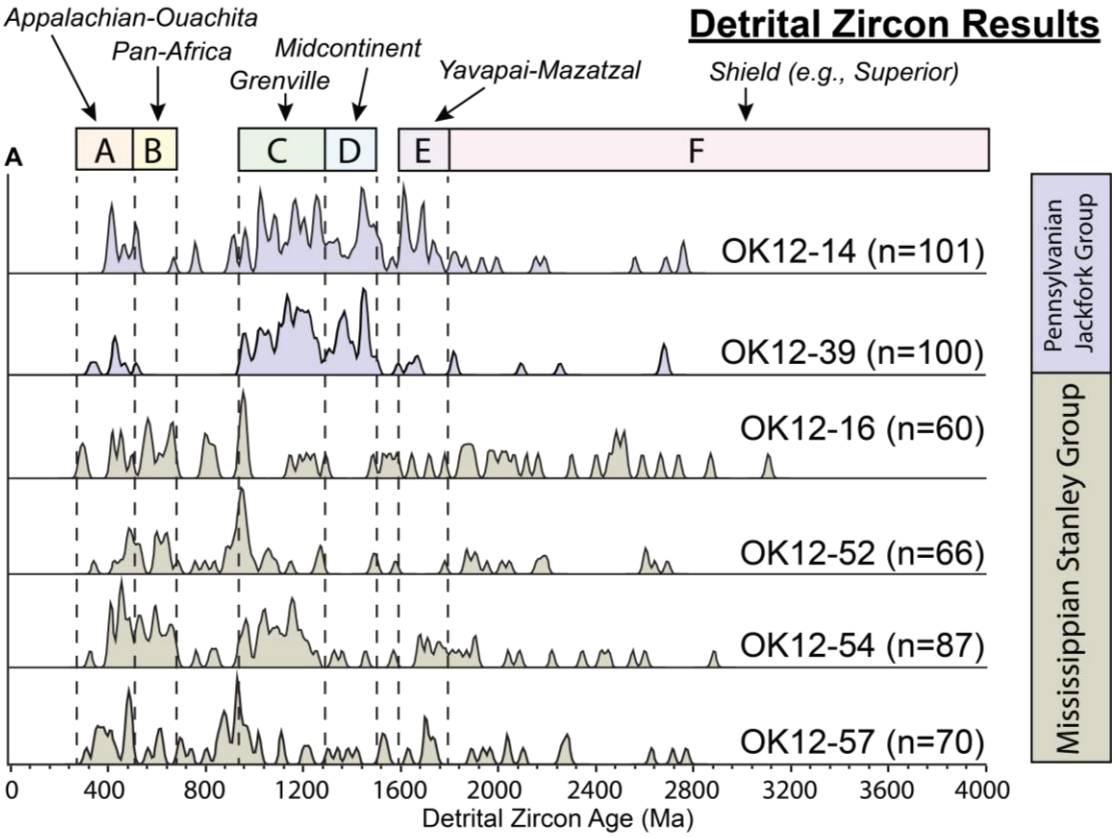
Detrital Zircon Results
Appalachian-Ouachita
Pan-Africa
Midcontinent
Grenville
Yavapai-Mazatzal
Shield (e.g., Superior)
A
A
B
C
D
E
F
OK12-14 (n=101)
OK12-39 (n=100)
OK12-16 (n=60)
OK12-52 (n=66)
OK12-54 (n=87)
OK12-57 (n=70)
Pennsylvanian Jackfork Group
Mississippian Stanley Group
0
400
800
1200
1600
2000
2400
2800
3200
3600
4000
Detrital Zircon Age (Ma)

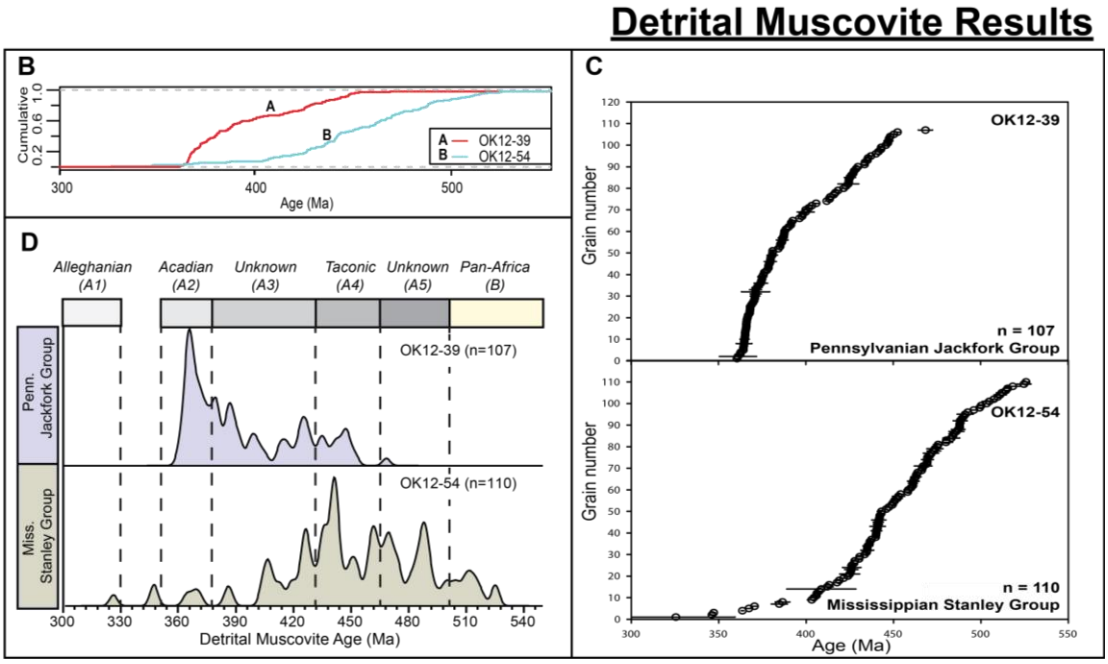
Detrital Muscovite Results
B
Cumulative
0.2
0.6
1.0
A
B
A OK12-39
B OK12-54
300
400
500
Age (Ma)
C
OK12-39
Grain number
n = 107
Pennsylvanian Jackfork Group
OK12-54
n = 110
Mississippian Stanley Group
300
350
400
450
500
550
Age (Ma)
D
Alleghanian (A1)
Acadian (A2)
Unknown (A3)
Taconic (A4)
Unknown (A5)
Pan-Africa (B)
Penn. Jackfork Group
Miss. Stanley Group
OK12-39 (n=107)
OK12-54 (n=110)
300
330
360
390
420
450
480
510
540
Detrital Muscovite Age (Ma)

Figure 7. Eastern North America basement provinces for Laurentian continental crust traversing the Canadian shield to Grenville. (Hoffman, 1989; Van Schmus et al., 1993; modified from Thomas et al., 2004). Approximate location of samples used in this study from the Stanley and Jackfork Groups are indicated by filled black triangle. Samples locations as presented by Thomas et al. (2004) shown in both present and palinspastic locations. Additional sample locations shown are from Northwest Arkansas (Xie et al., 2016b), Newfoundland (McLennan et al., 2001), and these basins: Illinois (Kissock, 2016), Ouachita (Gleason et al., 2001), Black Warrior (Becker et al., 2005; Xie et al., 2016a), Appalachian (Gray and Zeitler, 1997; Eriksson et al., 2004; Thomas et al., 2004; Becker et al., 2005; Park et al., 2010), and New England Foreland (Gray and Zeitler, 1997; McLennan et al., 2001). High sample density in the Appalachian Basin necessitated locality delineation by group on the figure. Bold letters on shaded basement indicate corresponding component to U-Pb zircon age populations of Laurentian crust.

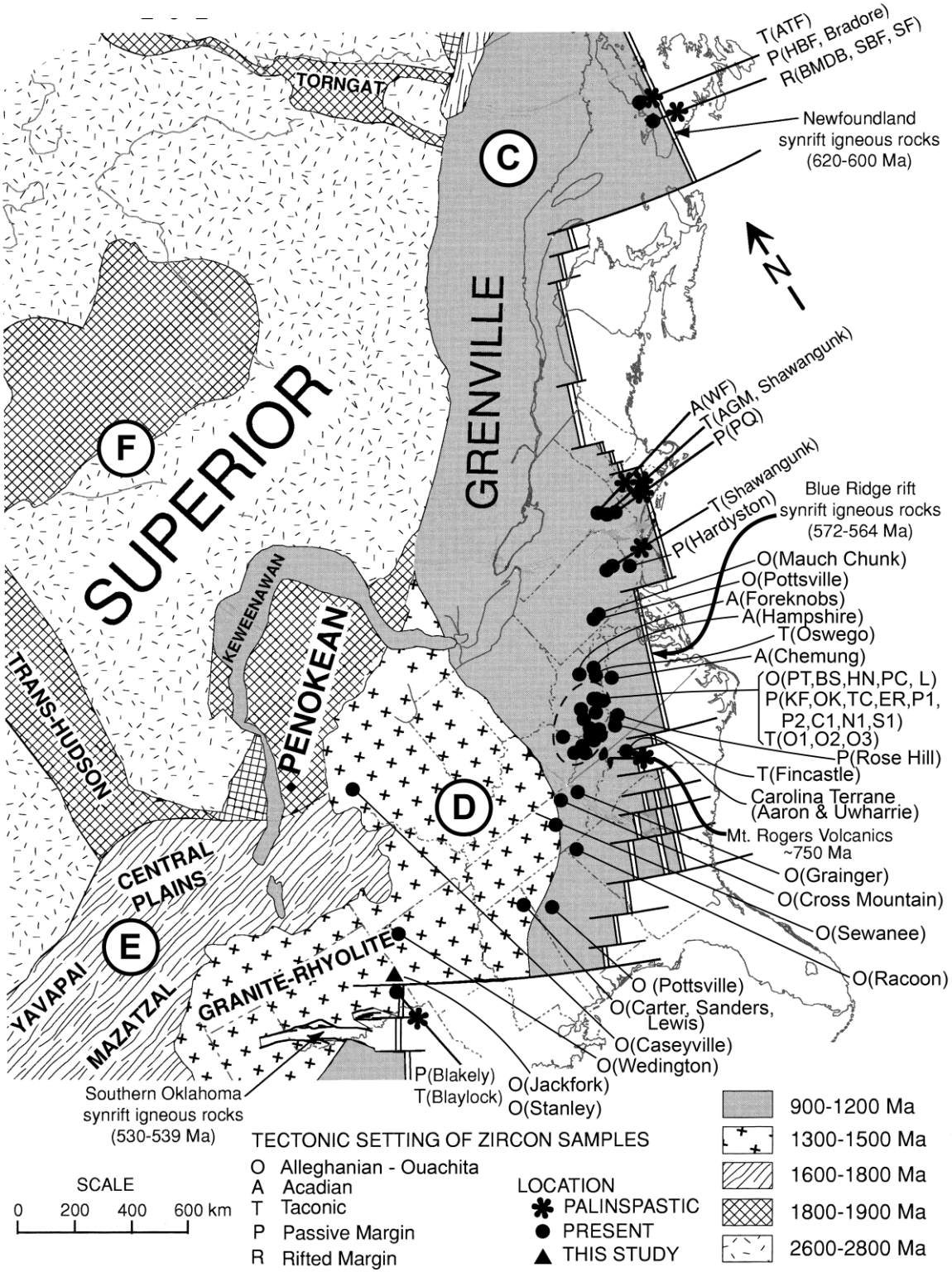
TORNGAT
C
GRENVILLE
SUPERIOR
F
KEWEENAWAN
PENOKEAN
TRANS-HUDSON
CENTRAL PLAINS
D
E
YAVAPAI
MAZATZAL
GRANITE-RHYOLITE
T(ATF)
P(HBF, Bradore)
R(BMDB, SBF, SF)
Newfoundland synrift igneous rocks (620-600 Ma)
N
A(WF)
T(AGM, Shawangunk)
P(PQ)
T(Shawangunk)
P(Hardyston)
Blue Ridge rift synrift igneous rocks (572-564 Ma)
O(Mauch Chunk)
O(Pottsville)
A(Foreknobs)
A(Hampshire)
T(Oswego)
A(Chemung)
O(PT,BS,HN,PC, L)
P(KF,OK,TC,ER,P1, P2,C1,N1,S1)
T(O1,O2,O3)
P(Rose Hill)
T(Fincastle)
Carolina Terrane (Aaron & Uwharrie)
Mt. Rogers Volcanics ~750 Ma
O(Grainger)
O(Cross Mountain)
O(Sewanee)
O(Racoon)
O (Pottsville)
O(Carter, Sanders, Lewis)
O(Caseyville)
O(Wedington)
P(Blakely)
T(Blaylock)
O(Jackfork)
O(Stanley)
Southern Oklahoma synrift igneous rocks (530-539 Ma)
SCALE
0 200 400 600 km
TECTONIC SETTING OF ZIRCON SAMPLES
O Alleghanian - Ouachita
A Acadian
T Taconic
P Passive Margin
R Rifted Margin
LOCATION
PALINSPASTIC
PRESENT
THIS STUDY
900-1200 Ma
1300-1500 Ma
1600-1800 Ma
1800-1900 Ma
2600-2800 Ma

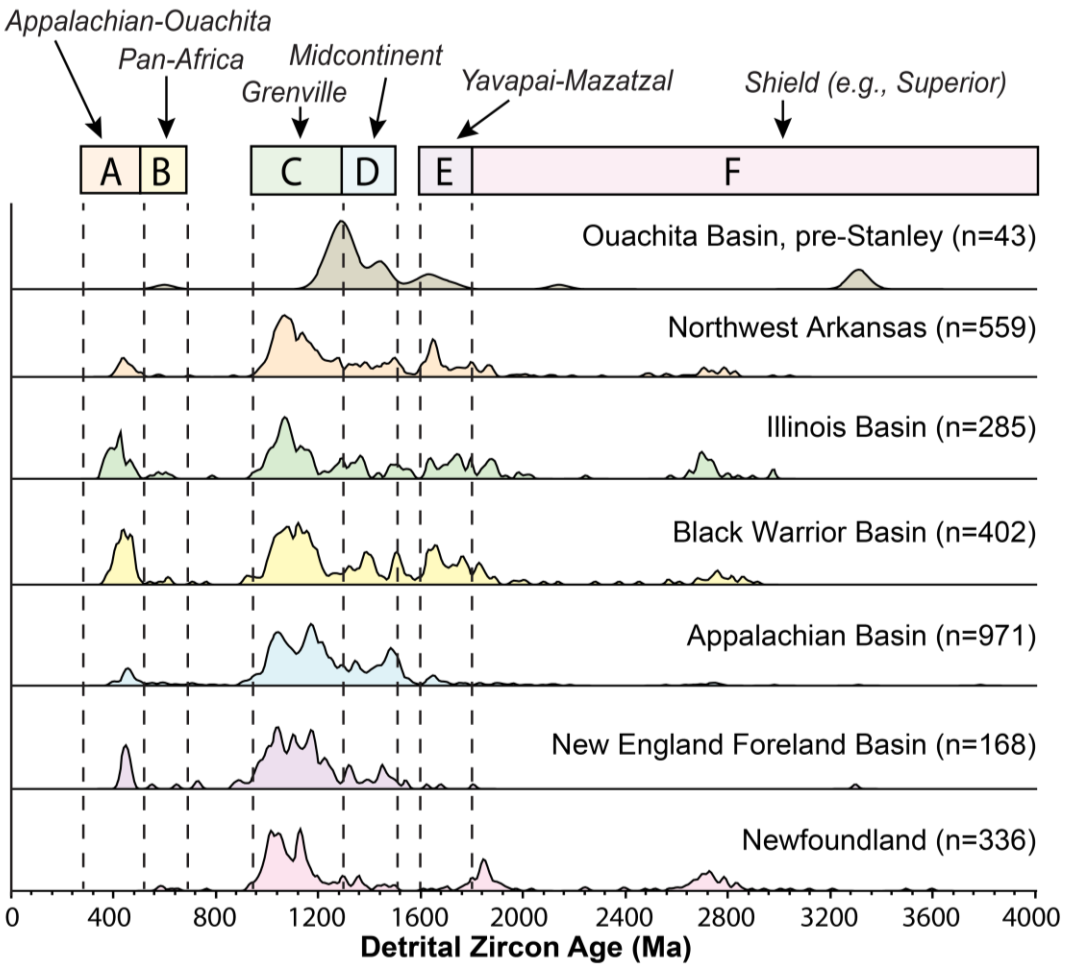

Figure 8. Normalized detrital zircon U-Pb age KDE plots for Ouachita Basin (Gleason et al., 2001; Shaulis et al., 2012), Northwest Arkansas (Xie et al., 2016b), Illinois Basin (Kissock, 2016), Black Warrior Basin (Becker et al., 2005; Xie et al., 2016a), Appalachian Basin (Gray and Zeitler, 1997; Eriksson et al., 2004, Thomas et al., 2004; Becker et al., 2005; Park et al., 2010), Newfoundland (Cawood and Nemchin, 2001), and New England Foreland Basin (Gray and Zeitler, 1997; McLennan et al., 2001). See Figure 6A for additional details. Individual KDE sample plots by each basin are in supplementary Figures 6-11.

Figure 9. Normalized detrital muscovite $^{40}Ar/^{39}Ar$ age KDE plots for surface and core samples of the Greater Black Warrior Basin (includes adjacent smaller-sized Cahaba and Coosa basins; Moore, 2012; Uddin et al., 2016). The Mary Lee Coal Zone is plotted twice because it is stratigraphically positioned in each core as shown, as surface sample is older than Brooks (BC) and Hendrix (HC) cores. Approximate deposition age is given by previous published work shown as solid black line for each sample. Locations of boreholes are indicated on Figure 3D, with KDE explanation in Figure 6D.

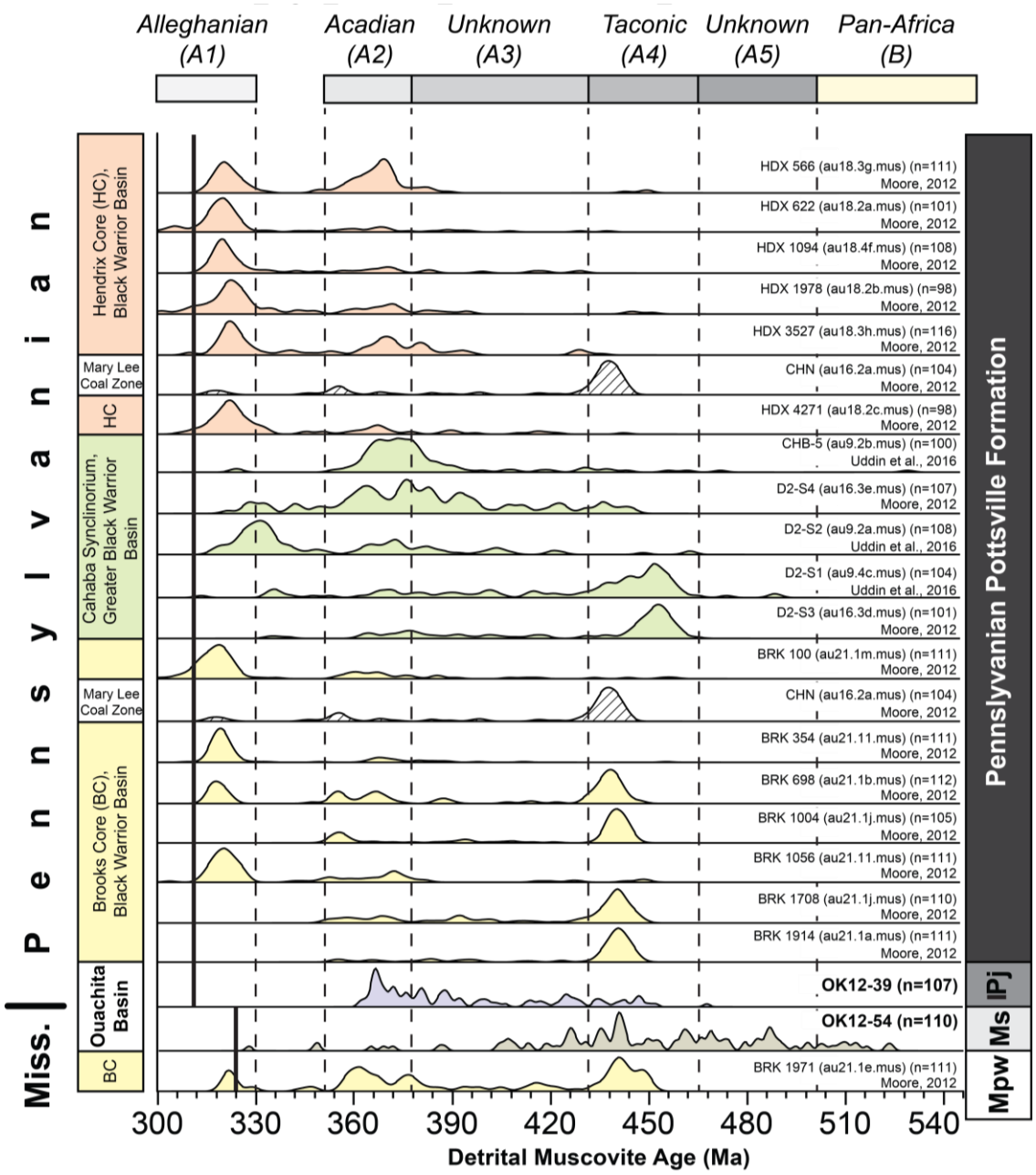
Alleghanian (A1)
Acadian (A2)
Unknown (A3)
Taconic (A4)
Unknown (A5)
Pan-Africa (B)
Miss.
Pennsylvanian
Hendrix Core (HC), Black Warrior Basin
Mary Lee Coal Zone
HC
Cahaba Synclinorium, Greater Black Warrior Basin
Mary Lee Coal Zone
Brooks Core (BC), Black Warrior Basin
Ouachita Basin
BC
HDX 566 (au18.3g.mus) (n=111) Moore, 2012
HDX 622 (au18.2a.mus) (n=101) Moore, 2012
HDX 1094 (au18.4f.mus) (n=108) Moore, 2012
HDX 1978 (au18.2b.mus) (n=98) Moore, 2012
HDX 3527 (au18.3h.mus) (n=116) Moore, 2012
CHN (au16.2a.mus) (n=104) Moore, 2012
HDX 4271 (au18.2c.mus) (n=98) Moore, 2012
CHB-5 (au9.2b.mus) (n=100) Uddin et al., 2016
D2-S4 (au16.3e.mus) (n=107) Moore, 2012
D2-S2 (au9.2a.mus) (n=108) Uddin et al., 2016
D2-S1 (au9.4c.mus) (n=104) Uddin et al., 2016
D2-S3 (au16.3d.mus) (n=101) Moore, 2012
BRK 100 (au21.1m.mus) (n=111) Moore, 2012
CHN (au16.2a.mus) (n=104) Moore, 2012
BRK 354 (au21.11.mus) (n=111) Moore, 2012
BRK 698 (au21.1b.mus) (n=112) Moore, 2012
BRK 1004 (au21.1j.mus) (n=105) Moore, 2012
BRK 1056 (au21.11.mus) (n=111) Moore, 2012
BRK 1708 (au21.1j.mus) (n=110) Moore, 2012
BRK 1914 (au21.1a.mus) (n=111) Moore, 2012
OK12-39 (n=107)
OK12-54 (n=110)
BRK 1971 (au21.1e.mus) (n=111) Moore, 2012
Pennsylvanian Pottsville Formation
Pj
Ms
Mpw
300
330
360
390
420
450
480
510
540
Detrital Muscovite Age (Ma)

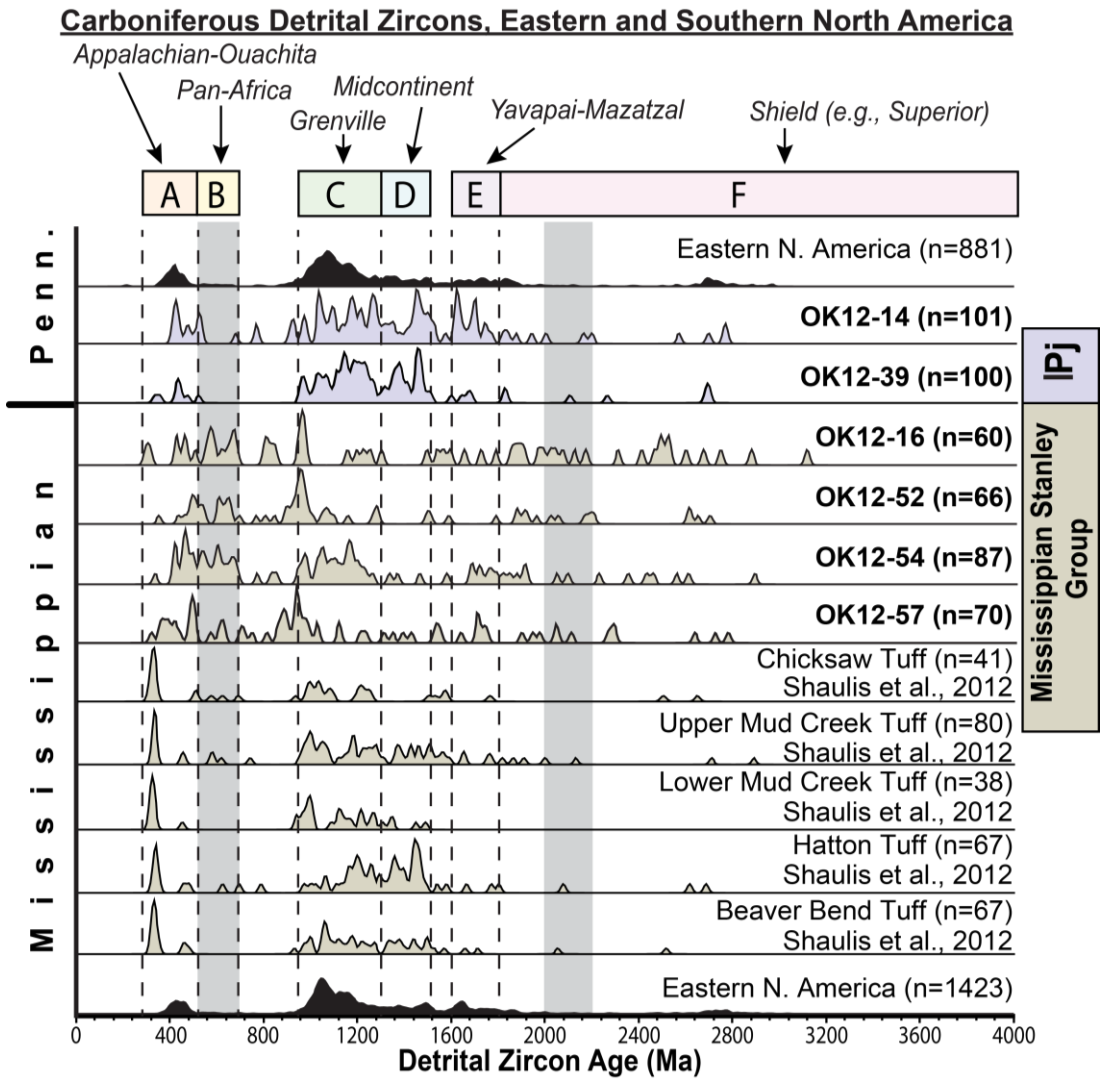

Figure 10. Comparison of published (combined by age) and new normalized detrital zircon U-Pb age KDE plots for Carboniferous stratigraphy in eastern and southern North America (Gray and Zeitler, 1997; Eriksson et al., 2004; Thomas et al., 2004; Becker et al., 2005; Park et al., 2010; Shaulis et al., 2012; Xie et al., 2016b). References are previously published Carbonifereous geochronologic data of Eastern North America, excluding the Ouachita Basin, as shown in black filled plots. Shaded plots are U-Pb data from the Stanley (tan) and Jackfork (violet) Groups are from Shaulis et al. (2012) and this study. See supplemental Figure 12 for individual KDEs by sample, rather than by a combined representation. Additional explanation in Figure 6A.

Figure 11. KDE plots of combined detrital U-Pb data from all samples of the Stanley and Jackfork Groups, with province indicated, along with crystallization and detrital zircon ages of peri-Gondwanan terranes and Laurentian crust (modified after Becker et al., 2005). Composite zircons ages are from peri-Gondwanan terranes (Mueller et al., 1994; Ingle-Jenkins et al., 1998; Coler and Samson, 2000; Wortman et al., 2000; Samson et al., 2001) and Laurentian crust (Hoffman, 1989; Van Schmus et al, 1993; Aleinikoff et al., 1995). Blue bar above each plot indicates the presence or higher abundance of detrital zircon ages when comparing the Stanley and Jackfork groups. KDE explanation is in Figure 6A and U-Pb data are in supplementary reference material.

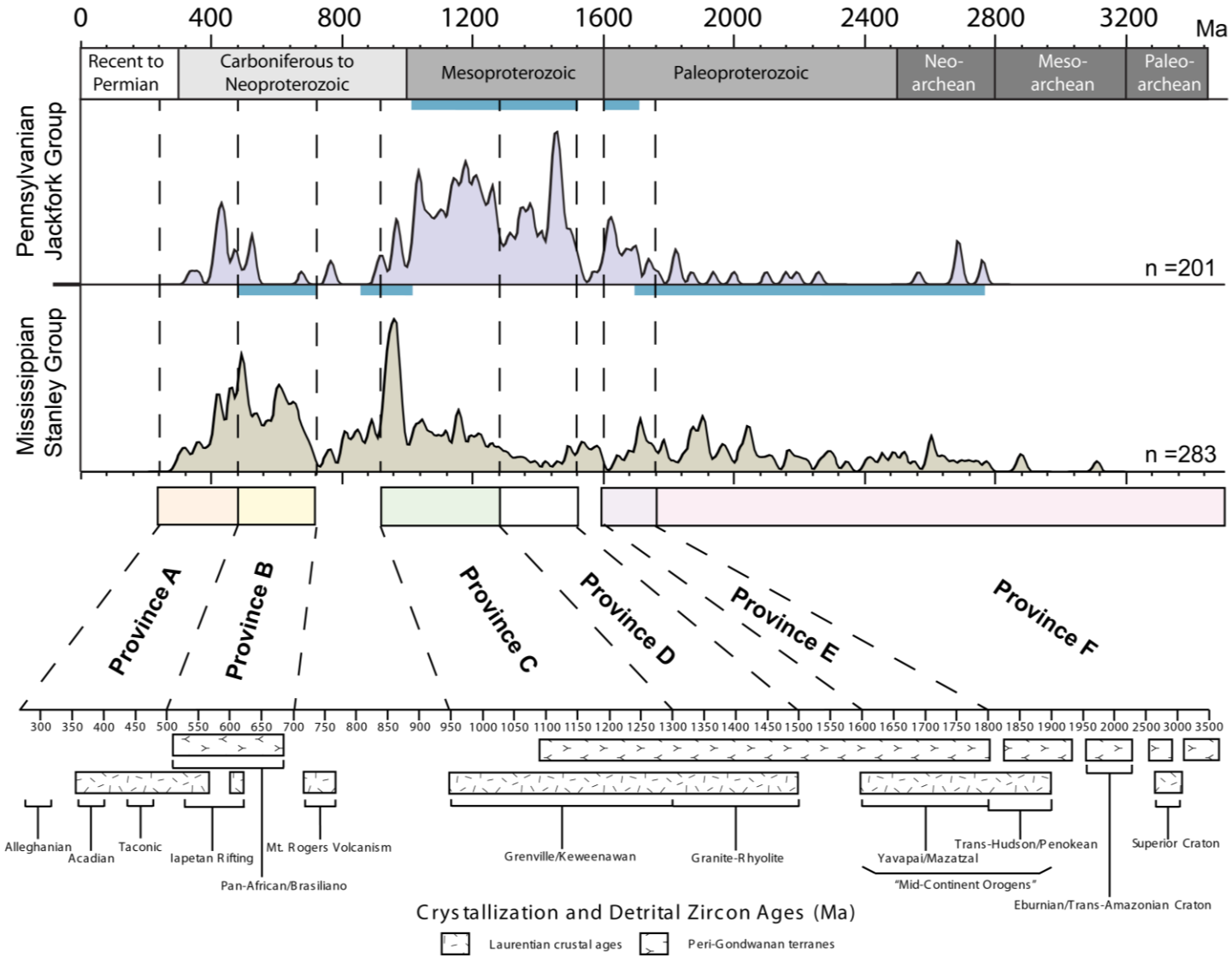
0
400
800
1200
1600
2000
2400
2800
3200
Ma
Recent to Permian
Carboniferous to Neoproterozoic
Mesoproterozoic
Paleoproterozoic
Neo-archean
Meso-archean
Paleo-archean
Pennsylvanian Jackfork Group
n =201
Mississippian Stanley Group
n =283
Province A
Province B
Province C
Province D
Province E
Province F
300 350 400 450 500 550 600 650 700 750 800 850 900 950 1000 1050 1100 1150 1200 1250 1300 1350 1400 1450 1500 1550 1600 1650 1700 1750 1800 1850 1900 1950 2000 2500 3000 3500
Alleghanian
Acadian
Taconic
Iapetan Rifting
Mt. Rogers Volcanism
Pan-African/Brasiliano
Grenville/Keweenawan
Granite-Rhyolite
Yavapai/Mazatzal
Trans-Hudson/Penokean
"Mid-Continent Orogens"
Eburnian/Trans-Amazonian Craton
Superior Craton
Crystallization and Detrital Zircon Ages (Ma)
Laurentian crustal ages
Peri-Gondwanan terranes

Figure 12. Multidimensional scaling (MDS) zircon plots based on distributional datasets and Kolmogorov-Smirnov dissimilarity, where the axes are dissimilarities measured between plotted samples. 'Provenance' in R programming environment is used to construct MDS plots for visualization and interpretation (Vermeech et al., 2016). Solid lines connect nearest-neighbors, whereas dashed lines connect second nearest-neighbors. Suggested groups of similar samples are shown by thick outline and labeled with roman numerals. A) Ouachita detrital zircon samples. Unfilled circles denote Mississippian Stanley Group samples (N = 4), and filled circles indicate Pennsylvanian Jackfork Group samples (N = 2). The first group (denoted by roman numeral 'I') is both Jackfork samples (filled dots) and sample OK12-54 from the Stanley Group (unfilled dot). B) Carboniferous detrital zircon samples from Ouachita Basin (N = 6), Illinois Basin (N = 1), Northwest Arkansas (N = 6) and Black Warrior Basin (N = 5; Becker et al., 2005; Kissock, 2016; Xie et al., 2016a; Xie et al., 2016b). Unfilled circles are Mississippian samples and filled circles are Pennsylvanian samples. C) Carboniferous detrital zircon samples for eastern North America. Filled circles represent all of the Ouachita samples, either Stanley (N = 4) or Jackfork (N = 2). Unfilled circles are detrital zircon samples from Appalachian Basin (N = 15), Black Warrior Basin (N = 6), Illinois Basin (N = 1), and Northwest Arkansas (N = 6; Gray and Zeitler, 1997; Eriksson et al., 2004; Thomas et al., 2004; Becker et al., 2005; Park et al., 2010; Shaulis et al., 2012; Xie et al., 2016b). D) Detrital zircon samples for eastern North America. Filled circles represent all of the Ouachita samples, either Stanley (N = 4) or Jackfork (N = 2). Unfilled circles are detrital zircon samples from Appalachian Basin (N = 33), Black Warrior Basin (N = 6), Illinois Basin (N = 1), Northwest Arkansas (N = 6), New England Foreland Basin (N = 5), Newfoundland (N = 6), and Ouachita Basin (N =2, excludes samples of this study; Gray and Zeitler, 1997; Gleason et al., 2001; Eriksson et al., 2004; Thomas et al., 2004; Becker et al., 2005; Park et al., 2010; Shaulis et al., 2012; Xie et al., 2016b). Sample/formation notation explanation – A, OK12-14; B, OK12-16; C, OK12-39; D, OK12-52; E, OK12-54; F, OK12-57; G, Bluestone; H, Princeton; I, Hinton; J, Mauch Chunk; K, Grainger; L, Price Sandstone; M, Hampshire; N, Chemung; O, Foreknobs; P, Oriskany; Q, Keefer; R, Rose Hill; S, Tuscarora; T, Oswego; U, Fincastle Member, Martinsburg Fm.; V, Aaron and Uwharrie; W, Uncoi; X, Erwin; Y, Hardyston; Z, Clasts in Bays Fm. (O1); a, Clasts in Bays Fm. (O2); b, Clasts in Bays Fm. (O3); c, Eagle Rock; d, Cloyd Conglomerate, Chemung Fm.; e, Lower Raleigh Sandstone, New River Fm.; f, Upper Raleigh Sandstone, New River Fm.; g, Sewanee Conglomerate; h, Cross Mountain; i, Shawangunk (Gray and Zeitler, 1997); j, Sharp Mountain Member, Pottsville Fm.; k, Poughquag Quartzite; l, Austin Glen Member, Normanskill Fm.; m, Shawangunk (McLennan et al., 2001); n, Walton Fm., Catskill Group; o, South Brook; p, Summerside; Q, Bradore; r, Hawke Bay; s, American Tickle; t, Caseyville; u, Lewis; v, Sanders; w, Carter Sandstone I; x, Carter Sandstone II; y, WD-1 (WD denotes Wedington Sandstone Member, Fayetteville Shale); z, WD-2;

Aa, WD-3; Bb, WD-5; Cc, WD-6; Dd, WD-8; Ee, Tumbling Run Member, Pottsville Fm.; Ff, Pottsville Fm., central Pennsylvania; Gg, Pocahontas; Hh, Lee; Ii, Raccoon Mountain; Jj, Montevallo coal zone, Pottsville Fm; Kk, Chicksaw Tuff, Stanley Group; Ll, Upper Mud Creek Tuff, Stanley Group; Mm, Lower Mud Creek Tuff, Stanley Group; Nn, Hatton Tuff, Stanley Group; Oo, Beaver Bend Tuff, Stanley Group. Sample locations provided in Figures 4 and 7. Normalized KDE combined plots for basins of eastern North America are presented in Figure 8, and for the Ouachita Basin in Figure 6.

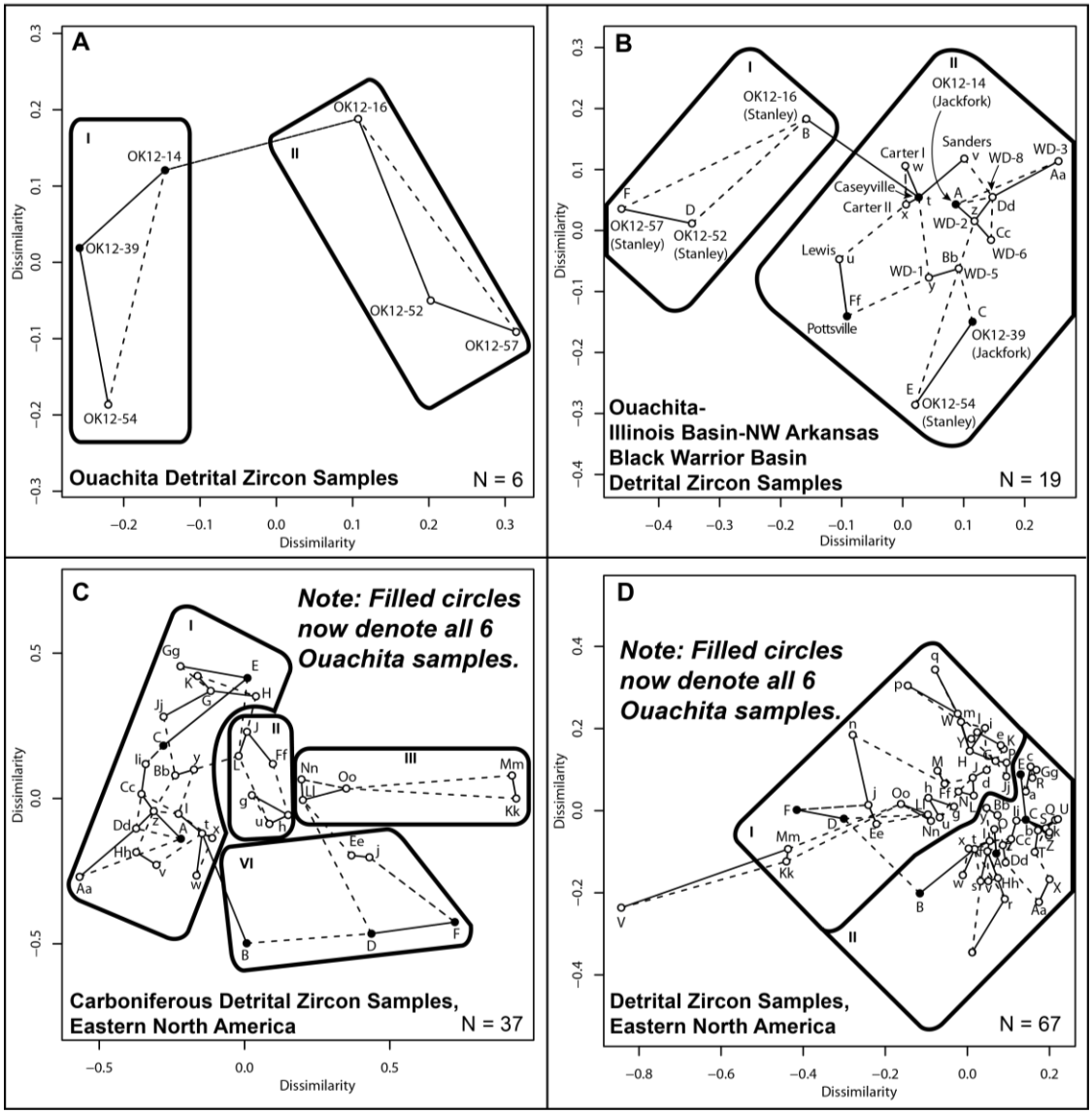
A
I
II
OK12-14
OK12-16
OK12-39
OK12-52
OK12-57
OK12-54
Ouachita Detrital Zircon Samples
N = 6
Dissimilarity
B
I
II
OK12-16 (Stanley)
OK12-14 (Jackfork)
OK12-57 (Stanley)
OK12-52 (Stanley)
Carter I
Carter II
Caseyville
Sanders
WD-3
WD-8
WD-2
WD-6
WD-5
WD-1
Lewis
Bb
Pottsville
OK12-39 (Jackfork)
OK12-54 (Stanley)
Ouachita-
Illinois Basin-NW Arkansas
Black Warrior Basin
Detrital Zircon Samples
N = 19
Dissimilarity
C
Note: Filled circles
now denote all 6
Ouachita samples.
I
II
III
VI
Carboniferous Detrital Zircon Samples,
Eastern North America
N = 37
Dissimilarity
D
Note: Filled circles
now denote all 6
Ouachita samples.
I
II
Detrital Zircon Samples,
Eastern North America
N = 67
Dissimilarity

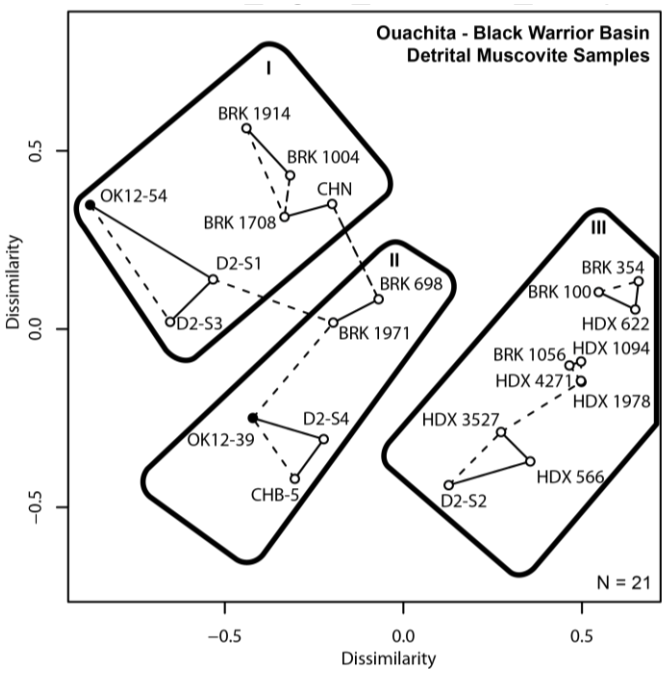

Figure 13. Multidimensional scaling (MDS) muscovite plots between Ouachita and Greater Black Warrior Basins, based on distributional datasets and Kolmogorov-Smirnov dissimilarity, where the axes are dissimilarities measured between plotted samples. Filled circles are Ouachita Basin samples, where unfilled circles are Greater Black Warrior Basin Samples. 'Provenance' in R programming environment is used to construct MDS plots for visualization and interpretation (Vermeech et al., 2016). Solid line connect nearest-neighbors, and dashed lines connect second nearest-neighbors. Suggested groups of similar samples shown by thick outline and labeled with roman numerals. Single-fused laser $^{40}Ar/^{39}Ar$ ages of detrital muscovite are from Moore, 2012 and Uddin et al., 2016. Surface sampling in Cahaba Synclinorium, Greater Black Warrior Basin includes: D2-S1, D2-S2, D2-S3, D2-S4, CHN, and CHB-5. Abbreviations – BRK, Brooks Core; HDX, Hendrix Core. Numbers after core names indicate sampled intervals. Borehole locations are shown on Figure 3D.

Figure 14. – - Paleogeography for the central portion of eastern North American from Late Mississippian - Early Pennsylvanian (modified from Donaldson and Shumaker, 1981). A) *Early Pennsylvanian* – Lowering of relative sea-level exposed sedimentary rocks in intracratonic basins and igneous basement rocks of the emergent Laurussian craton. A paleo-topographic high (i.e., Cincinnati Arch and Nashville Dome) is a major continental-scale drainage divide, and apparent boundary between the Appalachian and Ouachita basins. B) *Mid-Carboniferous* – A drop in sea-level occurred because of a major glaciation event, and craton tilt caused by Gondwanan land mass approach and subsequent erosion of the emergent craton. Generalized sediment dispersal paths are southwest directed based on paleoflow indicators. C) *Late Mississippian* – A shallow sea is present on lowlands of the craton. Sediment from distal sources was carried by large rivers: Michigan River to west, and Ontario River to east. The Michigan River carried sediments into the Michigan Basin (not shown), and then into the Illinois Basin. The Ontario River supplied sediment to Appalachian Basin (Potter and Siever, 1956; Meckel, 1967; Arkle, 1974; Bristol and Howard, 1974; Englund, 1974; Milici, 1974; Miller, 1974; Williamson, 1974; Dennison and Wheeler, 1975; Dever, 1977; Kepferle, 1977; Thomas, 1977a; Edmunds, 1979; Englund, 1979; Presley, 1979; Sable, 1979; Housekecht, 1980).

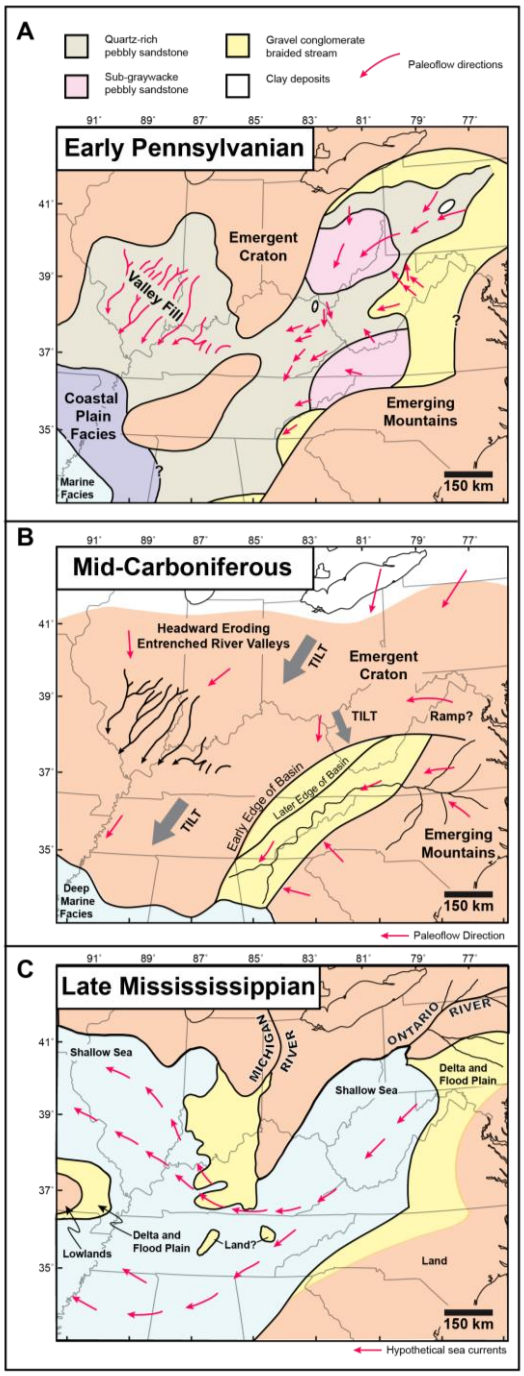
A
Quartz-rich pebbly sandstone
Sub-graywacke pebbly sandstone
Gravel conglomerate braided stream
Clay deposits
Paleoflow directions
91° 89° 87° 85° 83° 81° 79° 77°
Early Pennsylvanian
41° 39° 37° 35°
Emergent Craton
Valley Fill
Coastal Plain Facies
Marine Facies
Emerging Mountains
150 km
B
Mid-Carboniferous
Headward Eroding Entrenched River Valleys
TILT
Emergent Craton
TILT
Ramp?
Early Edge of Basin
Later Edge of Basin
TILT
Emerging Mountains
Deep Marine Facies
150 km
Paleoflow Direction
C
Late Mississisippian
MICHIGAN RIVER
ONTARIO RIVER
Shallow Sea
Shallow Sea
Delta and Flood Plain
Delta and Flood Plain
Land?
Lowlands
Land
150 km
Hypothetical sea currents

Sample	Latitude (ºN)	Longitude (ºW)	Elevation (m)	Age	Group	ISGN
OK12-14	34.6119	94.6595	610.4	Pennsylvanian	Jackfork	BVM00005T
OK12-16	34.4736	94.6603	220.4	Mississippian	Stanley	BVM00005V
OK12-39	34.2836	94.7781	265.6	Pennsylvanian	Jackfork	BVM00006P
OK12-52	34.3398	95.6422	153.9	Mississippian	Stanley	BVM000077
OK12-54	34.2794	95.5475	169.1	Mississippian	Stanley	BVM000079
OK12-57	34.2925	95.3014	193.2	Mississippian	Stanley	BVM00007D

Table 1. Sandstone sample locations with elevation, geologic age, and stratigraphic unit metadata. Additional attributes are provided by System for Earth Sample Registration (SESAR) using corresponding International Geo Sample Number (ISGN) at www.geosamples.org.

Sample	Formation	Age	Photomicrograph	Shape	Size	Color	Surfaces	FIs?	Other
OK12-14	Jackfork	Pennsylvanian	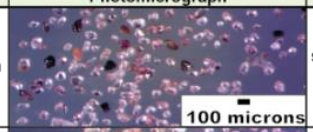	Well-rounded to sub-angular. Some grains are elongated.	Grains from 45 to 115 microns.	Most grains are transparent with slight pink hue. Some grains are of purple tint.	Most grains have smooth surfaces. Sub-angular grains tend to have slightly rougher surfaces.	Present mostly on sub-angular grains	Internal fractures occur in some grains. More fracturing in sub-angular grains
OK12-39	Jackfork	Pennsylvanian		Well-rounded to sub-rounded. Some elongated and equant grains.	Grains from 30 to 130 microns.	Most grains transparent with pink hue. Large amount of tanish grains.	Some rough surfaces on rounded grains. Elongated grains have smooth surfaces.	Present mostly on sub-angular grains	Grains show some internal fractures and/or opaque inclusions.
OK12-16	Stanley	Mississippian		Sub-rounded to sub-angular.	Grains from 50 to 165 microns.	Most grains are transparent with slight pink hue. Some grains show a tanish color. A few darker purple grains.	Well-rounded grains have smooth surfaces. Sub-rounded and sub-angular grains have slightly rough surfaces.	Present	Internal fractures present in most grains that are not well-rounded. Tan grains have more fracturing.
OK12-52	Stanley	Mississippian	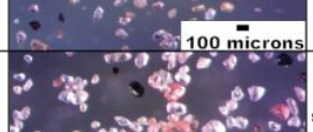	Well-rounded to sub-angular. Some grains elongated.	Grains from 55 to 190 microns.	Most grains transparent with pink hue. Some larger tan grains. A few darker purple grains present.	Most grains have slightly rough surfaces.	Present	Some grains show internal fractures. Large tan grains show more fracturing and/or opaque inclusions.
OK12-54	Stanley	Mississippian	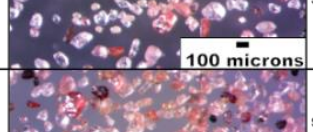	Sub-rounded to sub-angular. Some grains are elongated.	Grains from 45 to 140 microns.	Most grains transparent with pink hue. Some dark purple and red grains present.	Mostly smooth surfaces with some slightly rough surfaces.	Present	Some internal fractures present in grains.
OK12-57	Stanley	Mississippian	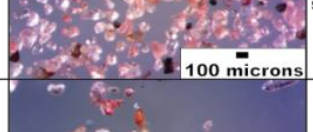	Well-rounded to sub-rounded grains. Some equant grains. Large elongated grain present.	Grains from 35 to 225 microns.	Most grains transparent with pink hue. A few grains with redish tint.	Mostly smooth surfaces. A few grains show rough surfaces.	None	Some grains show internal fractures.

Table 2. Characterization of representative zircon populations from each sample. Attributes for each sample are (left to right): Sample, Formation, Age, Photomicrograph, Shape of grains, Size of grains, Color of grains, Surfaces of grains, Fluid inclusion (FI) within grains, and other noted observations. Zircons in photomicrographs do not correspond to relative abundance of zircons between samples.

Sample name	Stratigraphic Period & Unit	Province A1 Alleghanian 265-327 Ma (%)	Province A2 Acadian 350-380 Ma (%)	Province A3 Unknown 381-439 Ma (%)	Province A4 Taconic 440-465 Ma (%)	Province A5 Unknown 466-499 Ma (%)	Province B Pan-Africa 500-700 Ma (%)	Province C Grenville 950-1300 Ma (%)	Province D Midcontinent 1300-1500 Ma (%)	Province E Yavapai-Mazatzal 1600-1800 Ma (%)	Province F >1800 Ma (%)	Others (%)
OK12-14 (n=101)	Pennsylvanian Jackfork Group	0	0	6	0	2	5	35	19	15	10	9
OK12-39 (n=100)		0	1	2	2	1	1	52	28	3	7	3
OK12-16 (n=60)	Mississippian Stanley Group	3	0	3	2	2	17	13	3	5	38	13
OK12-52 (n=66)		0	2	2	2	5	21	27	2	2	21	18
OK12-54 (n=87)		0	0	5	6	5	20	31	3	8	16	7
OK12-57 (n=70)		1	4	6	1	6	10	14	6	9	17	26

Table 3. Percentage of zircon U-Pb age component in each sample with total number of concordant grains indicated beneath sample name

Stratigraphic Period & Unit	Province A1 Alleghanian 265-327 Ma (%)	Province A2 Acadian 350-380 Ma (%)	Province A3 Unknown 381-439 Ma (%)	Province A4 Taconic 440-465 Ma (%)	Province A5 Unknown 466-499 Ma (%)	Province B Pan-Africa 500-700 Ma (%)	Province C Grenville 950-1300 Ma (%)	Province D Midcontinent 1300-1500 Ma (%)	Province E Yavapai-Mazatzal 1600-1800 Ma (%)	Province F >1800 Ma (%)	Others (%)
Pennsylvanian Jackfork Group (n = 201)	0	0	4	1	1	3	43	23	9	8	6
Mississippian Stanley Group (n = 283)	1	1	4	3	4	17	22	4	6	22	16

Table 4. Percentage of combined zircon U-Pb age component in the Mississippian Stanley Group and the Pennsylvanian Jackfork Group, respectively. Total numbers for combined concordant grains are indicated beneath each unit.

Sample name	Stratigraphic Period & Unit	Province A1 Alleghanian 265-327 Ma (%)	Province A2 Acadian 350-380 Ma (%)	Province A3 Unknown 381-439 Ma (%)	Province A4 Taconic 440-465 Ma (%)	Province A5 Unknown 466-499 Ma (%)	Province B Pan-Africa 500-700 Ma (%)	Province F >1800 Ma (%)
OK12-39 (n=107)	Pennsylvanian Jackfork Group	0	44	44	10	1	0	2
OK12-54 (n=110)	Mississippian Stanley Group	1	3	28	28	27	13	0

Table 5. Percentage of 40Ar/ 39Ar age component in each sample with total number of analyzed grains indicated beneath sample name.

APPENDIX B

MANUSCRIPT #1: ADDITIONAL REFERENCE MATERIAL

Detrital Zircon Uranium-Lead Isotope Data and Grain Ages

OK12-14, Pennsylvanian Jackfork Group – Detrital zircon

TABLE B1 - *Detrital zircon U-Pb geochronologic analyses of Pennsylvanian Jackfork Group (OK12-14) by LA-ICP-MS*

	Isotopic ratios							Isotopic ages (Ma)							
Analysis #	207/235	1 σ err.	206/238	1 σ err.	RHO	207/206	1 σ err.	% Dis.	207/235	1 σ err.	206/238	1 σ err.	207/206	1 σ err.	Best age	1 σ err.
OK12_14_46	0.5207	0.0307	0.0658	0.0015	0.6356	0.0573	0.0027	3.4	425.6	20.3	411.0	9.3	504.2	101.7	411.0	9.3
OK12_14_114	0.5583	0.0196	0.0670	0.0021	0.7969	0.0604	0.0013	7.1	450.4	12.7	418.2	12.6	618.4	45.7	418.2	12.6
OK12_14_2	0.5102	0.0518	0.0671	0.0060	0.8972	0.0551	0.0025	0.0	418.6	34.2	418.6	36.1	414.8	97.2	418.6	36.1
OK12_14_57	0.5724	0.0338	0.0688	0.0036	0.8779	0.0603	0.0017	6.7	459.5	21.6	428.9	21.7	615.0	59.9	428.9	21.7
OK12_14_3	0.5423	0.0550	0.0691	0.0062	0.8984	0.0569	0.0025	2.1	439.9	35.6	430.5	37.2	486.1	95.6	430.5	37.2
OK12_14_70	0.5631	0.0531	0.0705	0.0067	0.9610	0.0580	0.0015	3.2	453.5	33.9	439.0	39.9	528.2	56.8	439.0	39.9
OK12_14_80	0.6104	0.0682	0.0756	0.0058	0.6897	0.0585	0.0047	2.9	483.8	42.1	469.6	34.5	549.3	167.6	469.6	34.5
OK12_14_98	0.6521	0.0236	0.0770	0.0025	0.8288	0.0614	0.0013	6.1	509.8	14.4	478.5	15.1	652.8	43.3	478.5	15.1
OK12_14_43	0.6396	0.0384	0.0814	0.0019	0.6090	0.0569	0.0028	-0.5	502.1	23.5	504.7	11.5	488.7	105.4	504.7	11.5
OK12_14_35	0.6653	0.0401	0.0846	0.0030	0.6871	0.0570	0.0025	-1.1	517.9	24.2	523.3	17.7	493.2	94.6	523.3	17.7
OK12_14_108	0.6369	0.0247	0.0855	0.0027	0.6818	0.0540	0.0016	-5.7	500.4	15.2	528.7	16.2	373.0	63.7	528.7	16.2
OK12_14_103	0.7273	0.0278	0.0855	0.0029	0.7761	0.0617	0.0015	4.7	554.9	16.2	529.1	17.0	662.6	51.4	529.1	17.0
OK12_14_112	1.0989	0.0392	0.1109	0.0035	0.7902	0.0719	0.0016	9.9	752.8	18.8	678.0	20.3	982.0	44.4	678.0	20.3
OK12_14_102	1.1432	0.0508	0.1258	0.0048	0.7215	0.0659	0.0021	1.3	774.0	23.8	763.7	27.3	804.0	64.3	763.7	27.3
OK12_14_25	1.1383	0.0661	0.1271	0.0043	0.7166	0.0650	0.0027	0.1	771.7	30.9	771.1	24.7	772.7	84.4	771.1	24.7
OK12_14_101	1.6188	0.0529	0.1516	0.0047	0.9134	0.0774	0.0010	6.9	977.5	20.3	909.9	26.4	1132.7	26.4	909.9	26.4
OK12_14_9	1.5486	0.1556	0.1538	0.0137	0.9054	0.0729	0.0031	2.9	949.9	60.2	922.5	76.1	1010.9	84.2	922.5	76.1
OK12_14_8	1.5247	0.1531	0.1546	0.0138	0.9077	0.0714	0.0030	1.5	940.4	59.8	926.7	76.5	969.4	83.8	926.7	76.5
OK12_14_20	1.7052	0.1226	0.1614	0.0092	0.8391	0.0766	0.0030	4.6	1010.5	45.0	964.3	50.6	1111.1	76.5	964.3	50.6
OK12_14_94	1.6591	0.1492	0.1635	0.0058	0.5191	0.0735	0.0057	1.7	993.0	55.4	976.4	31.9	1027.3	149.7	976.4	31.9
OK12_14_54	1.7393	0.0980	0.1714	0.0087	0.9046	0.0736	0.0018	0.3	1023.2	35.7	1020.0	47.7	1029.5	47.8	1029.5	47.8
OK12_14_12	1.7437	0.1747	0.1716	0.0152	0.9056	0.0736	0.0031	0.4	1024.8	62.7	1021.0	83.2	1029.9	83.7	1029.9	83.7
OK12_14_81	1.9597	0.2194	0.1925	0.0148	0.6891	0.0738	0.0060	-3.0	1101.8	72.6	1135.0	79.3	1034.7	155.8	1034.7	155.8
OK12_14_26	1.8691	0.1081	0.1837	0.0062	0.7194	0.0738	0.0030	-1.6	1070.2	37.5	1086.9	33.8	1035.6	80.5	1035.6	80.5
OK12_14_90	2.0265	0.1835	0.1989	0.0071	0.5079	0.0738	0.0058	-4.0	1124.4	59.8	1169.5	38.0	1035.7	151.3	1035.7	151.3
OK12_14_21	1.9294	0.1342	0.1880	0.0104	0.8536	0.0744	0.0027	-1.7	1091.3	45.5	1110.3	56.0	1052.7	71.8	1052.7	71.8
OK12_14_5	1.8576	0.1867	0.1804	0.0161	0.9049	0.0746	0.0032	-0.3	1066.1	64.3	1069.2	87.1	1056.9	83.9	1056.9	83.9
OK12_14_84	2.1178	0.2374	0.2039	0.0157	0.6907	0.0753	0.0061	-3.6	1154.6	74.5	1196.0	83.4	1075.8	154.7	1075.8	154.7
OK12_14_32	2.1800	0.1315	0.2089	0.0076	0.7087	0.0757	0.0033	-4.1	1174.7	41.1	1222.8	40.4	1086.4	83.9	1086.4	83.9
OK12_14_14	1.9949	0.1406	0.1909	0.0106	0.8483	0.0757	0.0028	-1.1	1113.8	46.6	1126.4	57.3	1088.4	73.4	1088.4	73.4
OK12_14_50	1.8507	0.1131	0.1764	0.0094	0.8545	0.0761	0.0024	1.5	1063.7	39.5	1047.5	51.4	1096.5	62.3	1096.5	62.3
OK12_14_73	2.3360	0.2603	0.2220	0.0169	0.6931	0.0763	0.0061	-5.6	1223.3	76.3	1292.3	88.7	1101.7	152.8	1101.7	152.8

OK12-14, Pennsylvanian Jackfork Group – Detrital zircon, *continued*

OK12_14_97	2.1336	0.0888	0.2003	0.0070	0.7037	0.0772	0.0023	-1.5	1159.8	28.4	1177.0	37.6	1127.6	58.8	1127.6	58.8
OK12_14_33	1.8720	0.1095	0.1749	0.0060	0.7153	0.0776	0.0032	3.0	1071.2	38.0	1038.8	33.0	1137.2	80.4	1137.2	80.4
OK12_14_45	1.9037	0.1130	0.1760	0.0041	0.6250	0.0784	0.0038	3.4	1082.4	38.8	1045.3	22.4	1156.4	93.0	1156.4	93.0
OK12_14_19	1.9674	0.1443	0.1812	0.0103	0.8179	0.0787	0.0033	2.8	1104.4	48.2	1073.6	56.1	1164.6	81.6	1164.6	81.6
OK12_14_116	2.1171	0.0763	0.1950	0.0063	0.7980	0.0787	0.0017	0.5	1154.4	24.5	1148.5	33.6	1165.4	42.9	1165.4	42.9
OK12_14_111	1.9783	0.0664	0.1815	0.0056	0.8643	0.0791	0.0013	3.0	1108.1	22.4	1075.1	30.7	1173.6	33.3	1173.6	33.3
OK12_14_78	2.1888	0.2435	0.2002	0.0152	0.6931	0.0792	0.0064	0.1	1177.5	74.7	1176.4	81.3	1177.5	150.9	1177.5	150.9
OK12_14_56	1.8900	0.1137	0.1726	0.0092	0.8670	0.0794	0.0024	4.7	1077.6	39.2	1026.5	50.1	1181.9	58.2	1181.9	58.2
OK12_14_67	1.9632	0.1841	0.1786	0.0168	0.9632	0.0797	0.0020	3.9	1103.0	61.2	1059.5	91.1	1189.9	49.5	1189.9	49.5
OK12_14_7	2.3556	0.2382	0.2119	0.0189	0.8980	0.0805	0.0036	-0.8	1229.3	69.6	1239.1	99.6	1209.0	85.2	1209.0	85.2
OK12_14_118	2.0896	0.0724	0.1882	0.0060	0.8476	0.0805	0.0015	2.9	1145.4	23.5	1111.8	32.4	1209.6	36.1	1209.6	36.1
OK12_14_110	2.0672	0.0687	0.1858	0.0058	0.8890	0.0807	0.0012	3.4	1138.0	22.5	1098.8	31.5	1213.6	29.8	1213.6	29.8
OK12_14_29	2.1766	0.1324	0.1944	0.0070	0.6837	0.0812	0.0036	2.4	1173.6	41.5	1144.9	37.5	1226.2	85.5	1226.2	85.5
OK12_14_48	2.3437	0.1420	0.2067	0.0051	0.6055	0.0822	0.0041	1.2	1225.6	42.2	1211.4	27.0	1249.5	94.4	1249.5	94.4
OK12_14_105	2.2886	0.0756	0.2016	0.0063	0.9098	0.0823	0.0011	2.0	1208.8	23.1	1184.0	34.0	1253.3	26.7	1253.3	26.7
OK12_14_24	2.2661	0.1657	0.1993	0.0113	0.8155	0.0824	0.0035	2.5	1201.8	50.2	1171.4	60.3	1256.0	80.8	1256.0	80.8
OK12_14_58	1.9905	0.1148	0.1746	0.0089	0.8807	0.0827	0.0023	6.7	1112.3	38.2	1037.2	48.7	1261.6	52.5	1261.6	52.5
OK12_14_16	2.1277	0.1520	0.1859	0.0105	0.8410	0.0829	0.0032	5.0	1157.8	48.2	1099.4	56.7	1268.0	74.0	1268.0	74.0
OK12_14_62	2.1355	0.1988	0.1864	0.0174	0.9695	0.0831	0.0019	5.1	1160.4	62.4	1101.7	94.1	1271.9	44.3	1271.9	44.3
OK12_14_28	2.2793	0.1313	0.1982	0.0067	0.7212	0.0834	0.0034	3.3	1205.9	39.9	1165.8	35.9	1277.9	77.3	1277.9	77.3
OK12_14_119	2.3411	0.0777	0.2026	0.0064	0.9079	0.0838	0.0012	2.9	1224.8	23.3	1189.5	34.2	1287.6	27.0	1287.6	27.0
OK12_14_13	2.5757	0.1803	0.2208	0.0123	0.8531	0.0846	0.0031	0.6	1293.8	49.9	1286.3	64.4	1305.3	69.8	1305.3	69.8
OK12_14_17	3.0259	0.2128	0.2579	0.0144	0.8552	0.0851	0.0031	-4.6	1414.2	52.3	1478.9	73.6	1317.1	69.5	1317.1	69.5
OK12_14_63	2.5360	0.2366	0.2147	0.0201	0.9687	0.0857	0.0020	2.2	1282.4	65.8	1253.9	106.0	1330.8	44.6	1330.8	44.6
OK12_14_61	2.6916	0.2518	0.2262	0.0213	0.9700	0.0863	0.0020	0.9	1326.2	67.0	1314.5	111.0	1345.3	43.8	1345.3	43.8
OK12_14_39	2.7517	0.1601	0.2301	0.0051	0.6478	0.0867	0.0041	0.5	1342.5	42.4	1335.2	26.7	1353.0	88.0	1353.0	88.0
OK12_14_68	2.9821	0.2800	0.2464	0.0232	0.9634	0.0878	0.0022	-1.2	1403.1	69.0	1419.7	118.8	1378.0	48.1	1378.0	48.1
OK12_14_64	2.9646	0.2763	0.2417	0.0227	0.9700	0.0890	0.0020	0.2	1398.6	68.4	1395.4	116.6	1403.7	43.3	1403.7	43.3
OK12_14_82	2.4279	0.2710	0.1960	0.0150	0.6955	0.0897	0.0072	7.7	1250.9	77.3	1154.0	80.5	1420.0	146.0	1420.0	146.0
OK12_14_47	3.0689	0.1771	0.2459	0.0055	0.6633	0.0905	0.0042	0.6	1425.0	43.3	1417.1	28.2	1435.5	85.4	1435.5	85.4
OK12_14_44	2.9920	0.1739	0.2387	0.0055	0.6579	0.0908	0.0042	1.8	1405.6	43.3	1380.2	28.3	1443.0	85.9	1443.0	85.9
OK12_14_23	2.5537	0.1890	0.2038	0.0116	0.8040	0.0909	0.0040	7.1	1287.5	52.6	1195.5	61.7	1443.5	81.8	1443.5	81.8
OK12_14_42	2.6704	0.1550	0.2125	0.0048	0.6586	0.0911	0.0042	5.9	1320.3	42.0	1242.0	25.6	1448.5	85.8	1448.5	85.8
OK12_14_83	3.5124	0.3899	0.2784	0.0211	0.6941	0.0914	0.0073	-3.5	1530.0	84.2	1583.1	105.7	1455.4	144.8	1455.4	144.8
OK12_14_85	3.3826	0.3038	0.2678	0.0094	0.5190	0.0915	0.0071	-1.9	1500.4	68.0	1529.5	47.5	1457.0	140.8	1457.0	140.8
OK12_14_53	2.9492	0.1710	0.2332	0.0121	0.8955	0.0917	0.0024	3.1	1394.6	43.0	1351.5	63.1	1460.8	48.3	1460.8	48.3
OK12_14_79	3.4461	0.3822	0.2705	0.0205	0.6942	0.0923	0.0074	-1.9	1515.0	83.7	1543.5	103.2	1473.5	144.3	1473.5	144.3
OK12_14_18	3.0655	0.2156	0.2407	0.0135	0.8570	0.0923	0.0034	2.4	1424.1	52.5	1390.2	69.8	1474.4	67.7	1474.4	67.7

OK12-14, Pennsylvanian Jackfork Group – Detrital zircon, *continued*

OK12_14_86	3.3473	0.2996	0.2603	0.0090	0.5221	0.0931	0.0072	0.0	1492.2	67.7	1491.6	46.0	1490.5	139.6	1490.5	139.6
OK12_14_11	3.6037	0.3613	0.2794	0.0248	0.9064	0.0934	0.0040	-2.4	1550.3	76.7	1588.2	123.9	1496.2	78.1	1496.2	78.1
OK12_14_88	3.3955	0.3058	0.2625	0.0093	0.5162	0.0937	0.0073	0.1	1503.4	68.3	1502.4	47.1	1502.2	140.5	1502.2	140.5
OK12_14_115	2.9807	0.0980	0.2289	0.0072	0.9109	0.0944	0.0013	5.3	1402.7	24.7	1328.9	37.5	1516.8	25.5	1516.8	25.5
OK12_14_4	2.9661	0.2965	0.2263	0.0201	0.9104	0.0949	0.0039	6.0	1399.0	73.2	1315.0	104.9	1526.5	76.1	1526.5	76.1
OK12_14_89	4.4564	0.3989	0.3321	0.0115	0.5190	0.0972	0.0075	-7.3	1722.9	71.6	1848.3	55.2	1571.2	138.5	1571.2	138.5
OK12_14_100	3.6094	0.1173	0.2636	0.0081	0.9097	0.0993	0.0013	2.8	1551.6	25.5	1508.4	41.4	1611.0	25.1	1611.0	25.1
OK12_14_117	3.5811	0.1158	0.2613	0.0080	0.9088	0.0994	0.0013	3.2	1545.4	25.4	1496.4	40.9	1612.9	25.1	1612.9	25.1
OK12_14_60	3.7826	0.2167	0.2751	0.0142	0.9003	0.0997	0.0025	1.4	1589.1	45.0	1566.5	71.2	1618.6	45.7	1618.6	45.7
OK12_14_91	3.1934	0.2861	0.2319	0.0081	0.5229	0.0998	0.0077	7.6	1455.6	67.0	1344.3	42.2	1619.5	137.4	1619.5	137.4
OK12_14_109	3.5284	0.1171	0.2556	0.0081	0.9113	0.1001	0.0014	4.3	1533.6	25.9	1467.0	41.4	1626.6	25.3	1626.6	25.3
OK12_14_96	4.1999	0.3770	0.3036	0.0107	0.5230	0.1002	0.0078	-2.1	1674.0	71.1	1709.1	52.7	1627.9	137.4	1627.9	137.4
OK12_14_104	3.9482	0.1343	0.2845	0.0091	0.8822	0.1006	0.0016	0.6	1623.6	27.2	1614.1	45.4	1636.0	29.6	1636.0	29.6
OK12_14_95	4.2702	0.3848	0.3047	0.0109	0.5211	0.1015	0.0079	-1.6	1687.6	71.6	1714.4	53.5	1652.1	137.5	1652.1	137.5
OK12_14_38	4.2945	0.2480	0.3033	0.0068	0.6626	0.1026	0.0047	-0.9	1692.3	46.5	1707.5	33.3	1672.3	82.9	1672.3	82.9
OK12_14_120	4.0590	0.1321	0.2834	0.0086	0.8863	0.1039	0.0016	2.3	1646.1	26.2	1608.2	43.2	1694.8	27.7	1694.8	27.7
OK12_14_34	4.4509	0.2558	0.3098	0.0105	0.7254	0.1042	0.0042	-1.0	1721.9	46.6	1739.7	51.2	1699.7	72.6	1699.7	72.6
OK12_14_66	4.1521	0.3892	0.2889	0.0271	0.9614	0.1043	0.0027	1.7	1664.6	73.9	1635.8	134.1	1701.3	47.2	1701.3	47.2
OK12_14_71	4.6960	0.4364	0.3202	0.0300	0.9719	0.1064	0.0024	-1.4	1766.5	75.0	1790.6	144.7	1738.4	40.0	1738.4	40.0
OK12_14_22	4.4877	0.3144	0.3054	0.0171	0.8582	0.1065	0.0039	0.6	1728.7	56.6	1718.0	83.7	1740.8	64.9	1740.8	64.9
OK12_14_1	4.4284	0.4424	0.2971	0.0264	0.9096	0.1080	0.0045	2.4	1717.7	79.5	1676.7	129.7	1765.2	74.1	1765.2	74.1
OK12_14_106	4.7255	0.1582	0.3085	0.0097	0.8909	0.1111	0.0017	2.2	1771.8	27.7	1733.1	47.7	1817.7	27.5	1817.7	27.5
OK12_14_107	4.6231	0.1551	0.2928	0.0093	0.8950	0.1145	0.0017	5.6	1753.4	27.6	1655.4	46.1	1872.4	26.9	1872.4	26.9
OK12_14_37	4.9703	0.2900	0.3034	0.0073	0.6656	0.1187	0.0055	5.8	1814.3	48.2	1708.2	35.9	1937.2	80.1	1937.2	80.1
OK12_14_30	5.8943	0.3549	0.3477	0.0123	0.6873	0.1229	0.0054	1.9	1960.4	51.0	1923.8	58.4	1998.8	76.4	1998.8	76.4
OK12_14_41	7.7220	0.4471	0.4158	0.0092	0.6576	0.1346	0.0062	-1.9	2199.2	50.8	2241.2	42.0	2159.0	78.8	2159.0	78.8
OK12_14_113	7.4688	0.2443	0.3946	0.0121	0.8890	0.1373	0.0021	1.2	2169.2	28.9	2144.3	55.8	2193.0	25.9	2193.0	25.9
OK12_14_92	13.0147	1.1701	0.5521	0.0197	0.5250	0.1707	0.0132	-5.7	2680.7	81.4	2834.1	81.1	2564.8	123.9	2564.8	123.9
OK12_14_72	12.8773	1.1986	0.5074	0.0476	0.9723	0.1841	0.0041	0.9	2670.7	84.1	2645.4	200.3	2690.1	35.9	2690.1	35.9
OK12_14_59	12.8533	0.7409	0.4854	0.0253	0.9051	0.1920	0.0047	4.4	2669.0	52.9	2550.5	108.7	2759.5	39.7	2759.5	39.7
OK12_14_76	15.8541	1.7650	0.5964	0.0454	0.6929	0.1926	0.0155	-5.1	2868.0	101.1	3015.5	180.9	2764.4	126.0	2764.4	126.0

OK12-39, Pennsylvanian Jackfork Group – Detrital zircon

TABLE B2 - *Detrital zircon U-Pb geochronologic analyses of Pennsylvanian Jackfork Group (OK12-39) by LA-ICP-MS*

	Isotopic ratios								Isotopic ages (Ma)							
Analysis #	207/235	1 σ err.	206/238	1 σ err.	RHO	207/206	1 σ err.	% Dis.	207/235	1 σ err.	206/238	1 σ err.	207/206	1 σ err.	Best age	1 σ err.
OK12_39_18	0.4332	0.0190	0.0536	0.0019	0.8330	0.0585	0.0014	7.8	365.5	13.4	336.9	11.9	550.3	52.0	336.9	52.0
OK12_39_6	0.4291	0.0287	0.0573	0.0025	0.7841	0.0542	0.0023	0.9	362.5	20.2	359.3	15.0	380.5	92.9	359.3	92.9
OK12_39_13	0.5409	0.0224	0.0685	0.0024	0.8657	0.0573	0.0012	2.7	439.0	14.6	427.0	14.4	501.5	45.0	427.0	45.0
OK12_39_7	0.5681	0.0380	0.0698	0.0030	0.7798	0.0589	0.0025	4.7	456.8	24.3	435.2	17.9	564.4	90.8	435.2	90.8
OK12_39_26	0.5761	0.0344	0.0709	0.0041	0.9392	0.0589	0.0012	4.5	462.0	21.9	441.4	24.8	564.5	44.3	441.4	44.3
OK12_39_82	0.5848	0.0350	0.0715	0.0039	0.8696	0.0593	0.0018	4.8	467.5	22.2	445.3	23.3	579.0	63.2	445.3	63.2
OK12_39_38	0.6064	0.0364	0.0767	0.0042	0.9127	0.0573	0.0014	1.1	481.3	22.7	476.1	25.3	504.8	53.1	476.1	53.1
OK12_39_101	0.7210	0.0276	0.0848	0.0031	0.8992	0.0617	0.0010	4.8	551.2	16.2	524.5	18.2	662.7	35.7	524.5	35.7
OK12_39_118	1.7444	0.0702	0.1780	0.0066	0.8604	0.0710	0.0015	-3.0	1025.1	25.6	1056.3	36.1	958.7	41.7	958.7	36.1
OK12_39_5	1.6054	0.1075	0.1635	0.0071	0.7851	0.0711	0.0030	-0.4	972.3	41.0	976.3	39.0	961.0	84.5	961.0	39.0
OK12_39_88	1.8763	0.0751	0.1689	0.0071	0.9188	0.0714	0.0012	6.2	1072.8	26.2	1005.8	39.1	967.6	33.6	967.6	39.1
OK12_39_11	1.5129	0.1039	0.1531	0.0067	0.7631	0.0716	0.0032	1.8	935.6	41.2	918.5	37.4	973.8	89.6	973.8	37.4
OK12_39_108	1.6558	0.0637	0.1671	0.0061	0.9019	0.0719	0.0012	-0.4	991.8	24.1	996.0	33.5	982.1	33.6	982.1	33.5
OK12_39_70	1.5390	0.1500	0.1532	0.0141	0.9311	0.0727	0.0026	2.9	946.1	58.3	918.7	78.2	1005.3	70.5	1005.3	78.2
OK12_39_28	1.4235	0.0813	0.1410	0.0079	0.9533	0.0732	0.0013	5.4	898.8	33.5	850.1	44.8	1019.6	34.7	1019.6	44.8
OK12_39_79	1.9406	0.1100	0.1917	0.0101	0.9239	0.0734	0.0016	-3.2	1095.2	37.3	1130.6	54.7	1026.2	43.3	1026.2	54.7
OK12_39_110	1.6968	0.0637	0.1675	0.0060	0.9143	0.0735	0.0011	0.9	1007.3	23.7	998.1	33.0	1027.1	30.6	1027.1	33.0
OK12_39_109	1.7755	0.0694	0.1743	0.0064	0.8821	0.0739	0.0014	0.1	1036.5	25.1	1035.6	34.9	1037.9	37.0	1037.9	34.9
OK12_39_63	1.6205	0.1568	0.1584	0.0145	0.9372	0.0740	0.0025	3.1	978.2	59.0	948.0	80.3	1041.5	66.7	1041.5	80.3
OK12_39_103	1.7751	0.0691	0.1734	0.0064	0.8931	0.0742	0.0013	0.5	1036.4	25.0	1030.8	34.8	1047.7	35.1	1047.7	34.8
OK12_39_39	1.6966	0.1020	0.1647	0.0091	0.9146	0.0747	0.0018	2.4	1007.3	37.7	982.8	50.4	1059.9	48.2	1059.9	50.4
OK12_39_45	1.5504	0.0939	0.1500	0.0084	0.9130	0.0749	0.0019	5.2	950.7	36.7	900.8	46.8	1067.1	48.9	1067.1	46.8
OK12_39_72	1.7590	0.1709	0.1698	0.0156	0.9335	0.0750	0.0026	1.9	1030.5	61.0	1010.7	85.3	1067.5	68.5	1067.5	85.3
OK12_39_50	1.5674	0.1125	0.1509	0.0100	0.9212	0.0752	0.0021	5.3	957.4	43.6	906.2	56.0	1074.7	55.1	1074.7	56.0
OK12_39_73	2.0829	0.1190	0.1991	0.0106	0.9172	0.0759	0.0017	-2.4	1143.2	38.4	1170.6	56.7	1092.2	44.9	1092.2	56.7
OK12_39_33	2.0539	0.1154	0.1946	0.0109	0.9616	0.0765	0.0012	-1.1	1133.6	37.7	1146.2	58.4	1108.5	30.7	1108.5	58.4
OK12_39_97	2.0712	0.0774	0.1961	0.0070	0.9194	0.0766	0.0011	-1.3	1139.3	25.3	1154.5	37.6	1110.1	29.2	1110.1	37.6
OK12_39_78	1.8320	0.1050	0.1736	0.0093	0.9240	0.0766	0.0017	2.4	1057.0	37.0	1031.8	50.9	1110.1	43.2	1110.1	50.9
OK12_39_30	1.8581	0.1082	0.1755	0.0100	0.9383	0.0767	0.0016	2.2	1066.3	37.7	1042.4	54.5	1114.5	39.9	1114.5	54.5
OK12_39_55	1.5868	0.1163	0.1486	0.0101	0.9133	0.0773	0.0023	7.4	965.0	44.7	893.4	56.2	1129.9	58.4	1129.9	56.2
OK12_39_46	2.0273	0.1221	0.1897	0.0105	0.9140	0.0775	0.0019	0.4	1124.7	40.1	1120.0	56.8	1132.9	47.9	1132.9	56.8
OK12_39_86	2.1015	0.0836	0.1738	0.0072	0.9162	0.0777	0.0013	10.1	1149.3	27.0	1032.9	39.7	1138.0	33.0	1138.0	39.7

OK12-39, Pennsylvanian Jackfork Group – Detrital zircon, *continued*

OK12_39_4	1.8586	0.1247	0.1734	0.0075	0.7879	0.0777	0.0033	3.4	1066.5	43.4	1030.8	41.3	1138.0	82.1	1138.0	41.3
OK12_39_2	2.1188	0.1413	0.1967	0.0085	0.7880	0.0780	0.0033	-0.2	1155.0	45.0	1157.7	45.4	1147.6	81.5	1147.6	45.4
OK12_39_115	2.2024	0.0831	0.2046	0.0074	0.9216	0.0781	0.0011	-1.5	1181.8	26.0	1200.0	39.4	1148.3	28.9	1148.3	39.4
OK12_39_60	1.8663	0.1345	0.1732	0.0115	0.9171	0.0781	0.0022	3.7	1069.2	46.6	1029.7	63.0	1148.4	56.0	1148.4	63.0
OK12_39_68	1.8561	0.1793	0.1719	0.0157	0.9375	0.0781	0.0026	4.0	1065.6	61.8	1022.8	86.0	1149.1	65.4	1149.1	86.0
OK12_39_117	2.0800	0.0758	0.1925	0.0067	0.9175	0.0783	0.0011	0.6	1142.2	24.7	1135.1	36.0	1155.3	28.6	1155.3	36.0
OK12_39_75	2.1791	0.1252	0.2002	0.0107	0.9139	0.0790	0.0018	-0.2	1174.4	39.2	1176.6	57.2	1170.9	45.5	1170.9	57.2
OK12_39_10	1.9281	0.1312	0.1766	0.0078	0.7768	0.0791	0.0035	3.9	1090.9	44.5	1048.5	42.4	1174.3	84.2	1174.3	42.4
OK12_39_19	2.1832	0.0886	0.1999	0.0069	0.8780	0.0792	0.0015	0.1	1175.7	27.9	1175.0	37.1	1176.1	38.0	1176.1	37.1
OK12_39_66	2.0523	0.1981	0.1869	0.0171	0.9371	0.0795	0.0027	2.5	1133.1	63.8	1104.4	92.1	1183.5	65.2	1183.5	92.1
OK12_39_40	2.2922	0.1367	0.2091	0.0116	0.9213	0.0795	0.0018	-1.2	1209.9	41.3	1224.0	61.3	1183.9	45.1	1183.9	61.3
OK12_39_98	2.2087	0.0824	0.2012	0.0071	0.9019	0.0796	0.0013	0.2	1183.8	25.7	1182.0	37.9	1186.8	31.7	1186.8	37.9
OK12_39_23	2.0781	0.0870	0.1885	0.0068	0.8794	0.0799	0.0016	2.5	1141.6	28.3	1113.4	36.7	1194.7	38.8	1194.7	36.7
OK12_39_20	2.2785	0.0944	0.2059	0.0073	0.8777	0.0802	0.0016	-0.1	1205.7	28.8	1206.9	39.0	1202.5	38.7	1202.5	39.0
OK12_39_8	2.1321	0.1443	0.1924	0.0085	0.7891	0.0803	0.0034	2.1	1159.3	45.7	1134.4	45.9	1203.7	81.6	1203.7	45.9
OK12_39_36	1.6356	0.0933	0.1475	0.0084	0.9643	0.0804	0.0012	9.9	984.0	35.3	887.0	46.9	1206.3	29.7	1206.3	46.9
OK12_39_100	2.2553	0.0859	0.2030	0.0073	0.9091	0.0805	0.0013	0.6	1198.4	26.4	1191.6	39.2	1210.4	31.0	1210.4	39.2
OK12_39_37	2.2423	0.1404	0.2008	0.0114	0.8897	0.0809	0.0023	1.2	1194.4	43.0	1179.7	61.0	1220.1	55.2	1220.1	61.0
OK12_39_104	2.1565	0.0846	0.1931	0.0069	0.8482	0.0810	0.0017	2.5	1167.1	26.9	1138.3	37.3	1220.7	40.6	1220.7	37.3
OK12_39_64	2.0051	0.1939	0.1784	0.0163	0.9359	0.0813	0.0028	5.3	1117.3	63.5	1058.1	88.7	1229.2	65.5	1229.2	88.7
OK12_39_24	2.0531	0.0856	0.1828	0.0065	0.8697	0.0814	0.0017	4.5	1133.3	28.1	1082.0	35.3	1232.2	39.9	1232.2	35.3
OK12_39_15	2.0940	0.0870	0.1864	0.0066	0.8655	0.0814	0.0017	3.9	1146.8	28.2	1101.7	35.5	1232.3	40.3	1232.3	35.5
OK12_39_3	2.1524	0.1438	0.1907	0.0082	0.7879	0.0818	0.0035	3.5	1165.8	45.3	1125.2	44.4	1239.9	80.6	1239.9	44.4
OK12_39_116	2.5478	0.0951	0.2255	0.0081	0.9262	0.0819	0.0012	-1.9	1285.8	26.9	1310.6	42.3	1244.1	27.4	1244.1	42.3
OK12_39_61	2.1885	0.2117	0.1917	0.0176	0.9366	0.0826	0.0028	4.0	1177.4	65.3	1130.5	94.3	1259.7	64.9	1259.7	94.3
OK12_39_54	2.0897	0.1510	0.1829	0.0122	0.9194	0.0828	0.0024	5.5	1145.4	48.5	1083.0	66.4	1263.5	54.6	1263.5	66.4
OK12_39_49	1.9340	0.1393	0.1690	0.0113	0.9203	0.0829	0.0023	7.9	1092.9	47.1	1006.4	61.9	1267.3	54.1	1267.3	61.9
OK12_39_41	2.9309	0.1751	0.2528	0.0140	0.9201	0.0841	0.0020	-4.5	1389.9	44.2	1452.7	71.5	1294.0	44.9	1294.0	71.5
OK12_39_89	2.3379	0.0935	0.1767	0.0074	0.9079	0.0849	0.0015	14.3	1223.9	28.1	1049.1	40.3	1314.3	33.8	1314.3	40.3
OK12_39_65	2.2290	0.2157	0.1897	0.0174	0.9383	0.0850	0.0028	5.9	1190.2	65.7	1119.9	93.7	1315.4	63.6	1315.4	93.7
OK12_39_42	3.1122	0.1853	0.2626	0.0145	0.9218	0.0859	0.0020	-4.7	1435.7	44.7	1503.3	73.6	1336.1	44.0	1336.1	73.6
OK12_39_83	2.6063	0.1508	0.2188	0.0118	0.9117	0.0864	0.0021	2.1	1302.4	41.6	1275.3	61.9	1347.9	45.3	1347.9	61.9
OK12_39_113	2.6382	0.1001	0.2209	0.0080	0.9138	0.0866	0.0013	1.9	1311.4	27.6	1286.9	42.0	1351.2	29.6	1351.2	42.0
OK12_39_67	2.4220	0.2349	0.2021	0.0186	0.9371	0.0867	0.0029	5.0	1249.1	67.4	1186.4	98.8	1354.0	63.9	1354.0	98.8
OK12_39_52	2.6462	0.1905	0.2200	0.0147	0.9207	0.0871	0.0024	2.4	1313.6	51.7	1282.0	77.0	1363.4	53.2	1363.4	77.0
OK12_39_62	2.6872	0.2605	0.2231	0.0205	0.9356	0.0871	0.0030	2.0	1324.9	69.3	1298.1	107.0	1363.7	64.6	1363.7	107.0
OK12_39_69	2.5942	0.2507	0.2142	0.0196	0.9369	0.0876	0.0030	3.7	1299.0	68.5	1251.2	103.3	1374.1	63.7	1374.1	103.3
OK12_39_95	2.8106	0.1129	0.2053	0.0086	0.9061	0.0879	0.0016	11.4	1358.4	29.6	1203.6	45.8	1380.8	33.9	1380.8	45.8

OK12-39, Pennsylvanian Jackfork Group – Detrital zircon, *continued*

OK12_39_27	2.0437	0.1150	0.1685	0.0094	0.9642	0.0879	0.0013	11.2	1130.2	37.7	1003.7	51.9	1381.1	28.6	1381.1	51.9
OK12_39_48	2.8237	0.1677	0.2327	0.0128	0.9201	0.0880	0.0020	1.0	1361.9	43.6	1348.7	66.5	1381.6	44.0	1381.6	66.5
OK12_39_77	3.0681	0.1768	0.2526	0.0135	0.9114	0.0881	0.0021	-1.9	1424.8	43.2	1452.1	69.1	1384.8	44.9	1384.8	69.1
OK12_39_102	2.7814	0.1039	0.2267	0.0081	0.9148	0.0890	0.0013	2.5	1350.6	27.5	1317.3	42.2	1403.2	28.7	1403.2	42.2
OK12_39_119	2.8862	0.1090	0.2342	0.0083	0.8939	0.0893	0.0015	1.6	1378.3	28.1	1356.7	43.3	1411.6	32.2	1411.6	43.3
OK12_39_16	2.5706	0.1064	0.2084	0.0073	0.8670	0.0894	0.0018	5.6	1292.3	29.8	1220.2	38.9	1413.4	39.0	1413.4	38.9
OK12_39_105	2.9403	0.1110	0.2346	0.0085	0.9185	0.0909	0.0014	2.4	1392.4	28.2	1358.4	44.0	1444.4	28.3	1444.4	44.0
OK12_39_80	3.1009	0.1779	0.2474	0.0133	0.9255	0.0909	0.0020	0.6	1432.9	43.1	1424.9	68.3	1445.5	40.8	1445.5	68.3
OK12_39_25	3.1287	0.1775	0.2493	0.0141	0.9647	0.0910	0.0014	0.3	1439.8	42.7	1435.0	72.3	1445.8	28.4	1445.8	72.3
OK12_39_99	3.5056	0.1301	0.2785	0.0099	0.9249	0.0913	0.0013	-3.6	1528.5	28.9	1584.0	49.7	1452.0	26.7	1452.0	49.7
OK12_39_111	3.1384	0.1176	0.2488	0.0088	0.8946	0.0915	0.0015	0.7	1442.2	28.4	1432.3	45.1	1456.4	31.7	1456.4	45.1
OK12_39_57	2.7375	0.1969	0.2166	0.0145	0.9236	0.0916	0.0025	5.6	1338.7	52.1	1263.8	76.2	1458.4	51.6	1458.4	76.2
OK12_39_106	3.4383	0.1259	0.2718	0.0095	0.9181	0.0917	0.0013	-2.4	1513.2	28.4	1549.9	47.9	1461.8	27.4	1461.8	47.9
OK12_39_12	2.9051	0.1946	0.2291	0.0099	0.7846	0.0919	0.0039	3.9	1383.2	49.4	1329.6	51.6	1464.8	78.8	1464.8	51.6
OK12_39_81	2.8220	0.1610	0.2228	0.0119	0.9250	0.0919	0.0020	4.8	1361.4	41.9	1296.4	62.4	1465.5	40.6	1465.5	62.4
OK12_39_107	3.0538	0.1205	0.2402	0.0090	0.9103	0.0922	0.0015	2.4	1421.2	29.8	1387.7	46.8	1471.3	30.9	1471.3	46.8
OK12_39_35	3.0151	0.1698	0.2371	0.0132	0.9602	0.0922	0.0015	2.8	1411.4	42.1	1371.5	68.7	1471.3	29.8	1471.3	68.7
OK12_39_47	3.1201	0.1879	0.2423	0.0134	0.9128	0.0934	0.0023	2.7	1437.7	45.3	1398.6	69.4	1495.0	45.8	1495.0	69.4
OK12_39_58	2.9776	0.2148	0.2294	0.0153	0.9164	0.0940	0.0027	5.0	1401.9	53.4	1331.2	79.6	1509.0	53.6	1509.0	79.6
OK12_39_114	2.7359	0.1018	0.2014	0.0071	0.9135	0.0985	0.0015	11.6	1338.3	27.3	1182.8	38.1	1596.0	28.1	1596.0	38.1
OK12_39_59	3.6069	0.2598	0.2588	0.0173	0.9223	0.1010	0.0028	4.3	1551.1	55.7	1483.8	87.9	1641.8	50.8	1641.8	87.9
OK12_39_32	4.1462	0.2324	0.2937	0.0164	0.9646	0.1023	0.0015	0.2	1663.5	44.8	1659.9	81.1	1667.0	27.3	1667.0	81.1
OK12_39_56	3.6113	0.2595	0.2539	0.0170	0.9245	0.1030	0.0028	6.0	1552.0	55.6	1458.5	86.6	1679.6	49.8	1679.6	86.6
OK12_39_76	5.1131	0.2951	0.3325	0.0178	0.9128	0.1116	0.0026	-0.7	1838.3	47.9	1850.5	85.7	1825.1	42.2	1825.1	85.7
OK12_39_14	4.4709	0.1817	0.2904	0.0101	0.8791	0.1116	0.0022	4.8	1725.6	33.2	1643.4	50.2	1825.9	34.8	1825.9	50.2
OK12_39_87	6.2637	0.2522	0.3091	0.0131	0.9188	0.1301	0.0022	13.8	2013.4	34.7	1736.3	64.1	2099.7	29.2	2099.7	64.1
OK12_39_51	7.5357	0.5418	0.3828	0.0255	0.9223	0.1426	0.0040	4.0	2177.2	62.5	2089.5	117.9	2259.0	47.2	2259.0	117.9
OK12_39_92	13.0795	0.5274	0.4595	0.0193	0.9081	0.1828	0.0032	9.2	2685.4	37.3	2437.3	84.9	2678.3	29.1	2678.3	84.9
OK12_39_34	11.3162	0.6395	0.4464	0.0251	0.9643	0.1838	0.0028	6.7	2549.5	51.4	2379.0	111.0	2687.2	24.7	2687.2	111.0
OK12_39_43	13.4031	0.7945	0.5274	0.0289	0.9186	0.1842	0.0043	-0.8	2708.5	54.5	2730.7	120.8	2691.2	38.2	2691.2	120.8

OK12-16, Mississippian Stanley Group – Detrital zircon

TABLE B3 - *Detrital zircon U-Pb geochronologic analyses of Mississippian Stanley Group (OK12-16) by LA-ICP-MS*

	Isotopic ratios								Isotopic ages (Ma)							
Analysis #	207/235	1 σ err.	206/238	1 σ err.	RHO	207/206	1 σ err.	% Dis.	207/235	1 σ err.	206/238	1 σ err.	207/206	1 σ err.	Best age	1 σ err.
OK12_16_44	0.3730	0.0323	0.0471	0.0028	0.8815	0.0574	0.0025	7.8	321.8	23.6	296.7	17.2	508.0	94.3	296.7	17.2
OK12_16_34	0.4066	0.0515	0.0498	0.0034	0.9320	0.0591	0.0040	9.6	346.4	36.5	313.3	20.8	572.6	141.2	313.3	20.8
OK12_16_92	0.5708	0.0400	0.0684	0.0047	0.8911	0.0605	0.0020	7.0	458.5	25.6	426.4	28.5	619.8	68.7	426.4	28.5
OK12_16_120	0.5939	0.0272	0.0687	0.0031	0.7401	0.0626	0.0020	9.5	473.3	17.2	428.4	18.4	695.2	67.9	428.4	18.4
OK12_16_55	0.6426	0.0745	0.0741	0.0084	0.9648	0.0630	0.0019	8.6	503.9	45.1	460.6	50.5	706.7	63.7	460.6	50.5
OK12_16_7	0.5611	0.1002	0.0749	0.0070	0.9315	0.0543	0.0053	-3.0	452.2	63.2	465.8	42.1	384.0	204.7	465.8	42.1
OK12_16_18	0.7181	0.0938	0.0817	0.0062	0.9224	0.0638	0.0043	7.9	549.6	54.0	506.0	37.0	733.4	136.1	506.0	37.0
OK12_16_118	0.8212	0.0372	0.0897	0.0040	0.8033	0.0663	0.0019	9.0	608.7	20.5	553.9	23.6	816.0	57.9	553.9	23.6
OK12_16_75	0.7660	0.0466	0.0927	0.0045	0.6262	0.0600	0.0029	1.0	577.5	26.4	571.5	26.3	602.1	101.5	571.5	26.3
OK12_16_67	0.8092	0.0716	0.0929	0.0081	0.9579	0.0632	0.0016	4.9	602.0	39.4	572.5	47.8	715.2	53.4	572.5	47.8
OK12_16_47	0.8187	0.0671	0.0957	0.0054	0.8998	0.0621	0.0025	3.0	607.3	36.8	588.9	31.8	676.7	82.5	588.9	31.8
OK12_16_104	0.9465	0.0257	0.1010	0.0013	-0.9065	0.0680	0.0026	8.3	676.3	13.3	620.2	7.4	867.9	78.6	620.2	7.4
OK12_16_91	0.8613	0.0622	0.1054	0.0074	0.8225	0.0592	0.0025	-2.4	630.9	33.4	645.9	42.8	574.3	89.6	645.9	42.8
OK12_16_103	1.0605	0.0318	0.1086	0.0019	-0.3586	0.0708	0.0028	9.5	734.1	15.6	664.4	11.2	953.0	79.7	664.4	11.2
OK12_16_48	1.0731	0.0893	0.1097	0.0064	0.8990	0.0710	0.0028	9.4	740.3	42.8	671.0	36.9	956.2	79.9	671.0	36.9
OK12_16_73	1.0297	0.0631	0.1118	0.0054	0.5966	0.0668	0.0034	4.9	718.8	31.1	683.4	31.1	831.7	101.9	683.4	31.1
OK12_16_9	1.2804	0.2279	0.1326	0.0123	0.9321	0.0701	0.0068	4.1	837.0	96.7	802.6	69.7	930.0	188.0	802.6	69.7
OK12_16_30	1.3656	0.1773	0.1343	0.0100	0.9271	0.0737	0.0049	7.1	874.3	73.4	812.1	56.4	1032.8	130.0	812.1	56.4
OK12_16_69	1.3018	0.1126	0.1376	0.0120	0.9781	0.0686	0.0012	1.8	846.5	48.5	831.1	67.4	887.2	37.1	831.1	67.4
OK12_16_101	1.3773	0.0345	0.1408	0.0015	-0.8828	0.0710	0.0025	3.4	879.3	14.6	849.0	8.4	956.5	69.5	849.0	8.4
OK12_16_77	1.7558	0.1067	0.1580	0.0076	0.6143	0.0806	0.0040	8.1	1029.3	38.6	945.9	42.0	1211.9	93.7	945.9	42.0
OK12_16_68	1.7762	0.1553	0.1600	0.0140	0.9740	0.0805	0.0016	7.7	1036.8	55.3	957.0	77.5	1209.4	38.8	957.0	77.5
OK12_16_88	1.8588	0.1296	0.1613	0.0111	0.8990	0.0835	0.0026	9.6	1066.6	45.0	964.0	61.5	1280.1	59.6	964.0	61.5
OK12_16_114	1.6677	0.0752	0.1619	0.0072	0.8257	0.0746	0.0020	2.9	996.3	28.2	967.3	39.9	1058.4	52.4	967.3	39.9
OK12_16_106	1.6174	0.0428	0.1631	0.0020	-0.7743	0.0719	0.0027	0.3	977.0	16.5	974.2	11.2	983.4	73.4	974.2	11.2
OK12_16_66	1.9366	0.1683	0.1794	0.0157	0.9776	0.0783	0.0014	2.7	1093.8	56.6	1063.8	85.1	1154.2	36.2	1154.2	36.2
OK12_16_109	2.1609	0.0975	0.1961	0.0087	0.8266	0.0798	0.0021	1.2	1168.6	30.9	1154.2	46.9	1193.0	51.3	1193.0	51.3
OK12_16_107	2.2022	0.0580	0.1971	0.0024	-0.8612	0.0810	0.0030	1.9	1181.7	18.2	1159.7	12.7	1222.4	71.3	1222.4	71.3
OK12_16_3	2.4716	0.4324	0.2181	0.0195	0.9397	0.0822	0.0079	-0.6	1263.7	119.2	1271.9	102.4	1250.2	177.1	1250.2	177.1
OK12_16_76	2.1293	0.1293	0.1832	0.0087	0.6091	0.0843	0.0042	6.4	1158.4	41.1	1084.5	47.5	1300.1	93.0	1300.1	93.0
OK12_16_97	3.0964	0.0817	0.2409	0.0028	-0.9256	0.0932	0.0035	2.8	1431.8	20.0	1391.5	14.7	1492.4	69.4	1492.4	69.4
OK12_16_87	3.1016	0.2162	0.2354	0.0163	0.9038	0.0954	0.0029	4.9	1433.1	52.2	1362.8	84.3	1536.2	56.2	1536.2	56.2

OK12-16, Mississippian Stanley Group – Detrital zircon, *continued*

OK12_16_43	2.4378	0.1915	0.1827	0.0097	0.9036	0.0968	0.0037	13.7	1253.8	55.0	1082.0	52.6	1562.5	69.9	1562.5	69.9
OK12_16_64	2.3394	0.2015	0.1727	0.0150	0.9783	0.0982	0.0018	16.1	1224.3	59.5	1027.1	81.7	1590.9	33.3	1590.9	33.3
OK12_16_52	2.5953	0.2854	0.1855	0.0206	0.9903	0.1015	0.0016	15.6	1299.3	77.6	1096.9	110.8	1652.1	28.2	1652.1	28.2
OK12_16_89	4.6992	0.3269	0.3224	0.0222	0.9055	0.1056	0.0032	-1.9	1767.1	56.6	1801.3	107.5	1724.2	54.3	1724.2	54.3
OK12_16_6	2.9790	0.5220	0.1979	0.0178	0.9391	0.1092	0.0105	17.0	1402.3	125.2	1164.1	95.0	1785.8	165.2	1785.8	165.2
OK12_16_95	4.8200	0.3370	0.3083	0.0213	0.9009	0.1132	0.0035	3.1	1788.4	57.2	1732.2	104.3	1852.0	55.0	1852.0	55.0
OK12_16_72	4.6675	0.3938	0.2960	0.0252	0.9859	0.1144	0.0016	5.1	1761.4	68.2	1671.3	124.3	1870.2	25.5	1870.2	25.5
OK12_16_74	3.9291	0.2379	0.2467	0.0118	0.6286	0.1155	0.0056	12.2	1619.7	47.9	1421.6	60.9	1888.3	84.1	1888.3	84.1
OK12_16_46	4.6281	0.3609	0.2877	0.0149	0.9014	0.1167	0.0045	7.1	1754.4	63.1	1629.9	74.4	1906.1	67.5	1906.1	67.5
OK12_16_99	4.1881	0.1107	0.2517	0.0029	-0.9915	0.1207	0.0046	13.4	1671.7	21.4	1447.3	15.0	1966.2	66.2	1966.2	66.2
OK12_16_82	4.1622	0.2645	0.2473	0.0121	0.5234	0.1221	0.0069	14.5	1666.6	50.7	1424.4	62.3	1987.7	97.0	1987.7	97.0
OK12_16_33	3.7409	0.4568	0.2181	0.0138	0.9490	0.1242	0.0081	19.5	1580.2	93.4	1272.0	72.7	2017.9	111.2	2017.9	111.2
OK12_16_14	4.1385	0.5478	0.2384	0.0191	0.9237	0.1258	0.0083	17.1	1661.9	102.9	1378.6	98.7	2040.5	112.2	2040.5	112.2
OK12_16_93	5.5671	0.3920	0.3150	0.0219	0.8897	0.1280	0.0042	7.6	1911.0	58.9	1765.1	106.4	2070.7	56.8	2070.7	56.8
OK12_16_84	5.2526	0.3213	0.2895	0.0140	0.6157	0.1317	0.0065	11.9	1861.2	50.9	1638.9	69.5	2120.2	84.0	2120.2	84.0
OK12_16_60	5.1091	0.5568	0.2740	0.0302	0.9931	0.1353	0.0017	15.1	1837.6	88.6	1561.0	150.8	2167.9	22.3	2167.9	22.3
OK12_16_54	6.0192	0.6489	0.2980	0.0325	0.9944	0.1466	0.0017	15.0	1978.6	89.8	1681.4	159.4	2306.2	19.6	2306.2	19.6
OK12_16_38	6.1713	0.4985	0.2879	0.0160	0.9025	0.1555	0.0060	18.5	2000.4	68.2	1630.9	79.7	2407.1	64.5	2407.1	64.5
OK12_16_108	13.3315	0.3740	0.6031	0.0082	-0.8513	0.1603	0.0065	-12.5	2703.4	26.2	3042.2	33.0	2459.2	66.5	2459.2	66.5
OK12_16_40	6.9927	0.5541	0.3114	0.0166	0.8991	0.1628	0.0064	17.2	2110.5	68.1	1747.8	81.0	2485.4	64.4	2485.4	64.4
OK12_16_112	8.1819	0.3684	0.3626	0.0162	0.8455	0.1635	0.0041	11.4	2251.3	39.9	1994.3	76.1	2492.0	41.4	2492.0	41.4
OK12_16_94	10.8947	0.7598	0.4757	0.0329	0.9048	0.1659	0.0050	0.2	2514.2	62.9	2508.6	142.1	2516.2	50.1	2516.2	50.1
OK12_16_85	9.5086	0.6643	0.4136	0.0286	0.8986	0.1665	0.0052	6.6	2388.4	62.2	2231.2	129.0	2522.9	51.6	2522.9	51.6
OK12_16_80	10.7853	0.6526	0.4502	0.0216	0.6298	0.1738	0.0083	4.3	2504.8	54.7	2396.3	95.2	2594.7	77.9	2594.7	77.9
OK12_16_57	8.6115	0.9264	0.3436	0.0374	0.9955	0.1819	0.0019	17.1	2297.8	93.4	1903.8	177.0	2670.0	17.1	2670.0	17.1
OK12_16_63	13.3152	1.1509	0.5079	0.0442	0.9794	0.1902	0.0034	2.0	2702.3	78.5	2647.6	186.1	2743.5	28.7	2743.5	28.7
OK12_16_10	15.1279	2.6405	0.5332	0.0474	0.9408	0.2058	0.0197	2.4	2823.3	154.0	2755.1	196.4	2872.7	147.6	2872.7	147.6
OK12_16_22	14.2879	1.8047	0.4344	0.0312	0.9334	0.2385	0.0154	16.0	2769.0	113.3	2325.3	138.5	3109.8	99.4	3109.8	99.4

OK12-52, Mississippian Stanley Group – Detrital zircon

TABLE B4 - *Detrital zircon U-Pb geochronologic analyses of Mississippian Stanley Group (OK12-52) by LA-ICP-MS*

	Isotopic ratios								Isotopic ages (Ma)							
Analysis #	207/235	1 σ err.	206/238	1 σ err.	RHO	207/206	1 σ err.	% Dis.	207/235	1 σ err.	206/238	1 σ err.	207/206	1 σ err.	Best age	1 σ err.
OK12_52_108	0.4083	0.0159	0.0562	0.0018	0.6976	0.0527	0.0015	-1.4	347.7	11.4	352.5	11.1	314.0	63.5	352.5	11.1
OK12_52_101	0.5714	0.0221	0.0698	0.0023	0.7106	0.0593	0.0016	5.2	458.9	14.2	435.2	13.6	578.1	59.0	435.2	13.6
OK12_52_17	0.6216	0.0479	0.0743	0.0052	0.8740	0.0605	0.0023	5.8	490.9	29.6	462.2	30.9	622.1	79.0	462.2	30.9
OK12_52_20	0.6540	0.0500	0.0786	0.0054	0.8678	0.0602	0.0023	4.5	510.9	30.2	487.7	32.0	611.4	80.1	487.7	32.0
OK12_52_96	0.6282	0.0301	0.0791	0.0035	0.8430	0.0576	0.0015	0.8	495.0	18.6	490.9	21.1	513.5	56.4	490.9	21.1
OK12_52_92	0.6469	0.0295	0.0797	0.0035	0.9009	0.0589	0.0012	2.5	506.6	18.0	494.1	20.9	562.9	43.0	494.1	20.9
OK12_52_58	0.6176	0.1984	0.0815	0.0164	0.8126	0.0571	0.0112	-3.4	488.4	117.5	505.1	97.1	493.6	383.1	505.1	97.1
OK12_52_62	0.6052	0.1951	0.0827	0.0170	0.8136	0.0551	0.0108	-6.6	480.5	116.5	512.4	100.7	417.4	386.4	512.4	100.7
OK12_52_84	0.6743	0.0294	0.0848	0.0036	0.9087	0.0576	0.0011	-0.3	523.3	17.7	524.7	21.1	516.4	39.8	524.7	21.1
OK12_52_56	0.6146	0.1973	0.0870	0.0175	0.8132	0.0532	0.0104	-10.5	486.5	117.0	537.7	103.0	337.4	392.2	537.7	103.0
OK12_52_79	0.7600	0.0336	0.0880	0.0037	0.8971	0.0626	0.0012	5.3	574.0	19.2	543.4	22.0	696.3	41.4	543.4	22.0
OK12_52_114	0.8409	0.0415	0.0983	0.0044	0.8092	0.0620	0.0018	2.5	619.6	22.6	604.5	25.5	672.9	61.5	604.5	25.5
OK12_52_34	0.8033	0.0584	0.0984	0.0062	0.8504	0.0591	0.0023	-1.1	598.7	32.3	605.3	36.3	569.7	81.1	605.3	36.3
OK12_52_72	0.8026	0.2580	0.0993	0.0204	0.8153	0.0609	0.0119	-2.0	598.3	135.8	610.1	118.5	636.4	371.2	610.1	118.5
OK12_52_89	0.9728	0.0454	0.1015	0.0046	0.9268	0.0695	0.0012	9.7	689.9	23.1	623.1	27.0	914.1	35.9	623.1	27.0
OK12_52_80	0.9618	0.0432	0.1035	0.0044	0.8791	0.0673	0.0015	7.2	684.2	22.1	635.2	25.7	848.3	44.3	635.2	25.7
OK12_52_111	0.9570	0.0461	0.1055	0.0046	0.8262	0.0657	0.0018	5.1	681.8	23.6	646.8	26.7	796.4	56.4	646.8	26.7
OK12_52_119	0.9356	0.0441	0.1059	0.0045	0.8289	0.0640	0.0017	3.2	670.6	22.9	648.9	26.1	741.7	55.2	648.9	26.1
OK12_52_113	1.0223	0.0481	0.1072	0.0046	0.8393	0.0691	0.0018	8.2	715.1	23.9	656.3	26.5	901.6	52.2	656.3	26.5
OK12_52_23	1.0648	0.0818	0.1140	0.0078	0.8599	0.0676	0.0027	5.5	736.2	39.5	695.7	44.9	856.9	79.5	695.7	44.9
OK12_52_93	1.1004	0.0506	0.1262	0.0056	0.8903	0.0632	0.0013	-1.7	753.5	24.2	766.0	31.8	716.4	44.4	766.0	31.8
OK12_52_52	1.2633	0.4061	0.1330	0.0268	0.8123	0.0715	0.0141	2.9	829.4	167.6	805.2	150.8	971.4	356.7	805.2	150.8
OK12_52_65	1.4406	0.4632	0.1398	0.0287	0.8155	0.0777	0.0151	6.9	906.0	176.4	843.3	160.5	1138.4	344.9	843.3	160.5
OK12_52_66	1.3754	0.4423	0.1487	0.0306	0.8156	0.0697	0.0136	-1.8	878.5	173.4	893.9	169.4	918.8	355.8	893.9	169.4
OK12_52_25	1.5372	0.1117	0.1490	0.0094	0.8503	0.0747	0.0029	5.3	945.4	43.8	895.3	52.4	1060.1	75.2	895.3	52.4
OK12_52_102	1.4316	0.0594	0.1525	0.0052	0.6445	0.0681	0.0022	-1.4	902.2	24.5	914.7	28.8	870.4	66.0	914.7	28.8
OK12_52_40	1.5681	0.0595	0.1542	0.0043	0.7053	0.0737	0.0020	3.5	957.7	23.2	924.5	24.0	1034.0	53.4	924.5	24.0
OK12_52_53	1.5544	0.4996	0.1554	0.0313	0.8123	0.0753	0.0148	2.2	952.2	181.4	931.3	172.3	1076.6	351.4	931.3	172.3
OK12_52_16	1.8401	0.1408	0.1571	0.0108	0.8769	0.0848	0.0031	11.2	1059.9	49.1	940.8	60.0	1309.9	69.8	940.8	60.0
OK12_52_64	1.3700	0.4417	0.1575	0.0324	0.8126	0.0656	0.0129	-7.6	876.2	173.5	942.7	178.0	792.3	365.2	942.7	178.0
OK12_52_18	1.6017	0.1241	0.1590	0.0110	0.8584	0.0729	0.0029	2.1	970.9	47.3	951.0	60.7	1011.8	78.7	951.0	60.7
OK12_52_24	1.9155	0.1460	0.1597	0.0109	0.8712	0.0868	0.0033	12.1	1086.5	49.6	955.1	60.3	1356.0	70.5	955.1	60.3

OK12-52, Mississippian Stanley Group – Detrital zircon, *continued*

OK12_52_14	2.1912	0.1766	0.1600	0.0117	0.8820	0.0991	0.0038	18.8	1178.3	54.7	956.6	64.9	1607.9	69.3	956.6	64.9
OK12_52_54	1.5606	0.5012	0.1605	0.0323	0.8128	0.0732	0.0144	-0.5	954.7	181.5	959.5	177.0	1019.9	353.7	959.5	177.0
OK12_52_6	1.8179	0.0887	0.1608	0.0072	0.8675	0.0819	0.0020	8.6	1051.9	31.5	961.3	39.6	1243.4	47.0	961.3	39.6
OK12_52_83	1.6885	0.0742	0.1718	0.0072	0.8891	0.0712	0.0014	-1.8	1004.2	27.6	1022.2	39.5	964.4	40.9	964.4	40.9
OK12_52_47	1.7237	0.0649	0.1625	0.0045	0.7085	0.0769	0.0020	4.6	1017.4	23.9	970.6	24.9	1118.9	52.1	970.6	24.9
OK12_52_85	1.6841	0.0761	0.1640	0.0072	0.9092	0.0745	0.0014	2.3	1002.5	28.4	979.1	39.5	1053.8	37.8	979.1	39.5
OK12_52_107	1.7553	0.0639	0.1646	0.0052	0.8094	0.0773	0.0017	4.6	1029.1	23.3	982.1	29.0	1129.3	42.3	982.1	29.0
OK12_52_73	1.8202	0.0815	0.1817	0.0077	0.8844	0.0726	0.0015	-2.2	1052.7	28.9	1076.0	42.1	1004.1	42.3	1004.1	42.3
OK12_52_87	1.7677	0.0791	0.1728	0.0076	0.9295	0.0742	0.0012	0.6	1033.7	28.6	1027.7	41.4	1046.1	33.2	1046.1	33.2
OK12_52_88	1.8778	0.0880	0.1821	0.0081	0.8729	0.0748	0.0017	-0.5	1073.3	30.6	1078.5	44.1	1062.5	45.9	1062.5	45.9
OK12_52_70	2.0519	0.6595	0.2058	0.0423	0.8152	0.0751	0.0146	-6.5	1132.9	198.7	1206.5	222.1	1071.7	348.3	1071.7	348.3
OK12_52_109	1.8014	0.0861	0.1718	0.0075	0.8402	0.0760	0.0020	2.3	1046.0	30.7	1022.0	40.9	1093.9	51.4	1093.9	51.4
OK12_52_81	1.9666	0.0856	0.1820	0.0077	0.9272	0.0784	0.0013	2.4	1104.1	28.9	1077.7	41.9	1155.9	32.2	1155.9	32.2
OK12_52_43	2.2503	0.0923	0.1972	0.0058	0.6263	0.0828	0.0027	3.1	1196.9	28.4	1160.0	31.1	1263.4	61.6	1263.4	61.6
OK12_52_90	2.4269	0.1114	0.2109	0.0094	0.9157	0.0835	0.0016	1.4	1250.6	32.5	1233.5	49.8	1279.9	35.9	1279.9	35.9
OK12_52_117	2.4834	0.1168	0.2152	0.0092	0.8400	0.0836	0.0021	0.8	1267.2	33.5	1256.5	48.5	1283.1	49.3	1283.1	49.3
OK12_52_120	3.1008	0.1463	0.2410	0.0103	0.8394	0.0932	0.0024	2.9	1432.9	35.6	1391.9	53.3	1492.0	48.1	1492.0	48.1
OK12_52_97	2.8195	0.1075	0.2178	0.0071	0.7430	0.0939	0.0024	6.7	1360.7	28.2	1270.0	37.3	1505.1	48.1	1505.1	48.1
OK12_52_11	3.7165	0.1793	0.2750	0.0123	0.8951	0.0979	0.0021	0.5	1574.9	37.9	1566.3	62.0	1584.9	39.8	1584.9	39.8
OK12_52_63	4.4865	1.4414	0.3096	0.0635	0.8156	0.1092	0.0212	-0.6	1728.5	236.9	1738.5	305.5	1786.2	317.6	1786.2	317.6
OK12_52_95	5.4111	0.2422	0.3425	0.0150	0.9324	0.1146	0.0019	-0.6	1886.6	37.7	1898.9	71.6	1872.9	29.1	1872.9	29.1
OK12_52_57	5.1818	1.6632	0.3394	0.0683	0.8132	0.1150	0.0225	-1.8	1849.6	241.9	1883.8	320.5	1879.1	316.8	1879.1	316.8
OK12_52_59	3.7708	1.2106	0.2434	0.0490	0.8130	0.1166	0.0229	11.5	1586.6	229.6	1404.4	249.1	1905.4	316.0	1905.4	316.0
OK12_52_48	3.6410	0.1377	0.2248	0.0064	0.7297	0.1174	0.0030	16.1	1558.5	29.7	1307.2	33.4	1917.5	45.7	1917.5	45.7
OK12_52_91	6.3134	0.2804	0.3809	0.0165	0.9324	0.1202	0.0019	-3.0	2020.3	38.2	2080.6	76.8	1959.0	28.6	1959.0	28.6
OK12_52_39	6.1617	0.2351	0.3594	0.0102	0.7197	0.1243	0.0033	1.0	1999.0	32.8	1979.1	48.3	2019.1	46.2	2019.1	46.2
OK12_52_30	4.6269	0.3347	0.2644	0.0166	0.8589	0.1267	0.0047	13.8	1754.1	58.7	1512.2	84.3	2052.6	64.0	2052.6	64.0
OK12_52_94	7.9996	0.3571	0.4294	0.0188	0.9334	0.1351	0.0022	-3.2	2231.0	39.5	2303.1	84.0	2165.2	27.9	2165.2	27.9
OK12_52_49	5.4541	1.7520	0.3003	0.0605	0.8130	0.1367	0.0268	10.6	1893.4	243.9	1692.8	293.1	2186.4	306.7	2186.4	306.7
OK12_52_46	7.7396	0.2866	0.4064	0.0110	0.7064	0.1381	0.0036	0.1	2201.2	32.8	2198.5	50.1	2203.2	44.8	2203.2	44.8
OK12_52_7	9.0486	0.4389	0.3745	0.0170	0.9033	0.1751	0.0037	12.5	2342.9	43.4	2050.4	79.2	2607.0	34.3	2607.0	34.3
OK12_52_15	11.3772	0.8691	0.4695	0.0323	0.8779	0.1754	0.0064	2.9	2554.6	68.9	2481.2	140.1	2609.7	59.7	2609.7	59.7
OK12_52_98	11.1311	0.4015	0.4501	0.0143	0.8190	0.1793	0.0037	5.5	2534.2	33.1	2395.6	63.1	2646.0	34.1	2646.0	34.1
OK12_52_86	10.4865	0.4599	0.4116	0.0177	0.9354	0.1848	0.0029	10.3	2478.7	39.9	2222.2	80.2	2696.0	25.6	2696.0	25.6

OK12-54, Mississippian Stanley Group – Detrital zircon

TABLE B5 - *Detrital zircon U-Pb geochronologic analyses of Mississippian Stanley Group (OK12-54) by LA-ICP-MS*

	Isotopic ratios								Isotopic ages (Ma)							
Analysis #	207/235	1 σ err.	206/238	1 σ err.	RHO	207/206	1 σ err.	% Dis.	207/235	1 σ err.	206/238	1 σ err.	207/206	1 σ err.	Best age	1 σ err.
Ok12_54_31	0.3901	0.0144	0.0529	0.0015	0.5625	0.0535	0.0017	0.6	334.4	10.5	332.3	9.1	349.1	69.4	332.3	69.4
Ok12_54_91	0.5543	0.0284	0.0662	0.0033	0.9046	0.0590	0.0013	7.7	447.8	18.4	413.4	19.8	567.7	47.4	413.4	47.4
Ok12_54_95	0.5416	0.0270	0.0666	0.0032	0.9229	0.0573	0.0011	5.4	439.5	17.6	415.8	19.6	504.1	42.1	415.8	42.1
Ok12_54_90	0.5690	0.0286	0.0672	0.0033	0.9305	0.0597	0.0011	8.4	457.4	18.4	419.1	20.0	593.6	39.9	419.1	39.9
Ok12_54_37	0.5438	0.0313	0.0674	0.0028	0.7027	0.0585	0.0024	4.7	440.9	20.4	420.2	16.7	547.3	87.1	420.2	87.1
Ok12_54_69	0.6176	0.0584	0.0719	0.0053	0.8397	0.0625	0.0032	8.4	488.3	36.0	447.5	32.0	689.8	106.4	447.5	106.4
Ok12_54_66	0.5549	0.0529	0.0730	0.0054	0.8319	0.0552	0.0029	-1.4	448.2	34.0	454.4	32.6	422.0	114.4	454.4	114.4
Ok12_54_115	0.5772	0.0454	0.0742	0.0039	0.7430	0.0564	0.0030	0.3	462.6	28.8	461.3	23.4	468.8	113.2	461.3	113.2
Ok12_54_102	0.6315	0.0515	0.0747	0.0041	0.7196	0.0613	0.0035	6.6	497.0	31.5	464.2	24.3	651.1	117.4	464.2	117.4
Ok12_54_78	0.6495	0.0368	0.0747	0.0031	0.7705	0.0630	0.0023	8.6	508.2	22.4	464.5	18.5	709.6	75.2	464.5	75.2
Ok12_54_77	0.5843	0.0325	0.0749	0.0030	0.7626	0.0566	0.0020	0.4	467.2	20.6	465.5	17.9	475.1	77.9	465.5	77.9
Ok12_54_56	0.6518	0.0682	0.0788	0.0070	0.8578	0.0601	0.0032	4.0	509.6	41.1	489.1	41.8	605.6	112.3	489.1	112.3
Ok12_54_43	0.6714	0.0386	0.0789	0.0032	0.6807	0.0616	0.0026	6.1	521.5	23.2	489.7	18.9	660.3	87.8	489.7	87.8
Ok12_54_63	0.6591	0.0626	0.0801	0.0060	0.8371	0.0598	0.0031	3.4	514.1	37.6	496.8	35.5	596.8	109.2	496.8	109.2
Ok12_54_23	0.7038	0.0563	0.0838	0.0056	0.8313	0.0608	0.0027	4.1	541.1	33.0	518.6	33.1	630.4	93.0	518.6	93.0
Ok12_54_1	0.6981	0.0575	0.0856	0.0057	0.8197	0.0590	0.0028	1.6	537.6	33.8	529.2	33.9	567.0	99.6	529.2	99.6
Ok12_54_73	0.7439	0.0417	0.0865	0.0035	0.7524	0.0623	0.0023	5.2	564.7	24.0	535.1	20.5	685.3	77.1	535.1	77.1
Ok12_54_55	0.6831	0.0708	0.0878	0.0078	0.8647	0.0565	0.0029	-2.7	528.6	41.9	542.7	46.0	471.1	111.3	542.7	111.3
Ok12_54_68	0.7403	0.0705	0.0894	0.0066	0.8323	0.0602	0.0032	1.9	562.6	40.3	551.8	39.2	611.7	110.6	551.8	110.6
Ok12_54_83	0.7658	0.0433	0.0921	0.0037	0.7583	0.0603	0.0022	1.7	577.3	24.6	567.8	22.0	614.7	77.7	567.8	77.7
Ok12_54_27	0.7839	0.0223	0.0951	0.0025	0.8558	0.0598	0.0009	0.3	587.7	12.6	585.7	14.7	595.2	31.9	585.7	31.9
Ok12_54_105	0.8449	0.0660	0.0966	0.0051	0.7479	0.0634	0.0033	4.4	621.9	35.7	594.7	29.6	721.9	107.0	594.7	107.0
Ok12_54_25	0.8312	0.0263	0.0974	0.0027	0.7898	0.0619	0.0012	2.4	614.3	14.5	599.3	16.0	669.4	41.5	599.3	41.5
Ok12_54_74	0.7964	0.0438	0.0981	0.0039	0.7755	0.0589	0.0021	-1.4	594.8	24.5	603.1	22.8	562.7	74.2	603.1	74.2
Ok12_54_62	0.8482	0.0808	0.0996	0.0074	0.8320	0.0619	0.0033	1.9	623.7	43.5	611.8	43.3	672.1	109.7	611.8	109.7
Ok12_54_8	0.8166	0.0675	0.1023	0.0069	0.8158	0.0577	0.0028	-3.6	606.1	37.0	628.0	40.0	518.6	101.6	628.0	101.6
Ok12_54_58	0.8755	0.0903	0.1043	0.0092	0.8715	0.0609	0.0031	-0.2	638.6	47.7	639.8	53.6	636.8	105.3	639.8	105.3
Ok12_54_6	0.8942	0.0734	0.1075	0.0072	0.8250	0.0601	0.0028	-1.5	648.6	38.6	658.5	41.7	607.7	97.3	658.5	97.3
Ok12_54_106	0.9305	0.0732	0.1076	0.0056	0.7398	0.0627	0.0033	1.4	667.9	37.8	658.6	32.7	699.2	109.4	658.6	109.4
Ok12_54_52	1.0355	0.1067	0.1102	0.0097	0.8728	0.0682	0.0034	6.6	721.7	51.9	673.9	56.4	875.7	100.9	673.9	100.9
Ok12_54_76	1.0575	0.0605	0.1119	0.0045	0.7374	0.0685	0.0026	6.7	732.6	29.4	683.9	26.2	884.2	77.9	683.9	77.9
Ok12_54_82	1.2963	0.0720	0.1264	0.0051	0.7783	0.0744	0.0026	9.1	844.1	31.4	767.2	29.2	1051.6	69.0	767.2	69.0

OK12-54, Mississippian Stanley Group – Detrital zircon, *continued*

Ok12_54_7	1.2759	0.1049	0.1384	0.0092	0.8214	0.0667	0.0031	0.0	835.0	45.7	835.4	52.1	827.6	94.9	827.6	94.9
Ok12_54_113	1.3363	0.1033	0.1438	0.0074	0.7502	0.0674	0.0035	-0.5	861.6	43.9	866.1	41.6	850.1	103.6	850.1	103.6
Ok12_54_98	1.5506	0.1256	0.1598	0.0086	0.7140	0.0704	0.0040	-0.5	950.7	48.8	955.4	47.4	939.6	112.4	939.6	112.4
Ok12_54_72	1.6149	0.1536	0.1656	0.0124	0.8390	0.0709	0.0037	-1.2	976.0	58.0	988.1	68.1	953.8	102.9	953.8	102.9
Ok12_54_120	1.5450	0.1202	0.1570	0.0081	0.7468	0.0714	0.0037	0.9	948.5	46.8	940.0	45.2	968.1	102.8	968.1	102.8
Ok12_54_99	1.3467	0.1041	0.1365	0.0071	0.7529	0.0715	0.0037	4.8	866.1	44.1	825.0	39.9	972.7	101.3	972.7	101.3
Ok12_54_2	1.7015	0.1403	0.1713	0.0115	0.8226	0.0718	0.0034	-1.0	1009.1	51.4	1019.5	63.0	980.4	92.7	980.4	92.7
Ok12_54_15	1.8820	0.1501	0.1862	0.0124	0.8337	0.0731	0.0032	-2.4	1074.8	51.5	1100.8	66.8	1016.4	86.7	1016.4	86.7
Ok12_54_21	1.6243	0.1299	0.1602	0.0106	0.8301	0.0733	0.0033	2.2	979.7	49.0	957.8	58.8	1023.1	87.7	1023.1	87.7
Ok12_54_19	1.9132	0.1547	0.1874	0.0126	0.8250	0.0738	0.0034	-2.0	1085.7	52.6	1107.5	68.0	1036.4	89.7	1036.4	89.7
Ok12_54_13	1.6174	0.1302	0.1578	0.0106	0.8288	0.0741	0.0033	3.3	977.0	49.3	944.6	58.6	1044.6	88.3	1044.6	88.3
OK12_54_46	1.8646	0.1050	0.1816	0.0072	0.7064	0.0744	0.0030	-0.7	1068.6	36.6	1075.8	39.2	1051.0	78.3	1051.0	78.3
Ok12_54_93	1.5929	0.0794	0.1510	0.0074	0.9284	0.0744	0.0014	6.3	967.4	30.6	906.8	41.2	1051.3	37.2	1051.3	37.2
Ok12_54_114	1.7178	0.1338	0.1656	0.0086	0.7474	0.0752	0.0039	2.7	1015.2	48.8	987.7	47.5	1074.9	101.2	1074.9	101.2
Ok12_54_26	1.6132	0.0486	0.1552	0.0042	0.8283	0.0753	0.0013	4.6	975.3	18.7	930.3	23.7	1077.8	33.8	1077.8	33.8
Ok12_54_35	1.7631	0.0507	0.1681	0.0045	0.8852	0.0761	0.0010	2.9	1032.0	18.5	1001.6	25.1	1096.7	26.7	1096.7	26.7
Ok12_54_81	1.9650	0.1150	0.1872	0.0078	0.7244	0.0761	0.0031	-0.2	1103.6	38.6	1106.0	42.0	1098.4	78.7	1098.4	78.7
Ok12_54_65	1.7721	0.1685	0.1677	0.0126	0.8416	0.0768	0.0040	3.4	1035.3	59.9	999.7	68.9	1116.1	99.7	1116.1	99.7
Ok12_54_101	1.4519	0.1124	0.1364	0.0071	0.7531	0.0772	0.0040	9.5	910.7	45.5	824.2	40.0	1126.5	99.1	1126.5	99.1
Ok12_54_80	1.6107	0.0931	0.1499	0.0062	0.7371	0.0779	0.0030	7.6	974.4	35.6	900.3	34.5	1144.9	75.8	1144.9	75.8
Ok12_54_18	2.0935	0.1665	0.1935	0.0128	0.8357	0.0782	0.0034	0.5	1146.7	53.2	1140.5	68.9	1152.5	84.3	1152.5	84.3
Ok12_54_11	1.7607	0.1450	0.1626	0.0109	0.8241	0.0783	0.0037	5.8	1031.1	52.0	971.5	60.2	1153.8	89.9	1153.8	89.9
Ok12_54_22	1.6562	0.1323	0.1522	0.0102	0.8373	0.0787	0.0034	7.9	991.9	49.3	913.5	56.6	1163.8	84.2	1163.8	84.2
Ok12_54_42	2.1884	0.1220	0.2009	0.0079	0.7101	0.0789	0.0031	-0.2	1177.3	38.1	1180.3	42.2	1169.0	75.8	1169.0	75.8
Ok12_54_40	1.7835	0.1004	0.1636	0.0065	0.7099	0.0790	0.0031	6.0	1039.5	36.0	976.7	36.0	1170.9	76.6	1170.9	76.6
Ok12_54_32	2.1242	0.0653	0.1929	0.0053	0.8003	0.0799	0.0015	1.7	1156.7	21.0	1137.1	28.5	1193.3	36.3	1193.3	36.3
Ok12_54_38	1.7140	0.0967	0.1553	0.0062	0.7111	0.0799	0.0032	8.2	1013.8	35.6	930.9	34.6	1194.5	76.4	1194.5	76.4
Ok12_54_67	1.8441	0.1747	0.1661	0.0124	0.8401	0.0807	0.0042	6.6	1061.3	60.5	990.8	67.9	1213.9	98.3	1213.9	98.3
Ok12_54_9	2.6080	0.2133	0.2319	0.0154	0.8249	0.0813	0.0038	-3.2	1302.9	58.3	1344.6	80.3	1228.8	88.2	1228.8	88.2
Ok12_54_24	1.9956	0.1595	0.1750	0.0117	0.8359	0.0825	0.0036	6.7	1114.0	52.7	1039.4	63.7	1257.0	83.5	1257.0	83.5
Ok12_54_75	2.2557	0.1258	0.1910	0.0078	0.7781	0.0856	0.0030	6.0	1198.6	38.5	1126.7	41.8	1330.1	66.5	1330.1	66.5
Ok12_54_14	2.8988	0.2323	0.2404	0.0160	0.8320	0.0872	0.0039	-0.5	1381.6	58.8	1388.8	82.8	1364.9	83.3	1364.9	83.3
Ok12_54_4	1.9457	0.1629	0.1535	0.0105	0.8280	0.0916	0.0043	16.1	1097.0	54.7	920.6	58.7	1460.1	86.7	1460.1	86.7
OK12_54_45	2.8928	0.1625	0.2152	0.0086	0.7145	0.0974	0.0038	9.0	1380.0	41.5	1256.4	45.3	1574.0	71.8	1574.0	71.8
OK12_54_49	2.4403	0.2540	0.1720	0.0153	0.8594	0.1030	0.0055	18.4	1254.6	72.3	1023.2	83.4	1679.2	95.2	1679.2	95.2
Ok12_54_108	2.5071	0.1977	0.1764	0.0091	0.7253	0.1031	0.0056	17.8	1274.1	55.7	1047.1	49.9	1680.4	97.5	1680.4	97.5
Ok12_54_84	4.0514	0.2225	0.2805	0.0112	0.7823	0.1047	0.0036	3.1	1644.6	43.8	1593.8	56.0	1709.7	61.9	1709.7	61.9
Ok12_54_109	2.9481	0.2294	0.2030	0.0107	0.7580	0.1053	0.0054	14.6	1394.4	57.3	1191.2	56.9	1720.3	91.2	1720.3	91.2

OK12-54, Mississippian Stanley Group – Detrital zircon, *continued*

Ok12_54_117	3.9825	0.3086	0.2698	0.0140	0.7529	0.1070	0.0055	5.6	1630.6	61.0	1540.0	70.7	1749.4	91.3	1749.4	91.3
Ok12_54_110	3.7853	0.2950	0.2544	0.0133	0.7497	0.1079	0.0056	8.1	1589.6	60.7	1461.1	67.9	1764.4	92.0	1764.4	92.0
Ok12_54_61	2.9859	0.2818	0.1988	0.0148	0.8437	0.1092	0.0056	16.8	1404.0	69.4	1168.7	78.9	1786.2	90.1	1786.2	90.1
Ok12_54_10	3.7691	0.3101	0.2457	0.0165	0.8274	0.1109	0.0051	10.7	1586.2	64.0	1416.2	84.8	1814.6	81.6	1814.6	81.6
Ok12_54_20	4.9419	0.3951	0.3175	0.0211	0.8311	0.1126	0.0050	1.8	1809.4	65.4	1777.4	102.4	1841.3	78.4	1841.3	78.4
Ok12_54_107	4.7118	0.3648	0.2985	0.0155	0.7527	0.1145	0.0059	4.8	1769.3	62.9	1683.7	76.3	1871.8	89.9	1871.8	89.9
Ok12_54_12	6.1728	0.5062	0.3829	0.0256	0.8262	0.1166	0.0054	-4.5	2000.6	69.2	2089.9	118.2	1904.1	80.8	1904.1	80.8
Ok12_54_51	3.8382	0.3983	0.2383	0.0213	0.8756	0.1170	0.0059	13.9	1600.8	80.3	1377.8	110.0	1910.3	87.4	1910.3	87.4
Ok12_54_119	5.6930	0.4368	0.3276	0.0167	0.7510	0.1260	0.0064	5.4	1930.3	64.2	1826.9	80.5	2043.0	87.7	2043.0	87.7
Ok12_54_54	6.6337	0.6830	0.3726	0.0329	0.8735	0.1293	0.0065	1.1	2063.8	87.0	2041.5	152.9	2088.3	85.6	2088.3	85.6
Ok12_54_96	6.9132	0.3484	0.3491	0.0174	0.9359	0.1396	0.0025	8.1	2100.3	43.7	1930.4	82.4	2222.6	30.8	2222.6	30.8
Ok12_54_104	8.2710	0.6394	0.4000	0.0207	0.7537	0.1500	0.0077	4.1	2261.1	67.7	2169.0	94.6	2345.4	85.0	2345.4	85.0
Ok12_54_30	7.2496	0.2112	0.3348	0.0094	0.9118	0.1570	0.0019	13.1	2142.6	25.7	1861.6	45.0	2423.8	20.3	2423.8	20.3
Ok12_54_17	8.5321	0.6821	0.3866	0.0258	0.8384	0.1596	0.0070	8.0	2289.3	70.2	2107.2	119.0	2451.2	71.9	2451.2	71.9
Ok12_54_87	10.0400	0.4885	0.4179	0.0201	0.9414	0.1694	0.0028	7.7	2438.5	44.0	2250.8	90.8	2551.9	27.5	2551.9	27.5
Ok12_54_50	7.5475	0.7784	0.3140	0.0278	0.8702	0.1745	0.0089	19.2	2178.7	88.5	1760.5	134.8	2601.6	82.3	2601.6	82.3
Ok12_54_33	12.3914	0.3413	0.4336	0.0114	0.9154	0.2072	0.0023	11.9	2634.5	25.6	2322.1	51.3	2883.9	18.0	2883.9	18.0

OK12-57, Mississippian Stanley Group – Detrital zircon

TABLE B6 - *Detrital zircon U-Pb geochronologic analyses of Mississippian Stanley Group (OK12-57) by LA-ICP-MS*

	Isotopic ratios								Isotopic ages (Ma)							
Analysis #	207/235	1 σ err.	206/238	1 σ err.	RHO	207/206	1 σ err.	% Dis.	207/235	1 σ err.	206/238	1 σ err.	207/206	1 σ err.	Best age	1 σ err.
OK12_57_99	0.3634	0.1450	0.0509	0.0111	0.9974	0.0520	0.0094	-1.6	314.7	102.6	319.8	68.0	286.3	368.6	319.8	68.0
OK12_57_85	0.4672	0.1802	0.0568	0.0101	1.0478	0.0603	0.0116	8.5	389.2	117.6	356.2	61.2	615.5	367.8	356.2	61.2
OK12_57_116	0.3984	0.1137	0.0583	0.0055	0.9755	0.0500	0.0097	-7.3	340.5	79.3	365.3	33.2	194.1	399.7	365.3	33.2
OK12_57_40	0.4845	0.0833	0.0599	0.0081	0.8861	0.0582	0.0047	6.5	401.2	55.4	375.2	48.8	535.4	169.3	375.2	48.8
OK12_57_104	0.4112	0.1644	0.0623	0.0137	0.9971	0.0480	0.0087	-11.4	349.7	111.9	389.6	82.6	101.5	380.6	389.6	82.6
OK12_57_66	0.4846	0.0689	0.0632	0.0084	0.9737	0.0555	0.0018	1.5	401.2	46.0	395.1	50.8	433.3	71.5	395.1	50.8
OK12_57_93	0.5680	0.2187	0.0670	0.0118	1.0490	0.0622	0.0119	8.5	456.7	132.6	417.9	71.1	681.1	363.7	417.9	71.1
OK12_57_1	0.5266	0.0494	0.0672	0.0035	0.8738	0.0569	0.0031	2.4	429.5	32.3	419.3	21.1	487.8	116.0	419.3	21.1
OK12_57_117	0.4908	0.1402	0.0708	0.0067	0.9738	0.0507	0.0099	-8.8	405.5	91.2	441.0	40.0	227.4	397.6	441.0	40.0
OK12_57_92	0.5641	0.2173	0.0776	0.0138	1.0483	0.0533	0.0102	-6.1	454.2	132.1	481.8	81.8	342.3	383.3	481.8	81.8
OK12_57_95	0.6302	0.2428	0.0790	0.0140	1.0487	0.0586	0.0112	1.3	496.2	141.0	489.9	82.9	550.4	371.3	489.9	82.9
OK12_57_20	0.6248	0.0523	0.0791	0.0047	0.8496	0.0573	0.0026	0.5	492.8	32.2	490.6	28.0	504.8	97.5	490.6	28.0
OK12_57_90	0.6147	0.2369	0.0797	0.0141	1.0484	0.0565	0.0108	-1.7	486.5	139.0	494.6	83.8	473.8	375.6	494.6	83.8
OK12_57_56	0.6771	0.0463	0.0809	0.0038	0.8325	0.0607	0.0024	4.5	525.0	27.7	501.2	22.6	629.1	82.3	501.2	22.6
OK12_57_115	0.6188	0.1757	0.0820	0.0075	0.9838	0.0552	0.0107	-3.8	489.1	104.6	507.9	44.5	420.9	384.3	507.9	44.5
OK12_57_37	0.7110	0.1217	0.0928	0.0124	0.8868	0.0551	0.0045	-4.9	545.3	69.8	572.0	72.9	416.8	171.7	572.0	72.9
OK12_57_32	0.9215	0.1638	0.0990	0.0140	0.8911	0.0669	0.0055	8.2	663.2	83.1	608.7	81.8	835.6	162.8	608.7	81.8
OK12_57_109	0.9083	0.2582	0.1016	0.0093	0.9818	0.0654	0.0127	4.9	656.1	128.9	624.0	54.5	785.9	363.2	624.0	54.5
OK12_57_60	0.8500	0.0571	0.1022	0.0048	0.8527	0.0603	0.0022	-0.4	624.6	30.9	627.4	28.1	614.1	77.0	627.4	28.1
OK12_57_7	1.1058	0.1045	0.1149	0.0060	0.8696	0.0699	0.0039	7.3	756.2	49.2	700.9	34.8	926.1	109.7	700.9	34.8
OK12_57_100	1.0659	0.4252	0.1170	0.0257	0.9977	0.0663	0.0120	3.2	736.7	190.1	713.3	146.4	816.6	338.3	713.3	146.4
OK12_57_91	1.1294	0.4412	0.1230	0.0223	1.0398	0.0674	0.0132	2.6	767.5	191.2	747.8	126.7	849.0	361.1	747.8	126.7
OK12_57_75	1.3531	0.2131	0.1342	0.0198	0.9702	0.0733	0.0028	6.6	868.9	88.0	811.7	111.4	1022.9	76.0	811.7	111.4
OK12_57_106	1.2990	0.5180	0.1420	0.0311	0.9977	0.0666	0.0120	-1.3	845.3	206.3	856.2	173.3	824.6	337.8	856.2	173.3
OK12_57_76	1.7365	0.2669	0.1442	0.0207	0.9693	0.0875	0.0033	15.0	1022.2	94.5	868.5	115.5	1372.6	71.8	868.5	115.5
OK12_57_12	1.5643	0.1479	0.1463	0.0078	0.8736	0.0777	0.0042	8.0	956.2	56.9	879.9	43.8	1138.7	104.7	879.9	43.8
OK12_57_119	1.1643	0.3322	0.1472	0.0138	0.9752	0.0579	0.0113	-12.9	784.0	145.0	885.1	76.9	524.3	378.9	885.1	76.9
OK12_57_67	1.5213	0.2140	0.1483	0.0195	0.9724	0.0743	0.0025	5.1	939.0	82.7	891.5	108.5	1049.0	65.6	891.5	108.5
OK12_57_36	1.3897	0.2435	0.1500	0.0211	0.9001	0.0666	0.0052	-1.8	884.6	98.5	900.7	117.0	826.8	155.3	900.7	117.0
OK12_57_61	1.8963	0.2606	0.1546	0.0199	0.9760	0.0888	0.0027	14.2	1079.8	87.5	926.4	110.1	1400.7	57.2	926.4	110.1
OK12_57_118	1.2872	0.3701	0.1560	0.0150	0.9634	0.0603	0.0119	-11.3	840.0	152.3	934.6	83.1	615.7	376.0	934.6	83.1
OK12_57_47	1.7019	0.2916	0.1741	0.0233	0.8873	0.0703	0.0057	-2.5	1009.2	104.0	1034.8	126.9	937.0	157.8	937.0	157.8

OK12-57, Mississippian Stanley Group – Detrital zircon, *continued*

OK12_57_54	1.6435	0.1099	0.1570	0.0073	0.8455	0.0759	0.0028	4.8	987.1	41.3	939.9	40.3	1093.0	72.7	939.9	40.3
OK12_57_101	1.4937	0.5962	0.1573	0.0345	0.9975	0.0691	0.0125	-1.5	927.8	217.7	941.9	189.5	902.4	334.3	941.9	189.5
OK12_57_114	1.7074	0.4861	0.1768	0.0164	0.9791	0.0706	0.0138	-3.8	1011.3	167.7	1049.6	89.2	946.4	354.9	946.4	354.9
OK12_57_38	1.6813	0.2885	0.1703	0.0229	0.8877	0.0710	0.0058	-1.2	1001.5	103.8	1013.9	124.9	957.2	157.3	957.2	157.3
OK12_57_8	1.6558	0.1553	0.1683	0.0089	0.8765	0.0715	0.0039	-1.1	991.8	57.7	1002.5	48.7	970.9	106.3	970.9	106.3
OK12_57_39	1.6550	0.2832	0.1638	0.0219	0.8870	0.0727	0.0059	1.4	991.5	102.9	977.7	120.3	1005.0	156.2	977.7	120.3
OK12_57_33	1.6391	0.2882	0.1661	0.0235	0.9005	0.0709	0.0056	-0.6	985.4	105.2	990.8	128.4	956.0	152.5	990.8	128.4
OK12_57_59	1.9123	0.1248	0.1890	0.0085	0.8533	0.0733	0.0026	-2.8	1085.4	42.6	1116.2	46.0	1023.6	70.5	1023.6	70.5
OK12_57_44	1.7370	0.2969	0.1699	0.0227	0.8879	0.0735	0.0059	1.1	1022.4	104.6	1011.6	124.0	1028.5	155.1	1028.5	155.1
OK12_57_113	2.0172	0.5731	0.1918	0.0176	0.9828	0.0769	0.0150	-0.9	1121.3	176.6	1131.1	94.6	1119.1	346.0	1119.1	346.0
OK12_57_28	1.9639	0.3439	0.1836	0.0258	0.9013	0.0769	0.0060	1.5	1103.2	111.5	1086.6	139.0	1119.5	147.8	1119.5	147.8
OK12_57_102	2.3152	0.9254	0.2092	0.0460	0.9972	0.0806	0.0146	-0.6	1216.9	250.0	1224.5	240.7	1211.1	320.4	1211.1	320.4
OK12_57_105	2.4533	0.9795	0.2193	0.0482	0.9976	0.0815	0.0147	-1.6	1258.4	253.5	1278.0	249.7	1232.6	318.8	1232.6	318.8
OK12_57_14	2.0862	0.1664	0.1786	0.0102	0.8726	0.0848	0.0035	7.4	1144.3	53.3	1059.4	55.7	1310.2	77.3	1310.2	77.3
OK12_57_55	2.0036	0.1310	0.1681	0.0075	0.8451	0.0864	0.0032	10.3	1116.7	43.4	1001.6	41.2	1347.6	69.0	1347.6	69.0
OK12_57_5	2.1362	0.1981	0.1755	0.0089	0.8778	0.0884	0.0048	10.2	1160.6	62.2	1042.6	48.8	1390.7	100.0	1390.7	100.0
OK12_57_120	2.2526	0.6417	0.1831	0.0170	0.9783	0.0900	0.0176	9.5	1197.6	182.8	1083.8	91.9	1425.3	332.8	1425.3	332.8
OK12_57_34	3.5163	0.6152	0.2667	0.0374	0.9005	0.0948	0.0074	0.5	1530.9	129.7	1523.9	187.7	1524.7	140.3	1524.7	140.3
OK12_57_13	3.3550	0.2649	0.2551	0.0143	0.8707	0.0954	0.0039	1.9	1493.9	60.0	1464.9	73.2	1536.6	74.9	1536.6	74.9
OK12_57_26	2.2589	0.3951	0.1690	0.0237	0.9007	0.0961	0.0075	16.1	1199.6	116.2	1006.7	129.5	1550.2	139.6	1550.2	139.6
OK12_57_68	3.2880	0.4649	0.2362	0.0313	0.9746	0.1008	0.0032	7.5	1478.2	104.5	1367.0	161.1	1638.5	58.5	1638.5	58.5
OK12_57_71	3.1103	0.4255	0.2153	0.0276	0.9768	0.1046	0.0031	12.4	1435.2	100.0	1257.2	144.8	1706.9	53.8	1706.9	53.8
OK12_57_63	3.6503	0.5090	0.2524	0.0330	0.9748	0.1047	0.0033	7.0	1560.6	105.5	1451.1	167.4	1709.0	57.0	1709.0	57.0
OK12_57_43	5.1577	0.8777	0.3539	0.0471	0.8882	0.1048	0.0084	-5.8	1845.7	135.3	1953.2	220.4	1711.1	140.8	1711.1	140.8
OK12_57_25	4.9947	0.8756	0.3384	0.0477	0.9019	0.1062	0.0082	-3.3	1818.4	138.4	1879.0	225.6	1734.3	136.1	1734.3	136.1
OK12_57_111	3.9608	1.1254	0.2710	0.0250	0.9823	0.1069	0.0208	4.9	1626.2	207.6	1546.1	125.6	1746.8	319.0	1746.8	319.0
OK12_57_15	4.1276	0.3258	0.2580	0.0145	0.8721	0.1161	0.0047	10.9	1659.8	62.5	1479.4	74.0	1897.4	71.3	1897.4	71.3
OK12_57_19	3.3258	0.2616	0.2028	0.0111	0.8615	0.1190	0.0050	20.0	1487.1	59.6	1190.3	59.4	1941.6	73.2	1941.6	73.2
OK12_57_3	5.0096	0.4734	0.3003	0.0161	0.8753	0.1212	0.0066	7.0	1820.9	77.0	1692.6	79.5	1973.5	93.4	1973.5	93.4
OK12_57_22	5.0746	0.3988	0.2929	0.0164	0.8715	0.1257	0.0051	9.6	1831.9	64.6	1656.2	81.0	2039.0	70.0	2039.0	70.0
OK12_57_11	4.9643	0.4675	0.2853	0.0152	0.8754	0.1264	0.0068	10.8	1813.3	76.6	1618.0	75.6	2048.1	92.6	2048.1	92.6
OK12_57_69	4.6159	0.6396	0.2559	0.0331	0.9735	0.1306	0.0042	16.2	1752.1	109.5	1469.0	167.9	2105.9	55.4	2105.9	55.4
OK12_57_108	6.6239	2.6434	0.3372	0.0740	0.9977	0.1430	0.0259	9.2	2062.5	302.3	1873.0	347.2	2264.2	282.4	2264.2	282.4
OK12_57_29	6.4157	1.1224	0.3192	0.0447	0.8983	0.1445	0.0114	12.2	2034.4	143.1	1785.9	214.8	2282.4	129.6	2282.4	129.6
OK12_57_72	6.8920	0.9552	0.3432	0.0445	0.9751	0.1454	0.0045	9.3	2097.6	116.0	1901.8	210.2	2292.8	52.7	2292.8	52.7
OK12_57_16	11.2292	0.8839	0.4586	0.0257	0.8731	0.1777	0.0072	4.3	2542.3	70.9	2433.2	112.8	2631.7	65.6	2631.7	65.6
OK12_57_58	10.5005	0.6905	0.4063	0.0185	0.8516	0.1874	0.0068	11.4	2480.0	59.2	2198.0	84.2	2719.3	58.2	2719.3	58.2
OK12_57_50	9.5237	0.6355	0.3565	0.0161	0.8318	0.1937	0.0075	17.8	2389.8	59.5	1965.4	76.0	2774.0	61.7	2774.0	61.7

OK12-39, Pennsylvanian Jackfork Group – Detrital muscovite

au.28.5c.mus (OK12-39) Harold Johnson *j=0.0201310±0.000030* *Grain sizes = 0.177 - 0.42 mm*

#	40 V	39 V	38 V	37 V	36 V	Moles 40Ar*	%Rad	R	Age (Ma)	%-sd
Blank	*0.00745 ± 0.000085*	*0.00100 ± 0.000033*	*0.00018 ± 0.000013*	*0.00031 ± 0.000016*	*0.0000696 ± 0.000007*					
1	4.82010 ± 0.003021	0.42486 ± 0.000597	0.00542 ± 0.000049	-0.00206 ± 0.006663	0.000277 ± 0.000011	3.70E-14	98.3%	11.1523	365.40 ± 0.63	0.17%
2	3.80287 ± 0.002653	0.32212 ± 0.000452	0.00408 ± 0.000047	0.00631 ± 0.009788	0.000175 ± 0.000009	2.92E-14	98.7%	11.6467	380.00 ± 0.67	0.18%
3	7.08748 ± 0.006826	0.54195 ± 0.001041	0.00714 ± 0.000119	0.02126 ± 0.007379	0.000363 ± 0.000012	5.44E-14	98.5%	12.8837	416.03 ± 0.93	0.22%
4	1.48908 ± 0.001761	0.10420 ± 0.000537	0.00137 ± 0.000033	0.00747 ± 0.008175	0.000113 ± 0.000009	1.14E-14	97.8%	13.9770	447.29 ± 2.58	0.58%
5	1.29737 ± 0.001797	0.11206 ± 0.000294	0.00143 ± 0.000028	0.00460 ± 0.008863	0.000169 ± 0.000010	9.97E-15	96.2%	11.1351	364.88 ± 1.44	0.39%
6	3.50618 ± 0.001679	0.30016 ± 0.000696	0.00375 ± 0.000034	0.00310 ± 0.007630	0.000180 ± 0.000009	2.69E-14	98.5%	11.5042	375.80 ± 0.96	0.25%
7	1.15725 ± 0.000814	0.08187 ± 0.000287	0.00105 ± 0.000026	-0.01840 ± 0.009311	0.000079 ± 0.000011	8.89E-15	97.9%	13.8286	443.08 ± 2.15	0.49%
8	5.43993 ± 0.003951	0.48201 ± 0.000517	0.00621 ± 0.000079	-0.00191 ± 0.005354	0.000133 ± 0.000010	4.18E-14	99.3%	11.2038	366.92 ± 0.53	0.14%
9	3.04222 ± 0.001710	0.27261 ± 0.000715	0.00358 ± 0.000075	0.00307 ± 0.008482	0.000033 ± 0.000012	2.34E-14	99.7%	11.1249	364.58 ± 1.08	0.30%
10	1.99870 ± 0.001827	0.14363 ± 0.000371	0.00180 ± 0.000033	0.00516 ± 0.006262	0.000068 ± 0.000011	1.54E-14	99.0%	13.7790	441.66 ± 1.45	0.33%
11	1.77484 ± 0.001248	0.14708 ± 0.000373	0.00201 ± 0.000057	0.00357 ± 0.009151	0.000015 ± 0.000018	1.36E-14	99.8%	12.0390	391.50 ± 1.60	0.4%
12	2.14377 ± 0.002157	0.17027 ± 0.000474	0.00213 ± 0.000036	-0.00423 ± 0.007725	0.000031 ± 0.000011	1.65E-14	99.6%	12.5345	405.93 ± 1.37	0.3%
13	0.16601 ± 0.000379	0.01409 ± 0.000085	0.00022 ± 0.000022	0.01129 ± 0.008329	0.000024 ± 0.000010	1.28E-15	96.3%	11.3515	371.29 ± 8.02	2.2%
14	2.52196 ± 0.001578	0.21048 ± 0.000704	0.00263 ± 0.000041	0.00333 ± 0.007663	0.000052 ± 0.000019	1.94E-14	99.4%	11.9106	387.75 ± 1.61	0.4%
15	2.94450 ± 0.001551	0.21453 ± 0.000556	0.00293 ± 0.000079	0.01117 ± 0.005370	0.000127 ± 0.000012	2.26E-14	98.8%	13.5556	435.30 ± 1.29	0.3%
16	3.89367 ± 0.003077	0.29604 ± 0.000644	0.00389 ± 0.000050	-0.00780 ± 0.008556	0.000021 ± 0.000013	2.99E-14	99.8%	13.1291	423.09 ± 1.08	0.3%
17	0.71754 ± 0.000962	0.06059 ± 0.000285	0.00077 ± 0.000026	0.00669 ± 0.008424	0.000036 ± 0.000014	5.51E-15	98.6%	11.6769	380.89 ± 3.01	0.8%
18	1.17602 ± 0.001911	0.10273 ± 0.000261	0.00132 ± 0.000032	0.00005 ± 0.007819	0.000043 ± 0.000017	9.03E-15	98.9%	11.3246	370.50 ± 2.02	0.5%
19	3.90549 ± 0.004379	0.27786 ± 0.000625	0.00376 ± 0.000058	0.00352 ± 0.008363	0.000039 ± 0.000017	3.00E-14	99.7%	14.0154	448.37 ± 1.28	0.3%
20	2.74134 ± 0.001979	0.23970 ± 0.000771	0.00324 ± 0.000062	-0.01541 ± 0.014736	0.000212 ± 0.000022	2.11E-14	97.7%	11.1687	365.88 ± 1.55	0.4%
21	4.86487 ± 0.004067	0.41726 ± 0.000934	0.00523 ± 0.000047	-0.00661 ± 0.006919	0.000259 ± 0.000012	3.74E-14	98.4%	11.4741	374.91 ± 0.95	0.3%
22	1.57612 ± 0.001938	0.13904 ± 0.000365	0.00184 ± 0.000044	0.00275 ± 0.008898	0.000072 ± 0.000011	1.21E-14	98.7%	11.1841	366.34 ± 1.34	0.4%
23	1.77897 ± 0.001380	0.15805 ± 0.000572	0.00196 ± 0.000027	0.01080 ± 0.007636	0.000045 ± 0.000012	1.37E-14	99.3%	11.1790	366.19 ± 1.57	0.4%
24	0.82103 ± 0.000883	0.06855 ± 0.000281	0.00088 ± 0.000023	0.00596 ± 0.007157	0.000147 ± 0.000021	6.31E-15	94.8%	11.3516	371.29 ± 3.45	0.9%
25	1.90125 ± 0.001587	0.14090 ± 0.000392	0.00179 ± 0.000031	0.01272 ± 0.005979	0.000083 ± 0.000011	1.46E-14	98.8%	13.3279	428.80 ± 1.47	0.3%
26	3.60476 ± 0.002663	0.00260 ± 0.000100	0.00243 ± 0.000043	0.01545 ± 0.007989	0.012474 ± 0.000088	2.77E-14	-2.2%	-30.9152		
27	1.89883 ± 0.001303	0.15580 ± 0.000272	0.00198 ± 0.000028	0.00593 ± 0.010276	0.000104 ± 0.000018	1.46E-14	98.4%	11.9945	390.20 ± 1.38	3.53E-03
28	2.96054 ± 0.002798	0.25958 ± 0.000687	0.00329 ± 0.000024	0.00359 ± 0.007379	0.000204 ± 0.000012	2.27E-14	98.0%	11.1739	366.03 ± 1.16	0.32%
29	2.47894 ± 0.001394	0.18242 ± 0.000335	0.00231 ± 0.000017	0.01293 ± 0.008177	0.000057 ± 0.000012	1.90E-14	99.4%	13.5045	433.84 ± 1.06	0.24%
30	0.84695 ± 0.000850	0.07274 ± 0.000280	0.00097 ± 0.000025	0.00692 ± 0.005798	0.000059 ± 0.000011	6.51E-15	98.0%	11.4145	373.16 ± 2.15	0.58%
31	2.33560 ± 0.001113	0.18645 ± 0.000444	0.00238 ± 0.000034	0.00095 ± 0.007811	0.000161 ± 0.000012	1.79E-14	98.0%	12.2725	398.32 ± 1.17	0.29%
32	3.59933 ± 0.002298	0.31910 ± 0.000460	0.00412 ± 0.000043	0.00371 ± 0.008084	0.000090 ± 0.000008	2.76E-14	99.3%	11.1975	366.73 ± 0.64	0.17%
33	1.01871 ± 0.001274	0.07689 ± 0.000288	0.00103 ± 0.000029	-0.00243 ± 0.006310	0.000305 ± 0.000011	7.82E-15	91.1%	12.0752	392.56 ± 2.20	0.56%
34	0.63348 ± 0.000815	0.03957 ± 0.000196	0.00053 ± 0.000028	0.00951 ± 0.008607	0.000174 ± 0.000013	4.87E-15	92.0%	14.7313	468.54 ± 4.09	0.87%
35	1.33065 ± 0.001495	0.11793 ± 0.000227	0.00145 ± 0.000029	-0.01325 ± 0.009807	-0.000019 ± 0.000012	1.02E-14	100.3%	11.2728	368.97 ± 1.30	0.35%

OK12-39, Pennsylvanian Jackfork Group – Detrital muscovite, *continued*

36	0.29192 ± 0.000520	0.02590 ± 0.000186	0.00033 ± 0.000021	-0.01482 ± 0.008302	0.000007 ± 0.000009	2.24E-15	98.8%	11.1290	364.70 ± 4.58	1.26%
37	1.19570 ± 0.001116	0.10655 ± 0.000353	0.00137 ± 0.000040	-0.04226 ± 0.011864	0.000046 ± 0.000019	9.18E-15	98.6%	11.0558	362.53 ± 2.15	0.59%
38	0.89692 ± 0.001250	0.07860 ± 0.000371	0.00100 ± 0.000026	-0.00323 ± 0.006446	0.000007 ± 0.000018	6.89E-15	99.7%	11.3805	372.15 ± 2.85	0.77%
39	1.16923 ± 0.001592	0.10351 ± 0.000462	0.00134 ± 0.000029	0.01235 ± 0.010500	0.000111 ± 0.000011	8.98E-15	97.3%	10.9910	360.60 ± 2.05	0.57%
40	0.92078 ± 0.001272	0.08019 ± 0.000327	0.00104 ± 0.000031	-0.00105 ± 0.005758	-0.000008 ± 0.000016	7.07E-15	100.3%	11.4818	375.14 ± 2.56	0.68%
41	1.11725 ± 0.001216	0.07853 ± 0.000294	0.00104 ± 0.000027	-0.00028 ± 0.010039	0.000037 ± 0.000011	8.58E-15	99.0%	14.0877	450.42 ± 2.29	0.51%
42	2.53755 ± 0.001127	0.18526 ± 0.000530	0.00236 ± 0.000052	0.00147 ± 0.009068	0.000044 ± 0.000012	1.95E-14	99.5%	13.6277	437.36 ± 1.42	0.32%
43	1.86135 ± 0.001654	0.14358 ± 0.000479	0.00186 ± 0.000028	0.01815 ± 0.007189	0.000029 ± 0.000010	1.43E-14	99.6%	12.9167	416.98 ± 1.62	0.39%
44	4.04110 ± 0.003135	0.29303 ± 0.000572	0.00386 ± 0.000047	0.01932 ± 0.004464	0.000068 ± 0.000012	3.10E-14	99.5%	13.7287	440.23 ± 1.01	0.23%
45	2.08801 ± 0.002441	0.18535 ± 0.000559	0.00237 ± 0.000043	-0.00284 ± 0.008133	0.000075 ± 0.000015	1.60E-14	98.9%	11.1437	365.14 ± 1.44	0.39%
46	1.96189 ± 0.001661	0.14001 ± 0.000352	0.00179 ± 0.000036	-0.00126 ± 0.007265	0.000041 ± 0.000011	1.51E-14	99.4%	13.9255	445.83 ± 1.40	0.31%
47	2.43386 ± 0.002056	0.19649 ± 0.000418	0.00263 ± 0.000041	0.01205 ± 0.008206	0.000546 ± 0.000013	1.87E-14	93.4%	11.5714	377.78 ± 1.14	0.30%
48	0.91161 ± 0.001199	0.06733 ± 0.000326	0.00084 ± 0.000025	0.00131 ± 0.004509	0.000040 ± 0.000010	7.00E-15	98.7%	13.3651	429.86 ± 2.64	0.61%
49	1.95261 ± 0.001219	0.16222 ± 0.000291	0.00203 ± 0.000047	0.01189 ± 0.008338	-0.000003 ± 0.000017	1.50E-14	100.1%	12.0442	391.66 ± 1.27	0.32%
50	3.77963 ± 0.003038	0.26969 ± 0.000472	0.00342 ± 0.000058	0.03052 ± 0.005305	0.000033 ± 0.000021	2.90E-14	99.8%	13.9895	447.64 ± 1.13	0.25%
51	2.48814 ± 0.002215	0.21436 ± 0.000754	0.00270 ± 0.000035	0.01945 ± 0.009149	0.000112 ± 0.000012	1.91E-14	98.7%	11.4625	374.57 ± 1.48	0.39%
52	3.53711 ± 0.003197	0.29646 ± 0.000623	0.00375 ± 0.000033	0.00611 ± 0.005009	0.000018 ± 0.000017	2.72E-14	99.9%	11.9152	387.88 ± 1.05	0.27%
53	0.94488 ± 0.001174	0.07075 ± 0.000230	0.00090 ± 0.000031	-0.00431 ± 0.006516	0.000039 ± 0.000011	7.26E-15	98.7%	13.1864	424.74 ± 2.16	0.51%
54	1.09927 ± 0.001218	0.09059 ± 0.000346	0.00118 ± 0.000030	0.02062 ± 0.005731	0.000066 ± 0.000012	8.44E-15	98.4%	11.9416	388.65 ± 2.07	0.53%
55	1.10402 ± 0.001000	0.08336 ± 0.000267	0.00114 ± 0.000038	0.01575 ± 0.009406	0.000052 ± 0.000012	8.48E-15	98.7%	13.0777	421.61 ± 2.00	0.47%
56	2.68410 ± 0.001359	0.21901 ± 0.000454	0.00275 ± 0.000034	0.00930 ± 0.009129	0.000039 ± 0.000011	2.06E-14	99.6%	12.2072	396.41 ± 0.99	0.25%
57	1.75983 ± 0.002199	0.15515 ± 0.000447	0.00194 ± 0.000026	0.00527 ± 0.007272	0.000057 ± 0.000018	1.35E-14	99.1%	11.2377	367.92 ± 1.64	0.44%
58	3.60458 ± 0.003799	0.29052 ± 0.000788	0.00367 ± 0.000041	0.00338 ± 0.008837	0.000014 ± 0.000017	2.77E-14	99.9%	12.3941	401.86 ± 1.30	0.32%
59	2.43869 ± 0.002764	0.20690 ± 0.000325	0.00276 ± 0.000036	-0.00227 ± 0.007163	0.000071 ± 0.000010	1.87E-14	99.1%	11.6838	381.09 ± 0.89	0.23%
60	1.79994 ± 0.002239	0.13973 ± 0.000458	0.00176 ± 0.000041	0.01405 ± 0.006814	0.000043 ± 0.000016	1.38E-14	99.4%	12.8010	413.64 ± 1.82	0.44%
61	1.73934 ± 0.001899	0.12800 ± 0.000479	0.00166 ± 0.000037	0.00055 ± 0.007362	0.000039 ± 0.000011	1.34E-14	99.3%	13.4996	433.70 ± 1.90	0.44%
62	2.76580 ± 0.001296	0.23317 ± 0.000541	0.00290 ± 0.000039	0.01849 ± 0.004283	0.000058 ± 0.000011	2.12E-14	99.4%	11.7963	384.40 ± 1.03	0.27%
63	1.62313 ± 0.001515	0.13619 ± 0.000534	0.00170 ± 0.000031	-0.00244 ± 0.005471	0.000040 ± 0.000011	1.25E-14	99.3%	11.8291	385.36 ± 1.75	0.45%
64	2.66534 ± 0.002464	0.22356 ± 0.000469	0.00285 ± 0.000047	0.01137 ± 0.006739	0.000050 ± 0.000011	2.05E-14	99.5%	11.8609	386.29 ± 1.01	0.26%
65	0.27391 ± 0.000648	0.02147 ± 0.000114	0.00024 ± 0.000029	-0.01184 ± 0.007170	0.000031 ± 0.000010	2.10E-15	96.6%	12.3270	399.90 ± 4.93	1.23%
66	0.99839 ± 0.001074	0.07512 ± 0.000155	0.00102 ± 0.000042	-0.00807 ± 0.008830	-0.000002 ± 0.000015	7.67E-15	100.1%	13.2910	427.74 ± 2.16	0.50%
67	1.05255 ± 0.001723	0.07702 ± 0.000303	0.00095 ± 0.000026	-0.00747 ± 0.009374	0.000026 ± 0.000010	8.08E-15	99.3%	13.5680	435.65 ± 2.26	0.52%
68	0.84959 ± 0.000952	0.07491 ± 0.000277	0.00097 ± 0.000034	0.01264 ± 0.008184	-0.000001 ± 0.000018	6.53E-15	100.1%	11.3410	370.98 ± 2.74	0.74%
69	0.97044 ± 0.000871	0.07714 ± 0.000296	0.00101 ± 0.000029	0.02133 ± 0.008276	0.000065 ± 0.000011	7.45E-15	98.0%	12.3300	399.99 ± 2.12	0.53%
70	2.01590 ± 0.002337	0.17178 ± 0.000297	0.00216 ± 0.000037	-0.03418 ± 0.007843	0.000077 ± 0.000012	1.55E-14	98.9%	11.6025	378.70 ± 1.03	0.27%
71	0.86463 ± 0.001198	0.07313 ± 0.000278	0.00097 ± 0.000038	0.00108 ± 0.006985	0.000046 ± 0.000010	6.64E-15	98.4%	11.6391	379.77 ± 2.05	0.54%
72	2.02916 ± 0.002511	0.15209 ± 0.000377	0.00193 ± 0.000028	0.00097 ± 0.008746	0.000037 ± 0.000017	1.56E-14	99.5%	13.2704	427.15 ± 1.58	0.37%
73	0.69799 ± 0.001160	0.05629 ± 0.000353	0.00075 ± 0.000023	-0.03648 ± 0.005624	0.000200 ± 0.000010	5.36E-15	91.6%	11.3514	371.29 ± 3.18	0.86%
74	1.02629 ± 0.001163	0.09094 ± 0.000279	0.00105 ± 0.000047	-0.00813 ± 0.007580	0.000012 ± 0.000010	7.88E-15	99.7%	11.2475	368.22 ± 1.58	0.43%

OK12-39, Pennsylvanian Jackfork Group – Detrital muscovite, *continued*

75	1.71828 ± 0.001538	0.14600 ± 0.000429	0.00182 ± 0.000019	-0.04146 ± 0.014039	0.000044 ± 0.000010	1.32E-14	99.2%	11.6793	380.96 ± 1.36	0.36%
76	1.12270 ± 0.001545	0.10044 ± 0.000242	0.00125 ± 0.000034	0.00034 ± 0.009534	0.000021 ± 0.000009	8.62E-15	99.5%	11.1164	364.33 ± 1.35	0.37%
77	1.51662 ± 0.001360	0.13268 ± 0.000483	0.00167 ± 0.000031	-0.02105 ± 0.007342	0.000042 ± 0.000015	1.16E-14	99.2%	11.3362	370.84 ± 1.79	0.48%
78	0.84700 ± 0.000820	0.07525 ± 0.000471	0.00095 ± 0.000027	-0.01934 ± 0.006865	0.000030 ± 0.000009	6.51E-15	99.0%	11.1394	365.01 ± 2.62	0.72%
79	0.90397 ± 0.000912	0.08048 ± 0.000327	0.00104 ± 0.000028	-0.00397 ± 0.012026	-0.000011 ± 0.000014	6.94E-15	100.4%	11.2327	367.78 ± 2.24	0.61%
80	0.79243 ± 0.001255	0.07062 ± 0.000360	0.00090 ± 0.000028	-0.00608 ± 0.006670	0.000037 ± 0.000011	6.09E-15	98.6%	11.0680	362.89 ± 2.44	0.67%
81	1.02466 ± 0.001444	0.09002 ± 0.000354	0.00123 ± 0.000036	-0.00523 ± 0.007303	0.000041 ± 0.000009	7.87E-15	98.8%	11.2485	368.25 ± 1.82	0.49%
82	0.82463 ± 0.001415	0.06947 ± 0.000204	0.00089 ± 0.000025	0.00155 ± 0.007747	-0.000022 ± 0.000022	6.33E-15	100.8%	11.8701	386.56 ± 3.33	0.86%
83	0.85137 ± 0.001253	0.07568 ± 0.000272	0.00094 ± 0.000026	-0.00834 ± 0.007727	0.000023 ± 0.000010	6.54E-15	99.2%	11.1587	365.58 ± 1.89	0.52%
84	0.10788 ± 0.000464	0.00964 ± 0.000090	0.00015 ± 0.000018	-0.00420 ± 0.006846	0.000006 ± 0.000010	8.29E-16	98.4%	11.0118	361.22 ± 10.66	2.95%
85	2.99463 ± 0.002740	0.26622 ± 0.000408	0.00334 ± 0.000046	-0.00414 ± 0.008019	0.000071 ± 0.000010	2.30E-14	99.3%	11.1698	365.91 ± 0.75	0.21%
86	0.58737 ± 0.000986	0.05084 ± 0.000460	0.00064 ± 0.000031	-0.01282 ± 0.003480	0.000017 ± 0.000009	4.51E-15	99.1%	11.4506	374.22 ± 3.91	1.04%
87	0.66336 ± 0.001187	0.04984 ± 0.000276	0.00067 ± 0.000021	-0.00407 ± 0.004128	0.000017 ± 0.000011	5.10E-15	99.2%	13.2077	425.35 ± 3.20	0.75%
88	1.29769 ± 0.001218	0.09973 ± 0.000281	0.00126 ± 0.000027	-0.02285 ± 0.010690	0.000014 ± 0.000013	9.97E-15	99.7%	12.9702	418.52 ± 1.78	0.43%
89	1.91200 ± 0.001629	0.13498 ± 0.000319	0.00168 ± 0.000038	-0.01343 ± 0.007689	-0.000015 ± 0.000016	1.47E-14	100.2%	14.1647	452.60 ± 1.57	0.35%
90	0.47634 ± 0.000580	0.04055 ± 0.000251	0.00051 ± 0.000023	-0.07488 ± 0.013619	0.000015 ± 0.000011	3.66E-15	99.1%	11.6375	379.73 ± 3.56	0.94%
91	1.17329 ± 0.001449	0.08426 ± 0.000297	0.00110 ± 0.000030	-0.01094 ± 0.006767	0.000027 ± 0.000010	9.01E-15	99.3%	13.8319	443.17 ± 2.00	0.45%
92	1.49525 ± 0.000906	0.11229 ± 0.000362	0.00143 ± 0.000023	-0.00876 ± 0.004746	0.000051 ± 0.000010	1.15E-14	99.0%	13.1801	424.56 ± 1.65	0.39%
93	1.24229 ± 0.001934	0.10939 ± 0.000403	0.00141 ± 0.000033	-0.01289 ± 0.005472	0.000020 ± 0.000010	9.54E-15	99.5%	11.3014	369.81 ± 1.71	0.46%
94	0.20677 ± 0.000518	0.01570 ± 0.000105	0.00023 ± 0.000019	-0.01637 ± 0.006297	-0.000002 ± 0.000009	1.59E-15	100.3%	13.1735	424.37 ± 6.03	1.42%
95	1.67337 ± 0.001200	0.14020 ± 0.000282	0.00177 ± 0.000026	-0.01905 ± 0.005912	0.000050 ± 0.000010	1.29E-14	99.1%	11.8308	385.41 ± 1.07	0.28%
96	1.67399 ± 0.001445	0.13385 ± 0.000519	0.00182 ± 0.000038	0.00197 ± 0.008953	0.000025 ± 0.000009	1.29E-14	99.6%	12.4510	403.51 ± 1.74	0.43%
97	0.64609 ± 0.000798	0.04835 ± 0.000153	0.00063 ± 0.000023	-0.01773 ± 0.004522	0.000020 ± 0.000011	4.96E-15	99.1%	13.2388	426.24 ± 2.62	0.61%
98	2.22204 ± 0.002618	0.15880 ± 0.000517	0.00198 ± 0.000027	-0.01214 ± 0.005920	0.000013 ± 0.000010	1.71E-14	99.8%	13.9688	447.05 ± 1.66	0.37%
99	1.24336 ± 0.001183	0.10691 ± 0.000382	0.00138 ± 0.000028	-0.02284 ± 0.007715	0.000004 ± 0.000020	9.55E-15	99.9%	11.6176	379.14 ± 2.31	0.61%
100	0.23110 ± 0.000633	0.00422 ± 0.000079	0.00008 ± 0.000019	-0.02319 ± 0.009132	0.000024 ± 0.000011	1.78E-15	96.9%	53.0582	1310.91 ± 31.47	2.40%
101	2.18754 ± 0.001575	0.18194 ± 0.000463	0.00232 ± 0.000034	-0.01469 ± 0.008211	0.000074 ± 0.000010	1.68E-14	99.0%	11.9033	387.53 ± 1.16	0.30%
102	0.77200 ± 0.000647	0.06592 ± 0.000150	0.00088 ± 0.000024	-0.00695 ± 0.008714	0.000024 ± 0.000010	5.93E-15	99.1%	11.6037	378.73 ± 1.74	0.46%
103	2.10404 ± 0.001393	0.16479 ± 0.000327	0.00205 ± 0.000030	-0.01727 ± 0.010814	0.000013 ± 0.000009	1.62E-14	99.8%	12.7454	412.04 ± 1.00	0.24%
104	0.19699 ± 0.000479	0.00096 ± 0.000067	0.00009 ± 0.000020	-0.01872 ± 0.006820	0.000012 ± 0.000010	1.51E-15	98.1%	201.8349	2926 ± 212	7.25%
105	2.13700 ± 0.001281	0.18893 ± 0.000426	0.00256 ± 0.000048	-0.00782 ± 0.005938	0.000103 ± 0.000010	1.64E-14	98.6%	11.1494	365.31 ± 1.00	0.27%
106	1.99715 ± 0.002534	0.16273 ± 0.000393	0.00201 ± 0.000031	-0.01860 ± 0.007987	0.000007 ± 0.000015	1.53E-14	99.9%	12.2592	397.93 ± 1.40	0.35%
107	0.80613 ± 0.001062	0.06201 ± 0.000278	0.00080 ± 0.000023	-0.01665 ± 0.008488	0.000039 ± 0.000010	6.19E-15	98.6%	12.8124	413.97 ± 2.50	0.60%
108	0.96375 ± 0.001801	0.08111 ± 0.000319	0.00103 ± 0.000024	-0.00640 ± 0.006770	0.000000 ± 0.000018	7.40E-15	100.0%	11.8815	386.89 ± 2.70	0.70%
109	0.98793 ± 0.001118	0.08777 ± 0.000289	0.00112 ± 0.000029	-0.05219 ± 0.013162	0.000041 ± 0.000011	7.59E-15	98.8%	11.1184	364.39 ± 1.78	0.49%
110	1.02198 ± 0.001485	0.08866 ± 0.000330	0.00110 ± 0.000027	-0.00452 ± 0.006551	0.000002 ± 0.000009	7.85E-15	100.0%	11.5208	376.29 ± 1.81	0.48%

OK12-54, Mississippian Stanley Group -- Detrital muscovite

au.28.5e.mus (OK12-54) Harold Johnson *j=0.0201310±0.000030* *Grain sizes = 0.177 - 0.42 mm*

#	40 V	39 V	38 V	37 V	36 V	Moles 40Ar*	%Rad	R	Age (Ma)	%-sd
Blank	*0.00745 ± 0.000085*	*0.00100 ± 0.000033*	*0.00018 ± 0.000013*	*0.00031 ± 0.000016*	*0.0000696 ± 0.000007*					
1	7.90380 ± 0.005007	0.58290 ± 0.001093	0.00735 ± 0.000079	0.00004 ± 0.000016	0.000055 ± 0.000014	6.07E-14	99.8%	13.5314	434.61 ± 0.89	0.21%
2	3.85505 ± 0.004697	0.28857 ± 0.000630	0.00381 ± 0.000076	-0.00001 ± 0.000019	0.000074 ± 0.000009	2.96E-14	99.4%	13.2836	427.53 ± 1.12	0.26%
3	2.14224 ± 0.001505	0.14660 ± 0.000279	0.00198 ± 0.000030	0.00001 ± 0.000016	0.000486 ± 0.000011	1.65E-14	93.3%	13.6329	437.51 ± 1.18	0.27%
4	2.24077 ± 0.002022	0.14342 ± 0.000401	0.00181 ± 0.000035	0.00001 ± 0.000015	0.000074 ± 0.000009	1.72E-14	99.0%	15.4717	489.16 ± 1.57	0.32%
5	1.14253 ± 0.000924	0.07969 ± 0.000338	0.00101 ± 0.000024	0.00003 ± 0.000016	0.000032 ± 0.000013	8.78E-15	99.2%	14.2196	454.15 ± 2.53	0.56%
6	1.33414 ± 0.001222	0.10607 ± 0.000433	0.00136 ± 0.000030	0.00001 ± 0.000011	0.000034 ± 0.000016	1.02E-14	99.3%	12.4842	404.47 ± 2.25	0.56%
7	1.08069 ± 0.000957	0.07145 ± 0.000277	0.00102 ± 0.000038	0.00001 ± 0.000010	0.000039 ± 0.000009	8.30E-15	98.9%	14.9610	474.96 ± 2.28	0.48%
8	3.99416 ± 0.002272	0.24992 ± 0.000407	0.00319 ± 0.000028	0.00000 ± 0.000015	0.000330 ± 0.000011	3.07E-14	97.6%	15.5917	492.48 ± 0.96	0.19%
9	0.27283 ± 0.000575	0.02228 ± 0.000092	0.00027 ± 0.000016	0.00001 ± 0.000012	0.000028 ± 0.000009	2.10E-15	96.9%	11.8703	386.56 ± 4.23	1.09%
10	1.55378 ± 0.001556	0.09888 ± 0.000391	0.00127 ± 0.000031	-0.00002 ± 0.000016	0.000093 ± 0.000009	1.19E-14	98.2%	15.4369	488.20 ± 2.21	0.45%
11	3.20936 ± 0.002390	0.21137 ± 0.000404	0.00280 ± 0.000048	0.00001 ± 0.000010	0.000023 ± 0.000016	2.47E-14	99.8%	15.1516	480.27 ± 1.23	0.3%
12	1.13871 ± 0.002030	0.06984 ± 0.000336	0.00085 ± 0.000029	-0.00001 ± 0.000012	-0.000010 ± 0.000014	8.75E-15	100.3%	16.3047	512.08 ± 3.21	0.6%
13	1.54042 ± 0.000933	0.10562 ± 0.000561	0.00134 ± 0.000034	0.00002 ± 0.000012	0.000042 ± 0.000009	1.18E-14	99.2%	14.4677	461.14 ± 2.62	0.6%
14	0.88966 ± 0.001527	0.05711 ± 0.000393	0.00073 ± 0.000024	0.00003 ± 0.000016	0.000036 ± 0.000010	6.83E-15	98.8%	15.3939	487.01 ± 3.83	0.8%
15	2.89265 ± 0.002944	0.27214 ± 0.000661	0.00344 ± 0.000044	0.00001 ± 0.000015	0.000082 ± 0.000010	2.22E-14	99.2%	10.5407	347.16 ± 0.99	0.3%
16	3.82740 ± 0.002755	0.27808 ± 0.000693	0.00347 ± 0.000030	0.00000 ± 0.000015	0.000045 ± 0.000009	2.94E-14	99.7%	13.7155	439.86 ± 1.18	0.3%
17	2.06560 ± 0.001752	0.14278 ± 0.000461	0.00182 ± 0.000029	0.00004 ± 0.000011	-0.000008 ± 0.000013	1.59E-14	100.1%	14.4668	461.12 ± 1.75	0.4%
18	3.41030 ± 0.002095	0.24037 ± 0.000690	0.00301 ± 0.000018	0.00004 ± 0.000011	0.000072 ± 0.000009	2.62E-14	99.4%	14.0989	450.74 ± 1.37	0.3%
19	2.25074 ± 0.002336	0.16492 ± 0.000244	0.00216 ± 0.000035	0.00001 ± 0.000017	0.000026 ± 0.000015	1.73E-14	99.7%	13.5999	436.57 ± 1.15	0.3%
20	6.80613 ± 0.005818	0.41950 ± 0.000871	0.00555 ± 0.000074	0.00005 ± 0.000017	0.000011 ± 0.000017	5.23E-14	100.0%	16.2168	509.68 ± 1.21	0.2%
21	0.97416 ± 0.000947	0.09240 ± 0.000340	0.00117 ± 0.000029	0.00001 ± 0.000014	0.000011 ± 0.000010	7.48E-15	99.7%	10.5094	346.22 ± 1.66	0.5%
22	1.83807 ± 0.001139	0.13721 ± 0.000501	0.00174 ± 0.000030	0.00003 ± 0.000013	-0.000004 ± 0.000014	1.41E-14	100.1%	13.3962	430.75 ± 1.86	0.4%
23	1.03197 ± 0.001388	0.08181 ± 0.000247	0.00106 ± 0.000024	0.00000 ± 0.000014	0.000021 ± 0.000009	7.93E-15	99.4%	12.5399	406.09 ± 1.74	0.4%
24	1.16698 ± 0.001188	0.08259 ± 0.000239	0.00107 ± 0.000019	0.00001 ± 0.000016	0.000177 ± 0.000010	8.96E-15	95.5%	13.4956	433.59 ± 1.80	0.4%
25	2.99401 ± 0.002202	0.21559 ± 0.000571	0.00274 ± 0.000037	0.00001 ± 0.000015	0.000043 ± 0.000009	2.30E-14	99.6%	13.8289	443.08 ± 1.29	0.3%
26	1.43709 ± 0.001249	0.08890 ± 0.000256	0.00119 ± 0.000022	0.00004 ± 0.000016	0.000009 ± 0.000010	1.10E-14	99.8%	16.1356	507.45 ± 1.85	0.4%
27	1.02954 ± 0.001657	0.06988 ± 0.000312	0.00087 ± 0.000024	0.00001 ± 0.000013	0.000048 ± 0.000015	7.91E-15	98.6%	14.5309	462.92 ± 3.04	6.57E-03
28	2.66940 ± 0.001720	0.17168 ± 0.000570	0.00215 ± 0.000030	0.00002 ± 0.000021	0.000072 ± 0.000010	2.05E-14	99.2%	15.4243	487.85 ± 1.75	0.36%
29	0.77181 ± 0.000662	0.04603 ± 0.000326	0.00059 ± 0.000025	0.00000 ± 0.000011	0.000036 ± 0.000013	5.93E-15	98.6%	16.5324	518.30 ± 4.57	0.88%
30	1.18487 ± 0.001037	0.07160 ± 0.000288	0.00093 ± 0.000022	0.00002 ± 0.000016	0.000039 ± 0.000010	9.10E-15	99.0%	16.3878	514.35 ± 2.47	0.48%
31	0.73439 ± 0.001090	0.05349 ± 0.000298	0.00068 ± 0.000023	0.00001 ± 0.000011	-0.000025 ± 0.000010	5.64E-15	101.0%	13.7295	440.26 ± 3.10	0.71%
32	2.29317 ± 0.002672	0.17595 ± 0.000498	0.00237 ± 0.000056	0.00003 ± 0.000018	0.000027 ± 0.000010	1.76E-14	99.7%	12.9879	419.03 ± 1.40	0.33%
33	1.80875 ± 0.000958	0.11327 ± 0.000370	0.00148 ± 0.000023	0.00003 ± 0.000009	0.000038 ± 0.000009	1.39E-14	99.4%	15.8707	500.18 ± 1.82	0.36%
34	2.88052 ± 0.001747	0.19758 ± 0.000334	0.00252 ± 0.000031	0.00002 ± 0.000014	0.000056 ± 0.000014	2.21E-14	99.4%	14.4955	461.92 ± 1.06	0.23%
35	1.62406 ± 0.001067	0.10251 ± 0.000325	0.00133 ± 0.000026	0.00001 ± 0.000021	-0.000028 ± 0.000014	1.25E-14	100.5%	15.8429	499.41 ± 2.07	0.41%

OK12-54, Mississippian Stanley Group -- Detrital muscovite, *continued*

36	1.15565 ± 0.001163	0.08468 ± 0.000233	0.00104 ± 0.000023	0.00001 ± 0.000015	0.000015 ± 0.000009	8.88E-15	99.6%	13.5954	436.44 ± 1.62	0.37%
37	1.11043 ± 0.000964	0.07512 ± 0.000431	0.00096 ± 0.000021	0.00003 ± 0.000011	0.000005 ± 0.000016	8.53E-15	99.9%	14.7628	469.42 ± 3.38	0.72%
38	0.77467 ± 0.000967	0.05871 ± 0.000263	0.00078 ± 0.000019	0.00005 ± 0.000016	0.000007 ± 0.000008	5.95E-15	99.7%	13.1604	423.99 ± 2.38	0.56%
39	0.64689 ± 0.000966	0.04265 ± 0.000275	0.00054 ± 0.000025	0.00000 ± 0.000013	0.000003 ± 0.000008	4.97E-15	99.9%	15.1471	480.15 ± 3.65	0.76%
40	1.45291 ± 0.001933	0.10529 ± 0.000231	0.00135 ± 0.000032	0.00000 ± 0.000016	-0.000016 ± 0.000015	1.12E-14	100.3%	13.7994	442.25 ± 1.78	0.40%
41	2.06182 ± 0.001883	0.14883 ± 0.000448	0.00196 ± 0.000035	0.00000 ± 0.000014	0.000030 ± 0.000015	1.58E-14	99.6%	13.7942	442.10 ± 1.70	0.39%
42	0.28312 ± 0.000646	0.01890 ± 0.000083	0.00024 ± 0.000019	-0.00001 ± 0.000014	0.000019 ± 0.000009	2.17E-15	98.0%	14.6754	466.97 ± 5.14	1.10%
43	0.67061 ± 0.001042	0.04824 ± 0.000387	0.00061 ± 0.000020	0.00001 ± 0.000018	0.000020 ± 0.000009	5.15E-15	99.1%	13.7799	441.69 ± 4.06	0.92%
44	1.63459 ± 0.001487	0.10559 ± 0.000427	0.00134 ± 0.000033	0.00003 ± 0.000019	0.000021 ± 0.000010	1.26E-14	99.6%	15.4230	487.81 ± 2.22	0.45%
45	2.22855 ± 0.001896	0.15769 ± 0.000353	0.00206 ± 0.000024	-0.00002 ± 0.000016	0.000215 ± 0.000011	1.71E-14	97.1%	13.7288	440.24 ± 1.26	0.29%
46	1.23611 ± 0.001553	0.09078 ± 0.000264	0.00119 ± 0.000031	0.00003 ± 0.000011	0.000021 ± 0.000009	9.49E-15	99.5%	13.5477	435.08 ± 1.66	0.38%
47	1.72461 ± 0.002694	0.13155 ± 0.000545	0.00159 ± 0.000022	0.00001 ± 0.000021	0.000016 ± 0.000010	1.32E-14	99.7%	13.0731	421.48 ± 1.99	0.47%
48	0.45234 ± 0.000721	0.03316 ± 0.000218	0.00042 ± 0.000018	0.00002 ± 0.000017	0.000011 ± 0.000008	3.47E-15	99.3%	13.5463	435.04 ± 3.66	0.84%
49	0.78421 ± 0.000915	0.05258 ± 0.000201	0.00068 ± 0.000024	0.00003 ± 0.000013	0.000045 ± 0.000007	6.02E-15	98.3%	14.6601	466.54 ± 2.27	0.49%
50	0.29786 ± 0.000478	0.01905 ± 0.000085	0.00022 ± 0.000018	0.00002 ± 0.000015	0.000046 ± 0.000008	2.29E-15	95.4%	14.9178	473.76 ± 4.63	0.98%
51	1.31400 ± 0.001042	0.11458 ± 0.000441	0.00144 ± 0.000034	0.00002 ± 0.000012	0.000056 ± 0.000008	1.01E-14	98.7%	11.3232	370.46 ± 1.62	0.44%
52	0.63004 ± 0.001113	0.04484 ± 0.000264	0.00058 ± 0.000015	0.00004 ± 0.000008	0.000197 ± 0.000009	4.84E-15	90.7%	12.7495	412.15 ± 3.36	0.82%
53	1.65824 ± 0.001497	0.11540 ± 0.000292	0.00142 ± 0.000033	-0.00002 ± 0.000013	0.000003 ± 0.000016	1.27E-14	100.0%	14.3621	458.17 ± 1.80	0.39%
54	1.27412 ± 0.001076	0.08568 ± 0.000374	0.00112 ± 0.000032	0.00001 ± 0.000015	0.000237 ± 0.000009	9.79E-15	94.5%	14.0529	449.44 ± 2.34	0.52%
55	1.39168 ± 0.001758	0.06863 ± 0.000335	0.00085 ± 0.000024	0.00004 ± 0.000019	0.000016 ± 0.000010	1.07E-14	99.7%	20.2071	615.75 ± 3.37	0.55%
56	0.22671 ± 0.000300	0.01657 ± 0.000093	0.00023 ± 0.000016	0.00002 ± 0.000018	0.000025 ± 0.000008	1.74E-15	96.7%	13.2333	426.08 ± 5.24	1.23%
57	0.06009 ± 0.000297	0.00465 ± 0.000096	0.00007 ± 0.000019	0.00001 ± 0.000008	0.000004 ± 0.000009	4.62E-16	97.8%	12.6325	408.77 ± 19.80	4.84%
58	1.12760 ± 0.001146	0.08202 ± 0.000367	0.00105 ± 0.000029	-0.00001 ± 0.000009	-0.000012 ± 0.000009	8.66E-15	100.3%	13.7471	440.76 ± 2.30	0.52%
59	4.45166 ± 0.003114	0.30046 ± 0.000649	0.00401 ± 0.000063	0.00001 ± 0.000019	0.000055 ± 0.000009	3.42E-14	99.6%	14.7618	469.39 ± 1.11	0.24%
60	1.08096 ± 0.001007	0.06552 ± 0.000168	0.00082 ± 0.000036	0.00001 ± 0.000012	0.000017 ± 0.000009	8.30E-15	99.5%	16.4228	515.31 ± 1.86	0.36%
61	0.73494 ± 0.001147	0.04383 ± 0.000295	0.00052 ± 0.000024	-0.00001 ± 0.000013	-0.000006 ± 0.000008	5.65E-15	100.2%	16.7679	524.70 ± 4.01	0.77%
62	1.07262 ± 0.000843	0.09559 ± 0.000311	0.00127 ± 0.000034	-0.00001 ± 0.000018	-0.000027 ± 0.000015	8.24E-15	100.7%	11.2209	367.43 ± 1.92	0.52%
63	7.27714 ± 0.005279	0.51906 ± 0.000724	0.00691 ± 0.000077	0.00005 ± 0.000018	0.000165 ± 0.000009	5.59E-14	99.3%	13.9259	445.84 ± 0.72	0.16%
64	0.44722 ± 0.000527	0.03248 ± 0.000104	0.00044 ± 0.000029	0.00001 ± 0.000020	-0.000003 ± 0.000009	3.44E-15	100.2%	13.7670	441.32 ± 2.94	0.67%
65	1.08383 ± 0.001242	0.07055 ± 0.000228	0.00085 ± 0.000023	0.00004 ± 0.000017	0.000018 ± 0.000011	8.32E-15	99.5%	15.2882	484.07 ± 2.18	0.45%
66	1.14241 ± 0.001520	0.08629 ± 0.000292	0.00101 ± 0.000022	0.00000 ± 0.000012	0.000007 ± 0.000008	8.77E-15	99.8%	13.2152	425.57 ± 1.79	0.42%
67	1.31423 ± 0.001034	0.10459 ± 0.000463	0.00124 ± 0.000031	-0.00001 ± 0.000011	0.000008 ± 0.000008	1.01E-14	99.8%	12.5441	406.21 ± 1.96	0.48%
68	0.99864 ± 0.000957	0.06290 ± 0.000221	0.00081 ± 0.000022	-0.00001 ± 0.000013	0.000034 ± 0.000009	7.67E-15	99.0%	15.7174	495.95 ± 2.26	0.46%
69	0.29303 ± 0.000510	0.01876 ± 0.000078	0.00023 ± 0.000026	-0.00001 ± 0.000013	0.000005 ± 0.000008	2.25E-15	99.5%	15.5384	491.01 ± 4.70	0.96%
70	0.92648 ± 0.000799	0.06261 ± 0.000262	0.00074 ± 0.000026	0.00001 ± 0.000018	0.000010 ± 0.000009	7.12E-15	99.7%	14.7496	469.05 ± 2.38	0.51%
71	1.09638 ± 0.001301	0.06476 ± 0.000229	0.00084 ± 0.000025	0.00001 ± 0.000009	0.000206 ± 0.000010	8.42E-15	94.4%	15.9891	503.43 ± 2.46	0.49%
72	1.01328 ± 0.001796	0.07291 ± 0.000353	0.00091 ± 0.000031	0.00001 ± 0.000012	0.000034 ± 0.000009	7.78E-15	99.0%	13.7610	441.15 ± 2.58	0.59%
73	1.24334 ± 0.001259	0.09275 ± 0.000172	0.00116 ± 0.000021	0.00001 ± 0.000007	0.000007 ± 0.000010	9.55E-15	99.8%	13.3826	430.36 ± 1.34	0.31%
74	1.79830 ± 0.001092	0.10696 ± 0.000305	0.00130 ± 0.000030	0.00002 ± 0.000020	-0.000017 ± 0.000015	1.38E-14	100.3%	16.8128	525.92 ± 2.00	0.38%

OK12-54, Mississippian Stanley Group -- Detrital muscovite, *continued*

75	0.83409 ± 0.000379	0.05705 ± 0.000206	0.00069 ± 0.000020	0.00002 ± 0.000023	0.000010 ± 0.000010	6.41E-15	99.6%	14.5671	463.93 ± 2.34	0.51%
76	0.85867 ± 0.001226	0.06197 ± 0.000272	0.00076 ± 0.000020	0.00001 ± 0.000022	0.000005 ± 0.000008	6.60E-15	99.8%	13.8317	443.16 ± 2.38	0.54%
77	0.29940 ± 0.000683	0.02261 ± 0.000242	0.00028 ± 0.000023	0.00002 ± 0.000010	0.000004 ± 0.000008	2.30E-15	99.6%	13.1938	424.95 ± 5.80	1.36%
78	2.20093 ± 0.001306	0.15226 ± 0.000390	0.00190 ± 0.000028	0.00001 ± 0.000013	0.000013 ± 0.000015	1.69E-14	99.8%	14.4307	460.10 ± 1.53	0.33%
79	1.22178 ± 0.001262	0.09439 ± 0.000248	0.00120 ± 0.000022	0.00000 ± 0.000016	-0.000008 ± 0.000009	9.38E-15	100.2%	12.9435	417.75 ± 1.49	0.36%
80	2.08009 ± 0.001823	0.16162 ± 0.000674	0.00201 ± 0.000029	0.00002 ± 0.000016	0.000045 ± 0.000008	1.60E-14	99.4%	12.7880	413.27 ± 1.84	0.45%
81	0.02845 ± 0.000333	0.00278 ± 0.000104	0.00002 ± 0.000018	0.00003 ± 0.000014	0.000004 ± 0.000009	2.19E-16	96.0%	9.8208	325.47 ± 33.98	10.44%
82	2.51759 ± 0.001534	0.22622 ± 0.000409	0.00286 ± 0.000042	-0.00001 ± 0.000012	0.000028 ± 0.000009	1.93E-14	99.7%	11.0923	363.61 ± 0.79	0.22%
83	3.16727 ± 0.003630	0.21343 ± 0.000497	0.00266 ± 0.000034	0.00000 ± 0.000009	0.000052 ± 0.000009	2.43E-14	99.5%	14.7680	469.57 ± 1.29	0.27%
84	0.98805 ± 0.001328	0.06455 ± 0.000245	0.00082 ± 0.000030	0.00001 ± 0.000017	-0.000010 ± 0.000014	7.59E-15	100.3%	15.3061	484.57 ± 2.84	0.59%
85	1.09042 ± 0.001926	0.06703 ± 0.000326	0.00083 ± 0.000026	0.00001 ± 0.000009	-0.000011 ± 0.000017	8.38E-15	100.3%	16.2678	511.07 ± 3.51	0.69%
86	0.42430 ± 0.000782	0.03593 ± 0.000246	0.00045 ± 0.000025	0.00003 ± 0.000016	-0.000069 ± 0.000014	3.26E-15	104.8%	11.8078	384.73 ± 4.64	1.21%
87	0.91091 ± 0.001158	0.07258 ± 0.000373	0.00089 ± 0.000037	0.00002 ± 0.000015	0.000026 ± 0.000010	7.00E-15	99.1%	12.4423	403.26 ± 2.53	0.63%
88	1.02870 ± 0.000729	0.06943 ± 0.000270	0.00086 ± 0.000025	0.00001 ± 0.000012	0.000040 ± 0.000008	7.90E-15	98.9%	14.6486	466.22 ± 2.14	0.46%
89	0.99263 ± 0.000787	0.04762 ± 0.000248	0.00053 ± 0.000035	-0.00002 ± 0.000015	0.000007 ± 0.000009	7.62E-15	99.8%	20.7997	630.98 ± 3.70	0.59%
90	1.18615 ± 0.001419	0.07976 ± 0.000377	0.00099 ± 0.000030	0.00003 ± 0.000016	0.000015 ± 0.000009	9.11E-15	99.6%	14.8140	470.86 ± 2.53	0.54%
91	0.42353 ± 0.000624	0.02758 ± 0.000170	0.00031 ± 0.000020	0.00003 ± 0.000012	-0.000006 ± 0.000009	3.25E-15	100.4%	15.3572	485.99 ± 4.33	0.89%
92	0.97061 ± 0.001400	0.06936 ± 0.000282	0.00088 ± 0.000024	0.00000 ± 0.000016	0.000003 ± 0.000008	7.46E-15	99.9%	13.9794	447.35 ± 2.23	0.50%
93	0.40727 ± 0.000815	0.03035 ± 0.000165	0.00037 ± 0.000018	0.00001 ± 0.000018	0.000020 ± 0.000009	3.13E-15	98.6%	13.2271	425.90 ± 3.83	0.90%
94	0.29387 ± 0.000315	0.02121 ± 0.000091	0.00025 ± 0.000026	-0.00002 ± 0.000023	0.000007 ± 0.000009	2.26E-15	99.3%	13.7562	441.02 ± 4.42	1.00%
95	0.91510 ± 0.000666	0.05873 ± 0.000261	0.00073 ± 0.000030	-0.00001 ± 0.000011	0.000014 ± 0.000009	7.03E-15	99.5%	15.5085	490.18 ± 2.66	0.54%
96	0.29341 ± 0.000457	0.01906 ± 0.000079	0.00025 ± 0.000019	0.00000 ± 0.000009	0.000009 ± 0.000009	2.25E-15	99.1%	15.2546	483.14 ± 4.75	0.98%
97	0.56709 ± 0.001007	0.04163 ± 0.000170	0.00054 ± 0.000026	0.00000 ± 0.000017	0.000009 ± 0.000009	4.36E-15	99.5%	13.5594	435.41 ± 2.77	0.64%
98	0.51837 ± 0.000628	0.03347 ± 0.000198	0.00041 ± 0.000019	0.00000 ± 0.000018	0.000006 ± 0.000010	3.98E-15	99.7%	15.4382	488.23 ± 4.01	0.82%
99	0.79618 ± 0.000798	0.05272 ± 0.000255	0.00063 ± 0.000020	0.00001 ± 0.000014	0.000021 ± 0.000009	6.12E-15	99.2%	14.9848	475.63 ± 2.83	0.59%
100	0.66320 ± 0.000695	0.04654 ± 0.000188	0.00059 ± 0.000020	0.00002 ± 0.000007	0.000015 ± 0.000010	5.09E-15	99.3%	14.1540	452.30 ± 2.77	0.61%
101	0.93912 ± 0.001316	0.06411 ± 0.000254	0.00080 ± 0.000024	0.00001 ± 0.000006	0.000023 ± 0.000009	7.21E-15	99.3%	14.5419	463.23 ± 2.36	0.51%
102	0.51994 ± 0.000627	0.03666 ± 0.000222	0.00042 ± 0.000020	0.00002 ± 0.000016	0.000001 ± 0.000009	3.99E-15	100.0%	14.1766	452.94 ± 3.63	0.80%
103	0.83803 ± 0.000747	0.06640 ± 0.000240	0.00087 ± 0.000037	0.00003 ± 0.000012	0.000007 ± 0.000009	6.44E-15	99.7%	12.5888	407.50 ± 2.03	0.50%
104	0.70903 ± 0.000715	0.04885 ± 0.000297	0.00061 ± 0.000024	0.00000 ± 0.000015	0.000006 ± 0.000009	5.45E-15	99.7%	14.4780	461 ± 3	0.72%
105	1.13871 ± 0.000889	0.07875 ± 0.000362	0.00096 ± 0.000022	0.00001 ± 0.000012	0.000023 ± 0.000009	8.75E-15	99.4%	14.3738	458.50 ± 2.39	0.52%
106	0.95338 ± 0.001166	0.06757 ± 0.000285	0.00091 ± 0.000045	0.00001 ± 0.000016	0.000009 ± 0.000013	7.32E-15	99.7%	14.0674	449.85 ± 2.69	0.60%
107	1.23331 ± 0.000968	0.09201 ± 0.000183	0.00111 ± 0.000030	0.00006 ± 0.000015	0.000035 ± 0.000008	9.47E-15	99.2%	13.2934	427.81 ± 1.24	0.29%
108	0.52968 ± 0.000646	0.03547 ± 0.000218	0.00043 ± 0.000027	0.00000 ± 0.000012	0.000004 ± 0.000010	4.07E-15	99.8%	14.8976	473.19 ± 3.93	0.83%
109	1.12715 ± 0.000854	0.08185 ± 0.000214	0.00098 ± 0.000020	0.00001 ± 0.000014	0.000014 ± 0.000009	8.66E-15	99.6%	13.7212	440.02 ± 1.57	0.36%
110	0.34954 ± 0.000545	0.02143 ± 0.000094	0.00017 ± 0.000024	0.00000 ± 0.000013	0.000020 ± 0.000008	2.68E-15	98.3%	16.0398	504.83 ± 4.14	0.82%
111	0.38099 ± 0.000757	0.02568 ± 0.000144	0.00031 ± 0.000020	0.00000 ± 0.000013	-0.000008 ± 0.000009	2.93E-15	100.6%	14.8369	471.49 ± 4.40	0.93%
112	0.73002 ± 0.000887	0.05467 ± 0.000217	0.00062 ± 0.000021	0.00001 ± 0.000010	0.000021 ± 0.000008	5.61E-15	99.1%	13.2372	426.19 ± 2.30	0.54%

Additional Figures

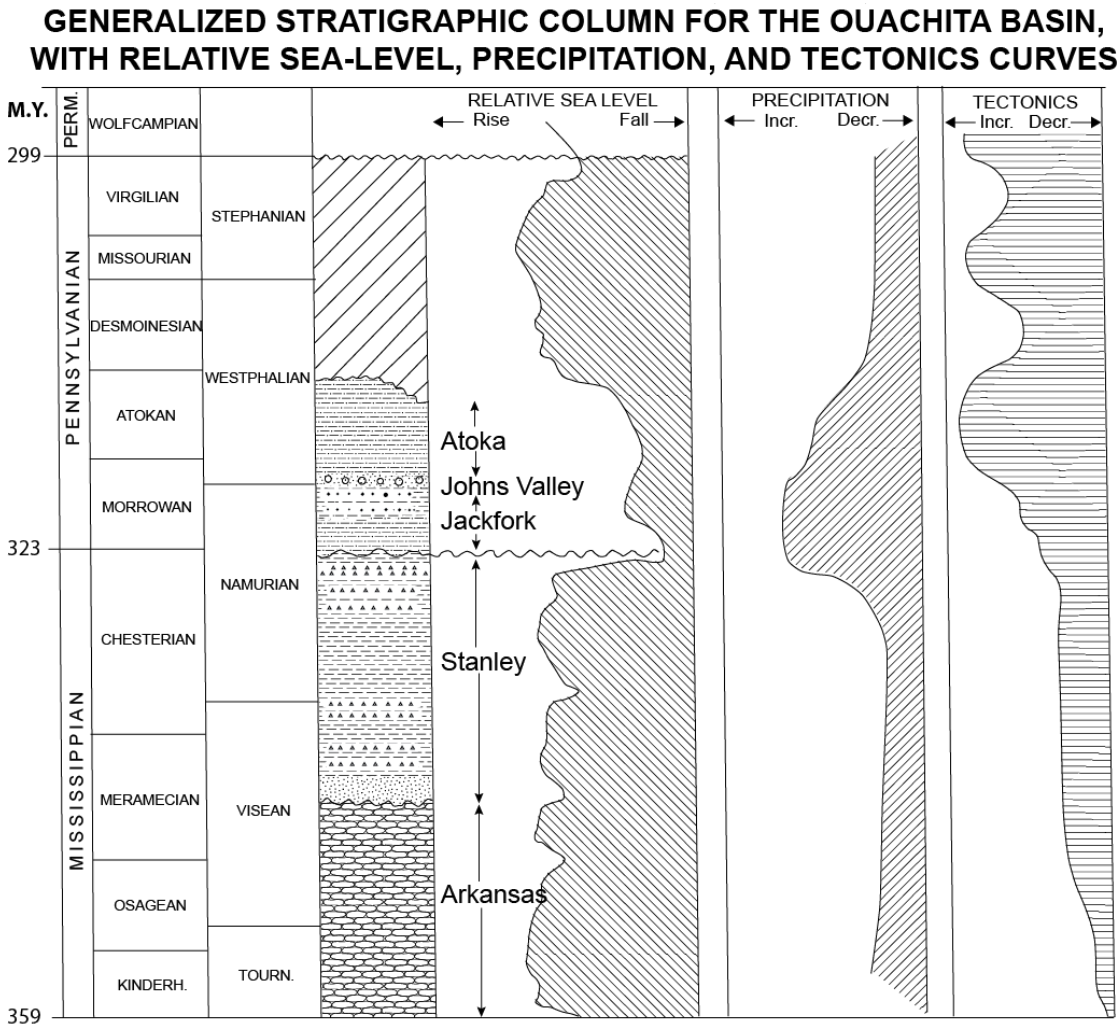

Figure S1. Generalized stratigraphic column for the Ouachita Basin, with relative sea-level, precipitation, and tectonic curves. Modified from Sutherland and Manger (1979), Arbenz (1989a), Cecil and Eble (1989), Ross and Ross (1987), and Coleman et al. (1994).

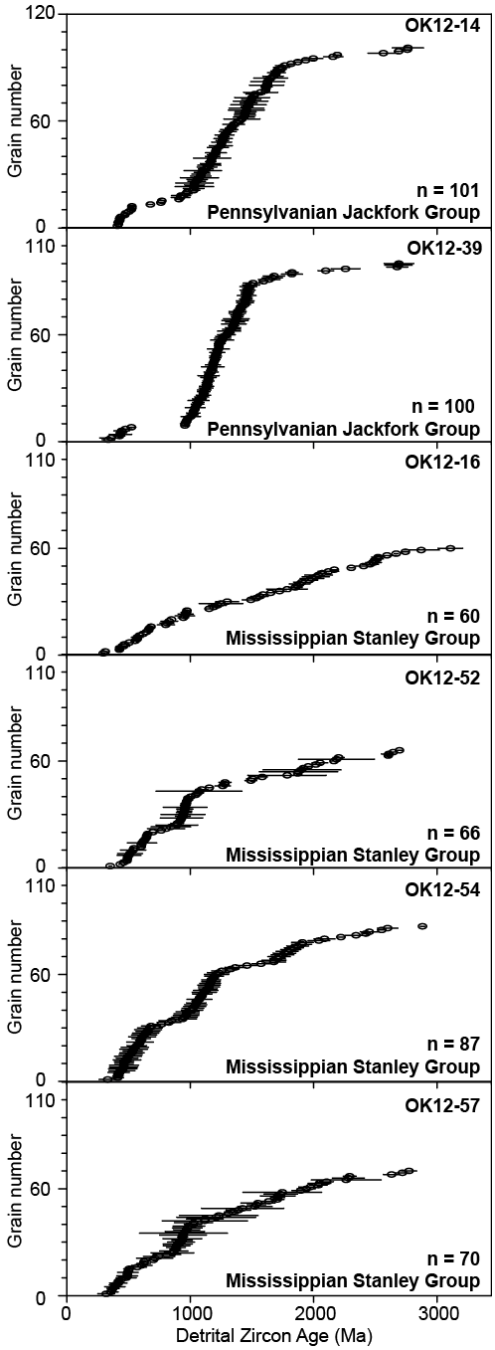

Figure S2. - Detrital zircon U-Pb grain ages (1σ error), from youngest to oldest; n is the number of grains analyzed with less than 10% discordance (younger than 1000 Ma) and less than 20% (older than 1000 Ma). Locations are shown in Figure 4, and U-Pb data given in supplemental reference material.

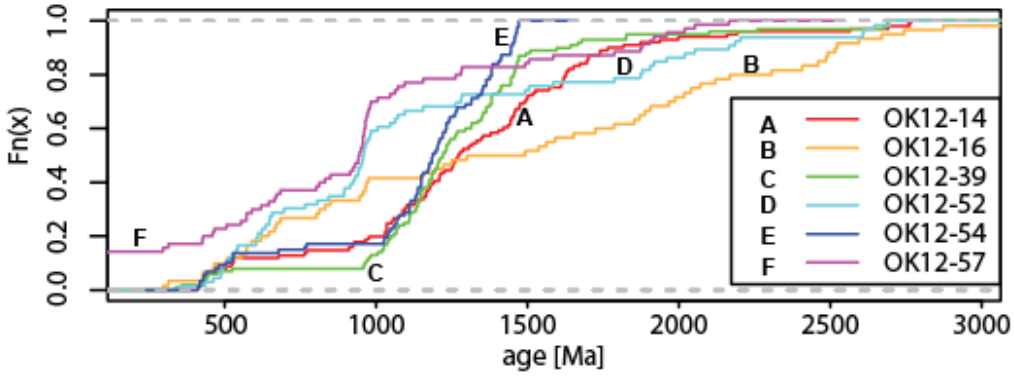

Figure S3. - Cumulative probability curves of detrital zircon ages from the Stanley Group and and Jackfork Groups. See supplemental Figure 2 for further information.

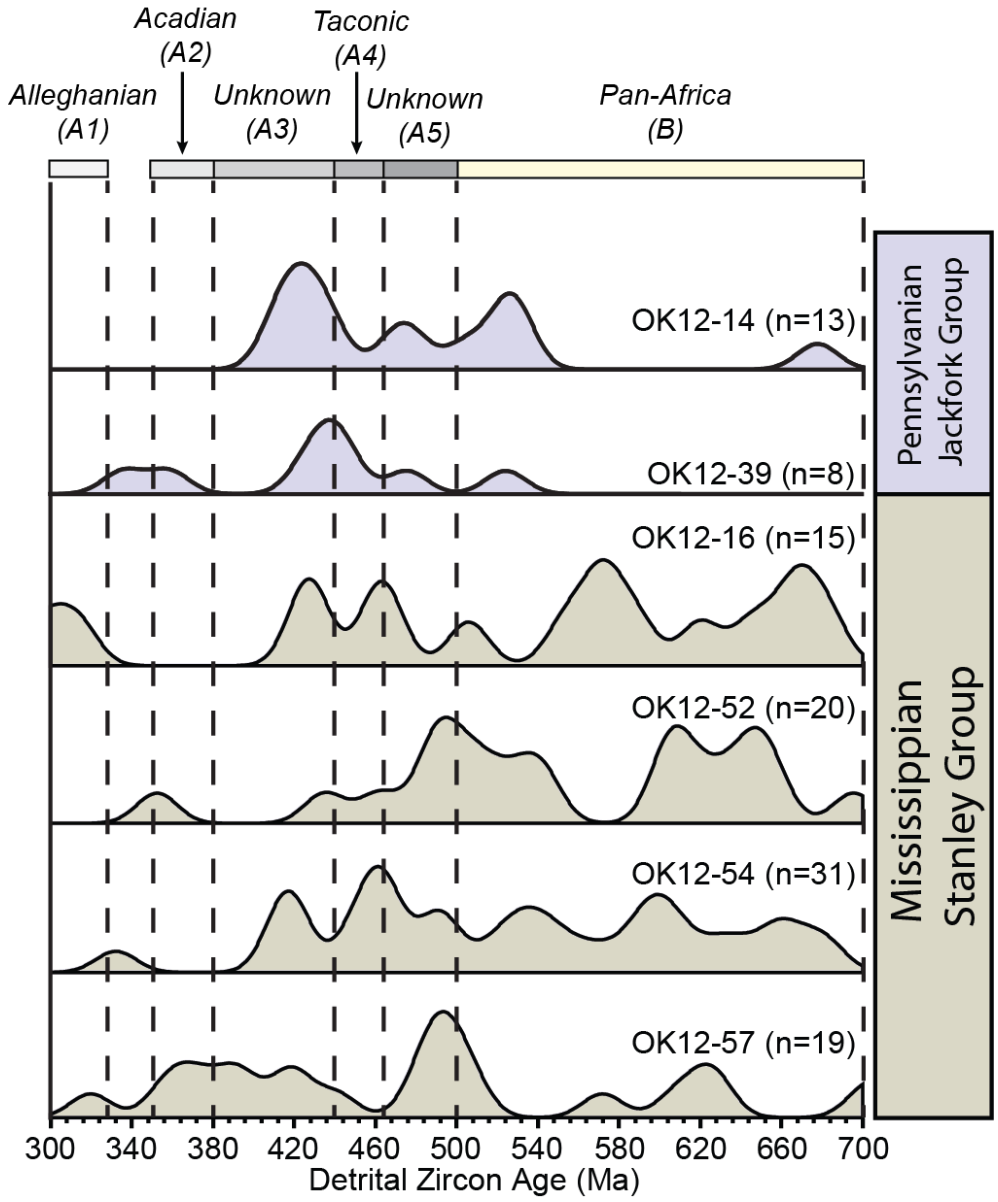

Figure S4. - Normalized detrital zircon U-Pb KDE plots for 4 Stanley Group samples and 2 Jackfork Group samples spanning 300-700 Ma. KDE bandwidth of 2 m.y. is used. Plot explanations are provided in Figure 6A.

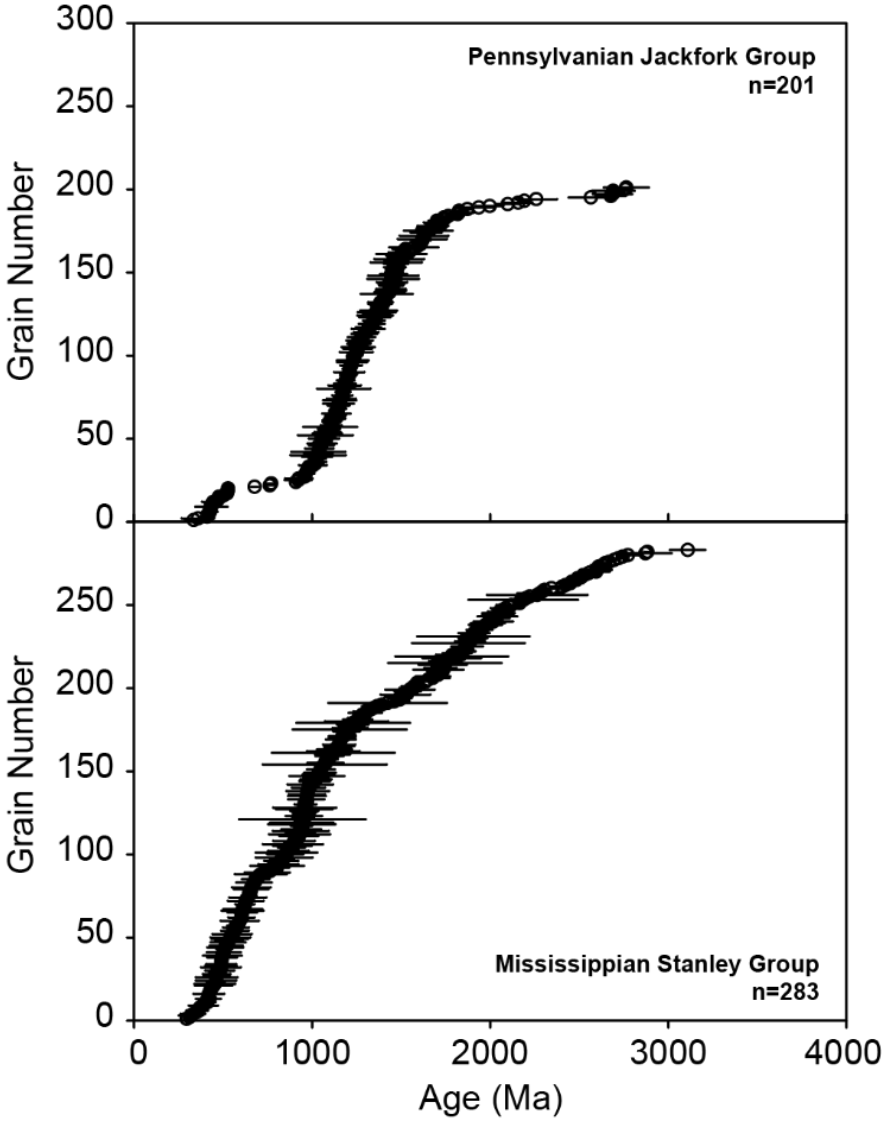

Figure S5. - U-Pb grain ages with 1σ error, from youngest to oldest, of combined detrital U-Pb data from all samples for both Mississippian Stanley Group and Pennsylvanian Jackfork group. n is the number of grains analyzed with less than 10% discordance on grains younger than 1000 Ma and less than 20% on grains older than 1000 Ma.

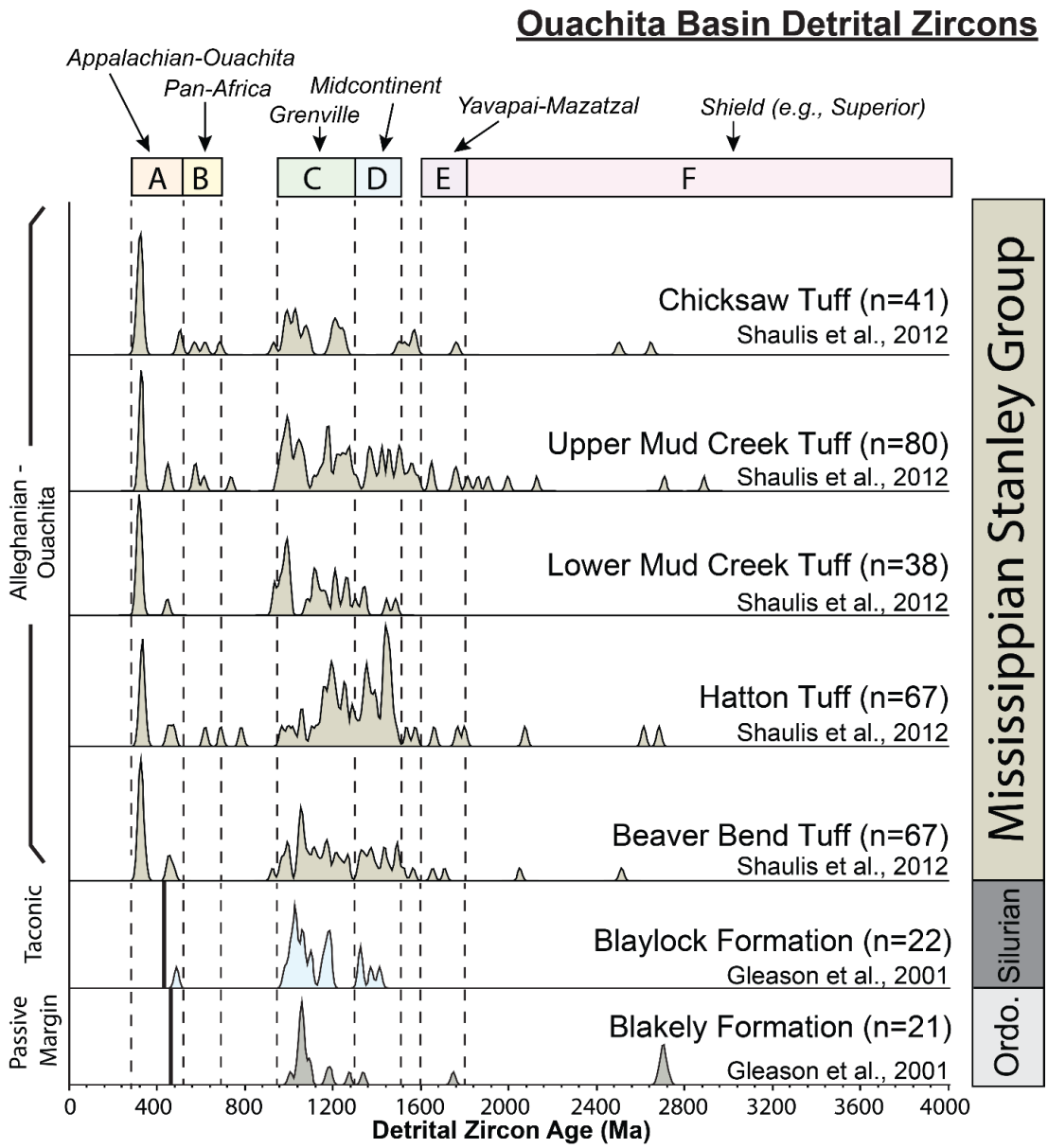

Figure S6. - Normalized detrital zircon U-Pb age KDE plots for Ouachita Basin (Gleason et al., 2001; Shaulis et al., 2012). Approximate deposition age given by published work is shown as a solid black line for each sample. KDE plot explanation and sample locations are provided in Figures 6 and 7, respectively.

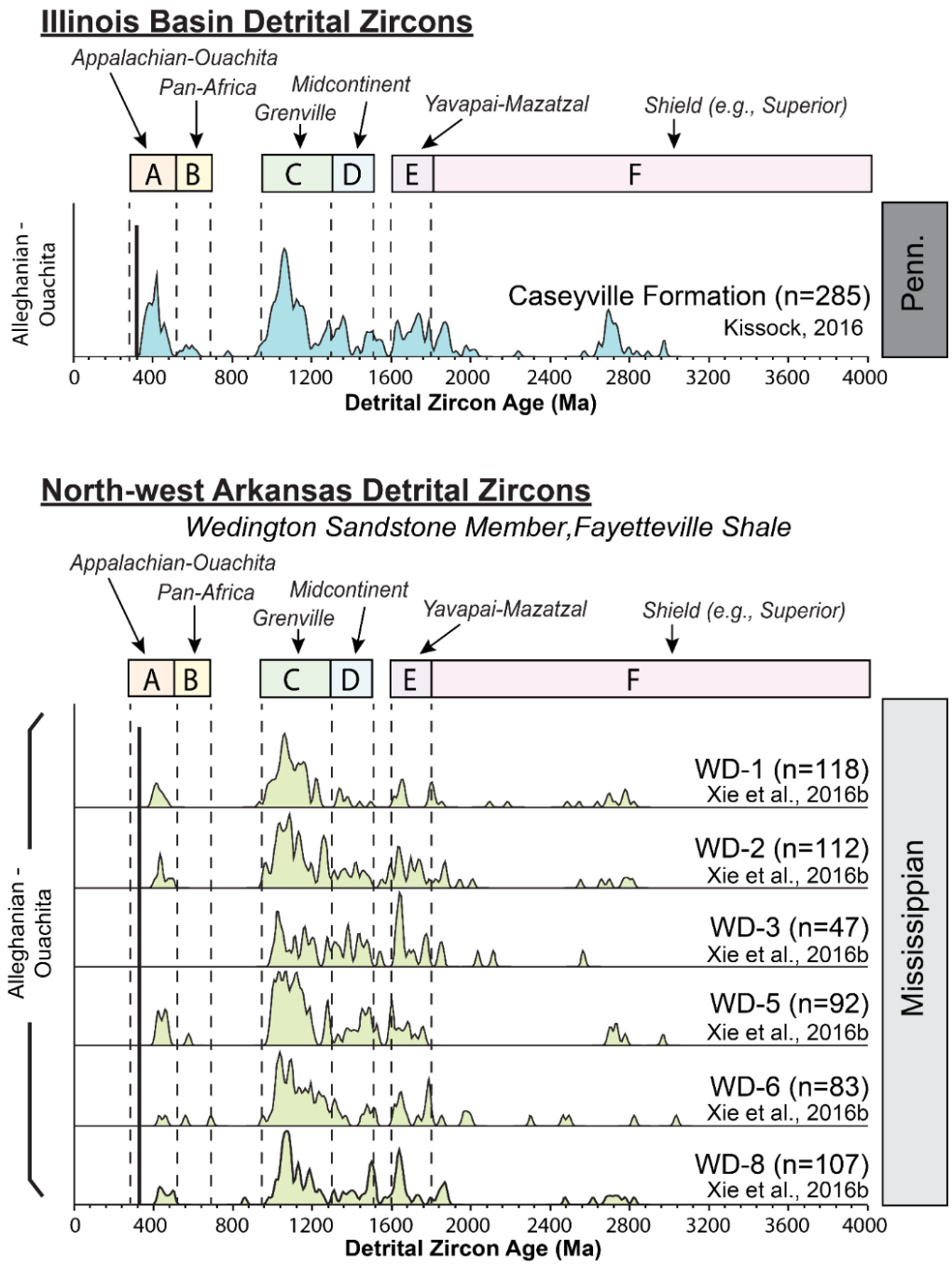

Figure S7. - Normalized detrital zircon U-Pb age KDE plots for the Caseyville Formation of the Illinois Basin and Wedington Sandstone Member, Fayetteville Shale of Northwest Arkansas (Xie et al., 2016b; Kissock, 2016). See supplemental Figure 6 for additional details.

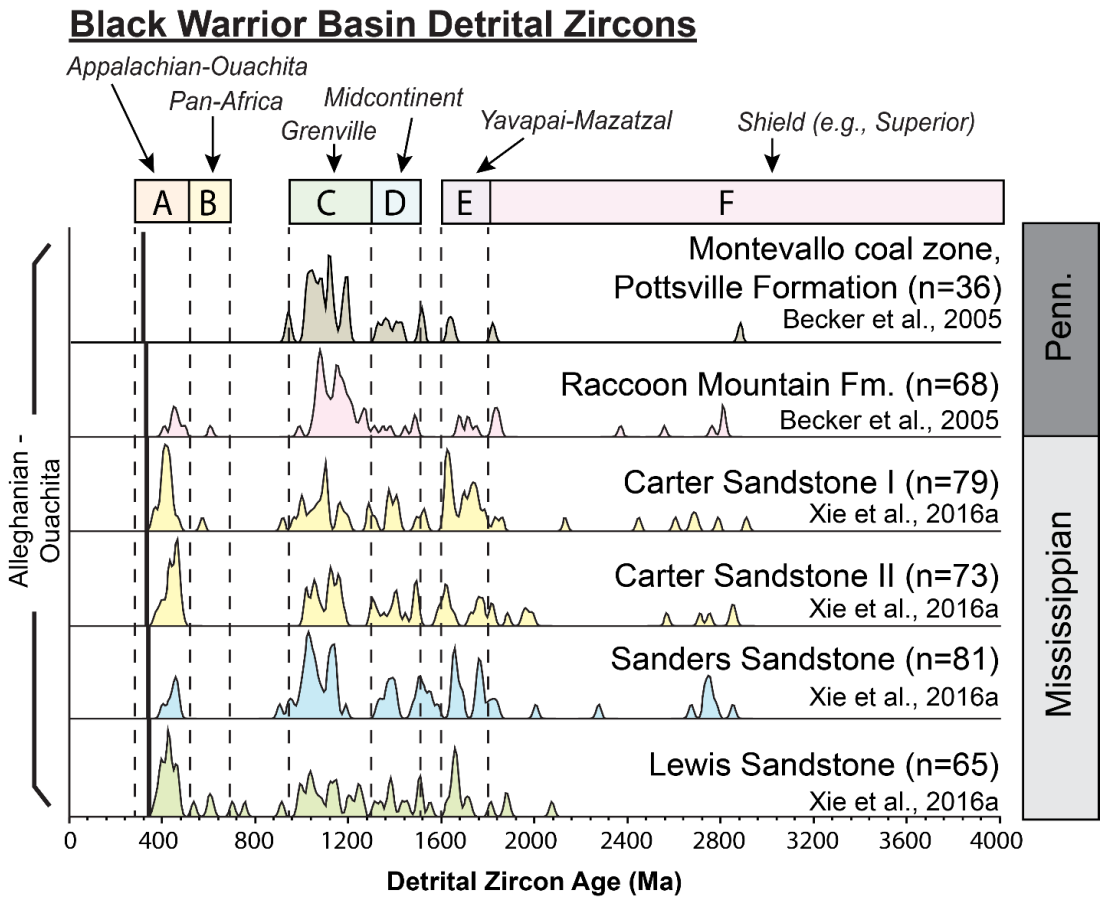

Figure S8. - Normalized detrital zircon U-Pb age KDE plots for the Black Warrior Basin (Becker et al., 2005; Xie et al., 2016a). See supplemental Figure 6 for additional details.

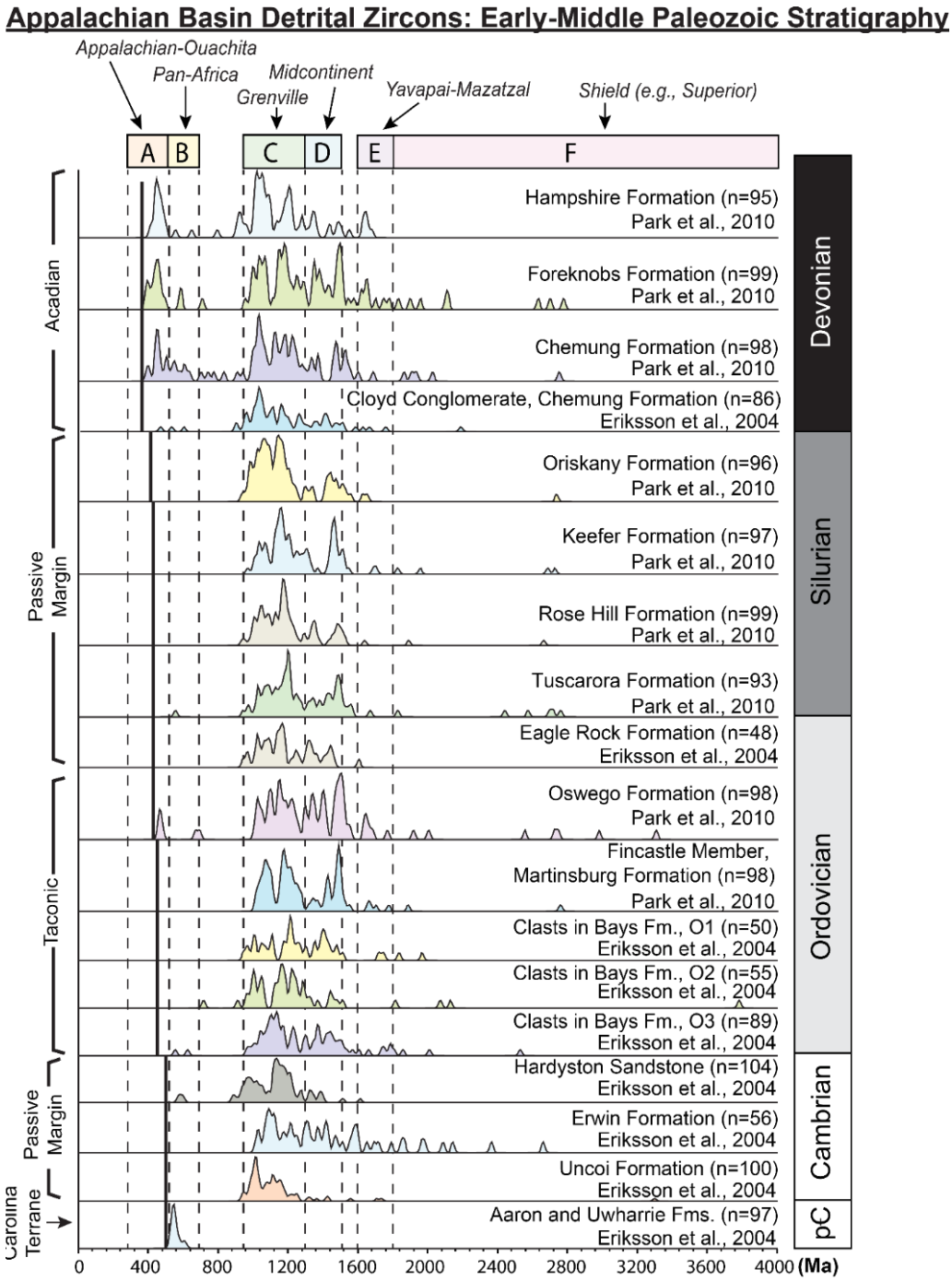

Figure S9. - Normalized detrital zircon U-Pb age KDE plots for Early to Middle Paleozoic stratigraphy in the Appalachian Foreland Basin (Eriksson et al., 2004; Park et al., 2010). See supplemental Figure 6 for additional details.

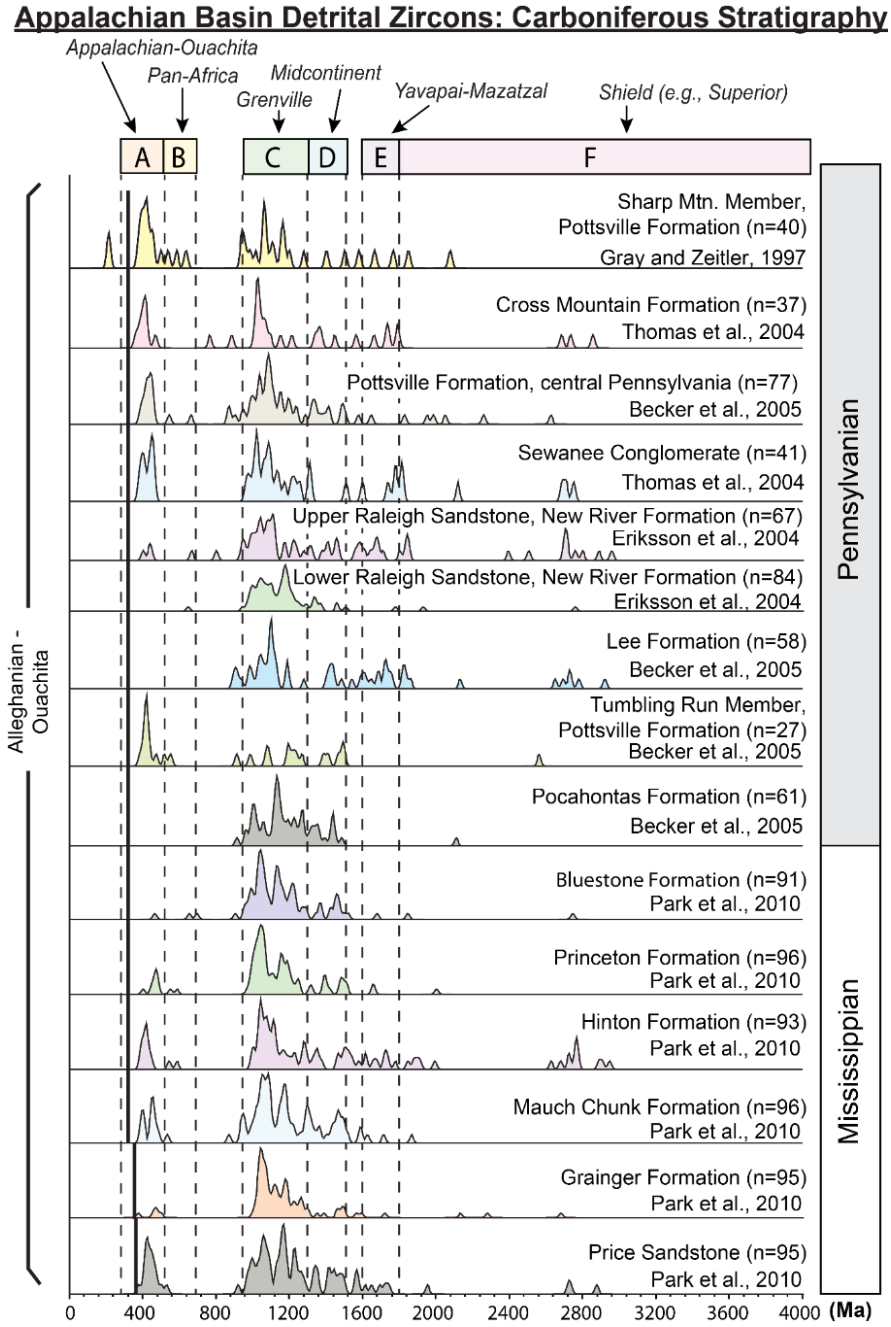

Figure S10. - Normalized detrital zircon U-Pb age kernel density estimate (KDE) plots for Carboniferous stratigraphy in the Appalachian Foreland Basin (Gray and Zeitler, 1997; Eriksson et al., 2004, Thomas et al., 2004; Becker et al., 2005; Park et al., 2010). See supplemental Figure 6 for additional details.

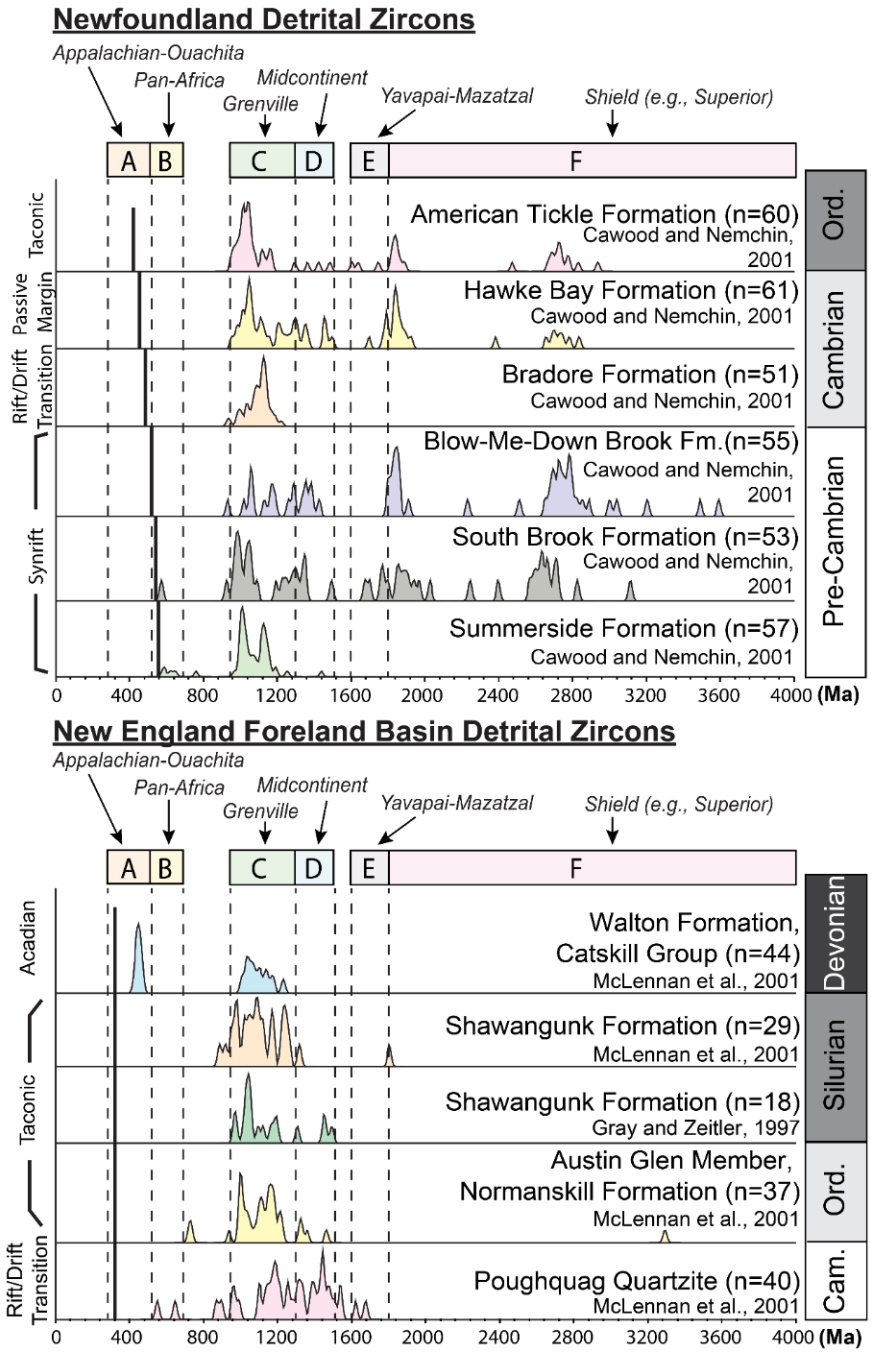

Figure S11. - Normalized detrital zircon U-Pb age KDE plots for Newfoundland (Cawood and Nemchin, 2001) and New England Foreland Basin (Gray and Zeitler, 1997; McLennan et al., 2001). See supplemental Figure 6 for additional details.

Figure S12. - Comparison of published and new normalized detrital zircon U-Pb age KDE plots for Carboniferous stratigraphy in eastern and southern North America (Gray and Zeitler, 1997; Eriksson et al., 2004; Thomas et al., 2004; Becker et al., 2005; Park et al., 2010; Shaulis et al., 2012; Xie et al., 2016b). Shaded plots are new U-Pb data from the Stanley and Jackfork Groups. See supplemental Figure 6 for additional details.

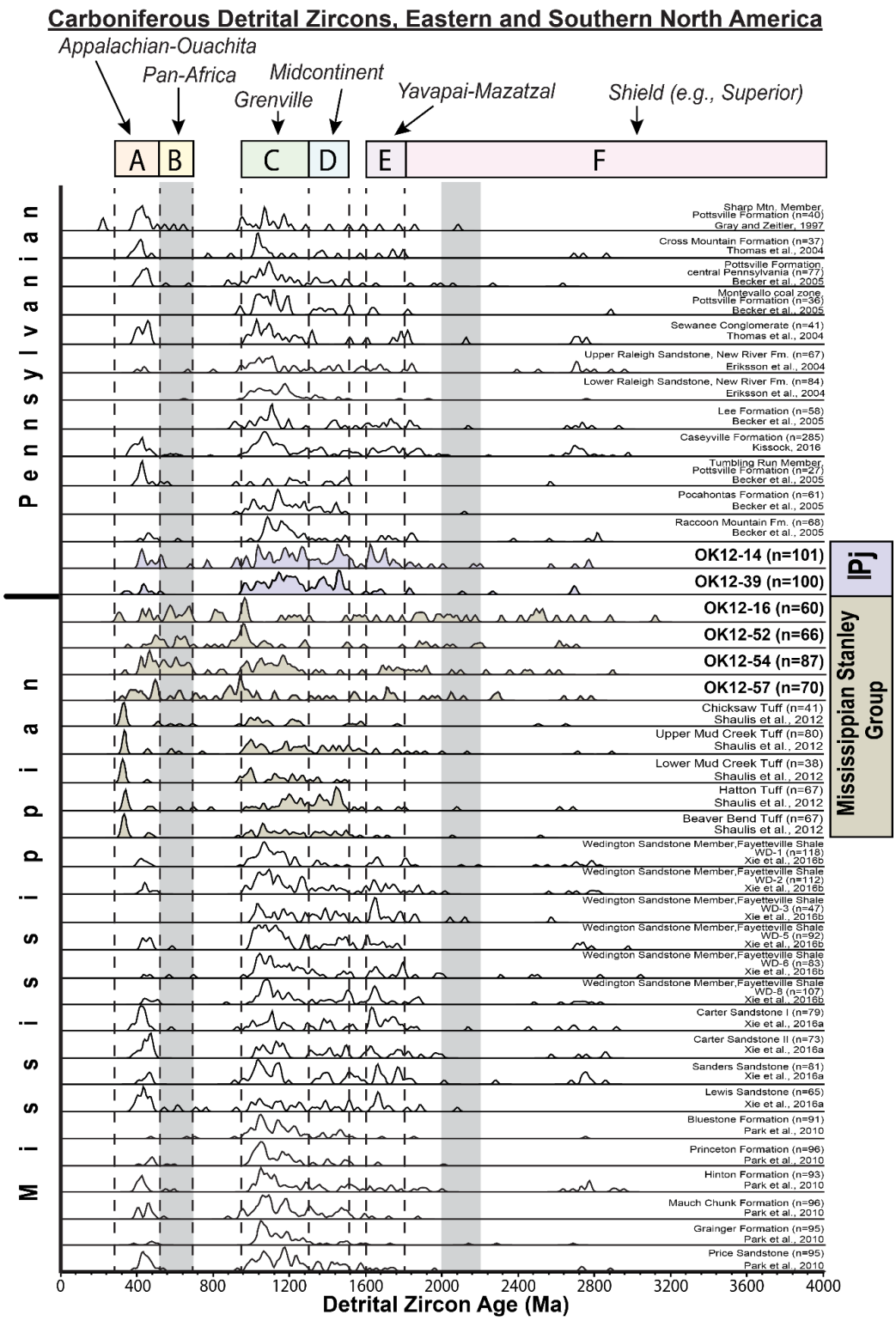
Carboniferous Detrital Zircons, Eastern and Southern North America
Appalachian-Ouachita
Pan-Africa
Grenville
Midcontinent
Yavapai-Mazatzal
Shield (e.g., Superior)
A
B
C
D
E
F
Pennsylvanian
Mississippian
Sharp Mtn. Member, Pottsville Formation (n=40) Gray and Zeitler, 1997
Cross Mountain Formation (n=37) Thomas et al., 2004
Pottsville Formation, central Pennsylvania (n=77) Becker et al., 2005
Montevallo coal zone, Pottsville Formation (n=36) Becker et al., 2005
Sewanee Conglomerate (n=41) Thomas et al., 2004
Upper Raleigh Sandstone, New River Fm. (n=67) Eriksson et al., 2004
Lower Raleigh Sandstone, New River Fm. (n=84) Eriksson et al., 2004
Lee Formation (n=56) Becker et al., 2005
Caseyville Formation (n=285) Kissock, 2016
Tumbling Run Member, Pottsville Formation (n=27) Becker et al., 2005
Pocahontas Formation (n=61) Becker et al., 2005
Raccoon Mountain Fm. (n=68) Becker et al., 2005
OK12-14 (n=101)
OK12-39 (n=100)
OK12-16 (n=60)
OK12-52 (n=66)
OK12-54 (n=87)
OK12-57 (n=70)
Chicksaw Tuff (n=41) Shaulis et al., 2012
Upper Mud Creek Tuff (n=80) Shaulis et al., 2012
Lower Mud Creek Tuff (n=38) Shaulis et al., 2012
Hatton Tuff (n=67) Shaulis et al., 2012
Beaver Bend Tuff (n=67) Shaulis et al., 2012
Wedington Sandstone Member,Fayetteville Shale WD-1 (n=118) Xie et al., 2016b
Wedington Sandstone Member,Fayetteville Shale WD-2 (n=112) Xie et al., 2016b
Wedington Sandstone Member,Fayetteville Shale WD-3 (n=47) Xie et al., 2016b
Wedington Sandstone Member,Fayetteville Shale WD-5 (n=92) Xie et al., 2016b
Wedington Sandstone Member,Fayetteville Shale WD-6 (n=83) Xie et al., 2016b
Wedington Sandstone Member,Fayetteville Shale WD-8 (n=107) Xie et al., 2016b
Carter Sandstone I (n=79) Xie et al., 2016a
Carter Sandstone II (n=73) Xie et al., 2016a
Sanders Sandstone (n=81) Xie et al., 2016a
Lewis Sandstone (n=65) Xie et al., 2016a
Bluestone Formation (n=91) Park et al., 2010
Princeton Formation (n=96) Park et al., 2010
Hinton Formation (n=93) Park et al., 2010
Mauch Chunk Formation (n=96) Park et al., 2010
Grainger Formation (n=95) Park et al., 2010
Price Sandstone (n=95) Park et al., 2010
IPj
Mississippian Stanley Group
0
400
800
1200
1600
2000
2400
2800
3200
3600
4000
Detrital Zircon Age (Ma)

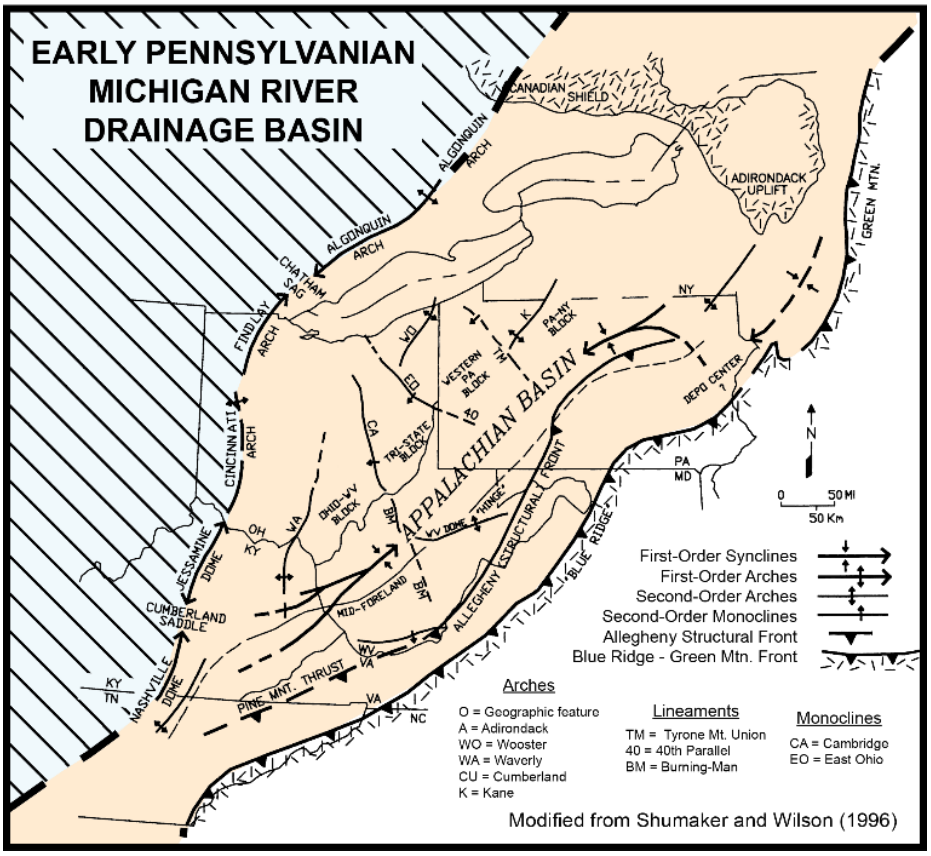

Figure S13. - Influence of basement structures on sediment dispersal during the Early Pennsylvanian for eastern North America (modified from Shumaker and Wilson, 1996). Diagonal lines represent a portion of the drainage basin for the continental-scale Michigan River system. The shaded area, including the Appalachian Basin, indicates the drainage area for the Ontario River system (see Figure 14C). A topographic low parallel and to either side of the curvilinear trend of basement arches served as two distinct drainage basins during the lowstand of the Early Pennsylvanian. Sediment into the Appalachian Basin includes proximal orogenic sources to the east from accreted terranes and distal sediment sources carried by the Ontario River from a region to the northeast. Abbreviations – KY, Kentucky; MD, Maryland; NC, North Carolina; NY, New York; OH, Ohio; PA, Pennsylvania; TN, Tennessee; VA, Virginia; WV, West Virginia.

APPENDIX C

MANUSCRIPT #2: FIGURES/TABLES

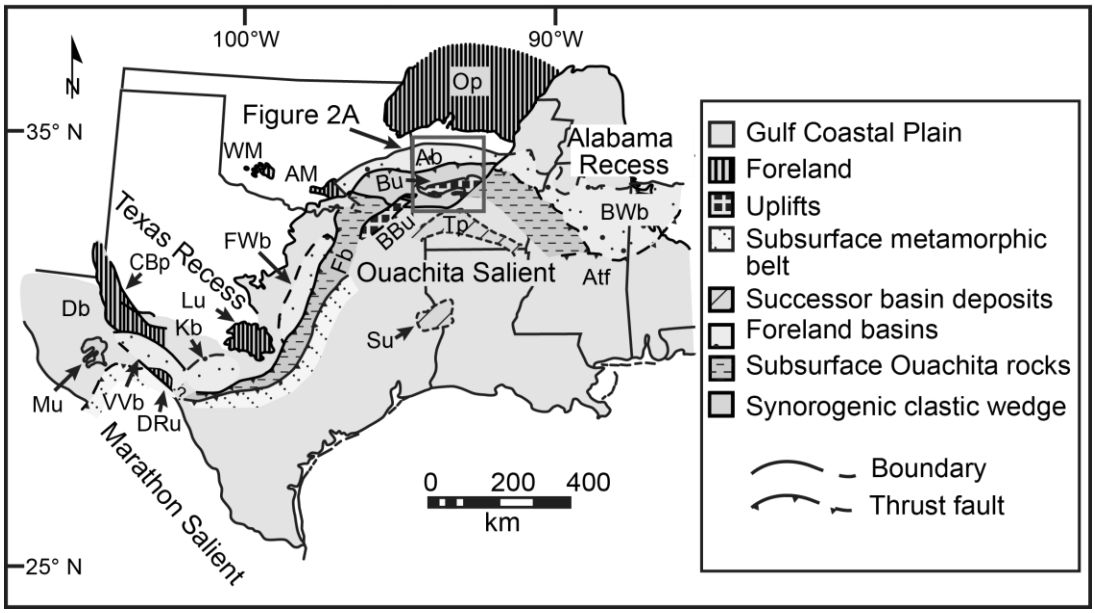

Figure 1. Tectonic overview map for the southern margin of North America (modified from Viele and Thomas, 1989). Abbreviations -- AtF- Appalachian tectonic front; Fb - Frontal belt; Basins: Ab - Arkoma, BWb - Black Warrior, Db - Deleware, FWb - Fort Worth, Kb - Kerr, VVb - Val Verde; Platforms: CBp - Central Basin, Op - Ozark, Tp - Texarkana; Mountains: AM - Arbuckle, WM - Wichita; Uplifts: BBu - Broken Bow, Bu - Benton, DRu - Devil's River, Lu - Llano, Mu - Marathon, Su - Sabine.

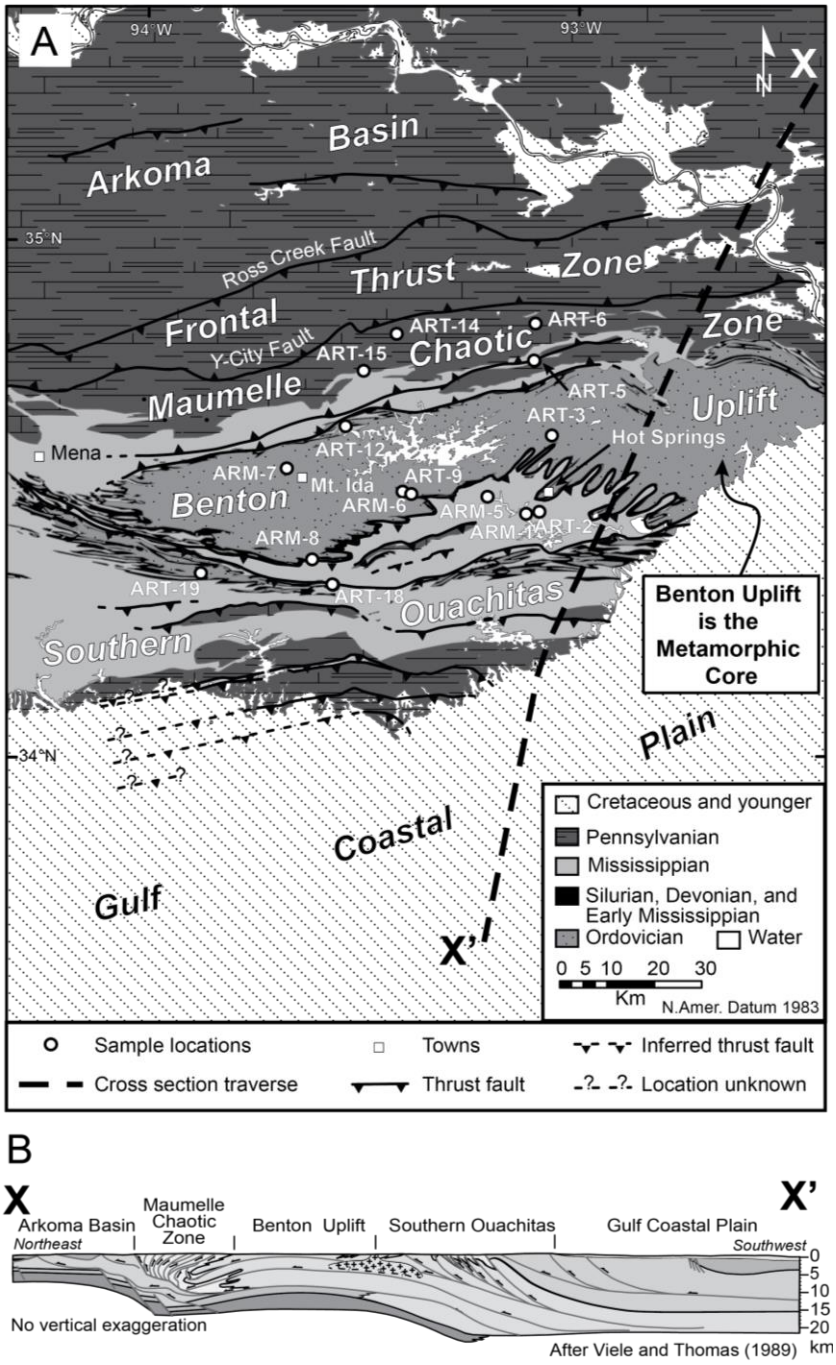

Figure 2. A. Geologic setting of western Arkansas with sample locations and cross section traverse. B. Representative cross section for eastern Ouachita orogen (after Viele and Thomas, 1989). Solid lines with arrows are thrust faults and motion direction, respectively.

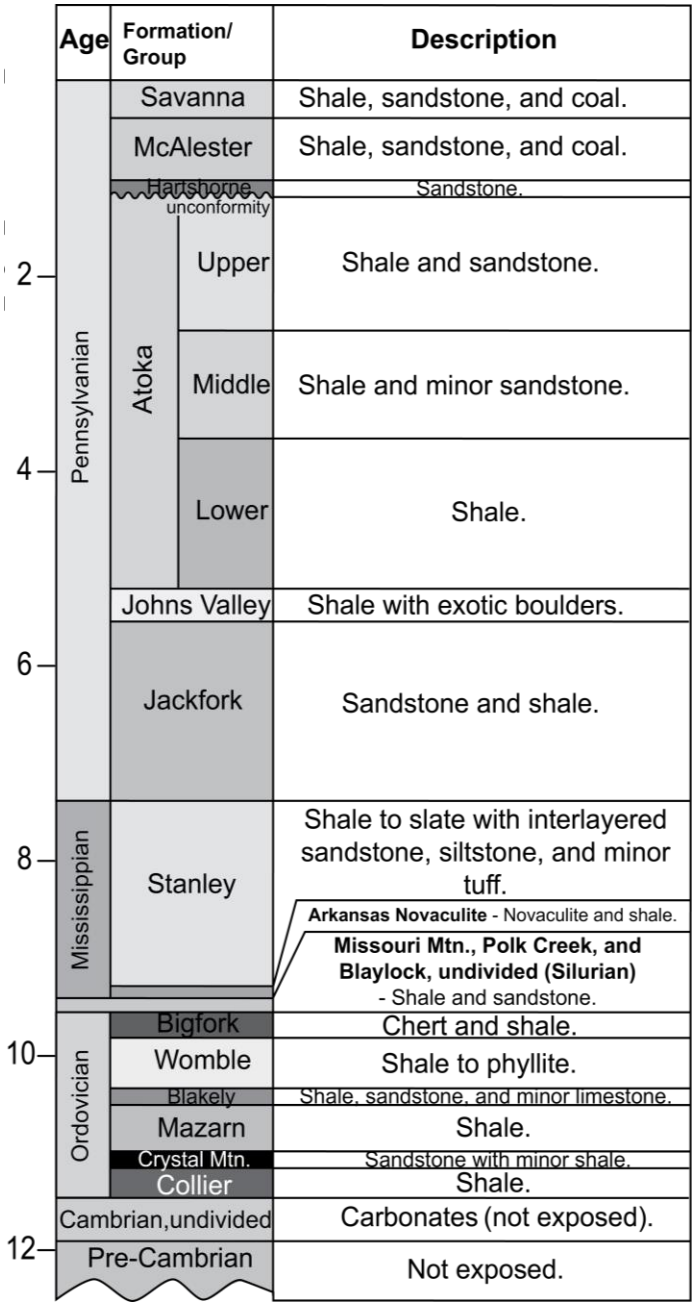

Figure 3. Simplified central Ouachita stratigraphy. Cumulative stratigraphic thickness is computed assuming the Savanna Formation is at the top of the stratigraphic section. The thickness range is compiled from Flawn et al. (1961); Briggs et al. (1975); Thomas (1977); Lowe (1989); Viele and Thomas (1989); Haley and Stone (2006); Arbenz (2008). The Cambrian carbonates are known from industry wells (Kruger, 1983).

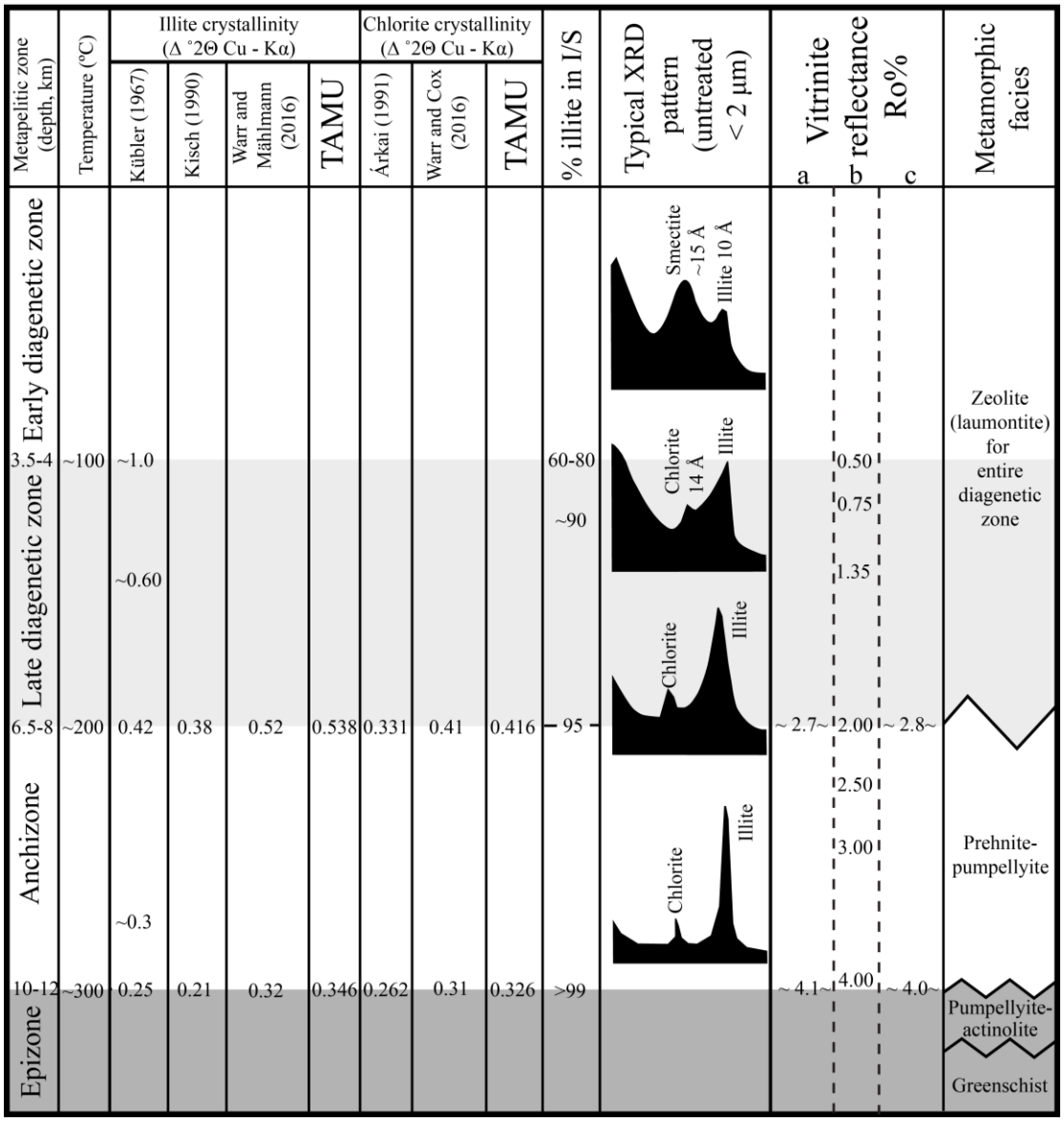

Figure 4. Metapelitic zones and thermal correlation diagram. Values for chlorite crystallinity are for the *d*(002) peak. Compiled from Árkai (1991), Merriman and Frey (1999), Merriman and Peacor (1999), Kübler and Jaboyedoff (2000), and War and Cox (2016). Vitrinite reflectance values: a, Árkai (1991); b, Merriman and Frey (1999); c, Kübler and Jaboyedoff (2000).

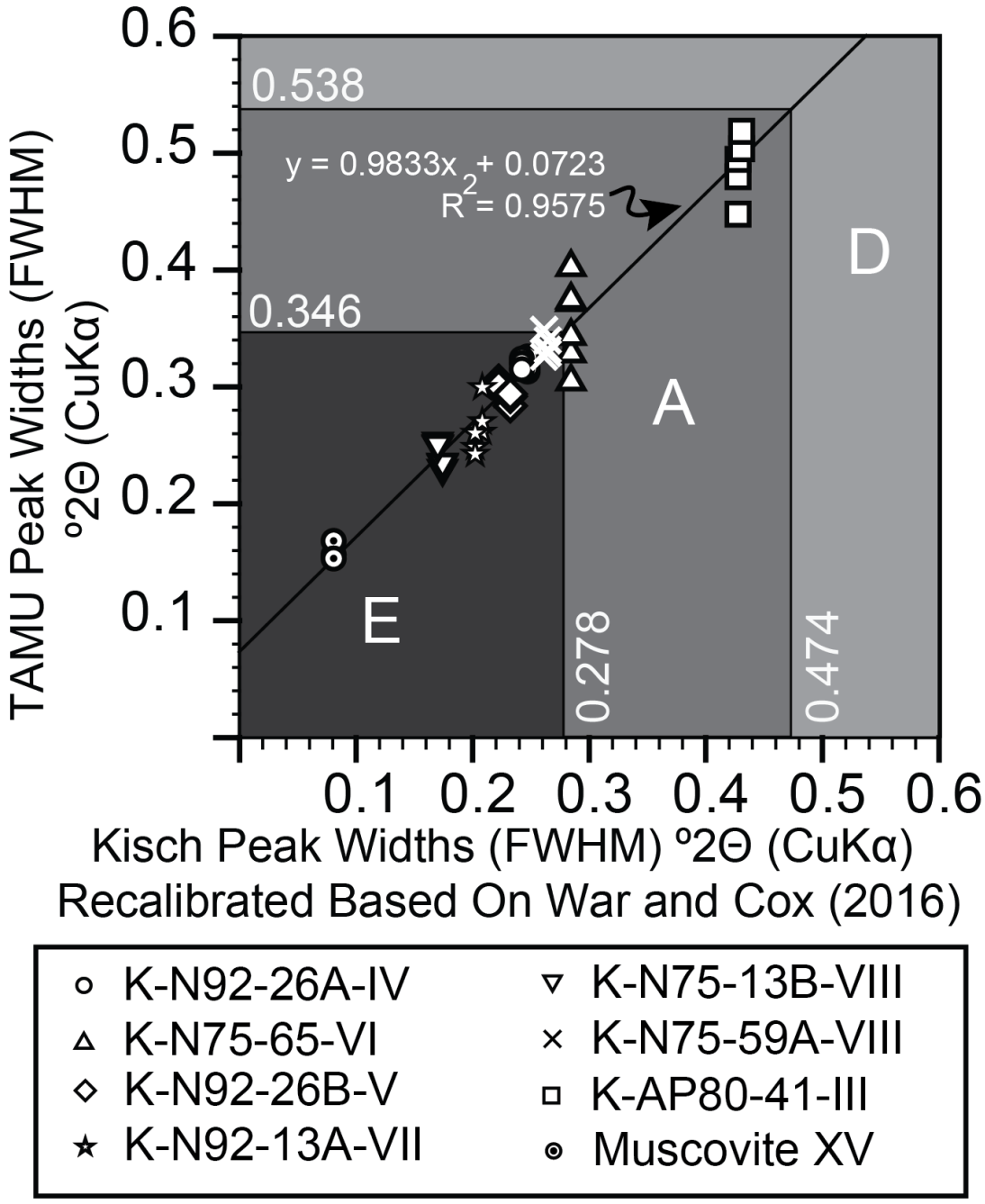

Figure 5. Calibration for illite crystallinity using polished slate standards and pegmatitic muscovite flake (Kisch, 1991). Kisch (1991) boundaries for crystallinity zones recalibrated following Warr and Cox (2016). Standards kindly provided by H. J. Kisch. Abbreviations: E, Epizone; A, Anchizone; D, Diagenetic Zone.

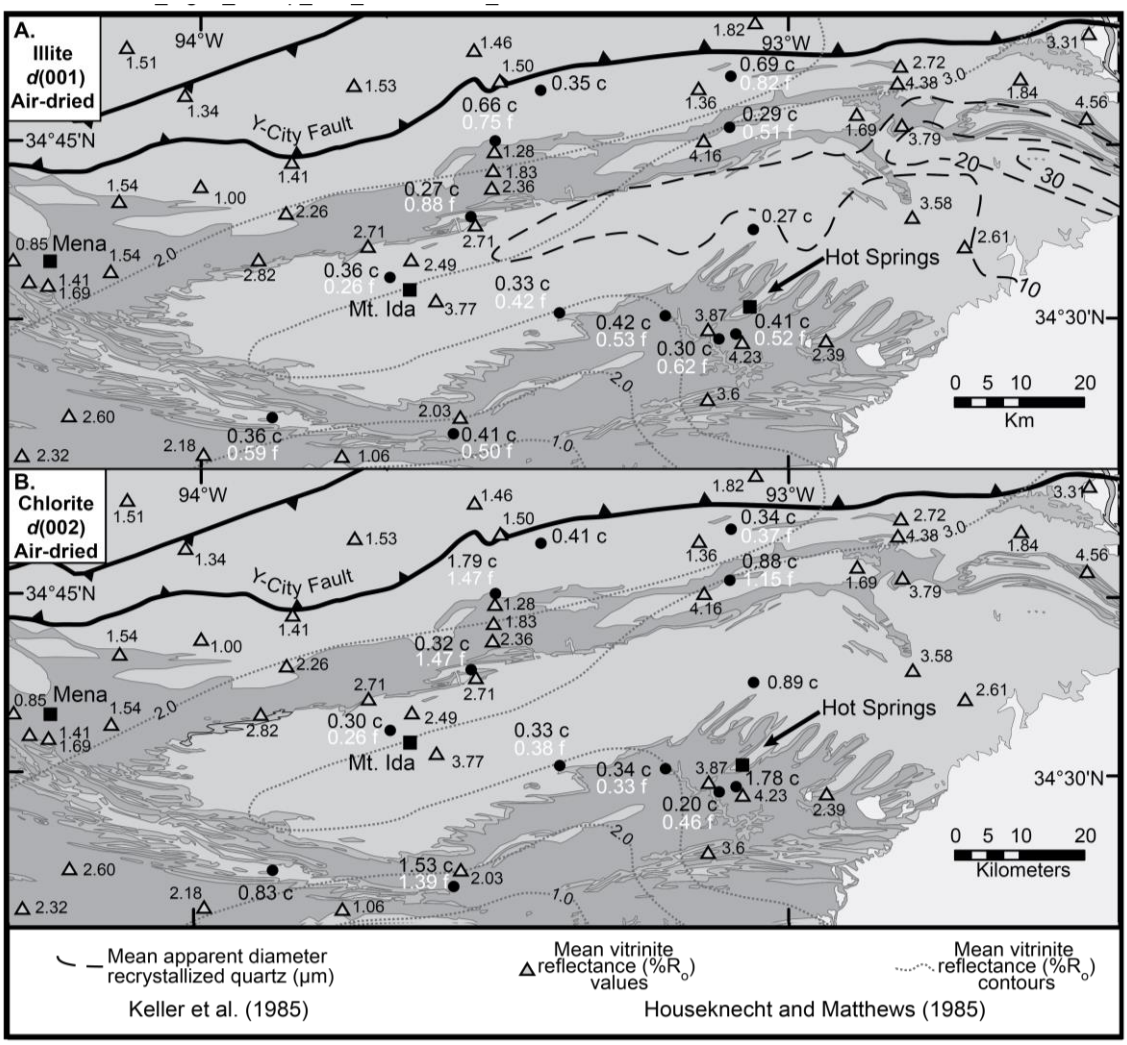

Figure 6. A. Crystallinity values for the air-dried coarse clay fraction and fine clay fraction of illite *d*(001). Crystallinity is given in FWHM °2Θ CuKα, where c denotes the coarse clay fraction and f denotes the fine clay fraction. The fine clay fraction indicates lower thermal maturation (~100°C) in comparison to the coarse clay fraction. Mean apparent diameter of recrystallized quartz are given by Keller et al. (1985). Mean vitrinite reflectance values and contours are given by Houseknecht and Matthews (1985). B. Crystallinity values for the air-dried coarse clay fraction and fine clay fraction of chlorite *d*(002). Crystallinity is given in FWHM °2Θ CuKα, where c denotes the coarse clay fraction and f denotes the fine clay fraction. Mean apparent diameter of recrystallized quartz are given by Keller et al. (1985). Mean vitrinite reflectance values and contours are given by Houseknecht and Matthews (1985).

Figure 7. Illite crystallinity of samples vs. the cumulative stratigraphic thickness for (A) fine clay and (B) coarse clay. All samples K-saturated, air-dried and X-rayed at room temperature. Cumulative stratigraphic thickness is the thickness of sediments above a particular sample that would have existed assuming no erosion (values determined from Fig. 3). Illite crystallinity increases with cumulative stratigraphic thickness.

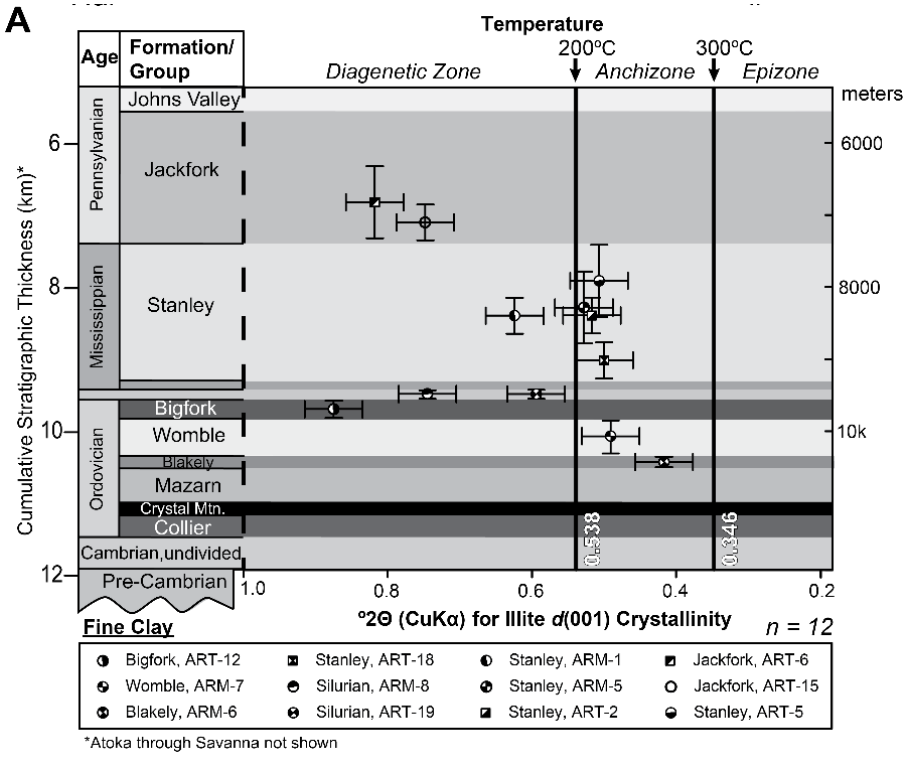
A
Temperature
200°C
300°C
Age
Formation/ Group
Diagenetic Zone
Anchizone
Epizone
meters
Johns Valley
Jackfork
Stanley
Bigfork
Womble
Blakely
Mazarn
Crystal Mtn.
Collier
Cambrian,undivided
Pre-Cambrian
Pennsylvanian
Mississippian
Ordovician
Cumulative Stratigraphic Thickness (km)*
6
8
10
12
6000
8000
10k
0.538
0.346
1.0
0.8
0.6
0.4
0.2
°2Θ (CuKα) for Illite d(001) Crystallinity
Fine Clay
n = 12
Bigfork, ART-12
Womble, ARM-7
Blakely, ARM-6
Stanley, ART-18
Silurian, ARM-8
Silurian, ART-19
Stanley, ARM-1
Stanley, ARM-5
Stanley, ART-2
Jackfork, ART-6
Jackfork, ART-15
Stanley, ART-5
*Atoka through Savanna not shown

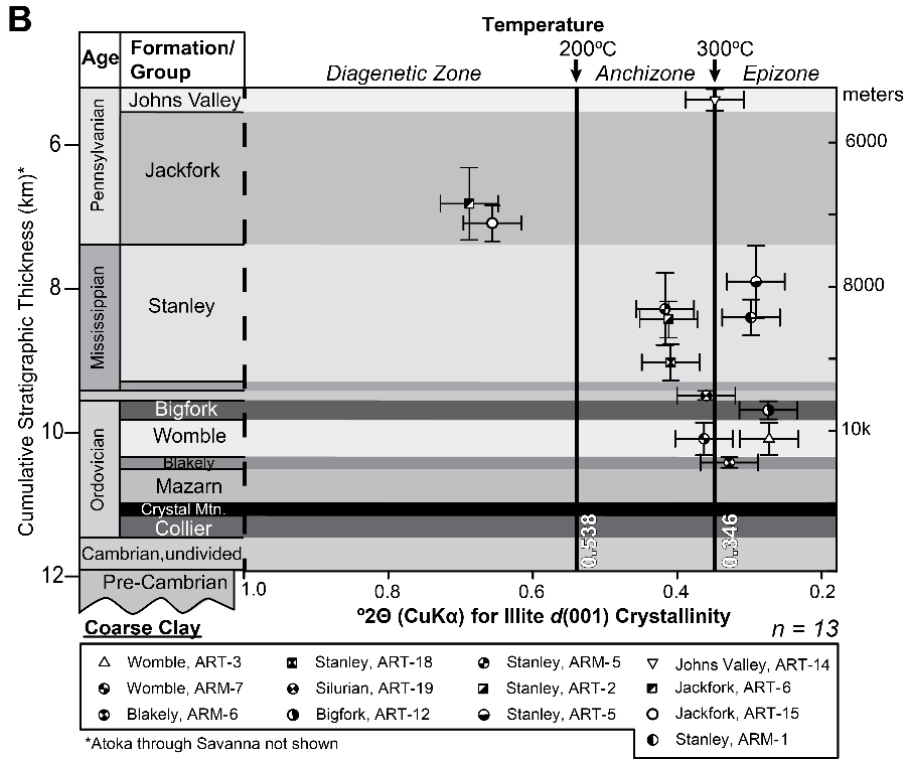
B
Temperature
200°C
300°C
Age
Formation/ Group
Diagenetic Zone
Anchizone
Epizone
meters
Johns Valley
Jackfork
Stanley
Bigfork
Womble
Blakely
Mazarn
Crystal Mtn.
Collier
Cambrian,undivided
Pre-Cambrian
Pennsylvanian
Mississippian
Ordovician
Cumulative Stratigraphic Thickness (km)*
6
8
10
12
6000
8000
10k
0.538
0.346
1.0
0.8
0.6
0.4
0.2
°2Θ (CuKα) for Illite d(001) Crystallinity
Coarse Clay
n = 13
Womble, ART-3
Womble, ARM-7
Blakely, ARM-6
Stanley, ART-18
Silurian, ART-19
Bigfork, ART-12
Stanley, ARM-5
Stanley, ART-2
Stanley, ART-5
Johns Valley, ART-14
Jackfork, ART-6
Jackfork, ART-15
Stanley, ARM-1
*Atoka through Savanna not shown

Figure 8. Chlorite crystallinity of samples vs. the cumulative stratigraphic thickness (see Fig. 3) for (A) fine clay and (B) coarse clay. Chlorite crystallinity does not increase with cumulative stratigraphic thickness. See Fig. 7 for further explanation.

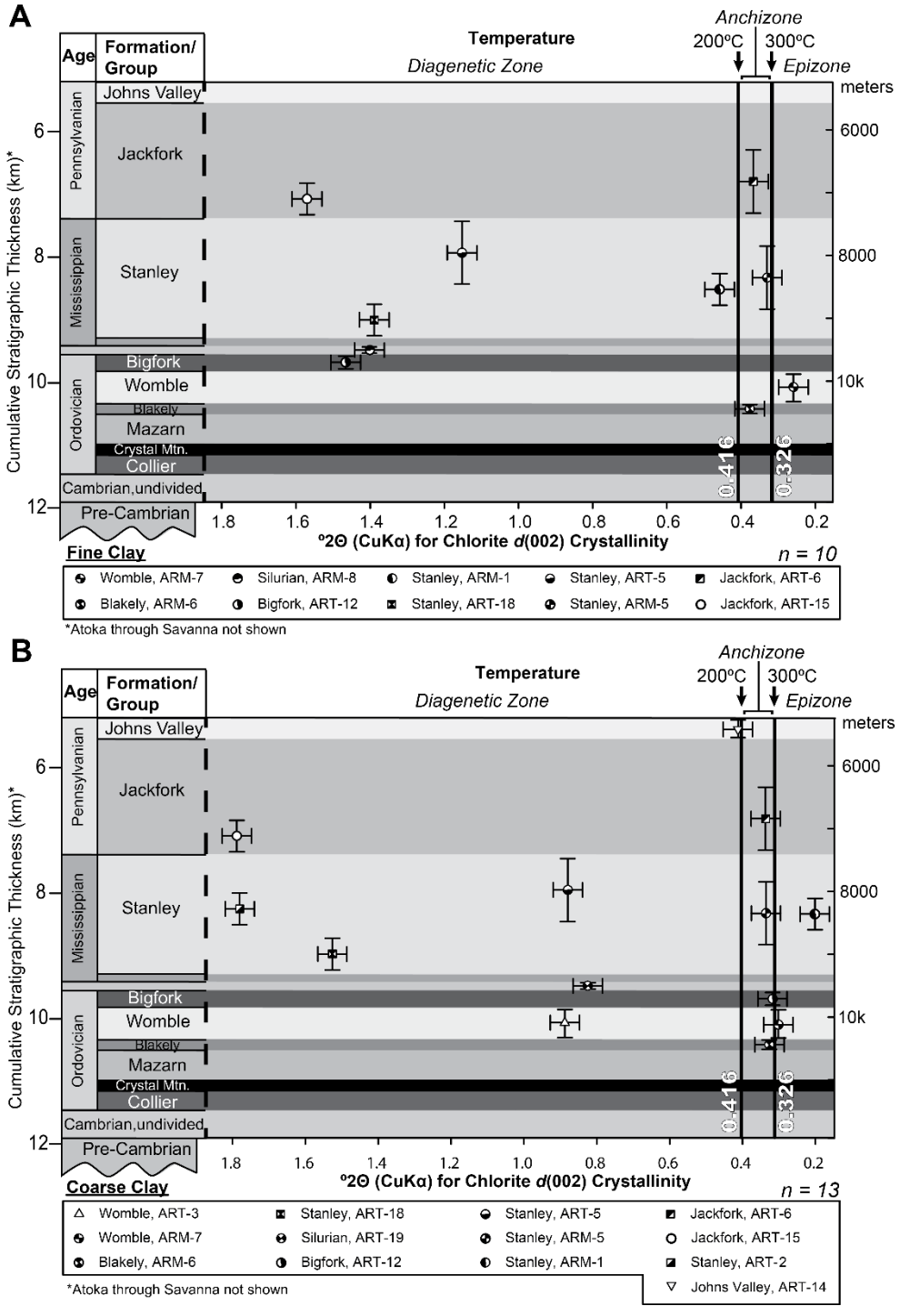
A
Age
Formation/ Group
Temperature
Diagenetic Zone
Anchizone
200ºC
300ºC
Epizone
meters
Johns Valley
Jackfork
Stanley
Bigfork
Womble
Blakely
Mazarn
Crystal Mtn.
Collier
Cambrian,undivided
Pre-Cambrian
Pennsylvanian
Mississippian
Ordovician
Cumulative Stratigraphic Thickness (km)*
6
8
10
12
6000
8000
10k
0.41
0.32
1.8
1.6
1.4
1.2
1.0
0.8
0.6
0.4
0.2
ºΘ (CuKα) for Chlorite d(002) Crystallinity
Fine Clay
n = 10
Womble, ARM-7
Silurian, ARM-8
Stanley, ARM-1
Stanley, ART-5
Jackfork, ART-6
Blakely, ARM-6
Bigfork, ART-12
Stanley, ART-18
Stanley, ARM-5
Jackfork, ART-15
*Atoka through Savanna not shown
B
Age
Formation/ Group
Temperature
Diagenetic Zone
Anchizone
200ºC
300ºC
Epizone
meters
Johns Valley
Jackfork
Stanley
Bigfork
Womble
Blakely
Mazarn
Crystal Mtn.
Collier
Cambrian,undivided
Pre-Cambrian
Pennsylvanian
Mississippian
Ordovician
Cumulative Stratigraphic Thickness (km)*
6
8
10
12
6000
8000
10k
0.41
0.32
1.8
1.6
1.4
1.2
1.0
0.8
0.6
0.4
0.2
ºΘ (CuKα) for Chlorite d(002) Crystallinity
Coarse Clay
n = 13
Womble, ART-3
Stanley, ART-18
Stanley, ART-5
Jackfork, ART-6
Womble, ARM-7
Silurian, ART-19
Stanley, ARM-5
Jackfork, ART-15
Blakely, ARM-6
Bigfork, ART-12
Stanley, ARM-1
Stanley, ART-2
Johns Valley, ART-14
*Atoka through Savanna not shown

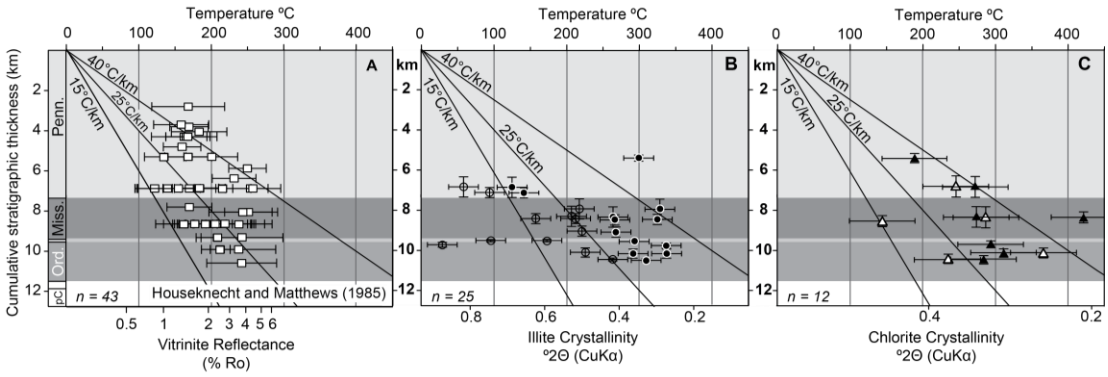

Figure 9. Comparison with different types of thermal maturation. A. Vitrinite reflectance. B. Illite crystallinity. C. Chlorite crystallinity. Plotted peak temperatures based on VR calculated using equation, T_{peak} = (ln(VR) + 1.680/0.0124, for burial-related maturation (Barker and Pawlewicz, 1994). Filled symbols are coarse clay data and open symbols are fine clay data. Not all crystallinity data are plotted because the FWHM exceed the X-axis at this scale, and see Figs. 7 and 8 for plots of all data. See Fig. 3 for cumulative stratigraphic thickness. Both measures of thermal maturation measures increase toward exposed eastern Ouachita metamorphic core to reach lower greenschist transition.

Table 1. Sample attributes

Sample	Latitude[a] (°N)	Longitude[a] (°W)	Elevation [b] (m)	Formation(s)[c]	Rock type collected
ARM-1	34.478615	-93.116110	147.00	Stanley	Shale
ARM-5	34.511394	-93.206393	141.00	Stanley	Shale
ARM-6	34.514999	-93.383061	199.00	Blakely	Shale
ARM-7	34.563613	-93.668333	200.00	Womble	Shale
ARM-8	34.389444	-93.608616	203.00	Missouri Mtn, Polk Creek, and Blaylock	Shale
ART-2	34.485835	-93.087226	170.00	Stanley	Sandstone
ART-3	34.633614	-93.058337	223.00	Womble	Sandstone
ART-5	34.777774	-93.098888	339.00	Stanley	Sandstone
ART-6	34.849999	-93.096666	189.00	Jackfork	Sandstone
ART-9	34.524444	-93.401671	235.00	Crystal Mountain	Sandstone
ART-12	34.650554	-93.532779	182.00	Bigfork	Sandstone
ART-14	34.829441	-93.416116	240.00	Johns Valley	Sandstone
ART-15	34.757782	-93.492504	309.00	Jackfork	Sandstone
ART-18	34.343611	-93.560001	195.00	Stanley	Sandstone
ART-19	34.364447	-93.863334	367.00	Missouri Mtn, Polk Creek, and Blaylock	Sandstone

[a] North American Datum 1983

[b] Elevation determined from USGS 30 m digital elevation model.

[c]Formation determined using 'Geologic Map of the Ouachita Mountain Region and a portion of the Arkansas Valley Region in Arkansas' (Haley and Stone, 2006)

APPENDIX D

MANUSCRIPT #2: ADDITIONAL REFERENCE MATERIAL

X-ray Diffraction Data

TABLE B1. Semi-quantitative mineralogical analysis using X-ray Diffraction[a]

Sample	Sand fraction		Silt fraction		Coarse clay fraction		Fine clay fraction		Carbonate, organic material, and procedural loss
	%	Mineralogy[b]	%	Mineralogy[b]	%	Mineralogy[b]	%	Mineralogy[b]	%
Pennsylvanian Johns Valley Formation									
ART-14	68.63	Q	27.13	C?,Q	0.15	C,I,Q	N.D.	N.D.[c]	4.09
Pennsylvanian Jackfork Formation									
ART-6	85.09	Q	12.37	C?,Q	1.02	S,C,I/S,I,Q	0.18	S,C,I/S,I,Q	1.34
ART-15	73.88	F,Q	21.06	F,Q	2.58	C,I,Q	0.12	C,I	2.35
Mississippian Stanley Formation									
ARM-1	46.60	C,I,F	38.69	C,I,F	10.69	C,I	1.20	C,I	2.81
ARM-5	36.66	C,I,F,Q	52.08	C,I,F,Q	9.15	C,I,Q	0.48	C,I,Q?	1.63
ART-2	80.26	C,I?,F,Q	15.64	C,I?,F,Q	1.66	C,I,Q	0.22	C?,I,Q	2.22
ART-5	69.51	I?F,Q	26.51	C,I,F,Q	2.42	C,I,Q	0.18	C,I	1.38
ART-18	67.68	C,I?,F,Q	26.54	C,I?,F,Q	3.09	C,I,Q	0.38	C,I,Q	2.31
Silurian-Ordovician, Undivided									
ARM-8	29.02	I?,Q	44.14	I?,Q	11.76	I,Q	3.63	I,Q	11.46
ART-19	80.58	I?,Q	12.86	C?,I?,Q	2.78	C?,I,Q	0.24	C,I,Q	3.53
Ordovician Bigfork Formation									
ART-12	83.29	Q	13.25	Q	0.76	C,I,Q	0.13	C,I,Q	2.57
Ordovician Womble Formation									
ARM-7	22.22	C,I,F,Q	59.19	C,I,F,Q	15.35	C,I	1.23	I,C	2.01
ART-3	82.43	Q	15.36	I?,Q	0.28	I,K,Q	N.D.[c]	N.D.[c]	1.93
Ordovician Blakely Formation									
ARM-6	26.37	C,I,Q	56.91	C,I,Q	12.72	C,I	1.01	C,I	3.00
Ordovician Crystal Mountain Formation									
ART-9	91.63	Q	6.97	Q	0.37	Q	N.D.[c]	N.D.[c]	1.03

[a] Sand and silt fractions are randomly oriented and side loaded into an aluminum holder. Both clay fractions are oriented and mineralogy determined from inspection of the diffractograms of each treatment type (i.e., ethylene glycol vapor solvation and heat treatments). Carbonate, organic material, and procedural loss determined by subtracting combined weight of the fractions from the initial sample weight prior to pretreatments.

[b] Minerals present denoted using the following abbreviations: C--chlorite, F--feldspars, I--illite, I/S--interlayered illite and smectite, K--kaolinite, and Q--quartz.

[c] N.D. =no data.

TABLE B2. CHLORITE 001 PEAK VALUES AT AIR DRIED, ETHYLENE GLYCOL VAPOR SOLVATED, HEATED 300°C, AND HEATED 550°C

Sample, clay fraction	2Θ (degrees)	D-spacing (angstroms)	Peak max counts (counts/second)	Peak area (integrated counts)	FWHM (degrees)	Sample, clay fraction	2Θ (degrees)	D-spacing (angstroms)	Peak max counts (counts/second)	Peak area (integrated counts)	FWHM (degrees)
Pennsylvanian Johns Valley Formation						Mississippian Stanley Formation					
ART-14, coarse						ARM-1, fine					
Air-dried	6.30	14.030	113.8	1224.5	0.472	Air-dried	6.40	13.811	62.7	709.3	0.560
Ethylene Glycol Vapor	6.45	13.704	106.1	1107.1	0.485	Ethylene Glycol Vapor	6.35	13.919	45.0	474.9	0.636
Heated 300°C	N.D.*	N.D.*	N.D.*	N.D.*	N.D.*	Heated 300°C	6.45	13.704	31.8	357.5	0.595
Heated 550°C	N.D.*	N.D.*	N.D.*	N.D.*	N.D.*	Heated 550°C	6.60†	13.393†	44.3†	711.4†	0.589†
Pennsylvanian Jackfork Formation						ARM-5, coarse					
ART-6, coarse§						Air-dried	6.50	13.598	15.8	73.8	0.226
Air-dried	6.35	13.919	259.2	2414.1	0.420	Ethylene Glycol Vapor	6.65	13.292	13.1	59.7	0.222
Ethylene Glycol Vapor	6.35	13.919	343.4	4255.0	0.511	Heated 300°C	6.90†	12.811†	17.2†	212.6†	0.828†
Heated 300°C	6.45	13.704	75.4	725.1	0.433	Heated 550°C	N.D.*	N.D.*	N.D.*	N.D.*	N.D.*
Heated 550°C	6.85†	12.904†	29.4†	472.6†	.788†	ARM-5, fine					
ART-6, fine§						Air-dried	6.25	14.142	39.8	239.5	0.240
Air-dried	6.40	13.811	71.1	729.0	0.541	Ethylene Glycol Vapor	6.35	13.919	45.9	320.4	0.374
Ethylene Glycol Vapor	N.D.*	N.D.*	N.D.*	N.D.*	N.D.*	Heated 300°C	6.35	13.919	35.8	282.8	0.516
Heated 300°C	N.D.*	N.D.*	N.D.*	N.D.*	N.D.*	Heated 550°C	6.65	13.292	53.8	528.8	0.480
Heated 550°C	N.D.*	N.D.*	N.D.*	N.D.*	N.D.*	ART-2, coarse					
Mississippian Stanley Formation						Air-dried	6.80†	12.999†	27.1†	346.5†	0.501†
ARM-1, coarse						Ethylene Glycol Vapor	6.65†	13.292†	22.2†	278.9†	0.498†
Air-dried	6.30	14.030	12.5	53.1	0.210	Heated 300°C	7.25†	12.193†	22.3†	160.5†	0.168†
Ethylene Glycol Vapor	6.30	14.030	14.7	69.0	0.173	Heated 550°C	7.65†	11.557†	64.1†	1138.7†	0.799†
Heated 300°C	N.D.*	N.D.*	N.D.*	N.D.*	N.D.*						
Heated 550°C	6.50	13.598	36.8	239.9	0.323						

Note: Samples without C_{001} data omitted.
*N.D. –no data.
†Broad peak measurement.
§Possible smectite interlayering, mainly with illite.

TABLE B3. CHLORITE 001 PEAK VALUES AT AIR DRIED, ETHYLENE GLYCOL VAPOR SOLVATED, HEATED 300˚C, AND HEATED 550˚C

Sample, clay fraction	2Θ (degrees)	D-spacing (angstroms)	Peak max counts (counts/second)	Peak area (integrated counts)	FWHM (degrees)	Sample, clay fraction	2Θ (degrees)	D-spacing (angstroms)	Peak max counts (counts/second)	Peak area (integrated counts)	FWHM (degrees)
Mississippian Stanley Formation						Ordovician Blakely Formation					
ART-2, fine						ARM-6, fine					
Air-dried	N.D.*	N.D.*	N.D.*	N.D.*	N.D.*	Air-dried	6.95†	12.719†	273.5†	7473.0†	1.286†
Ethylene Glycol Vapor	6.25	14.142	19.3	270.2	0.161	Ethylene Glycol Vapor	N.D.*	N.D.*	N.D.*	N.D.*	N.D.*
Heated 300˚C	N.D.*	N.D.*	N.D.*	N.D.*	N.D.*	Heated 300˚C	N.D.*	N.D.*	N.D.*	N.D.*	N.D.*
Heated 550˚C	7.65†	11.557†	63.6†	1125.5†	.963†	Heated 550˚C	6.70	13.193	83.7	626.8	0.471
ART-5, coarse											
Air-dried	6.40†	13.811†	25.3†	519†	1.027†						
Ethylene Glycol Vapor	6.65†	13.292†	25.3†	480.7†	1.101†						
Heated 300˚C	N.D.*	N.D.*	N.D.*	N.D.*	N.D.*						
Heated 550˚C	7.60†	11.633†	19.9†	124.1†	.241†						
Ordovician Bigfork Formation											
ART-12, course											
Air-dried	6.35	13.919	18.5	72.0	0.220						
Ethylene Glycol Vapor	6.35	13.919	26.9	85.1	0.111						
Heated 300˚C	6.40	13.811	15.7	42.3	0.060						
Heated 550˚C	6.50	13.598	38.4	217.6	0.289						
Ordovician Blakely Formation											
ARM-6, coarse											
Air-dried	N.D.*	N.D.*	N.D.*	N.D.*	N.D.*						
Ethylene Glycol Vapor	N.D.*	N.D.*	N.D.*	N.D.*	N.D.*						
Heated 300˚C	N.D.*	N.D.*	N.D.*	N.D.*	N.D.*						
Heated 550˚C	6.45	13.704	53.0	271.4	0.203						

Note: Samples without C_{001} data omitted.
*N.D. —no data.
†Broad peak measurement.
‡Possible smectite interlayering, mainly with illite.

TABLE B5. ILLITE 001 PEAK VALUES AT AIR DRIED, ETHYLENE GLYCOL VAPOR SOLVATED, HEATED 300°C, AND HEATED 550°C

Sample, clay fraction	2Θ (degrees)	D-spacing (angstroms)	Peak max counts (counts/second)	Peak area (integrated counts)	FWHM (degrees)
Mississippian Stanley Formation					
ARM-5, fine					
Air-dried	8.90	9.9361	628.9	7681.5	0.528
Ethylene Glycol Vapor	8.95	9.8807	586.6	7546.2	0.543
Heated 300°C	8.95	9.8807	667.2	7437.1	0.468
Heated 550°C	8.90	9.9361	348.2	3466.9	0.425
ART-2, coarse					
Air-dried	8.85	9.9922	319.2	3047.3	0.412
Ethylene Glycol Vapor	8.90	9.9361	311.7	3032.2	0.414
Heated 300°C	8.90	9.9361	212.9	1647.9	0.306
Heated 550°C	8.90	9.9361	99.3	948.9	0.361
ART-2, fine					
Air-dried	8.75	10.1060	35.6	395.9	0.517
Ethylene Glycol Vapor	8.80	10.0490	39.8	395.2	0.377
Heated 300°C	8.85	9.9922	35.2	391.8	0.551
Heated 550°C	8.85	9.9922	121.8	1475.0	0.532
ART-5, coarse					
Air-dried	8.95	9.8807	454.3	3207.0	0.291
Ethylene Glycol Vapor	8.95	9.8807	441.2	3236.3	0.301
Heated 300°C	8.90	9.9361	97.4	763.4	0.338
Heated 550°C	8.80	10.0490	60.7	423.6	0.310
Mississippian Stanley Formation					
ART-5, fine					
Air-dried	9.00	9.8259	54.3	475.2	0.507
Ethylene Glycol Vapor	9.00	9.8259	55.0	489.9	0.385
Heated 300°C	9.00	9.8259	33.3	253.4	0.394
Heated 550°C	8.85	9.9922	26.3	173.4	0.143
ART-18, coarse					
Air-dried	8.95	9.8807	162.5	2050.1	0.409
Ethylene Glycol Vapor	8.95	9.8807	162.3	2056.4	0.404
Heated 300°C	N.D.†	N.D.†	N.D.†	N.D.†	N.D.†
Heated 550°C	N.D.†	N.D.†	N.D.†	N.D.†	N.D.†
ART-18, fine					
Air-dried	9.05	9.7718	36.9	412.0	0.500
Ethylene Glycol Vapor	9.05*	9.7718*	37.1*	530.8*	0.677*
Heated 300°C	9.05*	9.7718*	17.9*	145.7*	0.173*
Heated 550°C	N.D.†	N.D.†	N.D.†	N.D.†	N.D.†
Silurian-Ordovician, Undivided					
ARM-8, coarse					
Air-dried	N.D.†	N.D.†	N.D.†	N.D.†	N.D.†
Ethylene Glycol Vapor	8.95	N.D.†	20.5	153.8	0.387
Heated 300°C	8.90	9.9361	24.6	318.6	0.656
Heated 550°C	N.D.†	N.D.†	N.D.†	N.D.†	N.D.†

Note: Samples without I_{001} data omitted.
*Broad peak measurement.
†N.D. = no data.
‡Possible smectite interlayering, mainly with illite.

TABLE B4. ILLITE 001 PEAK VALUES AT AIR DRIED, ETHYLENE GLYCOL VAPOR SOLVATED, HEATED 300˚C, AND HEATED 550˚C

Sample, clay fraction	2Θ (degrees)	D-spacing (angstroms)	Peak max counts (counts/second)	Peak area (integrated counts)	FWHM (degrees)
Pennsylvanian Johns Valley Formation					
ART-14, coarse					
Air-dried	8.95	9.8807	18.4	78.3	0.348
Ethylene Glycol Vapor	8.95*	9.8807*	14.3*	56.8*	0.317*
Heated 300˚C	N.D.†	N.D.†	N.D.†	N.D.†	N.D.†
Heated 550˚C	N.D.†	N.D.†	N.D.†	N.D.†	N.D.†
Pennsylvanian Jackfork Formation					
ART-6, coarse§					
Air-dried	8.15*	10.8490*	528.8*	8955.8*	0.688*
Ethylene Glycol Vapor	8.85*	9.9922*	145.7*	1425.0*	0.433*
Heated 300˚C	8.85*	9.9922*	241.6*	5864.8*	1.128*
Heated 550˚C	9.20*	9.6128*	50.9*	812.9*	0.757*
ART-6, fine§					
Air-dried	8.05	10.9830	516.7	11196.2	0.818
Ethylene Glycol Vapor	N.D.†	N.D.†	N.D.†	N.D.†	N.D.†
Heated 300˚C	8.25*	10.717*	195.4*	4264.7*	0.992*
Heated 550˚C	9.50*	9.3099*	59.3*	694.1*	0.555*
ART-15, coarse					
Air-dried	8.90	9.9361	207.3	3769.3	0.656
Ethylene Glycol Vapor	8.95	9.8807	212.8	3445.8	0.624
Heated 300˚C	9.00*	9.8259*	52.4*	1075.1*	0.833*
Heated 550˚C	8.30*	10.6530*	76.6*	2410.9*	1.571*

Sample, clay fraction	2Θ (degrees)	D-spacing (angstroms)	Peak max counts (counts/second)	Peak area (integrated counts)	FWHM (degrees)
Pennsylvanian Jackfork Formation					
ART-15, fine					
Air-dried	8.95*	9.8807*	55.2*	855.3*	0.748*
Ethylene Glycol Vapor	8.85	9.9922	49.1	849.1	0.562
Heated 300˚C	8.85*	9.9922*	67.9*	1105.9*	0.756*
Heated 550˚C	8.80*	10.049*	79.0*	2048.7*	1.308*
Mississippian Stanley Formation					
ARM-1, coarse					
Air-dried	8.90	9.9361	53.7	379.1	0.298
Ethylene Glycol Vapor	8.95	9.8807	49.7	353.6	0.274
Heated 300˚C	8.96	9.8751	36.6	205.9	0.241
Heated 550˚C	8.85	9.9922	65.6	364.4	0.244
ARM-1, fine					
Air-dried	8.85	9.9922	647.6	9230.5	0.624
Ethylene Glycol Vapor	8.90	9.9361	629.2	8836.2	0.613
Heated 300˚C	8.90	9.9361	705.8	9050.5	0.543
Heated 550˚C	8.90	9.9361	374.6	5054.8	0.549
ARM-5, coarse					
Air-dried	9.10	9.7182	192.7	1898.5	0.417
Ethylene Glycol Vapor	9.15	9.6652	197.9	2099.1	0.458
Heated 300˚C	9.25	9.5609	229.5	2109.8	0.389
Heated 550˚C	9.23	9.5868	61.4	719.7	0.522

Note: Samples without I_{001} data omitted.
*Broad peak measurement.
†N.D. = no data.
§Possible smectite interlayering, mainly with illite.

TABLE B6. ILLITE 001 PEAK VALUES AT AIR DRIED, ETHYLENE GLYCOL VAPOR SOLVATED, HEATED 300˚C, AND HEATED 550˚C

Sample, clay fraction	2Θ (degrees)	D-spacing (angstroms)	Peak max counts (counts/second)	Peak area (integrated counts)	FWHM (degrees)
Silurian-Ordovician, Undivided					
ARM-8, fine					
Air-dried	8.90	9.9361	1245.2	21144.1	0.745
Ethylene Glycol Vapor	8.90	9.9361	1119.4	19089.4	0.727
Heated 300˚C	8.95	9.8807	1218.2	18401.0	0.650
Heated 550˚C	8.90	9.9361	1229.7	17802.7	0.625
ART-19, coarse					
Air-dried	8.90	9.9361	775.4	6977.6	0.360
Ethylene Glycol Vapor	8.90	9.9361	784.8	7167.5	0.363
Heated 300˚C	9.00	9.8259	47.5	390.1	0.311
Heated 550˚C	8.95	9.8807	39.4	230.5	0.089
ART-19,fine					
Air-dried	8.85	9.9922	219.4	2892.5	0.594
Ethylene Glycol Vapor	8.90	9.9361	219.0	3050.3	0.615
Heated 300˚C	8.80	10.0490	437.0	5184.2	0.506
Heated 550˚C	8.85	9.9922	195.2	2407.9	0.527
Ordovician Bigfork Formation					
ART-12, coarse					
Air-dried	8.85	9.9922	61.1	415.1	0.274
Ethylene Glycol Vapor	8.90	9.9361	68.8	487.3	0.311
Heated 300˚C	8.90*	9.9361*	35.0*	244.5*	0.330*
Heated 550˚C	8.85	9.9922	14.8	71.2	0.241
Ordovician Bigfork Formation					
ART-12, fine					
Air-dried	8.90*	9.9361*	56.9*	1151.5*	0.875*
Ethylene Glycol Vapor	8.95*	9.8807*	49.9*	848.6*	0.780*
Heated 300˚C	9.00*	9.8259*	27.8*	500.2*	0.706*
Heated 550˚C	8.85*	9.9922*	22.7*	402.3*	1.130*
Ordovician Womble Formation					
ARM-7, coarse					
Air-dried	8.85	9.9922	4344.6	39109.5	0.363
Ethylene Glycol Vapor	8.90	9.9361	3978.2	38284.2	0.388
Heated 300˚C	8.95	9.8807	1723.4	13309.1	0.297
Heated 550˚C	9.40	9.4087	336.2	3167.6	0.371
ARM-7, fine					
Air-dried	8.85	9.9922	629.9	7379.7	0.491
Ethylene Glycol Vapor	8.90	9.9361	628.9	7660.3	0.498
Heated 300˚C	8.85	9.9922	600.2	6811.3	0.486
Heated 550˚C	8.90	9.9361	161.9	1860.0	0.528
ART-3, coarse					
Air-dried	8.95	9.8807	288.5	2026.2	0.273
Ethylene Glycol Vapor	8.95	9.8807	284.1	2171.5	0.303
Heated 300˚C	8.95	9.8807	86.6	580.7	0.234
Heated 550˚C	9.05	9.7718	34.3	317.2	0.515

Note: Samples without I_{001} data omitted.
*Broad peak measurement.
†N.D. = no data.
§Possible smectite interlayering, mainly with illite.

TABLE B7. ILLITE 001 PEAK VALUES AT AIR DRIED, ETHYLENE GLYCOL VAPOR SOLVATED, HEATED 300°C, AND HEATED 550°C

Sample, clay fraction	2Θ (degrees)	D-spacing (angstroms)	Peak max counts (counts/second)	Peak area (integrated counts)	FWHM (degrees)
Ordovician Blakely Formation					
ARM-6, coarse					
Air-dried	8.95	9.8807	478.2	3769.5	0.328
Ethylene Glycol Vapor	8.90	9.9361	459.1	3805.2	0.340
Heated 300°C	8.95	9.8807	459.8	3833.7	0.332
Heated 550°C	8.90	9.9361	252.8	2164.7	0.333
ARM-6, fine					
Air-dried	9.00	9.8259	1274.2	13740.7	0.417
Ethylene Glycol Vapor	9.05	9.7718	806.5	7860.0	0.398
Heated 300°C	9.05	9.7718	1230.5	14869.9	0.432
Heated 550°C	9.00	9.8259	1140.7	13494.3	0.443

Note: Samples without I_{001} data omitted.
*Broad peak measurement.
†N.D. – no data.
§Possible smectite interlayering, mainly with illite.

TABLE B8. CHLORITE 002 PEAK VALUES AT AIR DRIED, ETHYLENE GLYCOL VAPOR SOLVATED, HEATED 300°C, AND HEATED 550°C

Sample, clay fraction	2Θ (degrees)	D-spacing (angstroms)	Peak max counts (counts/second)	Peak area (integrated counts)	FWHM (degrees)	Sample, clay fraction	2Θ (degrees)	D-spacing (angstroms)	Peak max counts (counts/second)	Peak area (integrated counts)	FWHM (degrees)
Pennsylvanian Johns Valley Formation						Pennsylvanian Jackfork Formation					
ART-14, coarse						ART-15, fine					
Air-dried	12.65	6.9978	773.7	8828.4	0.413	Air-dried	11.90*	7.4371*	95.8*	3565.8*	1.570*
Ethylene Glycol Vapor	12.60	7.0255	793.9	8855.8	0.404	Ethylene Glycol Vapor	12.05*	7.3449*	91.7*	3042.0*	1.693*
Heated 300°C	12.55	7.0533	62.6	1005.4	0.598	Heated 300°C	11.95*	7.4061*	115.2*	3656.1*	1.369*
Heated 550°C	N.D.†	N.D.†	N.D.†	N.D.†	N.D.†	Heated 550°C	N.D.†	N.D.†	N.D.†	N.D.†	N.D.†
Pennsylvanian Jackfork Formation						Mississippian Stanley Formation					
ART-6, coarse§						ARM-1, coarse					
Air-dried	12.60	7.0255	2332.6	19790.4	0.337	Air-dried	12.60	7.0255	40	174.7	0.202
Ethylene Glycol Vapor	12.60	7.0255	2418.7	20459.0	0.336	Ethylene Glycol Vapor	12.60	7.0255	34.6	185.4	0.192
Heated 300°C	12.60	7.0255	1031.6	10743.0	0.420	Heated 300°C	12.65	6.9978	13.4?	83.9	0.226
Heated 550°C	N.D.†	N.D.†	N.D.†	N.D.†	N.D.†	Heated 550°C	N.D.†	N.D.†	N.D.†	N.D.†	N.D.†
ART-6, fine§						ARM-1, fine					
Air-dried	12.55	7.0533	405.7	3809.4	0.367	Air-dried	12.65	6.9978	307	3699.6	0.458
Ethylene Glycol Vapor	12.55	7.0533	361.7	3449.2	0.388	Ethylene Glycol Vapor	12.60	7.0255	294.8	3611.7	0.461
Heated 300°C	12.70	6.9704	163.1	1935.0	0.512	Heated 300°C	12.70	6.9704	150.2	2095.6	0.517
Heated 550°C	N.D.†	N.D.†	N.D.†	N.D.†	N.D.†	Heated 550°C	13.95*	6.3485*	50.8*	1160.3*	1.087*
ART-15, coarse						ARM-5, coarse					
Air-dried	11.85*	7.4684*	307.1*	11633.7*	1.788*	Air-dried	12.75	6.9432	125.2	1067.5	0.336
Ethylene Glycol Vapor	12.20*	7.2549*	286.4*	10970.5*	1.843*	Ethylene Glycol Vapor	12.85	6.8893	135.8	1193.0	0.383
Heated 300°C	12.10*	7.3146*	110.0*	3355.6*	1.161*	Heated 300°C	12.90	6.8628	104.1	983.0	0.394
Heated 550°C	N.D.†	N.D.†	N.D.†	N.D.†	N.D.†	Heated 550°C	N.D.†	N.D.†	N.D.†	N.D.†	N.D.†

Note: Samples without C_{002} data omitted.
*Broad peak measurement.
†N.D. = no data.
§Possible smectite interlayering, mainly with illite.

TABLE B9. CHLORITE 002 PEAK VALUES AT AIR DRIED, ETHYLENE GLYCOL VAPOR SOLVATED, HEATED 300˚C, AND HEATED 550˚C

Sample, clay fraction	2Θ (degrees)	D-spacing (angstroms)	Peak max counts (counts/second)	Peak area (integrated counts)	FWHM (degrees)
Mississippian Stanley Formation					
ARM-5, fine					
Air-dried	12.65	6.9978	224.5	2009.6	0.330
Ethylene Glycol Vapor	12.60	7.0255	224.0	1894.9	0.316
Heated 300˚C	12.65	6.9978	134.6	1355.6	0.375
Heated 550˚C	13.45*	6.5833*	45.1*	918.6*	1.003*
ART-2, coarse					
Air-dried	12.10*	7.3146*	80.1*	3267.3*	1.780*
Ethylene Glycol Vapor	12.20*	7.2549*	84.7*	3273.4*	1.866*
Heated 300˚C	12.05*	7.3449*	59.7*	1913.6*	1.699*
Heated 550˚C	N.D.†	N.D.†	N.D.†	N.D.†	N.D.†
ART-5, coarse					
Air-dried	12.20*	7.2549*	225.3*	5377.6*	0.880*
Ethylene Glycol Vapor	12.25*	7.2254*	235.4*	5518.1*	0.864*
Heated 300˚C	12.25*	7.2254*	79.6*	1828.6*	0.889*
Heated 550˚C	N.D.†	N.D.†	N.D.†	N.D.†	N.D.†
ART-5, fine					
Air-dried	12.35*	7.1671*	66.1*	1834.0*	1.152*
Ethylene Glycol Vapor	12.40*	7.1383*	76.4*	1933.6*	1.027*
Heated 300˚C	12.35*	7.1671*	47.1*	994.7*	0.778*
Heated 550˚C	N.D.†	N.D.†	N.D.†	N.D.†	N.D.†
Mississippian Stanley Formation					
ART-18, coarse					
Air-dried	12.20*	7.2549*	117.3*	3758.0*	1.526*
Ethylene Glycol Vapor	12.15*	7.2846*	119.4*	4167.8*	1.536*
Heated 300˚C	N.D.†	N.D.†	N.D.†	N.D.†	N.D.†
Heated 550˚C	N.D.†	N.D.†	N.D.†	N.D.†	N.D.†
ART-18, fine					
Air-dried	12.05*	7.3449*	52.4*	1551.3*	1.389*
Ethylene Glycol Vapor	12.30*	7.1961*	51.5*	1674.4*	1.269*
Heated 300˚C	12.50*	7.0814*	21.9*	347.5*	0.427*
Heated 550˚C	N.D.†	N.D.†	N.D.†	N.D.†	N.D.†
Silurian-Ordovician, Undivided					
ARM-8, fine					
Air-dried	13.80*	6.4171*	68.1*	1686.8*	1.402*
Ethylene Glycol Vapor	13.80*	6.4171*	54.7*	1168.1*	1.043*
Heated 300˚C	13.90*	6.3712*	71.9*	1512.5*	1.227*
Heated 550˚C	13.60*	6.5111*	103.3*	2750.5*	1.322*
ART-19, coarse					
Air-dried	12.00*	7.3754*	47.9*	945.2*	0.825*
Ethylene Glycol Vapor	12.25*	7.2257*	48.7*	1072.6*	1.128*
Heated 300˚C	N.D.†	N.D.†	N.D.†	N.D.†	N.D.†
Heated 550˚C	N.D.†	N.D.†	N.D.†	N.D.†	N.D.†

Note: Samples without C_{002} data omitted.
*Broad peak measurement.
†N.D. = no data.
§Possible smectite interlayering, mainly with illite.

TABLE B10. CHLORITE 002 PEAK VALUES AT AIR DRIED, ETHYLENE GLYCOL VAPOR SOLVATED, HEATED 300°C, AND HEATED 550°C

Sample, clay fraction	2Θ (degrees)	D-spacing (angstroms)	Peak max counts (counts/second)	Peak area (integrated counts)	FWHM (degrees)
Silurian-Ordovician, Undivided					
ART-19,fine					
Air-dried	N.D.†	N.D.†	N.D.†	N.D.†	N.D.†
Ethylene Glycol Vapor	N.D.†	N.D.†	N.D.†	N.D.†	N.D.†
Heated 300°C	12.40*	7.1383*	34.2*	572.6*	0.882*
Heated 550°C	N.D.†	N.D.†	N.D.†	N.D.†	N.D.†
Ordovician Bigfork Formation					
ART-12, coarse					
Air-dried	12.60	7.0255	74.4	623.8	0.318
Ethylene Glycol Vapor	12.60	7.0255	77.1	624.9	0.288
Heated 300°C	12.5*	7.0814*	46.6*	418.9*	0.451*
Heated 550°C	N.D.†	N.D.†	N.D.†	N.D.†	N.D.†
ART-12, fine					
Air-dried	12.25*	7.2254*	77.4*	2179.4*	1.466*
Ethylene Glycol Vapor	12.15*	7.2846*	59.4*	1914.4*	1.735*
Heated 300°C	12.40*	7.1383*	43.0*	1249.2*	1.377*
Heated 550°C	N.D.†	N.D.†	N.D.†	N.D.†	N.D.†
Ordovician Womble Formation					
ARM-7, coarse					
Air-dried	12.55	7.0533	181.1	1553.0	0.302
Ethylene Glycol Vapor	12.60	7.0255	164.0	1517.2	0.318
Heated 300°C	12.60	7.0255	92.8	622.5	0.254
Heated 550°C	N.D.†	N.D.†	N.D.†	N.D.†	N.D.†
Ordovician Womble Formation					
ARM-7, fine					
Air-dried	12.60	7.0255	31.8	227.1	0.259
Ethylene Glycol Vapor	12.55	7.0533	33.3	216.1	0.228
Heated 300°C	12.60	7.0255	18.5	128.5	0.212
Heated 550°C	N.D.†	N.D.†	N.D.†	N.D.†	N.D.†
ART-3, coarse					
Air-dried	12.3*	7.1961*	137.8*	3334.4*	0.888*
Ethylene Glycol Vapor	12.3*	7.1961*	149.2*	3765.3*	0.852*
Heated 300°C	12.35*	7.1671*	85.3*	1521.7*	0.553*
Heated 550°C	N.D.†	N.D.†	N.D.†	N.D.†	N.D.†
Ordovician Blakely Formation					
ARM-6, coarse					
Air-dried	12.55	7.0533	66.8	491.1	0.327
Ethylene Glycol Vapor	12.55	7.0533	65.4	587.5	0.355
Heated 300°C	12.50	7.0814	55.0	549.0	0.504
Heated 550°C	N.D.†	N.D.†	N.D.†	N.D.†	N.D.†
ARM-6, fine					
Air-dried	12.65	6.9978	57.4	512.6	0.377
Ethylene Glycol Vapor	12.70	6.9704	38.2	290.6	0.421
Heated 300°C	12.65	6.9978	31.5	213.7	0.319
Heated 550°C	13.85*	6.3941*	74.5*	1593.9*	1.094*

Note: Samples without C_{002} data omitted.
*Broad peak measurement.
†N.D. = no data.
§Possible smectite interlayering, mainly with illite.

TABLE B11. ILLITE 002 PEAK VALUES AT AIR DRIED, ETHYLENE GLYCOL VAPOR SOLVATED, HEATED 300˚C, AND HEATED 550˚C

Sample, clay fraction	2Θ (degrees)	D-spacing (angstroms)	Peak max counts (counts/second)	Peak area (integrated counts)	FWHM (degrees)	Sample, clay fraction	2Θ (degrees)	D-spacing (angstroms)	Peak max counts (counts/second)	Peak area (integrated counts)	FWHM (degrees)
Pennsylvanian Johns Valley Formation						Pennsylvanian Jackfork Formation					
ART-14, fine						ART-15, fine					
Air-dried	N.D.†	N.D.†	N.D.†	N.D.†	N.D.†	Air-dried	N.D.†	N.D.†	N.D.†	N.D.†	N.D.†
Ethylene Glycol Vapor	18.06*	4.9109*	19.6*	153.5*	0.458*	Ethylene Glycol Vapor	17.90	4.9555	62.9	911.3	0.637
Heated 300˚C	N.D.†	N.D.†	N.D.†	N.D.†	N.D.†	Heated 300˚C	17.90*	4.9555*	51.5*	912.4*	1.105*
Heated 550˚C	N.D.†	N.D.†	N.D.†	N.D.†	N.D.†	Heated 550˚C	17.50*	5.0678*	68.3*	1194.0*	0.904*
Pennsylvanian Jackfork Formation						Mississippian Stanley Formation					
ART-6, coarse§						ARM-1, coarse					
Air-dried	17.85	4.9692	72.7	707.2	0.505	Air-dried	18.10*	4.9012*	32.7*	767.0*	1.099*
Ethylene Glycol Vapor	17.95*	4.9431*	89.5*	1154.2*	0.894*	Ethylene Glycol Vapor	18.05*	4.9146*	34.5*	721.2*	1.133*
Heated 300˚C	17.85	4.9692	103.5	1513.9	0.727	Heated 300˚C	18.08	4.9079	52.4	633.8	0.55
Heated 550˚C	18.35*	4.835*	94*	1913.6*	1.094*	Heated 550˚C	17.85*	4.9692*	50.0*	1203.9*	1.484*
ART-6, fine§						ARM-1, fine					
Air-dried	N.D.†	N.D.†	N.D.†	N.D.†	N.D.†	Air-dried	17.75	4.9970	366.1	5656.5	0.641
Ethylene Glycol Vapor	18.70*	4.7452*	207.2*	4298.0*	0.780*	Ethylene Glycol Vapor	17.80	4.9831	422.3	5940.3	0.589
Heated 300˚C	N.D.†	N.D.†	N.D.†	N.D.†	N.D.†	Heated 300˚C	17.85	4.9692	445.8	6027.6	0.519
Heated 550˚C	18.60*	4.7705*	81.0*	3447.6*	0.769*	Heated 550˚C	17.80	4.9831	468.1	6207.8	0.528
ART-15, coarse						ARM-5, coarse					
Air-dried	17.90*	4.9555*	45.3*	585.8*	0.632*	Air-dried	17.95	4.9418	174.7	2290.6	0.521
Ethylene Glycol Vapor	17.95*	4.9418*	43.8*	659.4*	0.712*	Ethylene Glycol Vapor	18.00	4.9282	192.5	2390.1	0.494
Heated 300˚C	17.97	4.9365	28.4	401.3	0.681	Heated 300˚C	18.05	4.9146	176.1	2480.5	0.491
Heated 550˚C	17.80*	4.9822*	41.6*	739.0*	0.675*	Heated 550˚C	18.05	4.9146	145.2	2098.7	0.53

Note: Samples without I_{002} data omitted.
*Broad peak measurement.
†N.D. = no data.
§Possible smectite interlayering, mainly with illite.

TABLE B12. ILLITE 002 PEAK VALUES AT AIR DRIED, ETHYLENE GLYCOL VAPOR SOLVATED, HEATED 300˚C, AND HEATED 550˚C

Sample, clay fraction	2Θ (degrees)	D-spacing (angstroms)	Peak max counts (counts/second)	Peak area (integrated counts)	FWHM (degrees)
Mississippian Stanley Formation					
ARM-5, fine					
Air-dried	17.85	4.9692	370.0	4787.7	0.536
Ethylene Glycol Vapor	17.80	4.9831	385.8	4907.8	0.522
Heated 300˚C	17.85	4.9692	434.3	4949.4	0.470
Heated 550˚C	17.70	5.0110	472.6	5415.7	0.457
ART-2, coarse					
Air-dried	17.80	4.9831	155.5	1271.9	0.391
Ethylene Glycol Vapor	17.85	4.9692	148.2	1299.4	0.344
Heated 300˚C	17.85	4.9692	110.4	1105.3	0.322
Heated 550˚C	17.70	5.0110	115.6	1179.2	0.350
ART-2, fine					
Air-dried	N.D.†	N.D.†	N.D.†	N.D.†	N.D.†
Ethylene Glycol Vapor	17.78*	4.9900*	71.2*	1124.3*	.884*
Heated 300˚C	17.75	4.9970	73.4	962.9	0.750
Heated 550˚C	17.75	4.9970	120.6	1271.6	0.443
ART-5, coarse					
Air-dried	17.85	4.9692	234.5	1734.8	0.303
Ethylene Glycol Vapor	17.85	4.9692	240.8	1734.2	0.278
Heated 300˚C	N.D.†	N.D.†	N.D.†	N.D.†	N.D.†
Heated 550˚C	17.71	5.0092	129.7	1827.8	0.468
Mississippian Stanley Formation					
ART-5, fine					
Air-dried	17.90	4.9555	39.0	349.4	0.389
Ethylene Glycol Vapor	17.95	4.9418	35.3	356.8	0.402
Heated 300˚C	17.85	4.9692	56.8	621.5	0.388
Heated 550˚C	17.77*	4.9912*	49.3*	1381.6*	0.869*
ART-18, coarse					
Air-dried	17.85	4.9692	47.3	399.7	0.414
Ethylene Glycol Vapor	17.90	4.9555	60.3	456.8	0.485
Heated 300˚C	N.D.†	N.D.†	N.D.†	N.D.†	N.D.†
Heated 550˚C	N.D.†	N.D.†	N.D.†	N.D.†	N.D.†
ART-18, fine					
Air-dried	18.00	4.9282	27.0	418.8	0.702
Ethylene Glycol Vapor	18.10	4.9012	20.1	301.1	0.769
Heated 300˚C	N.D.†	N.D.†	N.D.†	N.D.†	N.D.†
Heated 550˚C	17.75*	4.996*	20.2*	213.6*	0.240*
Silurian-Ordovician, Undivided					
ARM-8, fine					
Air-dried	17.90	4.9555	687.9	13324.2	0.762
Ethylene Glycol Vapor	17.90	4.9555	711.9	12466.7	0.709
Heated 300˚C	17.95	4.9418	784.4	13325.8	0.654
Heated 550˚C	17.80	4.9831	1057.8	17501.7	0.636

Note: Samples without I_{002} data omitted.
*Broad peak measurement.
†N.D. = no data.
‡Possible smectite interlayering, mainly with illite.

TABLE B13. ILLITE 002 PEAK VALUES AT AIR DRIED, ETHYLENE GLYCOL VAPOR SOLVATED, HEATED 300˚C, AND HEATED 550˚C

Sample, clay fraction	2Θ (degrees)	D-spacing (angstroms)	Peak max counts (counts/second)	Peak area (integrated counts)	FWHM (degrees)
Silurian-Ordovician, Undivided					
ART-19, coarse					
Air-dried	17.80	4.9831	261.5	2265.8	0.383
Ethylene Glycol Vapor	17.80	4.9831	285.4	2313.1	0.343
Heated 300˚C	17.90*	4.9555*	60.9*	1875.6*	1.238*
Heated 550˚C	17.79*	4.9856*	61.4*	1459.2*	0.911
ART-19,fine					
Air-dried	17.85	4.9692	115.4	1272.2	0.502
Ethylene Glycol Vapor	17.80	4.9831	120.1	1353.7	0.530
Heated 300˚C	17.80	4.9831	257.5	3617.7	0.575
Heated 550˚C	17.80	4.9831	241.6	3494.7	0.554
Ordovician Bigfork Formation					
ART-12, coarse					
Air-dried	17.90	4.9555	38.6	267.8	0.321
Ethylene Glycol Vapor	17.90	4.9555	43.4	308.7	0.296
Heated 300˚C	17.95	4.9418	32.2	309.6	0.464
Heated 550˚C	17.70	5.0110	40.0	515.9	0.199
ART-12, fine					
Air-dried	17.95*	4.9418*	37.1*	543.1*	0.763*
Ethylene Glycol Vapor	17.90*	4.9555*	33.9*	716.6*	0.906*
Heated 300˚C	N.D.†	N.D.†	N.D.†	N.D.†	N.D.†
Heated 550˚C	N.D.†	N.D.†	N.D.†	N.D.†	N.D.†
Ordovician Womble Formation					
ARM-7, coarse					
Air-dried	17.80	4.9831	2626.8	25643.4	0.375
Ethylene Glycol Vapor	17.75	4.9970	2762.6	25505.6	0.347
Heated 300˚C	17.85	4.9692	1422.6	11894.0	0.313
Heated 550˚C	18.25	4.8612	738.4	6633.7	0.367
ARM-7, fine					
Air-dried	17.80	4.9831	365.8	4664.1	0.527
Ethylene Glycol Vapor	17.80	4.9831	416.4	4817.1	0.454
Heated 300˚C	17.75	4.9970	400.2	5325.0	0.472
Heated 550˚C	17.75	4.9970	322.4	4395.6	0.501
ART-3, coarse					
Air-dried	17.90	4.9555	154.4	973.1	0.280
Ethylene Glycol Vapor	17.90	4.9555	167.3	1095.4	0.281
Heated 300˚C	17.90	4.9555	64.7	717.6	0.349
Heated 550˚C	17.70*	5.0110*	61.3*	861.3*	0.576*
Ordovician Blakely Formation					
ARM-6, coarse					
Air-dried	17.90	4.9555	428.0	4051.1	0.357
Ethylene Glycol Vapor	17.90	4.9555	442.1	4045.6	0.349
Heated 300˚C	17.90	4.9555	445.3	3941.0	0.335
Heated 550˚C	17.75	7.9970	360.0	4042.4	0.378

Note: Samples without I_{002} data omitted.
*Broad peak measurement.
†N.D. = no data.
§Possible smectite interlayering, mainly with illite.

TABLE B14. ILLITE 002 PEAK VALUES AT AIR DRIED, ETHYLENE GLYCOL VAPOR SOLVATED, HEATED 300°C, AND HEATED 550°C

Sample, clay fraction	2Θ (degrees)	D-spacing (angstroms)	Peak max counts (counts/second)	Peak area (integrated counts)	FWHM (degrees)
Ordovician Blakely Formation					
ARM-6, fine					
Air-dried	17.95	4.9418	760.2	8199.5	0.440
Ethylene Glycol Vapor	18.00	4.9282	572.8	6427.3	0.413
Heated 300°C	18.00	4.9282	772.1	8616.5	0.425
Heated 550°C	17.80	4.9831	1038.4	11157.8	0.421

Note: Samples without I_{002} data omitted.
*Broad peak measurement.
†N.D. = no data.
§Possible smectite interlayering, mainly with illite.

Clay Diffractograms

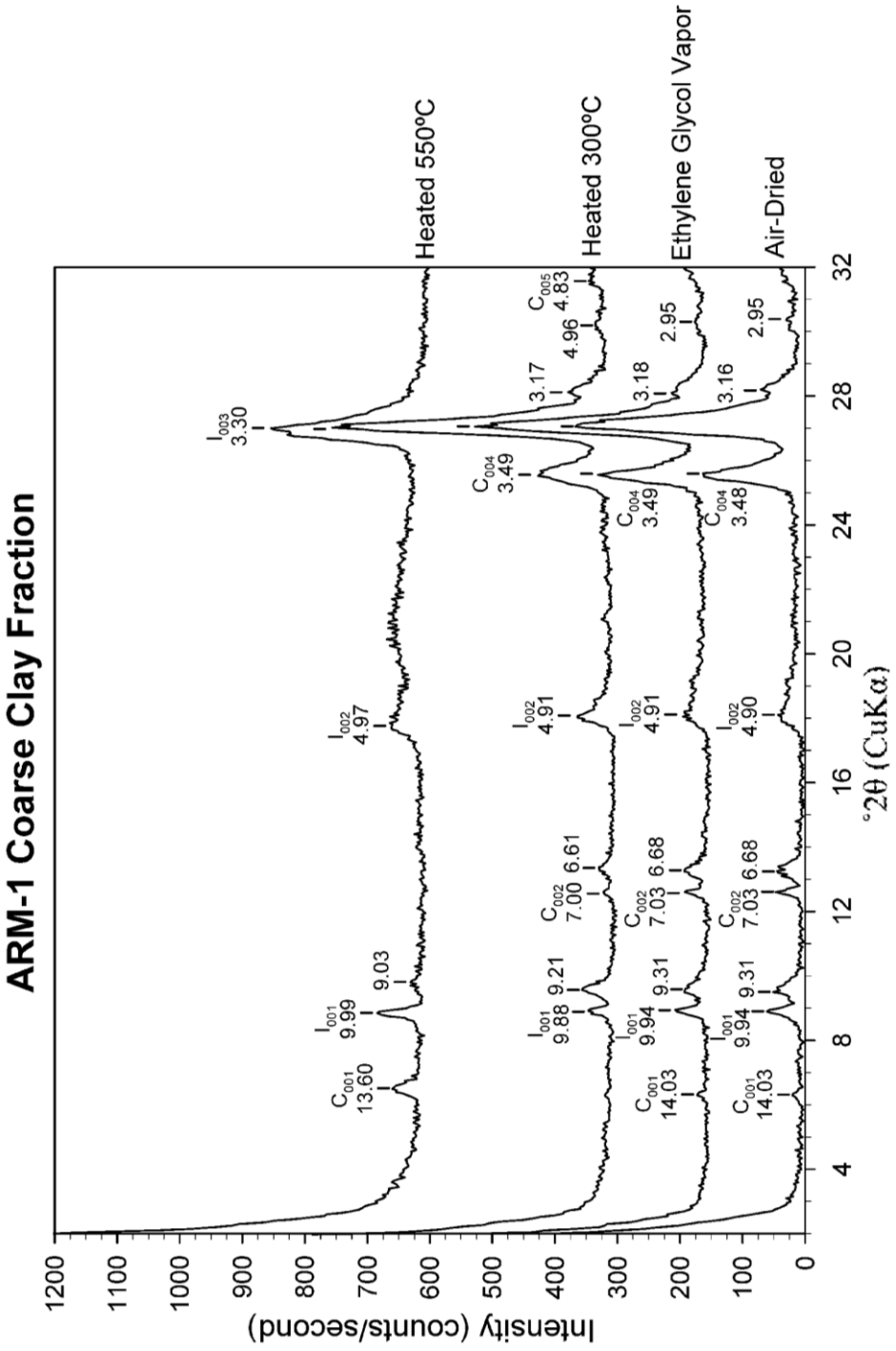

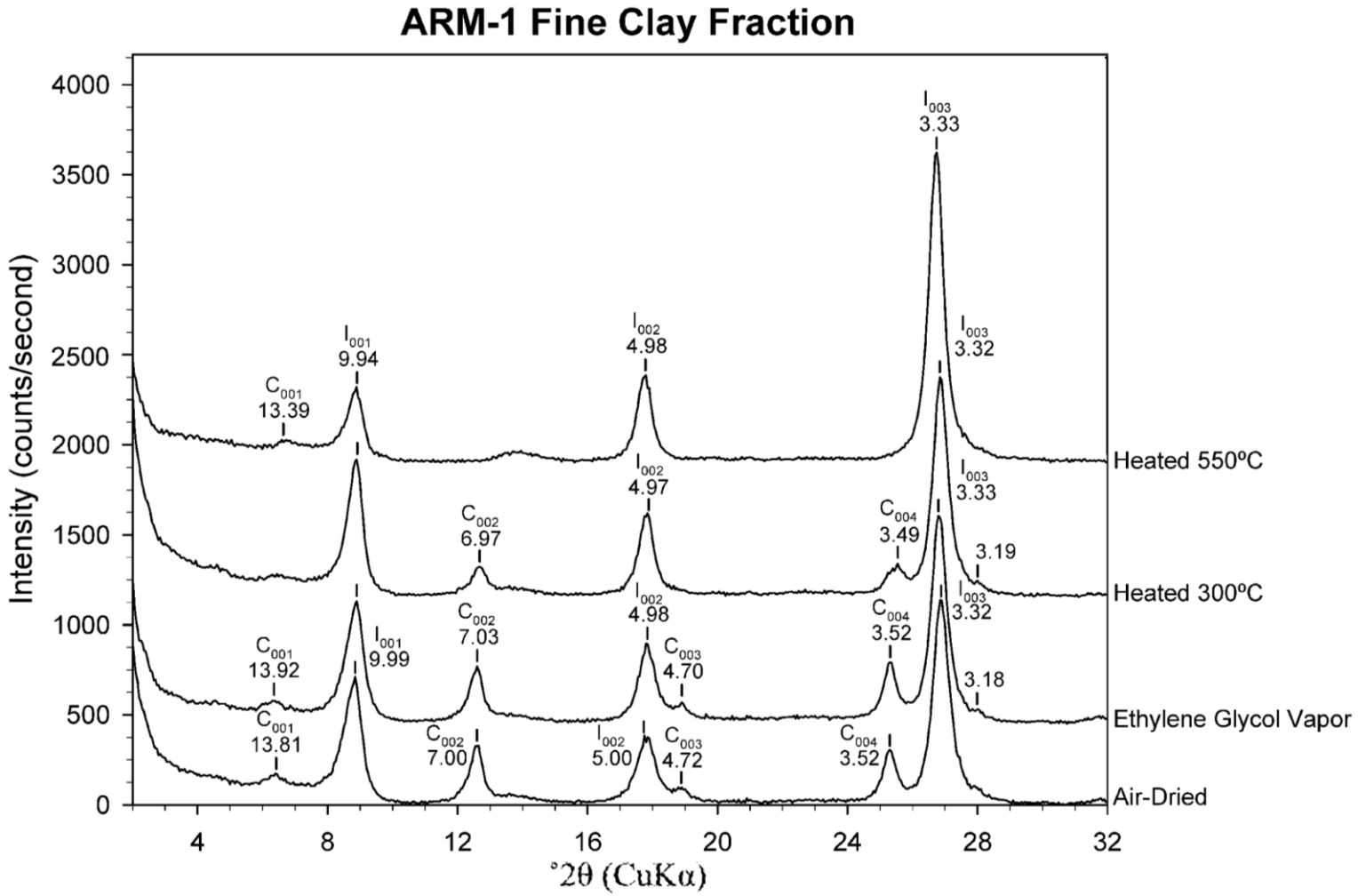
ARM-1 Fine Clay Fraction
Intensity (counts/second)
°2θ (CuKα)
Heated 550ºC
Heated 300ºC
Ethylene Glycol Vapor
Air-Dried
C001 13.39
I001 9.94
I002 4.98
I003 3.33
I003 3.32
C002 6.97
I002 4.97
C004 3.49
I003 3.33
3.19
C001 13.92
I001 9.99
C002 7.03
I002 4.98
C003 4.70
C004 3.52
I003 3.32
3.18
C001 13.81
C002 7.00
I002 5.00
C003 4.72
C004 3.52

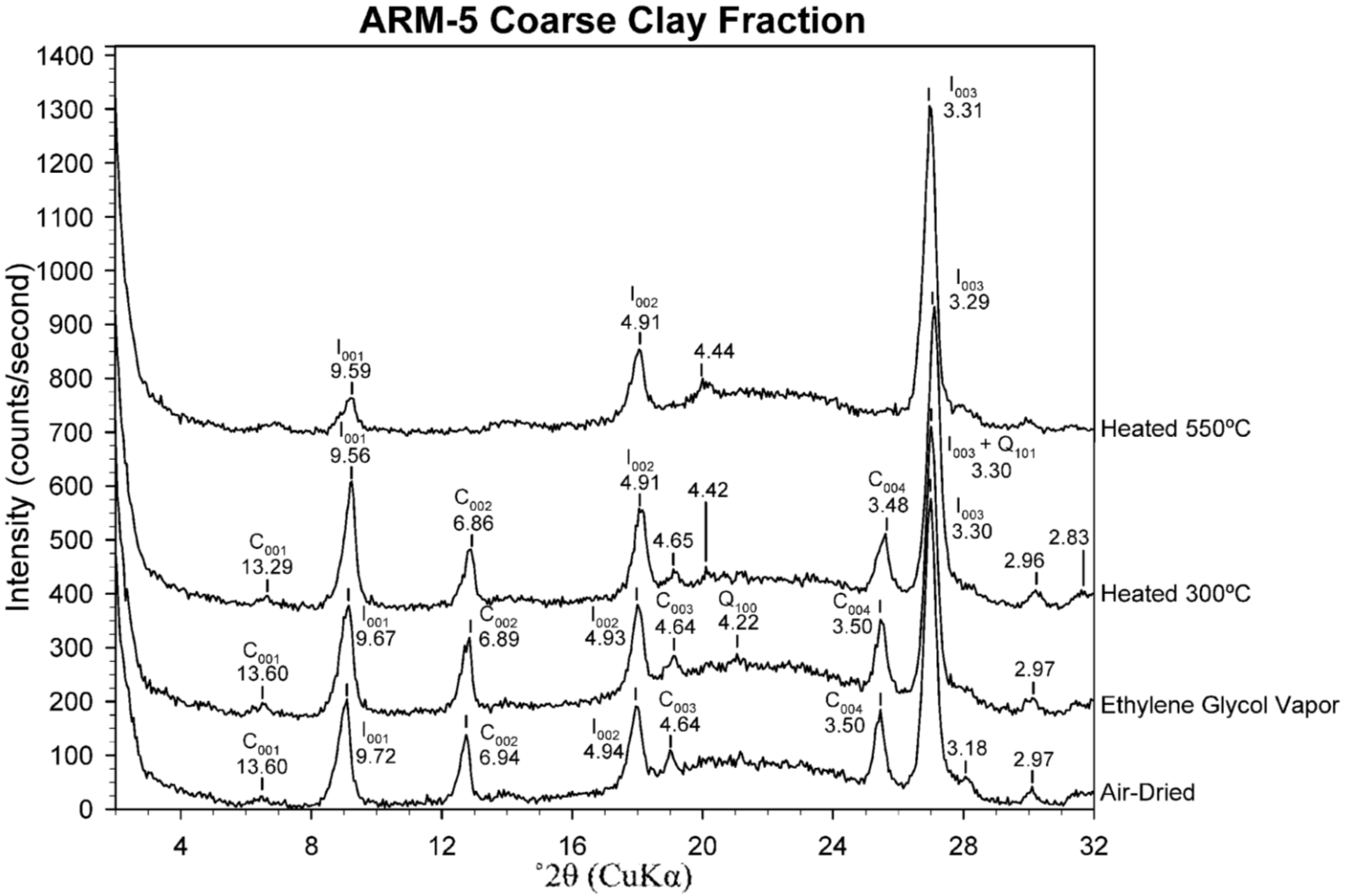
ARM-5 Coarse Clay Fraction
Intensity (counts/second)
°2θ (CuKα)
Heated 550ºC
Heated 300ºC
Ethylene Glycol Vapor
Air-Dried
I001 9.59
I001 9.56
I001 9.67
I001 9.72
I002 4.91
I002 4.91
I002 4.93
I002 4.94
4.44
4.42
4.65
C001 13.29
C001 13.60
C001 13.60
C002 6.86
C002 6.89
C002 6.94
C003 4.64
C003 4.64
Q100 4.22
C004 3.48
C004 3.50
C004 3.50
I003 3.31
I003 3.29
I003 3.30
I003 + Q101 3.30
3.18
2.97
2.96
2.97
2.83

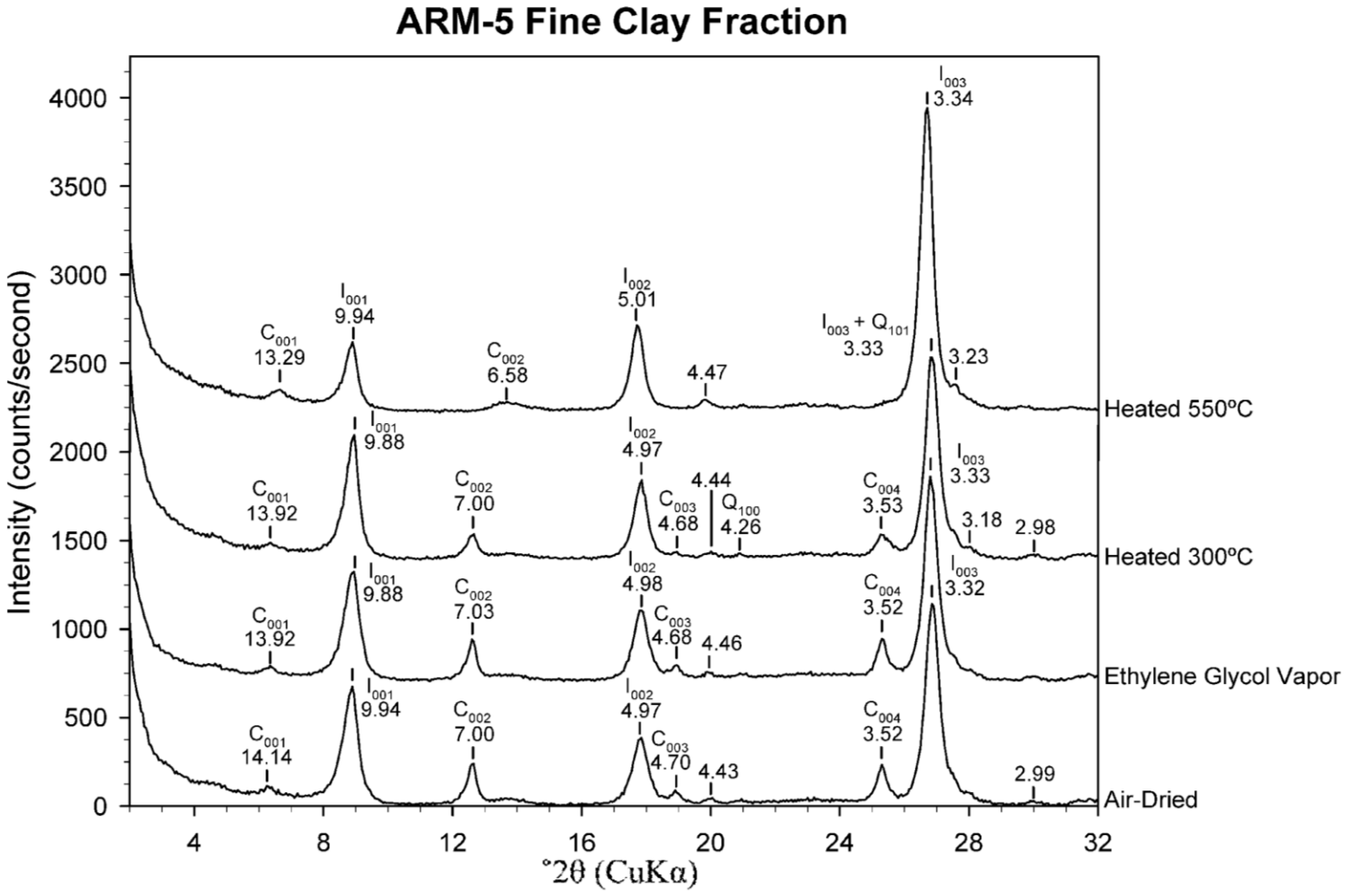
ARM-5 Fine Clay Fraction
Intensity (counts/second)
°2θ (CuKα)
Heated 550ºC
Heated 300ºC
Ethylene Glycol Vapor
Air-Dried
I003 3.34
I001 9.94
I002 5.01
C001 13.29
C002 6.58
4.47
I003 + Q101 3.33
3.23
I001 9.88
I002 4.97
I003 3.33
C001 13.92
C002 7.00
4.44
C003 4.68
Q100 4.26
C004 3.53
3.18
2.98
I001 9.88
I002 4.98
I003 3.32
C001 13.92
C002 7.03
C003 4.68
4.46
C004 3.52
I001 9.94
I002 4.97
C001 14.14
C002 7.00
C003 4.70
4.43
C004 3.52
2.99

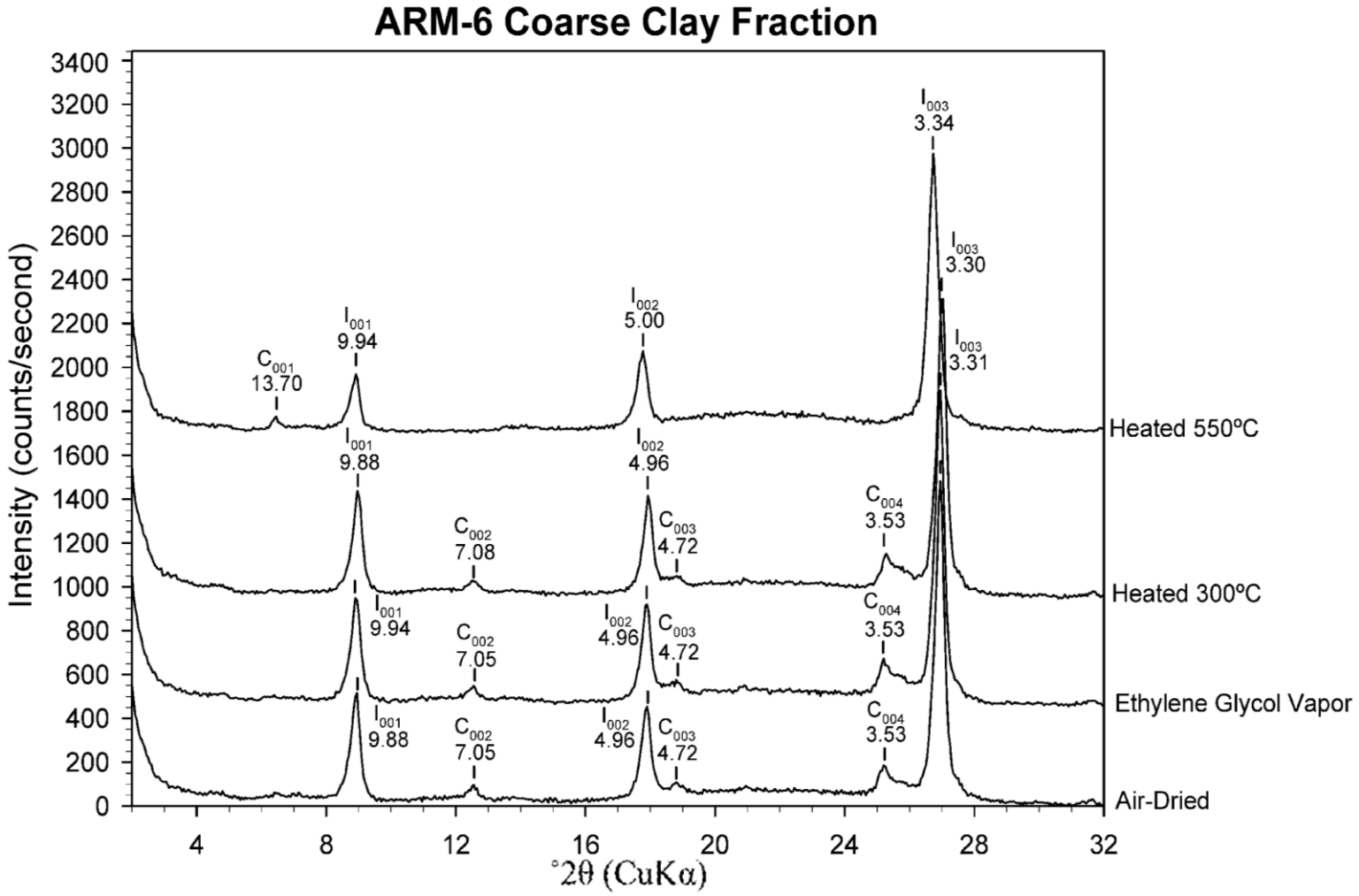
ARM-6 Coarse Clay Fraction
Intensity (counts/second)
°2θ (CuKα)
Heated 550ºC
Heated 300ºC
Ethylene Glycol Vapor
Air-Dried
C001 13.70
I001 9.94
I002 5.00
I003 3.34
I003 3.30
I003 3.31
I001 9.88
I002 4.96
C002 7.08
C003 4.72
C004 3.53
I001 9.94
C002 7.05
I002 4.96
C003 4.72
C004 3.53
I001 9.88
C002 7.05
I002 4.96
C003 4.72
C004 3.53

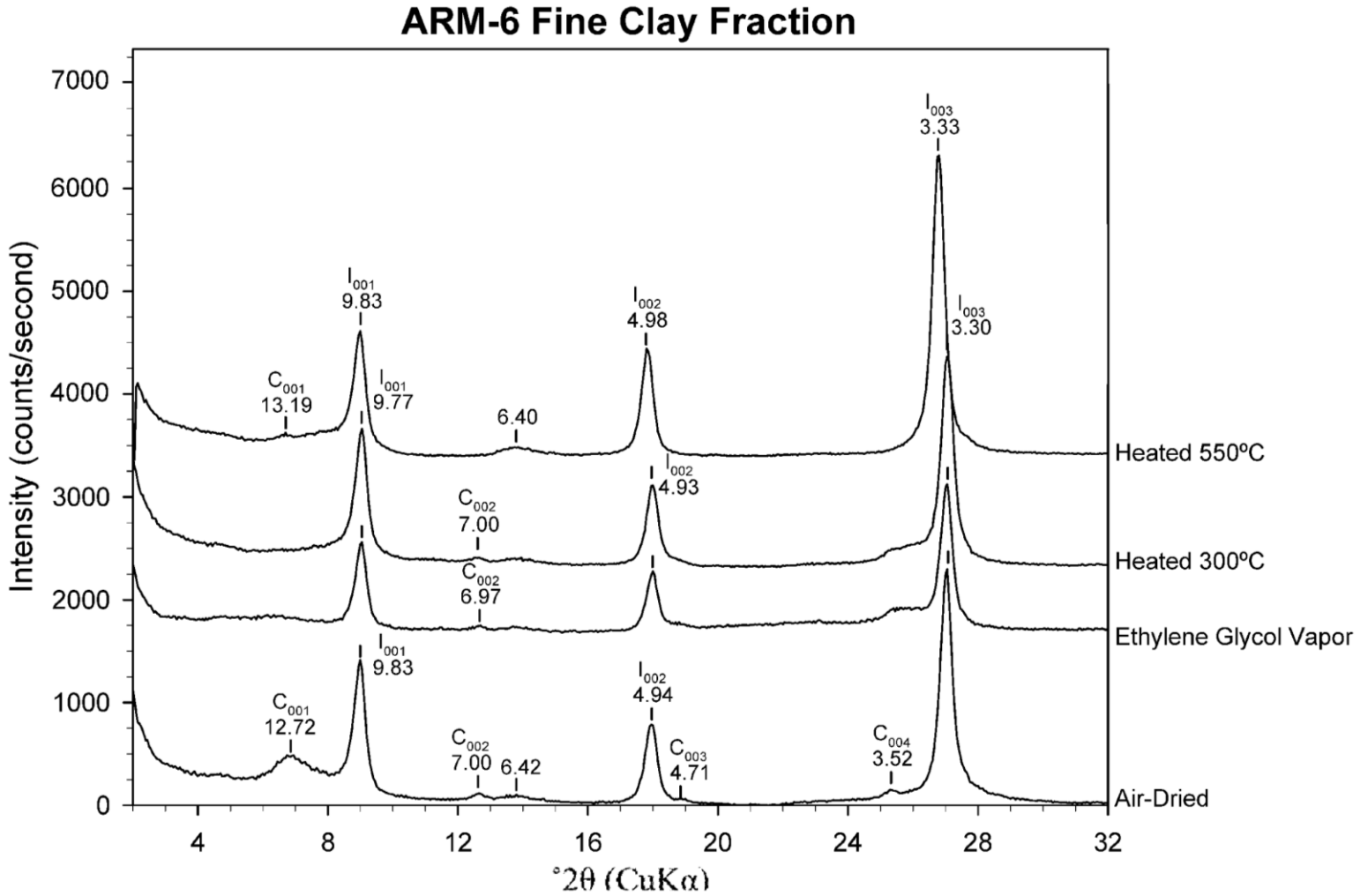
ARM-6 Fine Clay Fraction
Intensity (counts/second)
°2θ (CuKα)
Heated 550ºC
Heated 300ºC
Ethylene Glycol Vapor
Air-Dried
I003 3.33
I001 9.83
I002 4.98
I003 3.30
C001 13.19
I001 9.77
6.40
I002 4.93
C002 7.00
C002 6.97
I001 9.83
I002 4.94
C001 12.72
C002 7.00
6.42
C003 4.71
C004 3.52

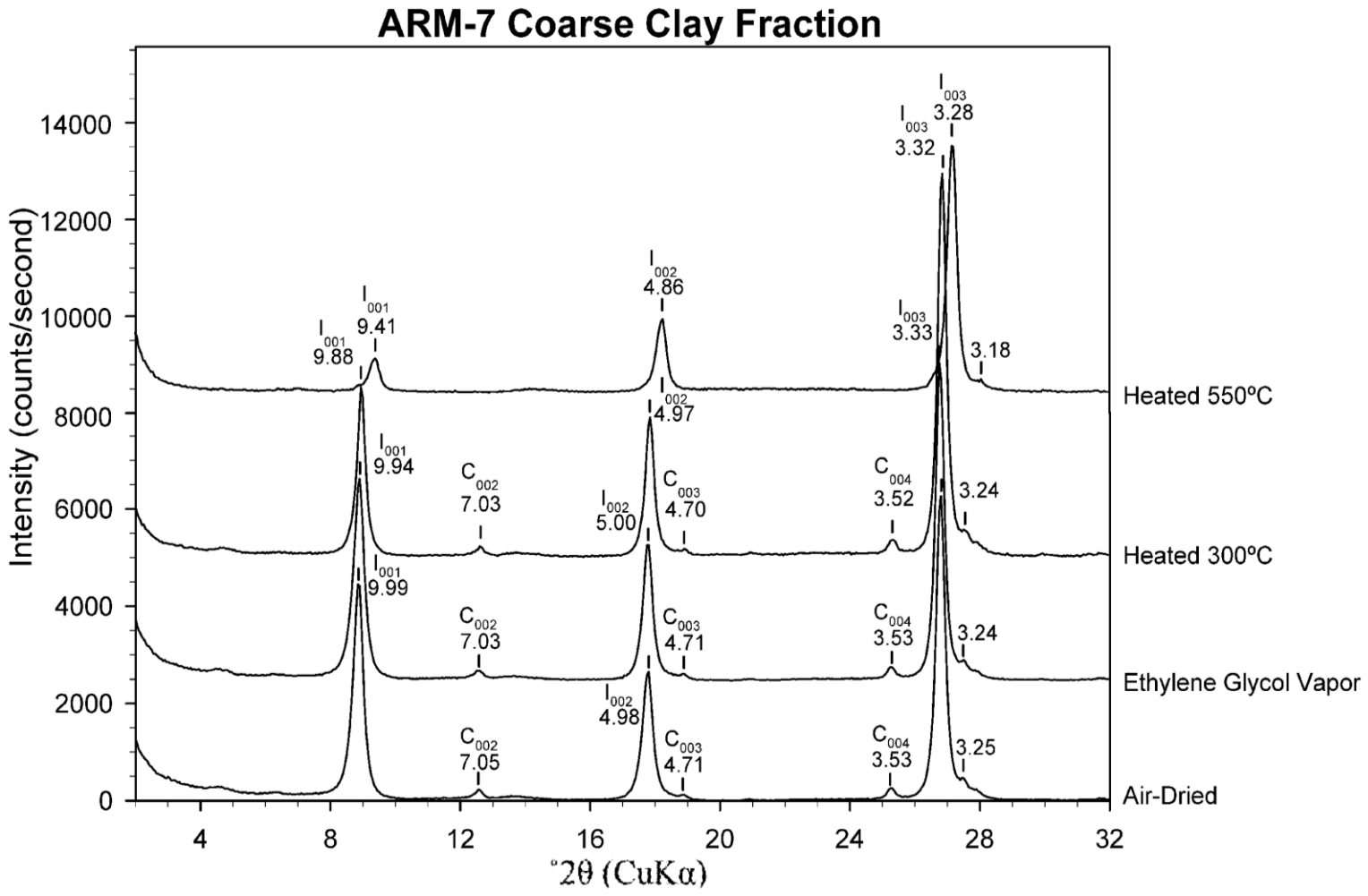
ARM-7 Coarse Clay Fraction
Intensity (counts/second)
°2θ (CuKα)
Heated 550ºC
Heated 300ºC
Ethylene Glycol Vapor
Air-Dried
I001 9.88
I001 9.41
I002 4.86
I003 3.32
I003 3.28
I003 3.33
3.18
I001 9.94
C002 7.03
I002 5.00
I002 4.97
C003 4.70
C004 3.52
3.24
I001 9.99
C002 7.03
C003 4.71
C004 3.53
3.24
I002 4.98
C002 7.05
C003 4.71
C004 3.53
3.25

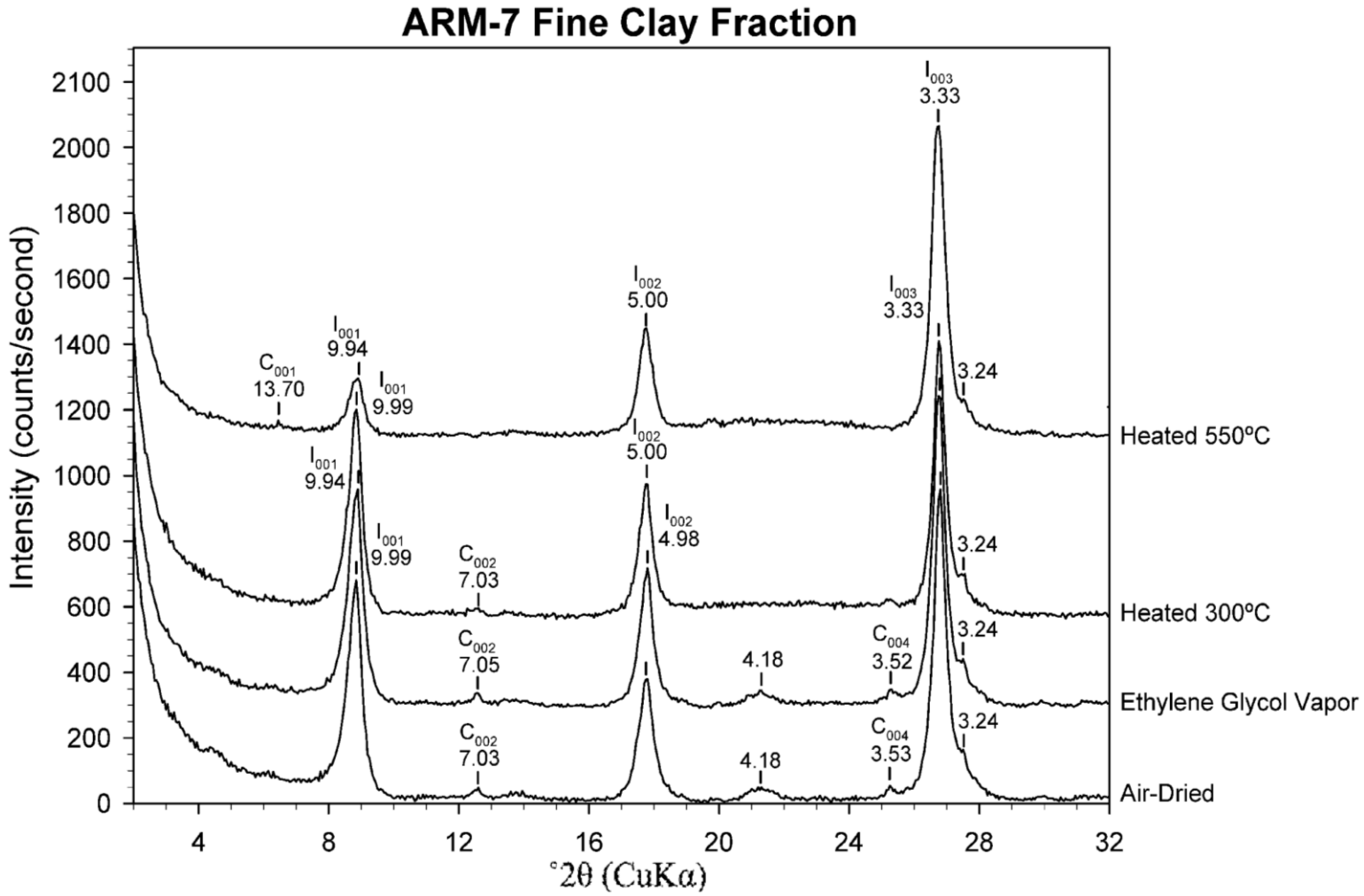
ARM-7 Fine Clay Fraction
Intensity (counts/second)
°2θ (CuKα)
Heated 550ºC
Heated 300ºC
Ethylene Glycol Vapor
Air-Dried
C001 13.70
I001 9.94
I001 9.99
I002 5.00
I003 3.33
3.24
I001 9.94
I001 9.99
C002 7.03
I002 5.00
I002 4.98
3.24
C002 7.05
4.18
C004 3.52
3.24
C002 7.03
4.18
C004 3.53
3.24

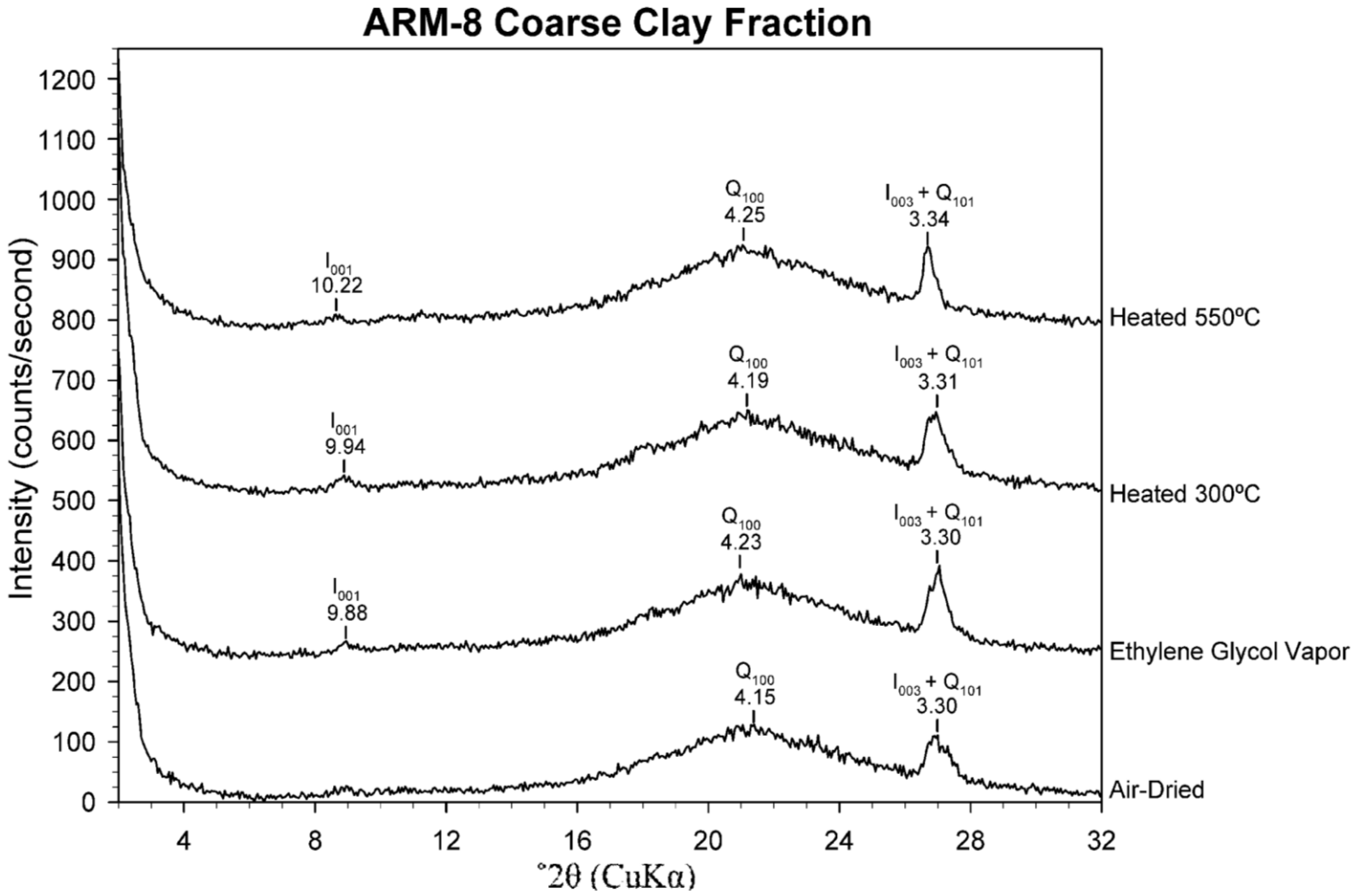
ARM-8 Coarse Clay Fraction
Intensity (counts/second)
°2θ (CuKα)
I001 10.22
Q100 4.25
I003 + Q101 3.34
Heated 550ºC
I001 9.94
Q100 4.19
I003 + Q101 3.31
Heated 300ºC
I001 9.88
Q100 4.23
I003 + Q101 3.30
Ethylene Glycol Vapor
Q100 4.15
I003 + Q101 3.30
Air-Dried

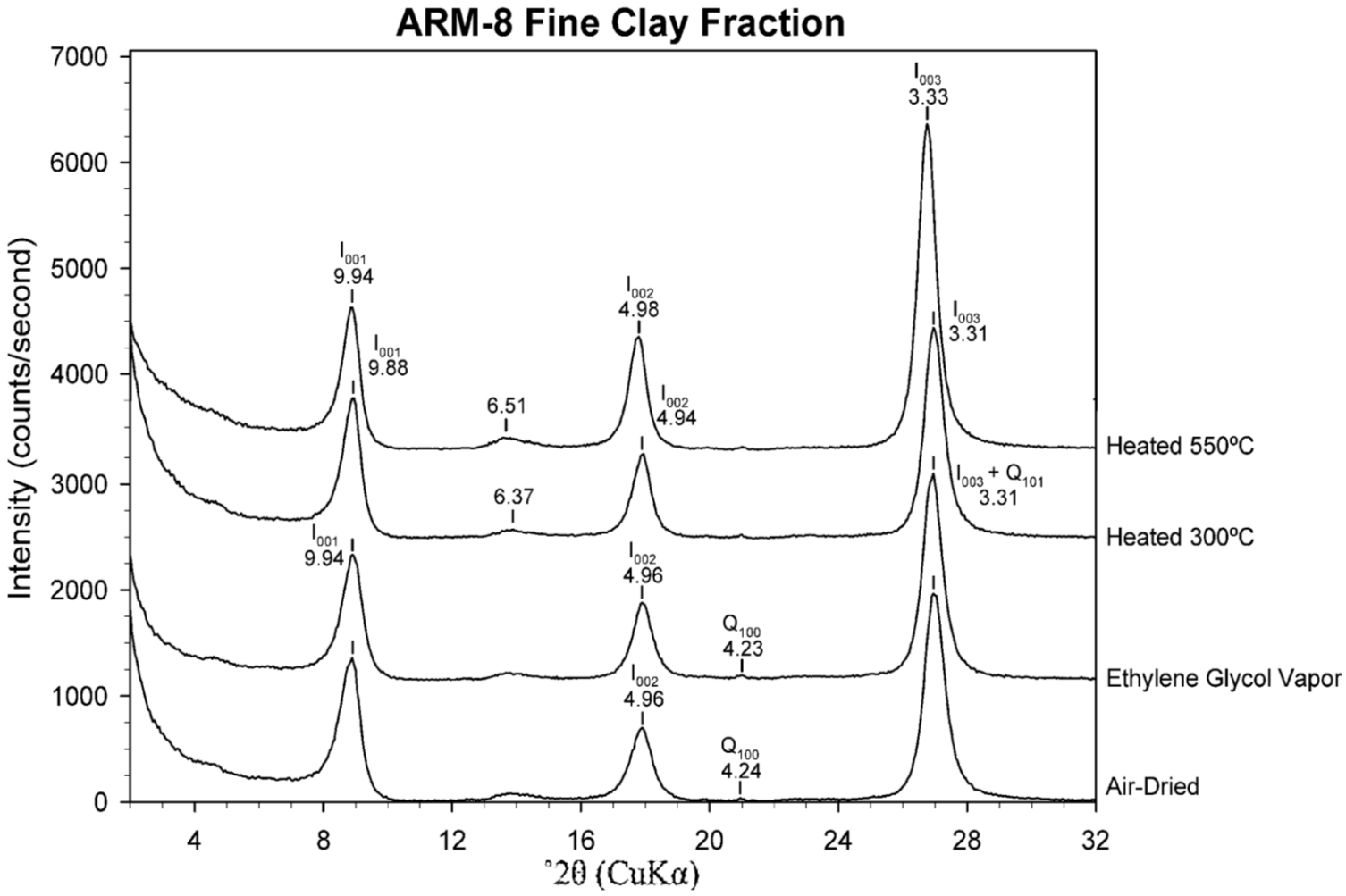
ARM-8 Fine Clay Fraction
Intensity (counts/second)
°2θ (CuKα)
I001 9.94
I001 9.88
6.51
I002 4.98
I002 4.94
I003 3.33
I003 3.31
Heated 550ºC
6.37
I003 + Q101 3.31
Heated 300ºC
I001 9.94
I002 4.96
Q100 4.23
Ethylene Glycol Vapor
I002 4.96
Q100 4.24
Air-Dried

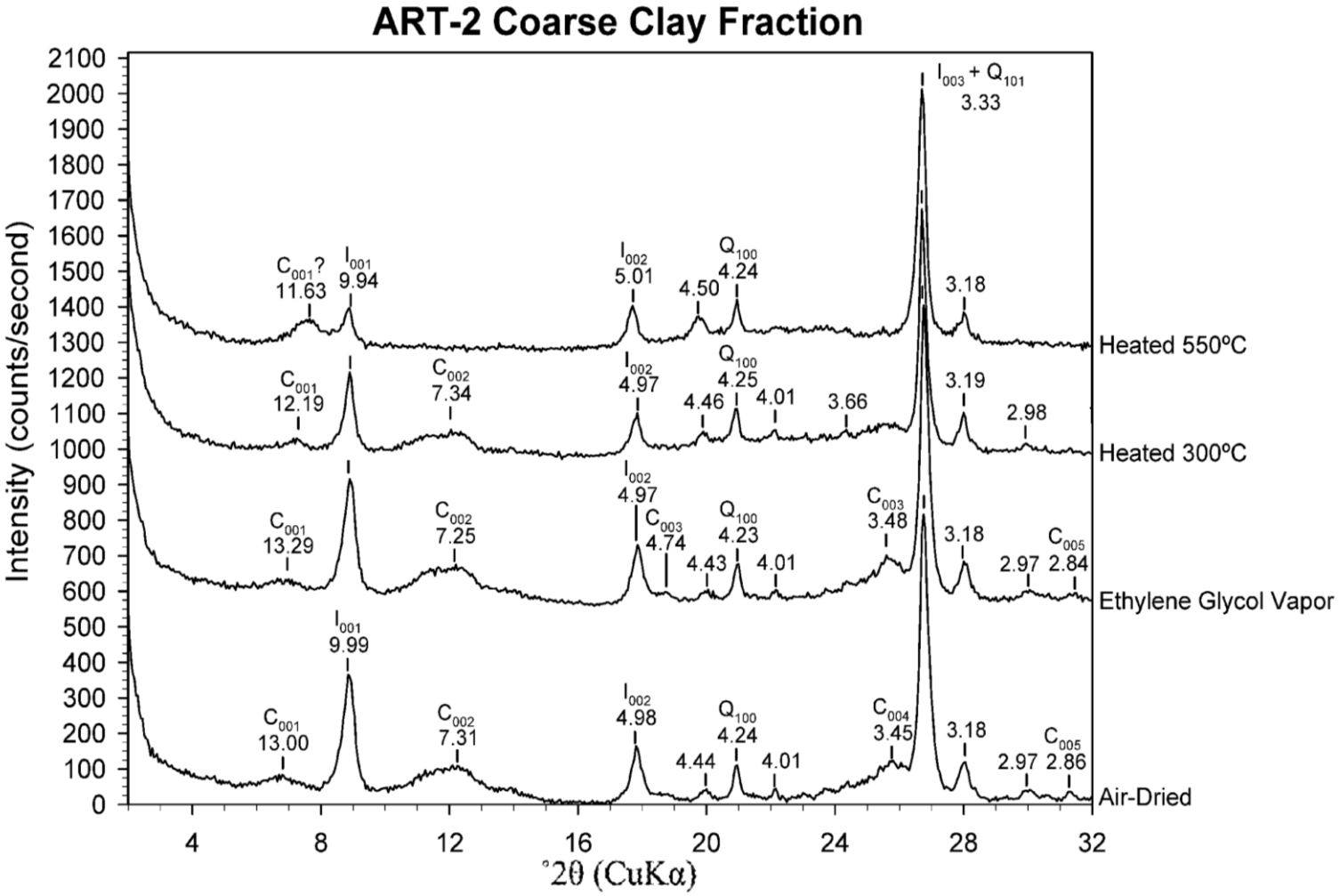
ART-2 Coarse Clay Fraction
Intensity (counts/second)
°2θ (CuKα)
Heated 550ºC
Heated 300ºC
Ethylene Glycol Vapor
Air-Dried
C001? 11.63
I001 9.94
I002 5.01
4.50
Q100 4.24
I003 + Q101 3.33
3.18
C001 12.19
C002 7.34
I002 4.97
4.46
Q100 4.25
4.01
3.66
3.19
2.98
C001 13.29
C002 7.25
I002 4.97
C003 4.74
4.43
Q100 4.23
4.01
C003 3.48
3.18
C005 2.97 2.84
I001 9.99
C001 13.00
C002 7.31
I002 4.98
4.44
Q100 4.24
4.01
C004 3.45
3.18
C005 2.97 2.86

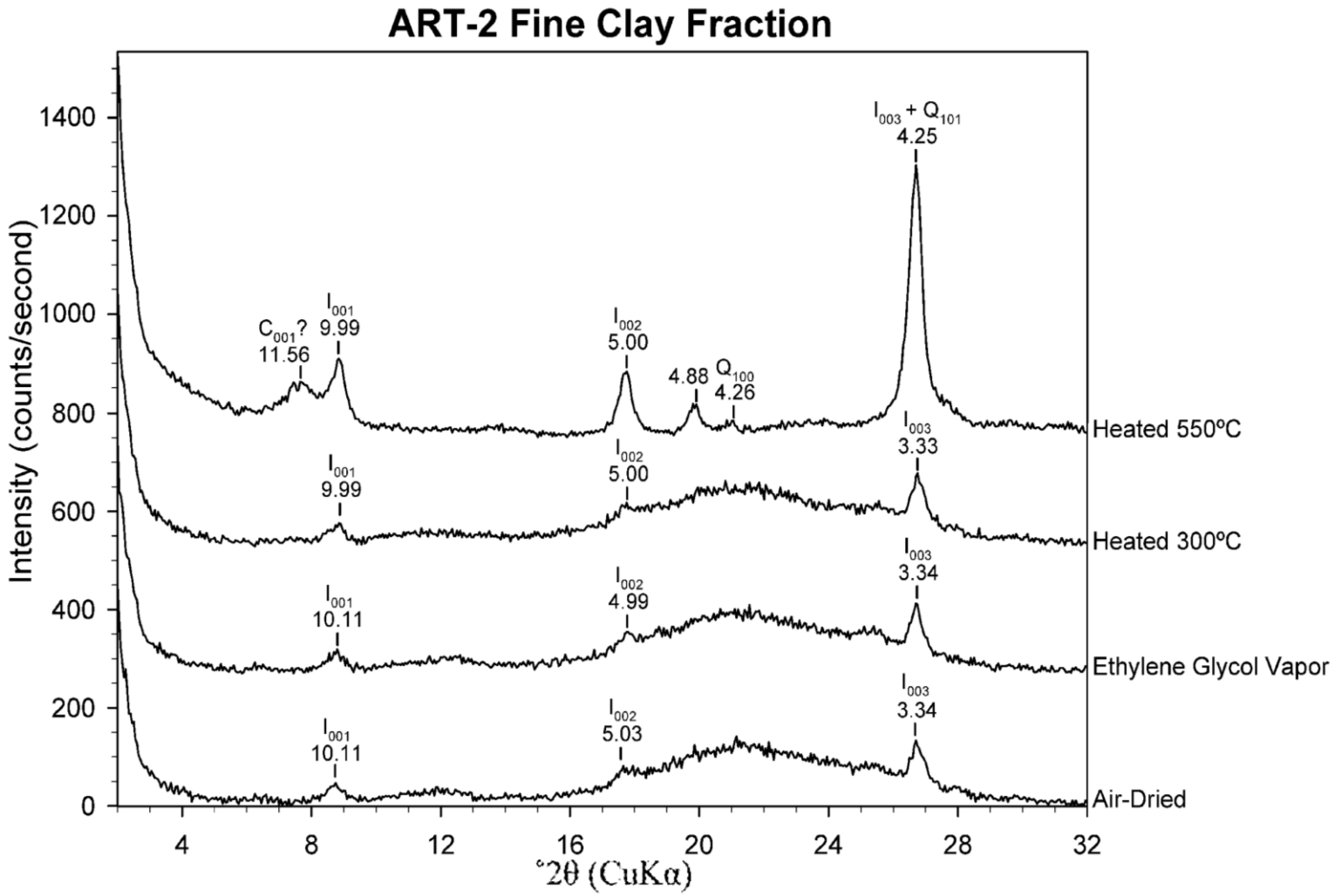
ART-2 Fine Clay Fraction
Intensity (counts/second)
°2θ (CuKα)
I003 + Q101
4.25
C001?
11.56
I001
9.99
I002
5.00
4.88
Q100
4.26
I003
3.33
Heated 550ºC
Heated 300ºC
I001
10.11
I002
4.99
I003
3.34
Ethylene Glycol Vapor
I001
10.11
I002
5.03
I003
3.34
Air-Dried

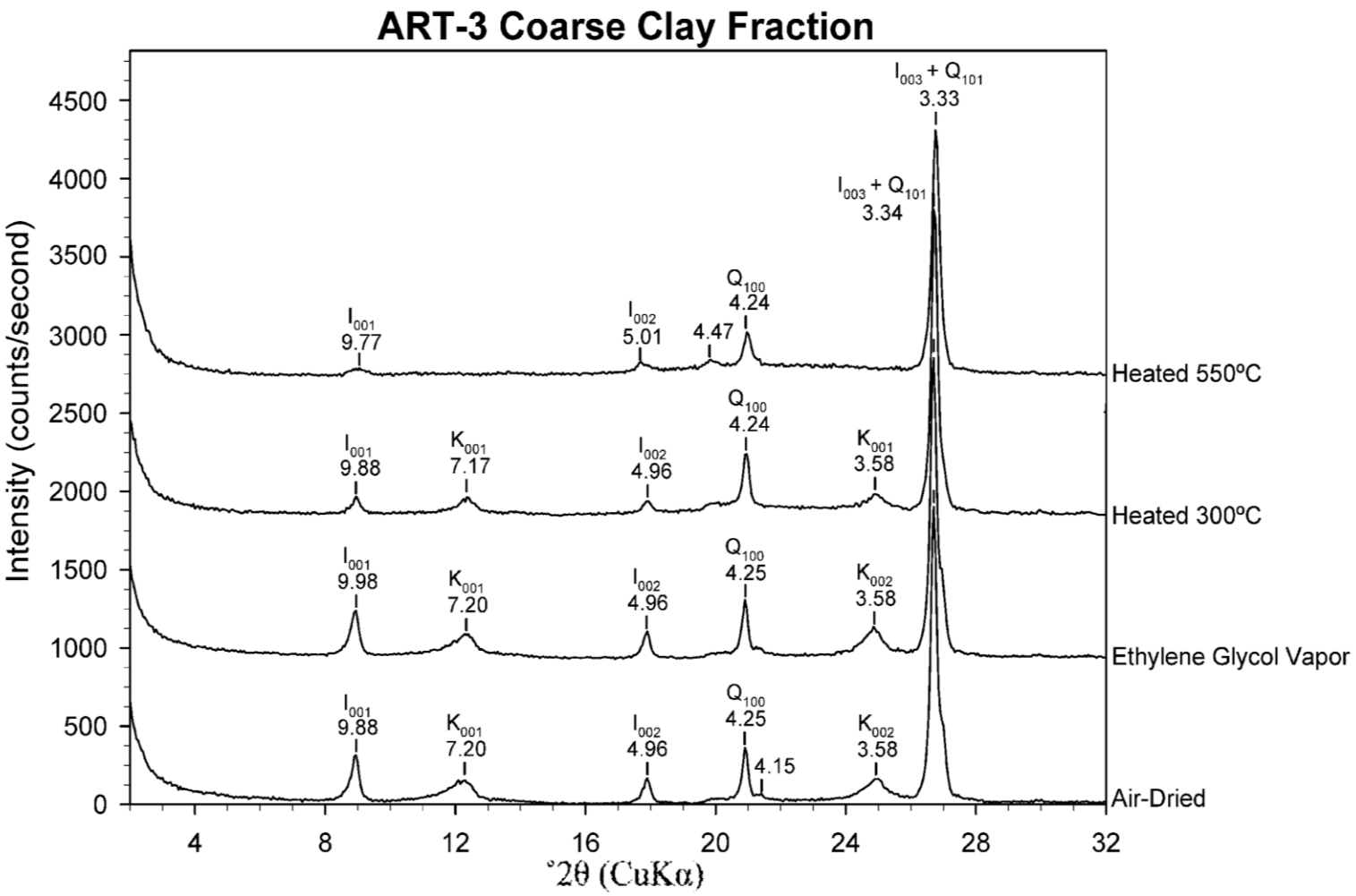
ART-3 Coarse Clay Fraction
Intensity (counts/second)
°2θ (CuKα)
Heated 550ºC
Heated 300ºC
Ethylene Glycol Vapor
Air-Dried
I001 9.77
I002 5.01
4.47
Q100 4.24
I003 + Q101 3.34
I003 + Q101 3.33
I001 9.88
K001 7.17
I002 4.96
Q100 4.24
K001 3.58
I001 9.98
K001 7.20
I002 4.96
Q100 4.25
K002 3.58
I001 9.88
K001 7.20
I002 4.96
Q100 4.25
4.15
K002 3.58

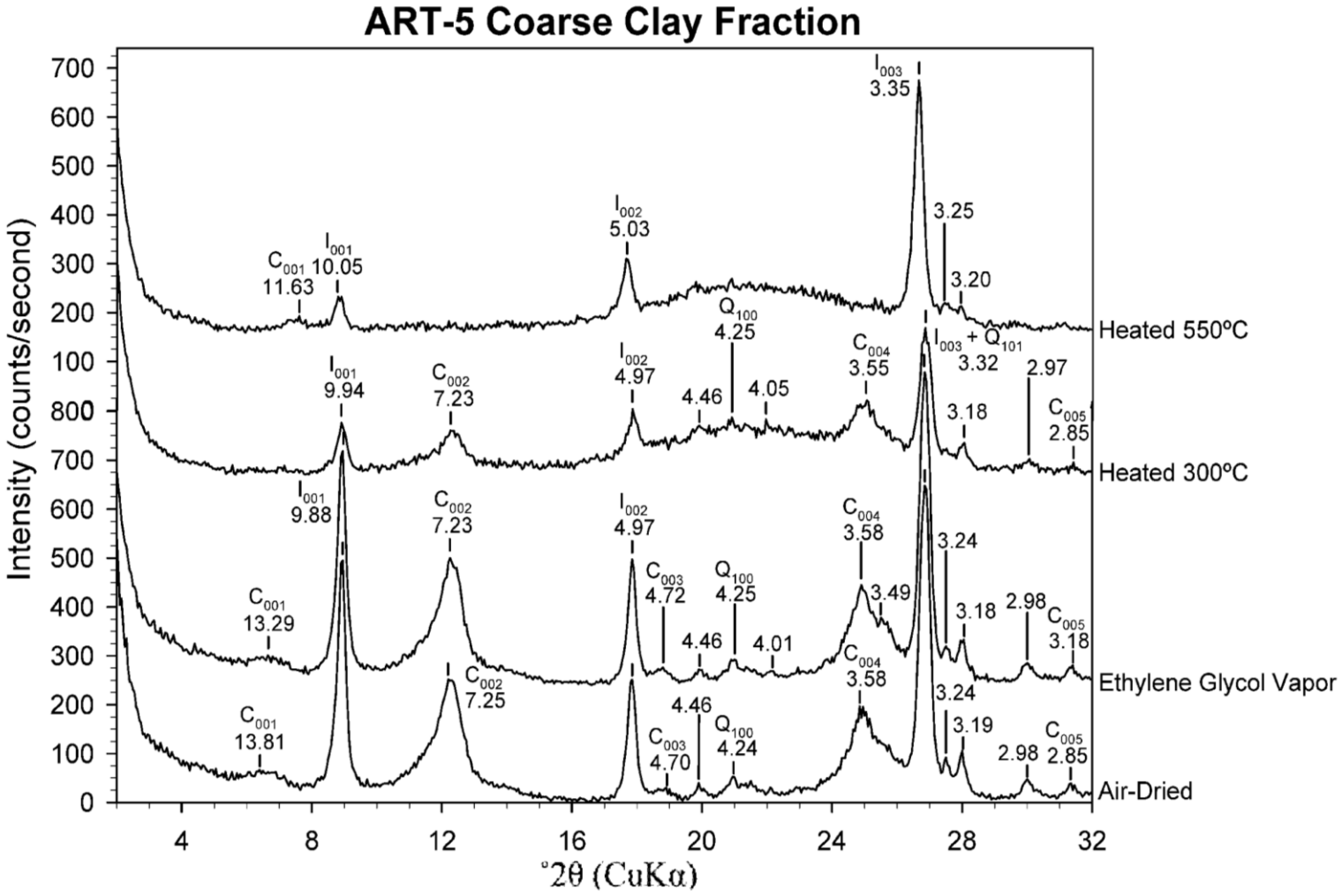
ART-5 Coarse Clay Fraction
Intensity (counts/second)
°2θ (CuKα)
Heated 550ºC
Heated 300ºC
Ethylene Glycol Vapor
Air-Dried
I003 3.35
I002 5.03
C001 11.63
I001 10.05
Q100 4.25
3.25
3.20
I003 + Q101 3.32
2.97
C004 3.55
I002 4.97
4.46
4.05
I001 9.94
C002 7.23
3.18
C005 2.85
I001 9.88
C002 7.23
I002 4.97
C004 3.58
3.24
C003 4.72
Q100 4.25
3.49
C001 13.29
3.18
2.98
C005 3.18
4.46
4.01
C004 3.58
C002 7.25
3.24
4.46
3.19
C001 13.81
C003 4.70
Q100 4.24
2.98
C005 2.85

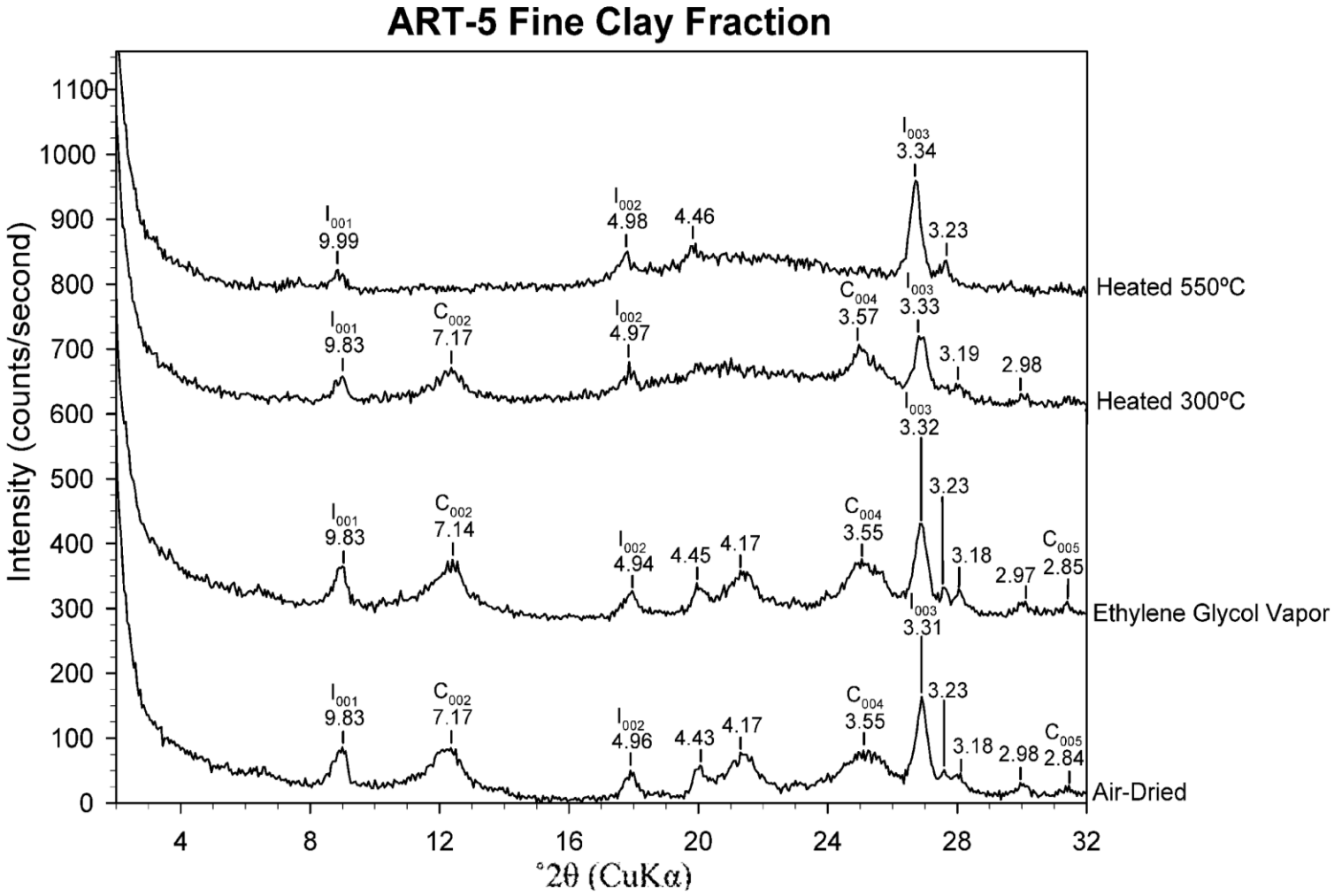
ART-5 Fine Clay Fraction
Intensity (counts/second)
°2θ (CuKα)
Heated 550ºC
Heated 300ºC
Ethylene Glycol Vapor
Air-Dried
I001 9.99
I002 4.98
4.46
I003 3.34
3.23
I003 3.33
C004 3.57
I001 9.83
C002 7.17
I002 4.97
3.19
2.98
I003 3.32
3.23
I001 9.83
C002 7.14
I002 4.94
4.45
4.17
C004 3.55
3.18
2.97
C005 2.85
I003 3.31
I001 9.83
C002 7.17
I002 4.96
4.43
4.17
C004 3.55
3.23
3.18
2.98
C005 2.84

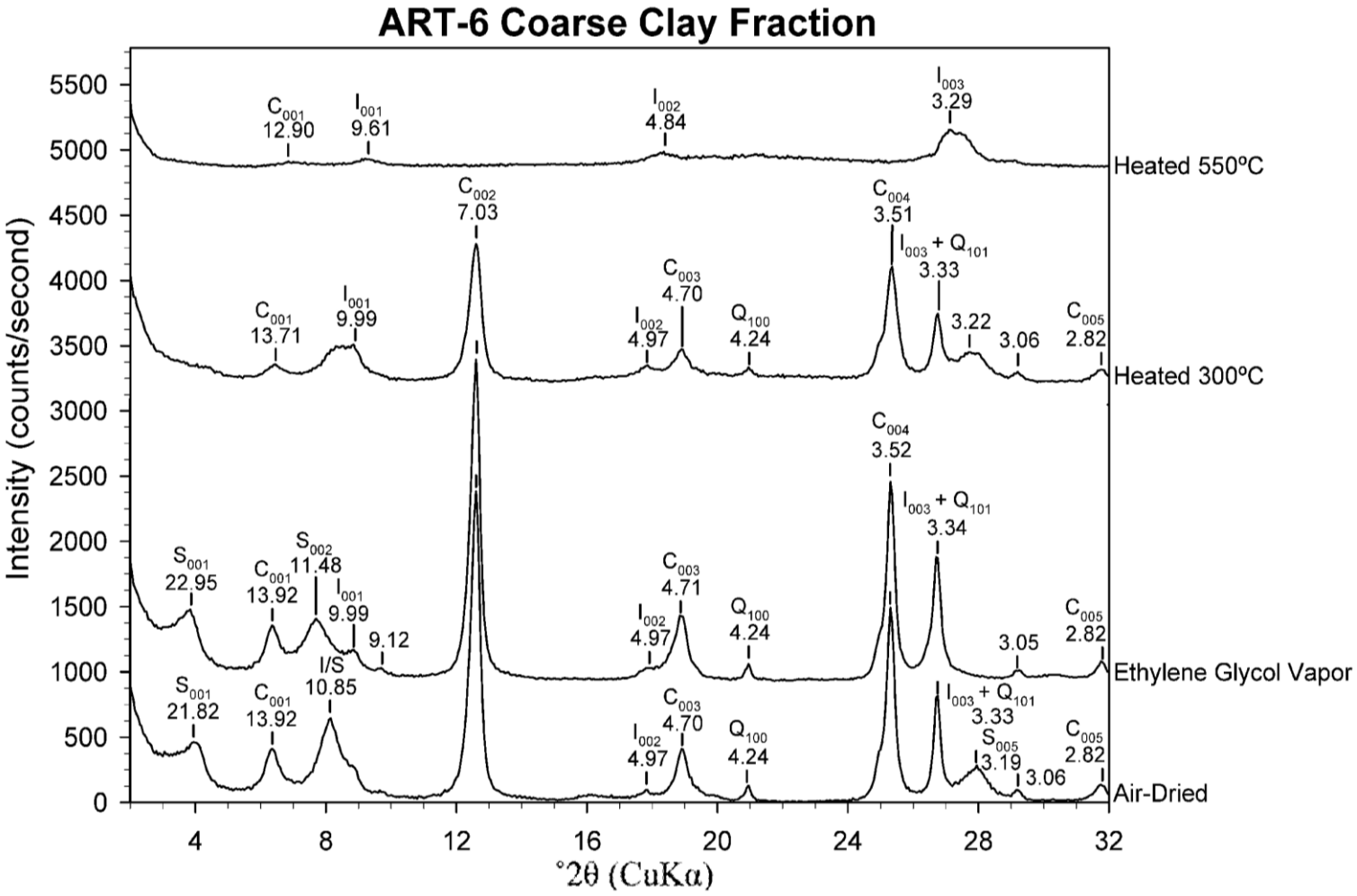
ART-6 Coarse Clay Fraction
Intensity (counts/second)
°2θ (CuKα)
Heated 550ºC
Heated 300ºC
Ethylene Glycol Vapor
Air-Dried
C001 12.90
I001 9.61
I002 4.84
I003 3.29
C002 7.03
C001 13.71
I001 9.99
C003 4.70
I002 4.97
Q100 4.24
C004 3.51
I003 + Q101 3.33
3.22
3.06
C005 2.82
C004 3.52
I003 + Q101 3.34
S001 22.95
C001 13.92
S002 11.48
I001 9.99
9.12
C003 4.71
I002 4.97
Q100 4.24
3.05
C005 2.82
S001 21.82
C001 13.92
I/S 10.85
C003 4.70
I002 4.97
Q100 4.24
I003 + Q101 3.33
S005 3.19
3.06
C005 2.82

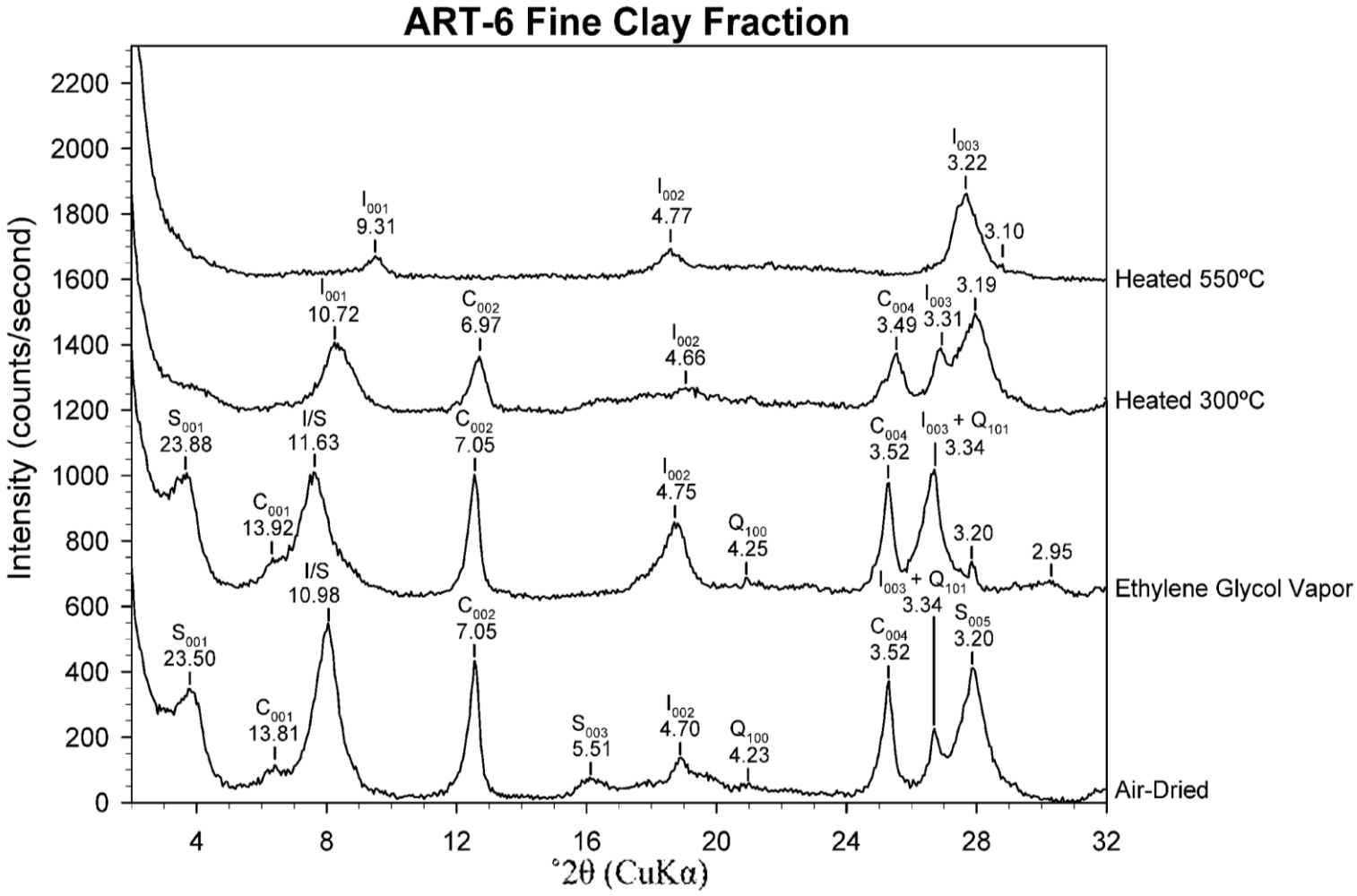
ART-6 Fine Clay Fraction
Intensity (counts/second)
°2θ (CuKα)
Heated 550ºC
Heated 300ºC
Ethylene Glycol Vapor
Air-Dried
I001 9.31
I002 4.77
I003 3.22
3.10
I001 10.72
C002 6.97
I002 4.66
C004 3.49
I003 3.31
3.19
S001 23.88
I/S 11.63
C002 7.05
C001 13.92
I002 4.75
Q100 4.25
C004 3.52
I003 + Q101 3.34
3.20
2.95
I/S 10.98
C002 7.05
I003 + Q101 3.34
S005 3.20
S001 23.50
C001 13.81
S003 5.51
I002 4.70
Q100 4.23
C004 3.52

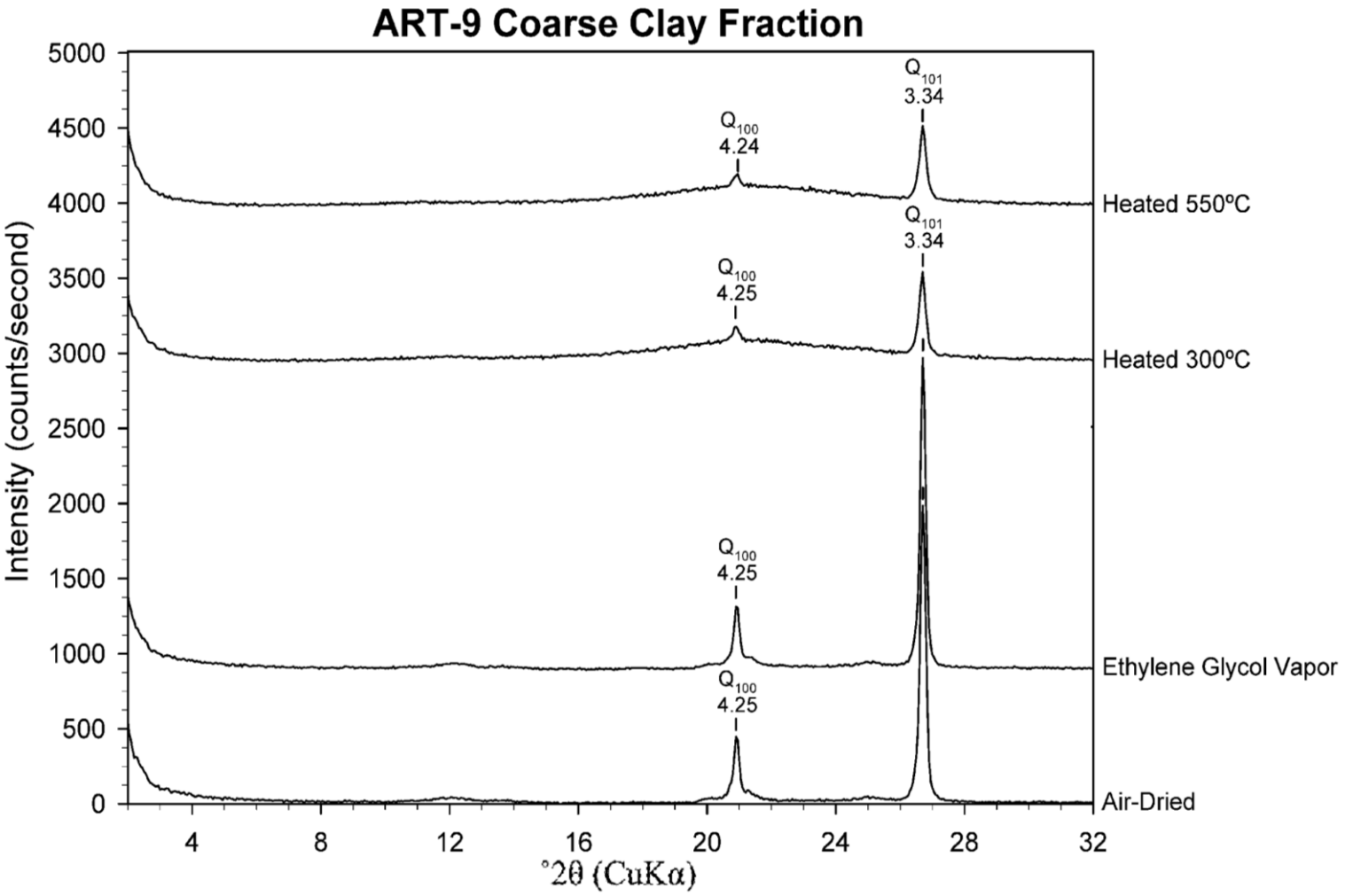
ART-9 Coarse Clay Fraction
Intensity (counts/second)
5000
4500
4000
3500
3000
2500
2000
1500
1000
500
0
4
8
12
16
20
24
28
32
°2θ (CuKα)
Q100 4.24
Q101 3.34
Heated 550ºC
Q100 4.25
Q101 3.34
Heated 300ºC
Q100 4.25
Ethylene Glycol Vapor
Q100 4.25
Air-Dried

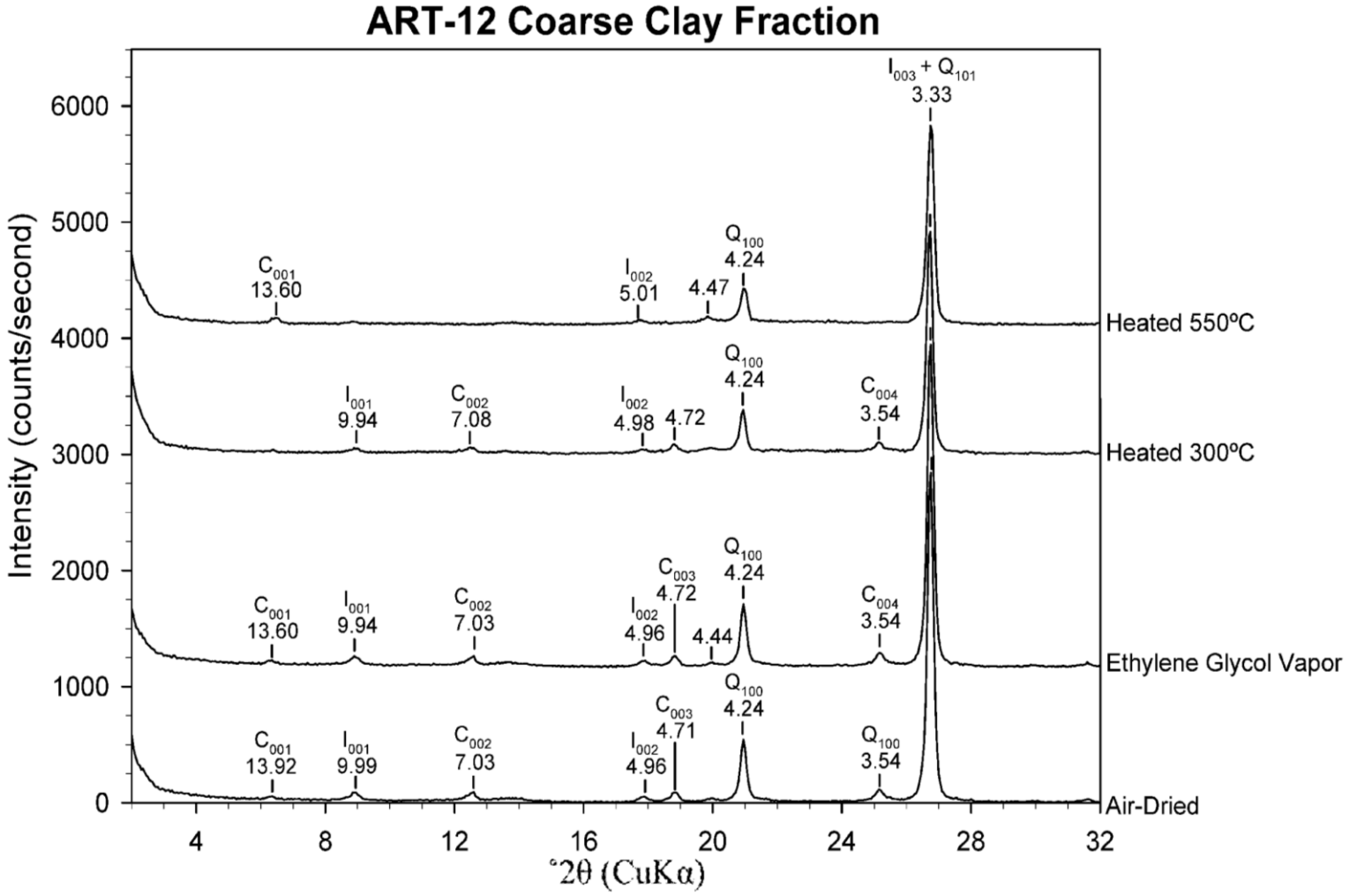
ART-12 Coarse Clay Fraction
Intensity (counts/second)
°2θ (CuKα)
Heated 550ºC
Heated 300ºC
Ethylene Glycol Vapor
Air-Dried
I003 + Q101 3.33
C001 13.60
I002 5.01
4.47
Q100 4.24
I001 9.94
C002 7.08
I002 4.98
4.72
Q100 4.24
C004 3.54
C001 13.60
I001 9.94
C002 7.03
C003 4.72
I002 4.96
4.44
Q100 4.24
C004 3.54
C001 13.92
I001 9.99
C002 7.03
C003 4.71
I002 4.96
Q100 4.24
Q100 3.54

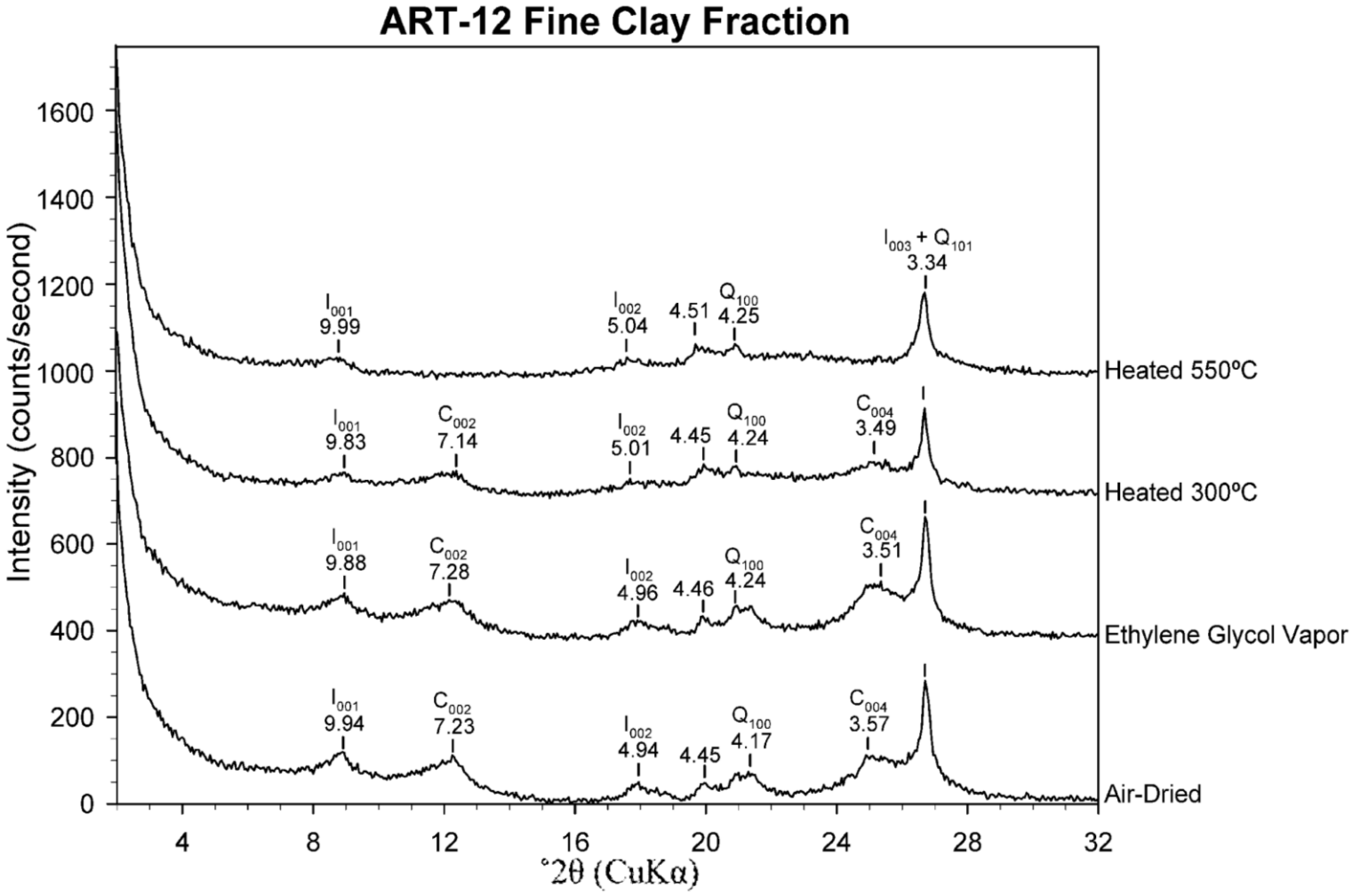
ART-12 Fine Clay Fraction
Intensity (counts/second)
°2θ (CuKα)
Heated 550ºC
Heated 300ºC
Ethylene Glycol Vapor
Air-Dried
I001 9.99
I002 5.04
4.51
Q100 4.25
I003 + Q101 3.34
I001 9.83
C002 7.14
I002 5.01
4.45
Q100 4.24
C004 3.49
I001 9.88
C002 7.28
I002 4.96
4.46
Q100 4.24
C004 3.51
I001 9.94
C002 7.23
I002 4.94
4.45
Q100 4.17
C004 3.57

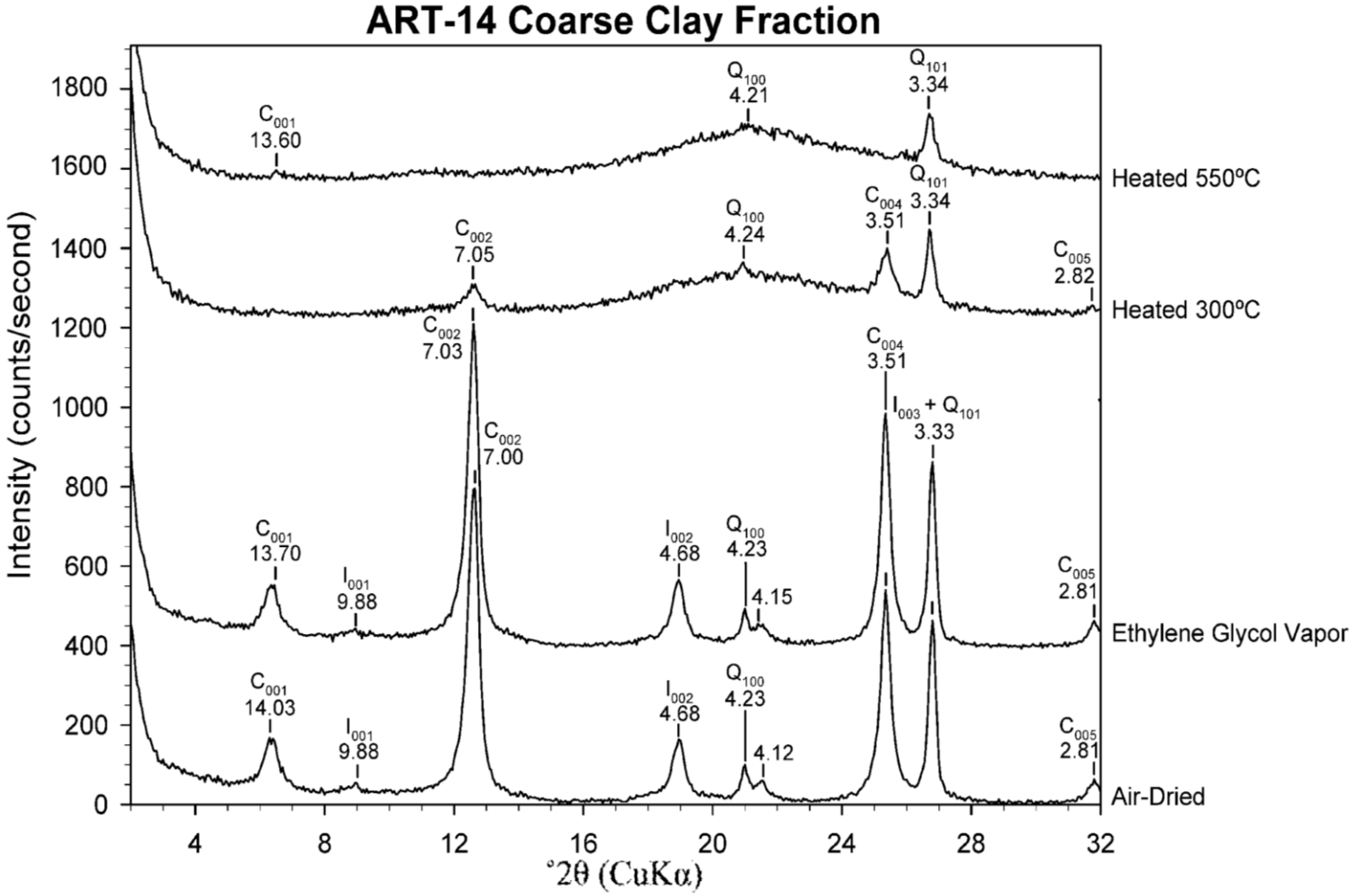
ART-14 Coarse Clay Fraction
Intensity (counts/second)
°2θ (CuKα)
Heated 550ºC
Heated 300ºC
Ethylene Glycol Vapor
Air-Dried
C001 13.60
Q100 4.21
Q101 3.34
C002 7.05
Q100 4.24
C004 3.51
Q101 3.34
C005 2.82
C002 7.03
C004 3.51
C002 7.00
I003 + Q101 3.33
C001 13.70
I001 9.88
I002 4.68
Q100 4.23
4.15
C005 2.81
C001 14.03
I001 9.88
I002 4.68
Q100 4.23
4.12
C005 2.81

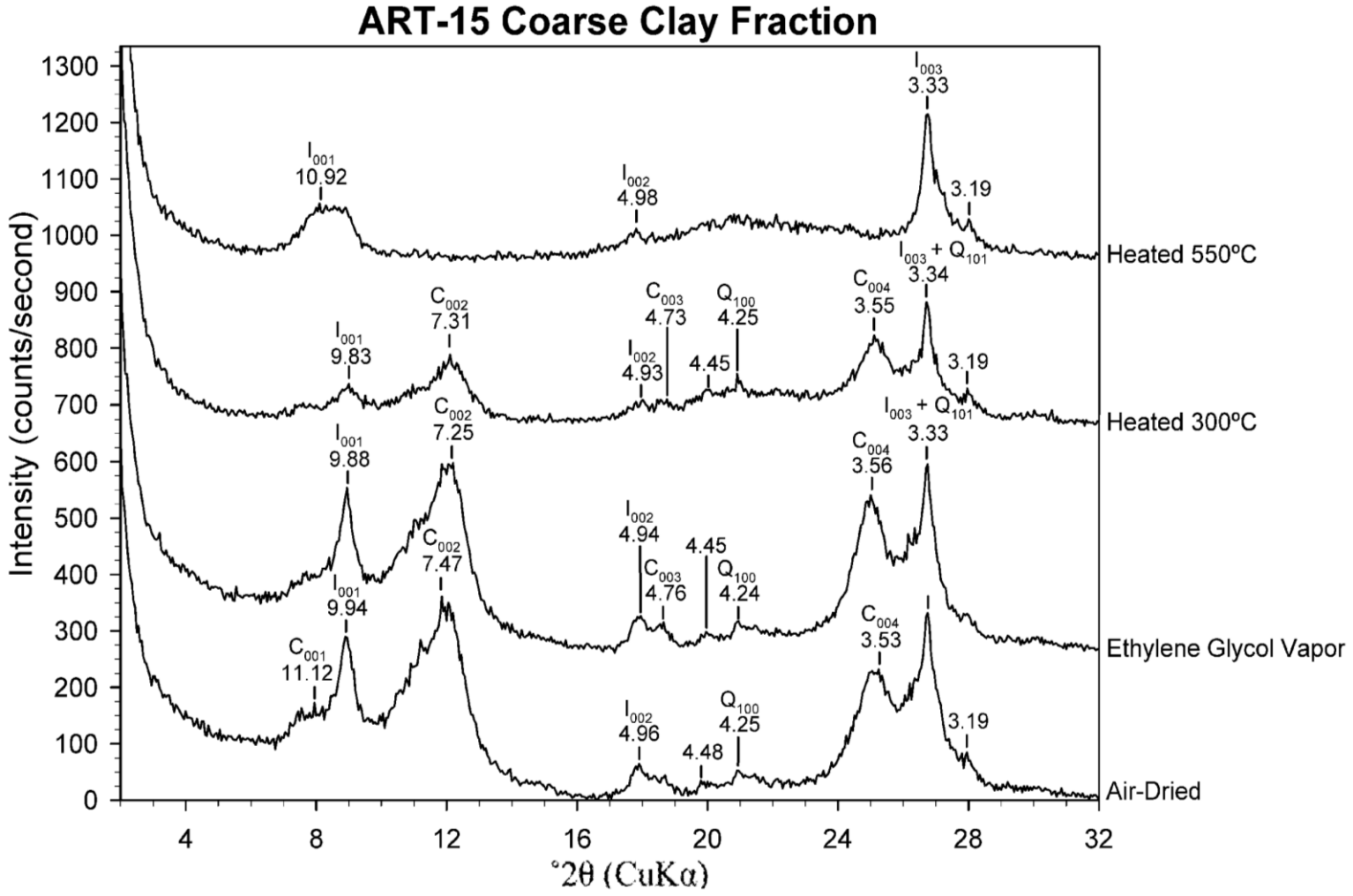
ART-15 Coarse Clay Fraction
Intensity (counts/second)
°2θ (CuKα)
Heated 550ºC
Heated 300ºC
Ethylene Glycol Vapor
Air-Dried
I001 10.92
I002 4.98
I003 3.33
3.19
I003 + Q101 3.34
C002 7.31
I001 9.83
C003 4.73
Q100 4.25
I002 4.93
4.45
C004 3.55
3.19
I003 + Q101
C002 7.25
I001 9.88
C004 3.56
3.33
I002 4.94
4.45
C002 7.47
C003 4.76
Q100 4.24
I001 9.94
C004 3.53
C001 11.12
I002 4.96
Q100 4.25
4.48
3.19

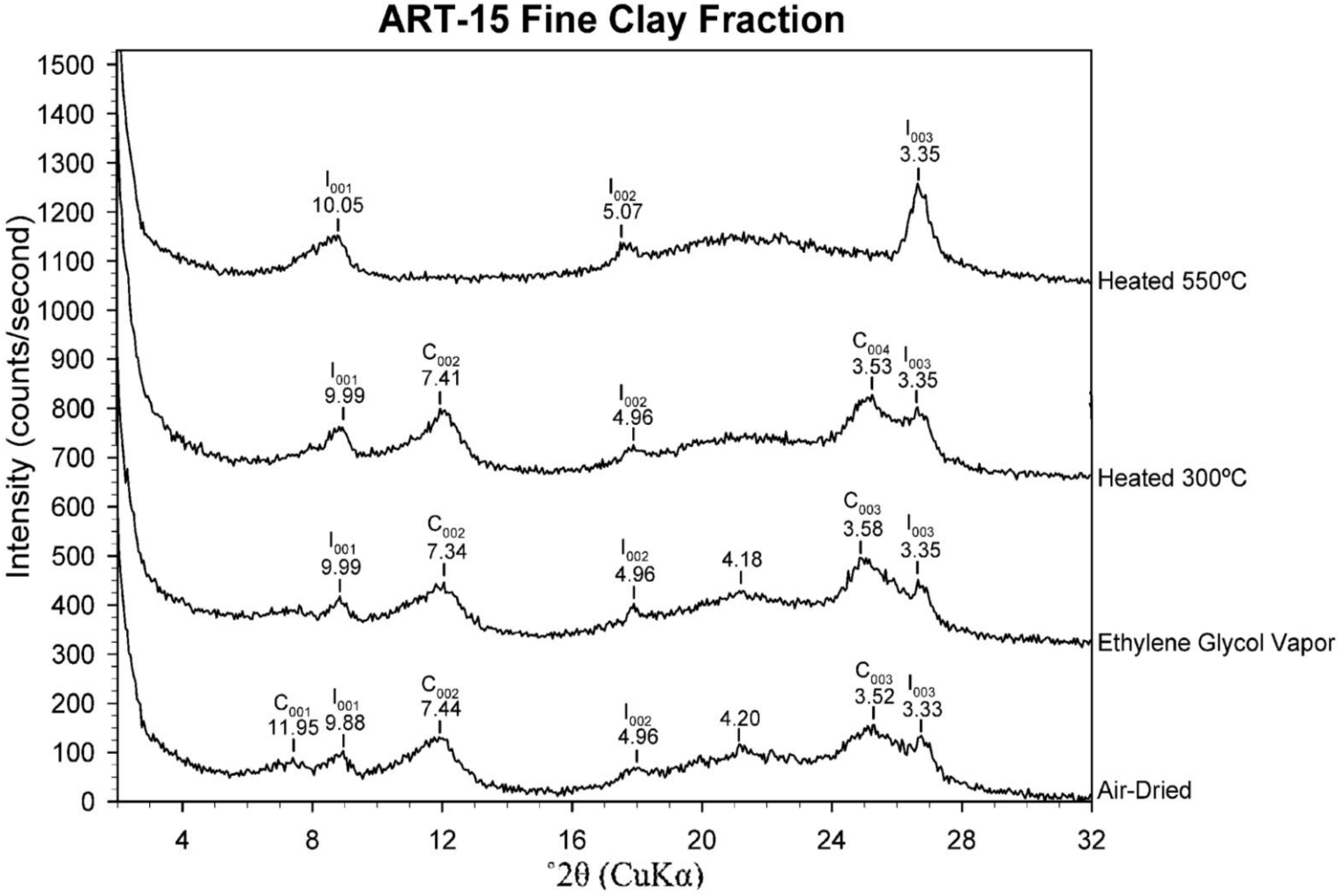
ART-15 Fine Clay Fraction
Intensity (counts/second)
°2θ (CuKα)
Heated 550ºC
Heated 300ºC
Ethylene Glycol Vapor
Air-Dried
I001 10.05
I002 5.07
I003 3.35
I001 9.99
C002 7.41
I002 4.96
C004 3.53
I003 3.35
I001 9.99
C002 7.34
I002 4.96
4.18
C003 3.58
I003 3.35
C001 11.95
I001 9.88
C002 7.44
I002 4.96
4.20
C003 3.52
I003 3.33

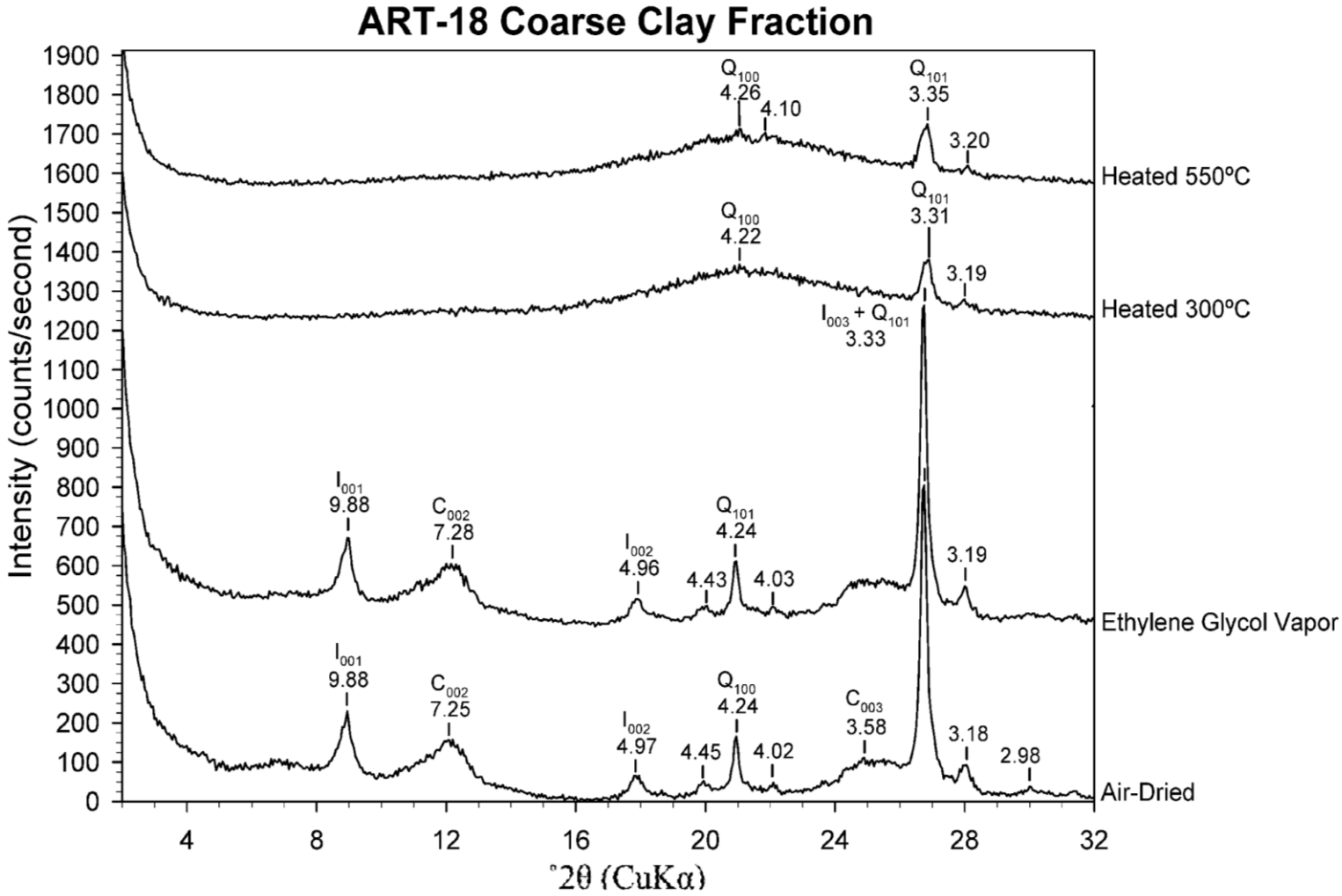
ART-18 Coarse Clay Fraction
Intensity (counts/second)
°2θ (CuKα)
Heated 550ºC
Heated 300ºC
Ethylene Glycol Vapor
Air-Dried
Q100 4.26
4.10
Q101 3.35
3.20
Q100 4.22
Q101 3.31
3.19
I003 + Q101 3.33
I001 9.88
C002 7.28
I002 4.96
4.43
Q101 4.24
4.03
3.19
I001 9.88
C002 7.25
I002 4.97
4.45
Q100 4.24
4.02
C003 3.58
3.18
2.98

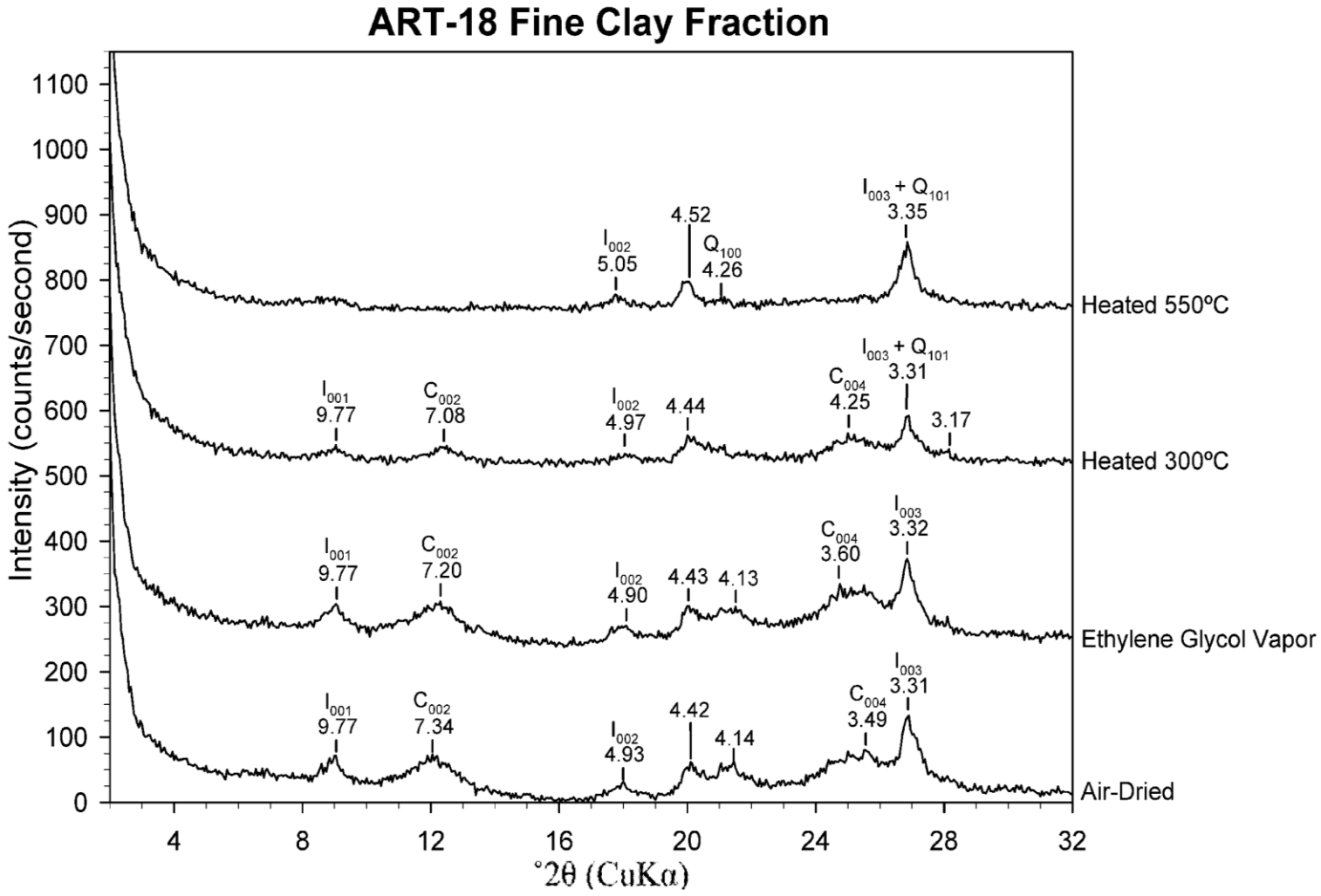
ART-18 Fine Clay Fraction
Intensity (counts/second)
°2θ (CuKα)
Heated 550ºC
Heated 300ºC
Ethylene Glycol Vapor
Air-Dried
I002 5.05
4.52
Q100 4.26
I003 + Q101 3.35
I001 9.77
C002 7.08
I002 4.97
4.44
C004 4.25
I003 + Q101 3.31
3.17
I001 9.77
C002 7.20
I002 4.90
4.43
4.13
C004 3.60
I003 3.32
I001 9.77
C002 7.34
I002 4.93
4.42
4.14
C004 3.49
I003 3.31

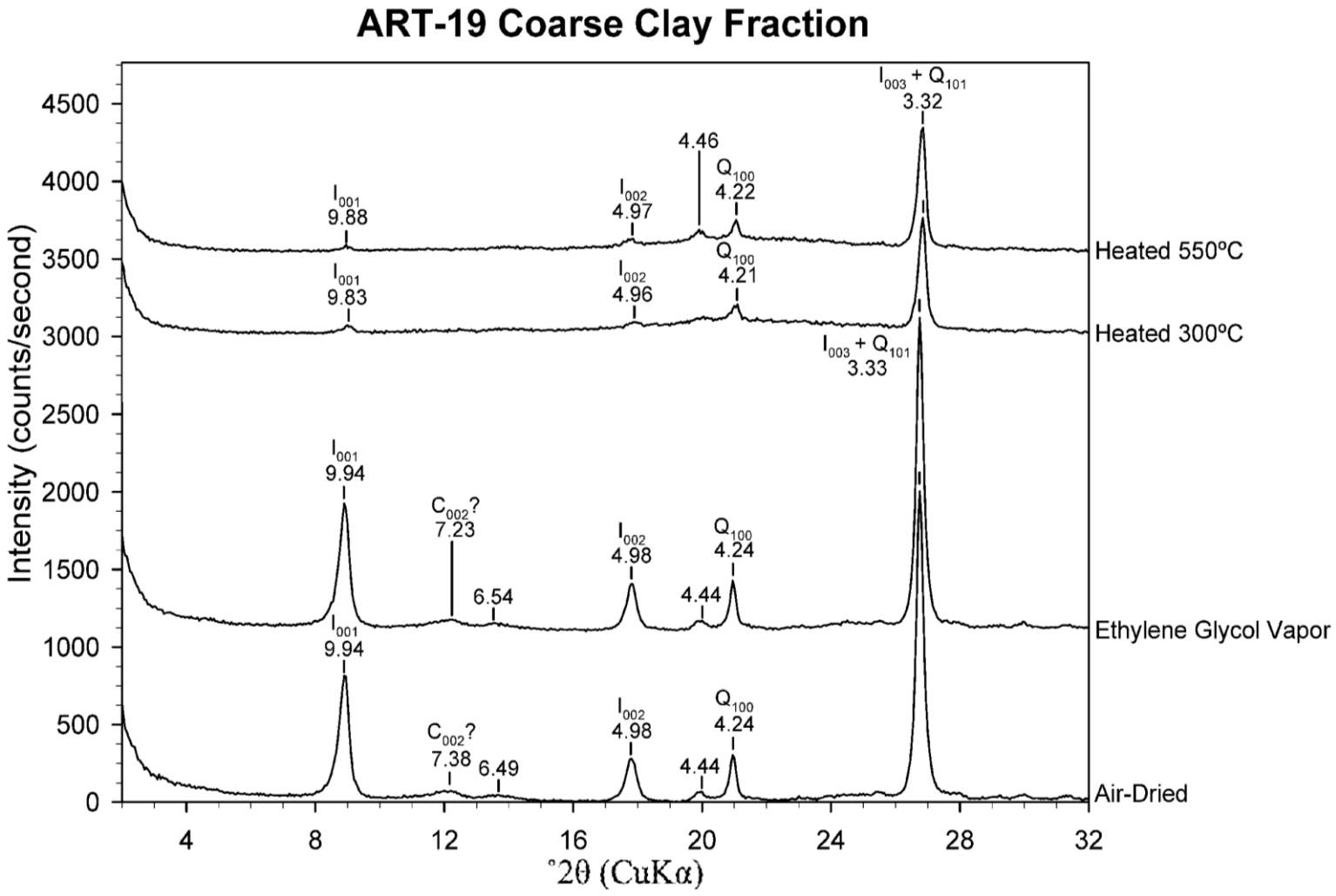
ART-19 Coarse Clay Fraction
Intensity (counts/second)
°2θ (CuKα)
I001 9.88
I002 4.97
4.46
Q100 4.22
I003 + Q101 3.32
Heated 550ºC
I001 9.83
I002 4.96
Q100 4.21
I003 + Q101 3.33
Heated 300ºC
I001 9.94
C002? 7.23
6.54
I002 4.98
4.44
Q100 4.24
Ethylene Glycol Vapor
I001 9.94
C002? 7.38
6.49
I002 4.98
4.44
Q100 4.24
Air-Dried

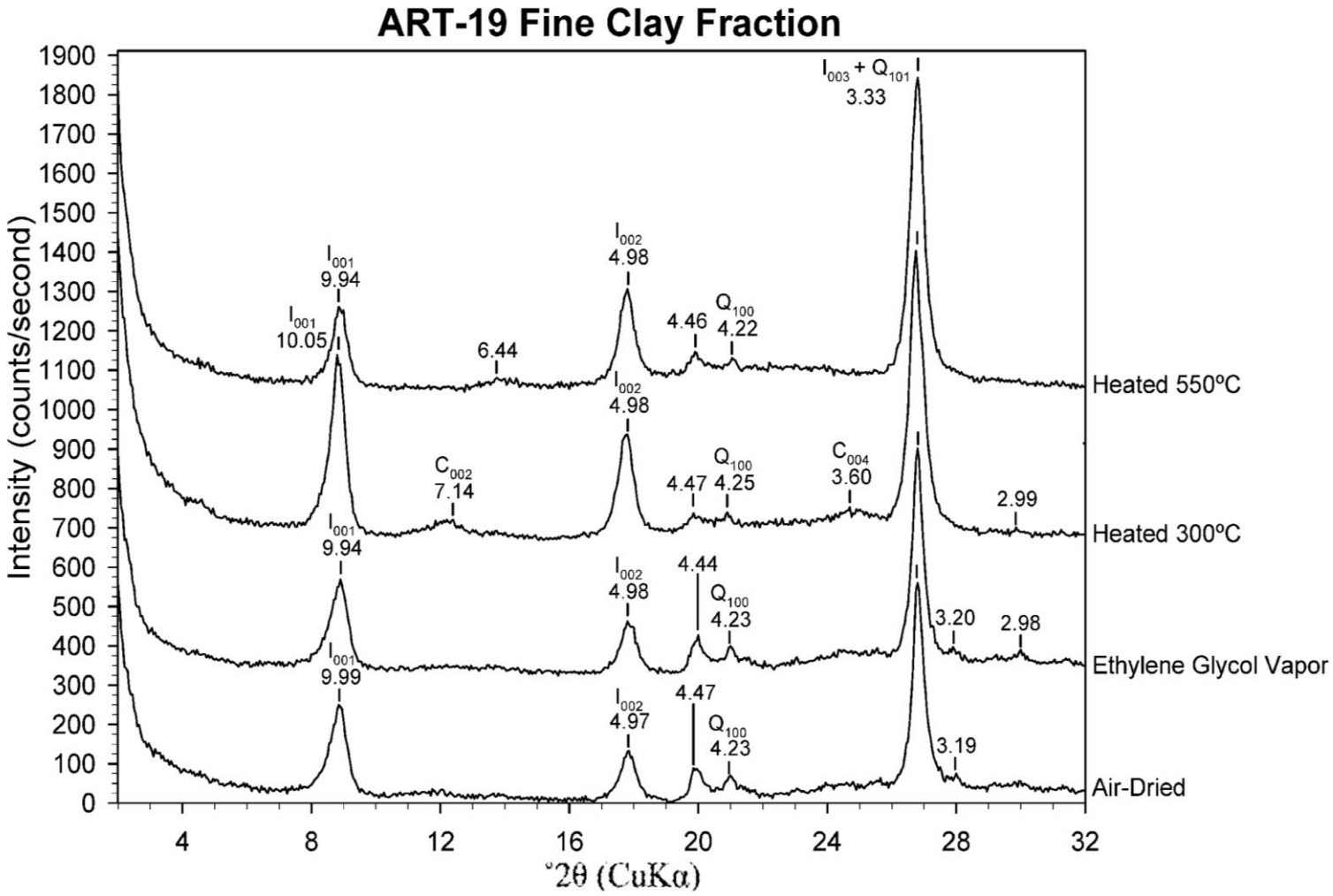
ART-19 Fine Clay Fraction
Intensity (counts/second)
°2θ (CuKα)
I001 9.94
I001 10.05
6.44
I002 4.98
4.46
Q100 4.22
I003 + Q101 3.33
Heated 550ºC
C002 7.14
I002 4.98
Q100 4.25
4.47
C004 3.60
2.99
Heated 300ºC
I001 9.94
I002 4.98
4.44
Q100 4.23
3.20
2.98
Ethylene Glycol Vapor
I001 9.99
I002 4.97
4.47
Q100 4.23
3.19
Air-Dried

APPENDIX E

MANUSCRIPT #3: FIGURES/TABLES

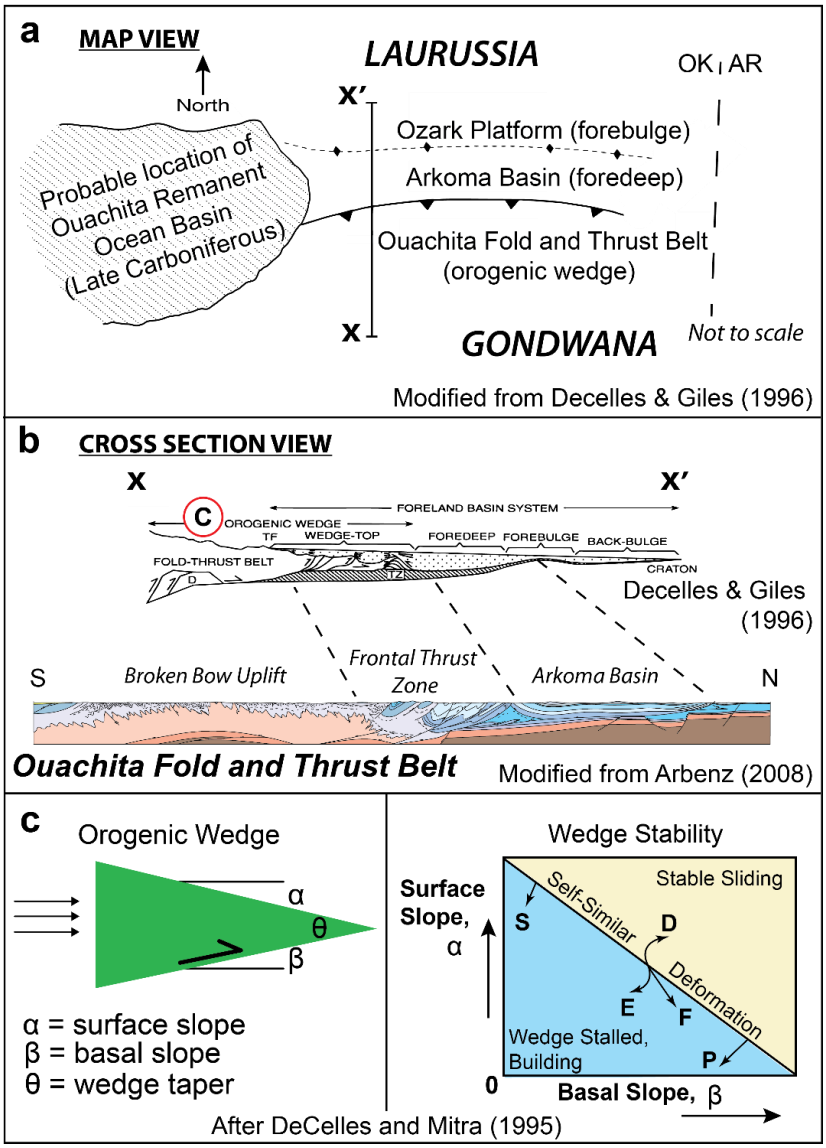

Figure 1. Generalized foreland basin system compared to the Ouachita FTB (Arbenz, 2008; DeCelles & Giles, 1996). (a) Map view and (b) Cross section view. Location of part C is indicated by letter outlined in red. Model for FTBs and development of orogenic (critical) wedge (c) and wedge stability (d), after Dahlen et al., (1984), Decelles & Mitra (1995), and Woodward (1987). Redrafted by D. Wiltschko. See text for explanation of (d).

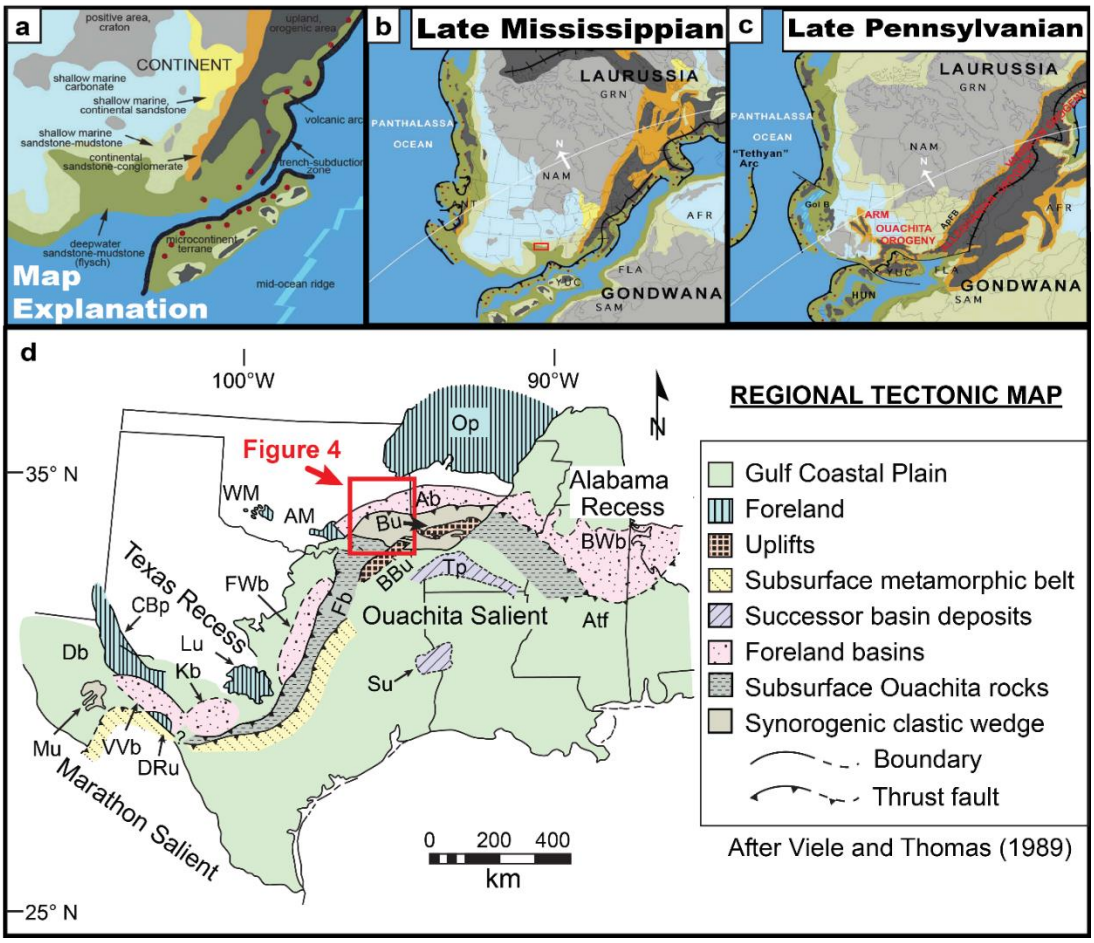

Figure 2. Plate tectonic setting of North America during the Carboniferous. (a) Explanation of elements in the plate tectonic maps. (b) Late Mississippian. (c) Late Pennsylvanian. These maps were created by Miall (2019) using data and ideas from Cook & Bally (1975), Ziegler (1988), Scotese (1998), Scotese & Golanka (1992), and Stampfli et al. (2002). Abbreviations -- AFR, Africa; ANT, Antler terrane; ARM, Ancestral Rocky Mountains; BAL, Baltica; FLA, Florida; GRN, Greenland; HUN, Hunic terranes; NAM, North America (Laurentia); NSL, North slope (Alaska); SAM, South America; YUC, Yucatan. (d) Tectonic overview map for the southern margin of North America (modified from Viele & Thomas, 1989). Study area is outlined. Abbreviations -- AtF, Appalachian tectonic front; Fb, Frontal belt. Basins: Ab, Arkoma; BWb, Black Warrior; Db, Deleware; FWb, Fort Worth; Kb, Kerr; VVb, Val Verde. Platforms: CBp, Central Basin; Op, Ozark; Tp, Texarkana. Mountains: AM, Arbuckle; WM, Wichita. Uplifts: BBu, Broken Bow; Bu, Benton; DRu, Devil's River; Lu, Llano; Mu, Marathon; Su, Sabine.

Figure 3. Sample locations in South-Eastern Oklahoma shown on simplified geologic map adapted from Arbenz (2008). Bulk sandstone collected at location marked by filled red dot. Sample number reference is "OK" = Oklahoma, "12" = 2012 collection year, and last number is sample identification. All samples are available in the SESAR database, with exception of sample BB-7. Surface geology modified from Haley et al., 1976; Stone et al., 1986; Johnson, 1988; Suneson et al., 1990; Suneson et al., 1994; Arbenz, 2008). Areas with sparse surface information or lack of space at this map scale have formations combined and youngest stratigraphy represented. Major tectonic features shown are Black Knob Ridge, Potato Hills, and Broken Bow Uplift. Mean vitrinite reflectance values have been contoured (Cardott, 2013; Houseknecht & Matthews, 1985).

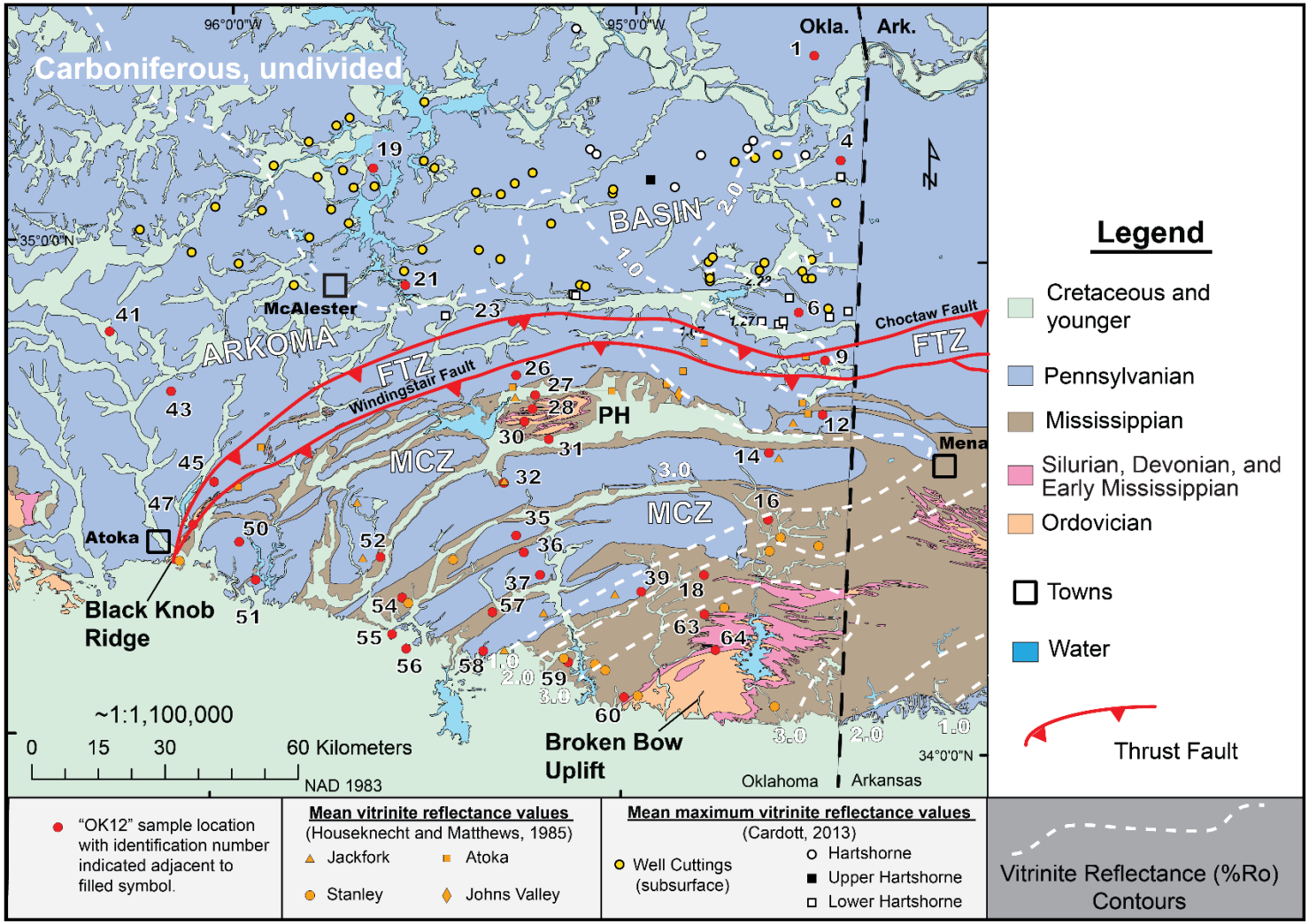
Carboniferous, undivided
96°0'0"W
95°0'0"W
35°0'0"N
34°0'0"N
Okla.
Ark.
BASIN
ARKOMA
McAlester
Atoka
Mena
FTZ
Windingstair Fault
Choctaw Fault
PH
MCZ
Black Knob Ridge
Broken Bow Uplift
~1:1,100,000
0 15 30 60 Kilometers
NAD 1983
Oklahoma
Arkansas
Legend
Cretaceous and younger
Pennsylvanian
Mississippian
Silurian, Devonian, and Early Mississippian
Ordovician
Towns
Water
Thrust Fault
"OK12" sample location with identification number indicated adjacent to filled symbol.
Mean vitrinite reflectance values
(Houseknecht and Matthews, 1985)
Jackfork
Atoka
Stanley
Johns Valley
Mean maximum vitrinite reflectance values
(Cardott, 2013)
Well Cuttings (subsurface)
Hartshorne
Upper Hartshorne
Lower Hartshorne
Vitrinite Reflectance (%Ro) Contours

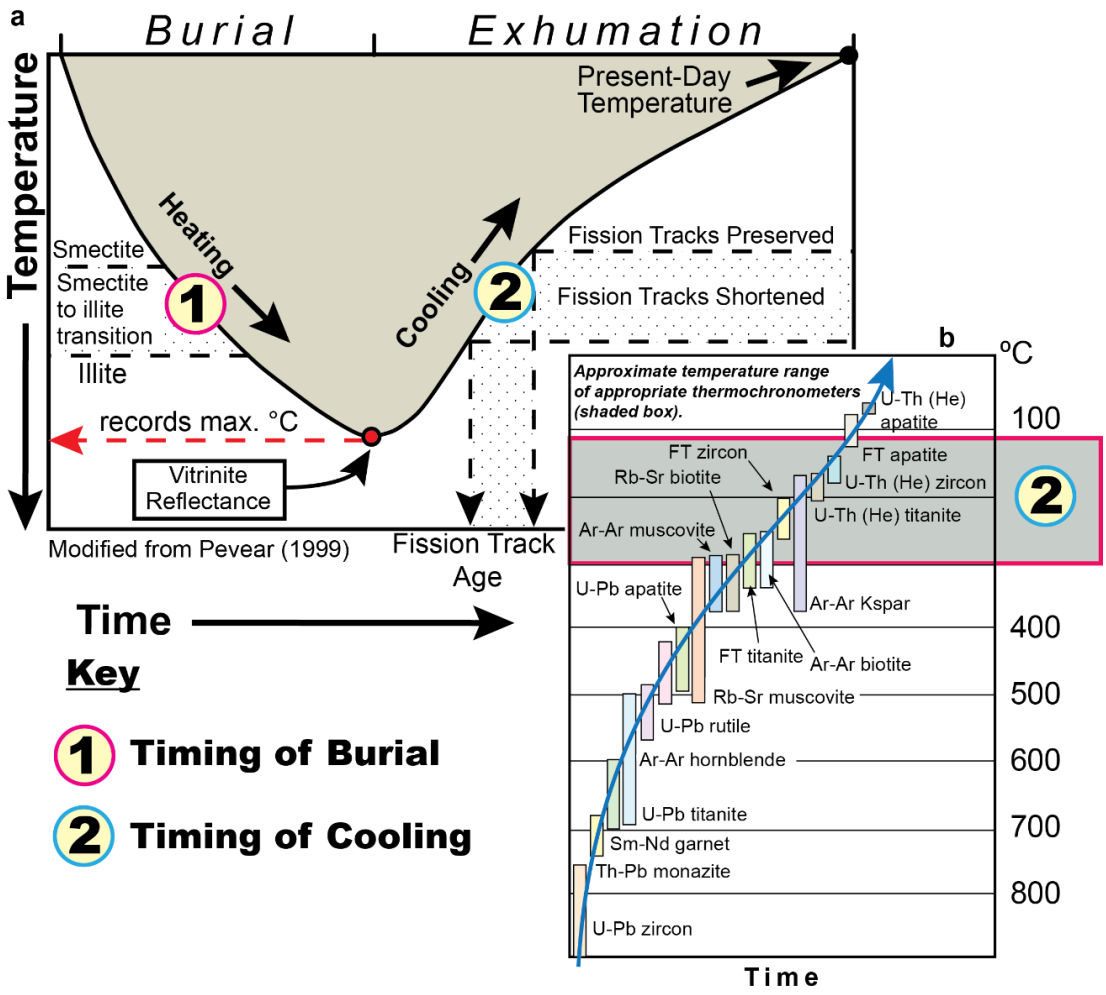

Figure 4. (a) Conceptual thermal diagram that illustrates use of paleothermometers to constrain burial and subsequent exhumation (Pevear, 1999). Smectite to illite transition (left) records the time of heating from increased burial because of overburden. The maximum or peak temperature inflection point at curve base) is known from vitrinite reflectance, a common measure of thermal maturation. Cooling history (right) represents the timing of uplift and cooling based on thermochronometric methods, including fission track ages and (U-Th)/He dates. (b) Effective closure temperatures of current thermochronometers (modified from Pollard, 2002 - http://pangea.stanford.edu/~dpollard/NSF/main.html, which was adapted from earlier work of P. Fitzgerald, S. Baldwin, G. Gehrels, P. Reiners, and M. Ducea). Range of thermochronometers (position 2, table and plot) that have potential to yield reset cooling ages for Ouachita orogen based on maximum temperatures calculated from vitrinite reflectance (Barker & Pawlewicz, 1994; Houseknecht & Matthews, 1985).

Figure 5. (a) Calculated central ages (N = 37) of zircon fission track data from each sample locality. Italicized indicates only sample to yield apatite for a new apatite fission track central age (N = 1). Ages calculated by Stuart N. Thomson (Univ. of Arizona) using statistics outlined in Galbraith (2005). Population are denoted as reset or mixed before age using "R" or "M", respectively. If more than one age was determined at a locality, all ages are given. (b) Calculated peak-fit ages of zircon fission track data from each sample locality. Ages calculated by BinomFit software (Brandon, 2011) and from utilizing the binomial peak-fitting algorithm of Galbraith & Green (1990) and Galbraith & Laslett (1993). Number within the parenthesis is the percent component of the entire population. Localities with multiple ages are grouped by stacking component percentages, where the next age starts after 100 percent is reached. Details on base map given in Figure 4.

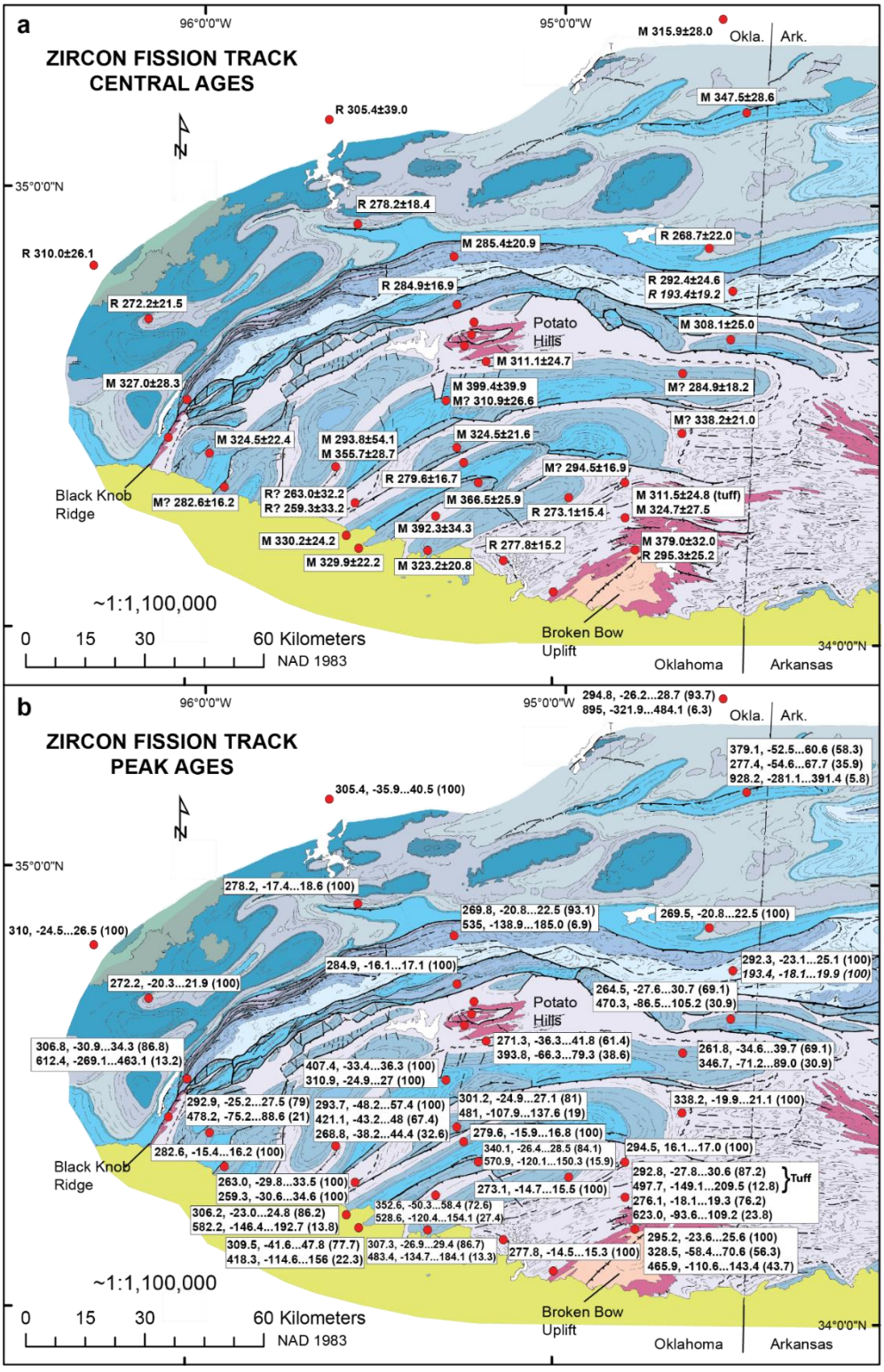
a
ZIRCON FISSION TRACK
CENTRAL AGES
96°0'0"W
95°0'0"W
35°0'0"N
34°0'0"N
M 315.9±28.0
Okla.
Ark.
M 347.5±28.6
R 305.4±39.0
R 278.2±18.4
R 310.0±26.1
M 285.4±20.9
R 268.7±22.0
R 284.9±16.9
R 292.4±24.6
R 193.4±19.2
R 272.2±21.5
Potato
Hills
M 308.1±25.0
M 311.1±24.7
M 327.0±28.3
M 399.4±39.9
M? 310.9±26.6
M? 284.9±18.2
M? 338.2±21.0
M 324.5±22.4
M 293.8±54.1
M 355.7±28.7
M 324.5±21.6
M? 294.5±16.9
R 279.6±16.7
Black Knob
Ridge
M? 282.6±16.2
R? 263.0±32.2
R? 259.3±33.2
M 366.5±25.9
R 273.1±15.4
M 311.5±24.8 (tuff)
M 324.7±27.5
M 392.3±34.3
M 330.2±24.2
R 277.8±15.2
M 379.0±32.0
R 295.3±25.2
M 329.9±22.2
M 323.2±20.8
~1:1,100,000
0 15 30 60 Kilometers
NAD 1983
Broken Bow
Uplift
Oklahoma
Arkansas
b
ZIRCON FISSION TRACK
PEAK AGES
96°0'0"W
95°0'0"W
294.8, -26.2...28.7 (93.7)
895, -321.9...484.1 (6.3)
Okla.
Ark.
379.1, -52.5...60.6 (58.3)
277.4, -54.6...67.7 (35.9)
928.2, -281.1...391.4 (5.8)
305.4, -35.9...40.5 (100)
35°0'0"N
278.2, -17.4...18.6 (100)
269.8, -20.8...22.5 (93.1)
535, -138.9...185.0 (6.9)
269.5, -20.8...22.5 (100)
310, -24.5...26.5 (100)
284.9, -16.1...17.1 (100)
292.3, -23.1...25.1 (100)
193.4, -18.1...19.9 (100)
272.2, -20.3...21.9 (100)
264.5, -27.6...30.7 (69.1)
470.3, -86.5...105.2 (30.9)
Potato
Hills
306.8, -30.9...34.3 (86.8)
612.4, -269.1...463.1 (13.2)
271.3, -36.3...41.8 (61.4)
393.8, -66.3...79.3 (38.6)
261.8, -34.6...39.7 (69.1)
346.7, -71.2...89.0 (30.9)
407.4, -33.4...36.3 (100)
310.9, -24.9...27 (100)
292.9, -25.2...27.5 (79)
478.2, -75.2...88.6 (21)
293.7, -48.2...57.4 (100)
421.1, -43.2...48 (67.4)
268.8, -38.2...44.4 (32.6)
301.2, -24.9...27.1 (81)
481, -107.9...137.6 (19)
338.2, -19.9...21.1 (100)
279.6, -15.9...16.8 (100)
282.6, -15.4...16.2 (100)
340.1, -26.4...28.5 (84.1)
570.9, -120.1...150.3 (15.9)
294.5, 16.1...17.0 (100)
Black Knob
Ridge
292.8, -27.8...30.6 (87.2)
497.7, -149.1...209.5 (12.8)
276.1, -18.1...19.3 (76.2)
623.0, -93.6...109.2 (23.8)
Tuff
263.0, -29.8...33.5 (100)
259.3, -30.6...34.6 (100)
273.1, -14.7...15.5 (100)
352.6, -50.3...58.4 (72.6)
528.6, -120.4...154.1 (27.4)
306.2, -23.0...24.8 (86.2)
582.2, -146.4...192.7 (13.8)
295.2, -23.6...25.6 (100)
328.5, -58.4...70.6 (56.3)
465.9, -110.6...143.4 (43.7)
309.5, -41.6...47.8 (77.7)
418.3, -114.6...156 (22.3)
307.3, -26.9...29.4 (86.7)
483.4, -134.7...184.1 (13.3)
277.8, -14.5...15.3 (100)
~1:1,100,000
0 15 30 60 Kilometers
NAD 1983
Broken Bow
Uplift
Oklahoma
Arkansas
34°0'0"N

Figure 6. (a) Calculated minimum ages of zircon fission track data from each sample locality using RadialPlotter software (Vermeesch, 2009). (b) Range of zircon (U-Th)/He dates and structural province given at each sample locality. Abbreviations: AB, Arkoma Basin; FTZ, Frontal Thrust Zone; BKR, Black Knob Ridge; PH, Potato Hills; MCZ, Maumelle Chaotic Zone; BBU, Broken Bow Uplift. Details on base map given in Figure 4.

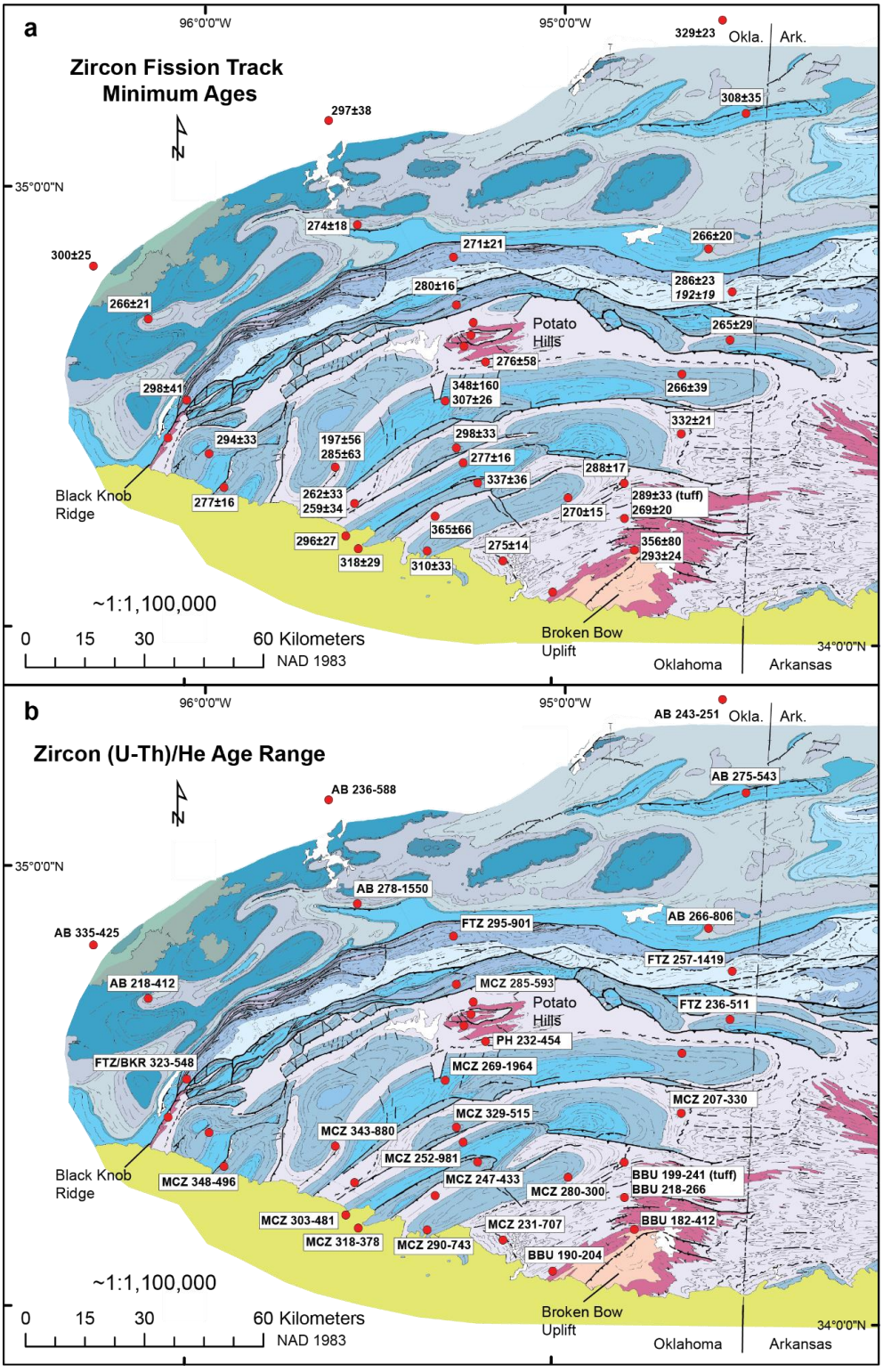
a
Zircon Fission Track
Minimum Ages
96°0'0"W
95°0'0"W
35°0'0"N
34°0'0"N
329±23
Okla.
Ark.
308±35
297±38
274±18
271±21
266±20
300±25
280±16
286±23
192±19
266±21
Potato
Hills
265±29
276±58
348±160
307±26
266±39
298±41
332±21
294±33
197±56
285±63
298±33
277±16
288±17
337±36
Black Knob
Ridge
277±16
262±33
259±34
289±33 (tuff)
269±20
270±15
365±66
296±27
275±14
356±80
293±24
318±29
310±33
~1:1,100,000
0 15 30 60 Kilometers
NAD 1983
Broken Bow
Uplift
Oklahoma
Arkansas
b
Zircon (U-Th)/He Age Range
AB 243-251
AB 275-543
AB 236-588
AB 278-1550
AB 266-806
AB 335-425
FTZ 295-901
FTZ 257-1419
AB 218-412
MCZ 285-593
FTZ 236-511
PH 232-454
FTZ/BKR 323-548
MCZ 269-1964
MCZ 207-330
MCZ 329-515
MCZ 343-880
MCZ 252-981
MCZ 247-433
BBU 199-241 (tuff)
BBU 218-266
MCZ 348-496
MCZ 280-300
MCZ 303-481
MCZ 231-707
BBU 182-412
MCZ 318-378
MCZ 290-743
BBU 190-204

Figure 7. Thermochronologic minimum age (fission track) and minimum date (zircon (U-Th)/He) comparison to peak temperature determined from the vitrinite reflectance (Houseknecht & Matthews, 1985). Peak temperature calculated from vitrinite reflectance using equation of Barker & Pawlewicz (1994). Geothermal gradients of 20°C/km, 30°C/km, and 40°C/km shown up to maximum temperature that the rocks reached to estimate burial depth range (km). Temperature error bars on plotted vitrinite reflectance may be used on plotted thermochronologic data because error bars not shown to aid in data presentation. X-axes are in different units of measure and correspond to each other. N = number of samples and n = number of minimum ages and minimum dates.

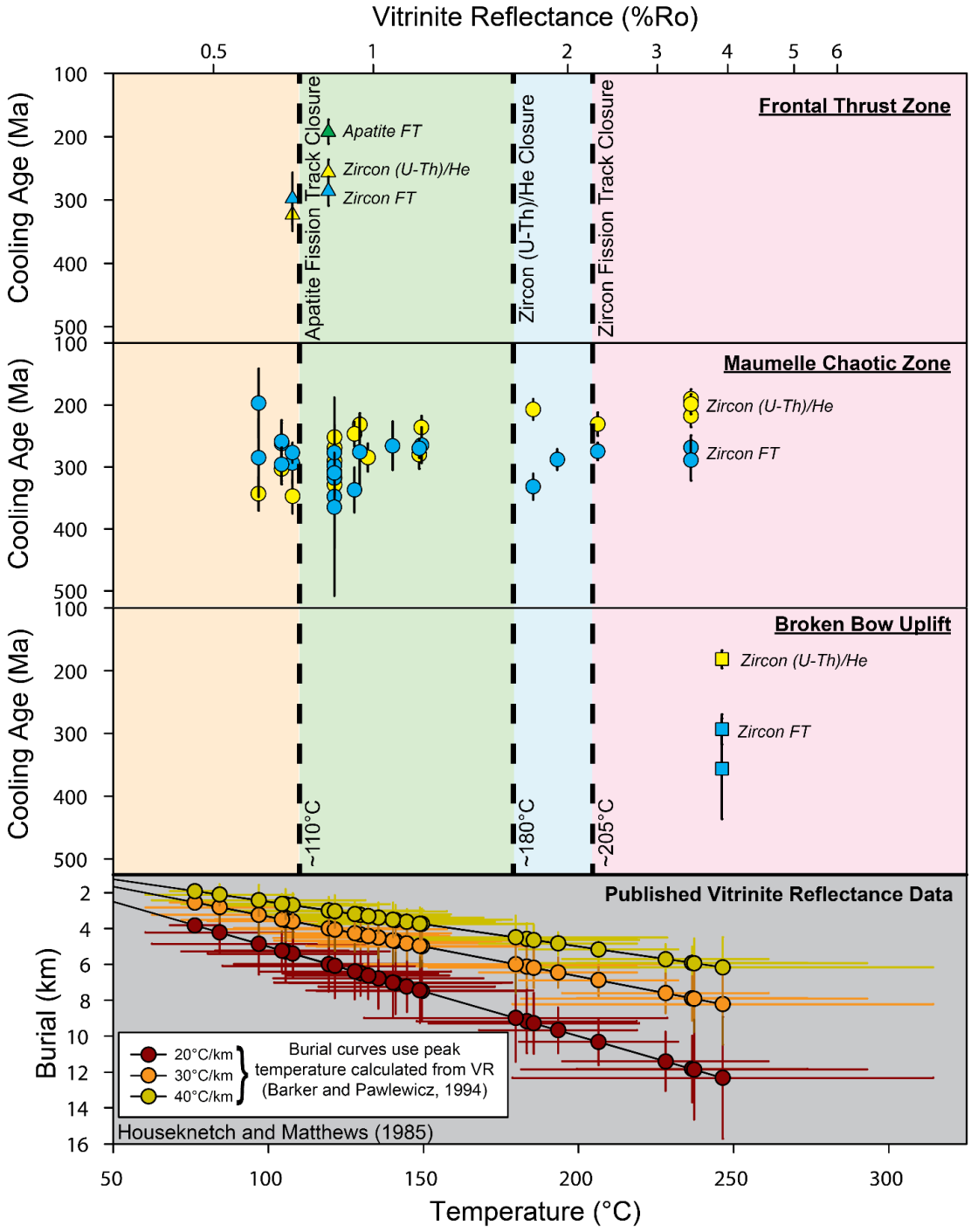
Vitrinite Reflectance (%Ro)
0.5
1
2
3
4
5
6
Cooling Age (Ma)
100
200
300
400
500
Apatite Fission Track Closure
Zircon (U-Th)/He Closure
Zircon Fission Track Closure
Frontal Thrust Zone
Apatite FT
Zircon (U-Th)/He
Zircon FT
Maumelle Chaotic Zone
Zircon (U-Th)/He
Zircon FT
Broken Bow Uplift
Zircon (U-Th)/He
Zircon FT
~110°C
~180°C
~205°C
Published Vitrinite Reflectance Data
Burial (km)
2
4
6
8
10
12
14
16
20°C/km
30°C/km
40°C/km
Burial curves use peak temperature calculated from VR (Barker and Pawlewicz, 1994)
Houseknetch and Matthews (1985)
50
100
150
200
250
300
Temperature (°C)

Figure 8. Thermochronology and thermal maturation plotted in comparison with sample elevation. Apatite fission track minimum ages (N = 14), with 1σ error, determined from reinterpreting published dates of Arne (1992) and from one new age given by OK12-9 (labeled on plot) determined by RadialPlotter software (Vermeesch, 2009). Elevation given in publication. Zircon (U-Th)/He dates (n =148), with 1σ error, are from 29 samples. Zircon fission track minimum ages (N = 50), with 1σ error, determined from 806 fission track grain dates, including dates for the Benton Uplift (Johnson, 2011). Elevation for samples in Oklahoma from global positioning system using an Xplore iX104C^4 tablet, and elevation for Benton Uplift samples provided by Johnson (2011). Vitrinite reflectance data (N = 31), with error, of southwestern Oklahoma indicate thermal maturation at the surface, where increase in %Ro is greater maturation (Houseknecht & Matthews, 1985). Elevation for each locality with vitrinite reflectance data determined with Google Earth (2018). Plotted symbols indicate structural provinces or Cretaceous intrusive rocks. All y-axes are scaled same for modern elevation in meters above sea level. Thermochronology plots (above key) use top x-axis (Ma), where vitrinite reflectance plot (below key) use bottom x-axis (%Ro). X-axes scales are different, and do not correspond to each other. N = number of samples, n = number of grain ages or dates.

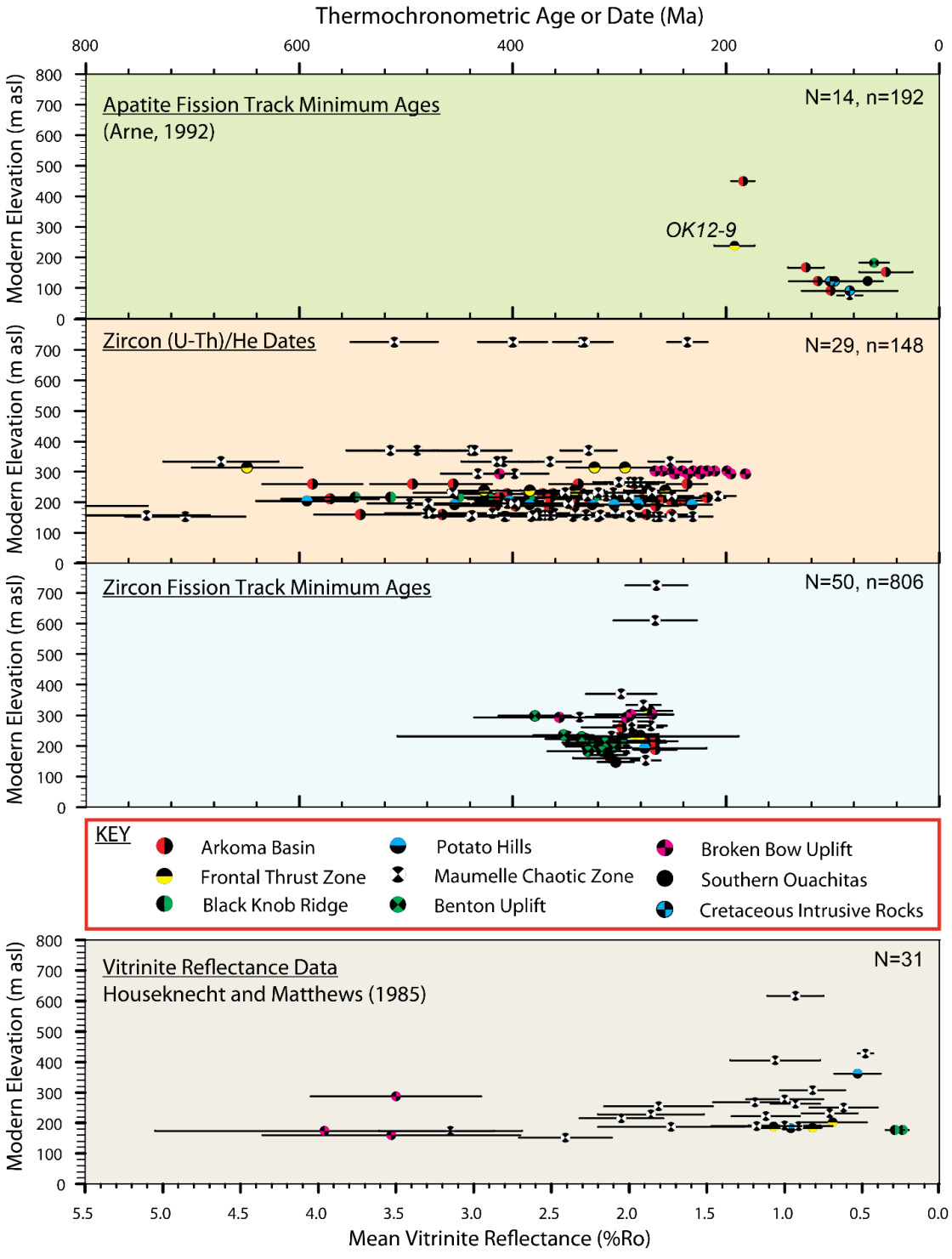
Thermochronometric Age or Date (Ma)
800
600
400
200
0
Modern Elevation (m asl)
Apatite Fission Track Minimum Ages
(Arne, 1992)
N=14, n=192
OK12-9
Zircon (U-Th)/He Dates
N=29, n=148
Zircon Fission Track Minimum Ages
N=50, n=806
KEY
Arkoma Basin
Frontal Thrust Zone
Black Knob Ridge
Potato Hills
Maumelle Chaotic Zone
Benton Uplift
Broken Bow Uplift
Southern Ouachitas
Cretaceous Intrusive Rocks
Vitrinite Reflectance Data
Houseknecht and Matthews (1985)
N=31
5.5
5.0
4.5
4.0
3.5
3.0
2.5
2.0
1.5
1.0
0.5
0.0
Mean Vitrinite Reflectance (%Ro)

Figure 9. Grain dates geochemistry and radial summary plots. (a) Uranium (ppm) of zircon grain compared to respectively fission track grain age (Ma), with 1σ error. Plotted symbols indicate structural provinces. n = number of grain ages. (b) Negative date – eU correlation of zircon (U-Th)/He dates (top plot). Lower plot compares Th/U radiometric ratios to corresponding zircon (U-Th)/He dates. (c) Radial summary plots by major provinces shown with abanico plot (i.e., kernel density estimate) on outside of logarithmic radial scale. Minimum age calculated for each province. Sample ID is approximated using the color bar. n = number of grain ages.

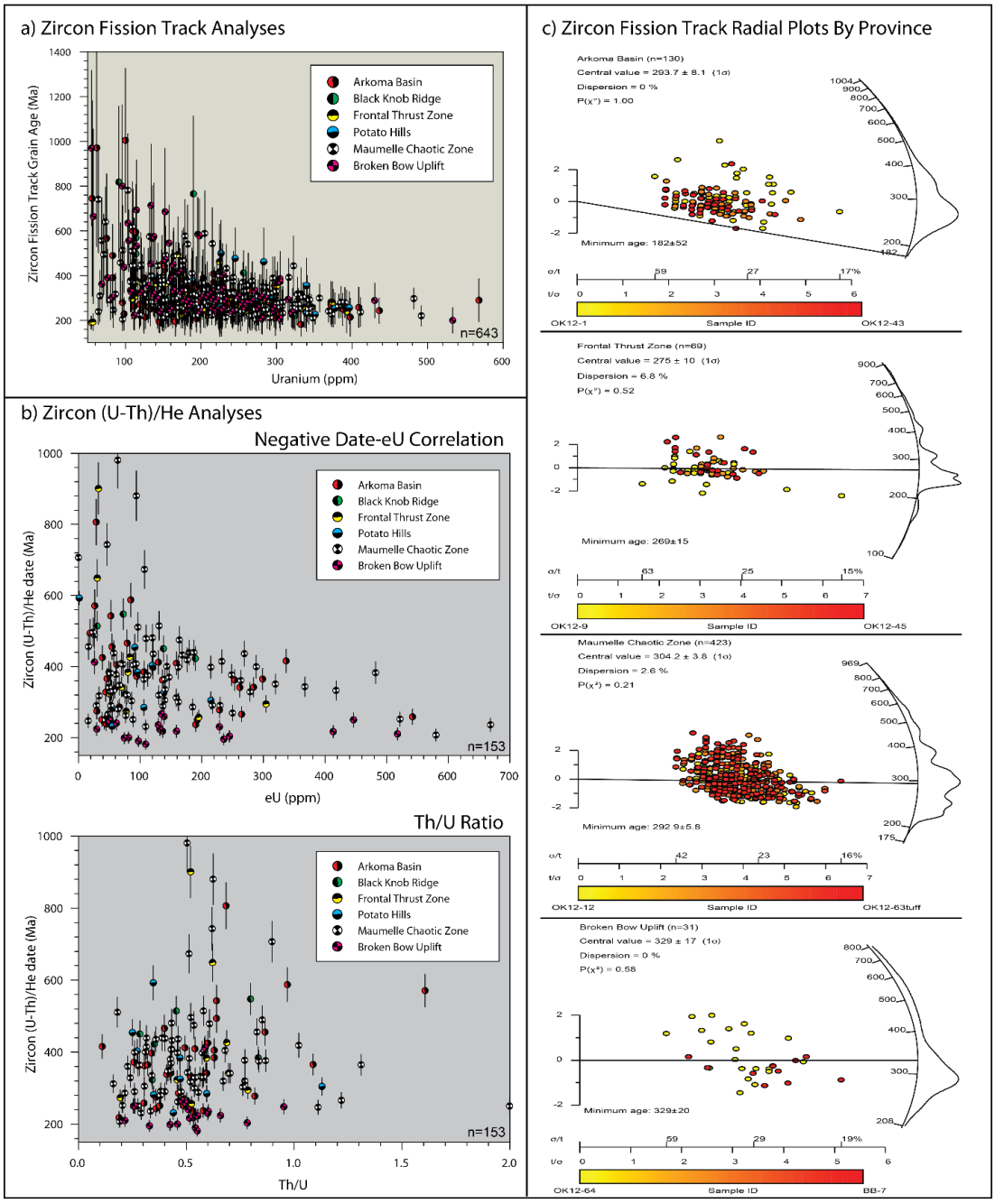
a) Zircon Fission Track Analyses
Zircon Fission Track Grain Age (Ma)
Uranium (ppm)
Arkoma Basin
Black Knob Ridge
Frontal Thrust Zone
Potato Hills
Maumelle Chaotic Zone
Broken Bow Uplift
n=643
b) Zircon (U-Th)/He Analyses
Negative Date-eU Correlation
Zircon (U-Th)/He date (Ma)
eU (ppm)
n=153
Th/U Ratio
Th/U
c) Zircon Fission Track Radial Plots By Province
Arkoma Basin (n=130)
Central value = 293.7 ± 8.1 (1σ)
Dispersion = 0 %
P(χ²) = 1.00
Minimum age: 182±52
Frontal Thrust Zone (n=69)
Central value = 275 ± 10 (1σ)
Dispersion = 6.8 %
P(χ²) = 0.52
Minimum age: 269±15
Maumelle Chaotic Zone (n=423)
Central value = 304.2 ± 3.8 (1σ)
Dispersion = 2.6 %
P(χ²) = 0.21
Minimum age: 292.9±5.8
Broken Bow Uplift (n=31)
Central value = 329 ± 17 (1σ)
Dispersion = 0 %
P(χ²) = 0.58
Minimum age: 329±20
Sample ID

Figure 10. Thermal maturation and thermochronology for the eastern traverse, Ouachita orogen, Oklahoma. Location shown by red line in the traverse index map of SE Oklahoma. Zircon (U-Th)/He dates (red filled circles) with error plotted for all of the structural provinces. Fission track minimum ages with error (see Figure 6A) plotted for zircon (gray filled circles) and apatite (black filled circles). Gray line with italicized number indicates youngest cooling age for given thermochronometer in that structural province because there is a mix of partially reset and reset grain ages. Vitrinite reflectance data (blue filled circles) with error given for the Frontal Thrust Zone, Maumelle Chaotic Zone, and the Broken Bow Uplift (Cardott, 2013; Houseknecht & Matthews, 1985). Published cross section illustrates structural position of each sample that were collected from outcrop and corresponding stratigraphic column given in Figure 4 (Arbenz, 2008). N = number of sample ages; n = number of grain dates. Abbreviations: AR, Arkansas; BBU, Broken Bow Uplift; BKR, Black Knob Ridge; PH, Potato Hills.

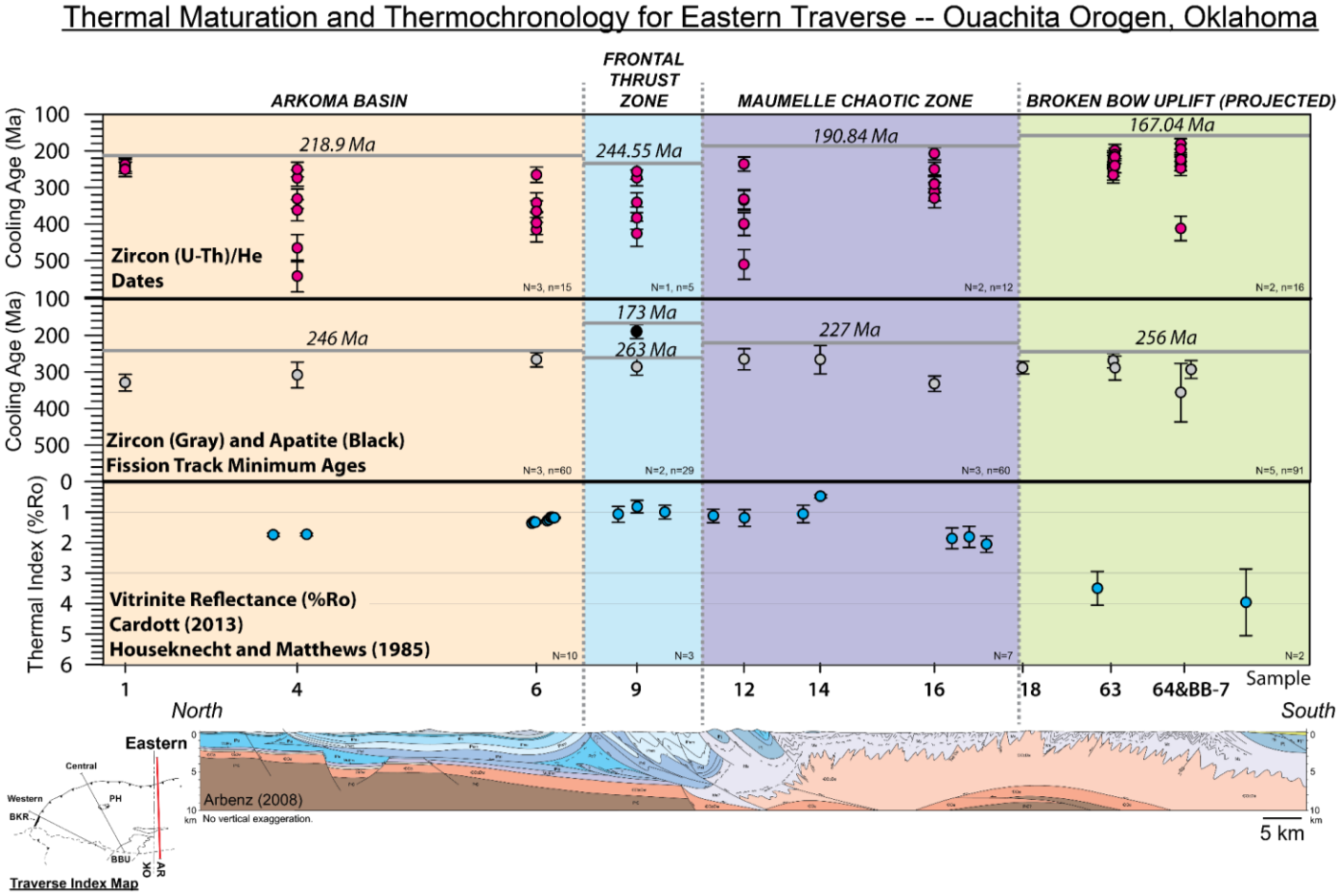
Thermal Maturation and Thermochronology for Eastern Traverse -- Ouachita Orogen, Oklahoma
ARKOMA BASIN
FRONTAL THRUST ZONE
MAUMELLE CHAOTIC ZONE
BROKEN BOW UPLIFT (PROJECTED)
Cooling Age (Ma)
Zircon (U-Th)/He Dates
218.9 Ma
244.55 Ma
190.84 Ma
167.04 Ma
N=3, n=15
N=1, n=5
N=2, n=12
N=2, n=16
Zircon (Gray) and Apatite (Black) Fission Track Minimum Ages
246 Ma
173 Ma
263 Ma
227 Ma
256 Ma
N=3, n=60
N=2, n=29
N=3, n=60
N=5, n=91
Thermal Index (%Ro)
Vitrinite Reflectance (%Ro)
Cardott (2013)
Houseknecht and Matthews (1985)
N=10
N=3
N=7
N=2
Sample
1
4
6
9
12
14
16
18
63
64&BB-7
North
South
Eastern
Central
Western
PH
BKR
BBU
OK
AR
Traverse Index Map
Arbenz (2008)
No vertical exaggeration.
km
5 km

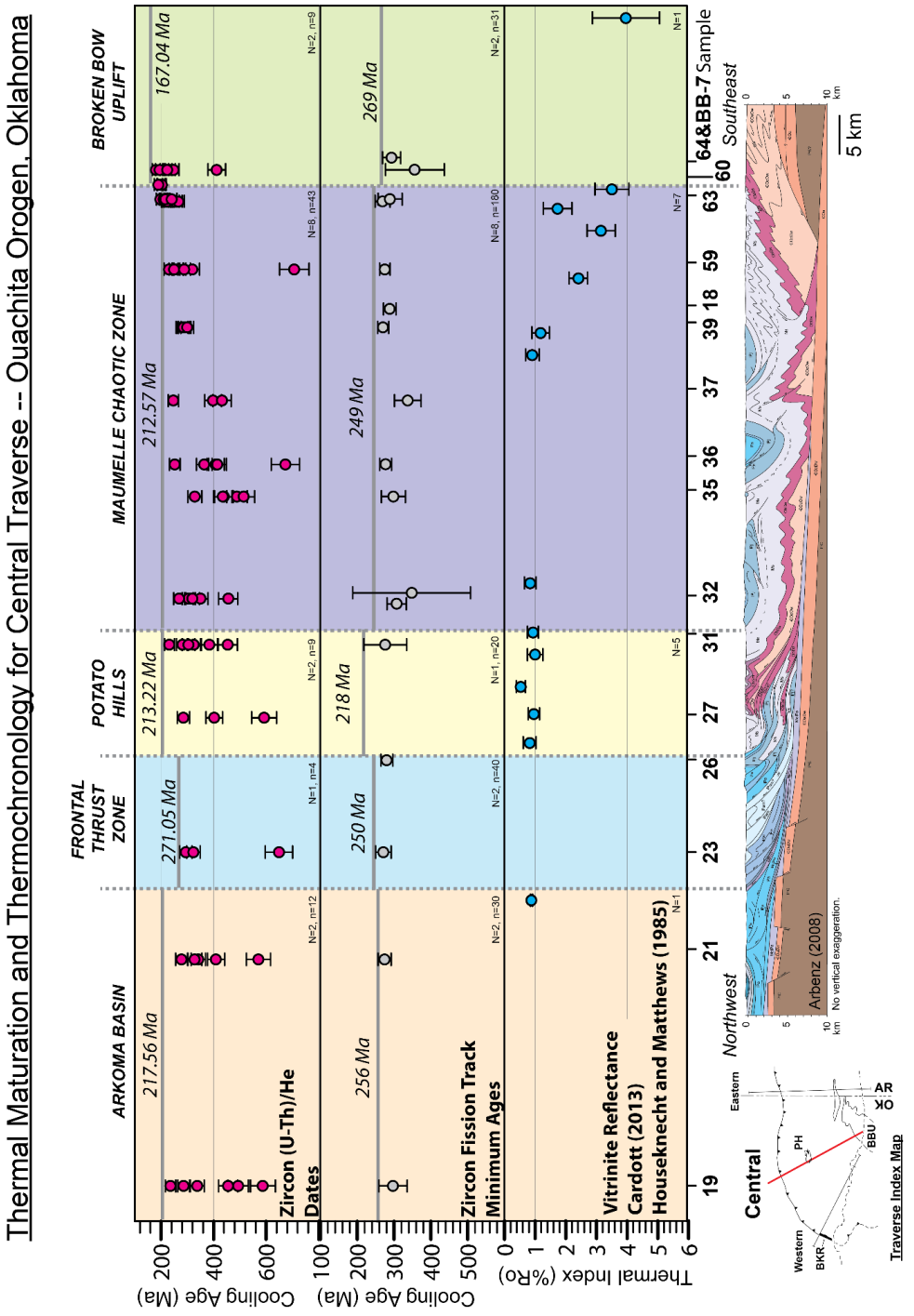

Figure 11. Thermal maturation and thermochronology for the central traverse, Ouachita orogen, Oklahoma. Location shown by red line in the traverse index map of SE Oklahoma. See Figure 9 for further explanation.

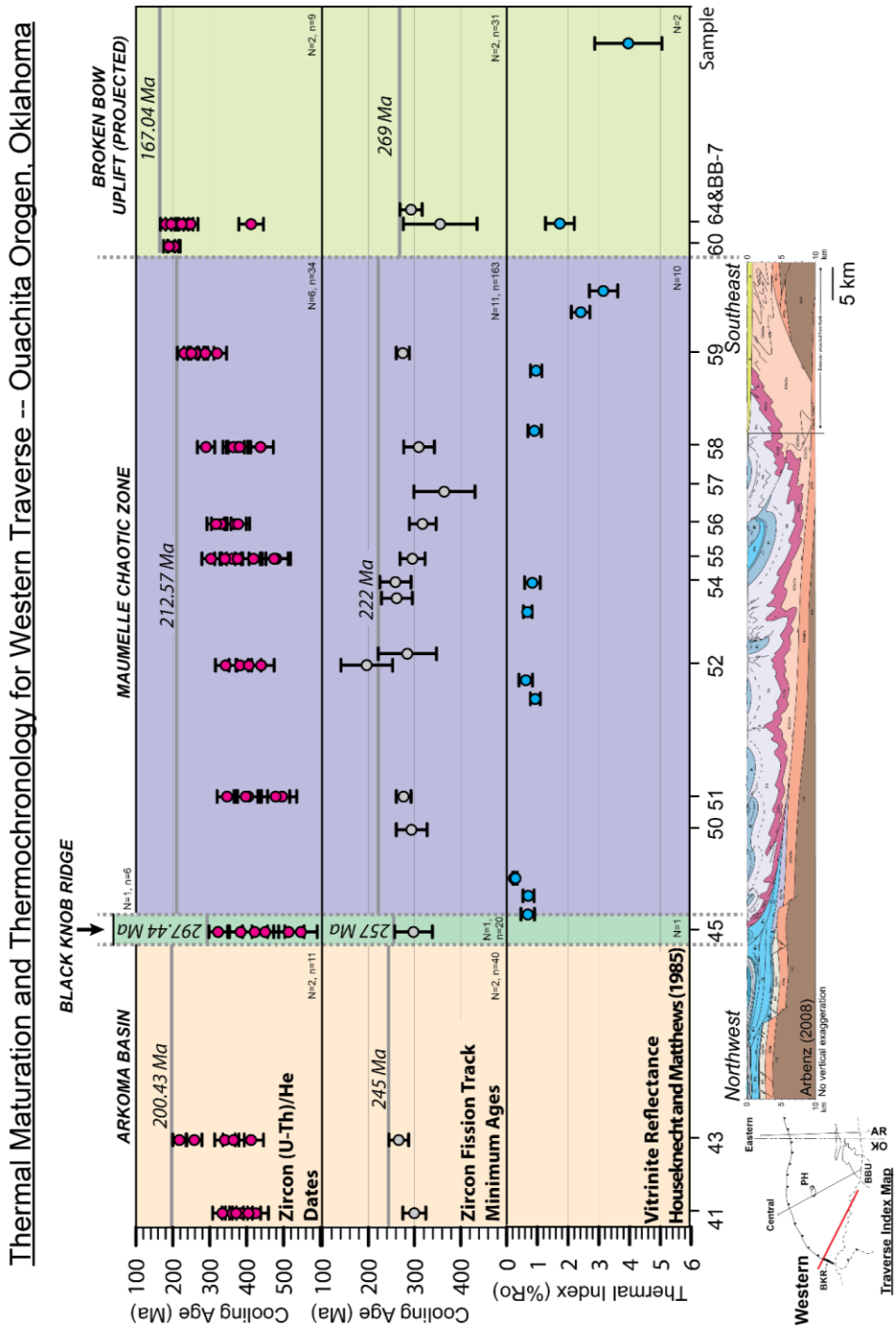

Figure 12. Thermal maturation and thermochronology for the western traverse, Ouachita orogen, Oklahoma. Location shown by red line in the traverse index map of SE Oklahoma. See Figure 9 for further explanation.

Figure 13. (a) Generalized thermal evolution diagram for the Ouachita orogen, with new thermochronologic constraints (adapted from Pevear, 1999). Base of Mississippian Stanley Group sediments (black filled circle) has assumed sediment deposition age (i.e., ~360 Ma). Burial is relatively unknown up until Late Mississippian when the sedimentation rate dramatically increased (Shaulis et al., 2012). Maximum temperature (filled red circle/black outline) based on vitrinite reflectance of ~4% R_o at base of Stanley Group that flanks the Broken Bow Uplift (see Figure 4). Zircon fission track ages from Late Pennsylvanian to Permian record the first episode of cooling, in part from thrust activity of the Ouachita orogenesis. The change in slope for the cooling pathway is steeper at first to illustrate interaction with major thrust fault activity that exhumes rocks toward surface, but the actual change of slope or position of slope change is not constrained by the thermochronologic data. Zircon (U-Th)/He dates are from Late Triassic to Middle Jurassic, which overlaps with timing of major rifting event during opening of Gulf of Mexico (GOM). Apatite fission track ages, both new and publish, have been reset in the Cretaceous (Arne, 1992). The present-day average surface temperature of ~15°C is shown by the unfilled circle outlined in red. Timing of major tectonic events as indicated by crosshatch pattern from Corrigan et al. (1998). (b) Summary diagram of cooling and denudation rates for outcrops along the Ouachita Trend (modified from Corrigan et al., 1998). Figure 2d has location of Benton Uplift (Ouachitas), Marathon Uplift, Llano Uplift, and Arbuckle Mountains. (Arne, 1992; Johnson 2011).

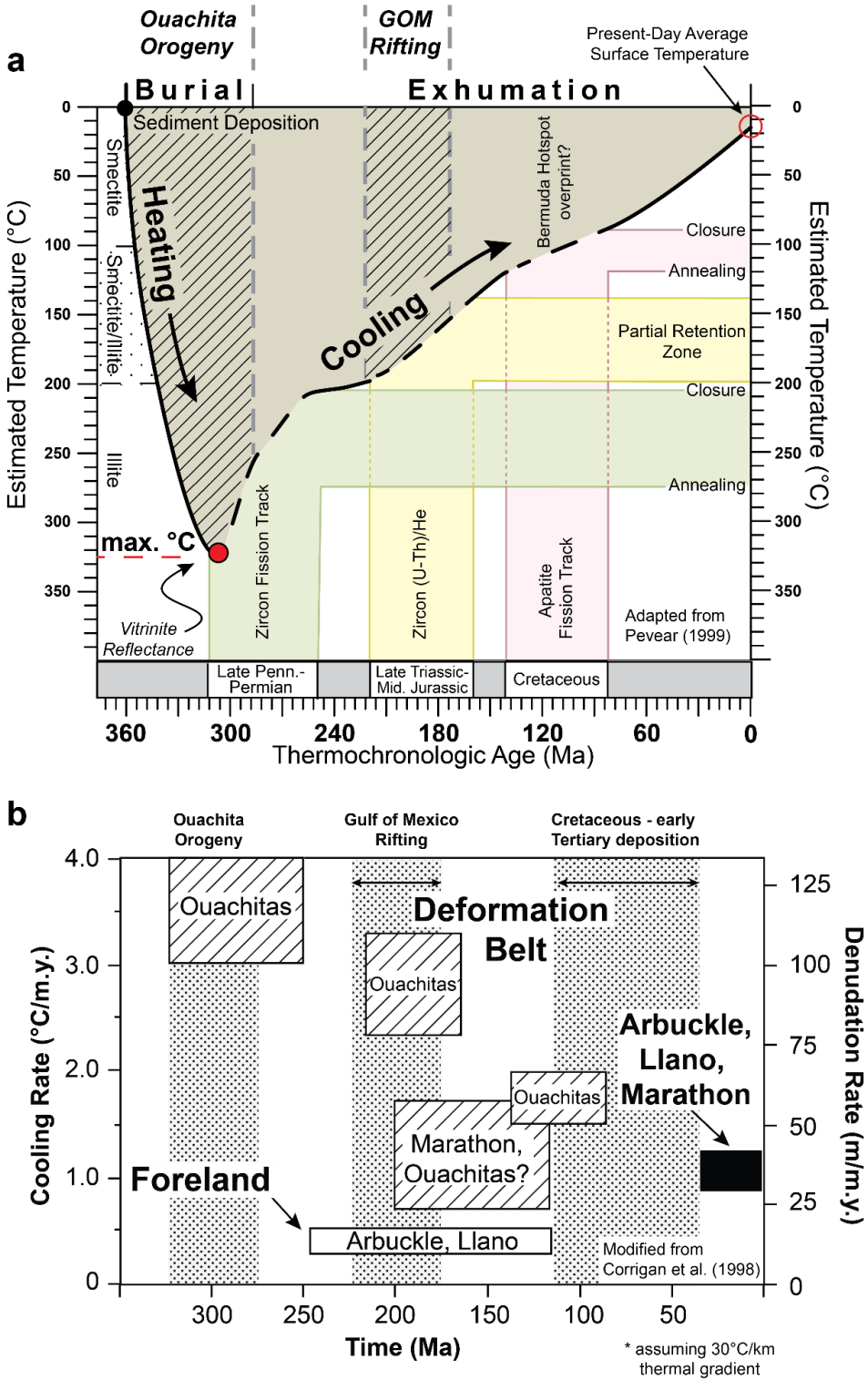
a
Ouachita Orogeny
GOM Rifting
Present-Day Average Surface Temperature
Burial
Exhumation
Sediment Deposition
Smectite
Smectite/Illite
Illite
Heating
Cooling
Bermuda Hotspot overprint?
Closure
Annealing
Partial Retention Zone
Closure
Annealing
max. °C
Vitrinite Reflectance
Zircon Fission Track
Zircon (U-Th)/He
Apatite Fission Track
Adapted from Pevear (1999)
Late Penn.-Permian
Late Triassic-Mid. Jurassic
Cretaceous
Estimated Temperature (°C)
Thermochronologic Age (Ma)
b
Ouachita Orogeny
Gulf of Mexico Rifting
Cretaceous - early Tertiary deposition
Ouachitas
Deformation Belt
Ouachitas
Arbuckle, Llano, Marathon
Ouachitas
Marathon, Ouachitas?
Foreland
Arbuckle, Llano
Modified from Corrigan et al. (1998)
Cooling Rate (°C/m.y.)
Denudation Rate (m/m.y.)
Time (Ma)
* assuming 30°C/km thermal gradient

APPENDIX F

MANUSCRIPT #3: ADDITIONAL REFERENCE MATERIAL

Introduction

The enclosed supporting information is primarily the data sets and suite of radial (abanico) plots. A complete morphological description with a representative photomicrograph of zircons for each sample is given in Table S1. Zircons in photomicrographs do not correspond to relative abundance of zircons between samples. Tables provide sample metadata, summary of fission track data, and youngest/min/peak ages as indicated in figure caption. Datasets S1-S2 are excel files with fission track data of each grain separated by sample. Dataset 3 lists (U-Th)/He aliquots by sample within sample table using a blank row to delineate each data suite.

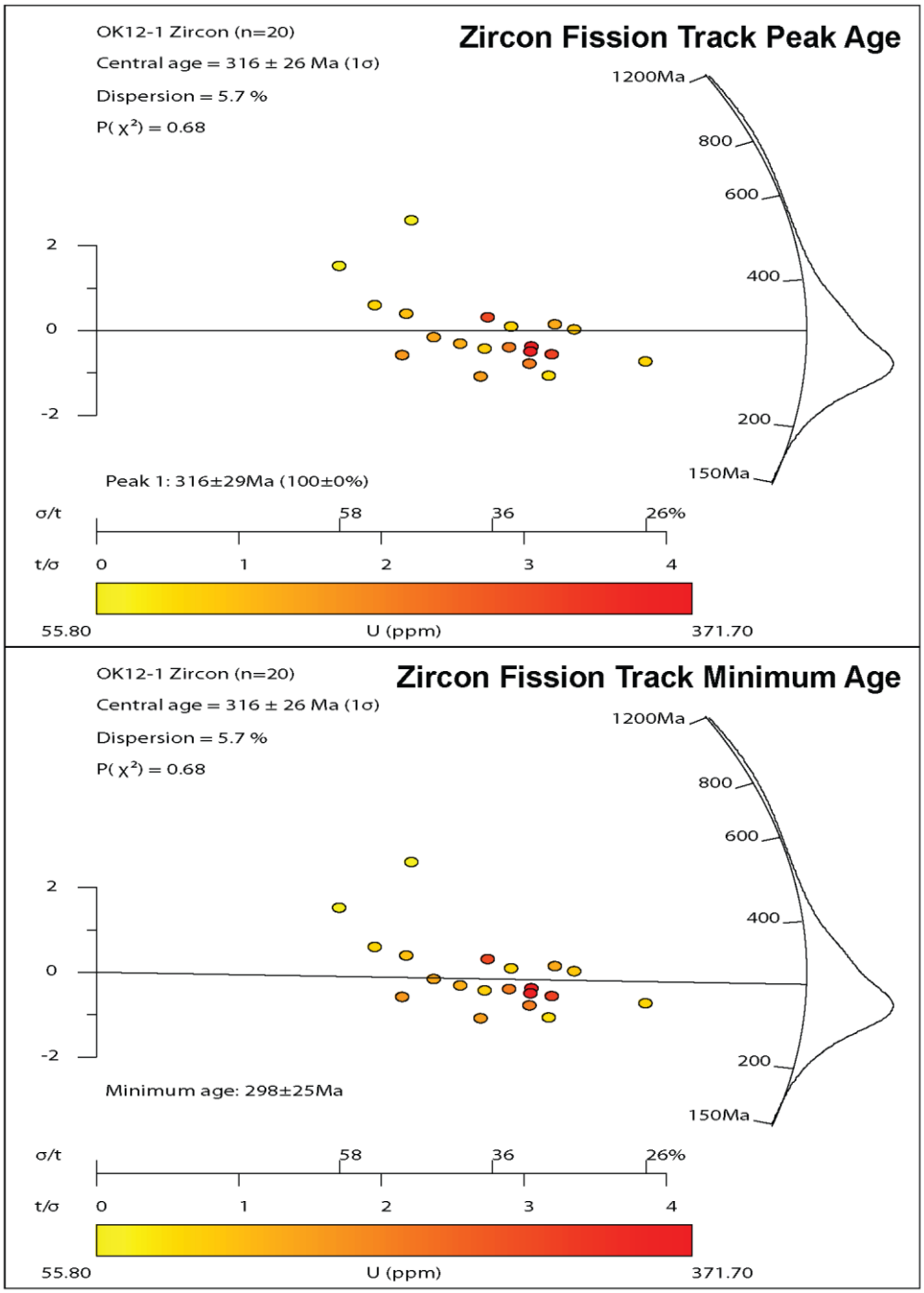

Figure S1. Radial (abanico) plots for OK12-1 zircon fission track ages: peak and minimum. Uranium (ppm) for each grain indicated by color scale, where yellow is lower U and red is higher U.

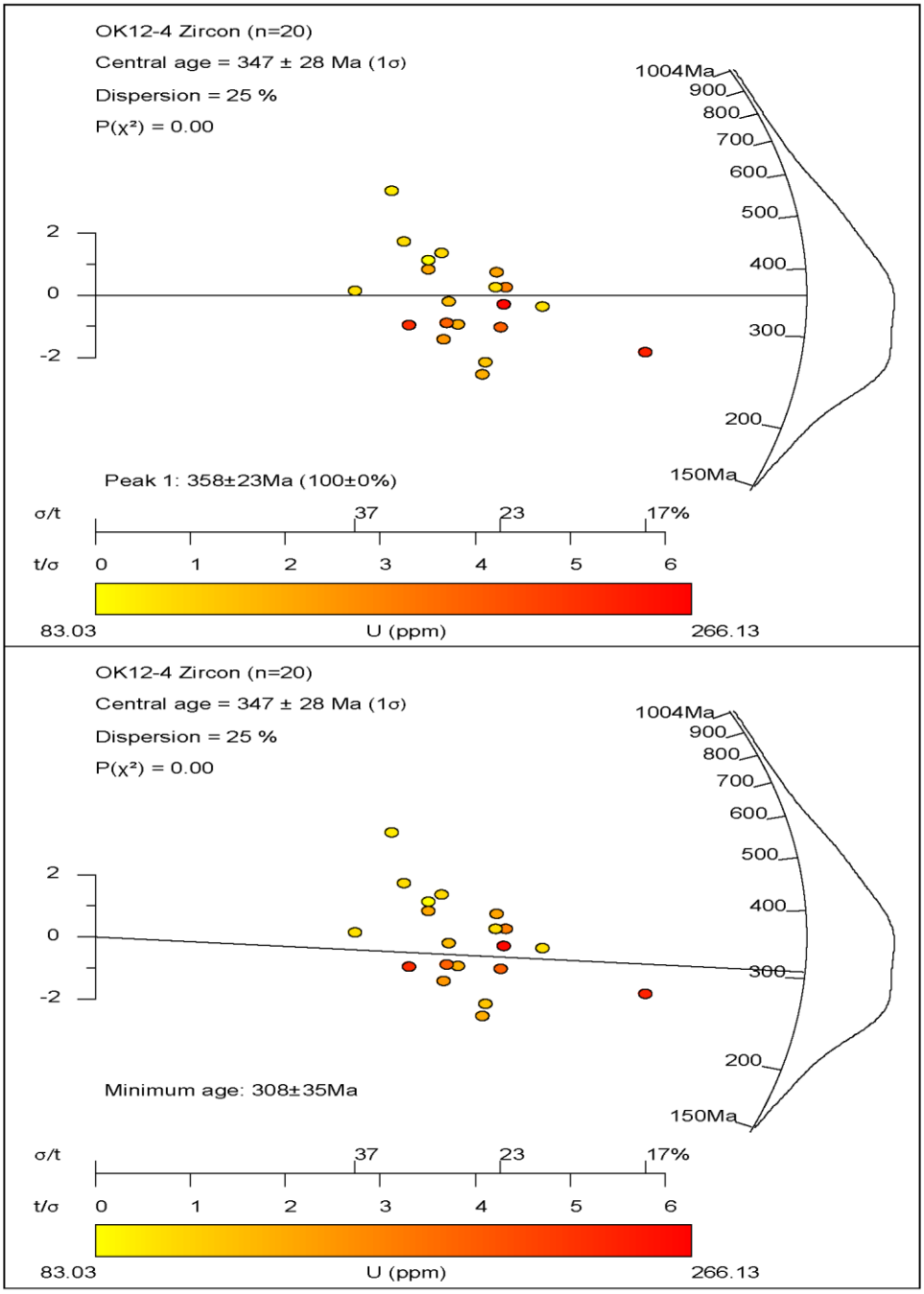

Figure S2. Radial (abanico) plots for OK12-4 zircon fission track ages: peak and minimum. Uranium (ppm) for each grain indicated by color scale, where yellow is lower U and red is higher U.

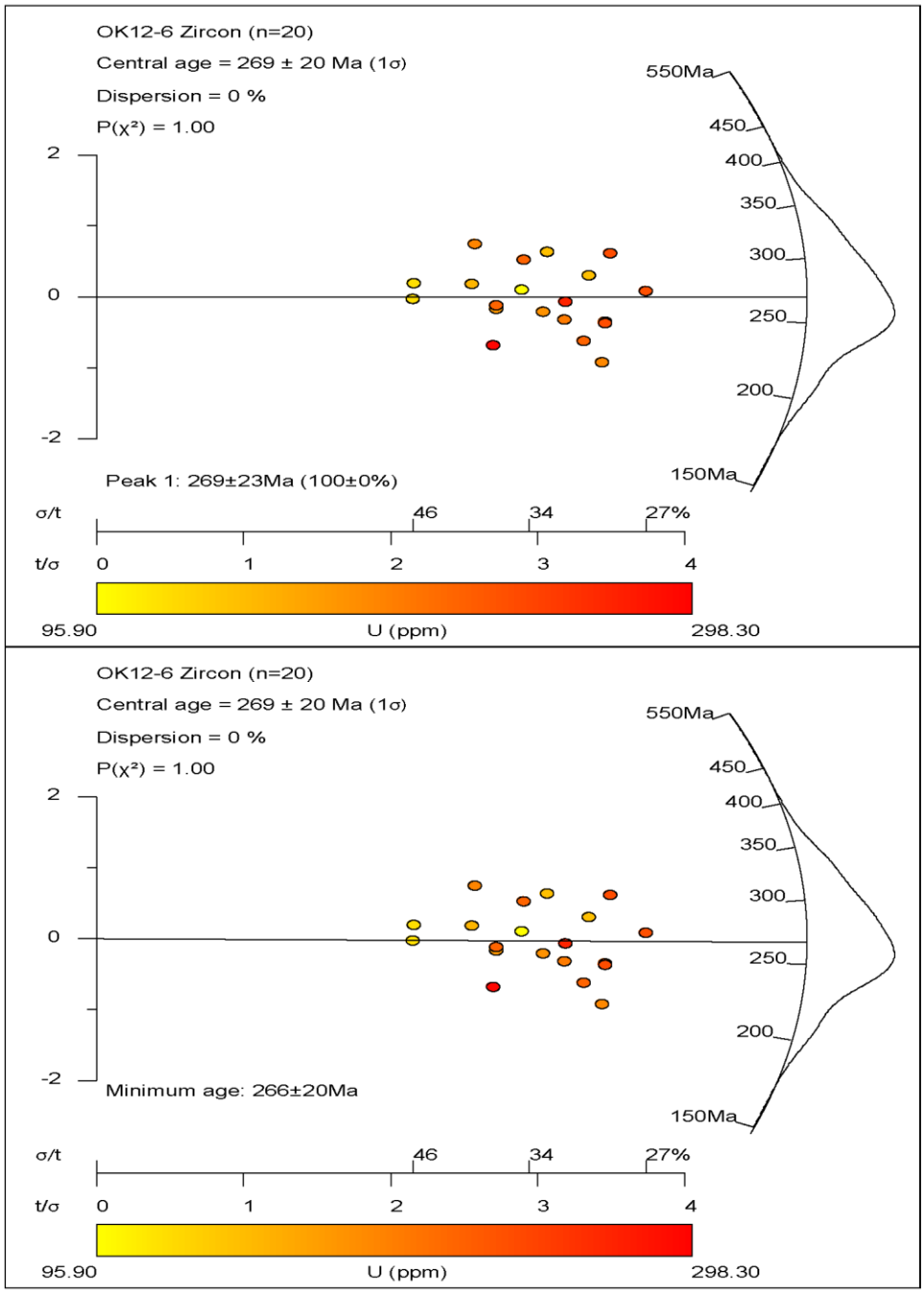

Figure S3. Radial (abanico) plots for OK12-6 zircon fission track ages: peak and minimum. Uranium (ppm) for each grain indicated by color scale, where yellow is lower U and red is higher U.

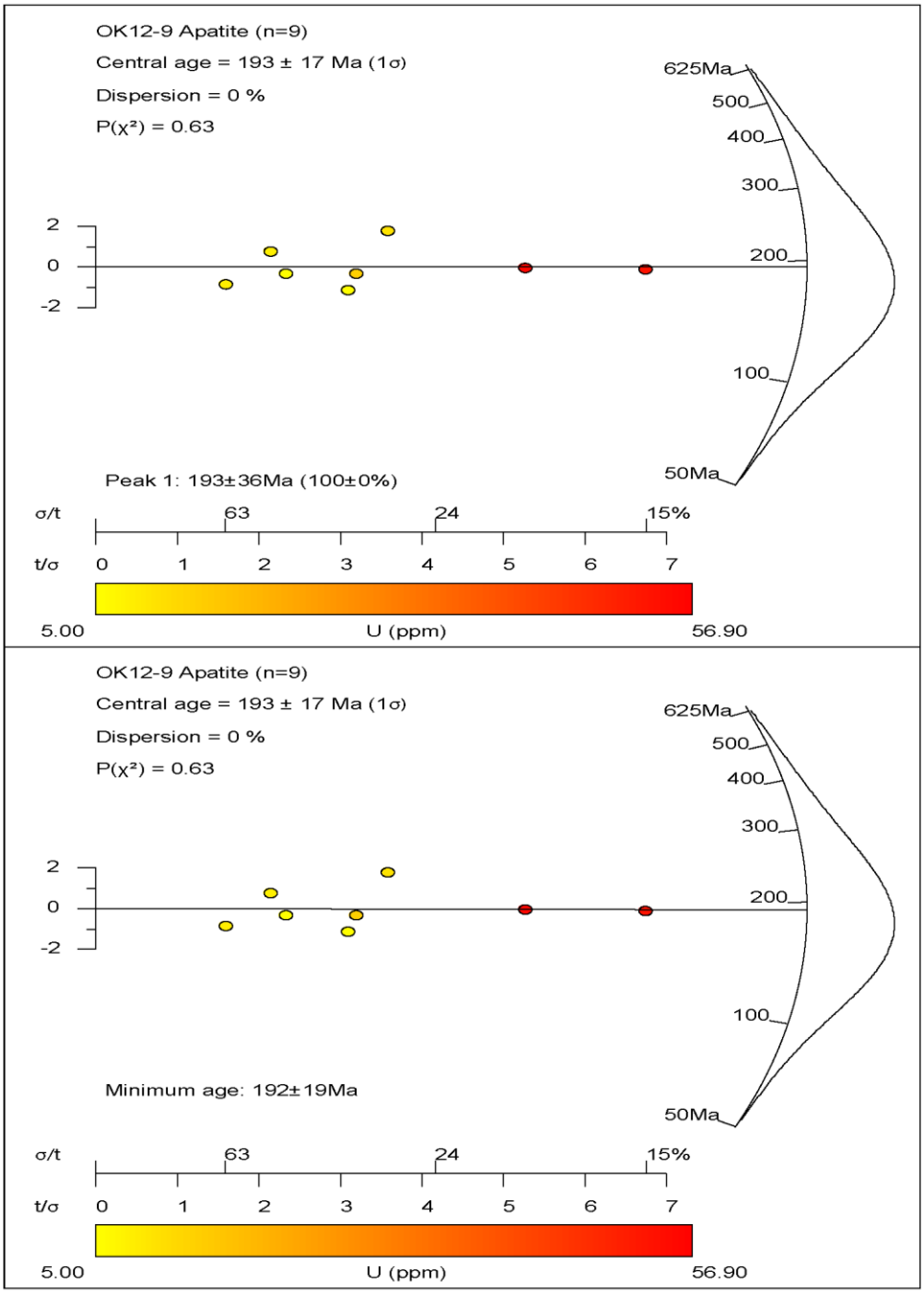

Figure S4. Radial (abanico) plots for OK12-9 apatite fission track ages: peak and minimum. Uranium (ppm) for each grain indicated by color scale, where yellow is lower U and red is higher U.

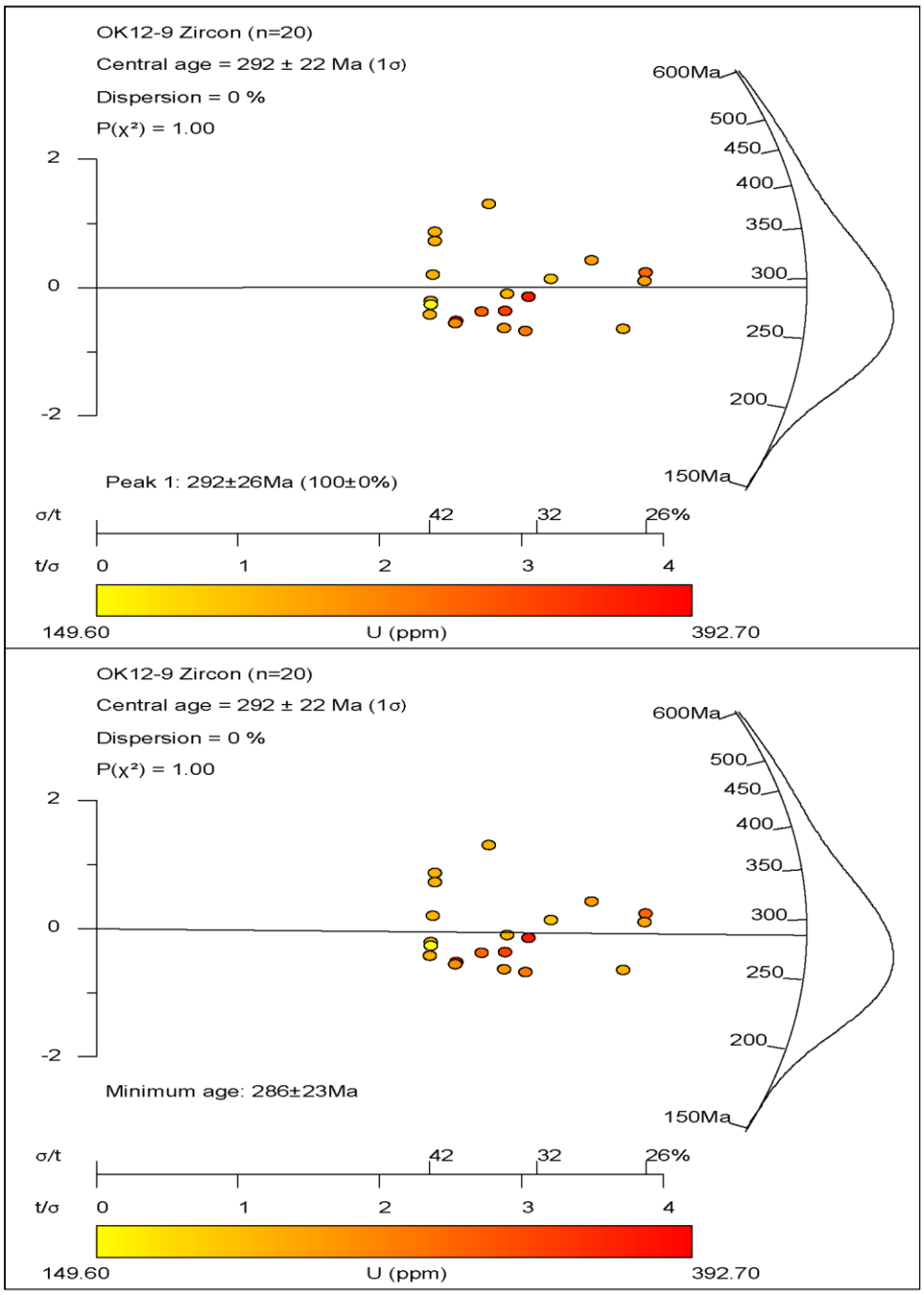

Figure S5. Radial (abanico) plots for OK12-9 zircon fission track ages: peak and minimum. Uranium (ppm) for each grain indicated by color scale, where yellow is lower U and red is higher U.

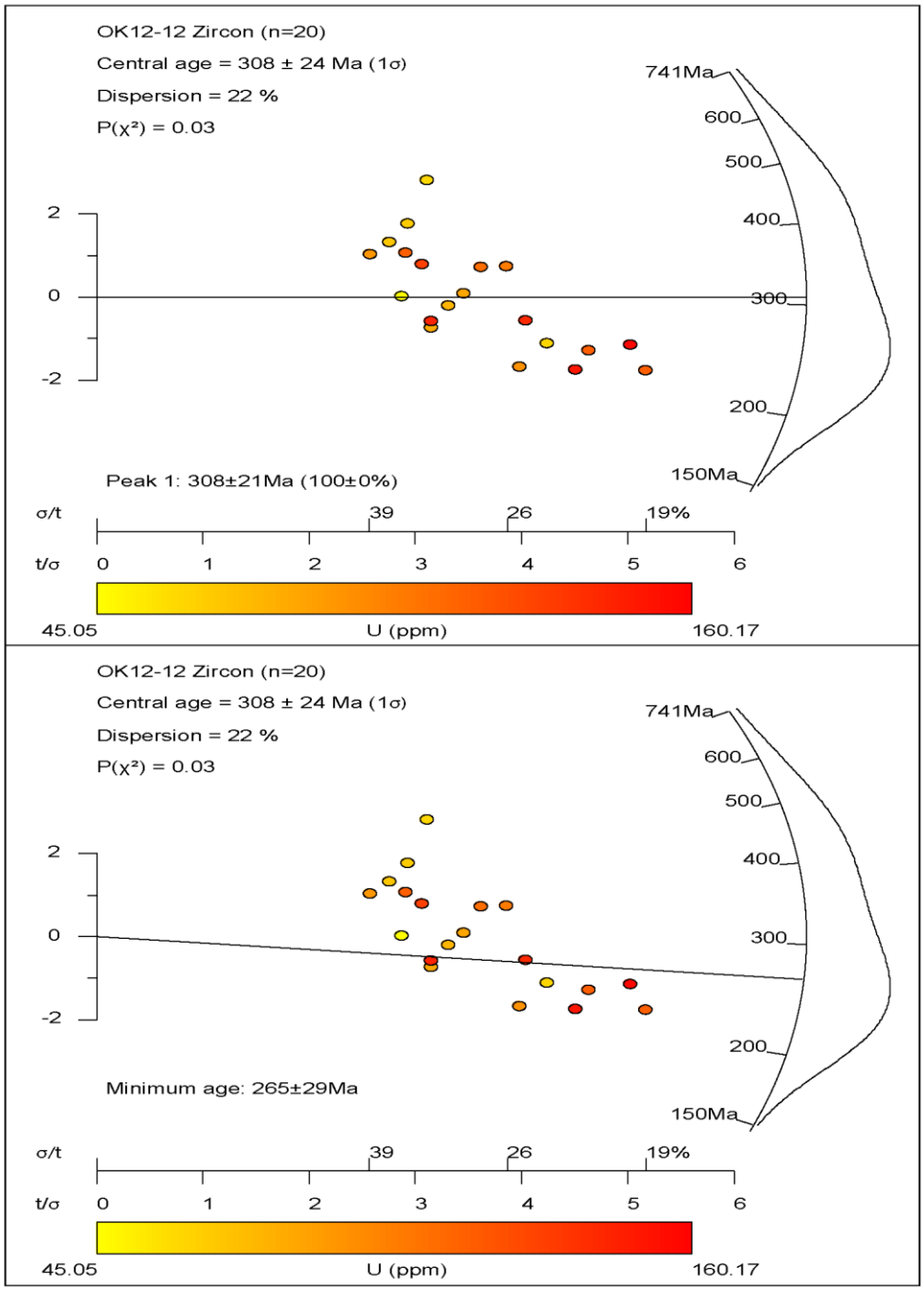

Figure S6. Radial (abanico) plots for OK12-12 zircon fission track ages: peak and minimum. Uranium (ppm) for each grain indicated by color scale, where yellow is lower U and red is higher U.

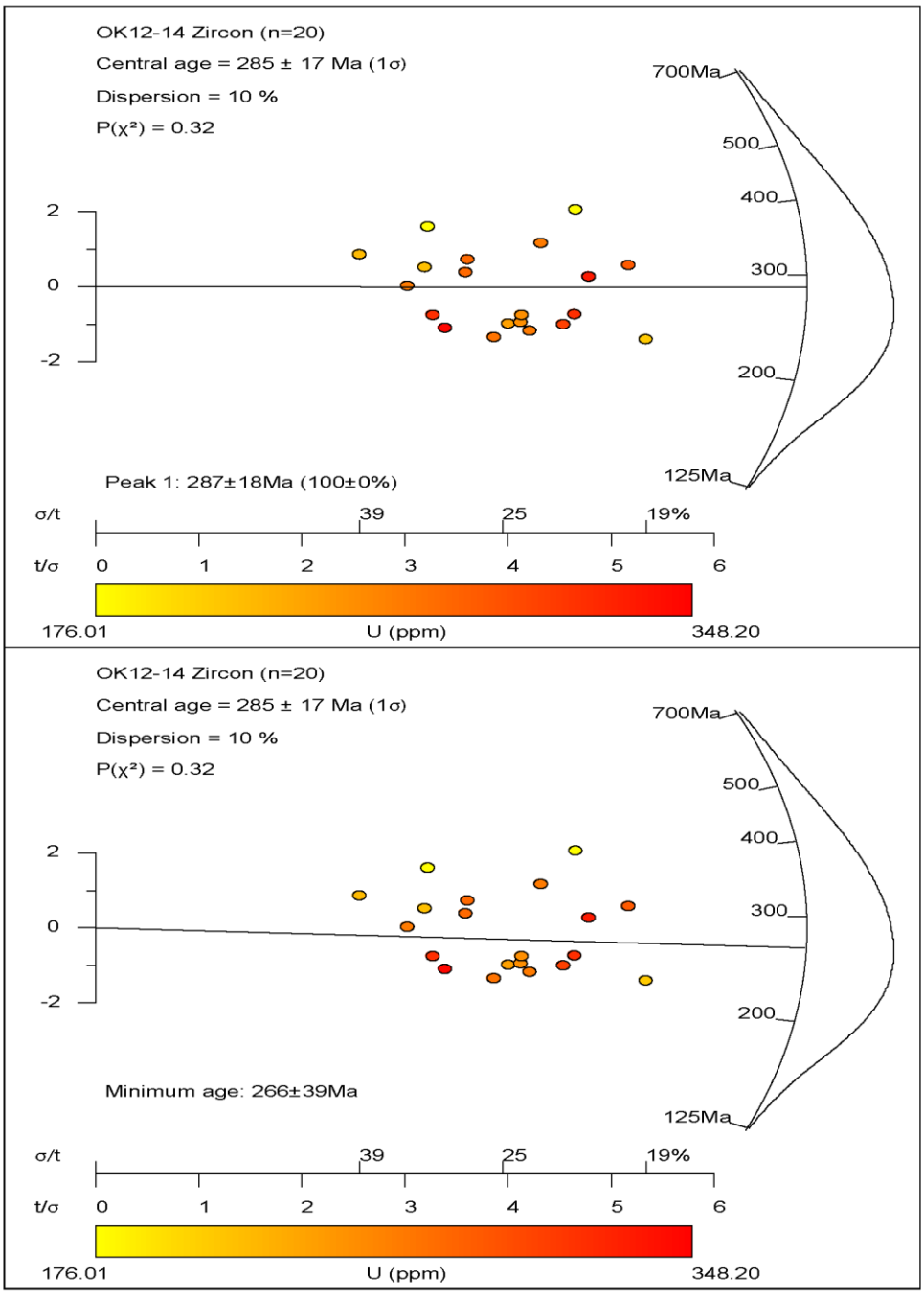

Figure S7. Radial (abanico) plots for OK12-14 zircon fission track ages: peak and minimum. Uranium (ppm) for each grain indicated by color scale, where yellow is lower U and red is higher U.

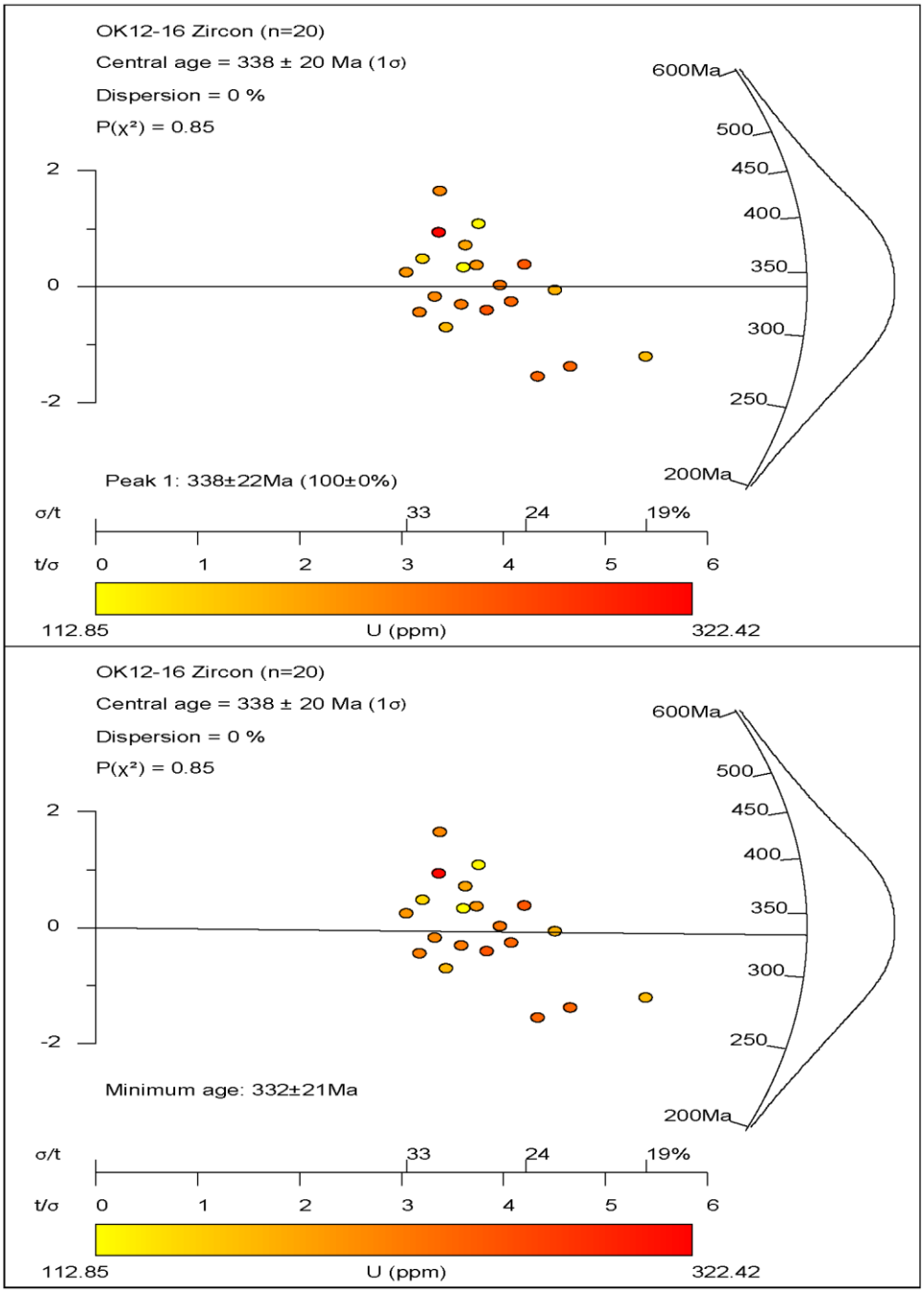

Figure S8. Radial (abanico) plots for OK12-16 zircon fission track ages: peak and minimum. Uranium (ppm) for each grain indicated by color scale, where yellow is lower U and red is higher U.

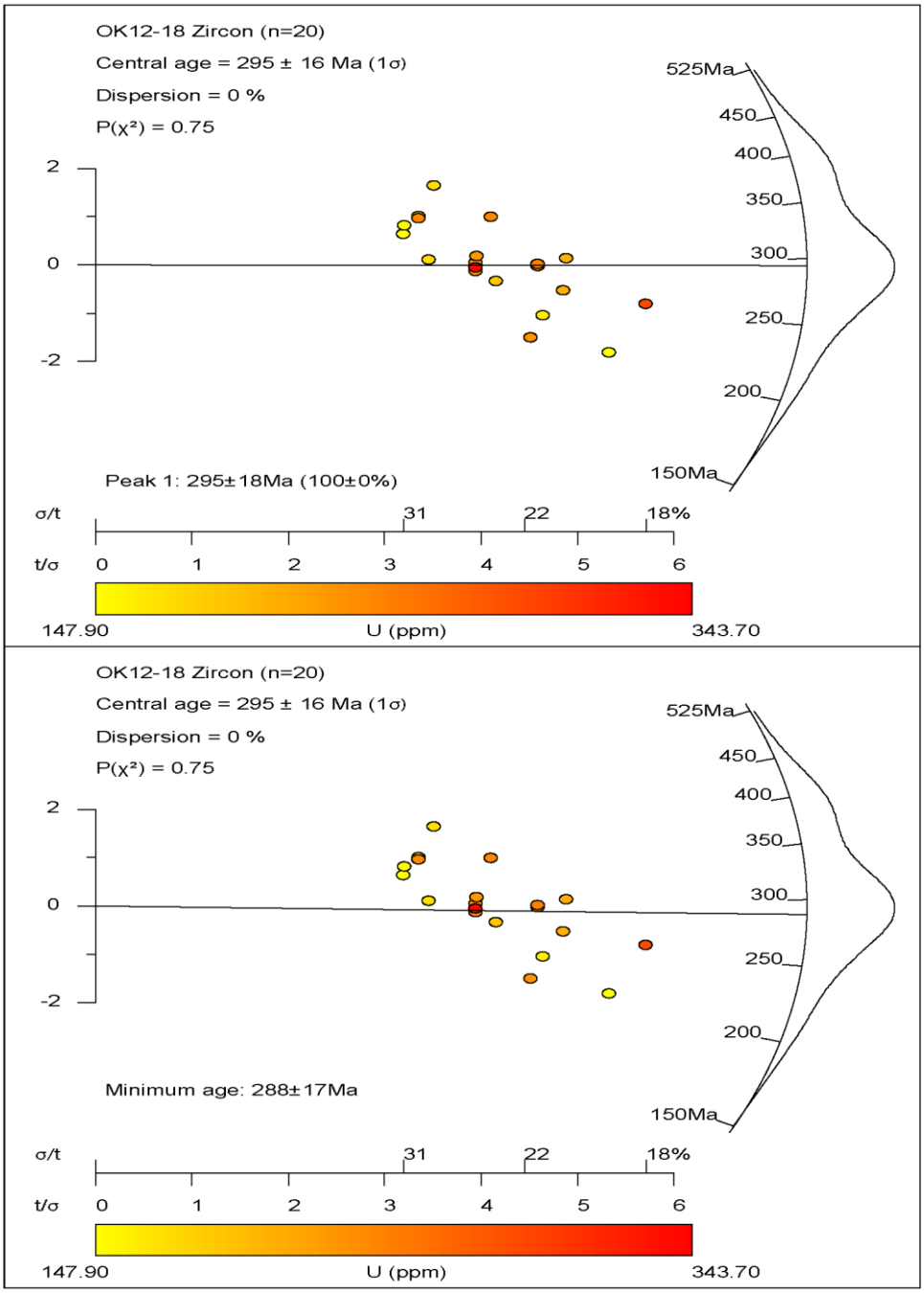

Figure S9. Radial (abanico) plots for OK12-18 zircon fission track ages: peak and minimum. Uranium (ppm) for each grain indicated by color scale, where yellow is lower U and red is higher U.

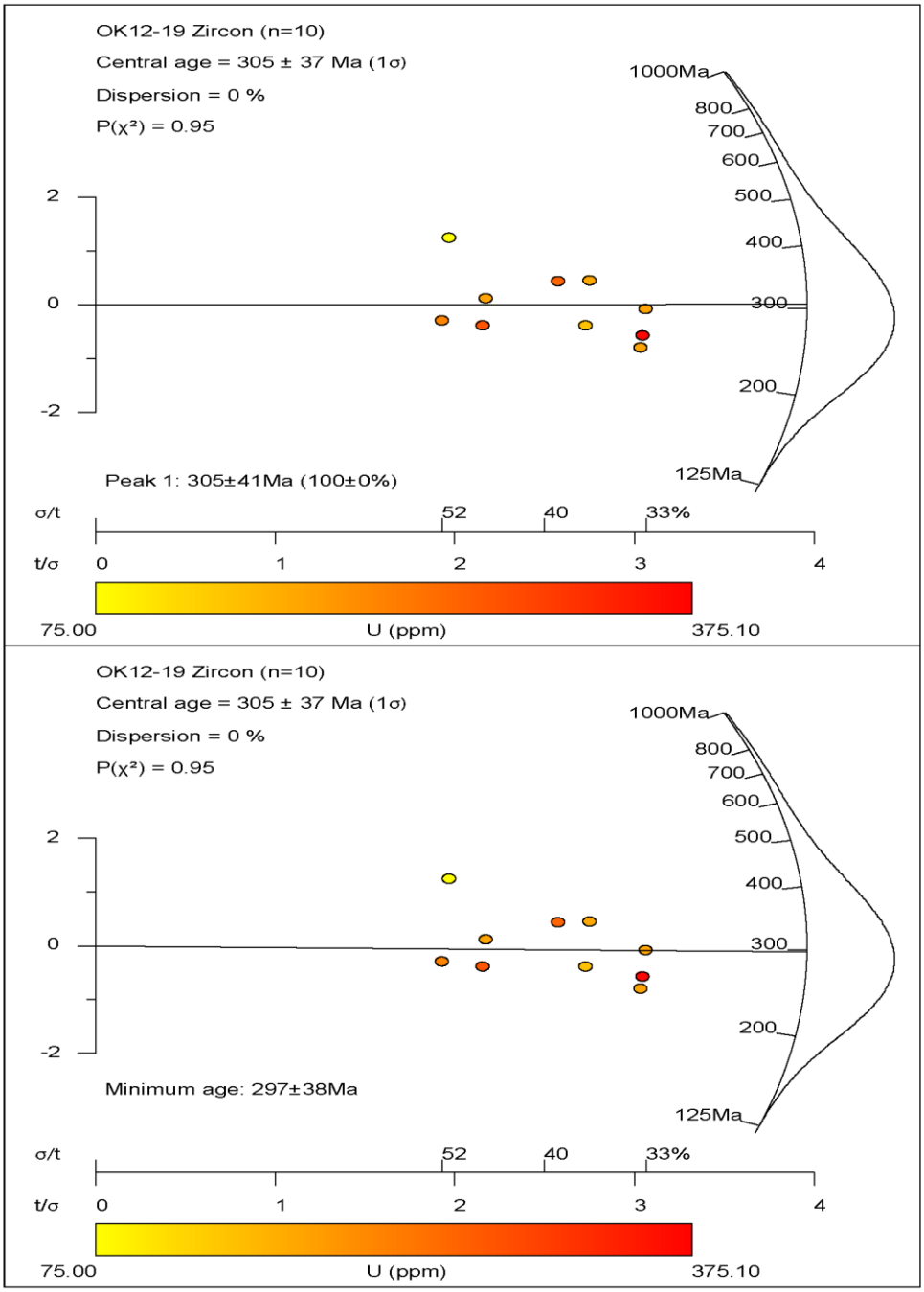

Figure S10. Radial (abanico) plots for OK12-19 zircon fission track ages: peak and minimum. Uranium (ppm) for each grain indicated by color scale, where yellow is lower U and red is higher U.

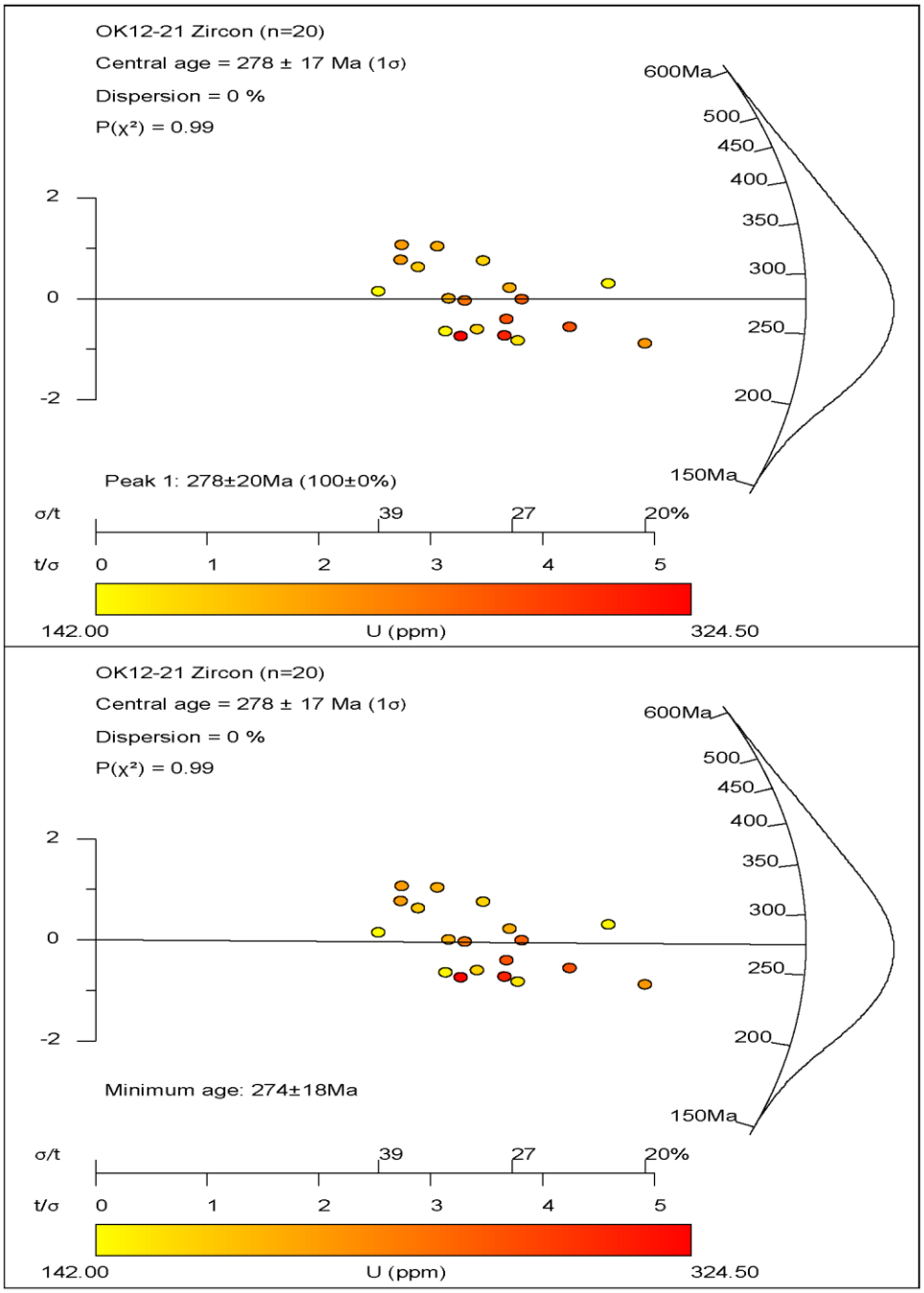

Figure S11. Radial (abanico) plots for OK12-21 zircon fission track ages: peak and minimum. Uranium (ppm) for each grain indicated by color scale, where yellow is lower U and red is higher U.

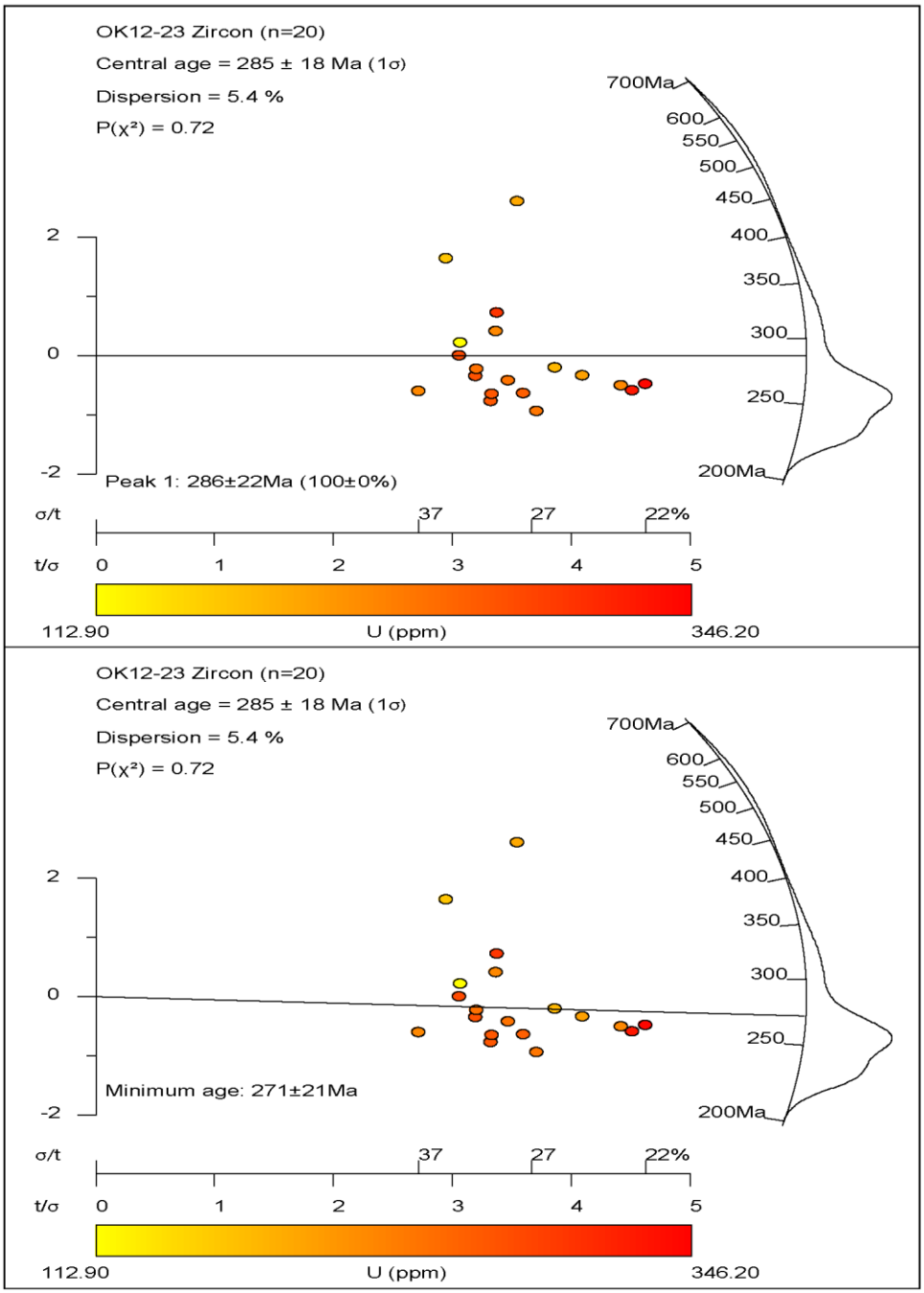

Figure S12. Radial (abanico) plots for OK12-23 zircon fission track ages: peak and minimum. Uranium (ppm) for each grain indicated by color scale, where yellow is lower U and red is higher U.

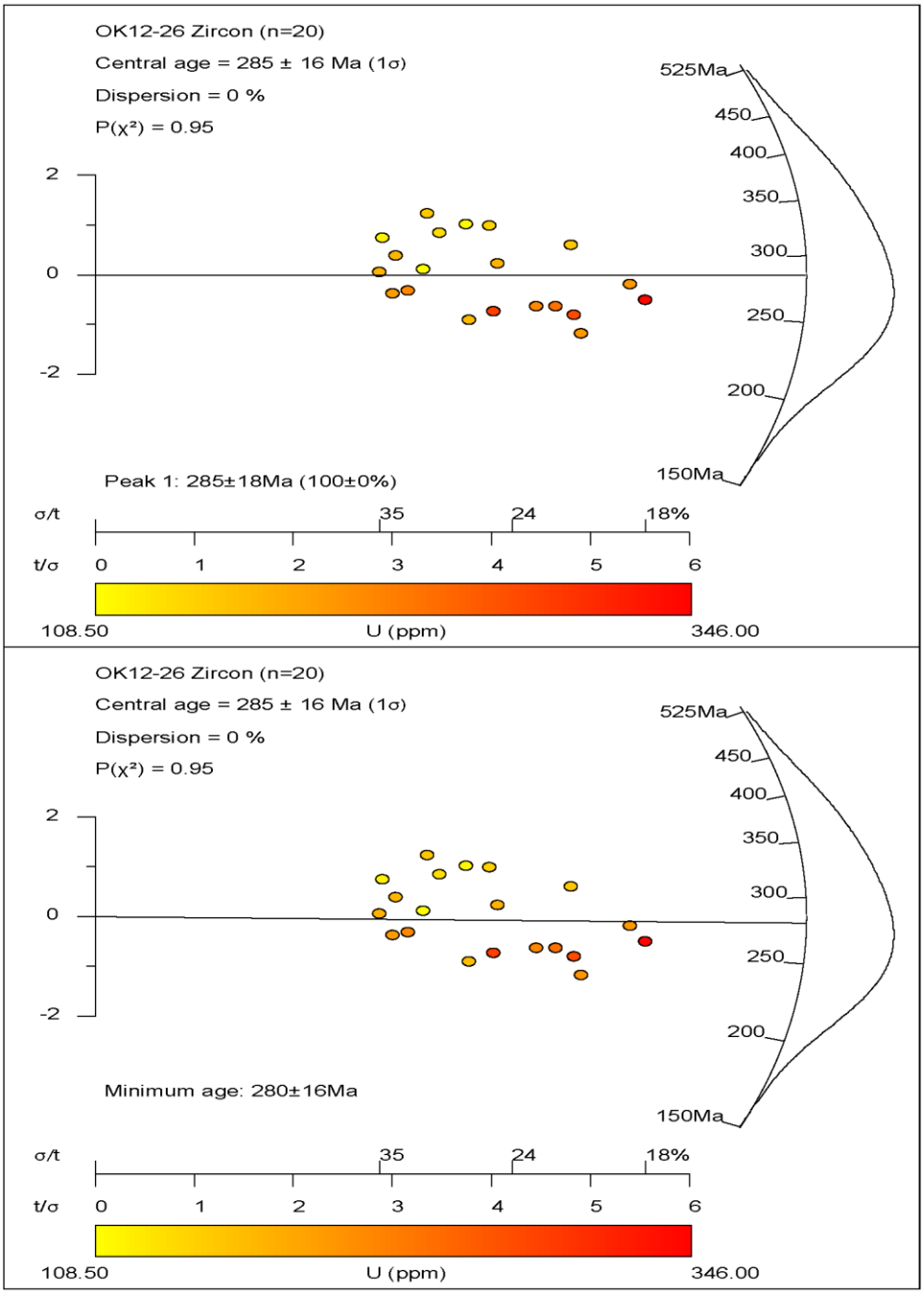

Figure S13. Radial (abanico) plots for OK12-26 zircon fission track ages: peak and minimum. Uranium (ppm) for each grain indicated by color scale, where yellow is lower U and red is higher U.

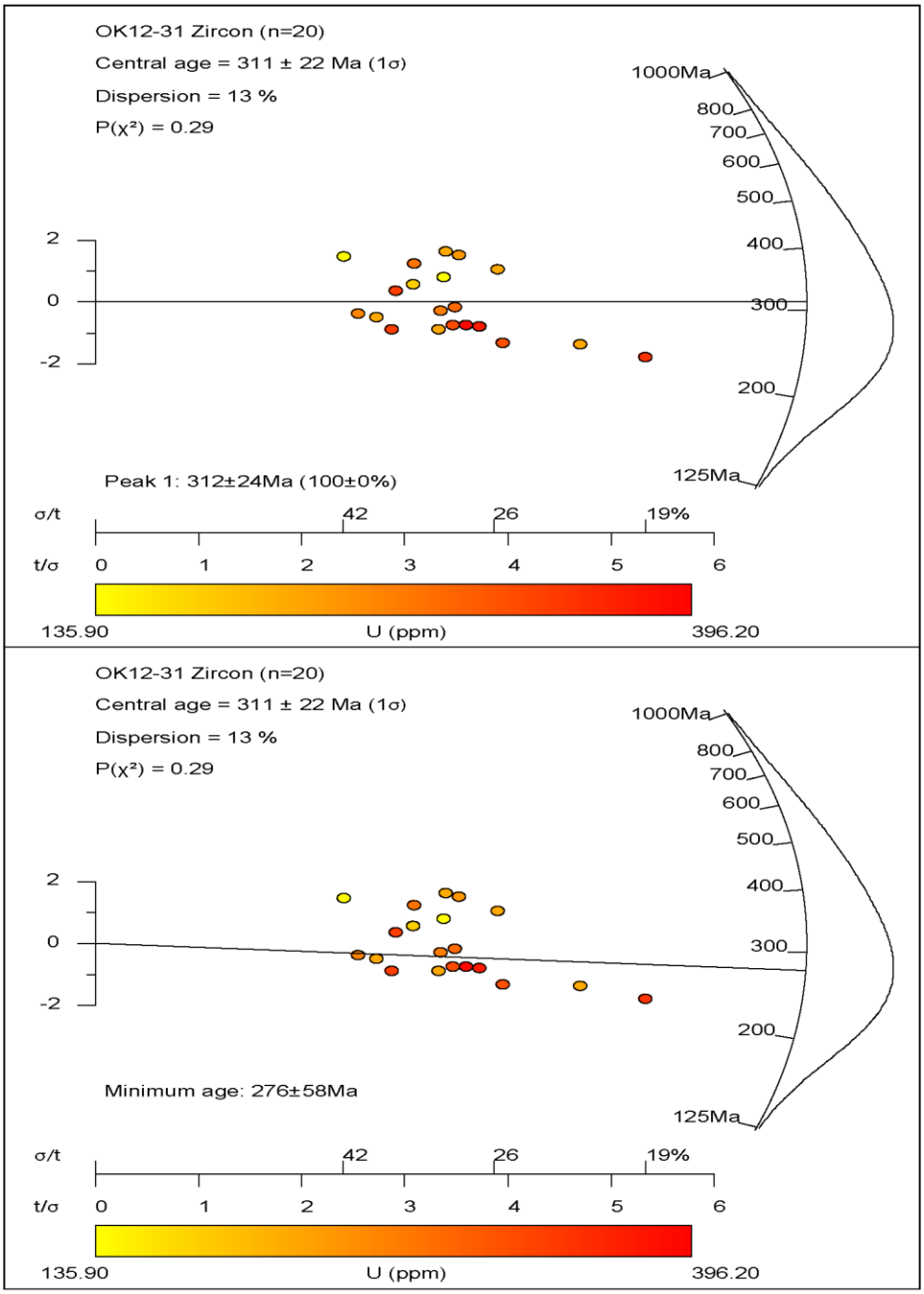

Figure S14. Radial (abanico) plots for OK12-31 zircon fission track ages: peak and minimum. Uranium (ppm) for each grain indicated by color scale, where yellow is lower U and red is higher U.

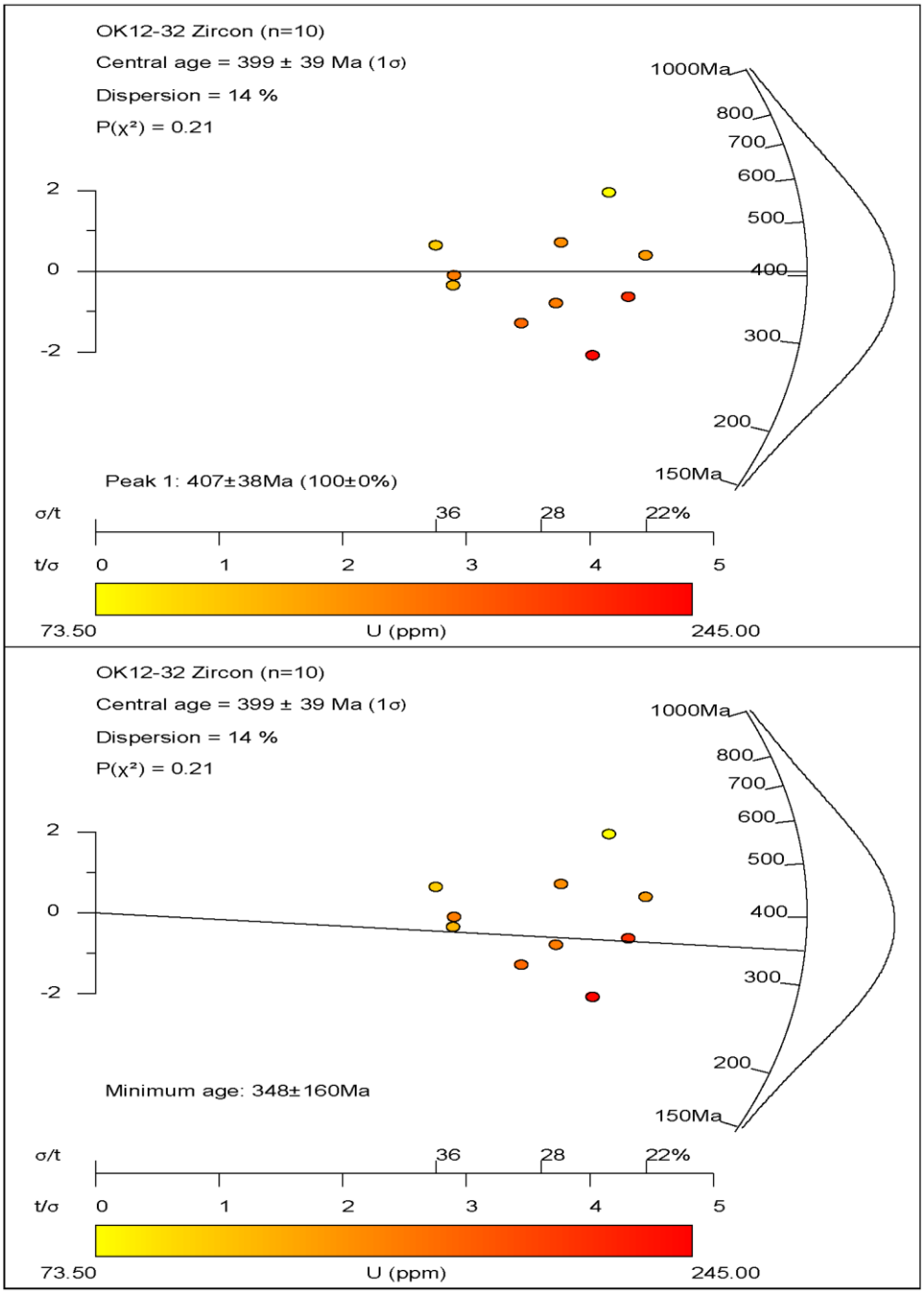

Figure S15. Radial (abanico) plots for OK12-32 zircon fission track ages: peak and minimum. Uranium (ppm) for each grain indicated by color scale, where yellow is lower U and red is higher U.

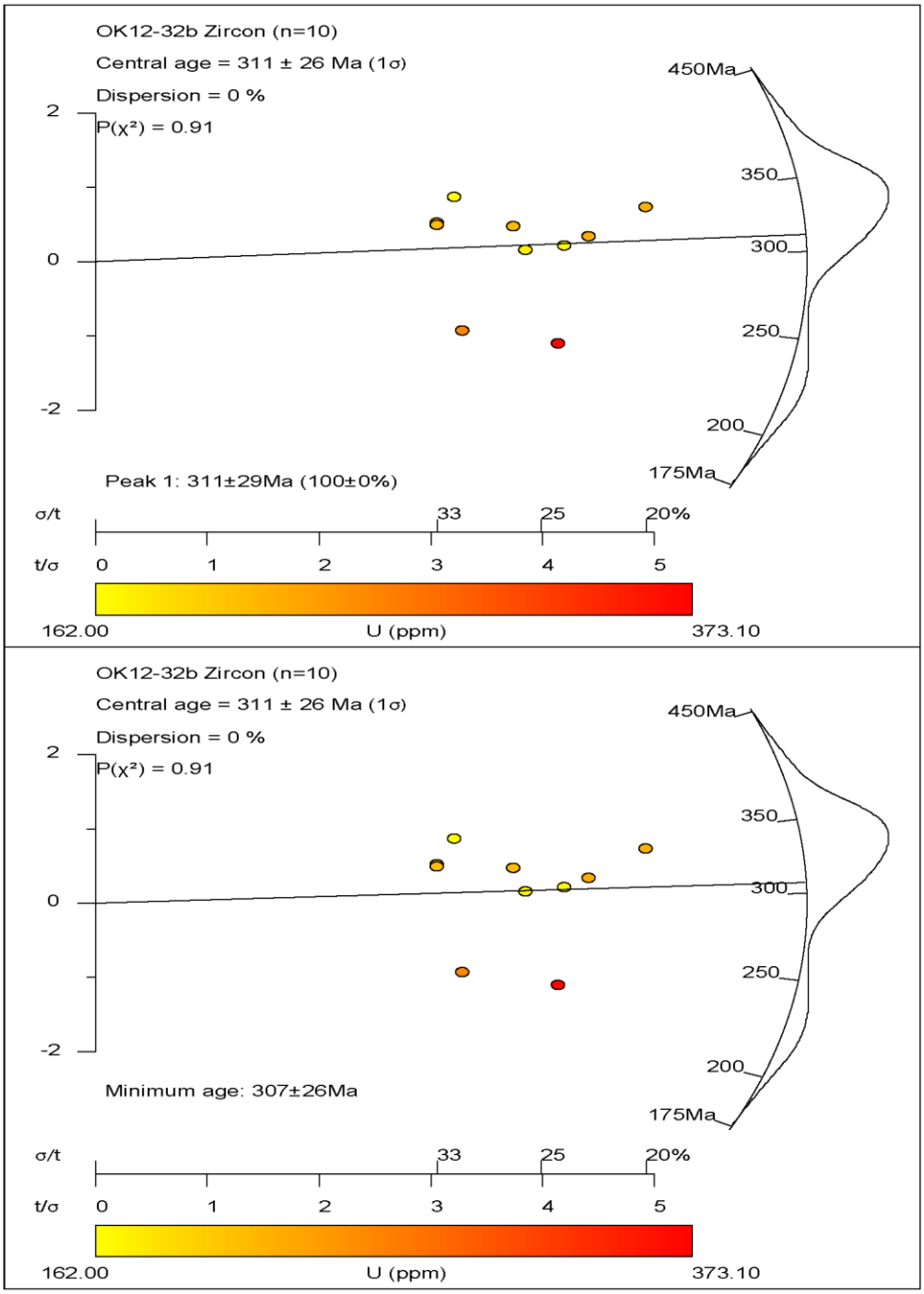

Figure S16. Radial (abanico) plots for OK12-32b zircon fission track ages: peak and minimum. Uranium (ppm) for each grain indicated by color scale, where yellow is lower U and red is higher U.

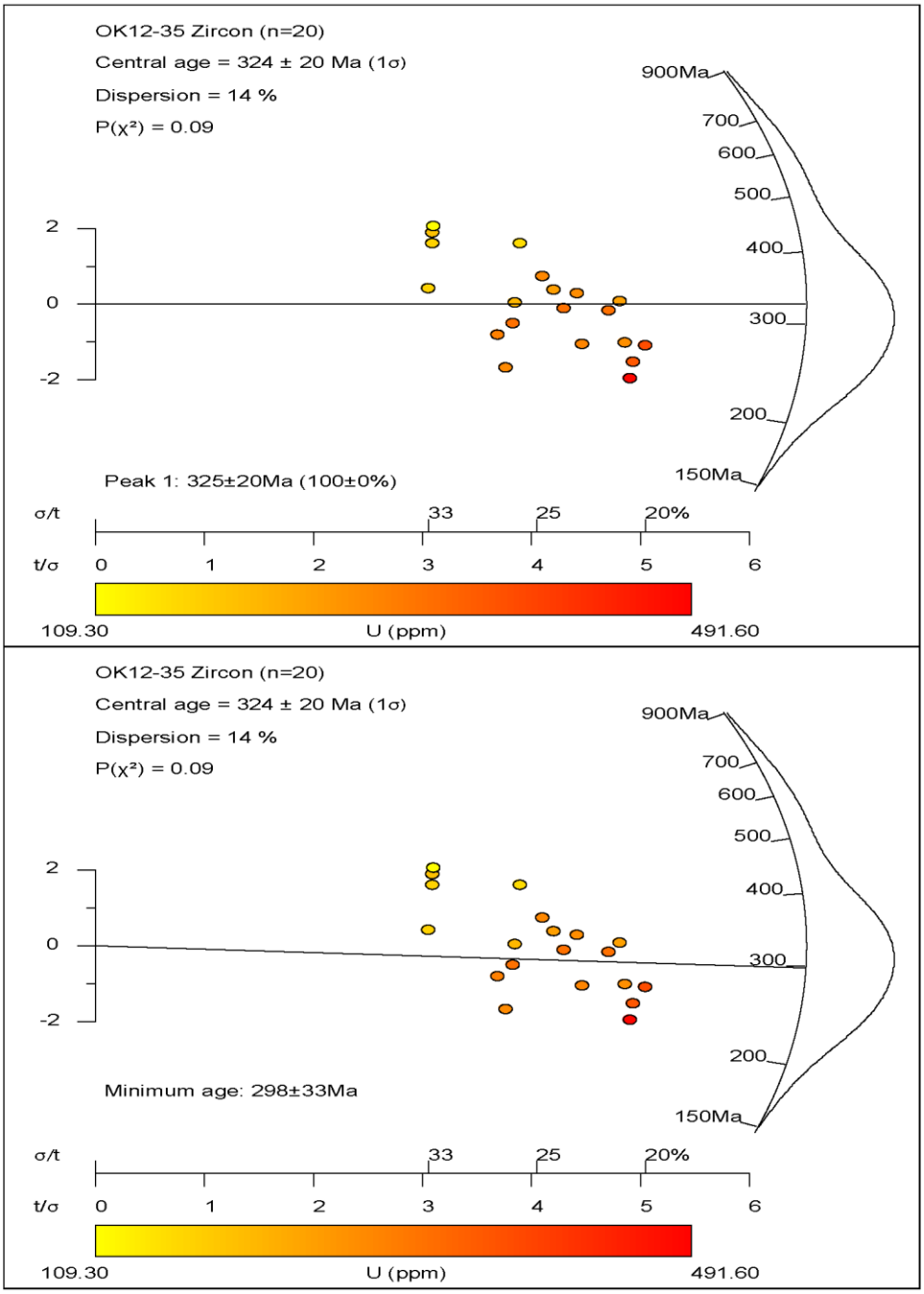

Figure S17. Radial (abanico) plots for OK12-35 zircon fission track ages: peak and minimum. Uranium (ppm) for each grain indicated by color scale, where yellow is lower U and red is higher U.

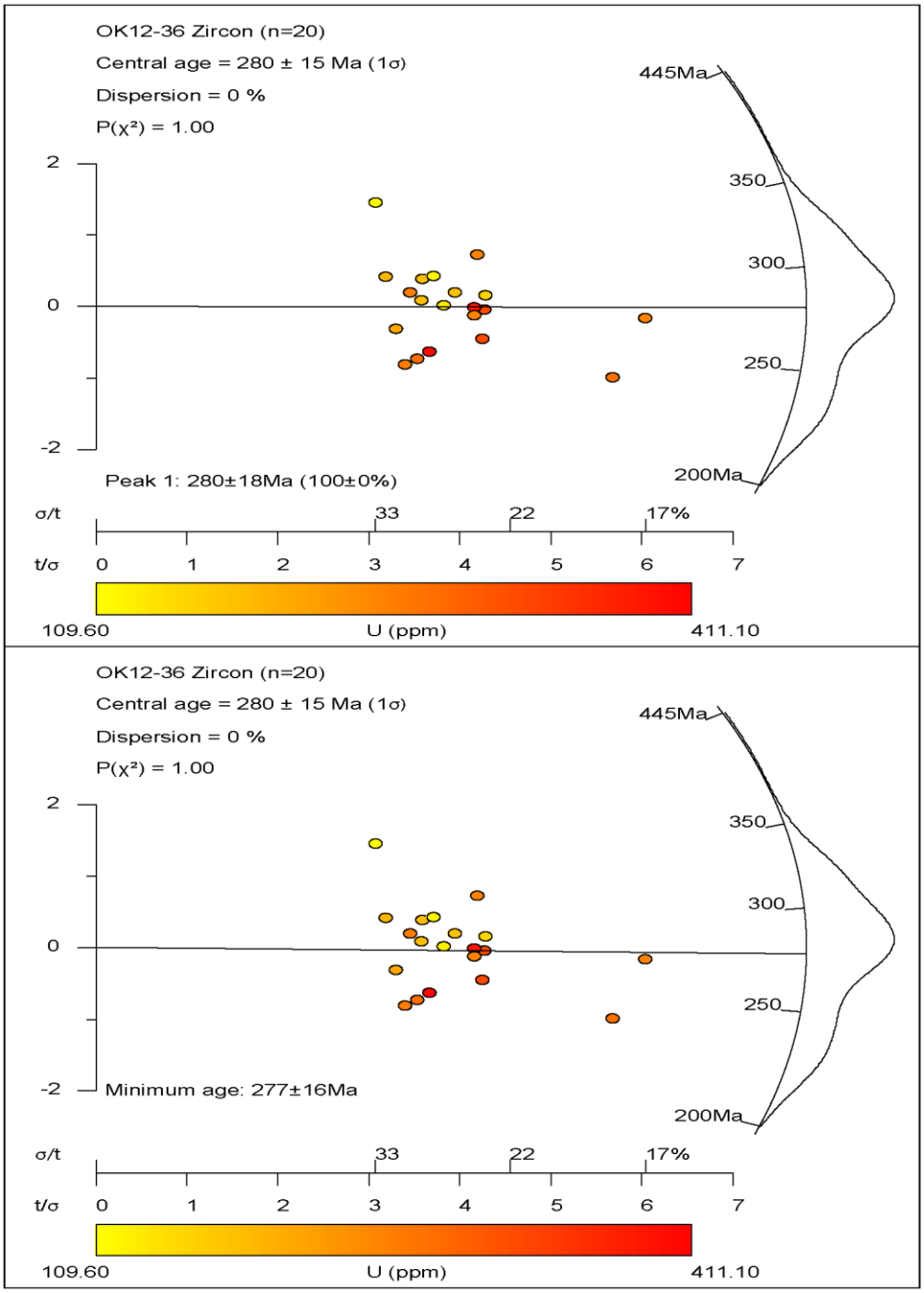

Figure S18. Radial (abanico) plots for OK12-36 zircon fission track ages: peak and minimum. Uranium (ppm) for each grain indicated by color scale, where yellow is lower U and red is higher U.

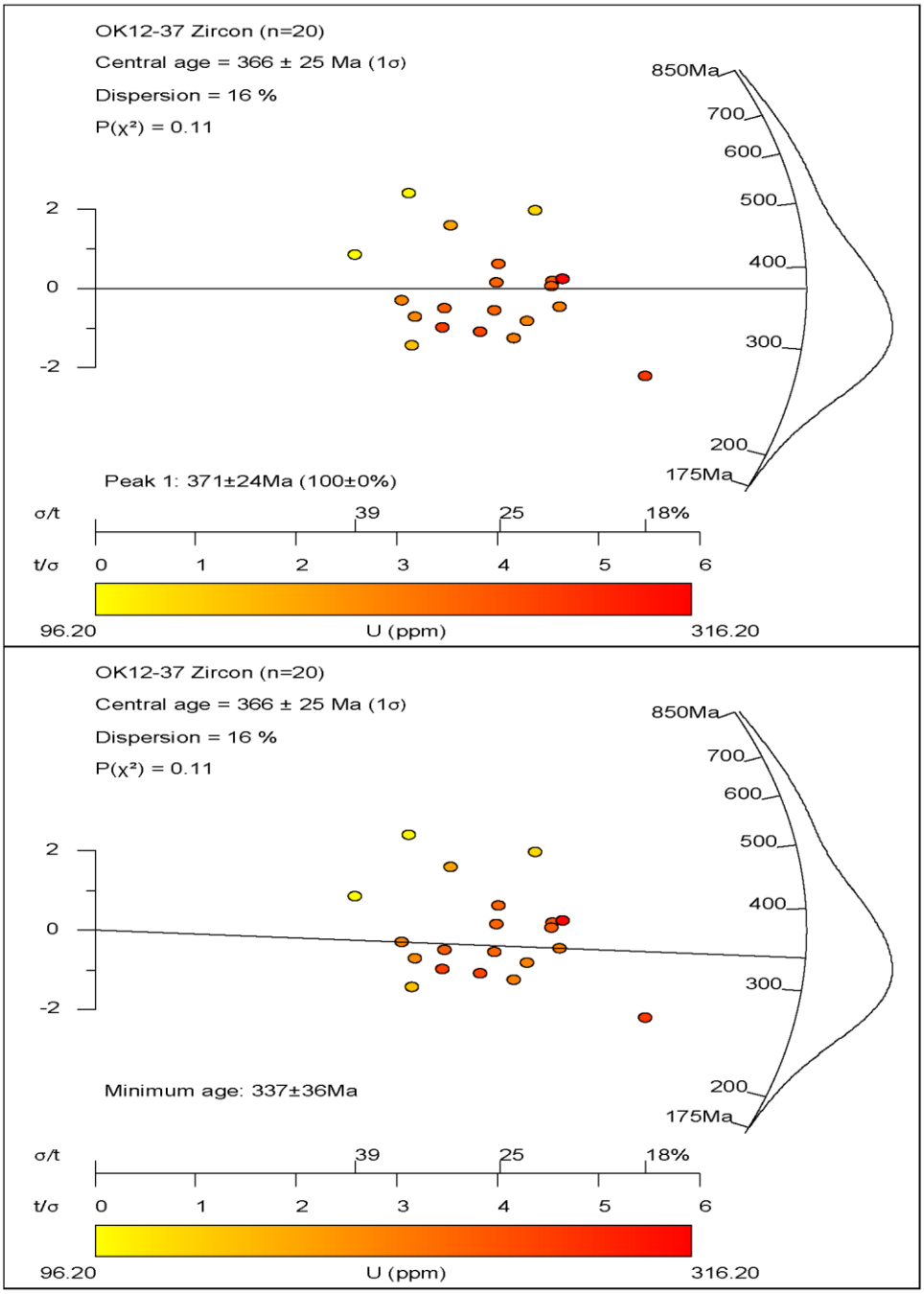

Figure S19. Radial (abanico) plots for OK12-37 zircon fission track ages: peak and minimum. Uranium (ppm) for each grain indicated by color scale, where yellow is lower U and red is higher U.

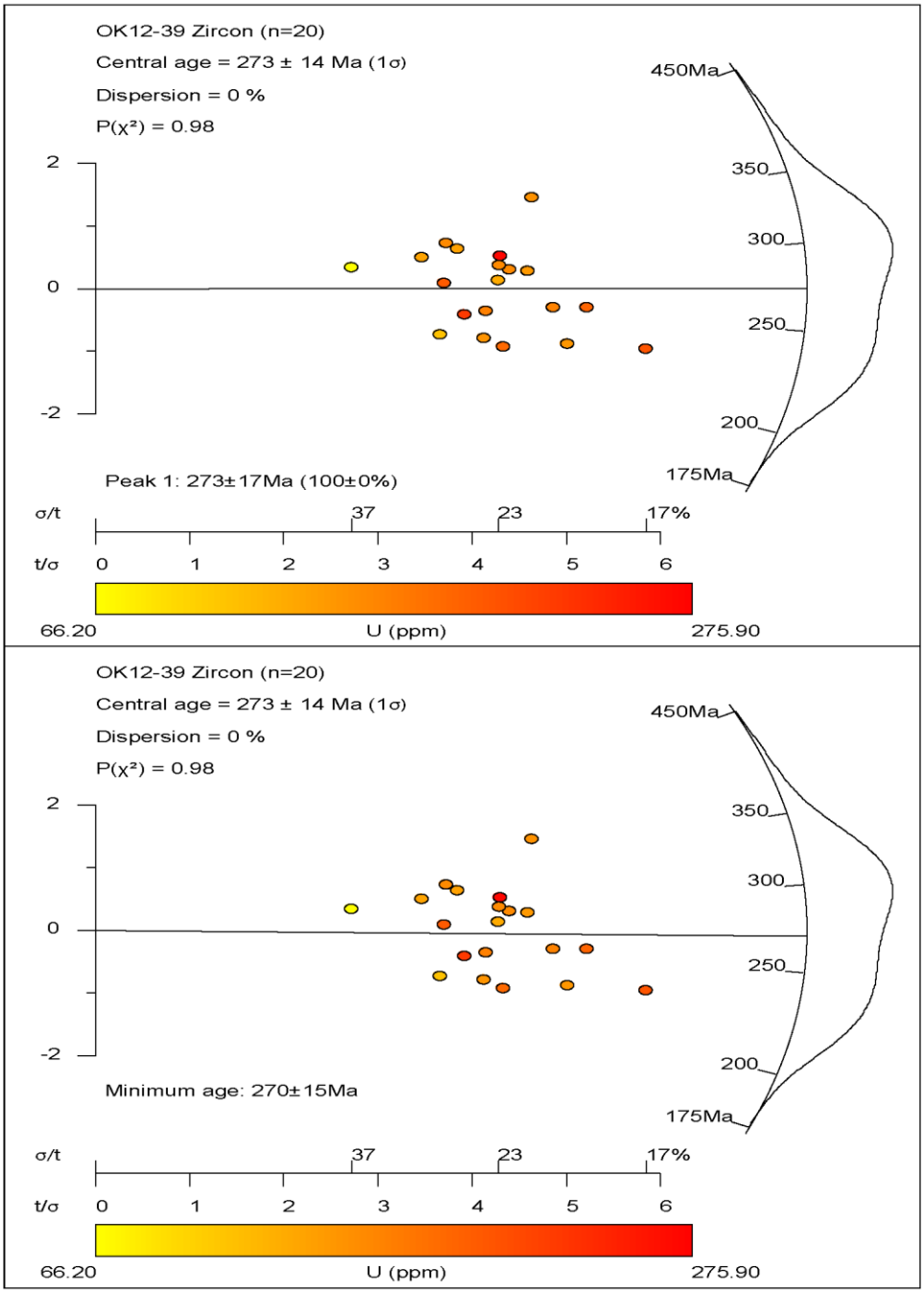

Figure S20. Radial (abanico) plots for OK12-39 zircon fission track ages: peak and minimum. Uranium (ppm) for each grain indicated by color scale, where yellow is lower U and red is higher U.

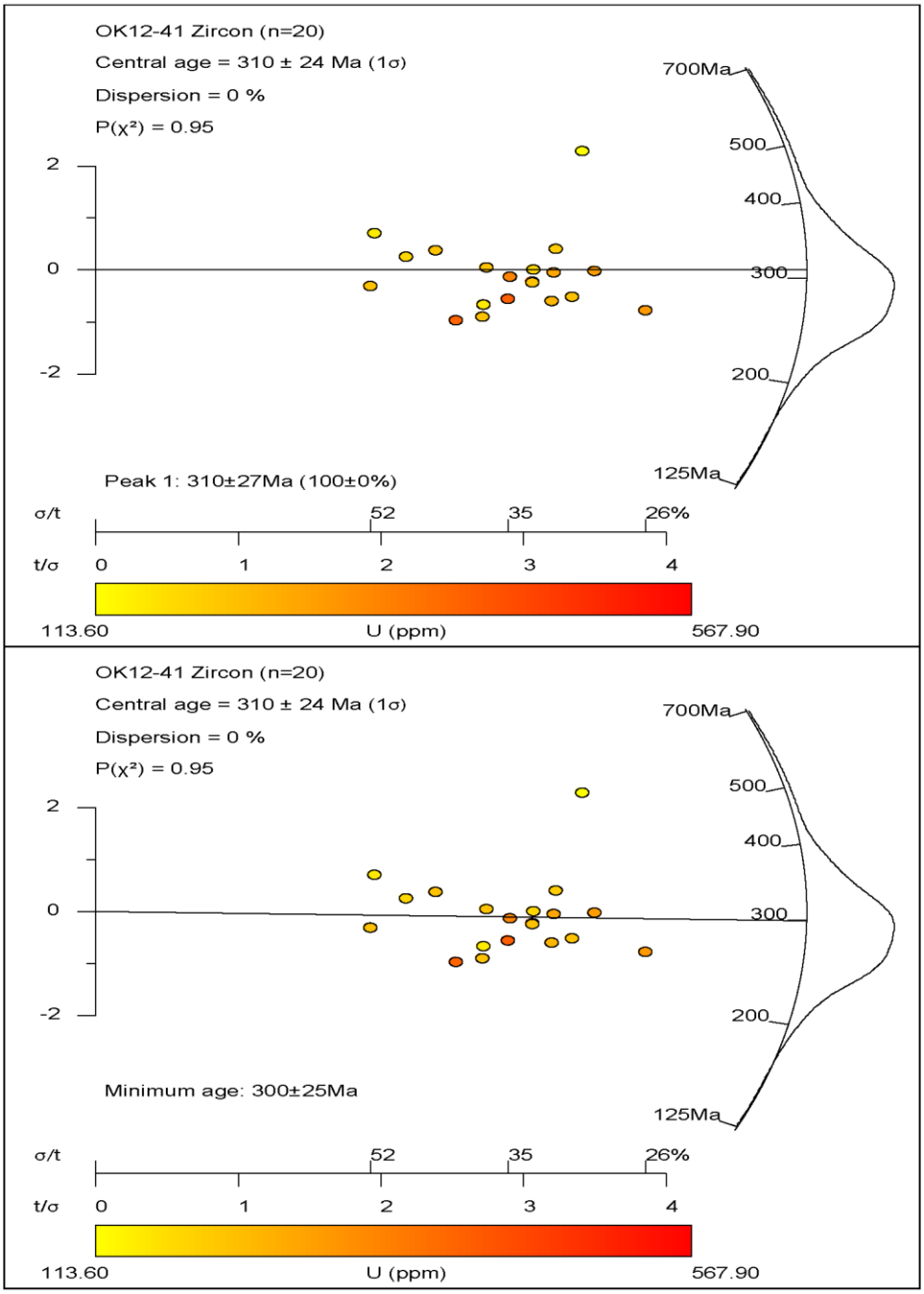

Figure S21. Radial (abanico) plots for OK12-41 zircon fission track ages: peak and minimum. Uranium (ppm) for each grain indicated by color scale, where yellow is lower U and red is higher U.

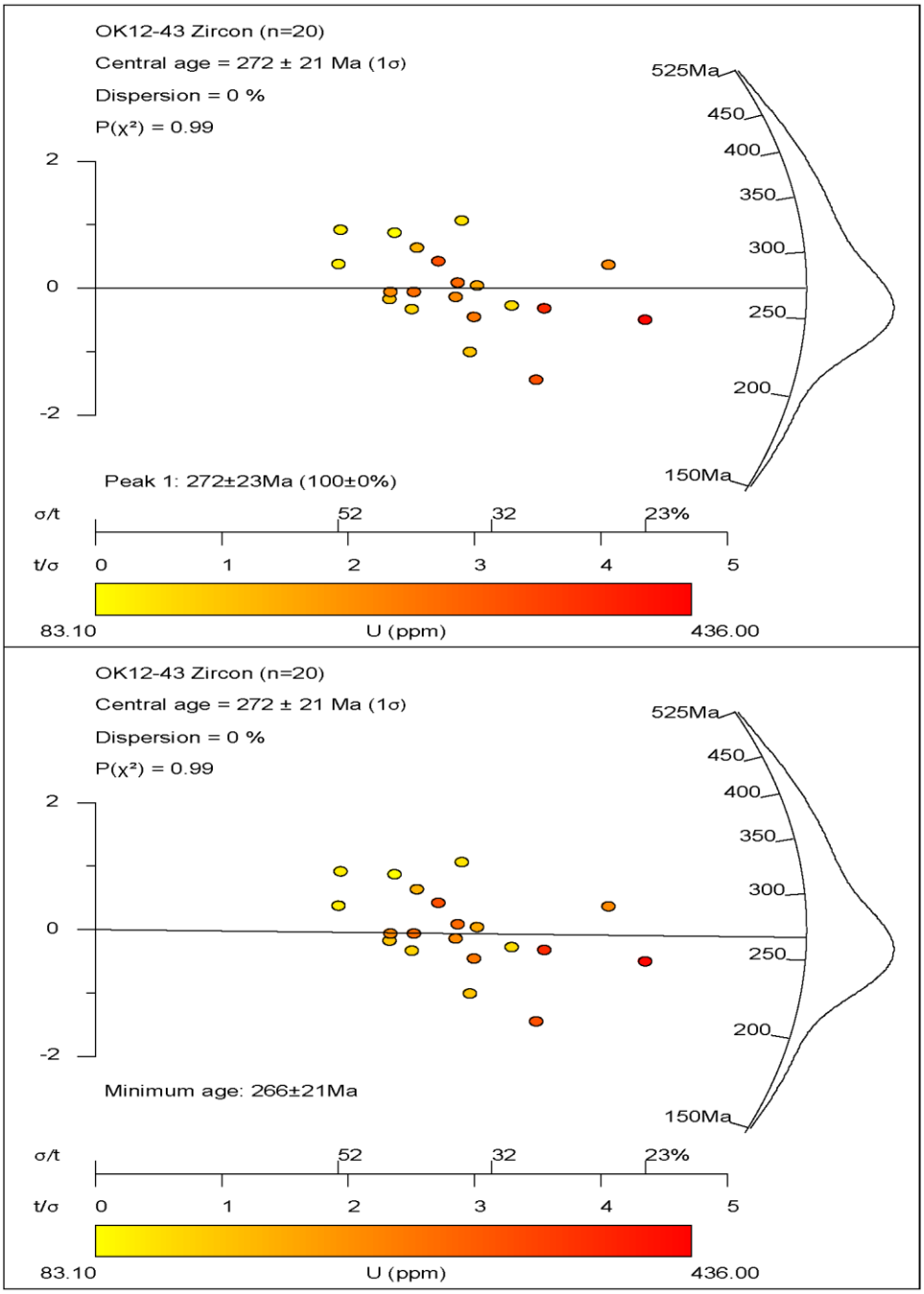

Figure S22. Radial (abanico) plots for OK12-43 zircon fission track ages: peak and minimum. Uranium (ppm) for each grain indicated by color scale, where yellow is lower U and red is higher U.

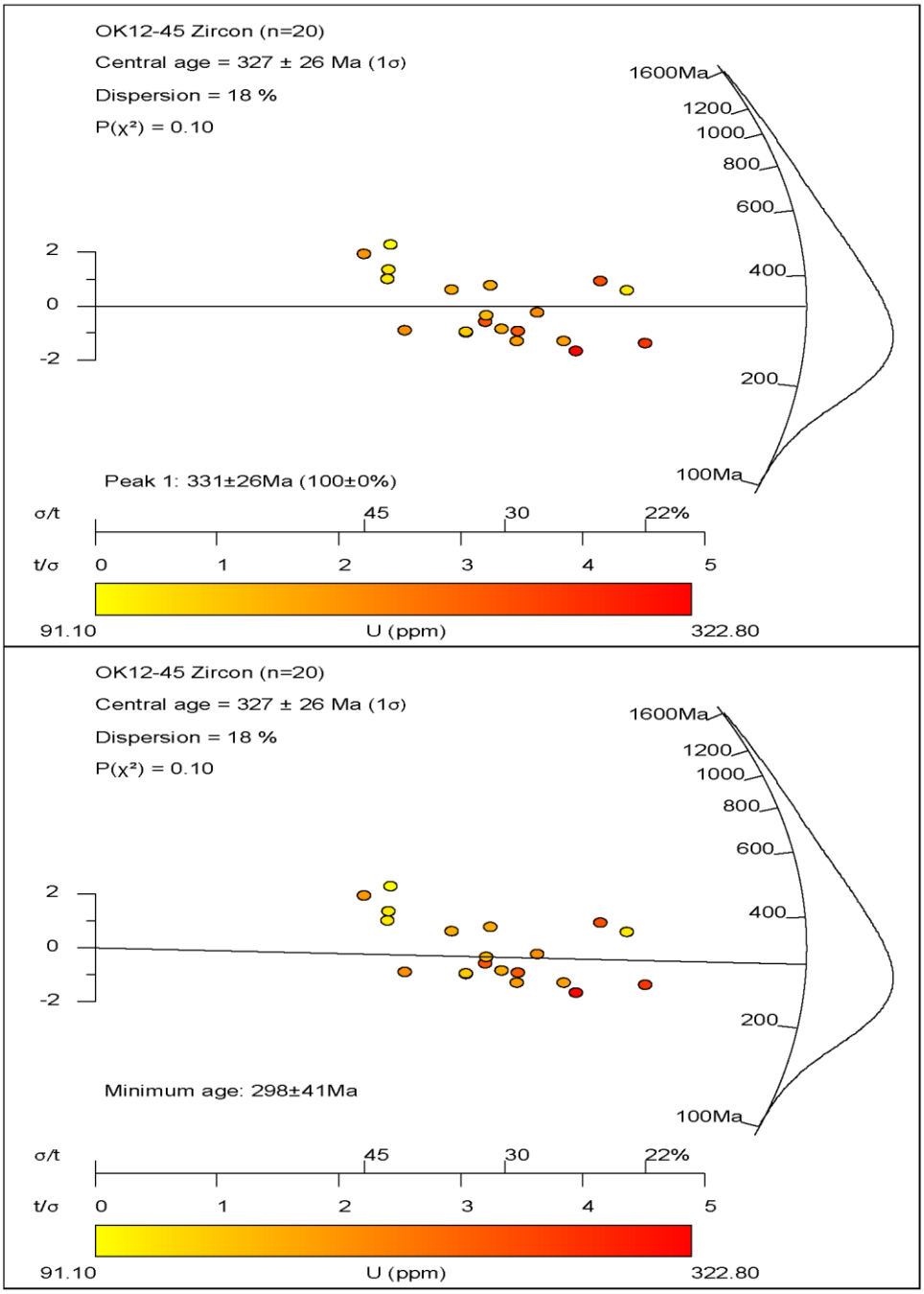

Figure S23. Radial (abanico) plots for OK12-45 zircon fission track ages: peak and minimum. Uranium (ppm) for each grain indicated by color scale, where yellow is lower U and red is higher U.

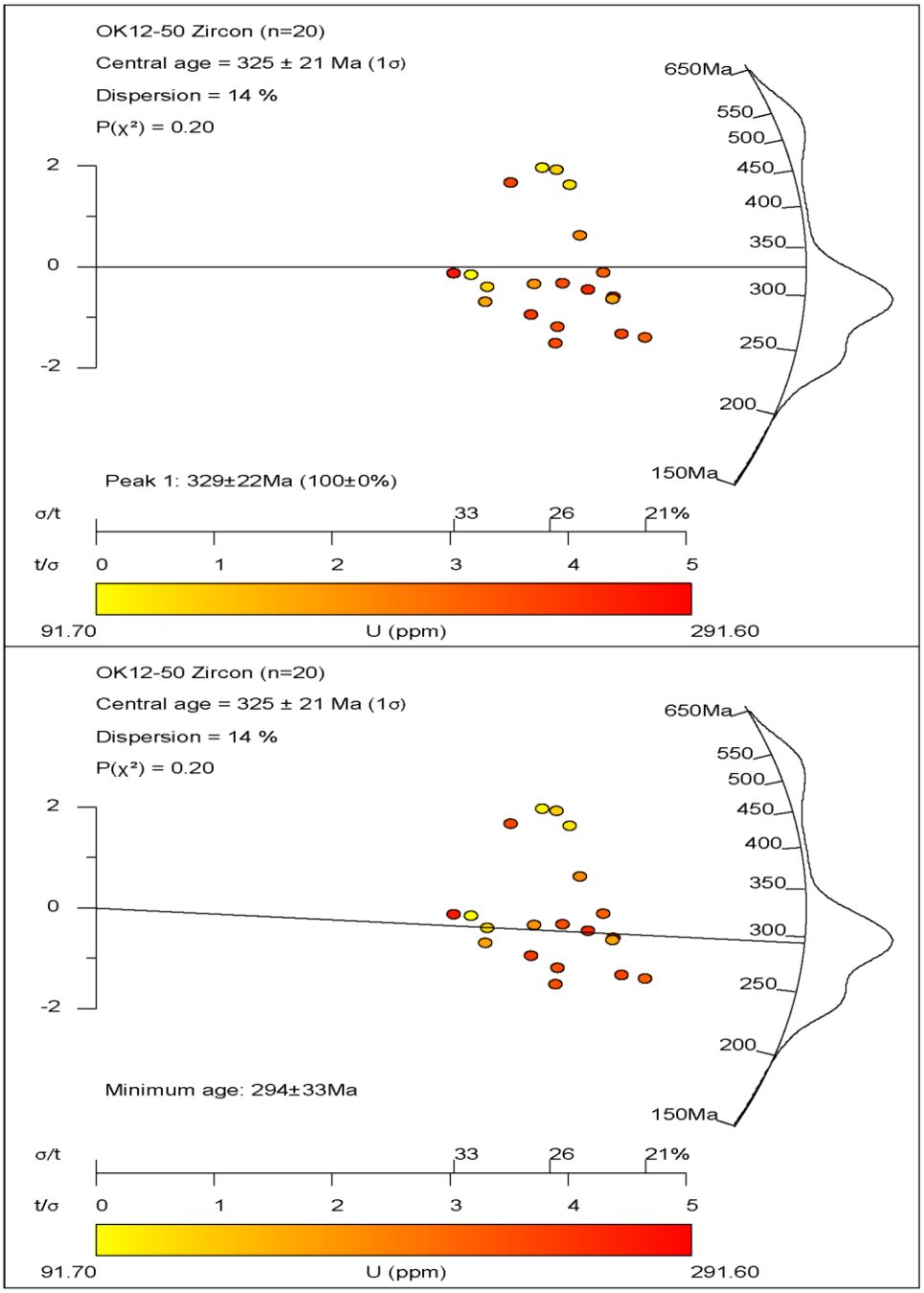

Figure S24. Radial (abanico) plots for OK12-50 zircon fission track ages: peak and minimum. Uranium (ppm) for each grain indicated by color scale, where yellow is lower U and red is higher U.

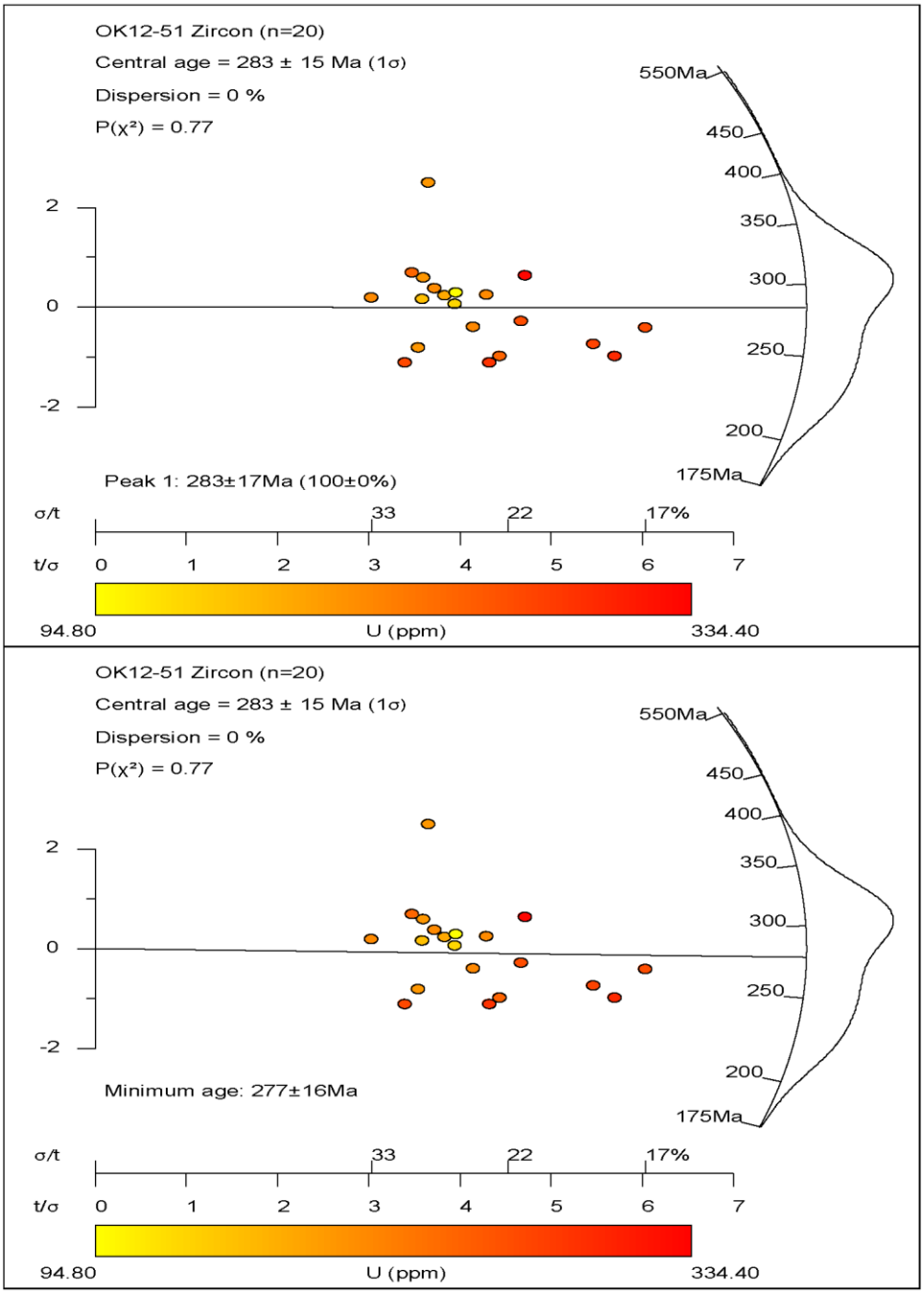

Figure S25. Radial (abanico) plots for OK12-51 zircon fission track ages: peak and minimum. Uranium (ppm) for each grain indicated by color scale, where yellow is lower U and red is higher U.

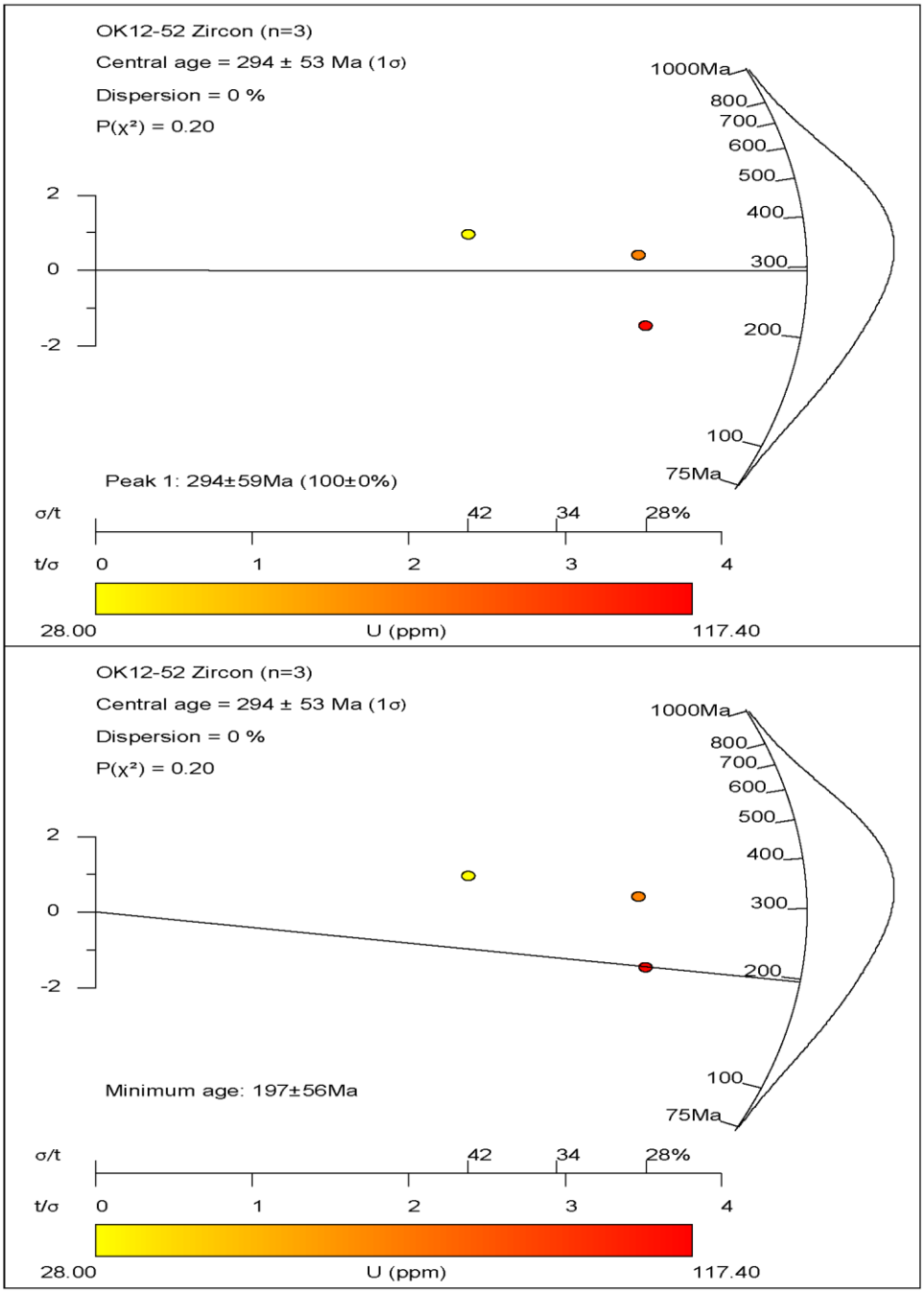

Figure S26. Radial (abanico) plots for OK12-52 zircon fission track ages: peak and minimum. Uranium (ppm) for each grain indicated by color scale, where yellow is lower U and red is higher U.

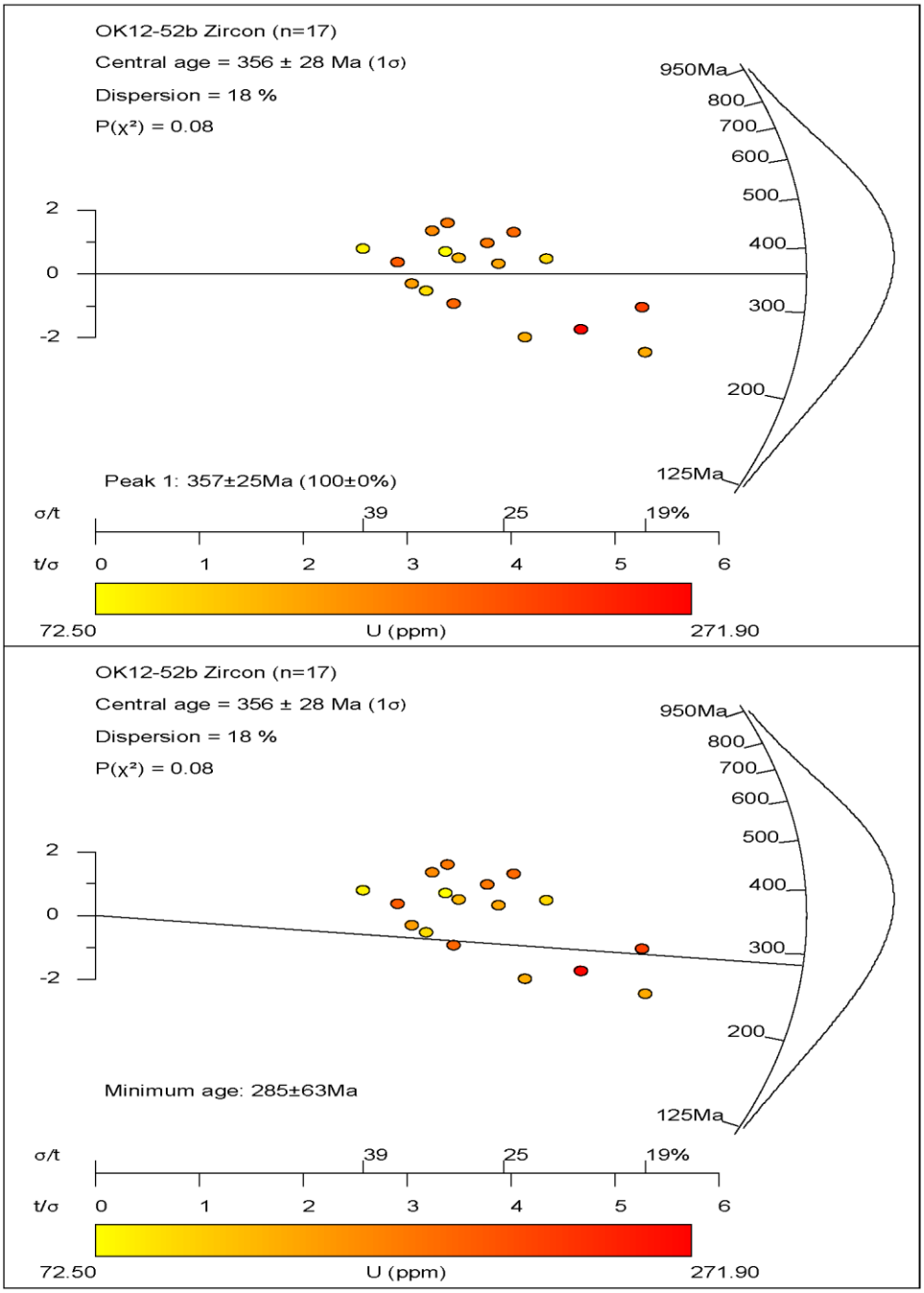

Figure S27. Radial (abanico) plots for OK12-52b zircon fission track ages: peak and minimum. Uranium (ppm) for each grain indicated by color scale, where yellow is lower U and red is higher U.

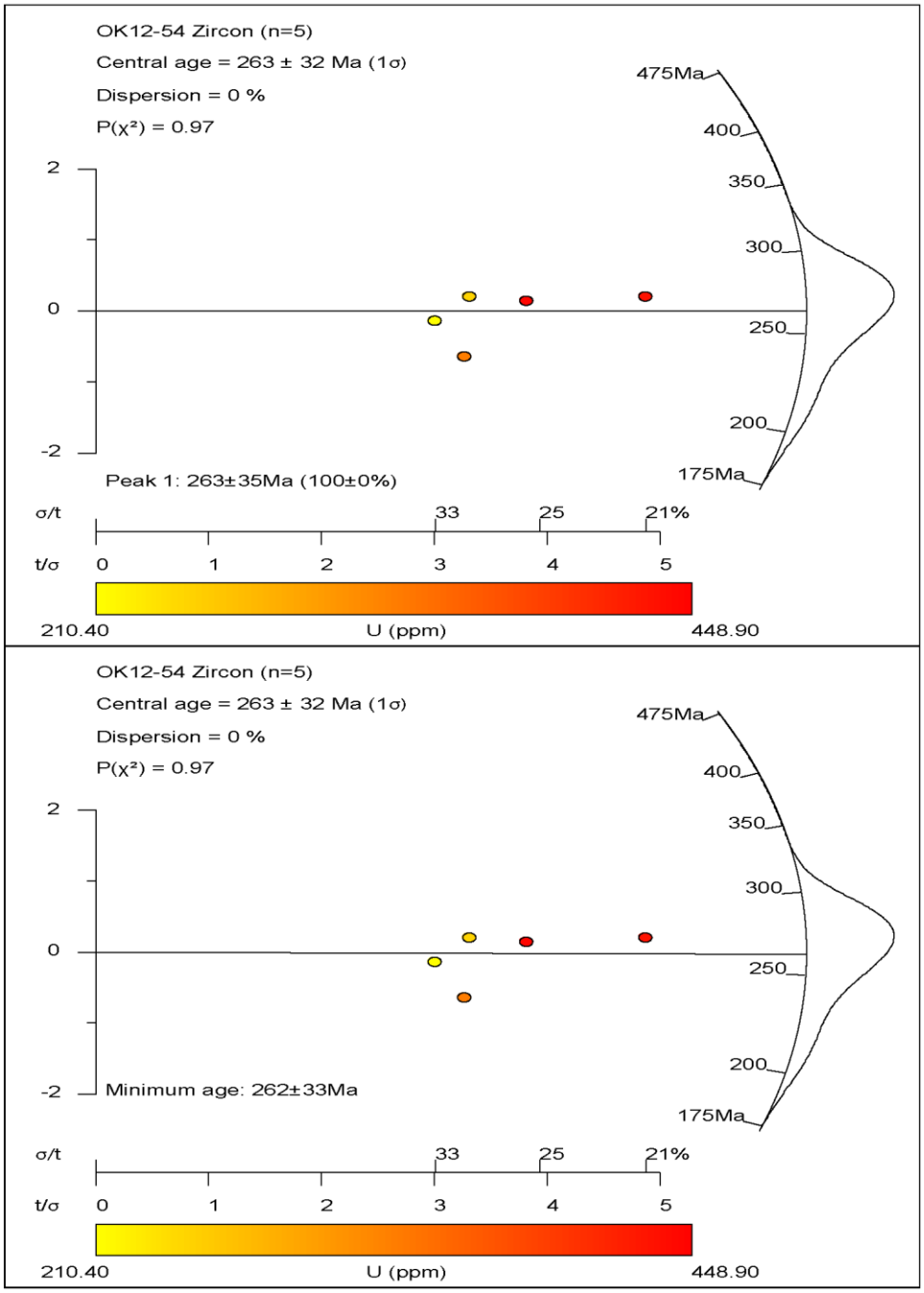

Figure S28. Radial (abanico) plots for OK12-54 zircon fission track ages: peak and minimum. Uranium (ppm) for each grain indicated by color scale, where yellow is lower U and red is higher U.

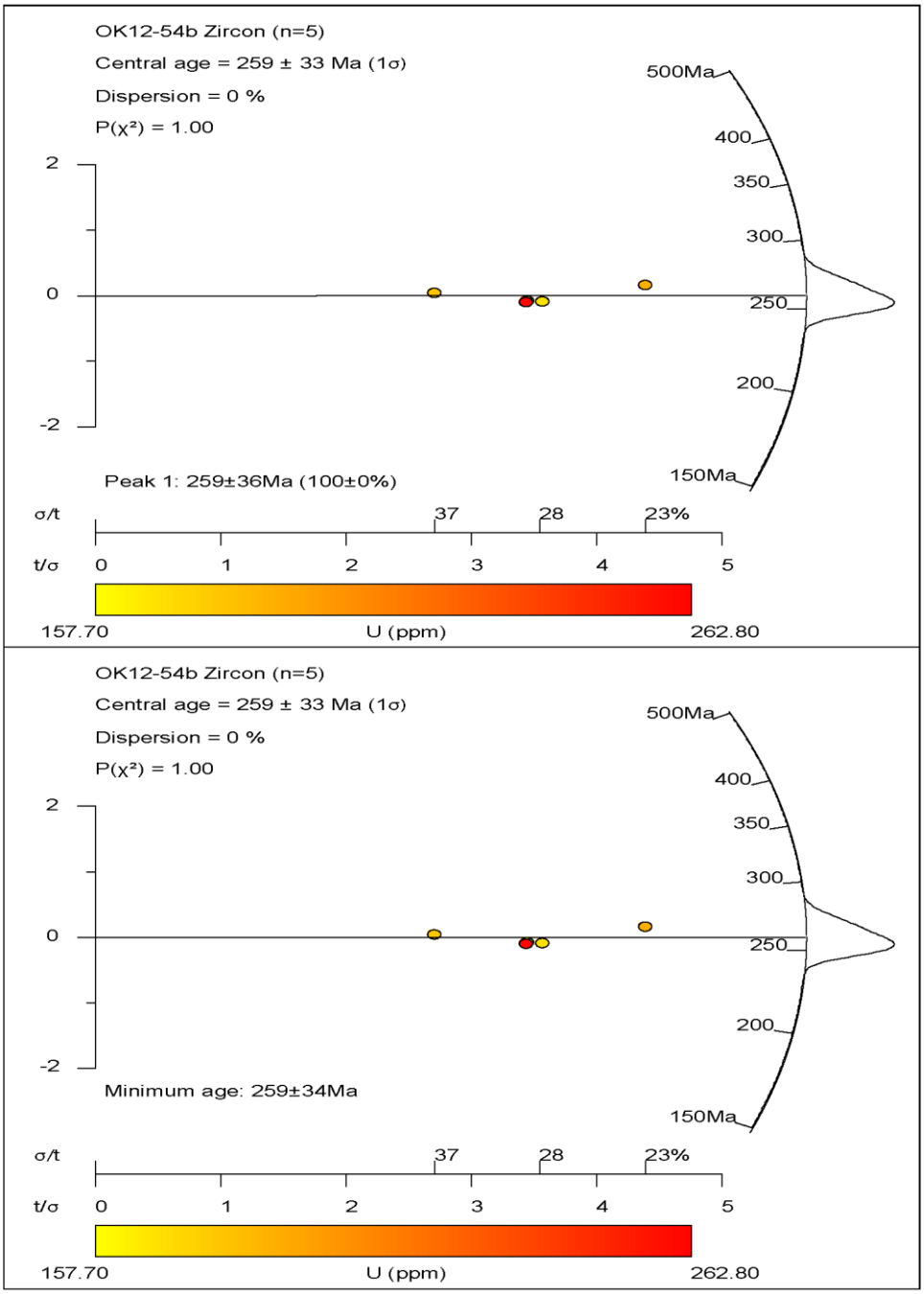

Figure S29. Radial (abanico) plots for OK12-54b zircon fission track ages: peak and minimum. Uranium (ppm) for each grain indicated by color scale, where yellow is lower U and red is higher U.

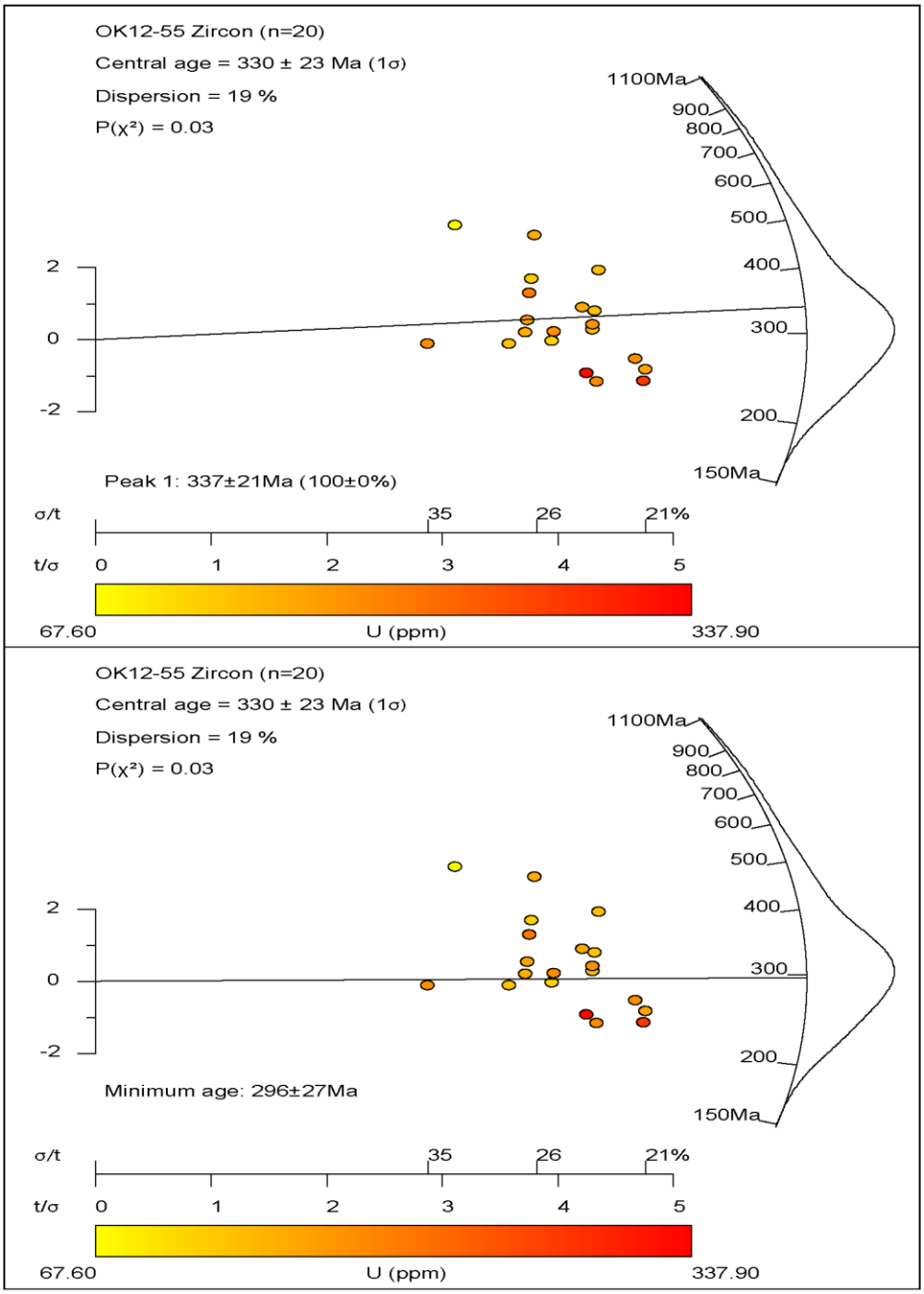

Figure S30. Radial (abanico) plots for OK12-55 zircon fission track ages: peak and minimum. Uranium (ppm) for each grain indicated by color scale, where yellow is lower U and red is higher U.

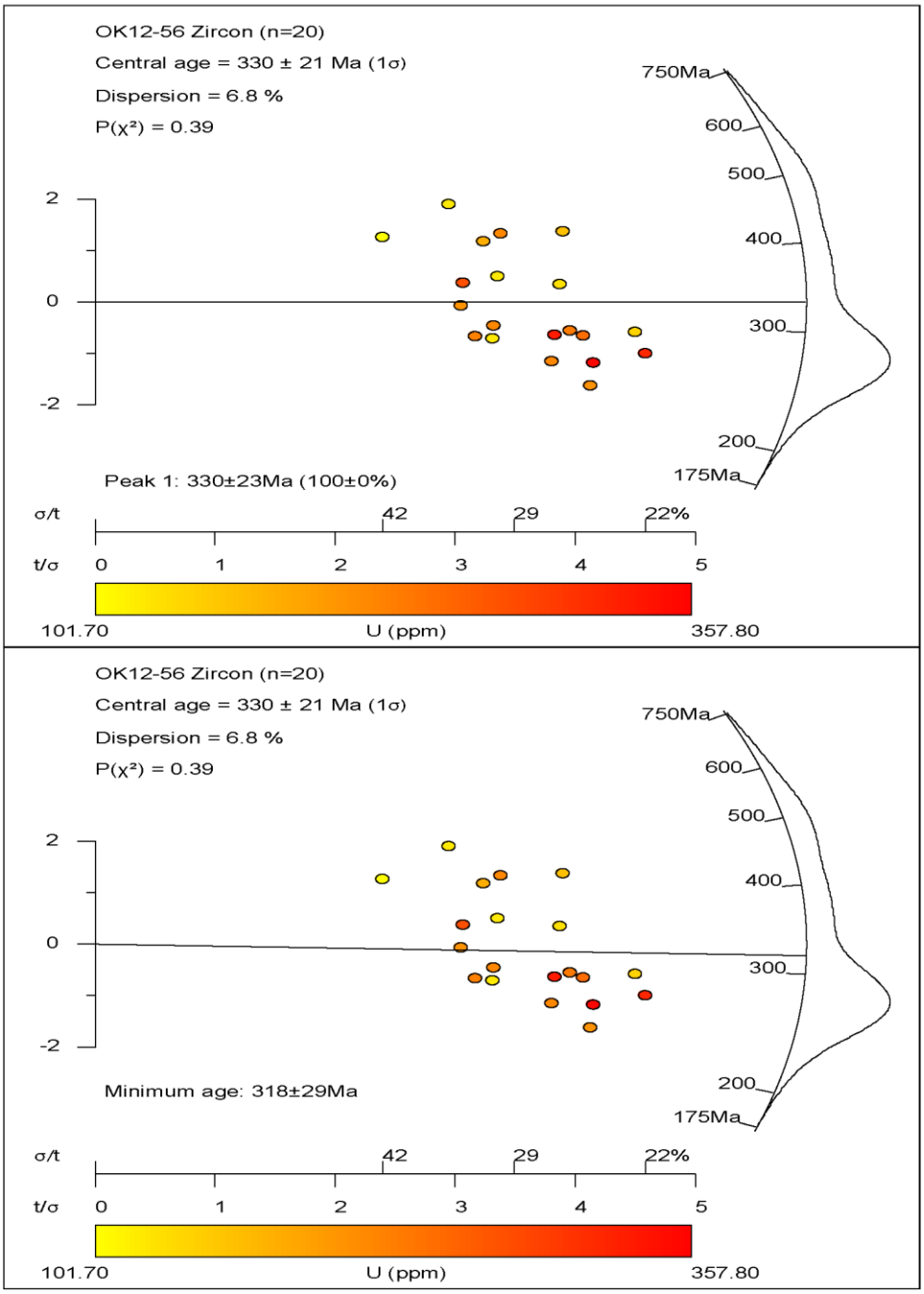

Figure S31. Radial (abanico) plots for OK12-56 zircon fission track ages: peak and minimum. Uranium (ppm) for each grain indicated by color scale, where yellow is lower U and red is higher U.

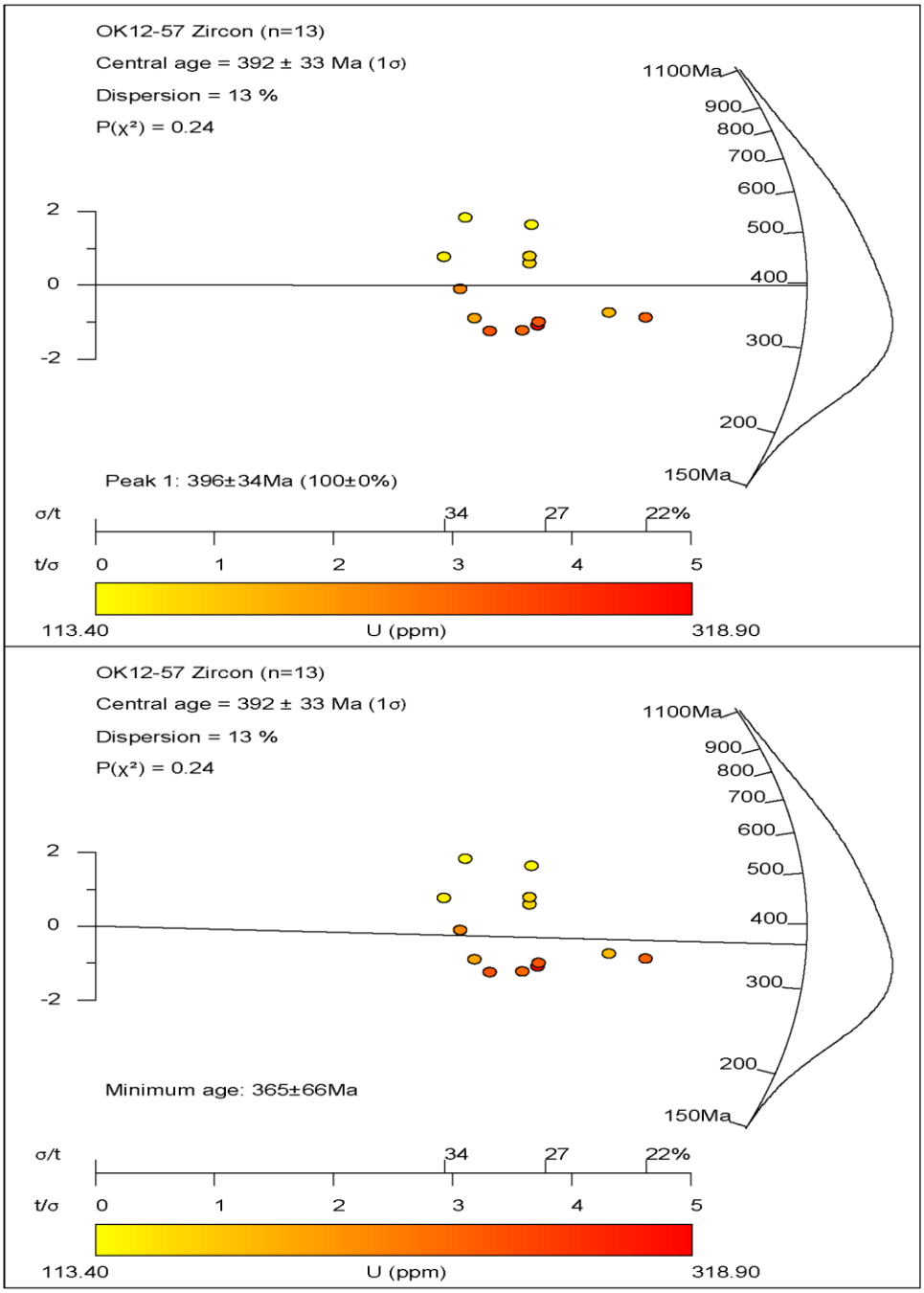

Figure S32. Radial (abanico) plots for OK12-57 zircon fission track ages: peak and minimum. Uranium (ppm) for each grain indicated by color scale, where yellow is lower U and red is higher U.

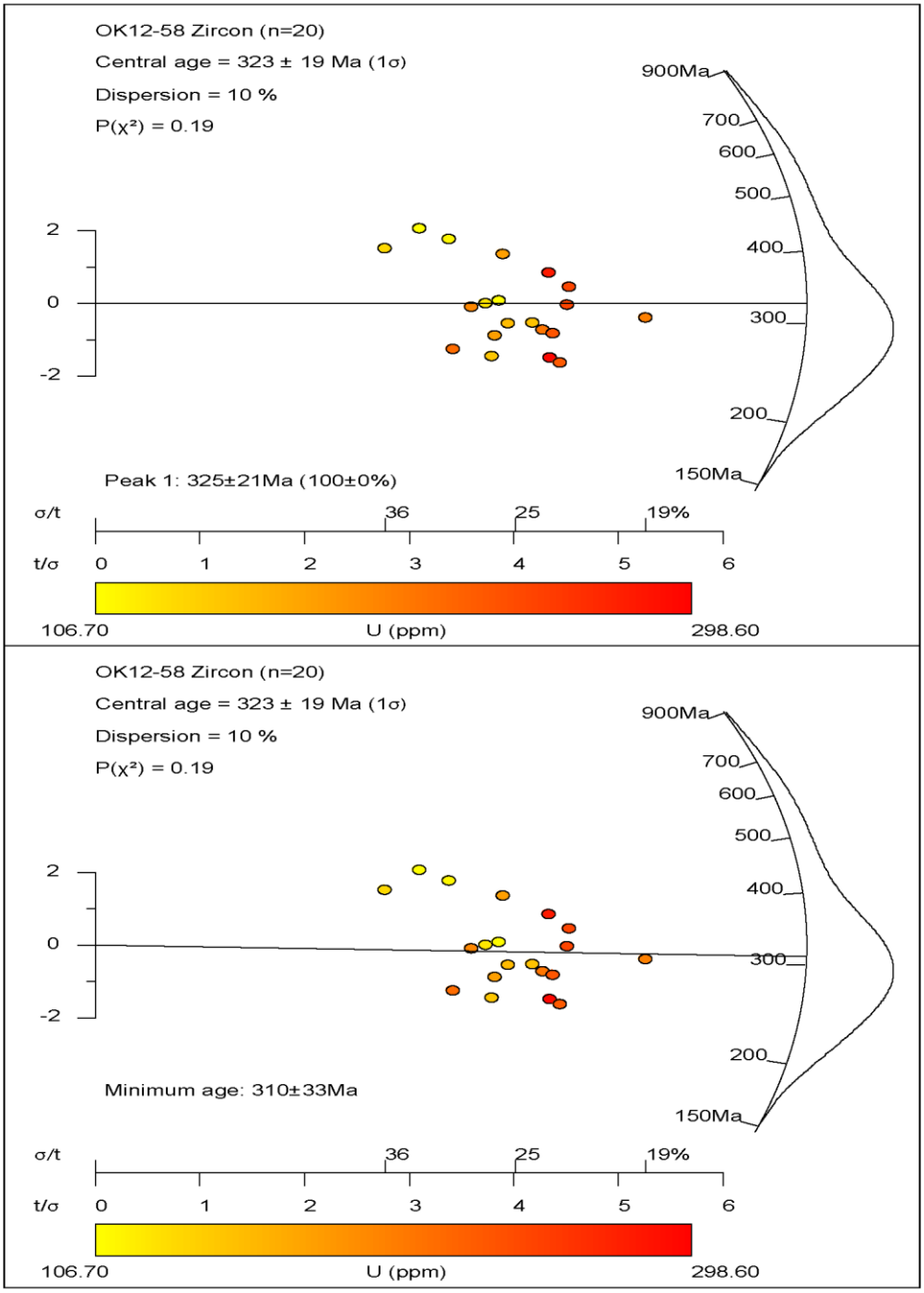

Figure S33. Radial (abanico) plots for OK12-58 zircon fission track ages: peak and minimum. Uranium (ppm) for each grain indicated by color scale, where yellow is lower U and red is higher U.

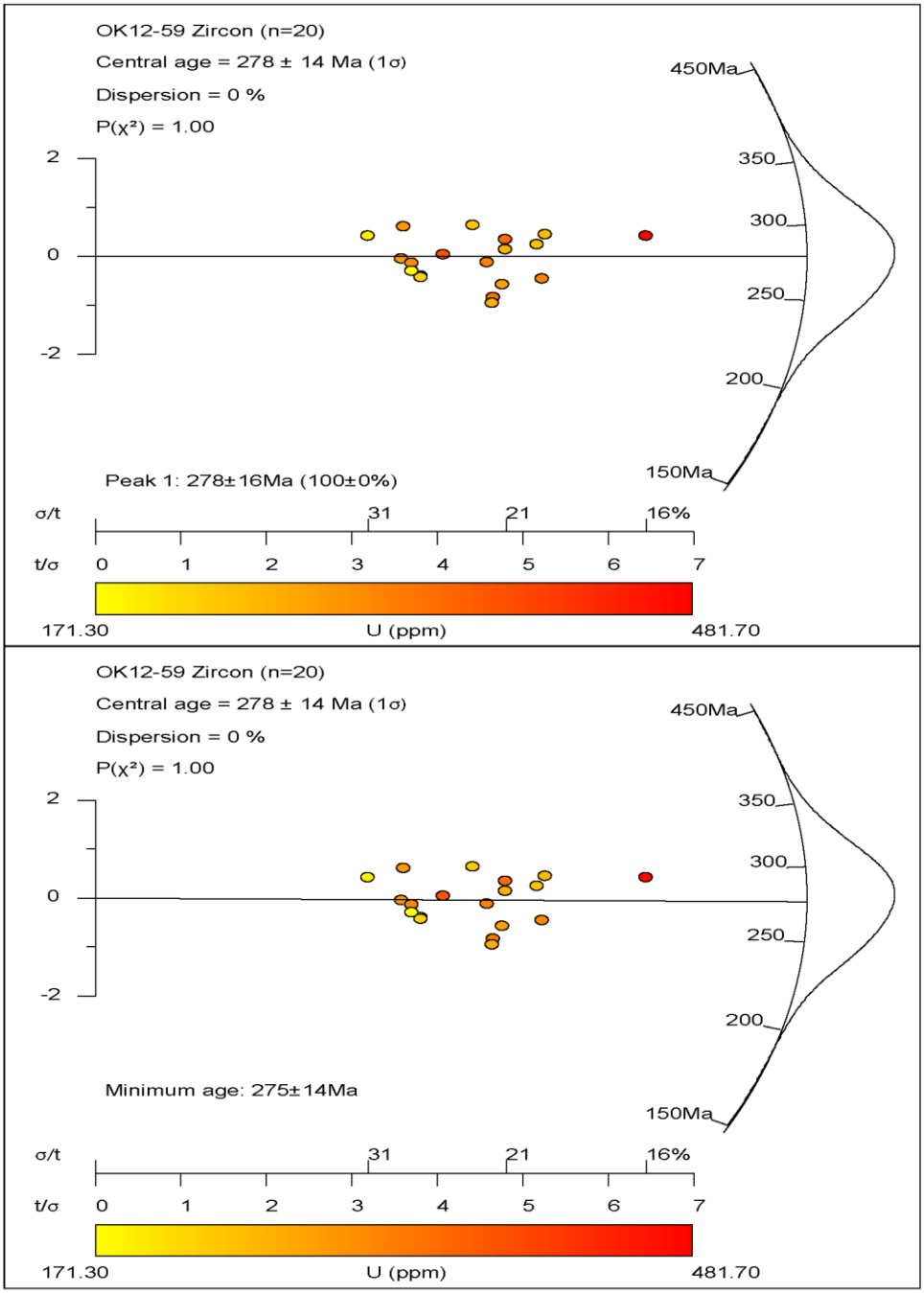

Figure S34. Radial (abanico) plots for OK12-59 zircon fission track ages: peak and minimum. Uranium (ppm) for each grain indicated by color scale, where yellow is lower U and red is higher U.

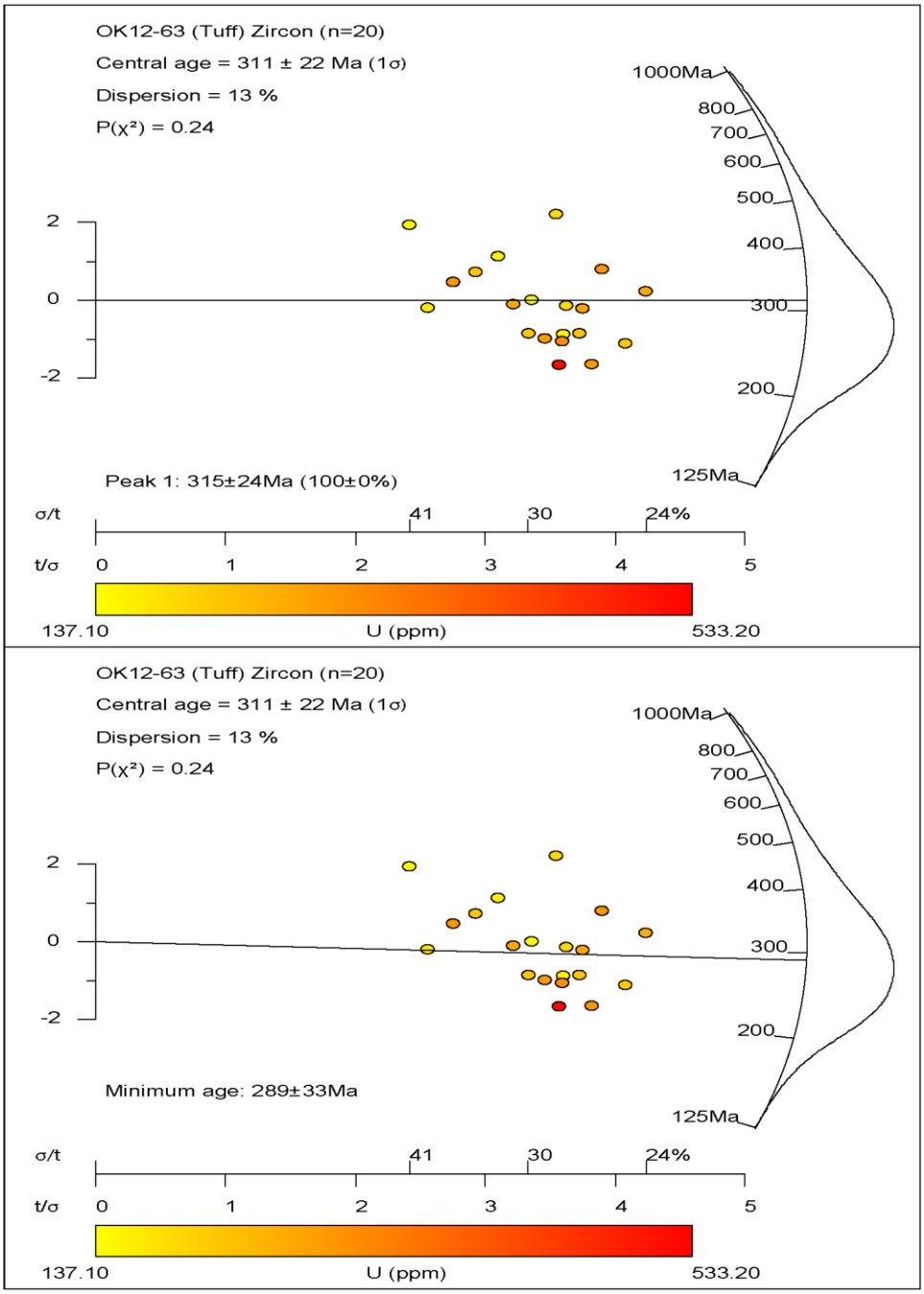

Figure S35. Radial (abanico) plots for OK12-63 (Tuff) zircon fission track ages: peak and minimum. Uranium (ppm) for each grain indicated by color scale, where yellow is lower U and red is higher U.

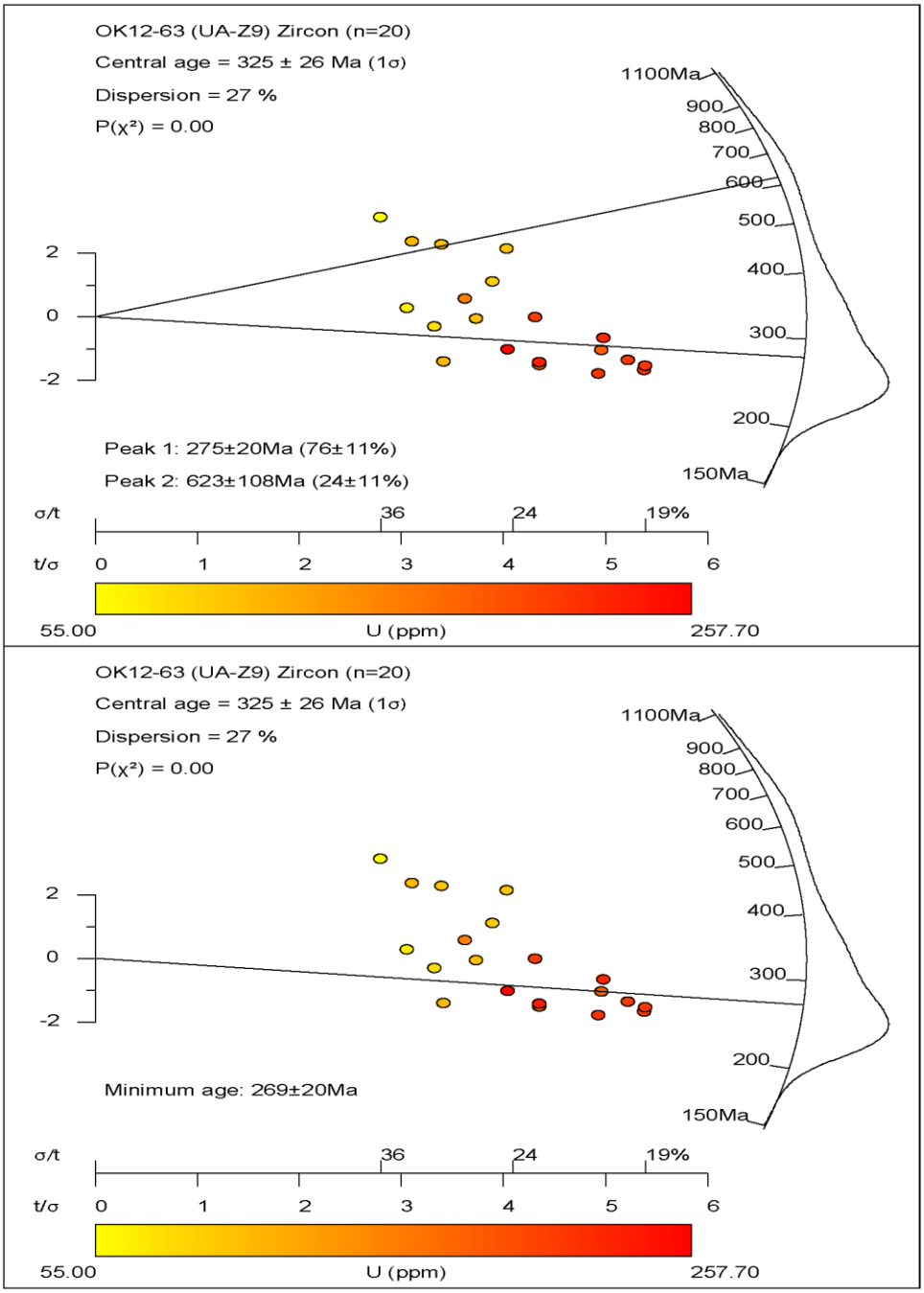

Figure S36. Radial (abanico) plots for OK12-63 (UA-Z9) zircon fission track ages: peak and minimum. Uranium (ppm) for each grain indicated by color scale, where yellow is lower U and red is higher U.

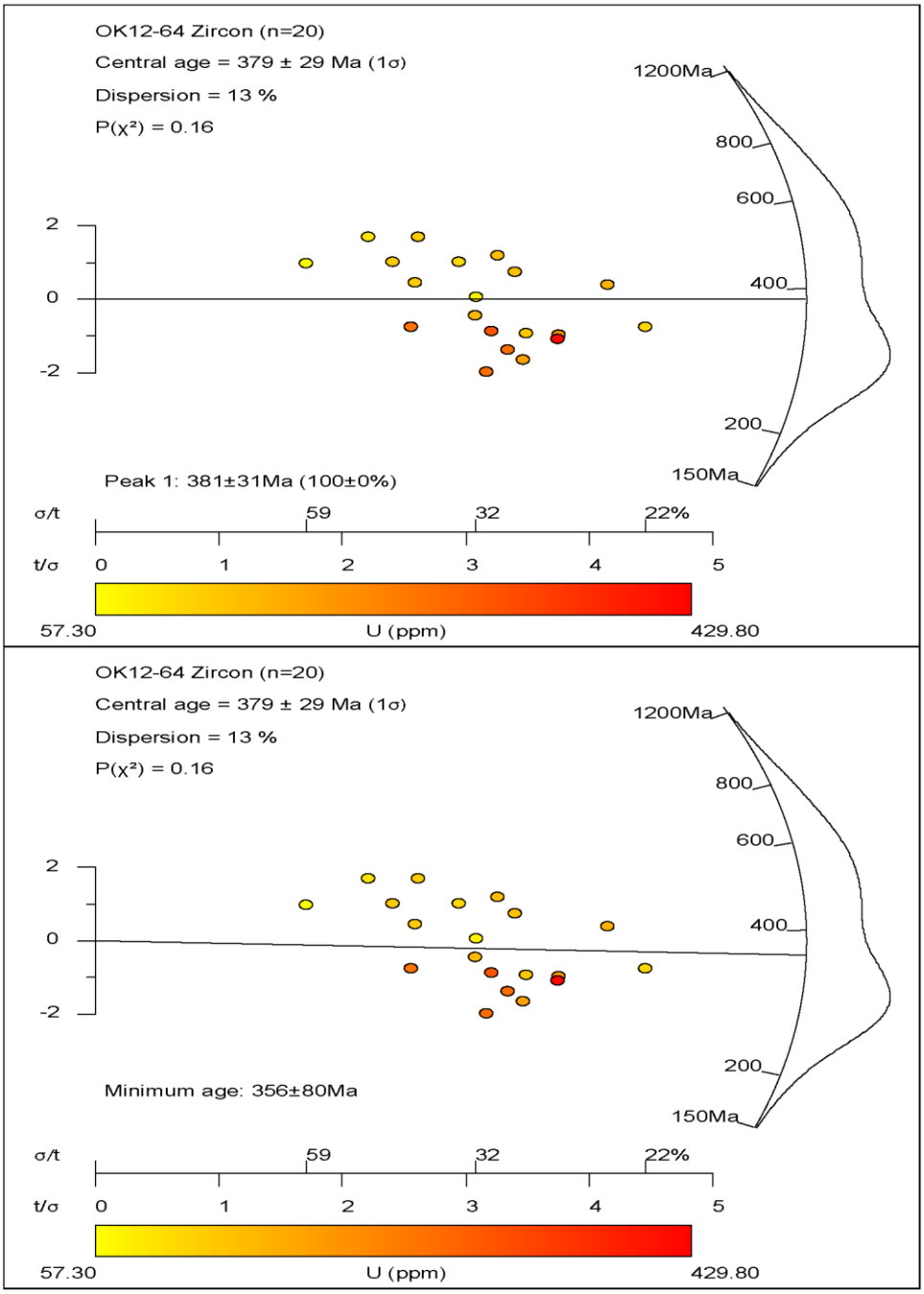

Figure S37. Radial (abanico) plots for OK12-64 zircon fission track ages: peak and minimum. Uranium (ppm) for each grain indicated by color scale, where yellow is lower U and red is higher U.

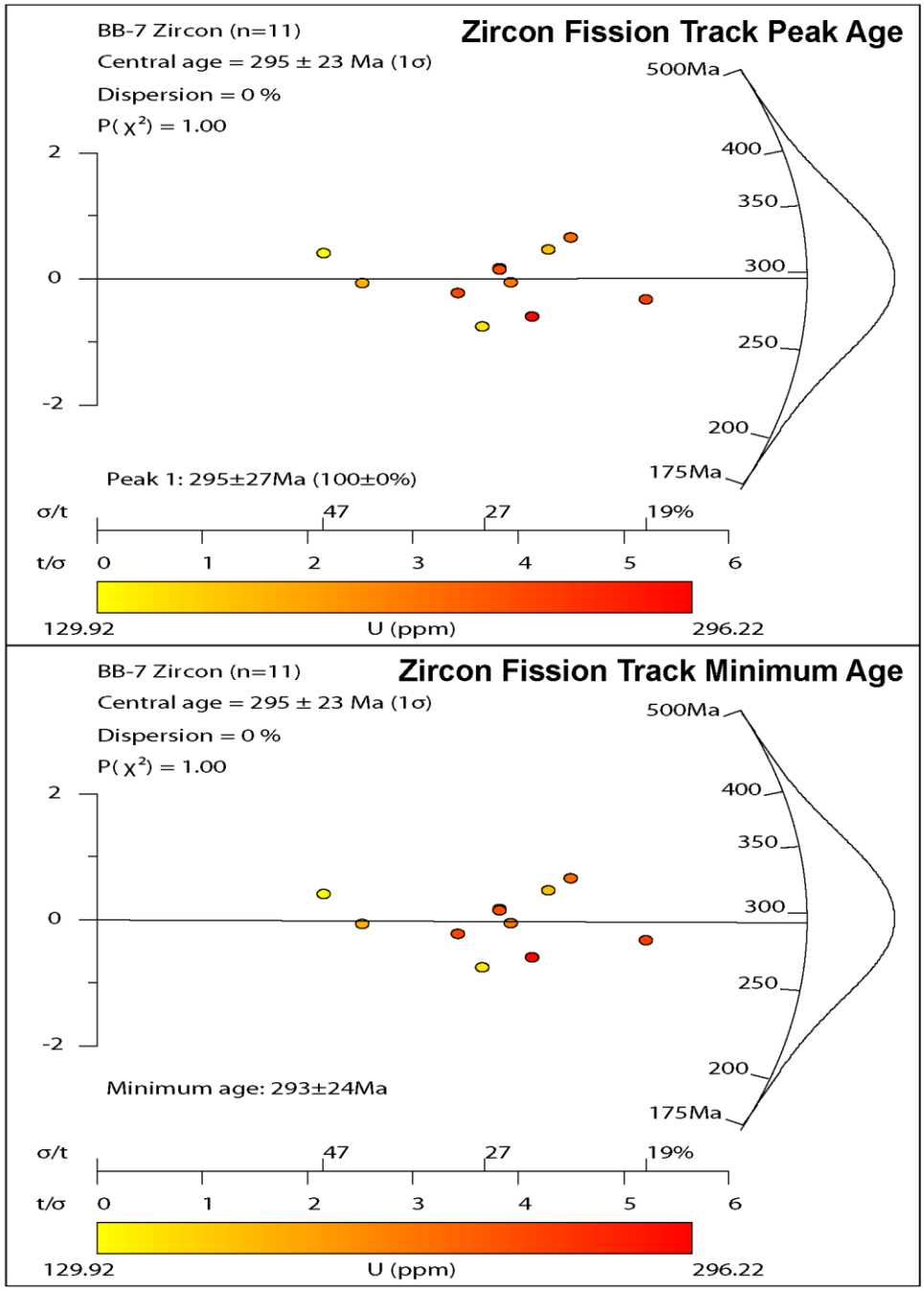

Figure S38. Radial (abanico) plots for BB-7 zircon fission track ages: peak and minimum. Uranium (ppm) for each grain indicated by color scale, where yellow is lower U and red is higher U.

Sample	*Latitude (°N)*	*Longitude (°W)*	*Elevation (m)*	*Age*	*Group/ Formation*	*Structural Province*	*ISGN*
OK12-1	35.4200	94.5614	205.1	Penn.	McAlester?	AB	BVM00005B
OK12-4	35.2084	94.4922	160.0	Penn.	Atoka, Lower	AB	BVM00005F
OK12-6	35.0582	94.5169	167.2	Penn.	McAlester	AB	BVM00005H
OK12-9	34.8017	94.5230	238.4	Penn.	Atoka, Middle	FTZ	BVM00005N
OK12-12	34.6920	94.5266	724.9	Penn.	Jackfork	MCZ	BVM00005Q
OK12-14	34.6119	94.6595	610.4	Penn.	Jackfork	MCZ	BVM00005T
OK12-16	34.4736	94.6603	220.4	Miss.	Stanley	MCZ	BVM00005V
OK12-18	34.3622	94.8113	280.1	Miss.	Stanley	MCZ	BVM00005Y
OK12-19	35.1726	95.6470	260.1	Penn.	Boggy	AB	BVM000059
OK12-21	34.9371	95.5603	211.3	Penn.	Savanna	AB	BVM000063
OK12-23	34.8693	95.2932	314.2	Penn.	Atoka, Lower	FTZ	BVM000065
OK12-26	34.7601	95.2819	234.2	Penn.	Atoka	MCZ	BVM000068
OK12-27	34.7210	95.2340	204.6	Penn.	Stanley	MCZ/PH	BVM00006A
OK12-28	34.6923	95.2395	240.2	Ord.-Dev.	Undifferentiated	PH	BVM00006C
OK12-31	34.6319	95.1980	192.4	Miss.	Stanley	MCZ/PH	BVM00006F
OK12-32	34.5411	95.3064	231.4	Penn.	Atoka	MCZ	BVM00006H
OK12-35	34.4350	95.2735	370.2	Penn.	Jackfork	MCZ	BVM00006L
OK12-36	34.4021	95.2738	333.6	Penn.	Jackfork	MCZ	BVM00006M
OK12-37	34.3564	95.2125	293.8	Penn.	Jackfork	MCZ	BVM00006N
OK12-39	34.2836	94.7781	265.6	Penn.	Jackfork	MCZ	BVM00006P
OK12-41	34.8262	96.2842	228.2	Penn.	Thurman?	AB	BVM00006T
OK12-43	34.7091	96.1286	214.9	Penn.	Savanna	AB	BVM00006V
OK12-45	34.5282	96.0163	216.5	Penn.	Atoka, Lower	BKR/FTZ	BVM00006X
OK12-50	34.4077	95.9509	241.3	Penn.	Jackfork	MCZ	BVM000075
OK12-51	34.3318	95.9074	196.1	Penn.	Jackfork	MCZ	BVM000075
OK12-52	34.3398	95.6422	153.9	Miss.	Stanley	MCZ	BVM000077
OK12-54	34.2794	95.5475	169.1	Miss.	Stanley	MCZ	BVM000079
OK12-55	34.2292	95.5706	163.9	Penn.	Atoka?	MCZ	BVM00007B
OK12-56	34.2004	95.5354	157.8	Penn.	Jackfork?	MCZ	BVM00007C
OK12-57	34.2925	95.3014	193.2	Miss.	Stanley	MCZ	BVM00007D
OK12-58	34.1995	95.3469	156.7	Miss.	Stanley	MCZ	BVM00007E
OK12-59	34.1804	95.1391	152.7	Miss.	Stanley	MCZ	BVM00007G
OK12-60	34.1117	95.0012	155.0	Miss.	Stanley	MCZ/BBU	BVM00007H
OK12-63	34.2825	94.8086	302.5	Miss.	Stanley	MCZ/BBU	BVM00007N
OK12-63tuff	34.2825	94.8086	302.5	Miss.	Stanley	MCZ/BBU	Not Registered
OK12-64	34.2106	94.7804	293.0	Ord.	Blaylock	BBU	BVM00007P
BB-7	34.2117	94.7802	290.0	Ord.	Blaylock	BBU	Not Registered

Note. All coordinates reported in reference to 1983 North American Datum. Abbreviations: Penn., Pennsylvanian; Miss., Mississippian; Ord., Ordovician; Dev., Devonian; AB, Arkoma Basin; FTZ, Frontal Thrust Zone; MCZ, Maumelle Chaotic Zone; PH, Potato Hills; BKR, Black Knob Ridge; BBU, Broken Bow Uplift. Additional metadata provided by System for Earth Sample Registration (SESAR) using corresponding International Geo Sample Number (ISGN) at www.geosamples.org.

Table S1. Sample locations with attributes.

Sample	Group/ Formation	Age	Photomicrograph	Shape	Size	Color	Surfaces	Fluid Inclusions?	Other
OK12-1	McAlester?	Pennslyvanian	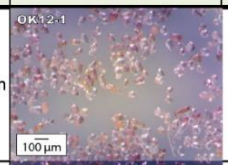	Well-rounded to sub-angular, mostly equant grains. Some grains are elongated.	Grains from 40 to 190 microns.	Most grains are transparent with pink hue.	Rough surfaces on a majority of grains. Smooth surfaces present on a small number of grains.	Present.	Some grains show minor internal fractures.
OK12-4	Atoka	Pennslyvanian	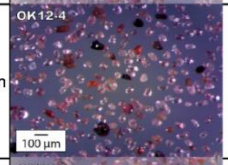	Well-rounded to sub-rounded equant grains.	Grains from 40 to 130 microns.	Most grains are transparent with pink hue. Few very well-rounded grains that are purple.	Irregular "pitted" surfaces.	Present in a few number of grains.	None.
OK12-6	McAlester	Pennslyvanian	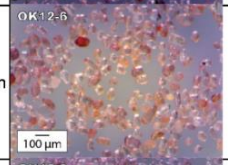	Well-rounded to sub-rounded equant and elongate grains.	Grains from 60 to 175 microns.	Most grains are transparent with pink hue.	Smooth to rough surfaces.	Present.	Some grains show minor internal fractures.
OK12-9	Atoka, Middle	Pennslyvanian	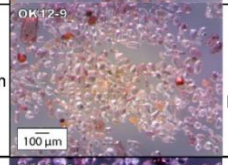	Well-rounded to sub-rounded equant grains. Minor sub-rounded elongate grains.	Grains from 40 to 150 microns.	Most grains are transparent with pink hue.	Smooth to rough surfaces.	Present.	A significantly larger, 120um X 235um, grain present. Some grains have internal fractures.
OK12-12	Jackfork	Pennsylvanian	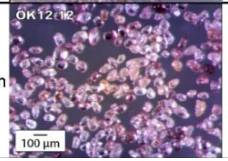	Well-rounded to sub-rounded. Some grains are elongated/equant	Grains from 45 to 150 microns.	Grains are mostly transparent with varying degree of pink hue. Some larger grains are a darker purple color.	Most well-rounded grains have smooth surfaces. Sub-rounded grains have slightly rough surfaces.	Present	Internal fractures present in most grains.

Table S2. Morphological descriptions of zircons, Ouachita FTB, Oklahoma. Separates may include minor grains of other heavy or opaque minerals.

Sample	Group/ Formation	Age	Photomicrograph	Shape	Size	Color	Surfaces	Fluid Inclusions?	Other
OK12-14	Jackfork	Pennsylvanian	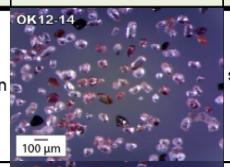	Well-rounded to sub-angular. Some grains are elongated.	Grains from 45 to 115 microns.	Most grains are transparent with slight pink hue. Some grains are of purple tint.	Most grains have smooth surfaces. Sub-angular grains tend to have slightly rougher surfaces.	Present mostly on sub-angular grains	Internal fractures occur in some grains. More fracturing in sub-angular grains. --Morphological description by Jacob T. Thompson.
OK12-16	Stanley	Mississippian	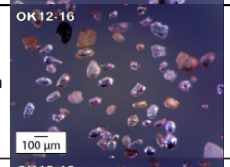	Sub-rounded to sub-angular.	Grains from 50 to 165 microns.	Most grains are transparent with slight pink hue. Some grains show a tanish color. A few darker purple grains.	Well-rounded grains have smooth surfaces. Sub-rounded and sub-angular grains have slightly rough surfaces.	Present	Internal fractures present in most grains that are not well-rounded. Tan grains have more fracturing. --Morphological description by Jacob T. Thompson.
OK12-18	Stanley	Mississippian		Well-rounded to sub-rounded.	Grains from 30 to 135 microns.	Grains are transparent with slight pink and purple hues.	Rough to slightly rough.	Present.	None.
OK12-19	Boggy	Pennsylvanian	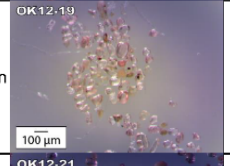	Well-rounded to sub-rounded.	Grains from 35 to 115 microns.	Grains are transparent with slight pink hue.	Smooth to slightly rough.	Present in few grains.	Internal fractures present in a majority of grains.
OK12-21	Savanna	Pennsylvanian	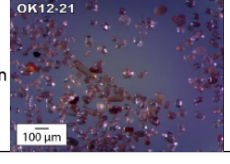	Well-rounded to sub-angular. Several elongate grains.	Grains from 30 to 210 microns.	Majority of grains are transparent with slight pink hue. Minor purple grains present.	Rough to smooth.	Present.	A small number of grains show internal fractures present.

Table S2, continued.

Sample	Group/ Formation	Age	Photomicrograph	Shape	Size	Color	Surfaces	Fluid Inclusions?	Other
OK12-23	Atoka, Lower	Pennsylvanian	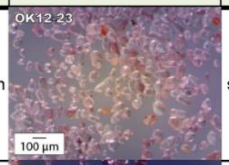	Well-rounded to sub-angular. Many elongate grains.	Grains from 30 to 135 microns.	Grains are a mostly transparent and pink. Few grains are purple.	Smooth to slightly rough.	Present.	Internal fractures present on several grains.
OK12-26	Atoka	Pennsylvanian	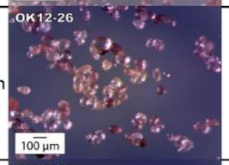	Well-rounded to sub-rounded.	Grains from 45 to 140 microns.	Grains are transparent with slight pink and purple hues.	Rough to slightly rough.	None.	None.
OK12-28	Bigfork to Arkansas Novaculite, undivided	Middle Ordovician to Devonian		Sub-angular.	Grain is approximately 50 microns.	Grain is transparent pink.	Rough?	None.	Poor zircon yield of only a few grains. Description is based on single grain shown in photomicrograph.
OK12-31	Stanley	Mississippian	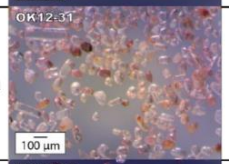	Well-rounded to sub-angular. Several elongate grains.	Grains from 50 to 335 microns.	Grains are a mostly transparent and pink. Few grains are purple.	Smooth to rough.	Present.	Possible fractures in a few number of grains.
OK12-32	Atoka	Pennsylvanian	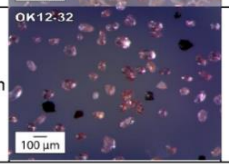	Well-rounded to sub-angular.	Grains from 50 to 135 microns.	Grains are transparent and pink.	Rough to smooth.	None.	None.

Table S2, continued.

Sample	Group/ Formation	Age	Photomicrograph	Shape	Size	Color	Surfaces	Fluid Inclusions?	Other
OK12-35	Jackfork	Pennsylvanian	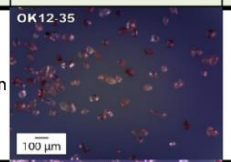	Well-rounded to sub-angular.	Grains from 35 to 135 microns.	Pink and purple transparent grains.	Rough to slightly rough.	Present.	None.
OK12-36	Jackfork	Pennsylvanian	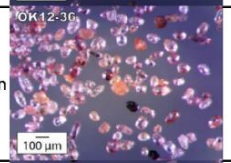	Well-rounded to sub-rounded. Some grains are elongated.	Grains from 55 to 125 microns.	Most grains transparent with darker pink hue. Some dark purple to reddish grains present. A few large tan tinted grains.	Slightly rough surfaces on the majority of grains. Elongated and some well-rounded grains have smooth surfaces.	Present.	Internal fractures present in sub-rounded grains. --Morphological description by Jacob T. Thompson.
OK12-37	Jackfork	Pennsylvanian	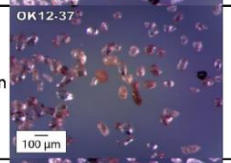	Well-rounded to sub-angular.	Grains from 40 to 150 microns.	Grains are transparent and pink. Sparse purple grains may be present.	Rough to slightly rough.	Present.	None.
OK12-39	Jackfork	Pennsylvanian	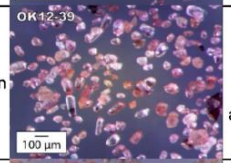	Well-rounded to sub-rounded. Some elongated and equant grains.	Grains from 30 to 130 microns.	Most grains transparent with pink hue. Large amount of tanish grains.	Some rough surfaces on rounded grains. Elongated grains have smooth surfaces.	Present mostly on sub-angular grains.	Grains show some internal fractures and/or opaque inclusions. --Morphological description by Jacob T. Thompson.
OK12-41	Thurman?	Pennsylvanian	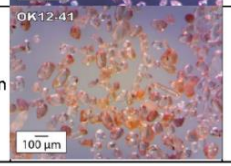	Well-rounded to sub-rounded. Some grains are elongated.	Grains from 60 to 235 microns.	Grains are transparent and pink. Few grains are purple.	Smooth to slightly rough.	Present.	None.

Table S2, continued.

Sample	Group/ Formation	Age	Photomicrograph	Shape	Size	Color	Surfaces	Fluid Inclusions?	Other
OK12-43	Savanna	Pennsylvanian	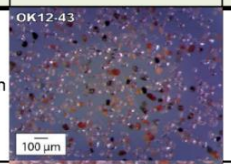	Well-rounded to sub-rounded.	Grains from 35 to 85 microns.	Grains are transparent, with minor pink hue.	Smooth to rough.	Present?	None.
OK12-45	Atoka, Lower *or* Johns Valley	Pennsylvanian	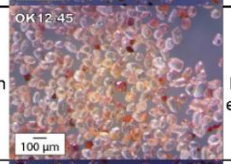	Well-rounded to sub-rounded. Mostly equant, but elongate grains are present.	Grains from 55 to 160 microns.	Grains are transparent and commonly pink.	Smooth to slightly rough.	Present.	Fractured grains are present.
OK12-50	Jackfork	Pennsylvanian	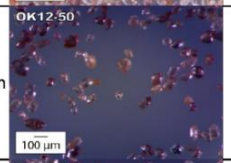	Well-rounded to sub-rounded.	Grains from 50 to 155 microns.	Grains are transparent, and typically have a minor pink hue.	Rough to slightly smooth.	Present?	None.
OK12-51	Jackfork	Pennsylvanian	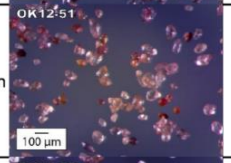	Rounded to sub-angular. Few elongate grains.	Grains from 50 to 135 microns.	Grains are transparent and pink.	Rough to slightly smooth.	None.	None.
OK12-52	Stanley	Mississippian	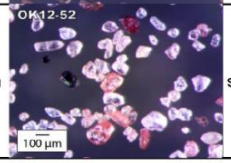	Well-rounded to sub-angular. Some grains elongated.	Grains from 55 to 190 microns.	Most grains transparent with pink hue. Some larger tan grains. A few darker purple grains present.	Most grains have slightly rough surfaces.	Present	Some grains show internal fractures. Large tan grains show more fracturing and/or opaque inclusions. -Morphological description by Jacob T. Thompson.

Table S2, continued.

Sample	Group/ Formation	Age	Photomicrograph	Shape	Size	Color	Surfaces	Fluid Inclusions?	Other
OK12-54	Stanley	Mississippian	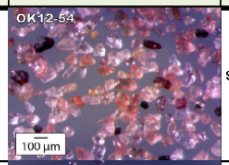	Sub-rounded to sub-angular. Some grains are elongated.	Grains from 45 to 140 microns.	Most grains transparent with pink hue. Some dark purple and red grains present.	Mostly smooth surfaces with some slightly rough surfaces.	Present.	Some internal fractures present in grains. --Morphological description by Jacob T. Thompson.
OK12-55	Jackfork?	Pennsylvanian	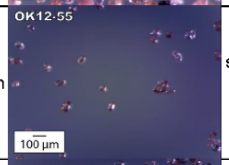	Well-rounded to sub-angular. Some grains elongated and others are equant.	Grains from 55 to 115 microns.	Grains are transparent, and typically have a minor pink hue.	Slightly rough to smooth.	Present.	None.
OK12-56	Jackfork?	Pennsylvanian	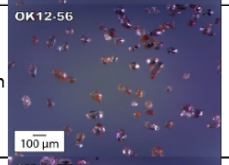	Well-rounded to sub-rounded. Mostly equant grains.	Grains from 45 to 140 microns.	Grains are transparent, and typically have a minor pink hue.	Smooth to slightly rough.	Present?	Several grains may have internal fractures.
OK12-57	Stanley	Mississippian	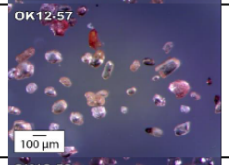	Well-rounded to sub-rounded grains. Some equant grains. Large elongated grain present.	Grains from 35 to 225 microns.	Most grains transparent with pink hue. A few grains with redish tint.	Mostly smooth surfaces. A few grains show rough surfaces.	None	Some grains show internal fractures. --Morphological description by Jacob T. Thompson.
OK12-58	Stanley	Mississippian	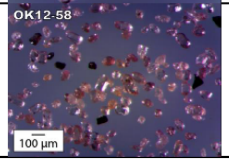	Well-rounded to sub-angular. Mostly equant grains.	Grains from 40 to 200 microns.	Grains are transparent and a majority are pink.	Smooth to rough.	Present.	None.

Table S2, continued.

Sample	Group/ Formation	Age	Photomicrograph	Shape	Size	Color	Surfaces	Fluid Inclusions?	Other
OK12-59	Stanley	Mississippian	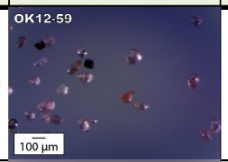	Well-rounded to rounded.	Grains from 40 to 200 microns.	Grains are transparent, mostly with a pink hue.	Rough to smooth.	None.	None.
OK12-60	Stanley	Mississippian	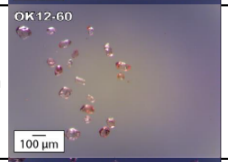	Well-rounded to rounded.	Grains from 50 to 100 microns.	Grains are transparent, mostly with a pink hue.	Slightly rough to smooth.	Present.	None.
OK12-63	Stanley	Mississippian	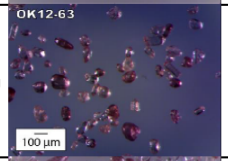	Well-rounded to sub-rounded. Mostly equant grains, and minor elongate grains.	Grains from 45 to 145 microns.	Grains are transparent and pink. Minor purple grains.	Rough to smooth.	Present.	None.
OK12-63 tuff	Stanley	Mississippian	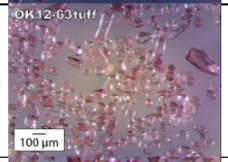	Well-rounded to sub-rounded. Mostly equant grains, and minor elongate grains.	Grains from 35 to 285 microns.	Grains are transparent and pink.	Smooth to slightly rough.	Present.	Many grains have internal fractures.
OK12-64	Ordovician	Blaylock	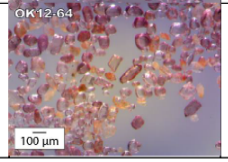	Well-rounded to sub-rounded. Mostly equant grains, and minor elongate grains.	Grains from 30 to 200 microns.	Grains are transparent. Most grains are pink, and purple is common.	Smooth to slightly rough.	Present.	None.

Table S2, continued.

Sample	Group/ Formation	Age	Photomicrograph	Shape	Size	Color	Surfaces	Fluid Inclusions?	Other
BB-7	Ordovician	Blaylock	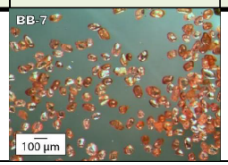	Well-rounded to sub-rounded. Mostly equant grains.	Grains from 45 to 135 microns.	Grains are transparent and pink.	Smooth to slightly rough.	None.	Several grains have internal fractures.

Table S2, continued.

Sample	Mineral	Grains (n)	Number of Tracks			Track Density ($x\ 10^6$ tr cm^{-2})			Age Dispersion (%)	P(χ2)	Central Age (Ma) (±1σ)	Comments
			N_s	N_i	N_d	ρ_s	ρ_i	ρ_d				
OK12-1	Zircon	20	2600	168	2215	16.190	1.046	0.3461	6.38	0.685	315.9±28.0†	mixed
OK12-4	Zircon	20	4418	339	3094	18.510	1.420	0.4834	24.70	0.003	347.5±28.6	mixed
OK12-6	Zircon	20	2614	199	2208	17.380	1.323	0.3460	<0.01	0.999	268.7±22.0†	reset
OK12-9	Apatite	9	257	336	3582	1.139	1.195	1.1190	<0.01	0.632	193.4±19.2	reset
OK12-9	Zircon	20	2642	184	2202	24.870	1.732	0.3440	<0.01	0.999	292.4±24.6†	reset
OK12-12	Zircon	20	3366	300	3084	10.930	0.975	0.4819	21.70	0.031	308.1±25.0	mixed
OK12-14	Zircon	20	3774	361	3074	26.310	2.518	0.4803	10.00	0.316	284.9±18.2	mixed
OK12-16	Zircon	20	3999	322	3064	23.670	1.906	0.4788	0.10	0.846	338.2±21.0	mixed?
OK12-18	Zircon	20	4217	390	3054	21.530	1.991	0.4772	0.10	0.747	294.5±16.9	mixed?
OK12-19	Zircon	10	1069	71	2195	19.880	1.321	0.3430	<0.01	0.948	305.4±39.0†	1 older grain
OK12-21	Zircon	20	2906	284	3044	20.000	1.955	0.4757	<0.01	0.988	278.2±18.4	reset
OK12-23	Zircon	20	3870	274	2188	23.260	1.647	0.3419	5.66	0.722	285.4±20.9†	mixed
OK12-26	Zircon	20	3787	360	3034	19.460	1.850	0.4741	<0.01	0.948	284.9±16.9	reset
OK12-31	Zircon	20	4077	263	2182	27.700	1.787	0.3409	13.30	0.294	311.1±24.7†	mixed
OK12-32	Zircon	10	2225	146	3024	20.820	1.366	0.4725	14.20	0.205	399.4±39.9	mixed
OK12-32b	Zircon	10	1986	1.59	2795	24.060	1.926	0.4367	<0.01	0.911	310.9±26.6	mixed?
OK12-35	Zircon	20	4558	376	3014	31.510	2.600	0.4710	14.30	0.092	324.5±21.6	mixed
OK12-36	Zircon	20	3721	357	3004	22.360	2.145	0.4694	<0.01	0.997	279.6±16.7	reset
OK12-37	Zircon	20	4716	337	2994	27.500	1.965	0.4679	15.70	0.111	366.5±25.9	mixed
OK12-39	Zircon	20	4170	407	2984	16.090	1.570	0.4663	<0.01	0.984	273.1±15.4	reset
OK12-41	Zircon	20	2840	184	2175	24.650	1.597	0.3398	0.84	0.947	310.0±26.1†	1 older grain
OK12-43	Zircon	20	1957	191	2974	20.250	1.978	0.4647	<0.01	0.990	272.2±21.5	reset
OK12-45	Zircon	20	3922	237	2168	20.560	1.243	0.3388	18.00	0.104	327.0±28.3†	mixed
OK12-50	Zircon	20	4144	332	2964	21.440	1.718	0.4632	14.00	0.197	324.5±22.4	mixed
OK12-51	Zircon	20	4243	396	2954	21.810	2.035	0.4616	0.30	0.774	282.6±16.2	1 older grain?
OK12-52	Zircon	3	369	33	2944	6.704	0.600	0.4601	3.50	0.199	293.8±54.1	mixed
OK12-52b	Zircon	17	3981	270	2725	18.850	1.278	0.4258	18.10	0.080	355.7±28.7	mixed
OK12-54	Zircon	5	762	76	2934	31.330	3.125	4.5850	<0.01	0.970	263.0±32.2	reset?
OK12-54b	Zircon	5	737	69	2715	17.190	1.609	0.4242	<0.01	0.999	259.3±33.2	reset?
OK12-55	Zircon	20	4610	356	2954	19.310	1.491	0.4569	19.20	0.034	330.2±24.2	mixed
OK12-56	Zircon	20	3655	287	2914	23.310	1.830	0.4554	7.20	0.393	329.9±22.2	mixed
OK12-57	Zircon	13	2788	181	2904	25.780	1.673	0.4538	12.50	0.240	392.3±34.3	mixed
OK12-58	Zircon	20	4412	350	2895	21.280	1.688	0.4523	10.10	0.191	323.2±20.8	mixed
OK12-59	Zircon	20	4724	438	2885	28.330	2.673	0.4507	<0.01	0.999	277.8±15.2	reset
OK12-63tuff	Zircon	20	4037	256	2162	25.230	1.600	0.3378	13.20	0.242	311.5±24.8†	mixed
OK12-63b	Zircon	20	4932	382	2875	18.010	1.395	0.4492	27.40	0.001	324.7±27.5	mixed
OK12-64	Zircon	20	4160	216	2155	20.900	1.085	0.3367	13.30	0.157	379.0±32.0†	mixed
BB-7	Zircon	11	1814	180	3168	21.640	2.147	0.4951	<0.01	0.997	295.3±25.2	reset

Note. Analyses by external detector method using 0.5 for the 4π/2π geometry correction factor. Ages calculated using dosimeter glasses: IRMM540R with ζ540R = 368.1±14.9 (apatite) and IRMM541 with ζ541 = 116.8±1.5 (121.1±3.5†) (zircon). $P\chi^2$ is the probability of obtaining a χ^2 value for v degrees of freedom where v = number of grains - 1. Abbreviations -- N_s and ρ_s, number and density, respectively, of spontaneous tracks in either apatite or zircon grains; N_i and ρ_i, number and density, respectively, number of induced tracks in detectors covering either apatite or zircon grains; N_d and ρ_d, number and density, respectively, of induced tracks in detectors covering fluence monitors. Analyst: Stuart N. Thomson.

Table S3. Fission track data summary for apatite and zircon, Ouachita orogen, SE Oklahoma.

Youngest Zircon (U-Th)/He Aliquot By Sample, Ouachita orogen, Southeastern Oklahoma

Sample	*Corrected Age (Ma)*	*Error, 1σ (Ma)*	*U (ppm)*	*Th (ppm)*	*147Sm (ppm)*	*[U]e*	*Th/U*	*He (nmol/g)*	*mass (µg)*	*Ft*	*ESR (µm)*
zOK12-1-3	237.9	19.03	40.0	23.1	0.8	45.3	0.58	41.7	2.75	0.71	39.09
zOK12-4-5	250.9	20.08	35.0	13.2	2.8	38.1	0.38	39.9	5.61	0.76	48.68
zOK12-6-3	265.8	21.27	237.3	119.1	3.7	264.8	0.50	299.8	6.19	0.77	52.11
zOK12-9-6	256.9	20.55	174.0	91.2	6.8	195.1	0.52	197.0	2.82	0.72	40.62
zOK12-12-3	236.2	18.89	620.5	207.3	32.4	668.3	0.33	676.8	6.32	0.78	53.30
zOK12-16-5	207.4	16.59	555.4	106.1	23.1	580.0	0.19	507.0	5.38	0.77	50.21
zOK12-19-1	236.5	18.92	169.5	90.1	0.5	190.2	0.53	170.3	2.47	0.69	36.92
zOK12-21-4	278.0	22.24	192.5	157.4	14.9	228.8	0.82	252.9	3.07	0.72	42.18
zOK12-23-2	294.6	23.57	257.6	202.4	7.3	304.3	0.79	367.4	3.91	0.74	45.91
zOK12-27-4	284.9	22.79	93.4	55.5	3.9	106.2	0.59	105.1	1.23	0.63	30.49
zOK12-31-2	231.8	18.54	49.6	21.8	1.4	54.6	0.44	56.1	10.57	0.81	61.90
zOK12-32-3	269.3	21.54	224.7	109.7	9.7	250.0	0.49	275.5	4.92	0.74	45.53
zOK12-35-1	328.7	26.29	263.7	63.4	12.0	278.4	0.24	357.8	2.34	0.71	38.91
zOK12-36-3	252.2	20.17	497.7	101.7	77.8	521.5	0.20	547.2	5.18	0.76	47.30
zOK12-37-1	247.0	19.76	12.6	14.0	3.9	15.9	1.11	17.1	7.71	0.79	57.04
zOK12-39-3	280.3	22.42	59.2	22.5	4.4	64.4	0.38	78.8	8.16	0.79	56.98
zOK12-41-2	334.6	26.77	48.0	24.9	0.3	53.7	0.52	77.3	7.30	0.78	53.18
zOK12-43-3	217.9	17.43	130.9	24.6	4.5	136.6	0.19	110.5	1.86	0.68	34.69
zOK12-45-3	323.3	25.86	70.4	24.1	1.0	75.9	0.34	104.4	6.14	0.77	50.69
zOK12-51-4	347.6	27.81	60.6	25.2	3.7	66.4	0.41	91.2	3.17	0.72	40.31
zOK12-52-3	343.4	27.47	328.6	166.3	72.1	367.2	0.51	534.6	5.96	0.77	50.14
zOK12-55-2	303.4	24.27	73.4	55.9	6.0	86.3	0.76	115.5	8.38	0.80	59.51
zOK12-56-3	317.5	25.40	29.8	15.5	3.7	33.4	0.52	46.1	7.69	0.79	55.64
zOK12-58-1	290.0	23.20	26.3	12.5	2.9	29.2	0.48	39.2	16.50	0.84	73.27
zOK12-59-3	231.0	18.48	102.2	29.7	2.5	109.0	0.29	107.4	6.96	0.78	52.28
zOK12-60-3	190.1	15.21	86.6	46.9	1.7	97.4	0.54	68.9	1.86	0.68	35.75
zOK12-63-2	218.1	17.45	141.7	75.6	3.4	159.2	0.53	150.1	6.94	0.79	55.90
zOK12-63tuff-1	198.8	15.90	67.8	28.8	5.0	74.5	0.42	66.2	12.32	0.82	64.63
zOK12-64-2	181.6	14.53	96.7	53.3	2.4	109.0	0.55	86.6	9.15	0.80	59.48

Note. eU = [U] + 0.235 [Th] +0.0053 [Sm] with concentrations in weight %. Abbreviations: F_t, α-ejection correction factor; ESR, equivalent spherical radius. See Appendix C for compiled and reduced (U-Th)/He data.

Table S4. Youngest zircon (U-Th)/He aliquot by sample, Ouachita orogen, SE Oklahoma.

		BinomFit										Radial Plotter	
Sample	*Total Grains*	*Peak Age "A" (Ma)*	*(-) 1σ* error (Ma)	*(+) 1σ* error (Ma)	*Grain Count*	*Fraction (%)*	*Peak Age "B" (Ma)*	*(-) 1σ* error (Ma)	*(+) 1σ* error (Ma)	*Grain Count*	*Fraction (%)*	*Minimum Age (Ma)*	*1σ* error (Ma)
OK12-1	20	294.8	26.2	28.7	18.7	93.7	895.6	321.9	484.1	1.3	6.3	329	23
OK12-4*	20	277.4	54.6	67.7	7.2	35.9	379.1	52.5	60.6	11.7	58.3	308	35
OK12-6	20	269.5	20.8	22.5	20.0	100.0						266	20
OK12-9 (apatite)	9	193.4	18.1	19.9	9.0	100.0						192	19
OK12-9	20	292.3	23.1	25.1	20.0	100.0						286	23
OK12-12	20	264.5	27.6	30.7	13.8	69.1	470.3	86.5	105.2	6.2	30.9	265	29
OK12-14	20	261.8	34.6	39.7	13.8	69.1	346.7	71.2	89.0	6.2	30.9	266	39
OK12-16	20	338.2	19.9	21.1	20.0	100.0						332	21
OK12-18	20	294.5	16.1	17.0	20.0	100.0						288	17
OK12-19	10	305.4	35.9	40.5	10.0	100.0						297	38
OK12-21	20	278.2	17.4	18.6	20.0	100.0						274	18
OK12-23	20	269.8	20.8	22.5	18.6	93.1	535.5	138.9	185.0	1.4	6.9	271	21
OK12-26	20	284.9	16.1	17.1	20.0	100.0						280	16
OK12-31	20	271.3	36.3	41.8	12.3	61.4	393.8	66.3	79.3	7.7	38.6	276	58
OK12-32	10	407.4	33.4	36.3	10.0	100.0						348	160
OK12-32b	10	310.9	24.9	27.0	10.0	100.0						307	26
OK12-35	20	301.2	24.9	27.1	16.2	81.0	481.0	107.9	137.6	3.8	19.0	298	33
OK12-36	20	279.6	15.9	16.8	20.0	100.0						277	16
OK12-37	20	340.1	26.4	28.5	16.8	84.1	570.9	120.1	150.3	3.2	15.9	337	36
OK12-39	20	273.1	14.7	15.5	20.0	100.0						270	15
OK12-41	20	310.0	24.5	26.5	20.0	100.0						300	25
OK12-43	20	272.2	20.3	21.9	20.0	100.0						266	21
OK12-45	20	306.8	30.9	34.3	17.4	86.8	612.4	269.1	463.1	2.6	13.2	298	41
OK12-50	20	292.9	25.2	27.5	15.8	79.0	478.2	75.2	88.6	4.2	21.0	294	33
OK12-51	20	282.6	15.4	16.2	20.0	100.0						277	16
OK12-52	3	293.7	48.2	57.4	3.0	100.0						197	56
OK12-52b	17	268.8	38.2	44.4	5.5	32.6	421.1	43.2	48.0	11.5	67.4	285	63
OK12-54	5	263.0	29.8	33.5	5.0	100.0						262	33
OK12-54b	5	259.3	30.6	34.6	5.0	100.0						259	34
OK12-55	20	306.2	23.0	24.8	17.2	86.2	582.2	146.4	192.7	2.8	13.8	296	27
OK12-56	20	309.5	41.6	47.8	15.5	77.7	418.3	114.6	156.0	4.5	22.3	318	29
OK12-57	13	352.6	50.3	58.4	9.4	72.6	528.6	120.4	154.1	3.6	27.4	365	66
OK12-58	20	307.3	26.9	29.4	17.3	86.7	483.4	134.7	184.1	2.7	13.3	310	33
OK12-59	20	277.8	14.5	15.3	20	100.0						275	14
OK12-63tuff	20	292.8	27.8	30.6	17.4	87.2	497.7	149.1	209.5	2.6	12.8	289	33
OK12-63b	20	276.1	18.1	19.3	15.2	76.2	623.0	93.6	109.2	4.8	23.8	269	20
OK12-64	20	328.5	58.4	70.6	11.3	56.3	465.9	110.6	143.4	8.7	43.7	356	80
BB-7	11	295.2	23.6	25.6	11	100.0						293	24

Note. *OK12-4 third population is 928.2 Ma, -281.1 Ma, +391.4Ma, 1.2 grain count, 5.8%. Peak ages calculated by BinomFit (Brandon, 2002) and minimum ages determined using Radial Plotter (Vermeesch, 2009).

Table S5. Fission track peak ages and minimum ages, Ouachita orogen, SE Oklahoma.

Data Set S1. Apatite Fission Track Data and Cooling Ages

Sample Number	**OK12-9**											
Position (#)	25											
Area of Graticule Square	6.400E-07											
No. of Crystals	9											
Zeta Factor ± Error	368.1	14.9										
Rho d (% Relative Error)	1.119E+06	1.67										
N d	3582											
N s	N i	N g	Dpar	Dper	Rmr0	ρ s	ρ i	ρ s / ρ i	U ppm	Age (Ma)	Age error	
16	24	100	1.63	0.38	0.838	2.500E+05	3.750E+05	0.6667	5.0	**135.86**	**44.25**	
88	94	36	2.06	0.51	0.811	3.819E+06	4.080E+06	0.9362	54.7	**189.98**	**29.38**	
4	7	16	2.06	0.46	0.811	3.906E+05	6.836E+05	0.5714	9.2	**116.63**	**73.28**	
54	57	21	1.80	0.56	0.828	4.018E+06	4.241E+06	0.9474	56.9	**192.22**	**37.46**	
33	21	40	2.92	0.86	0.743	1.289E+06	8.203E+05	1.5714	11.0	**315.78**	**89.23**	
19	22	30	1.68	0.67	0.835	9.896E+05	1.146E+06	0.8636	15.4	**175.46**	**55.49**	
11	8	20	2.00	0.49	0.815	8.594E+05	6.250E+05	1.3750	8.4	**277.14**	**129.35**	
10	12	24	1.98	0.65	0.816	6.510E+05	7.813E+05	0.8333	10.5	**169.38**	**72.90**	
10	12	49	1.99	0.48	0.816	3.189E+05	3.827E+05	0.8333	5.1	**169.38**	**72.90**	
**********	**********	**********	**********	**********	**********	**********	**********	**********	**********	**********	**********	
245	257	336	2.01	0.56	0.813	1.139E+06	1.195E+06	0.9533	16.0	**193.41**	**19.23**	
Pooled Ratio		0.9533	±	0.0948								
Mean Ratio		0.9554	±	0.1070								
Pooled Age		193.41	±	19.23	1 S.E.							
Mean Crystal Age		193.82	±	22.01	1 S.E.							
Binomial Age		**194.17**	**+**	**36.46**	**"+95%"**							
			-	**32.09**	**"-95%"**							
Central Age		**193.41**	**±**	**19.23**								
Age Dispersion		**0.00** %										
Chi-squared		**6.137**	with	8	degrees of freedom							
P (Chi-Sq)		**63.19 %**										
MSWD		**0.68**										

Data Set S2. Zircon Fission Track Data and Cooling Ages

Sample Number		**OK12-1**						
Position (#)		30						
Area of Graticule Square		6.400E-07						
No. of Crystals		20						
Zeta Factor ± Error		121.1	3.5					
Rho d (% Relative Error)		3.461E+05	2.12					
N d		2215						
N s	N i	N g	ρ s	ρ i	ρ s / ρ i	U ppm	Age (Ma)	Age error
139	8	6	3.620E+07	2.083E+06	17.3750	297.4	**354.20**	**129.41**
137	10	6	3.568E+07	2.604E+06	13.7000	371.7	**280.89**	**92.56**
132	10	6	3.438E+07	2.604E+06	13.2000	371.7	**270.85**	**89.37**
59	5	6	1.536E+07	1.302E+06	11.8000	185.9	**242.66**	**113.36**
106	8	15	1.104E+07	8.333E+05	13.2500	118.9	**271.86**	**100.15**
120	10	10	1.875E+07	1.563E+06	12.0000	223.0	**246.70**	**81.68**
122	9	9	2.118E+07	1.563E+06	13.5556	223.0	**277.99**	**96.54**
87	6	8	1.699E+07	1.172E+06	14.5000	167.3	**296.92**	**125.78**
84	4	8	1.641E+07	7.813E+05	21.0000	111.5	**425.71**	**218.40**
83	8	10	1.297E+07	1.250E+06	10.3750	178.4	**213.84**	**79.53**
144	9	18	1.250E+07	7.813E+05	16.0000	111.5	**326.87**	**112.92**
122	11	25	7.625E+06	6.875E+05	11.0909	98.1	**228.33**	**72.35**
96	7	10	1.500E+07	1.094E+06	13.7143	156.1	**281.18**	**110.54**
187	12	21	1.391E+07	8.929E+05	15.5833	127.4	**318.57**	**95.55**
93	5	8	1.816E+07	9.766E+05	18.6000	139.4	**378.46**	**174.27**
178	11	15	1.854E+07	1.146E+06	16.1818	163.5	**330.49**	**103.36**
143	11	8	2.793E+07	2.148E+06	13.0000	306.7	**266.83**	**84.04**
250	5	18	2.170E+07	4.340E+05	50.0000	62.0	**970.89**	**439.90**
113	3	12	1.471E+07	3.906E+05	37.6667	55.8	**744.64**	**436.41**
205	16	32	1.001E+07	7.813E+05	12.8125	111.5	**263.06**	**68.93**
**********	**********	**********	**********	**********	**********	**********	**********	**********
2600	168	251	1.619E+07	1.046E+06	15.4762	149.3	**316.43**	**27.63**
Pooled Ratio		15.4762	±	1.3513				
Mean Ratio		17.2703	±	2.1580				
Pooled Age		316.43	±	27.63	1 S.E.			
Mean Crystal Age		352.13	±	45.07	1 S.E.			
Binomial Age		**317.12**	**+**	**53.40**	**"+95%"**			
			-	**45.54**	**"-95%"**			
Central Age		**315.94**	**±**	**27.98**				
Age Dispersion		**6.38**	%					
Chi-squared		**15.588**	with	19	degrees of freedom			
P (Chi-Sq)		**68.45**	**%**					
MSWD		**0.93**						

Sample Number		**OK12-4**						
Position (#)		3						
Area of Graticule Square		6.400E-07						
No. of Crystals		20						
Zeta Factor ± Error		116.8	1.5					
Rho d (% Relative Error)		4.834E+05	1.80					
N d		3094						
N s	N i	N g	ρ s	ρ i	ρ s / ρ i	U ppm	Age (Ma)	Age error
147	19	24	9.570E+06	1.237E+06	7.7368	126.4	**214.80**	**52.58**
186	15	18	1.615E+07	1.302E+06	12.4000	133.1	**340.88**	**91.81**
296	19	20	2.313E+07	1.484E+06	15.5789	151.7	**425.45**	**101.13**
215	13	14	2.400E+07	1.451E+06	16.5385	148.3	**450.76**	**129.13**
117	12	8	2.285E+07	2.344E+06	9.7500	239.5	**269.53**	**81.92**
277	20	18	2.405E+07	1.736E+06	13.8500	177.4	**379.59**	**88.29**
244	20	12	3.177E+07	2.604E+06	12.2000	266.1	**335.53**	**78.39**
133	15	15	1.385E+07	1.563E+06	8.8667	159.7	**245.57**	**67.11**
110	8	12	1.432E+07	1.042E+06	13.7500	106.5	**376.93**	**138.28**
266	14	20	2.078E+07	1.094E+06	19.0000	111.8	**515.23**	**141.74**
205	20	16	2.002E+07	1.953E+06	10.2500	199.6	**283.06**	**66.60**
385	10	16	3.760E+07	9.766E+05	38.5000	99.8	**1004.40**	**322.48**
234	13	25	1.463E+07	8.125E+05	18.0000	83.0	**489.12**	**139.79**
164	16	18	1.424E+07	1.389E+06	10.2500	141.9	**283.06**	**74.40**
133	19	21	9.896E+06	1.414E+06	7.0000	144.5	**194.65**	**47.93**
291	24	36	1.263E+07	1.042E+06	12.1250	106.5	**333.52**	**71.21**
245	11	16	2.393E+07	1.074E+06	22.2727	109.8	**599.97**	**185.39**
264	19	28	1.473E+07	1.060E+06	13.8947	108.4	**380.79**	**90.84**
352	37	24	2.292E+07	2.409E+06	9.5135	246.2	**263.13**	**45.84**
154	15	12	2.005E+07	1.953E+06	10.2667	199.6	**283.51**	**76.94**
**********	**********	**********	**********	**********	**********	**********	**********	**********
4418	339	373	1.851E+07	1.420E+06	13.0324	145.1	**357.80**	**21.66**
Pooled Ratio		13.0324	±	0.7889				
Mean Ratio		14.0872	±	1.5583				
Pooled Age		357.80	±	21.66	1 S.E.			
Mean Crystal Age		385.90	±	43.84	1 S.E.			
Binomial Age		**358.19**	**+**	**41.27**	**"+95%"**			
			-	**36.97**	**"-95%"**			
Central Age		**347.49**	**±**	**28.62**				
Age Dispersion		**24.66**	%					
Chi-squared		**40.852**	with	19	degrees of freedom			
P (Chi-Sq)		**0.25**	**%**					
MSWD		**2.85**						

Sample Number		**OK12-5**						
Position (#)		31						
Area of Graticule Square		6.400E-07						
No. of Crystals		20						
Zeta Factor ± Error		121.1	3.5					
Rho d (% Relative Error)		3.450E+05	2.13					
N d		2208						
N s	N i	N g	ρ s	ρ i	ρ s / ρ i	U ppm	Age (Ma)	Age error
202	15	14	2.254E+07	1.674E+06	13.4667	239.7	**275.35**	**74.35**
142	9	9	2.465E+07	1.563E+06	15.7778	223.7	**321.44**	**111.09**
123	7	8	2.402E+07	1.367E+06	17.5714	195.8	**356.99**	**139.31**
204	13	12	2.656E+07	1.693E+06	15.6923	242.4	**319.75**	**92.18**
131	11	12	1.706E+07	1.432E+06	11.9091	205.1	**244.10**	**77.13**
72	5	9	1.250E+07	8.681E+05	14.4000	124.3	**294.00**	**136.38**
155	13	14	1.730E+07	1.451E+06	11.9231	207.8	**244.38**	**71.11**
131	13	15	1.365E+07	1.354E+06	10.0769	193.9	**207.14**	**60.69**
99	8	10	1.547E+07	1.250E+06	12.3750	179.0	**253.46**	**93.61**
173	12	18	1.502E+07	1.042E+06	14.4167	149.2	**294.34**	**88.50**
123	9	21	9.152E+06	6.696E+05	13.6667	95.9	**279.35**	**96.98**
123	10	12	1.602E+07	1.302E+06	12.3000	186.4	**251.96**	**83.34**
131	12	12	1.706E+07	1.563E+06	10.9167	223.7	**224.11**	**68.07**
142	11	9	2.465E+07	1.910E+06	12.9091	273.5	**264.18**	**83.22**
65	5	9	1.128E+07	8.681E+05	13.0000	124.3	**266.00**	**123.82**
82	8	6	2.135E+07	2.083E+06	10.2500	298.3	**210.64**	**78.39**
162	10	15	1.688E+07	1.042E+06	16.2000	149.2	**329.83**	**108.12**
99	7	10	1.547E+07	1.094E+06	14.1429	156.6	**288.87**	**113.45**
101	8	8	1.973E+07	1.563E+06	12.6250	223.7	**258.48**	**95.39**
154	13	12	2.005E+07	1.693E+06	11.8462	242.4	**242.83**	**70.67**
**********	**********	**********	**********	**********	**********	**********	**********	**********
2614	199	235	1.738E+07	1.323E+06	13.1357	189.5	**268.72**	**21.99**
Pooled Ratio		13.1357	±	1.0749				
Mean Ratio		13.2733	±	0.4463				
Pooled Age		268.72	±	21.99	1 S.E.			
Mean Crystal Age		271.48	±	9.32	1 S.E.			
Binomial Age		**269.23**	**+**	**41.70**	**"+95%"**			
			-	**36.01**	**"-95%"**			
Central Age		**268.72**	**±**	**21.99**				
Age Dispersion		**0.00**	%					
Chi-squared		**3.931**	with	19	degrees of freedom			
P (Chi-Sq)		**99.99**	**%**					
MSWD		**0.21**						

Sample Number		**OK12-9**						
Position (#)		32						
Area of Graticule Square		6.400E-07						
No. of Crystals		20						
Zeta Factor ± Error		121.1	3.5					
Rho d (% Relative Error)		3.440E+05	2.13					
N d		2202						
N s	N i	N g	ρ s	ρ i	ρ s / ρ i	U ppm	Age (Ma)	Age error
79	6	6	2.057E+07	1.563E+06	13.1667	224.4	**268.58**	**114.14**
77	6	9	1.337E+07	1.042E+06	12.8333	149.6	**261.91**	**111.41**
100	8	6	2.604E+07	2.083E+06	12.5000	299.2	**255.24**	**94.23**
114	9	6	2.969E+07	2.344E+06	12.6667	336.6	**258.58**	**90.01**
244	16	12	3.177E+07	2.083E+06	15.2500	299.2	**310.07**	**80.79**
94	6	6	2.448E+07	1.563E+06	15.6667	224.4	**318.33**	**134.53**
125	9	9	2.170E+07	1.563E+06	13.8889	224.4	**282.99**	**98.19**
72	6	6	1.875E+07	1.563E+06	12.0000	224.4	**245.23**	**104.57**
137	10	6	3.568E+07	2.604E+06	13.7000	374.0	**279.22**	**92.01**
82	7	4	3.203E+07	2.734E+06	11.7143	392.7	**239.49**	**94.70**
165	11	12	2.148E+07	1.432E+06	15.0000	205.7	**305.10**	**95.64**
115	10	8	2.246E+07	1.953E+06	11.5000	280.5	**235.19**	**78.00**
236	16	15	2.458E+07	1.667E+06	14.7500	239.3	**300.13**	**78.28**
81	7	6	2.109E+07	1.823E+06	11.5714	261.8	**236.63**	**93.61**
211	13	12	2.747E+07	1.693E+06	16.2308	243.1	**329.51**	**94.90**
104	9	8	2.031E+07	1.758E+06	11.5556	252.4	**236.31**	**82.54**
124	6	6	3.229E+07	1.563E+06	20.6667	224.4	**416.71**	**174.83**
184	8	8	3.594E+07	1.563E+06	23.0000	224.4	**462.11**	**167.72**
181	15	15	1.885E+07	1.563E+06	12.0667	224.4	**246.56**	**66.84**
117	6	6	3.047E+07	1.563E+06	19.5000	224.4	**393.89**	**165.48**
**********	**********	**********	**********	**********	**********	**********	**********	**********
2642	184	166	2.487E+07	1.732E+06	14.3587	248.7	**292.35**	**24.64**
Pooled Ratio		14.3587	±	1.2101				
Mean Ratio		14.4614	±	0.7247				
Pooled Age		292.35	±	24.64	1 S.E.			
Mean Crystal Age		294.39	±	15.08	1 S.E.			
Binomial Age		**292.94**	**+**	**47.13**	**"+95%"**			
			-	**40.47**	**"-95%"**			
Central Age		**292.35**	**±**	**24.64**				
Age Dispersion		**0.00**	%					
Chi-squared		**5.783**	with	19	degrees of freedom			
P (Chi-Sq)		**99.84**	**%**					
MSWD		**0.27**						

Sample Number		**OK12-12**						
Position (#)		4						
Area of Graticule Square		6.400E-07						
No. of Crystals		20						
Zeta Factor ± Error		116.8	1.5					
Rho d (% Relative Error)		4.819E+05	1.80					
N d		3084						
N s	N i	N g	ρ s	ρ i	ρ s / ρ i	U ppm	Age (Ma)	Age error
98	11	21	7.292E+06	8.185E+05	8.9091	83.9	**245.98**	**78.40**
176	23	24	1.146E+07	1.497E+06	7.6522	153.5	**211.84**	**47.20**
146	9	12	1.901E+07	1.172E+06	16.2222	120.1	**441.10**	**151.81**
146	10	12	1.901E+07	1.302E+06	14.6000	133.5	**398.32**	**130.50**
176	18	20	1.375E+07	1.406E+06	9.7778	144.2	**269.46**	**66.95**
118	7	12	1.536E+07	9.115E+05	16.8571	93.4	**457.77**	**178.36**
186	9	21	1.384E+07	6.696E+05	20.6667	68.6	**556.86**	**190.46**
102	9	32	4.980E+06	4.395E+05	11.3333	45.0	**311.31**	**108.47**
251	28	28	1.401E+07	1.563E+06	8.9643	160.2	**247.47**	**49.61**
193	14	20	1.508E+07	1.094E+06	13.7857	112.1	**376.74**	**104.61**
146	8	18	1.267E+07	6.944E+05	18.2500	71.2	**494.17**	**179.77**
103	11	12	1.341E+07	1.432E+06	9.3636	146.8	**258.28**	**82.13**
218	16	24	1.419E+07	1.042E+06	13.6250	106.8	**372.48**	**96.83**
127	12	24	8.268E+06	7.813E+05	10.5833	80.1	**291.17**	**88.17**
173	20	50	5.406E+06	6.250E+05	8.6500	64.1	**238.95**	**56.68**
150	13	24	9.766E+06	8.464E+05	11.5385	86.8	**316.81**	**91.86**
133	18	30	6.927E+06	9.375E+05	7.3889	96.1	**204.66**	**51.60**
205	24	32	1.001E+07	1.172E+06	8.5417	120.1	**236.01**	**51.19**
240	30	40	9.375E+06	1.172E+06	8.0000	120.1	**221.30**	**43.13**
279	10	25	1.744E+07	6.250E+05	27.9000	64.1	**740.93**	**239.03**
**********	**********	**********	**********	**********	**********	**********	**********	**********
3366	300	481	1.093E+07	9.745E+05	11.2200	99.9	**308.27**	**19.79**
Pooled Ratio		11.2200	±	0.7201				
Mean Ratio		12.6305	±	1.1762				
Pooled Age		308.27	±	19.79	1 S.E.			
Mean Crystal Age		346.00	±	33.02	1 S.E.			
Binomial Age		**308.67**	**+**	**38.36**	**"+95%"**			
			-	**34.09**	**"-95%"**			
Central Age		**308.09**	**±**	**24.99**				
Age Dispersion		**21.68**	%					
Chi-squared		**31.980**	with	19	degrees of freedom			
P (Chi-Sq)		**3.14**	**%**					
MSWD		**2.45**						

Sample Number		**OK12-14**						
Position (#)		5						
Area of Graticule Square		6.400E-07						
No. of Crystals		20						
Zeta Factor ± Error		116.8	1.5					
Rho d (% Relative Error)		4.803E+05	1.80					
N d		3074						
N s	N i	N g	ρ s	ρ i	ρ s / ρ i	U ppm	Age (Ma)	Age error
164	14	8	3.203E+07	2.734E+06	11.7143	281.2	**320.48**	**89.51**
180	14	8	3.516E+07	2.734E+06	12.8571	281.2	**350.91**	**97.67**
194	23	12	2.526E+07	2.995E+06	8.4348	308.0	**232.35**	**51.50**
276	20	12	3.594E+07	2.604E+06	13.8000	267.8	**375.91**	**87.44**
106	10	6	2.760E+07	2.604E+06	10.6000	267.8	**290.67**	**96.37**
103	7	5	3.219E+07	2.188E+06	14.7143	225.0	**400.05**	**156.51**
258	32	24	1.680E+07	2.083E+06	8.0625	214.3	**222.27**	**41.95**
148	18	12	1.927E+07	2.344E+06	8.2222	241.1	**226.60**	**56.79**
159	20	12	2.070E+07	2.604E+06	7.9500	267.8	**219.22**	**52.24**
190	11	10	2.969E+07	1.719E+06	17.2727	176.8	**467.15**	**145.24**
377	23	21	2.805E+07	1.711E+06	16.3913	176.0	**444.11**	**95.89**
100	12	6	2.604E+07	3.125E+06	8.3333	321.4	**229.61**	**70.33**
278	25	12	3.620E+07	3.255E+06	11.1200	334.8	**304.60**	**63.96**
215	24	12	2.799E+07	3.125E+06	8.9583	321.4	**246.50**	**53.33**
340	29	16	3.320E+07	2.832E+06	11.7241	291.3	**320.74**	**62.45**
99	13	6	2.578E+07	3.385E+06	7.6154	348.2	**210.15**	**62.17**
136	11	8	2.656E+07	2.148E+06	12.3636	221.0	**337.79**	**106.15**
126	17	10	1.969E+07	2.656E+06	7.4118	273.2	**204.61**	**53.06**
159	19	12	2.070E+07	2.474E+06	8.3684	254.5	**230.56**	**56.20**
166	19	12	2.161E+07	2.474E+06	8.7368	254.5	**240.52**	**58.49**
**********	**********	**********	**********	**********	**********	**********	**********	**********
3774	361	224	2.633E+07	2.518E+06	10.4543	259.0	**286.76**	**17.03**
Pooled Ratio		10.4543	±	0.6207				
Mean Ratio		10.7326	±	0.6787				
Pooled Age		286.76	±	17.03	1 S.E.			
Mean Crystal Age		294.23	±	19.01	1 S.E.			
Binomial Age		**287.07**	**+**	**32.46**	**"+95%"**			
			-	**29.15**	**"-95%"**			
Central Age		**284.84**	**±**	**18.18**				
Age Dispersion		**10.01**	%					
Chi-squared		**21.380**	with	19	degrees of freedom			
P (Chi-Sq)		**31.62**	**%**					
MSWD		**1.17**						

Sample Number		**OK12-16**						
Position (#)		6						
Area of Graticule Square		6.400E-07						
No. of Crystals		20						
Zeta Factor ± Error		116.8	1.5					
Rho d (% Relative Error)		4.788E+05	1.81					
N d		3064						
N s	N i	N g	ρ s	ρ i	ρ s / ρ i	U ppm	Age (Ma)	Age error
119	11	8	2.324E+07	2.148E+06	10.8182	221.7	**295.61**	**93.39**
243	12	9	4.219E+07	2.083E+06	20.2500	214.9	**542.73**	**160.94**
213	17	12	2.773E+07	2.214E+06	12.5294	228.4	**341.16**	**86.31**
142	12	9	2.465E+07	2.083E+06	11.8333	214.9	**322.67**	**97.27**
212	14	12	2.760E+07	1.823E+06	15.1429	188.1	**410.10**	**113.53**
210	18	12	2.734E+07	2.344E+06	11.6667	241.8	**318.24**	**78.48**
160	14	10	2.500E+07	2.188E+06	11.4286	225.7	**311.90**	**87.20**
183	21	14	2.042E+07	2.344E+06	8.7143	241.8	**239.18**	**55.36**
222	24	16	2.168E+07	2.344E+06	9.2500	241.8	**253.59**	**54.78**
259	19	12	3.372E+07	2.474E+06	13.6316	255.2	**370.32**	**88.40**
197	12	6	5.130E+07	3.125E+06	16.4167	322.4	**443.43**	**132.22**
132	13	12	1.719E+07	1.693E+06	10.1538	174.6	**277.85**	**81.00**
191	14	20	1.492E+07	1.094E+06	13.6429	112.8	**370.62**	**102.95**
206	15	12	2.682E+07	1.953E+06	13.7333	201.5	**373.01**	**100.10**
159	11	12	2.070E+07	1.432E+06	14.4545	147.8	**392.01**	**122.52**
179	16	10	2.797E+07	2.500E+06	11.1875	257.9	**305.47**	**79.99**
135	10	8	2.637E+07	1.953E+06	13.5000	201.5	**366.85**	**120.50**
249	15	20	1.945E+07	1.172E+06	16.6000	120.9	**448.22**	**119.58**
270	22	20	2.109E+07	1.719E+06	12.2727	177.3	**334.35**	**74.50**
318	32	30	1.656E+07	1.667E+06	9.9375	172.0	**272.05**	**50.81**
**********	**********	**********	**********	**********	**********	**********	**********	**********
3999	322	264	2.367E+07	1.906E+06	12.4193	196.6	**338.24**	**20.98**
Pooled Ratio		12.4193	±	0.7703				
Mean Ratio		12.8582	±	0.6271				
Pooled Age		338.24	±	20.98	1 S.E.			
Mean Crystal Age		349.87	±	17.51	1 S.E.			
Binomial Age		**338.63**	**+**	**40.25**	**"+95%"**			
			-	**35.93**	**"-95%"**			
Central Age		**338.24**	**±**	**20.98**				
Age Dispersion		**0.07**	%					
Chi-squared		**12.857**	with	19	degrees of freedom			
P (Chi-Sq)		**84.58**	**%**					
MSWD		**0.76**						

Sample Number		**OK12-18**						
Position (#)		7						
Area of Graticule Square		6.400E-07						
No. of Crystals		20						
Zeta Factor ± Error		116.8	1.5					
Rho d (% Relative Error)		4.772E+05	1.81					
N d		3054						
N s	N i	N g	ρ s	ρ i	ρ s / ρ i	U ppm	Age (Ma)	Age error
226	13	12	2.943E+07	1.693E+06	17.3846	175.2	**467.14**	**133.64**
187	17	12	2.435E+07	2.214E+06	11.0000	229.1	**299.49**	**76.16**
146	11	12	1.901E+07	1.432E+06	13.2727	148.3	**359.67**	**112.74**
193	17	12	2.513E+07	2.214E+06	11.3529	229.1	**308.87**	**78.44**
249	18	12	3.242E+07	2.344E+06	13.8333	242.6	**374.43**	**91.76**
248	23	16	2.422E+07	2.246E+06	10.7826	232.5	**293.70**	**64.35**
290	26	20	2.266E+07	2.031E+06	11.1538	210.3	**303.58**	**62.51**
179	23	16	1.748E+07	2.246E+06	7.7826	232.5	**213.32**	**47.49**
247	32	35	1.103E+07	1.429E+06	7.7188	147.9	**211.60**	**40.03**
176	12	12	2.292E+07	1.563E+06	14.6667	161.8	**396.30**	**118.57**
154	11	12	2.005E+07	1.432E+06	14.0000	148.3	**378.81**	**118.52**
251	23	15	2.615E+07	2.396E+06	10.9130	248.0	**297.17**	**65.08**
146	13	12	1.901E+07	1.693E+06	11.2308	175.2	**305.62**	**88.72**
179	17	12	2.331E+07	2.214E+06	10.5294	229.1	**286.96**	**73.10**
190	19	16	1.855E+07	1.855E+06	10.0000	192.1	**272.83**	**65.92**
253	26	20	1.977E+07	2.031E+06	9.7308	210.3	**265.63**	**55.02**
208	24	24	1.354E+07	1.563E+06	8.6667	161.8	**237.11**	**51.39**
174	12	8	3.398E+07	2.344E+06	14.5000	242.6	**391.93**	**117.30**
182	17	8	3.555E+07	3.320E+06	10.7059	343.7	**291.66**	**74.25**
339	36	20	2.648E+07	2.813E+06	9.4167	291.2	**257.23**	**45.45**
**********	**********	**********	**********	**********	**********	**********	**********	**********
4217	390	306	2.153E+07	1.991E+06	10.8128	206.2	**294.51**	**16.90**
Pooled Ratio		10.8128	±	0.6205				
Mean Ratio		11.4321	±	0.5553				
Pooled Age		294.51	±	16.90	1 S.E.			
Mean Crystal Age		310.97	±	15.46	1 S.E.			
Binomial Age		**294.80**	**+**	**31.91**	**"+95%"**			
			-	**28.78**	**"-95%"**			
Central Age		**294.51**	**±**	**16.90**				
Age Dispersion		**0.13**	%					
Chi-squared		**14.612**	with	19	degrees of freedom			
P (Chi-Sq)		**74.69**	**%**					
MSWD		**0.98**						

Sample Number		**OK12-19**						
Position (#)		33						
Area of Graticule Square		6.400E-07						
No. of Crystals		10						
Zeta Factor ± Error		121.1	3.5					
Rho d (% Relative Error)		3.430E+05	2.13					
N d		2195						
N s	N i	N g	ρ s	ρ i	ρ s / ρ i	U ppm	Age (Ma)	Age error
147	10	12	1.914E+07	1.302E+06	14.7000	187.5	**298.29**	**98.07**
52	4	4	2.031E+07	1.563E+06	13.0000	225.0	**264.49**	**137.57**
63	5	4	2.461E+07	1.953E+06	12.6000	281.3	**256.51**	**119.54**
125	10	6	3.255E+07	2.604E+06	12.5000	375.1	**254.52**	**84.14**
125	7	6	3.255E+07	1.823E+06	17.8571	262.5	**360.59**	**140.65**
105	8	12	1.367E+07	1.042E+06	13.1250	150.0	**266.98**	**98.39**
114	4	12	1.484E+07	5.208E+05	28.5000	75.0	**566.29**	**288.79**
116	10	12	1.510E+07	1.302E+06	11.6000	187.5	**236.52**	**78.41**
142	8	10	2.219E+07	1.250E+06	17.7500	180.0	**358.49**	**130.90**
80	5	6	2.083E+07	1.302E+06	16.0000	187.5	**324.02**	**149.82**
**********	**********	**********	**********	**********	**********	**********	**********	**********
1069	71	84	1.988E+07	1.321E+06	15.0563	190.2	**305.35**	**39.00**
Pooled Ratio		15.0563	±	1.9229				
Mean Ratio		15.7632	±	1.5788				
Pooled Age		305.35	±	39.00	1 S.E.			
Mean Crystal Age		319.34	±	32.71	1 S.E.			
Binomial Age		**306.94**	**+**	**84.37**	**"+95%"**			
			-	**65.72**	**"-95%"**			
Central Age		**305.35**	**±**	**39.00**				
Age Dispersion		**0.00**	%					
Chi-squared		**3.369**	with	9	degrees of freedom			
P (Chi-Sq)		**94.79**	**%**					
MSWD		**0.38**						

Sample Number		**OK12-21**						
Position (#)		8						
Area of Graticule Square		6.400E-07						
No. of Crystals		20						
Zeta Factor ± Error		116.8	1.5					
Rho d (% Relative Error)		4.757E+05	1.81					
N d		3044						
N s	N i	N g	ρ s	ρ i	ρ s / ρ i	U ppm	Age (Ma)	Age error
109	8	6	2.839E+07	2.083E+06	13.6250	216.3	**367.82**	**134.98**
98	12	6	2.552E+07	3.125E+06	8.1667	324.5	**222.98**	**68.37**
138	15	9	2.396E+07	2.604E+06	9.2000	270.4	**250.65**	**68.37**
180	20	12	2.344E+07	2.604E+06	9.0000	270.4	**245.30**	**58.07**
231	27	20	1.805E+07	2.109E+06	8.5556	219.1	**233.40**	**47.75**
121	8	6	3.151E+07	2.083E+06	15.1250	216.3	**407.06**	**148.87**
252	23	20	1.969E+07	1.797E+06	10.9565	186.6	**297.41**	**65.12**
76	7	8	1.484E+07	1.367E+06	10.8571	142.0	**294.78**	**116.62**
113	11	9	1.962E+07	1.910E+06	10.2727	198.3	**279.25**	**88.42**
115	9	8	2.246E+07	1.758E+06	12.7778	182.5	**345.55**	**119.85**
132	16	16	1.289E+07	1.563E+06	8.2500	162.3	**225.21**	**59.83**
252	23	25	1.575E+07	1.438E+06	10.9565	149.3	**297.41**	**65.12**
126	15	8	2.461E+07	2.930E+06	8.4000	304.2	**229.23**	**62.82**
92	11	12	1.198E+07	1.432E+06	8.3636	148.7	**228.26**	**73.00**
144	10	8	2.813E+07	1.953E+06	14.4000	202.8	**388.12**	**127.22**
112	13	12	1.458E+07	1.693E+06	8.6154	175.8	**235.01**	**69.06**
122	12	8	2.383E+07	2.344E+06	10.1667	243.4	**276.43**	**83.86**
166	13	12	2.161E+07	1.693E+06	12.7692	175.8	**345.32**	**99.75**
163	15	12	2.122E+07	1.953E+06	10.8667	202.8	**295.03**	**79.87**
164	16	10	2.563E+07	2.500E+06	10.2500	259.6	**278.64**	**73.24**
**********	**********	**********	**********	**********	**********	**********	**********	**********
2906	284	227	2.000E+07	1.955E+06	10.2324	203.0	**278.18**	**18.37**
Pooled Ratio		10.2324	±	0.6755				
Mean Ratio		10.5787	±	0.4819				
Pooled Age		278.18	±	18.37	1 S.E.			
Mean Crystal Age		287.38	±	13.37	1 S.E.			
Binomial Age		**278.56**	**+**	**35.89**	**"+95%"**			
			-	**31.77**	**"-95%"**			
Central Age		**278.18**	**±**	**18.37**				
Age Dispersion		**0.00**	%					
Chi-squared		**7.862**	with	19	degrees of freedom			
P (Chi-Sq)		**98.80**	**%**					
MSWD		**0.44**						

Sample Number		**OK12-23**						
Position (#)		34						
Area of Graticule Square		6.400E-07						
No. of Crystals		20						
Zeta Factor ± Error		121.1	3.5					
Rho d (% Relative Error)		3.419E+05	2.14					
N d		2188						
N s	N i	N g	ρ s	ρ i	ρ s / ρ i	U ppm	Age (Ma)	Age error
192	12	12	2.500E+07	1.563E+06	16.0000	225.8	**323.00**	**96.81**
140	12	8	2.734E+07	2.344E+06	11.6667	338.6	**237.11**	**71.83**
135	12	10	2.109E+07	1.875E+06	11.2500	270.9	**228.79**	**69.41**
235	18	20	1.836E+07	1.406E+06	13.0556	203.2	**264.76**	**65.45**
163	13	12	2.122E+07	1.693E+06	12.5385	244.6	**254.48**	**73.91**
273	22	15	2.844E+07	2.292E+06	12.4091	331.1	**251.91**	**56.56**
152	10	20	1.188E+07	7.813E+05	15.2000	112.9	**307.23**	**100.91**
165	15	14	1.842E+07	1.674E+06	11.0000	241.9	**223.79**	**60.89**
384	13	15	4.000E+07	1.354E+06	29.5385	195.7	**584.22**	**166.09**
211	12	9	3.663E+07	2.083E+06	17.5833	301.0	**354.10**	**105.86**
265	21	21	1.972E+07	1.563E+06	12.6190	225.8	**256.09**	**58.78**
166	14	12	2.161E+07	1.823E+06	11.8571	263.4	**240.91**	**67.60**
215	16	20	1.680E+07	1.250E+06	13.4375	180.6	**272.35**	**71.25**
140	12	10	2.188E+07	1.875E+06	11.6667	270.9	**237.11**	**71.83**
140	11	9	2.431E+07	1.910E+06	12.7273	275.9	**258.24**	**81.39**
223	9	12	2.904E+07	1.172E+06	24.7778	169.3	**493.56**	**168.74**
142	10	8	2.773E+07	1.953E+06	14.2000	282.2	**287.46**	**94.62**
91	8	8	1.777E+07	1.563E+06	11.3750	225.8	**231.29**	**85.70**
293	23	15	3.052E+07	2.396E+06	12.7391	346.2	**258.47**	**56.74**
145	11	10	2.266E+07	1.719E+06	13.1818	248.3	**267.27**	**84.14**
**********	**********	**********	**********	**********	**********	**********	**********	**********
3870	274	260	2.326E+07	1.647E+06	14.1241	237.9	**285.96**	**20.62**
Pooled Ratio		14.1241	±	1.0185				
Mean Ratio		14.4411	±	1.0546				
Pooled Age		285.96	±	20.62	1 S.E.			
Mean Crystal Age		292.24	±	21.80	1 S.E.			
Binomial Age		**286.35**	**+**	**37.12**	**"+95%"**			
			-	**32.79**	**"-95%"**			
Central Age		**285.39**	**±**	**20.92**				
Age Dispersion		**5.66**	%					
Chi-squared		**15.017**	with	19	degrees of freedom			
P (Chi-Sq)		**72.15**	**%**					
MSWD		**0.60**						

Sample Number		**OK12-26**						
Position (#)		9						
Area of Graticule Square		6.400E-07						
No. of Crystals		20						
Zeta Factor ± Error		116.8	1.5					
Rho d (% Relative Error)		4.741E+05	1.82					
N d		3034						
N s	N i	N g	ρ s	ρ i	ρ s / ρ i	U ppm	Age (Ma)	Age error
175	13	15	1.823E+07	1.354E+06	13.4615	141.1	**362.34**	**104.47**
221	24	16	2.158E+07	2.344E+06	9.2083	244.2	**250.04**	**54.03**
131	12	18	1.137E+07	1.042E+06	10.9167	108.5	**295.38**	**89.33**
232	26	15	2.417E+07	2.708E+06	8.9231	282.2	**242.44**	**50.43**
299	25	25	1.869E+07	1.563E+06	11.9600	162.8	**322.92**	**67.61**
93	10	8	1.816E+07	1.953E+06	9.3000	203.5	**252.48**	**84.21**
133	16	15	1.385E+07	1.667E+06	8.3125	173.7	**226.14**	**60.05**
224	27	21	1.667E+07	2.009E+06	8.2963	209.3	**225.71**	**46.25**
123	9	12	1.602E+07	1.172E+06	13.6667	122.1	**367.71**	**127.24**
97	9	8	1.895E+07	1.758E+06	10.7778	183.2	**291.71**	**101.85**
158	18	10	2.469E+07	2.813E+06	8.7778	293.1	**238.56**	**59.58**
326	32	25	2.038E+07	2.000E+06	10.1875	208.4	**276.07**	**51.51**
230	17	18	1.997E+07	1.476E+06	13.5294	153.8	**364.12**	**91.87**
201	22	16	1.963E+07	2.148E+06	9.1364	223.9	**248.13**	**55.99**
208	15	21	1.548E+07	1.116E+06	13.8667	116.3	**372.93**	**100.05**
120	10	9	2.083E+07	1.736E+06	12.0000	180.9	**323.97**	**106.87**
105	11	8	2.051E+07	2.148E+06	9.5455	223.9	**259.02**	**82.29**
327	34	16	3.193E+07	3.320E+06	9.6176	346.0	**260.94**	**47.38**
183	12	12	2.383E+07	1.563E+06	15.2500	162.8	**408.98**	**122.21**
201	18	16	1.963E+07	1.758E+06	11.1667	183.2	**301.99**	**74.60**
**********	**********	**********	**********	**********	**********	**********	**********	**********
3787	360	304	1.946E+07	1.850E+06	10.5194	192.8	**284.87**	**16.94**
Pooled Ratio		10.5194	±	0.6256				
Mean Ratio		10.8950	±	0.4748				
Pooled Age		284.87	±	16.94	1 S.E.			
Mean Crystal Age		294.81	±	13.13	1 S.E.			
Binomial Age		**285.18**	**+**	**32.29**	**"+95%"**			
			-	**28.99**	**"-95%"**			
Central Age		**284.87**	**±**	**16.94**				
Age Dispersion		**0.00**	%					
Chi-squared		**10.204**	with	19	degrees of freedom			
P (Chi-Sq)		**94.77**	**%**					
MSWD		**0.58**						

Sample Number		**OK12-31**						
Position (#)		35						
Area of Graticule Square		6.400E-07						
No. of Crystals		20						
Zeta Factor ± Error		121.1	3.5					
Rho d (% Relative Error)		3.409E+05	2.14					
N d		2182						
N s	N i	N g	ρ s	ρ i	ρ s / ρ i	U ppm	Age (Ma)	Age error
232	10	8	4.531E+07	1.953E+06	23.2000	283.0	**461.93**	**150.11**
103	9	6	2.682E+07	2.344E+06	11.4444	339.6	**232.01**	**81.07**
94	7	6	2.448E+07	1.823E+06	13.4286	264.2	**271.39**	**106.77**
143	12	12	1.862E+07	1.563E+06	11.9167	226.4	**241.40**	**73.07**
188	10	12	2.448E+07	1.302E+06	18.8000	188.7	**376.83**	**123.04**
193	13	10	3.016E+07	2.031E+06	14.8462	294.3	**299.39**	**86.46**
279	24	24	1.816E+07	1.563E+06	11.6250	226.4	**235.60**	**50.83**
159	9	6	4.141E+07	2.344E+06	17.6667	339.6	**354.73**	**122.21**
188	15	9	3.264E+07	2.604E+06	12.5333	377.4	**253.65**	**68.66**
236	12	20	1.844E+07	9.375E+05	19.6667	135.9	**393.68**	**117.36**
104	8	8	2.031E+07	1.563E+06	13.0000	226.4	**262.90**	**96.92**
312	13	12	4.063E+07	1.693E+06	24.0000	245.3	**477.28**	**136.19**
327	16	16	3.193E+07	1.563E+06	20.4375	226.4	**408.63**	**105.65**
302	12	12	3.932E+07	1.563E+06	25.1667	226.4	**499.61**	**148.16**
345	31	20	2.695E+07	2.422E+06	11.1290	351.0	**225.72**	**43.09**
189	17	12	2.461E+07	2.214E+06	11.1176	320.8	**225.49**	**57.67**
163	13	9	2.830E+07	2.257E+06	12.5385	327.1	**253.75**	**73.70**
171	12	10	2.672E+07	1.875E+06	14.2500	271.7	**287.63**	**86.52**
177	14	8	3.457E+07	2.734E+06	12.6429	396.2	**255.82**	**71.62**
172	6	10	2.688E+07	9.375E+05	28.6667	135.9	**566.12**	**235.99**
**********	**********	**********	**********	**********	**********	**********	**********	**********
4077	263	230	2.770E+07	1.787E+06	15.5019	258.9	**312.29**	**22.82**
Pooled Ratio		15.5019	±	1.1329				
Mean Ratio		16.4038	±	1.2142				
Pooled Age		312.29	±	22.82	1 S.E.			
Mean Crystal Age		330.01	±	25.01	1 S.E.			
Binomial Age		**312.73**	**+**	**41.24**	**"+95%"**			
			-	**36.34**	**"-95%"**			
Central Age		**311.13**	**±**	**24.70**				
Age Dispersion		**13.33**	%					
Chi-squared		**21.806**	with	19	degrees of freedom			
P (Chi-Sq)		**29.40**	**%**					
MSWD		**1.33**						

Sample Number		**OK12-32**						
Position (#)		10						
Area of Graticule Square		6.400E-07						
No. of Crystals		10						
Zeta Factor ± Error		116.8	1.5					
Rho d (% Relative Error)		4.725E+05	1.82					
N d		3024						
N s	N i	N g	ρ s	ρ i	ρ s / ρ i	U ppm	Age (Ma)	Age error
122	9	12	1.589E+07	1.172E+06	13.5556	122.5	**363.60**	**125.85**
185	15	15	1.927E+07	1.563E+06	12.3333	163.4	**331.65**	**89.34**
133	9	9	2.309E+07	1.563E+06	14.7778	163.4	**395.40**	**136.47**
350	21	24	2.279E+07	1.367E+06	16.6667	142.9	**444.24**	**100.29**
277	15	16	2.705E+07	1.465E+06	18.4667	153.1	**490.43**	**130.47**
164	18	12	2.135E+07	2.344E+06	9.1111	245.0	**246.63**	**61.48**
154	8	12	2.005E+07	1.042E+06	19.2500	108.9	**510.43**	**185.44**
137	13	12	1.784E+07	1.693E+06	10.5385	177.0	**284.43**	**82.79**
264	20	15	2.750E+07	2.083E+06	13.2000	217.8	**354.32**	**82.55**
439	18	40	1.715E+07	7.031E+05	24.3889	73.5	**640.13**	**154.60**
**********	**********	**********	**********	**********	**********	**********	**********	**********
2225	146	167	2.082E+07	1.366E+06	15.2397	142.8	**407.38**	**35.97**
Pooled Ratio		15.2397	±	1.3455				
Mean Ratio		15.2288	±	1.4436				
Pooled Age		407.38	±	35.97	1 S.E.			
Mean Crystal Age		407.10	±	39.71	1 S.E.			
Binomial Age		**408.40**	**+**	**73.76**	**"+95%"**			
			-	**62.30**	**"-95%"**			
Central Age		**399.39**	**±**	**39.89**				
Age Dispersion		**14.22**	%					
Chi-squared		**12.149**	with	9	degrees of freedom			
P (Chi-Sq)		**20.50**	**%**					
MSWD		**1.49**						

Sample Number		**OK12-32b**						
Position (#)		33						
Area of Graticule Square		6.400E-07						
No. of Crystals		10						
Zeta Factor ± Error		116.8	1.5					
Rho d (% Relative Error)		4.367E+05	1.89					
N d		2795						
N s	N i	N g	ρ s	ρ i	ρ s / ρ i	U ppm	Age (Ma)	Age error
356	26	20	2.781E+07	2.031E+06	13.6923	229.8	**340.07**	**69.52**
170	11	12	2.214E+07	1.432E+06	15.4545	162.0	**382.56**	**119.34**
268	21	16	2.617E+07	2.051E+06	12.7619	232.0	**317.52**	**72.32**
197	16	16	1.924E+07	1.563E+06	12.3125	176.8	**306.60**	**80.01**
140	10	8	2.734E+07	1.953E+06	14.0000	220.9	**347.51**	**114.03**
236	19	20	1.844E+07	1.484E+06	12.4211	167.9	**309.24**	**74.08**
172	19	9	2.986E+07	3.299E+06	9.0526	373.1	**226.83**	**55.08**
107	12	8	2.090E+07	2.344E+06	8.9167	265.1	**223.49**	**68.23**
201	15	12	2.617E+07	1.953E+06	13.4000	220.9	**332.99**	**89.45**
139	10	8	2.715E+07	1.953E+06	13.9000	220.9	**345.09**	**113.26**
**********	**********	**********	**********	**********	**********	**********	**********	**********
1986	159	129	2.406E+07	1.926E+06	12.4906	217.9	**310.93**	**26.59**
Pooled Ratio		12.4906	±	1.0683				
Mean Ratio		12.5912	±	0.6660				
Pooled Age		310.93	±	26.59	1 S.E.			
Mean Crystal Age		313.37	±	16.96	1 S.E.			
Binomial Age		**311.67**	**+**	**54.52**	**"+95%"**			
			-	**46.29**	**"-95%"**			
Central Age		**310.93**	**±**	**26.59**				
Age Dispersion		**0.00**	%					
Chi-squared		**4.011**	with	9	degrees of freedom			
P (Chi-Sq)		**91.07**	**%**					
MSWD		**0.55**						

Sample Number		**OK12-35**						
Position (#)		11						
Area of Graticule Square		6.400E-07						
No. of Crystals		20						
Zeta Factor ± Error		116.8	1.5					
Rho d (% Relative Error)		4.710E+05	1.82					
N d		3014						
N s	N i	N g	ρ s	ρ i	ρ s / ρ i	U ppm	Age (Ma)	Age error
220	27	9	3.819E+07	4.688E+06	8.1481	491.6	**220.32**	**45.19**
171	16	8	3.340E+07	3.125E+06	10.6875	327.8	**287.47**	**75.43**
274	28	12	3.568E+07	3.646E+06	9.7857	382.4	**263.70**	**52.65**
237	20	10	3.703E+07	3.125E+06	11.8500	327.8	**317.98**	**74.38**
197	16	12	2.565E+07	2.083E+06	12.3125	218.5	**330.08**	**86.12**
125	16	9	2.170E+07	2.778E+06	7.8125	291.3	**211.39**	**56.33**
205	10	9	3.559E+07	1.736E+06	20.5000	182.1	**540.57**	**175.48**
309	25	16	3.018E+07	2.441E+06	12.3600	256.1	**331.32**	**69.29**
257	26	15	2.677E+07	2.708E+06	9.8846	284.1	**266.31**	**55.13**
294	16	16	2.871E+07	1.563E+06	18.3750	163.9	**486.59**	**125.38**
140	10	9	2.431E+07	1.736E+06	14.0000	182.1	**374.03**	**122.71**
224	10	8	4.375E+07	1.953E+06	22.4000	204.9	**588.45**	**190.64**
236	10	15	2.458E+07	1.042E+06	23.6000	109.3	**618.51**	**200.17**
147	15	8	2.871E+07	2.930E+06	9.8000	307.3	**264.08**	**71.82**
241	27	12	3.138E+07	3.516E+06	8.9259	368.7	**240.96**	**49.20**
273	21	12	3.555E+07	2.734E+06	13.0000	286.8	**348.02**	**79.19**
282	24	12	3.672E+07	3.125E+06	11.7500	327.8	**315.36**	**67.42**
262	18	10	4.094E+07	2.813E+06	14.5556	295.0	**388.43**	**95.04**
253	19	12	3.294E+07	2.474E+06	13.3158	259.5	**356.24**	**85.11**
211	22	12	2.747E+07	2.865E+06	9.5909	300.4	**258.56**	**58.21**
**********	**********	**********	**********	**********	**********	**********	**********	**********
4558	376	226	3.151E+07	2.600E+06	12.1223	272.6	**325.10**	**18.89**
Pooled Ratio		12.1223	±	0.7043				
Mean Ratio		13.1327	±	1.0350				
Pooled Age		325.10	±	18.89	1 S.E.			
Mean Crystal Age		351.48	±	28.41	1 S.E.			
Binomial Age		**325.43**	**+**	**35.67**	**"+95%"**			
			-	**32.12**	**"-95%"**			
Central Age		**324.45**	**±**	**21.59**				
Age Dispersion		**14.32**	%					
Chi-squared		**27.576**	with	19	degrees of freedom			
P (Chi-Sq)		**9.19**	**%**					
MSWD		**1.90**						

Sample Number		**OK12-36**						
Position (#)		12						
Area of Graticule Square		6.400E-07						
No. of Crystals		20						
Zeta Factor ± Error		116.8	1.5					
Rho d (% Relative Error)		4.694E+05	1.82					
N d		3004						
N s	N i	N g	ρ s	ρ i	ρ s / ρ i	U ppm	Age (Ma)	Age error
144	13	8	2.813E+07	2.539E+06	11.0769	267.2	**296.72**	**86.18**
168	10	15	1.750E+07	1.042E+06	16.8000	109.6	**444.83**	**145.13**
131	11	9	2.274E+07	1.910E+06	11.9091	201.0	**318.47**	**100.22**
114	12	9	1.979E+07	2.083E+06	9.5000	219.3	**255.30**	**77.69**
168	16	20	1.313E+07	1.250E+06	10.5000	131.6	**281.60**	**73.94**
407	40	25	2.544E+07	2.500E+06	10.1750	263.1	**273.06**	**45.65**
107	13	8	2.090E+07	2.539E+06	8.2308	267.2	**221.77**	**65.33**
188	20	10	2.938E+07	3.125E+06	9.4000	328.9	**252.66**	**59.69**
163	14	12	2.122E+07	1.823E+06	11.6429	191.8	**311.52**	**87.04**
187	17	15	1.948E+07	1.771E+06	11.0000	186.4	**294.70**	**74.94**
207	20	10	3.234E+07	3.125E+06	10.3500	328.9	**277.66**	**65.31**
119	14	8	2.324E+07	2.734E+06	8.5000	287.8	**228.90**	**64.88**
198	19	8	3.867E+07	3.711E+06	10.4211	390.5	**279.52**	**67.42**
150	14	12	1.953E+07	1.823E+06	10.7143	191.8	**287.22**	**80.52**
132	15	6	3.438E+07	3.906E+06	8.8000	411.1	**236.83**	**64.75**
316	36	21	2.351E+07	2.679E+06	8.7778	281.9	**236.24**	**41.89**
176	15	20	1.375E+07	1.172E+06	11.7333	123.3	**313.88**	**84.72**
217	20	20	1.695E+07	1.563E+06	10.8500	164.4	**290.77**	**68.26**
193	19	12	2.513E+07	2.474E+06	10.1579	260.4	**272.61**	**65.83**
236	19	12	3.073E+07	2.474E+06	12.4211	260.4	**331.81**	**79.47**
**********	**********	**********	**********	**********	**********	**********	**********	**********
3721	357	260	2.236E+07	2.145E+06	10.4230	225.8	**279.57**	**16.70**
Pooled Ratio		10.4230	±	0.6226				
Mean Ratio		10.6480	±	0.4167				
Pooled Age		279.57	±	16.70	1 S.E.			
Mean Crystal Age		285.48	±	11.41	1 S.E.			
Binomial Age		**279.88**	**+**	**31.86**	**"+95%"**			
			-	**28.59**	**"-95%"**			
Central Age		**279.57**	**±**	**16.70**				
Age Dispersion		**0.00**	%					
Chi-squared		**6.231**	with	19	degrees of freedom			
P (Chi-Sq)		**99.73**	**%**					
MSWD		**0.32**						

Sample Number		**OK12-37**						
Position (#)		13						
Area of Graticule Square		6.400E-07						
No. of Crystals		20						
Zeta Factor ± Error		116.8	1.5					
Rho d (% Relative Error)		4.679E+05	1.83					
N d		2994						
N s	N i	N g	ρ s	ρ i	ρ s / ρ i	U ppm	Age (Ma)	Age error
207	17	12	2.695E+07	2.214E+06	12.1765	233.7	**324.42**	**82.17**
248	17	12	3.229E+07	2.214E+06	14.5882	233.7	**386.79**	**97.36**
98	11	12	1.276E+07	1.432E+06	8.9091	151.2	**238.96**	**76.17**
322	22	15	3.354E+07	2.292E+06	14.6364	241.9	**388.03**	**85.95**
292	23	18	2.535E+07	1.997E+06	12.6957	210.8	**337.90**	**73.57**
137	7	12	1.784E+07	9.115E+05	19.5714	96.2	**513.77**	**199.42**
197	19	15	2.052E+07	1.979E+06	10.3684	209.0	**277.27**	**66.89**
287	13	12	3.737E+07	1.693E+06	22.0769	178.7	**576.68**	**164.03**
123	11	9	2.135E+07	1.910E+06	11.1818	201.6	**298.53**	**94.18**
304	10	16	2.969E+07	9.766E+05	30.4000	103.1	**781.36**	**251.73**
340	23	12	4.427E+07	2.995E+06	14.7826	316.2	**391.79**	**84.86**
158	13	9	2.743E+07	2.257E+06	12.1538	238.3	**323.84**	**93.72**
127	10	8	2.480E+07	1.953E+06	12.7000	206.2	**338.01**	**111.27**
232	20	16	2.266E+07	1.953E+06	11.6000	206.2	**309.43**	**72.44**
312	22	15	3.250E+07	2.292E+06	14.1818	241.9	**376.32**	**83.44**
169	16	10	2.641E+07	2.500E+06	10.5625	263.9	**282.35**	**74.12**
308	33	20	2.406E+07	2.578E+06	9.3333	272.2	**250.12**	**46.15**
278	17	12	3.620E+07	2.214E+06	16.3529	233.7	**432.04**	**108.37**
440	20	25	2.750E+07	1.250E+06	22.0000	132.0	**574.76**	**132.03**
137	13	8	2.676E+07	2.539E+06	10.5385	268.1	**281.72**	**82.00**
**********	**********	**********	**********	**********	**********	**********	**********	**********
4716	337	268	2.750E+07	1.965E+06	13.9941	207.4	**371.48**	**22.53**
Pooled Ratio		13.9941	±	0.8487				
Mean Ratio		14.5405	±	1.1908				
Pooled Age		371.48	±	22.53	1 S.E.			
Mean Crystal Age		385.56	±	32.46	1 S.E.			
Binomial Age		**371.89**	**+**	**42.83**	**"+95%"**			
			-	**38.36**	**"-95%"**			
Central Age		**366.47**	**±**	**25.90**				
Age Dispersion		**15.71**	%					
Chi-squared		**26.719**	with	19	degrees of freedom			
P (Chi-Sq)		**11.14**	**%**					
MSWD		**1.50**						

Sample Number		**OK12-39**						
Position (#)		14						
Area of Graticule Square		6.400E-07						
No. of Crystals		20						
Zeta Factor ± Error		116.8	1.5					
Rho d (% Relative Error)		4.663E+05	1.83					
N d		2984						
N s	N i	N g	ρ s	ρ i	ρ s / ρ i	U ppm	Age (Ma)	Age error
126	15	21	9.375E+06	1.116E+06	8.4000	118.2	**224.78**	**61.60**
323	23	24	2.103E+07	1.497E+06	14.0435	158.6	**371.52**	**80.61**
174	21	18	1.510E+07	1.823E+06	8.2857	193.1	**221.78**	**51.47**
331	38	30	1.724E+07	1.979E+06	8.7105	209.7	**232.94**	**40.24**
157	17	12	2.044E+07	2.214E+06	9.2353	234.5	**246.71**	**63.23**
231	21	21	1.719E+07	1.563E+06	11.0000	165.5	**292.80**	**67.06**
241	28	30	1.255E+07	1.458E+06	8.6071	154.5	**230.23**	**46.25**
161	19	20	1.258E+07	1.484E+06	8.4737	157.3	**226.72**	**55.23**
251	26	25	1.569E+07	1.625E+06	9.6538	172.2	**257.67**	**53.40**
93	8	20	7.266E+06	6.250E+05	11.6250	66.2	**309.04**	**114.08**
194	16	18	1.684E+07	1.389E+06	12.1250	147.1	**322.01**	**84.07**
154	13	15	1.604E+07	1.354E+06	11.8462	143.5	**314.78**	**91.19**
179	19	18	1.554E+07	1.649E+06	9.4211	174.7	**251.58**	**60.96**
158	15	12	2.057E+07	1.953E+06	10.5333	206.9	**280.64**	**76.08**
224	20	20	1.750E+07	1.563E+06	11.2000	165.5	**298.00**	**69.87**
212	20	24	1.380E+07	1.302E+06	10.6000	137.9	**282.38**	**66.36**
291	30	25	1.819E+07	1.875E+06	9.7000	198.6	**258.88**	**49.98**
187	15	15	1.948E+07	1.563E+06	12.4667	165.5	**330.85**	**89.09**
232	20	12	3.021E+07	2.604E+06	11.6000	275.9	**308.39**	**72.20**
251	23	25	1.569E+07	1.438E+06	10.9130	152.3	**290.54**	**63.63**
**********	**********	**********	**********	**********	**********	**********	**********	**********
4170	407	405	1.609E+07	1.570E+06	10.2457	166.3	**273.14**	**15.44**
Pooled Ratio		10.2457	±	0.5793				
Mean Ratio		10.4220	±	0.3572				
Pooled Age		273.14	±	15.44	1 S.E.			
Mean Crystal Age		277.74	±	9.72	1 S.E.			
Binomial Age		**273.40**	**+**	**29.05**	**"+95%"**			
			-	**26.25**	**"-95%"**			
Central Age		**273.14**	**±**	**15.44**				
Age Dispersion		**0.00**	%					
Chi-squared		**8.230**	with	19	degrees of freedom			
P (Chi-Sq)		**98.42**	**%**					
MSWD		**0.44**						

Sample Number		**OK12-41**						
Position (#)		36						
Area of Graticule Square		6.400E-07						
No. of Crystals		20						
Zeta Factor ± Error		121.1	3.5					
Rho d (% Relative Error)		3.398E+05	2.14					
N d		2175						
N s	N i	N g	ρ s	ρ i	ρ s / ρ i	U ppm	Age (Ma)	Age error
89	4	6	2.318E+07	1.042E+06	22.2500	151.4	**442.27**	**226.61**
144	10	4	5.625E+07	3.906E+06	14.4000	567.9	**289.67**	**95.30**
363	12	24	2.363E+07	7.813E+05	30.2500	113.6	**594.15**	**175.63**
141	11	10	2.203E+07	1.719E+06	12.8182	249.9	**258.48**	**81.45**
53	4	4	2.070E+07	1.563E+06	13.2500	227.2	**267.01**	**138.78**
200	13	10	3.125E+07	2.031E+06	15.3846	295.3	**309.01**	**89.14**
159	12	12	2.070E+07	1.563E+06	13.2500	227.2	**267.01**	**80.51**
74	7	4	2.891E+07	2.734E+06	10.5714	397.5	**213.92**	**84.94**
97	8	12	1.263E+07	1.042E+06	12.1250	151.4	**244.76**	**90.46**
202	16	12	2.630E+07	2.083E+06	12.6250	302.9	**254.66**	**66.77**
126	8	8	2.461E+07	1.563E+06	15.7500	227.2	**316.17**	**115.84**
143	10	10	2.234E+07	1.563E+06	14.3000	227.2	**287.70**	**94.68**
89	8	8	1.738E+07	1.563E+06	11.1250	227.2	**224.93**	**83.41**
168	11	9	2.917E+07	1.910E+06	15.2727	277.6	**306.82**	**96.13**
193	11	12	2.513E+07	1.432E+06	17.5455	208.2	**351.25**	**109.61**
115	9	5	3.594E+07	2.813E+06	12.7778	408.9	**257.68**	**89.67**
133	9	6	3.464E+07	2.344E+06	14.7778	340.7	**297.10**	**102.89**
109	6	6	2.839E+07	1.563E+06	18.1667	227.2	**363.34**	**152.92**
155	10	12	2.018E+07	1.302E+06	15.5000	189.3	**311.27**	**102.17**
87	5	6	2.266E+07	1.302E+06	17.4000	189.3	**348.42**	**160.72**
**********	**********	**********	**********	**********	**********	**********	**********	**********
2840	184	180	2.465E+07	1.597E+06	15.4348	232.2	**309.99**	**26.09**
Pooled Ratio		15.4348	±	1.2989				
Mean Ratio		15.4770	±	0.9856				
Pooled Age		309.99	±	26.09	1 S.E.			
Mean Crystal Age		310.82	±	20.25	1 S.E.			
Binomial Age		**310.61**	**+**	**49.78**	**"+95%"**			
			-	**42.76**	**"-95%"**			
Central Age		**309.97**	**±**	**26.09**				
Age Dispersion		**0.84**	%					
Chi-squared		**10.242**	with	19	degrees of freedom			
P (Chi-Sq)		**94.67**	**%**					
MSWD		**0.43**						

Sample Number		**OK12-43**						
Position (#)		15						
Area of Graticule Square		6.400E-07						
No. of Crystals		20						
Zeta Factor ± Error		116.8	1.5					
Rho d (% Relative Error)		4.647E+05	1.83					
N d		2974						
N s	N i	N g	ρ s	ρ i	ρ s / ρ i	U ppm	Age (Ma)	Age error
113	12	15	1.177E+07	1.250E+06	9.4167	132.9	**250.62**	**76.30**
89	6	12	1.159E+07	7.813E+05	14.8333	83.1	**390.49**	**164.93**
92	7	6	2.396E+07	1.823E+06	13.1429	193.8	**347.16**	**136.34**
57	6	6	1.484E+07	1.563E+06	9.5000	166.1	**252.79**	**108.65**
63	7	8	1.230E+07	1.367E+06	9.0000	145.3	**239.73**	**95.66**
73	10	10	1.141E+07	1.563E+06	7.3000	166.1	**195.13**	**65.94**
104	10	8	2.031E+07	1.953E+06	10.4000	207.6	**276.24**	**91.67**
95	9	5	2.969E+07	2.813E+06	10.5556	299.0	**280.28**	**97.95**
66	4	6	1.719E+07	1.042E+06	16.5000	110.7	**432.92**	**223.13**
95	14	7	2.121E+07	3.125E+06	6.7857	332.2	**181.57**	**52.14**
96	8	4	3.750E+07	3.125E+06	12.0000	332.2	**317.70**	**117.13**
70	7	4	2.734E+07	2.734E+06	10.0000	290.7	**265.83**	**105.55**
192	21	8	3.750E+07	4.102E+06	9.1429	436.0	**243.47**	**56.22**
133	9	12	1.732E+07	1.172E+06	14.7778	124.6	**389.07**	**134.29**
202	18	12	2.630E+07	2.344E+06	11.2222	249.2	**297.58**	**73.50**
131	14	6	3.411E+07	3.646E+06	9.3571	387.6	**249.06**	**70.25**
88	9	6	2.292E+07	2.344E+06	9.7778	249.2	**260.04**	**91.19**
50	4	6	1.302E+07	1.042E+06	12.5000	110.7	**330.61**	**171.95**
60	6	4	2.344E+07	2.344E+06	10.0000	249.2	**265.83**	**113.98**
88	10	6	2.292E+07	2.604E+06	8.8000	276.8	**234.50**	**78.43**
**********	**********	**********	**********	**********	**********	**********	**********	**********
1957	191	151	2.025E+07	1.976E+06	10.2461	210.1	**272.23**	**21.52**
Pooled Ratio		10.2461	±	0.8099				
Mean Ratio		10.7506	±	0.5645				
Pooled Age		272.23	±	21.52	1 S.E.			
Mean Crystal Age		285.35	±	15.30	1 S.E.			
Binomial Age		**272.79**	**+**	**43.63**	**"+95%"**			
			-	**37.57**	**"-95%"**			
Central Age		**272.23**	**±**	**21.52**				
Age Dispersion		**0.00**	%					
Chi-squared		**7.597**	with	19	degrees of freedom			
P (Chi-Sq)		**99.03**	**%**					
MSWD		**0.50**						

Sample Number		**OK12-45**						
Position (#)		37						
Area of Graticule Square		6.400E-07						
No. of Crystals		20						
Zeta Factor ± Error		121.1	3.5					
Rho d (% Relative Error)		3.388E+05	2.15					
N d		2168						
N s	N i	N g	ρ s	ρ i	ρ s / ρ i	U ppm	Age (Ma)	Age error
121	10	10	1.891E+07	1.563E+06	12.1000	227.8	**243.56**	**80.62**
174	6	12	2.266E+07	7.813E+05	29.0000	113.9	**569.04**	**237.17**
166	13	12	2.161E+07	1.693E+06	12.7692	246.8	**256.77**	**74.53**
149	13	16	1.455E+07	1.270E+06	11.4615	185.1	**230.94**	**67.30**
82	7	8	1.602E+07	1.367E+06	11.7143	199.3	**235.94**	**93.29**
190	16	20	1.484E+07	1.250E+06	11.8750	182.3	**239.12**	**62.84**
379	20	40	1.480E+07	7.813E+05	18.9500	113.9	**377.48**	**87.66**
184	9	12	2.396E+07	1.172E+06	20.4444	170.9	**406.33**	**139.48**
152	11	10	2.375E+07	1.719E+06	13.8182	250.6	**277.42**	**87.19**
373	18	16	3.643E+07	1.758E+06	20.7222	256.3	**411.67**	**100.45**
198	5	6	5.156E+07	1.302E+06	39.6000	189.9	**765.11**	**347.56**
270	22	18	2.344E+07	1.910E+06	12.2727	278.5	**246.97**	**55.48**
255	6	15	2.656E+07	6.250E+05	42.5000	91.1	**817.73**	**339.02**
151	6	12	1.966E+07	7.813E+05	25.1667	113.9	**496.65**	**207.52**
232	11	15	2.417E+07	1.146E+06	21.0909	167.1	**418.77**	**130.10**
155	12	16	1.514E+07	1.172E+06	12.9167	170.9	**259.68**	**78.37**
165	11	16	1.611E+07	1.074E+06	15.0000	156.6	**300.60**	**94.23**
186	17	12	2.422E+07	2.214E+06	10.9412	322.8	**220.63**	**56.46**
218	14	16	2.129E+07	1.367E+06	15.5714	199.3	**311.78**	**86.69**
122	10	16	1.191E+07	9.766E+05	12.2000	142.4	**245.54**	**81.25**
**********	**********	**********	**********	**********	**********	**********	**********	**********
3922	237	298	2.056E+07	1.243E+06	16.5485	181.2	**330.85**	**25.13**
Pooled Ratio		16.5485	±	1.2571				
Mean Ratio		18.5057	±	2.0611				
Pooled Age		330.85	±	25.13	1 S.E.			
Mean Crystal Age		368.87	±	42.14	1 S.E.			
Binomial Age		**331.35**	**+**	**46.07**	**"+95%"**			
			-	**40.32**	**"-95%"**			
Central Age		**327.00**	**±**	**28.30**				
Age Dispersion		**17.99**	%					
Chi-squared		**27.047**	with	19	degrees of freedom			
P (Chi-Sq)		**10.36**	**%**					
MSWD		**1.99**						

Sample Number		**OK12-50**						
Position (#)		16						
Area of Graticule Square		6.400E-07						
No. of Crystals		20						
Zeta Factor ± Error		116.8	1.5					
Rho d (% Relative Error)		4.632E+05	1.84					
N d		2964						
N s	N i	N g	ρ s	ρ i	ρ s / ρ i	U ppm	Age (Ma)	Age error
229	21	12	2.982E+07	2.734E+06	10.9048	291.6	**288.43**	**66.08**
222	24	18	1.927E+07	2.083E+06	9.2500	222.2	**245.49**	**53.04**
133	12	16	1.299E+07	1.172E+06	11.0833	125.0	**293.05**	**88.57**
122	12	12	1.589E+07	1.563E+06	10.1667	166.6	**269.31**	**81.70**
316	15	25	1.975E+07	9.375E+05	21.0667	100.0	**546.08**	**144.82**
131	11	20	1.023E+07	8.594E+05	11.9091	91.7	**314.36**	**98.93**
261	13	9	4.531E+07	2.257E+06	20.0769	240.7	**521.43**	**148.64**
196	17	12	2.552E+07	2.214E+06	11.5294	236.1	**304.57**	**77.31**
262	18	16	2.559E+07	1.758E+06	14.5556	187.5	**382.18**	**93.52**
120	10	6	3.125E+07	2.604E+06	12.0000	277.7	**316.70**	**104.48**
213	19	12	2.773E+07	2.474E+06	11.2105	263.8	**296.34**	**71.26**
171	15	14	1.908E+07	1.674E+06	11.4000	178.5	**301.23**	**81.40**
144	17	12	1.875E+07	2.214E+06	8.4706	236.1	**225.16**	**57.96**
204	22	15	2.125E+07	2.292E+06	9.2727	244.4	**246.08**	**55.50**
227	21	21	1.689E+07	1.563E+06	10.8095	166.6	**285.97**	**65.54**
328	16	20	2.563E+07	1.250E+06	20.5000	133.3	**531.98**	**136.72**
145	15	10	2.266E+07	2.344E+06	9.6667	250.0	**256.33**	**69.76**
319	17	25	1.994E+07	1.063E+06	18.7647	113.3	**488.61**	**122.11**
244	20	15	2.542E+07	2.083E+06	12.2000	222.2	**321.85**	**75.21**
157	17	12	2.044E+07	2.214E+06	9.2353	236.1	**245.10**	**62.82**
**********	**********	**********	**********	**********	**********	**********	**********	**********
4144	332	302	2.144E+07	1.718E+06	12.4819	183.2	**329.10**	**20.17**
Pooled Ratio		12.4819	±	0.7649				
Mean Ratio		12.7036	±	0.9042				
Pooled Age		329.10	±	20.17	1 S.E.			
Mean Crystal Age		334.80	±	24.41	1 S.E.			
Binomial Age		**329.48**	**+**	**38.54**	**"+95%"**			
			-	**34.47**	**"-95%"**			
Central Age		**324.53**	**±**	**22.40**				
Age Dispersion		**14.04**	%					
Chi-squared		**23.979**	with	19	degrees of freedom			
P (Chi-Sq)		**19.70**	**%**					
MSWD		**1.19**						

Sample Number		**OK12-51**						
Position (#)		17						
Area of Graticule Square		6.400E-07						
No. of Crystals		20						
Zeta Factor ± Error		116.8	1.5					
Rho d (% Relative Error)		4.616E+05	1.84					
N d		2954						
N s	N i	N g	ρ s	ρ i	ρ s / ρ i	U ppm	Age (Ma)	Age error
243	24	15	2.531E+07	2.500E+06	10.1250	267.5	**267.32**	**57.51**
115	10	8	2.246E+07	1.953E+06	11.5000	209.0	**302.79**	**100.06**
183	16	15	1.906E+07	1.667E+06	11.4375	178.4	**301.18**	**78.81**
299	14	12	3.893E+07	1.823E+06	21.3571	195.1	**551.46**	**151.30**
228	20	16	2.227E+07	1.953E+06	11.4000	209.0	**300.21**	**70.34**
171	13	9	2.969E+07	2.257E+06	13.1538	241.5	**345.19**	**99.61**
101	13	8	1.973E+07	2.539E+06	7.7692	271.7	**206.11**	**60.91**
197	17	30	1.026E+07	8.854E+05	11.5882	94.8	**305.06**	**77.42**
120	14	12	1.563E+07	1.823E+06	8.5714	195.1	**227.02**	**64.32**
190	22	15	1.979E+07	2.292E+06	8.6364	245.3	**228.71**	**51.76**
326	36	20	2.547E+07	2.813E+06	9.0556	301.0	**239.61**	**42.42**
175	21	12	2.279E+07	2.734E+06	8.3333	292.6	**220.82**	**51.24**
310	33	20	2.422E+07	2.578E+06	9.3939	275.9	**248.39**	**45.82**
179	15	12	2.331E+07	1.953E+06	11.9333	209.0	**313.92**	**84.68**
158	14	15	1.646E+07	1.458E+06	11.2857	156.1	**297.27**	**83.16**
186	19	15	1.938E+07	1.979E+06	9.7895	211.8	**258.64**	**62.56**
296	24	12	3.854E+07	3.125E+06	12.3333	334.4	**324.19**	**69.19**
402	40	25	2.513E+07	2.500E+06	10.0500	267.5	**265.38**	**44.40**
186	17	21	1.384E+07	1.265E+06	10.9412	135.4	**288.40**	**73.36**
178	14	12	2.318E+07	1.823E+06	12.7143	195.1	**333.94**	**93.00**
**********	**********	**********	**********	**********	**********	**********	**********	**********
4243	396	304	2.181E+07	2.035E+06	10.7146	217.8	**282.56**	**16.14**
Pooled Ratio		10.7146	±	0.6122				
Mean Ratio		11.0684	±	0.6427				
Pooled Age		282.56	±	16.14	1 S.E.			
Mean Crystal Age		291.68	±	17.30	1 S.E.			
Binomial Age		**282.83**	**+**	**30.41**	**"+95%"**			
			-	**27.45**	**"-95%"**			
Central Age		**282.56**	**±**	**16.15**				
Age Dispersion		**0.31**	%					
Chi-squared		**14.164**	with	19	degrees of freedom			
P (Chi-Sq)		**77.41**	**%**					
MSWD		**0.71**						

Sample Number		**OK12-52**						
Position (#)		18						
Area of Graticule Square		6.400E-07						
No. of Crystals		3						
Zeta Factor ± Error		116.8	1.5					
Rho d (% Relative Error)		4.601E+05	1.84					
N d		2944						
N s	N i	N g	ρ s	ρ i	ρ s / ρ i	U ppm	Age (Ma)	Age error
164	13	30	8.542E+06	6.771E+05	12.6154	72.7	**330.36**	**95.48**
101	6	36	4.384E+06	2.604E+05	16.8333	28.0	**437.15**	**183.95**
104	14	20	8.125E+06	1.094E+06	7.4286	117.4	**196.58**	**56.14**
**********	**********	**********	**********	**********	**********	**********	**********	**********
369	33	86	6.704E+06	5.996E+05	11.1818	64.4	**293.66**	**53.76**
Pooled Ratio		11.1818	±	2.0471				
Mean Ratio		12.2924	±	2.7197				
Pooled Age		293.66	±	53.76	1 S.E.			
Mean Crystal Age		322.11	±	72.67	1 S.E.			
Binomial Age		**297.11**	**+**	**131.38**	**"+95%"**			
			-	**90.29**	**"-95%"**			
Central Age		**293.61**	**±**	**54.12**				
Age Dispersion		**3.53**	%					
Chi-squared		**3.229**	with	2	degrees of freedom			
P (Chi-Sq)		**19.90**	**%**					
MSWD		**2.70**						

Sample Number		**OK12-52b**						
Position (#)		40						
Area of Graticule Square		6.400E-07						
No. of Crystals		17						
Zeta Factor ± Error		116.8	1.5					
Rho d (% Relative Error)		4.258E+05	1.92					
N d		2725						
N s	N i	N g	ρ s	ρ i	ρ s / ρ i	U ppm	Age (Ma)	Age error
141	7	15	1.469E+07	7.292E+05	20.1429	84.6	**482.38**	**187.12**
285	12	12	3.711E+07	1.563E+06	23.7500	181.3	**565.08**	**167.03**
223	13	18	1.936E+07	1.128E+06	17.1538	130.9	**413.04**	**118.23**
364	30	24	2.370E+07	1.953E+06	12.1333	226.6	**294.87**	**56.42**
287	15	15	2.990E+07	1.563E+06	19.1333	181.3	**459.04**	**122.04**
330	20	35	1.473E+07	8.929E+05	16.5000	103.6	**397.77**	**92.06**
174	19	25	1.088E+07	1.188E+06	9.1579	137.8	**223.80**	**54.32**
134	10	12	1.745E+07	1.302E+06	13.4000	151.1	**324.89**	**106.77**
245	24	16	2.393E+07	2.344E+06	10.2083	271.9	**248.98**	**53.56**
247	11	12	3.216E+07	1.432E+06	22.4545	166.2	**535.50**	**165.48**
151	9	8	2.949E+07	1.758E+06	16.7778	203.9	**404.26**	**139.03**
138	11	20	1.078E+07	8.594E+05	12.5455	99.7	**304.65**	**95.70**
147	13	12	1.914E+07	1.693E+06	11.3077	196.4	**275.23**	**79.89**
349	17	16	3.408E+07	1.660E+06	20.5294	192.6	**491.29**	**122.55**
219	12	30	1.141E+07	6.250E+05	18.2500	72.5	**438.56**	**130.42**
258	16	20	2.016E+07	1.250E+06	16.1250	145.0	**389.00**	**100.62**
289	31	40	1.129E+07	1.211E+06	9.3226	140.5	**227.75**	**43.36**
**********	**********	**********	**********	**********	**********	**********	**********	**********
3981	270	330	1.885E+07	1.278E+06	14.7444	148.3	**356.60**	**23.89**
Pooled Ratio		14.7444	±	0.9876				
Mean Ratio		15.8172	±	1.1123				
Pooled Age		356.60	±	23.89	1 S.E.			
Mean Crystal Age		381.79	±	27.60	1 S.E.			
Binomial Age		**357.09**	**+**	**46.31**	**"+95%"**			
			-	**40.92**	**"-95%"**			
Central Age		**355.68**	**±**	**28.73**				
Age Dispersion		**18.08**	%					
Chi-squared		**24.469**	with	16	degrees of freedom			
P (Chi-Sq)		**7.97**	**%**					
MSWD		**2.26**						

Sample Number		**OK12-54**						
Position (#)		19						
Area of Graticule Square		6.400E-07						
No. of Crystals		5						
Zeta Factor ± Error		116.8	1.5					
Rho d (% Relative Error)		4.585E+05	1.85					
N d		2934						
N s	N i	N g	ρ s	ρ i	ρ s / ρ i	U ppm	Age (Ma)	Age error
167	16	6	4.349E+07	4.167E+06	10.4375	448.9	**273.59**	**71.86**
96	10	8	1.875E+07	1.953E+06	9.6000	210.4	**252.06**	**83.95**
272	26	10	4.250E+07	4.063E+06	10.4615	437.7	**274.21**	**56.62**
99	12	6	2.578E+07	3.125E+06	8.2500	336.7	**217.20**	**66.57**
128	12	8	2.500E+07	2.344E+06	10.6667	252.5	**279.47**	**84.61**
**********	**********	**********	**********	**********	**********	**********	**********	**********
762	76	38	3.133E+07	3.125E+06	10.0263	336.7	**263.03**	**32.19**
Pooled Ratio		10.0263	±	1.2270				
Mean Ratio		9.8831	±	0.4474				
Pooled Age		263.03	±	32.19	1 S.E.			
Mean Crystal Age		259.35	±	11.97	1 S.E.			
Binomial Age		**264.39**	**+**	**71.22**	**"+95%"**			
			-	**55.92**	**"-95%"**			
Central Age		**263.03**	**±**	**32.19**				
Age Dispersion		**0.00**	%					
Chi-squared		**0.534**	with	4	degrees of freedom			
P (Chi-Sq)		**97.01**	**%**					
MSWD		**0.14**						

Sample Number		**OK12-54b**						
Position (#)		41						
Area of Graticule Square		6.400E-07						
No. of Crystals		5						
Zeta Factor ± Error		116.8	1.5					
Rho d (% Relative Error)		4.242E+05	1.92					
N d		2715						
N s	N i	N g	ρ s	ρ i	ρ s / ρ i	U ppm	Age (Ma)	Age error
136	13	15	1.417E+07	1.354E+06	10.4615	157.7	**254.09**	**74.00**
146	14	15	1.521E+07	1.458E+06	10.4286	169.8	**253.31**	**71.11**
87	8	8	1.699E+07	1.563E+06	10.8750	182.0	**263.93**	**97.70**
135	13	9	2.344E+07	2.257E+06	10.3846	262.8	**252.26**	**73.49**
233	21	20	1.820E+07	1.641E+06	11.0952	191.1	**269.17**	**61.64**
**********	**********	**********	**********	**********	**********	**********	**********	**********
737	69	67	1.719E+07	1.609E+06	10.6812	187.4	**259.32**	**33.19**
Pooled Ratio		10.6812	±	1.3671				
Mean Ratio		10.6490	±	0.1421				
Pooled Age		259.32	±	33.19	1 S.E.			
Mean Crystal Age		258.56	±	3.52	1 S.E.			
Binomial Age		**260.78**	**+**	**74.15**	**"+95%"**			
			-	**57.47**	**"-95%"**			
Central Age		**259.32**	**±**	**33.19**				
Age Dispersion		**0.00**	%					
Chi-squared		**0.052**	with	4	degrees of freedom			
P (Chi-Sq)		**99.97**	**%**					
MSWD		**0.01**						

Sample Number		**OK12-55**						
Position (#)		20						
Area of Graticule Square		6.400E-07						
No. of Crystals		20						
Zeta Factor ± Error		116.8	1.5					
Rho d (% Relative Error)		4.569E+05	1.84					
N d		2954						
N s	N i	N g	ρ s	ρ i	ρ s / ρ i	U ppm	Age (Ma)	Age error
263	15	21	1.957E+07	1.116E+06	17.5333	120.7	**451.64**	**120.32**
180	20	10	2.813E+07	3.125E+06	9.0000	337.9	**235.78**	**55.83**
180	21	18	1.563E+07	1.823E+06	8.5714	197.1	**224.75**	**52.07**
152	14	18	1.319E+07	1.215E+06	10.8571	131.4	**283.38**	**79.40**
239	20	25	1.494E+07	1.250E+06	11.9500	135.1	**311.23**	**72.78**
189	17	25	1.181E+07	1.063E+06	11.1176	114.9	**290.03**	**73.73**
194	15	15	2.021E+07	1.563E+06	12.9333	168.9	**336.18**	**90.41**
97	9	8	1.895E+07	1.758E+06	10.7778	190.1	**281.35**	**98.24**
263	19	20	2.055E+07	1.484E+06	13.8421	160.5	**359.15**	**85.70**
247	20	18	2.144E+07	1.736E+06	12.3500	187.7	**321.39**	**75.06**
235	25	25	1.469E+07	1.563E+06	9.4000	168.9	**246.06**	**52.06**
311	10	25	1.944E+07	6.250E+05	31.1000	67.6	**780.61**	**251.40**
350	20	25	2.188E+07	1.250E+06	17.5000	135.1	**450.81**	**104.14**
240	24	21	1.786E+07	1.786E+06	10.0000	193.1	**261.46**	**56.28**
202	17	15	2.104E+07	1.771E+06	11.8824	191.5	**309.51**	**78.47**
220	25	15	2.292E+07	2.604E+06	8.8000	281.6	**230.63**	**48.95**
238	15	12	3.099E+07	1.953E+06	15.8667	211.2	**410.05**	**109.55**
270	20	25	1.688E+07	1.250E+06	13.5000	135.1	**350.52**	**81.61**
178	15	16	1.738E+07	1.465E+06	11.8667	158.4	**309.11**	**83.39**
362	15	16	3.535E+07	1.465E+06	24.1333	158.4	**613.78**	**162.31**
**********	**********	**********	**********	**********	**********	**********	**********	**********
4610	356	373	1.931E+07	1.491E+06	12.9494	161.2	**336.59**	**20.00**
Pooled Ratio		12.9494	±	0.7693				
Mean Ratio		13.6491	±	1.2412				
Pooled Age		336.59	±	20.00	1 S.E.			
Mean Crystal Age		354.28	±	33.04	1 S.E.			
Binomial Age		**336.94**	**+**	**37.89**	**"+95%"**			
			-	**34.03**	**"-95%"**			
Central Age		**330.22**	**±**	**24.23**				
Age Dispersion		**19.17**	%					
Chi-squared		**31.704**	with	19	degrees of freedom			
P (Chi-Sq)		**3.37**	**%**					
MSWD		**1.82**						

Sample Number		**OK12-56**						
Position (#)		21						
Area of Graticule Square		6.400E-07						
No. of Crystals		20						
Zeta Factor ± Error		116.8	1.5					
Rho d (% Relative Error)		4.554E+05	1.85					
N d		2914						
N s	N i	N g	ρ s	ρ i	ρ s / ρ i	U ppm	Age (Ma)	Age error
130	6	10	2.031E+07	9.375E+05	21.6667	101.7	**551.92**	**230.80**
124	12	16	1.211E+07	1.172E+06	10.3333	127.1	**269.12**	**81.59**
164	19	15	1.708E+07	1.979E+06	8.6316	214.7	**225.57**	**54.90**
196	18	12	2.552E+07	2.344E+06	10.8889	254.2	**283.28**	**70.06**
189	17	12	2.461E+07	2.214E+06	11.1176	240.1	**289.10**	**73.49**
247	22	25	1.544E+07	1.375E+06	11.2273	149.2	**291.88**	**65.27**
134	12	9	2.326E+07	2.083E+06	11.1667	226.0	**290.34**	**87.73**
220	9	12	2.865E+07	1.172E+06	24.4444	127.1	**619.38**	**211.10**
125	10	8	2.441E+07	1.953E+06	12.5000	211.9	**324.15**	**106.78**
236	23	12	3.073E+07	2.995E+06	10.2609	324.9	**267.27**	**58.69**
203	11	10	3.172E+07	1.719E+06	18.4545	186.4	**473.02**	**146.82**
151	16	12	1.966E+07	2.083E+06	9.4375	226.0	**246.23**	**64.97**
291	16	16	2.842E+07	1.563E+06	18.1875	169.5	**466.42**	**120.23**
224	16	20	1.750E+07	1.250E+06	14.0000	135.6	**361.98**	**94.03**
178	12	16	1.738E+07	1.172E+06	14.8333	127.1	**382.90**	**114.52**
183	19	9	3.177E+07	3.299E+06	9.6316	357.8	**251.20**	**60.81**
145	10	6	3.776E+07	2.604E+06	14.5000	282.5	**374.54**	**122.75**
114	11	8	2.227E+07	2.148E+06	10.3636	233.1	**269.90**	**85.43**
228	12	9	3.958E+07	2.083E+06	19.0000	226.0	**486.48**	**144.50**
173	16	8	3.379E+07	3.125E+06	10.8125	339.0	**281.33**	**73.79**
**********	**********	**********	**********	**********	**********	**********	**********	**********
3655	287	245	2.331E+07	1.830E+06	12.7352	198.5	**330.10**	**21.56**
Pooled Ratio		12.7352	±	0.8318				
Mean Ratio		13.5729	±	1.0040				
Pooled Age		330.10	±	21.56	1 S.E.			
Mean Crystal Age		351.23	±	26.65	1 S.E.			
Binomial Age		**330.53**	**+**	**41.78**	**"+95%"**			
			-	**37.04**	**"-95%"**			
Central Age		**329.68**	**±**	**22.20**				
Age Dispersion		**7.18**	%					
Chi-squared		**20.028**	with	19	degrees of freedom			
P (Chi-Sq)		**39.29**	**%**					
MSWD		**1.23**						

Sample Number		**OK12-57**						
Position (#)		22						
Area of Graticule Square		6.400E-07						
No. of Crystals		13						
Zeta Factor ± Error		116.8	1.5					
Rho d (% Relative Error)		4.538E+05	1.86					
N d		2904						
N s	N i	N g	ρ s	ρ i	ρ s / ρ i	U ppm	Age (Ma)	Age error
150	10	8	2.930E+07	1.953E+06	15.0000	212.6	**385.75**	**126.29**
255	14	16	2.490E+07	1.367E+06	18.2143	148.8	**465.49**	**128.21**
173	15	8	3.379E+07	2.930E+06	11.5333	318.9	**298.63**	**80.66**
128	12	8	2.500E+07	2.344E+06	10.6667	255.1	**276.66**	**83.76**
154	14	10	2.406E+07	2.188E+06	11.0000	238.1	**285.12**	**79.85**
339	14	20	2.648E+07	1.094E+06	24.2143	119.1	**611.76**	**167.41**
129	11	10	2.016E+07	1.719E+06	11.7273	187.1	**303.54**	**95.59**
260	20	20	2.031E+07	1.563E+06	13.0000	170.1	**335.63**	**78.25**
294	23	16	2.871E+07	2.246E+06	12.7826	244.5	**330.16**	**71.87**
278	10	15	2.896E+07	1.042E+06	27.8000	113.4	**697.61**	**225.09**
178	15	10	2.781E+07	2.344E+06	11.8667	255.1	**307.06**	**82.85**
269	14	16	2.627E+07	1.367E+06	19.2143	148.8	**490.10**	**134.81**
181	9	12	2.357E+07	1.172E+06	20.1111	127.6	**512.09**	**175.27**
**********	**********	**********	**********	**********	**********	**********	**********	**********
2788	181	169	2.578E+07	1.673E+06	15.4033	182.2	**395.81**	**31.65**
Pooled Ratio		15.4033	±	1.2316				
Mean Ratio		15.9331	±	1.5356				
Pooled Age		395.81	±	31.65	1 S.E.			
Mean Crystal Age		409.00	±	40.57	1 S.E.			
Binomial Age		**396.61**	**+**	**63.66**	**"+95%"**			
			-	**54.71**	**"-95%"**			
Central Age		**392.26**	**±**	**34.29**				
Age Dispersion		**12.54**	%					
Chi-squared		**15.025**	with	12	degrees of freedom			
P (Chi-Sq)		**24.01**	**%**					
MSWD		**1.30**						

Sample Number		**OK12-58**						
Position (#)		23						
Area of Graticule Square		6.400E-07						
No. of Crystals		20						
Zeta Factor ± Error		116.8	1.5					
Rho d (% Relative Error)		4.523E+05	1.86					
N d		2895						
N s	N i	N g	ρ s	ρ i	ρ s / ρ i	U ppm	Age (Ma)	Age error
353	30	25	2.206E+07	1.875E+06	11.7667	204.8	**303.55**	**58.13**
257	12	18	2.231E+07	1.042E+06	21.4167	113.8	**542.25**	**160.61**
114	13	10	1.781E+07	2.031E+06	8.7692	221.9	**227.57**	**66.82**
287	16	15	2.990E+07	1.667E+06	17.9375	182.0	**457.20**	**117.90**
308	22	15	3.208E+07	2.292E+06	14.0000	250.3	**359.58**	**79.77**
189	21	12	2.461E+07	2.734E+06	9.0000	298.6	**233.45**	**53.96**
308	20	12	4.010E+07	2.604E+06	15.4000	284.4	**394.46**	**91.46**
190	15	20	1.484E+07	1.172E+06	12.6667	128.0	**326.19**	**87.79**
214	20	16	2.090E+07	1.953E+06	10.7000	213.3	**276.61**	**64.98**
220	21	15	2.292E+07	2.188E+06	10.4762	238.9	**270.95**	**62.19**
188	17	18	1.632E+07	1.476E+06	11.0588	161.2	**285.69**	**72.64**
193	22	16	1.885E+07	2.148E+06	8.7727	234.7	**227.66**	**51.49**
247	10	16	2.412E+07	9.766E+05	24.7000	106.7	**621.49**	**200.96**
173	14	12	2.253E+07	1.823E+06	12.3571	199.1	**318.41**	**88.77**
161	16	15	1.677E+07	1.667E+06	10.0625	182.0	**260.46**	**68.53**
207	16	25	1.294E+07	1.000E+06	12.9375	109.2	**332.99**	**86.73**
138	16	18	1.198E+07	1.389E+06	8.6250	151.7	**223.89**	**59.34**
212	19	21	1.577E+07	1.414E+06	11.1579	154.4	**288.19**	**69.32**
176	8	10	2.750E+07	1.250E+06	22.0000	136.5	**556.40**	**201.53**
277	22	15	2.885E+07	2.292E+06	12.5909	250.3	**324.29**	**72.20**
**********	**********	**********	**********	**********	**********	**********	**********	**********
4412	350	324	2.128E+07	1.688E+06	12.6057	184.4	**324.66**	**19.46**
Pooled Ratio		12.6057	±	0.7557				
Mean Ratio		13.3198	±	1.0493				
Pooled Age		324.66	±	19.46	1 S.E.			
Mean Crystal Age		342.57	±	27.66	1 S.E.			
Binomial Age		**325.01**	**+**	**36.96**	**"+95%"**			
			-	**33.15**	**"-95%"**			
Central Age		**323.35**	**±**	**20.77**				
Age Dispersion		**10.13**	%					
Chi-squared		**24.134**	with	19	degrees of freedom			
P (Chi-Sq)		**19.11**	**%**					
MSWD		**1.45**						

Sample Number		**OK12-59**						
Position (#)		24						
Area of Graticule Square		6.400E-07						
No. of Crystals		20						
Zeta Factor ± Error		116.8	1.5					
Rho d (% Relative Error)		4.507E+05	1.86					
N d		2885						
N s	N i	N g	ρ s	ρ i	ρ s / ρ i	U ppm	Age (Ma)	Age error
136	11	10	2.125E+07	1.719E+06	12.3636	188.4	**317.47**	**99.78**
180	14	8	3.516E+07	2.734E+06	12.8571	299.7	**329.83**	**91.82**
150	14	8	2.930E+07	2.734E+06	10.7143	299.7	**276.02**	**77.39**
279	25	16	2.725E+07	2.441E+06	11.1600	267.6	**287.25**	**60.32**
520	45	16	5.078E+07	4.395E+06	11.5556	481.7	**297.20**	**46.67**
329	29	20	2.570E+07	2.266E+06	11.3448	248.3	**291.90**	**56.93**
217	24	12	2.826E+07	3.125E+06	9.0417	342.5	**233.70**	**50.55**
243	23	12	3.164E+07	2.995E+06	10.5652	328.3	**272.25**	**59.71**
156	16	8	3.047E+07	3.125E+06	9.7500	342.5	**251.65**	**66.31**
197	18	10	3.078E+07	2.813E+06	10.9444	308.3	**281.82**	**69.69**
212	24	15	2.208E+07	2.500E+06	8.8333	274.0	**228.41**	**49.46**
155	16	12	2.018E+07	2.083E+06	9.6875	228.3	**250.07**	**65.91**
157	15	8	3.066E+07	2.930E+06	10.4667	321.1	**269.77**	**73.16**
263	21	15	2.740E+07	2.188E+06	12.5238	239.8	**321.49**	**73.26**
298	30	16	2.910E+07	2.930E+06	9.9333	321.1	**256.29**	**49.43**
291	25	12	3.789E+07	3.255E+06	11.6400	356.8	**299.32**	**62.75**
354	30	20	2.766E+07	2.344E+06	11.8000	256.9	**303.34**	**58.09**
240	25	15	2.500E+07	2.604E+06	9.6000	285.4	**247.85**	**52.39**
150	15	15	1.563E+07	1.563E+06	10.0000	171.3	**257.98**	**70.10**
197	18	8	3.848E+07	3.516E+06	10.9444	385.3	**281.82**	**69.69**
**********	**********	**********	**********	**********	**********	**********	**********	**********
4724	438	256	2.883E+07	2.673E+06	10.7854	293.0	**277.81**	**15.23**
Pooled Ratio		10.7854	±	0.5914				
Mean Ratio		10.7863	±	0.2549				
Pooled Age		277.81	±	15.23	1 S.E.			
Mean Crystal Age		277.83	±	6.71	1 S.E.			
Binomial Age		**278.05**	**+**	**28.34**	**"+95%"**			
			-	**25.71**	**"-95%"**			
Central Age		**277.81**	**±**	**15.23**				
Age Dispersion		**0.00**	%					
Chi-squared		**4.127**	with	19	degrees of freedom			
P (Chi-Sq)		**99.99**	**%**					
MSWD		**0.22**						

Sample Number		OK12-63 (UA-Z9)						
Position (#)		25						
Area of Graticule Square		6.400E-07						
No. of Crystals		20						
Zeta Factor ± Error		116.8	1.5					
Rho d (% Relative Error)		4.492E+05	1.87					
N d		2875						
N s	N i	N g	ρ s	ρ i	ρ s / ρ i	U ppm	Age (Ma)	Age error
213	14	15	2.219E+07	1.458E+06	15.2143	160.4	**387.25**	**107.20**
142	12	25	8.875E+06	7.500E+05	11.8333	82.5	**303.18**	**91.40**
284	27	25	1.775E+07	1.688E+06	10.5185	185.6	**270.19**	**54.76**
276	16	28	1.540E+07	8.929E+05	17.2500	98.2	**437.35**	**112.90**
376	17	28	2.098E+07	9.487E+05	22.1176	104.3	**555.57**	**138.33**
300	30	24	1.953E+07	1.953E+06	10.0000	214.8	**257.14**	**49.58**
181	18	12	2.357E+07	2.344E+06	10.0556	257.7	**258.54**	**64.16**
243	27	21	1.808E+07	2.009E+06	9.0000	220.9	**231.88**	**47.33**
303	32	25	1.894E+07	2.000E+06	9.4688	219.9	**243.73**	**45.64**
306	27	20	2.391E+07	2.109E+06	11.3333	232.0	**290.66**	**58.72**
192	15	24	1.250E+07	9.766E+05	12.8000	107.4	**327.33**	**88.07**
112	13	20	8.750E+06	1.016E+06	8.6154	111.7	**222.14**	**65.28**
305	12	20	2.383E+07	9.375E+05	25.4167	103.1	**634.49**	**187.28**
312	32	25	1.950E+07	2.000E+06	9.7500	219.9	**250.83**	**46.90**
192	21	20	1.500E+07	1.641E+06	9.1429	180.4	**235.49**	**54.39**
319	8	25	1.994E+07	5.000E+05	39.8750	55.0	**969.37**	**347.69**
259	20	16	2.529E+07	1.953E+06	12.9500	214.8	**331.07**	**77.20**
279	10	15	2.906E+07	1.042E+06	27.9000	114.6	**693.26**	**223.67**
196	21	15	2.042E+07	2.188E+06	9.3333	240.6	**240.31**	**55.45**
142	10	25	8.875E+06	6.250E+05	14.2000	68.7	**362.15**	**118.77**
**********	**********	**********	**********	**********	**********	**********	**********	**********
4932	382	428	1.801E+07	1.395E+06	12.9110	153.4	**330.10**	**19.06**
Pooled Ratio		12.9110	±	0.7454				
Mean Ratio		14.8387	±	1.8158				
Pooled Age		330.10	±	19.06	1 S.E.			
Mean Crystal Age		377.97	±	47.46	1 S.E.			
Binomial Age		**330.42**	**+**	**35.81**	**"+95%"**			
			-	**32.27**	**"-95%"**			
Central Age		**324.69**	**±**	**27.47**				
Age Dispersion		**27.36**	%					
Chi-squared		**47.987**	with	19	degrees of freedom			
P (Chi-Sq)		**0.03**	**%**					
MSWD		**3.67**						

Sample Number		**OK12-63**						
Position (#)		38						
Area of Graticule Square		6.400E-07						
No. of Crystals		20						
Zeta Factor ± Error		121.1	3.5					
Rho d (% Relative Error)		3.378E+05	2.15					
N d		2162						
N s	N i	N g	ρ s	ρ i	ρ s / ρ i	U ppm	Age (Ma)	Age error
103	7	9	1.788E+07	1.215E+06	14.7143	177.7	**294.15**	**115.38**
165	16	12	2.148E+07	2.083E+06	10.3125	304.7	**207.55**	**54.86**
139	14	6	3.620E+07	3.646E+06	9.9286	533.2	**199.94**	**56.52**
311	16	12	4.049E+07	2.083E+06	19.4375	304.7	**385.79**	**99.87**
212	6	9	3.681E+07	1.042E+06	35.3333	152.3	**684.98**	**284.64**
174	14	20	1.359E+07	1.094E+06	12.4286	160.0	**249.33**	**69.84**
183	9	9	3.177E+07	1.563E+06	20.3333	228.5	**403.03**	**138.37**
384	13	15	4.000E+07	1.354E+06	29.5385	198.0	**577.51**	**164.19**
150	8	6	3.906E+07	2.083E+06	18.7500	304.7	**372.53**	**135.84**
228	10	14	2.545E+07	1.116E+06	22.8000	163.2	**450.25**	**146.37**
217	18	18	1.884E+07	1.563E+06	12.0556	228.5	**241.98**	**59.99**
225	15	12	2.930E+07	1.953E+06	15.0000	285.6	**299.73**	**80.65**
155	13	10	2.422E+07	2.031E+06	11.9231	297.1	**239.37**	**69.65**
169	11	9	2.934E+07	1.910E+06	15.3636	279.3	**306.83**	**96.11**
213	14	16	2.080E+07	1.367E+06	15.2143	199.9	**303.91**	**84.56**
191	12	20	1.492E+07	9.375E+05	15.9167	137.1	**317.60**	**95.21**
147	12	12	1.914E+07	1.563E+06	12.2500	228.5	**245.81**	**74.33**
317	19	16	3.096E+07	1.855E+06	16.6842	271.3	**332.53**	**79.45**
165	14	10	2.578E+07	2.188E+06	11.7857	319.9	**236.66**	**66.43**
189	15	15	1.969E+07	1.563E+06	12.6000	228.5	**252.70**	**68.40**
**********	**********	**********	**********	**********	**********	**********	**********	**********
4037	256	250	2.523E+07	1.600E+06	15.7695	234.0	**314.74**	**23.24**
Pooled Ratio		15.7695	±	1.1644				
Mean Ratio		16.6185	±	1.4469				
Pooled Age		314.74	±	23.24	1 S.E.			
Mean Crystal Age		331.25	±	29.53	1 S.E.			
Binomial Age		**315.19**	**+**	**42.14**	**"+95%"**			
			-	**37.07**	**"-95%"**			
Central Age		**311.48**	**±**	**24.82**				
Age Dispersion		**13.19**	%					
Chi-squared		**22.891**	with	19	degrees of freedom			
P (Chi-Sq)		**24.22**	**%**					
MSWD		**1.37**						

Sample Number		**OK12-64**						
Position (#)		39						
Area of Graticule Square		6.400E-07						
No. of Crystals		20						
Zeta Factor ± Error		121.1	3.5					
Rho d (% Relative Error)		3.367E+05	2.15					
N d		2155						
N s	N i	N g	ρ s	ρ i	ρ s / ρ i	U ppm	Age (Ma)	Age error
288	12	18	2.500E+07	1.042E+06	24.0000	152.8	**471.61**	**139.99**
101	7	6	2.630E+07	1.823E+06	14.4286	267.5	**287.64**	**112.90**
245	9	18	2.127E+07	7.813E+05	27.2222	114.6	**532.38**	**181.71**
209	5	12	2.721E+07	6.510E+05	41.8000	95.5	**800.38**	**363.34**
162	11	8	3.164E+07	2.148E+06	14.7273	315.2	**293.47**	**92.05**
197	10	30	1.026E+07	5.208E+05	19.7000	76.4	**389.61**	**127.07**
114	11	9	1.979E+07	1.910E+06	10.3636	280.2	**207.90**	**66.06**
224	15	16	2.188E+07	1.465E+06	14.9333	214.9	**297.48**	**80.06**
382	18	24	2.487E+07	1.172E+06	21.2222	171.9	**418.76**	**102.12**
343	21	40	1.340E+07	8.203E+05	16.3333	120.4	**324.68**	**73.92**
193	13	21	1.436E+07	9.673E+05	14.8462	141.9	**295.78**	**85.42**
161	7	12	2.096E+07	9.115E+05	23.0000	133.7	**452.64**	**175.52**
103	3	12	1.341E+07	3.906E+05	34.3333	57.3	**664.50**	**389.93**
168	10	14	1.875E+07	1.116E+06	16.8000	163.7	**333.72**	**109.29**
217	15	8	4.238E+07	2.930E+06	14.4667	429.8	**288.39**	**77.69**
259	7	12	3.372E+07	9.115E+05	37.0000	133.7	**713.36**	**274.45**
154	12	10	2.406E+07	1.875E+06	12.8333	275.1	**256.47**	**77.42**
177	6	10	2.766E+07	9.375E+05	29.5000	137.5	**575.00**	**239.59**
156	13	15	1.625E+07	1.354E+06	12.0000	198.7	**240.12**	**69.85**
307	11	16	2.998E+07	1.074E+06	27.9091	157.6	**545.26**	**168.47**
**********	**********	**********	**********	**********	**********	**********	**********	**********
4160	216	311	2.090E+07	1.085E+06	19.2593	159.2	**381.15**	**29.94**
Pooled Ratio		19.2593	±	1.5127				
Mean Ratio		21.3710	±	2.0113				
Pooled Age		381.15	±	29.94	1 S.E.			
Mean Crystal Age		421.60	±	40.88	1 S.E.			
Binomial Age		**381.78**	**+**	**55.36**	**"+95%"**			
			-	**48.19**	**"-95%"**			
Central Age		**378.98**	**±**	**31.99**				
Age Dispersion		**13.34**	%					
Chi-squared		**25.117**	with	19	degrees of freedom			
P (Chi-Sq)		**15.67**	**%**					
MSWD		**2.06**						

Sample Number		**BB7**			Mineral	**Zircon**					
Position (#)		39			Glass (U ppm	49.4					
Area of Graticule Square		6.400E-07			Irradiation	UA-Z4					
No. of Crystals		11			Analyst	SNT					
Zeta Factor ± Error		121.1	3.5		Count Date	12.4.2012					
Rho d (% Relative Error)		4.951E+05	1.78		Locality						
N d		3168			Rock Type						
N s	N i	N g	Rho s	Rho i	Rho s / Rho i	U ppm	Age (Ma)	Age error	50% Age	"+95%"	"-95%"
123	13	8	2.402E+07	2.539E+06	9.4615	253.3	**277.58**	**81.50**	286.20	239.58	128.28
169	17	12	2.201E+07	2.214E+06	9.9412	220.9	**291.34**	**74.78**	298.15	205.33	119.95
166	19	10	2.594E+07	2.969E+06	8.7368	296.2	**256.73**	**62.79**	262.24	169.06	101.73
225	20	18	1.953E+07	1.736E+06	11.2500	173.2	**328.73**	**77.51**	335.11	204.43	125.32
257	22	15	2.677E+07	2.292E+06	11.6818	228.7	**341.02**	**76.63**	346.99	198.00	124.52
284	30	18	2.465E+07	2.604E+06	9.4667	259.8	**277.73**	**54.14**	281.42	133.40	89.85
169	16	12	2.201E+07	2.083E+06	10.5625	207.9	**309.11**	**81.53**	316.72	226.42	130.05
69	7	6	1.797E+07	1.823E+06	9.8571	181.9	**288.93**	**115.03**	305.76	414.73	171.17
168	16	10	2.625E+07	2.500E+06	10.5000	249.4	**307.33**	**81.08**	314.90	225.23	129.35
61	5	6	1.589E+07	1.302E+06	12.2000	129.9	**355.74**	**165.92**	384.10	688.08	237.33
123	15	16	1.201E+07	1.465E+06	8.2000	146.2	**241.25**	**66.49**	247.92	189.46	106.12
**********	**********	**********	**********	**********	**********	**********	**********	**********	**********	**********	**********
1814	180	131	2.164E+07	2.147E+06	10.0778	214.2	**295.25**	**25.15**	295.89	48.83	41.88
Pooled Ratio		10.0778	±	0.8586							
Mean Ratio		10.1689	±	0.3683							
Pooled Age		295.25	±	25.15	1 S.E.						
Mean Crystal Age		297.86	±	11.03	1 S.E.						
Binomial Age		295.89	+	48.83	"+95%"						
			-	41.88	"-95%"						
Central Age		**295.25**	**±**	**25.15**							
Age Dispersion		**0.00**	%								
Chi-squared		**1.969**	with	10	degrees of freedom						
P (Chi-Sq)		**99.66**	**%**								

Data Set S3. Zircon (U-Th)/He Data and Cooling Ages

Sample	Age, Ma	err., Ma	U (ppm)	Th (ppm)	147Sm (ppm)	[U]e	Th/U	He (nmol/g)	mass (ug)	Ft	ESR
OK12-1											
OK12-1-1	242.94	19.44	38.8	13.94	0.87	42.0	0.36	40.4	3.78	0.72	41.32
OK12-1-3	237.93	19.03	40.0	23.13	0.83	45.3	0.58	41.7	2.75	0.71	39.09
OK12-1-5	250.21	20.02	182.1	46.46	5.88	192.9	0.26	193.3	2.93	0.73	42.25
OK12-1-6	251.25	20.10	46.3	22.48	1.32	51.5	0.49	52.0	3.13	0.73	43.27
OK12-4											
OK12-4-1	465.95	37.28	72.4	28.86	2.47	79.1	0.40	152.7	4.19	0.74	44.94
OK12-4-2	362.19	28.98	236.8	72.24	4.23	253.4	0.31	390.0	5.56	0.77	49.80
OK12-4-3	274.62	21.97	27.7	9.94	4.44	30.0	0.36	37.6	15.04	0.83	68.65
OK12-4-4	542.67	43.41	45.8	29.31	3.47	52.6	0.64	126.4	7.17	0.79	56.02
OK12-4-5	250.95	20.08	35.0	13.19	2.79	38.1	0.38	39.9	5.61	0.76	48.68
OK12-4-6	331.04	26.48	46.1	26.72	2.31	52.3	0.58	78.7	12.73	0.82	66.75
OK12-6											
OK12-6-1	806.46	64.52	25.0	17.08	0.54	28.9	0.68	99.1	4.21	0.74	45.38
OK12-6-2	342.25	27.38	63.9	27.39	0.65	70.2	0.43	101.1	5.49	0.76	48.94
OK12-6-3	265.82	21.27	237.3	119.09	3.68	264.8	0.50	299.8	6.19	0.77	52.11
OK12-6-4	415.81	33.27	328.5	36.23	1.50	336.9	0.11	585.0	4.14	0.75	45.74
OK12-6-5	365.82	29.27	36.9	40.16	5.90	46.2	1.09	67.3	3.27	0.72	41.86
OK12-6-6	397.27	31.78	112.1	38.00	3.47	120.9	0.34	202.5	4.77	0.76	48.33
OK12-9											
OK12-9-1	383.71	30.70	70.7	42.01	1.00	80.4	0.59	125.5	3.41	0.73	43.83
OK12-9-2	1419.27	113.54	11.0	4.51	0.16	12.0	0.41	77.1	3.46	0.74	44.19
OK12-9-3	426.60	34.13	72.1	49.54	0.39	83.5	0.69	148.8	3.99	0.75	47.23
OK12-9-4	341.53	27.32	60.4	41.97	2.36	70.0	0.70	92.9	2.62	0.70	39.04
OK12-9-5	273.77	21.90	74.1	14.38	2.27	77.4	0.19	83.1	2.42	0.71	39.50
OK12-9-6	256.89	20.55	174.0	91.24	6.84	195.1	0.52	197.0	2.82	0.72	40.62
OK12-12											
OK12-12-1	335.15	26.81	130.5	44.39	2.09	140.7	0.34	205.1	6.95	0.79	54.89
OK12-12-2	510.80	40.86	92.6	16.75	1.33	96.5	0.18	204.4	4.65	0.74	43.88
OK12-12-3	236.16	18.89	620.5	207.25	32.38	668.3	0.33	676.8	6.32	0.78	53.30
OK12-12-4	400.38	32.03	134.0	41.62	4.81	143.6	0.31	249.5	7.05	0.78	53.07
OK12-12-5	399.58	31.97	272.2	70.84	1.18	288.5	0.26	523.0	9.79	0.81	63.66
OK12-12-6	332.64	26.61	369.9	208.54	2.09	417.9	0.56	535.9	2.28	0.70	38.13

Sample	Age, Ma	err., Ma	U (ppm)	Th (ppm)	147Sm (ppm)	[U]e	Th/U	He (nmol/g)	mass (ug)	Ft	ESR
OK12-16											
OK12-16-1	312.21	24.98	153.0	24.72	1.05	158.7	0.16	215.5	6.48	0.79	54.41
OK12-16-2	329.62	26.37	46.6	25.16	3.63	52.4	0.54	73.7	6.57	0.77	51.78
OK12-16-3	290.56	23.25	210.3	84.30	2.07	229.7	0.40	276.2	4.28	0.75	46.74
OK12-16-4	291.29	23.30	199.8	76.13	4.35	217.3	0.38	266.2	5.64	0.76	49.23
OK12-16-5	207.43	16.59	555.4	106.14	23.13	580.0	0.19	507.0	5.38	0.77	50.21
OK12-16-6	250.82	20.07	83.3	22.97	1.39	88.5	0.28	97.1	7.34	0.80	57.03
OK12-19											
OK12-19-1	236.48	18.92	169.5	90.06	0.52	190.2	0.53	170.3	2.47	0.69	36.92
OK12-19-2	493.79	39.50	16.4	10.49	0.29	18.8	0.64	41.4	7.39	0.79	57.99
OK12-19-3	338.41	27.07	54.0	22.05	0.36	59.1	0.41	83.5	3.99	0.76	47.52
OK12-19-4	286.07	22.89	60.1	27.88	1.99	66.5	0.46	71.2	1.73	0.68	35.45
OK12-19-5	455.76	36.46	45.3	39.23	4.68	54.4	0.87	94.6	2.06	0.69	36.87
OK12-19-6	587.56	47.00	69.4	67.22	6.45	84.9	0.97	179.7	1.28	0.64	31.94
OK12-21											
OK12-21-1	341.90	27.35	250.1	147.53	8.03	284.1	0.59	374.5	2.41	0.70	38.05
OK12-21-2	409.36	32.75	141.4	76.35	3.14	159.0	0.54	255.7	2.86	0.71	39.46
OK12-21-3	570.92	45.67	19.3	31.06	5.49	26.5	1.61	60.6	3.02	0.71	41.43
OK12-21-4	277.99	22.24	192.5	157.35	14.91	228.8	0.82	252.9	3.07	0.72	42.18
OK12-21-5	328.20	26.26	39.2	22.55	3.00	44.4	0.58	56.2	2.27	0.70	38.18
OK12-21-6	1550.25	124.02	48.3	31.04	4.44	55.5	0.64	375.5	2.76	0.71	39.65
OK12-23											
OK12-23-1	900.88	72.07	29.0	15.07	0.93	32.4	0.52	135.9	8.52	0.80	58.82
OK12-23-2	294.62	23.57	257.6	202.36	7.31	304.3	0.79	367.4	3.91	0.74	45.91
OK12-23-3	323.36	25.87	45.8	20.94	0.89	50.6	0.46	68.6	4.87	0.76	48.51
OK12-23-6	648.82	51.91	26.7	16.58	2.09	30.5	0.62	90.2	8.56	0.80	60.48
OK12-27											
OK12-27-1	403.08	32.25	112.7	30.66	3.89	119.7	0.27	195.7	2.84	0.73	42.40
OK12-27-2	592.77	47.42	1.2	0.42	0.09	1.3	0.35	3.5	7.66	0.80	58.12
OK12-27-4	284.92	22.79	93.4	55.53	3.92	106.2	0.59	105.1	1.23	0.63	30.49

Zircon (U-Th)/He Data and Cooling Ages, continued.

Sample	Age, Ma	err., Ma	U (ppm)	Th (ppm)	147Sm (ppm)	[U]e	Th/U	He (nmol/g)	mass (ug)	Ft	ESR
OK12-31											
OK12-31-1	325.35	26.03	124.7	58.85	0.56	138.3	0.47	191.2	6.15	0.77	50.78
OK12-31-2	231.76	18.54	49.6	21.80	1.40	54.6	0.44	56.1	10.57	0.81	61.90
OK12-31-3	282.03	22.56	51.2	17.85	2.99	55.3	0.35	68.1	8.61	0.79	56.31
OK12-31-4	454.36	36.35	86.5	21.71	1.75	91.5	0.25	185.9	7.87	0.80	58.40
OK12-31-5	304.74	24.38	170.5	192.44	7.64	214.9	1.13	258.0	3.07	0.71	41.26
OK12-31-6	384.10	30.73	86.2	40.55	4.72	95.5	0.47	153.8	5.84	0.76	47.72
OK12-32											
OK12-32-1	305.46	24.44	130.5	39.96	4.07	139.7	0.31	173.2	3.39	0.74	43.61
OK12-32-2	350.58	28.05	290.7	123.39	76.54	319.5	0.42	446.1	3.17	0.72	41.07
OK12-32-3	269.27	21.54	224.7	109.68	9.73	250.0	0.49	275.5	4.92	0.74	45.53
OK12-32-4	319.57	25.57	113.1	75.93	7.94	130.7	0.67	181.7	7.79	0.79	55.94
OK12-32-5	456.11	36.49	13.8	11.39	2.18	16.4	0.83	34.2	12.51	0.82	66.01
OK12-32-7	1964.15	157.13	15.3	6.78	1.16	16.9	0.44	195.3	11.13	0.82	64.67
OK12-35											
OK12-35-1	328.68	26.29	263.7	63.41	11.96	278.4	0.24	357.8	2.34	0.71	38.91
OK12-35-2	436.35	34.91	243.2	112.43	22.47	269.2	0.46	447.8	2.04	0.69	36.22
OK12-35-3	489.47	39.16	21.8	18.54	0.00	26.0	0.85	49.3	2.18	0.69	37.93
OK12-35-4	439.19	35.14	167.4	52.81	1.31	179.5	0.32	312.5	2.59	0.71	39.66
OK12-35-5	514.53	41.16	115.4	66.88	1.32	130.8	0.58	264.4	2.57	0.70	38.75
OK12-35-6	435.45	34.84	112.1	40.30	0.66	121.4	0.36	203.3	2.05	0.69	36.79
OK12-36											
OK12-36-1	980.80	78.46	57.1	28.76	9.52	63.8	0.50	276.8	5.25	0.76	48.06
OK12-36-2	673.32	53.87	95.8	49.13	3.74	107.2	0.51	317.2	6.57	0.77	51.86
OK12-36-3	252.18	20.17	497.7	101.70	77.81	521.5	0.20	547.2	5.18	0.76	47.30
OK12-36-5	408.36	32.67	63.2	27.35	4.91	69.5	0.43	116.0	3.89	0.74	43.69
OK12-36-6	364.84	29.19	107.7	141.04	11.03	140.2	1.31	208.5	4.03	0.74	45.05
OK12-36-7	414.54	33.16	216.8	68.35	20.46	232.6	0.32	433.2	10.97	0.81	60.91

Zircon (U-Th)/He Data and Cooling Ages, continued.

Sample	Age, Ma	err., Ma	U (ppm)	Th (ppm)	147Sm (ppm)	[U]e	Th/U	He (nmol/g)	mass (ug)	Ft	ESR
OK12-37											
OK12-37-1	247.04	19.76	12.6	14.04	3.86	15.9	1.11	17.1	7.71	0.79	57.04
OK12-37-2	398.01	31.84	146.5	67.26	6.52	162.0	0.46	281.0	6.91	0.78	54.44
OK12-37-3	20.86	1.67	36.8	5.43	0.71	38.0	0.15	3.4	8.72	0.80	58.23
OK12-37-4	432.58	34.61	153.0	66.32	9.70	168.3	0.43	331.0	10.29	0.81	63.89
OK12-39											
OK12-39-1	290.20	23.22	49.6	12.90	3.91	52.6	0.26	64.7	5.64	0.77	50.17
OK12-39-3	280.30	22.42	59.2	22.50	4.40	64.4	0.38	78.8	8.16	0.79	56.98
OK12-39-4	286.01	22.88	176.3	37.91	15.68	185.1	0.21	217.1	4.20	0.75	44.93
OK12-39-5	300.37	24.03	144.4	77.61	11.22	162.3	0.54	178.8	2.15	0.67	33.94
OK12-41											
OK12-41-1	362.21	28.98	128.2	35.43	2.48	136.4	0.28	220.3	9.13	0.80	59.89
OK12-41-2	334.57	26.77	48.0	24.86	0.30	53.7	0.52	77.3	7.30	0.78	53.18
OK12-41-3	384.76	30.78	93.1	58.63	3.06	106.6	0.63	178.8	6.87	0.78	55.28
OK12-41-4	371.99	29.76	89.3	22.95	2.19	94.6	0.26	154.8	7.55	0.79	56.38
OK12-41-6	425.19	34.01	34.1	20.46	2.07	38.8	0.60	68.9	4.66	0.75	46.82
OK12-41-7	405.14	32.41	54.3	34.20	2.58	62.2	0.63	112.8	9.34	0.80	60.64
OK12-43											
OK12-43-1	412.07	32.97	116.6	57.52	5.24	129.8	0.49	200.4	2.24	0.68	34.99
OK12-43-2	341.26	27.30	230.1	136.96	7.35	261.7	0.60	311.3	1.22	0.63	30.48
OK12-43-3	217.86	17.43	130.9	24.62	4.45	136.6	0.19	110.5	1.86	0.68	34.69
OK12-43-6	364.73	29.18	278.0	89.35	38.95	298.8	0.32	327.4	0.49	0.55	23.32
OK12-43-7	258.60	20.69	505.8	153.75	159.02	542.0	0.30	453.6	0.77	0.59	26.43
OK12-45											
OK12-45-1	384.20	30.74	41.7	34.75	0.61	49.7	0.83	81.9	5.71	0.77	52.34
OK12-45-2	547.50	43.80	61.4	49.00	1.38	72.7	0.80	167.9	5.34	0.75	47.45
OK12-45-3	323.28	25.86	70.4	24.11	0.96	75.9	0.34	104.4	6.14	0.77	50.69
OK12-45-4	422.58	33.81	175.4	61.80	1.80	189.6	0.35	324.3	3.06	0.73	42.24
OK12-45-5	450.52	36.04	129.4	36.87	4.40	137.9	0.28	259.0	4.07	0.75	45.65
OK12-45-6	514.28	41.14	27.7	12.57	2.44	30.6	0.45	67.7	5.07	0.77	50.08

Zircon (U-Th)/He Data and Cooling Ages, continued.

Sample	Age, Ma	err., Ma	U (ppm)	Th (ppm)	147Sm (ppm)	[U]e	Th/U	He (nmol/g)	mass (ug)	Ft	ESR
OK12-51											
OK12-51-1	20.81	1.66	85.1	93.70	2.49	106.7	1.10	9.0	4.72	0.75	47.40
OK12-51-2	496.49	39.72	21.5	11.18	1.93	24.1	0.52	48.0	3.21	0.72	41.15
OK12-51-3	404.75	32.38	77.1	52.42	4.11	89.2	0.68	150.8	5.64	0.75	47.48
OK12-51-4	347.58	27.81	60.6	25.15	3.65	66.4	0.41	91.2	3.17	0.72	40.31
OK12-51-5	478.84	38.31	96.1	58.42	2.08	109.6	0.61	215.9	3.60	0.74	44.32
OK12-51-6	398.10	31.85	189.6	108.79	6.89	214.7	0.57	354.7	4.96	0.75	46.26
OK12-52											
OK12-52-1	880.46	70.44	82.0	51.15	9.86	93.8	0.62	369.7	6.75	0.77	52.02
OK12-52-2	382.58	30.61	430.4	221.30	121.82	482.0	0.51	775.4	7.59	0.76	48.26
OK12-52-3	343.35	27.47	328.6	166.33	72.08	367.2	0.51	534.6	5.96	0.77	50.14
OK12-52-4	406.07	32.49	63.8	37.26	1.89	72.4	0.58	122.9	4.31	0.75	47.40
OK12-52-6	439.56	35.16	171.9	66.74	16.98	187.4	0.39	352.3	5.68	0.77	50.13
OK12-52-7	407.57	32.61	85.0	36.55	2.73	93.5	0.43	167.8	8.24	0.79	56.57
OK12-55											
OK12-55-1	480.77	38.46	109.2	47.14	4.51	120.1	0.43	257.7	8.03	0.80	58.25
OK12-55-2	303.42	24.27	73.4	55.89	5.96	86.3	0.76	115.5	8.38	0.80	59.51
OK12-55-3	360.62	28.85	250.0	56.99	48.45	263.3	0.23	416.5	7.11	0.79	55.66
OK12-55-4	418.95	33.52	142.9	145.89	6.64	176.5	1.02	350.4	22.87	0.85	81.15
OK12-55-5	376.38	30.11	207.0	179.61	7.05	248.4	0.87	379.5	3.87	0.73	43.91
OK12-55-6	474.81	37.98	145.7	78.00	10.11	163.7	0.54	291.2	2.09	0.67	34.67
OK12-55-7	341.17	27.29	42.8	30.11	10.15	49.8	0.70	73.3	6.63	0.78	53.73
OK12-56											
OK12-56-1	369.77	29.58	133.7	57.49	8.14	146.9	0.43	233.5	5.71	0.77	52.23
OK12-56-2	331.36	26.51	49.8	28.90	3.52	56.5	0.58	82.5	8.65	0.80	58.40
OK12-56-3	317.52	25.40	29.8	15.45	3.69	33.4	0.52	46.1	7.69	0.79	55.64
OK12-56-4	377.50	30.20	51.8	39.94	3.08	61.0	0.77	102.0	7.86	0.80	59.07

Zircon (U-Th)/He Data and Cooling Ages, continued.

Sample	Age, Ma	err., Ma	U (ppm)	Th (ppm)	147Sm (ppm)	[U]e	Th/U	He (nmol/g)	mass (ug)	Ft	ESR
OK12-58											
OK12-58-1	290.00	23.20	26.3	12.54	2.86	29.2	0.48	39.2	16.50	0.84	73.27
OK12-58-2	437.95	35.04	52.3	20.99	2.57	57.2	0.40	108.6	5.92	0.78	52.61
OK12-58-3	374.73	29.98	94.3	78.88	4.64	112.5	0.84	184.0	8.06	0.79	56.02
OK12-58-4	364.22	29.14	99.8	28.21	2.06	106.3	0.28	174.4	10.04	0.81	62.59
OK12-58-5	381.04	30.48	47.6	20.33	3.18	52.3	0.43	92.9	18.53	0.84	73.44
OK12-58-6	743.01	59.44	40.5	25.11	2.68	46.3	0.62	166.6	18.10	0.84	76.56
OK12-59											
OK12-59-1	266.17	21.29	37.6	45.77	9.89	48.1	1.22	54.7	6.52	0.77	53.26
OK12-59-2	262.16	20.97	69.3	31.93	1.43	76.7	0.46	92.7	14.76	0.84	73.26
OK12-59-3	231.05	18.48	102.2	29.68	2.55	109.0	0.29	107.4	6.96	0.78	52.28
OK12-59-4	706.77	56.54	0.0	0.03	0.01	0.0	0.90	0.2	96.70	0.91	135.85
OK12-59-5	320.03	25.60	67.1	51.79	3.53	79.0	0.77	112.8	10.44	0.81	62.07
OK12-59-6	250.37	20.03	30.0	59.98	10.47	43.9	2.00	46.7	7.88	0.77	53.20
OK12-59-7	288.43	23.07	121.3	67.45	5.50	136.9	0.56	169.4	7.46	0.78	53.27
OK12-60											
OK12-60-1	200.07	16.01	73.7	33.80	3.50	81.5	0.46	58.7	1.61	0.66	32.96
OK12-60-2	203.77	16.30	207.6	162.50	3.44	245.1	0.78	187.2	2.10	0.68	36.57
OK12-60-3	190.11	15.21	86.6	46.92	1.71	97.4	0.54	68.9	1.86	0.68	35.75
OK12-63											
OK12-63-1	259.48	20.76	124.6	61.67	16.59	138.9	0.50	160.9	12.43	0.81	63.15
OK12-63-2	218.09	17.45	141.7	75.62	3.38	159.2	0.53	150.1	6.94	0.79	55.90
OK12-63-3	249.98	20.00	420.9	109.95	4.45	446.2	0.26	485.7	8.54	0.79	56.30
OK12-63-4	230.43	18.43	200.9	120.36	8.47	228.7	0.60	219.1	6.21	0.76	48.49
OK12-63-5	266.35	21.31	121.3	57.97	11.12	134.7	0.48	147.5	5.23	0.75	46.07
OK12-63-6	223.28	17.86	117.1	64.83	4.56	132.1	0.55	132.7	14.30	0.82	66.53

Zircon (U-Th)/He Data and Cooling Ages, continued.

Sample	Age, Ma	err., Ma	U (ppm)	Th (ppm)	147Sm (ppm)	[U]e	Th/U	He (nmol/g)	mass (ug)	Ft	ESR
OK12-63tuff											
OK12-63tuff-1	198.78	15.90	67.8	28.79	4.96	74.5	0.42	66.2	12.32	0.82	64.63
OK12-63tuff-2	210.42	16.83	493.0	106.14	14.58	517.5	0.22	426.3	2.90	0.72	39.85
OK12-63tuff-3	216.83	17.35	369.4	190.29	6.59	413.2	0.52	361.6	4.62	0.74	44.19
OK12-63tuff-4	240.82	19.27	55.1	28.06	6.56	61.6	0.51	62.5	7.83	0.77	50.63
OK12-64											
OK12-64-1	235.68	18.85	113.8	68.55	1.02	129.6	0.60	132.3	9.07	0.79	56.26
OK12-64-2	181.57	14.53	96.7	53.30	2.42	109.0	0.55	86.6	9.15	0.80	59.48
OK12-64-3	195.53	15.64	219.1	72.18	1.25	235.8	0.33	190.8	4.55	0.76	47.60
OK12-64-4	412.22	32.98	23.1	13.56	1.83	26.2	0.59	44.7	4.50	0.74	45.43
OK12-64-5	248.24	19.86	41.2	39.22	2.14	50.3	0.95	54.8	9.35	0.80	59.90
OK12-64-6	224.04	17.92	25.8	17.02	1.67	29.8	0.66	29.8	10.29	0.81	64.50

Zircon (U-Th)/He Data and Cooling Ages, continued.